Small x physics at an Electron Ion Collider

Anna Staśto

PennState
Eberly College of Science

CFNS Summer School, Stony Brook University, August 7-8, 2019

Outline

Outline

- I will focus on some personal selection of topics, not really completely representative for all the physics that can be done at an Electron Ion Collider. This can or has been hopefully complemented by other lectures.

Outline

- ✦ I will focus on some personal selection of topics, not really completely representative for all the physics that can be done at an Electron Ion Collider. This can or has been hopefully complemented by other lectures.

- ✦ It will be mix of phenomenology and also some formal developments in small x physics.

Outline

- I will focus on some personal selection of topics, not really completely representative for all the physics that can be done at an Electron Ion Collider. This can or has been hopefully complemented by other lectures.

- It will be mix of phenomenology and also some formal developments in small x physics.

- The Electron Ion Collider in this lecture is not only US EIC but can be a ‘generic’ Deep Inelastic ep-eA machine. Some simulations shown will be for other projects Large Hadron electron Collider and Future Circular Collider - electron hadron option which are CERN proposals. Many of the physics topics can be investigated by any of these machines - complementarity.

Outline

- ✦ I will focus on some personal selection of topics, not really completely representative for all the physics that can be done at an Electron Ion Collider. This can or has been hopefully complemented by other lectures.

- ✦ It will be mix of phenomenology and also some formal developments in small x physics.

- ✦ The Electron Ion Collider in this lecture is not only US EIC but can be a ‘generic’ Deep Inelastic ep-eA machine. Some simulations shown will be for other projects Large Hadron electron Collider and Future Circular Collider - electron hadron option which are CERN proposals. Many of the physics topics can be investigated by any of these machines - complementarity.

- ✦ **Lecture 1:** will focus on introduction to DIS, with a little bit of history, parton distribution functions, starting from electron-proton and then moving onto electron-ion. Physics of shadowing will be discussed.

Outline

- I will focus on some personal selection of topics, not really completely representative for all the physics that can be done at an Electron Ion Collider. This can or has been hopefully complemented by other lectures.

- It will be mix of phenomenology and also some formal developments in small x physics.

- The Electron Ion Collider in this lecture is not only US EIC but can be a ‘generic’ Deep Inelastic ep-eA machine. Some simulations shown will be for other projects Large Hadron electron Collider and Future Circular Collider - electron hadron option which are CERN proposals. Many of the physics topics can be investigated by any of these machines - complementarity.

- **Lecture 1:** will focus on introduction to DIS, with a little bit of history, parton distribution functions, starting from electron-proton and then moving onto electron-ion. Physics of shadowing will be discussed.

- **Lecture 2:** Continue on shadowing. Discuss the physics of diffraction, inclusive as well as exclusive diffraction of vector mesons. Nucleon, nuclear tomography in the context of the dipole picture of high energy scattering. Ideas of parton saturation will be discussed here.

Outline

- I will focus on some personal selection of topics, not really completely representative for all the physics that can be done at an Electron Ion Collider. This can or has been hopefully complemented by other lectures.

- It will be mix of phenomenology and also some formal developments in small x physics.

- The Electron Ion Collider in this lecture is not only US EIC but can be a ‘generic’ Deep Inelastic ep-eA machine. Some simulations shown will be for other projects Large Hadron electron Collider and Future Circular Collider - electron hadron option which are CERN proposals. Many of the physics topics can be investigated by any of these machines - complementarity.

- **Lecture 1:** will focus on introduction to DIS, with a little bit of history, parton distribution functions, starting from electron-proton and then moving onto electron-ion. Physics of shadowing will be discussed.

- **Lecture 2:** Continue on shadowing. Discuss the physics of diffraction, inclusive as well as exclusive diffraction of vector mesons. Nucleon, nuclear tomography in the context of the dipole picture of high energy scattering. Ideas of parton saturation will be discussed here.

- **Lecture 3:** small x physics, in particular resummation. This lecture will be most formal and technical of all three. I will discuss the issues of the theoretical formalism of high energy scattering, problems of stability and the resummation which is needed.

Why electron ion collisions?

Standard Model of Particle Physics

Why electron ion collisions?

Standard Model of Particle Physics

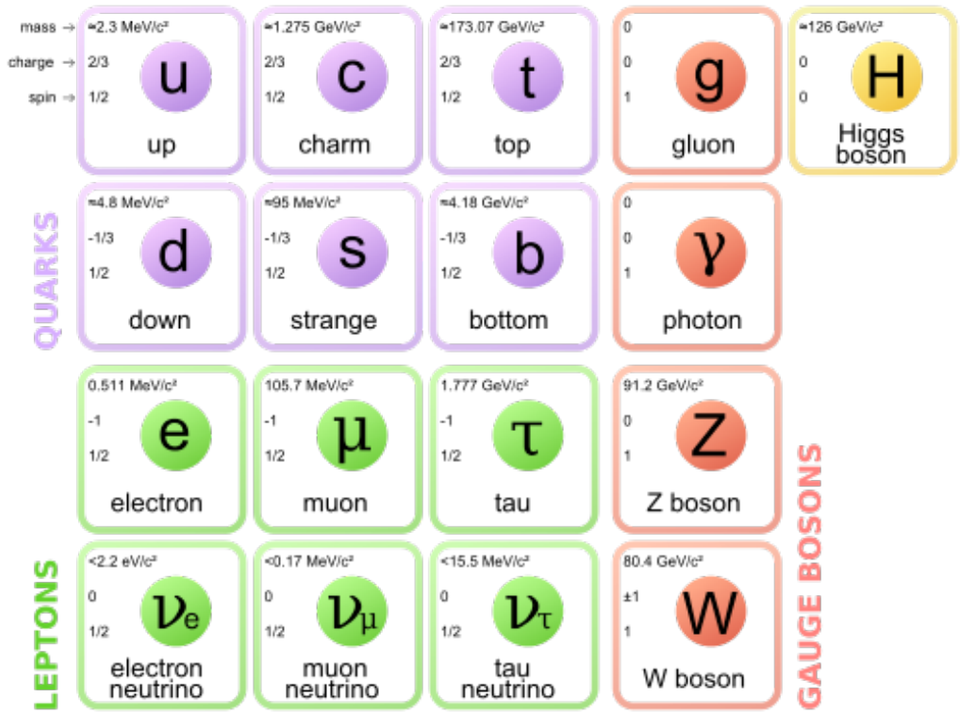

Why electron ion collisions?

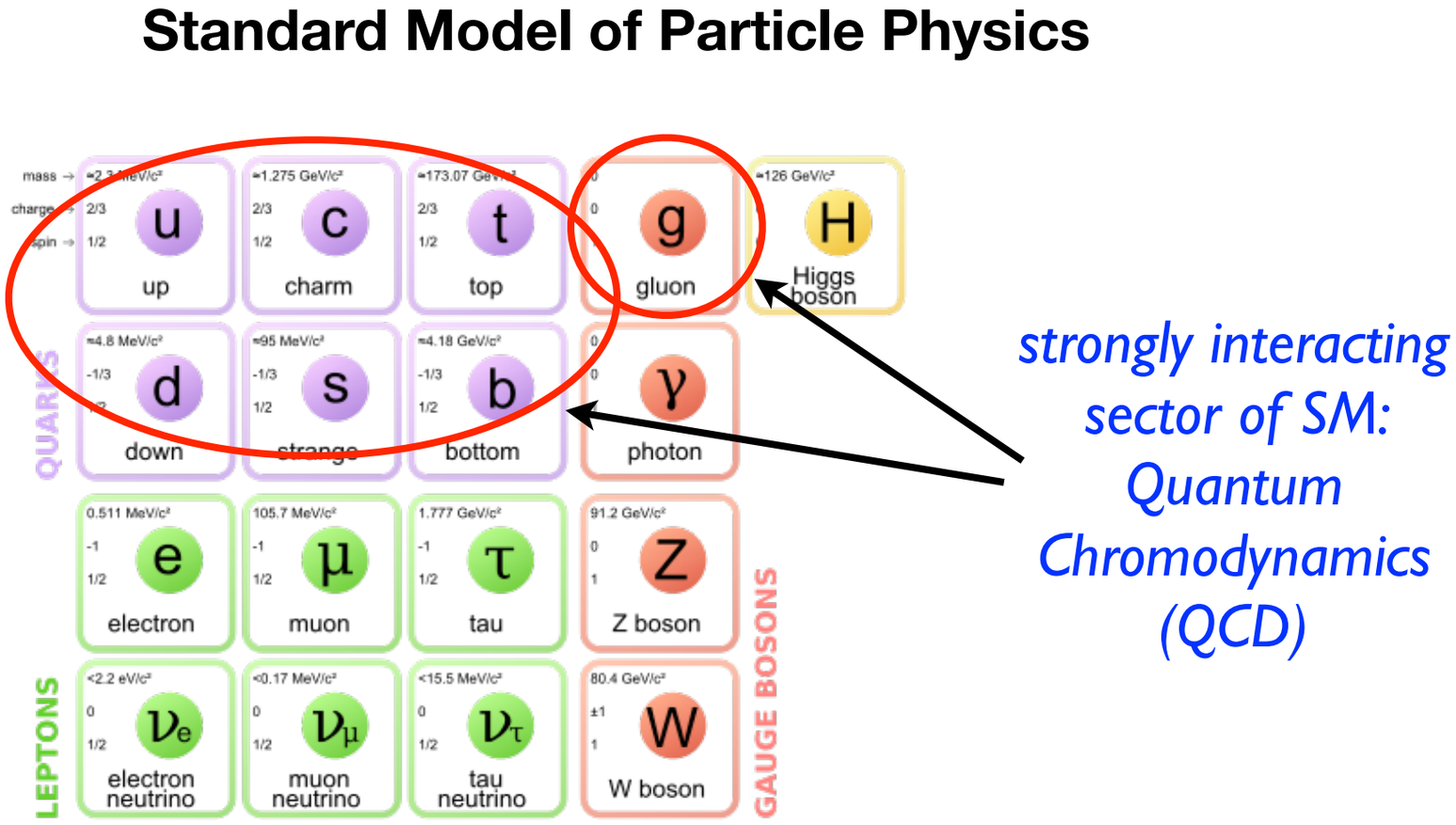

strongly interacting sector of SM: Quantum Chromodynamics (QCD)

Why electron ion collisions?

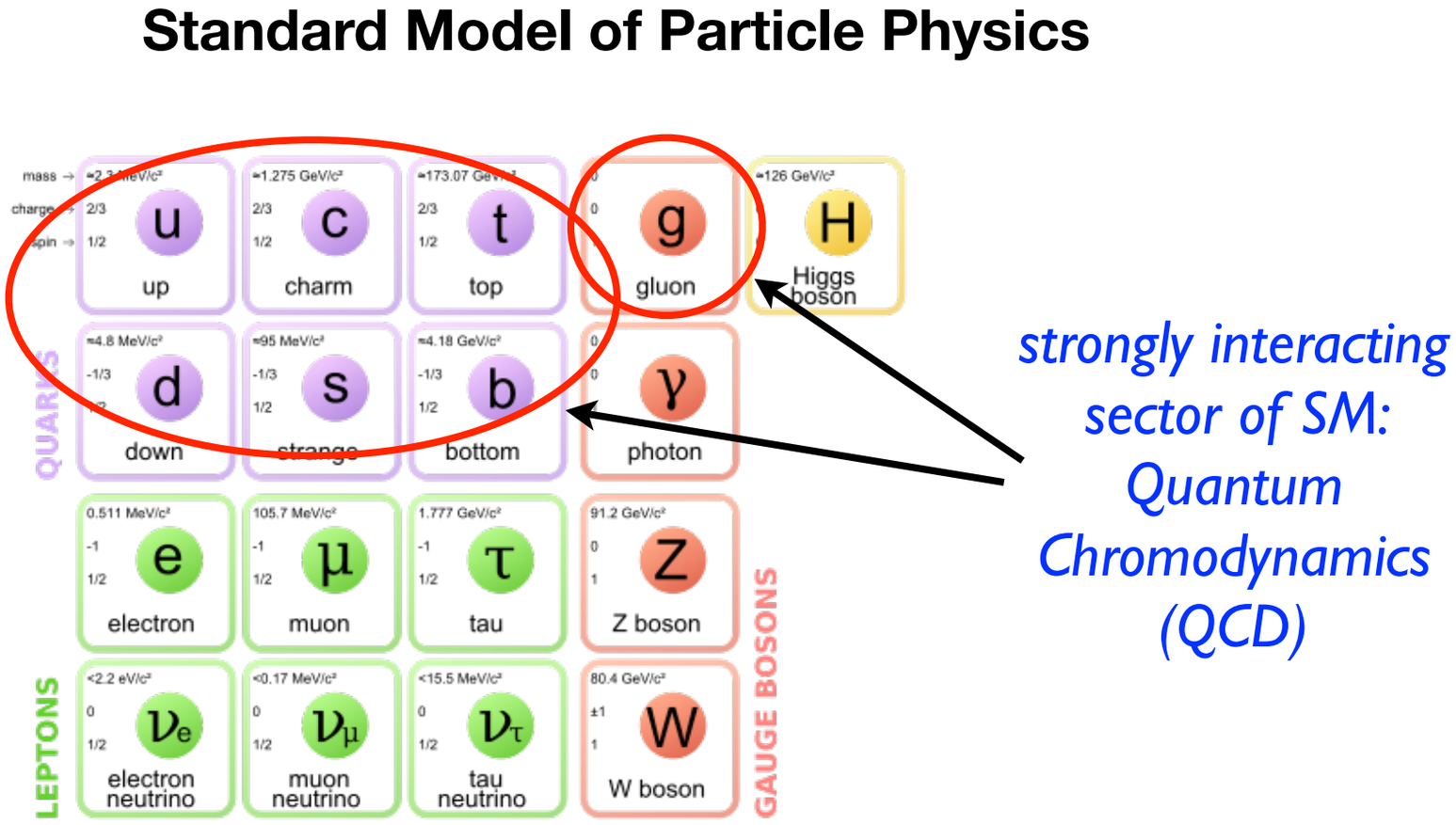

strongly interacting sector of SM: Quantum Chromodynamics (QCD)

But quarks are not free: **color is confined**
Bound in colorless hadrons: **protons, neutrons, mesons**
Protons and neutrons form **nuclei**
These are very complex bound states !

Why electron ion collisions?

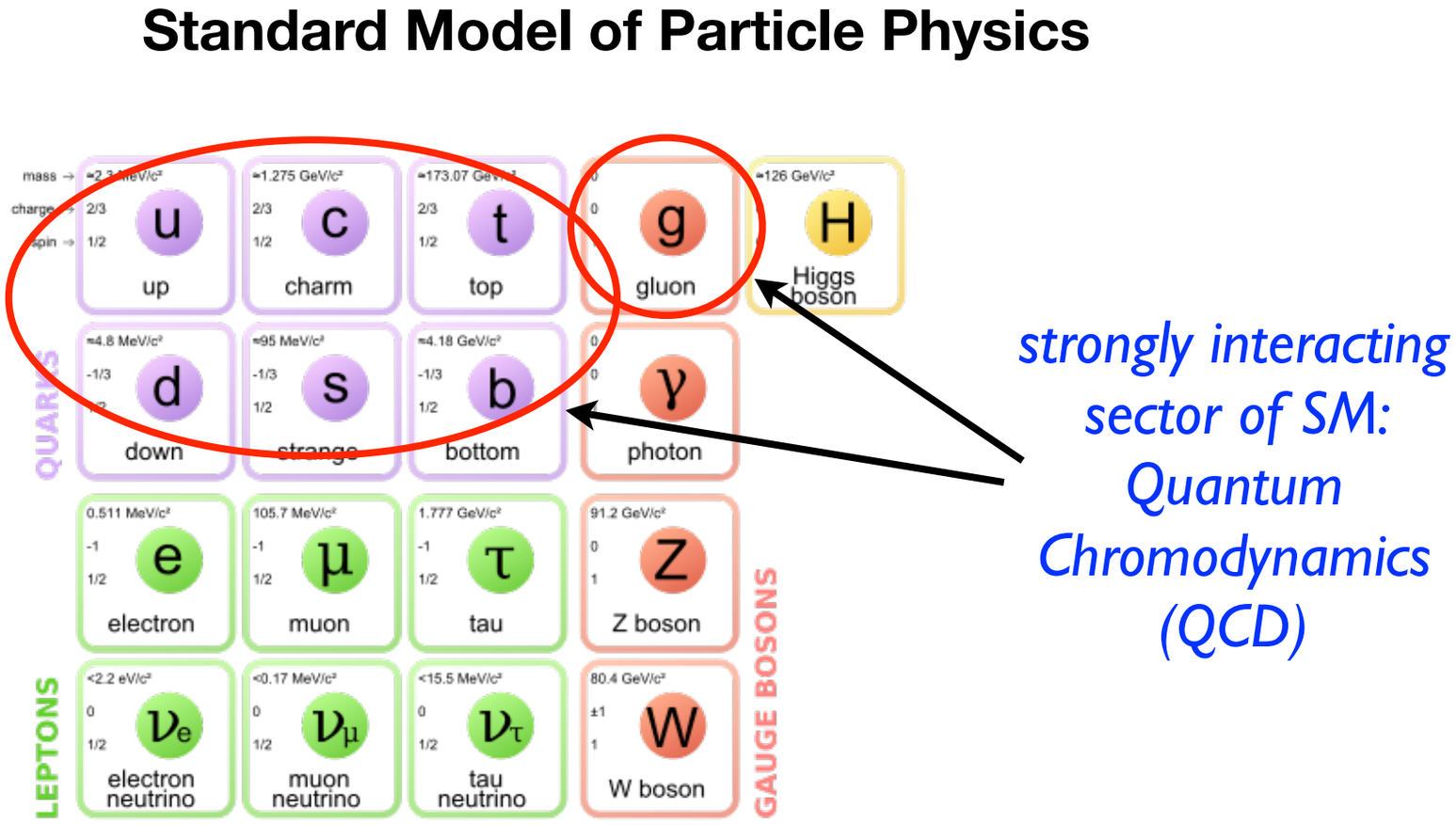

strongly interacting sector of SM: Quantum Chromodynamics (QCD)

But quarks are not free: **color is confined**
Bound in colorless hadrons: **protons, neutrons, mesons**
Protons and neutrons form **nuclei**
These are very complex bound states !

Leptons do not have substructure (*as far as we know)
Electroweak interactions

Why electron ion collisions?

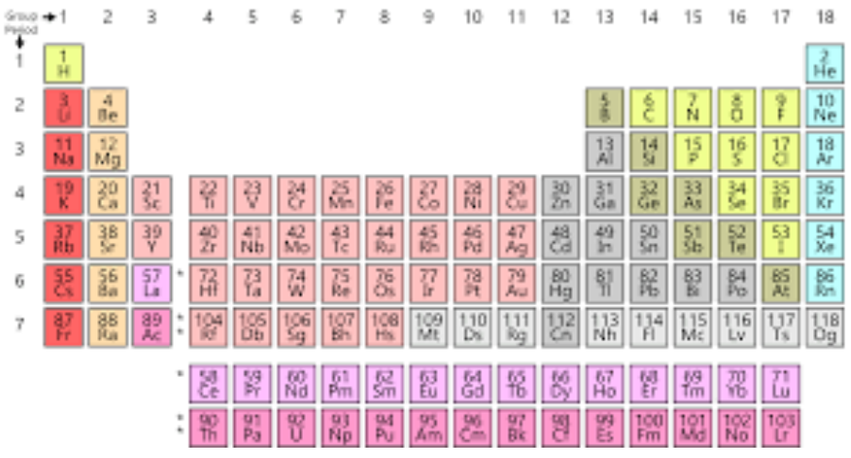

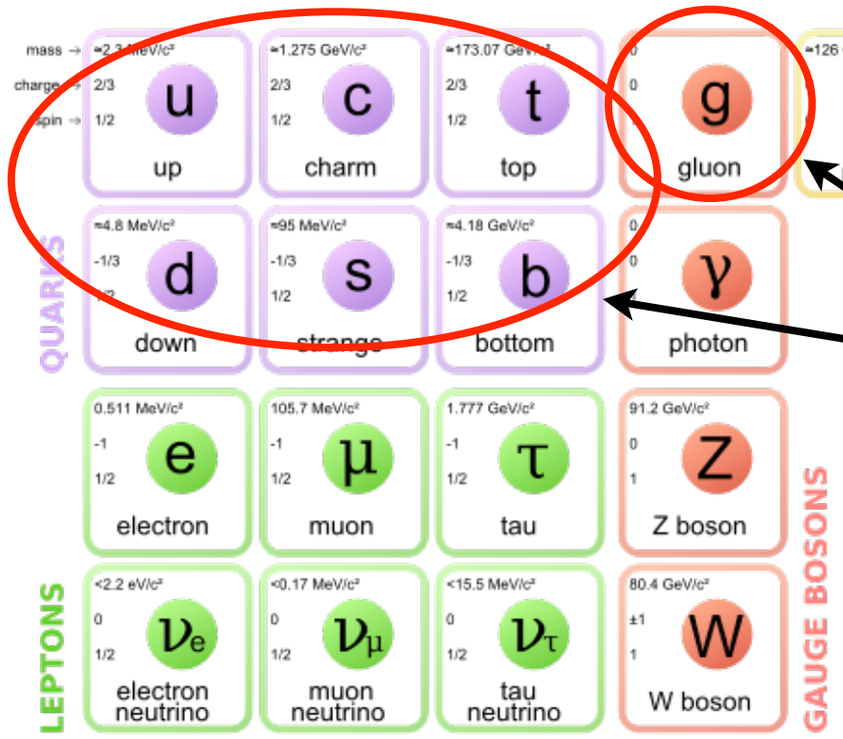

strongly interacting sector of SM: Quantum Chromodynamics (QCD)

But quarks are not free: **color is confined**
Bound in colorless hadrons: **protons, neutrons, mesons**
Protons and neutrons form **nuclei**
These are very complex bound states !

Leptons do not have substructure (*as far as we know)
Electroweak interactions

pp vs ep collisions

proton-proton collisions

Complicated hadronic environment

High multiplicity

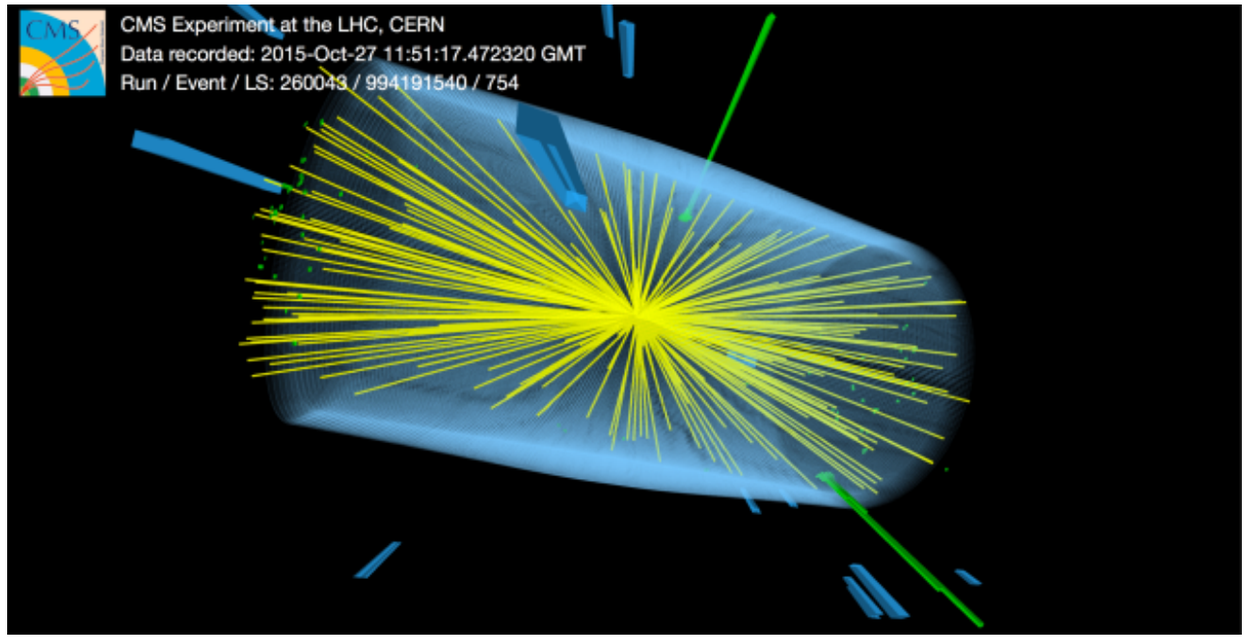

pp vs ep collisions

proton-proton collisions

Complicated hadronic environment

High multiplicity

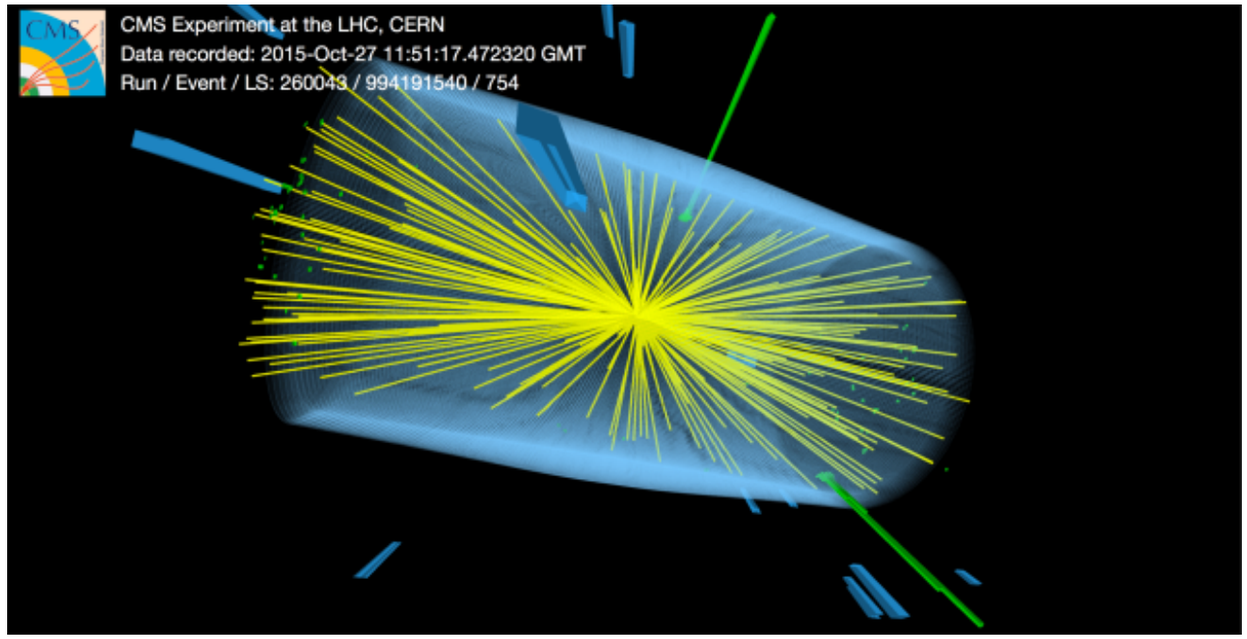

electron-proton collisions

Lepton-Hadron characterized by much cleaner events

Low multiplicity

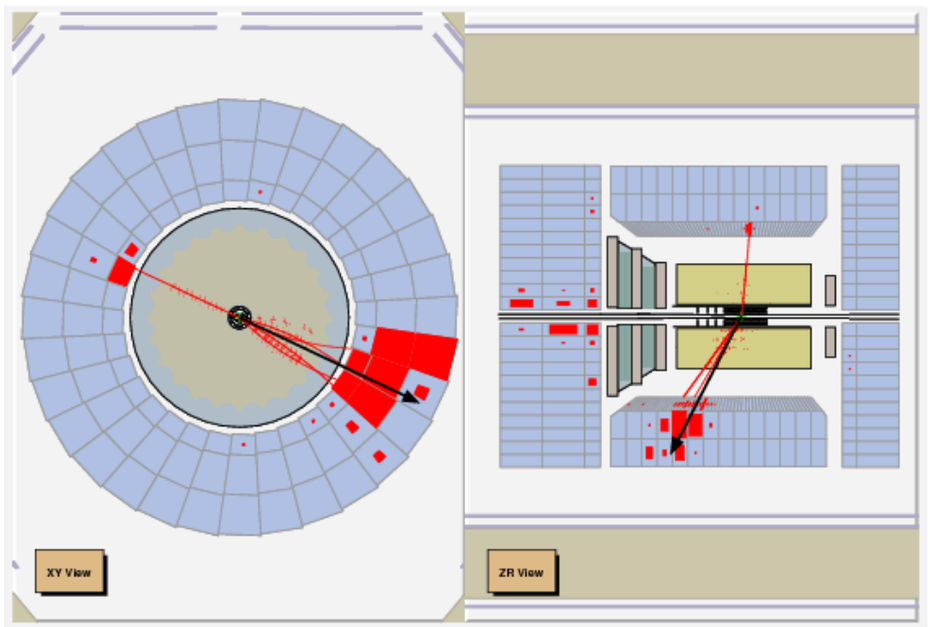

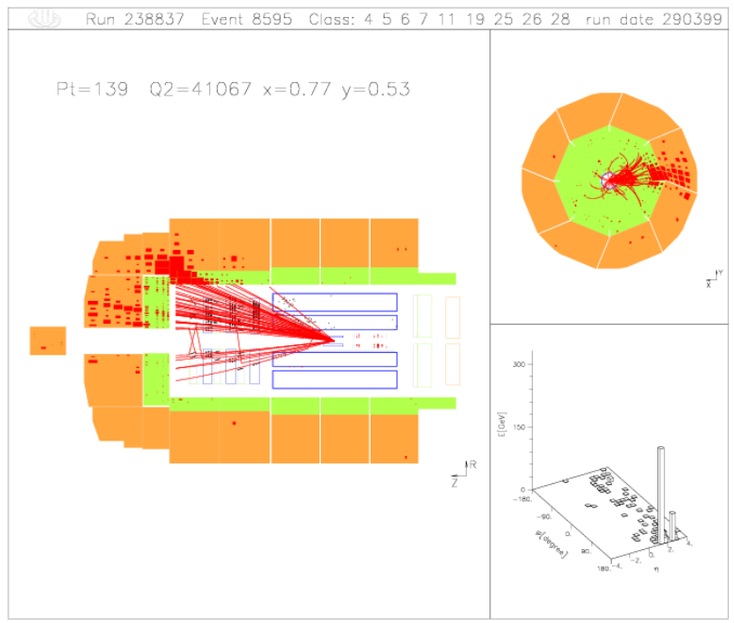

From protons to ions

proton-lead collisions

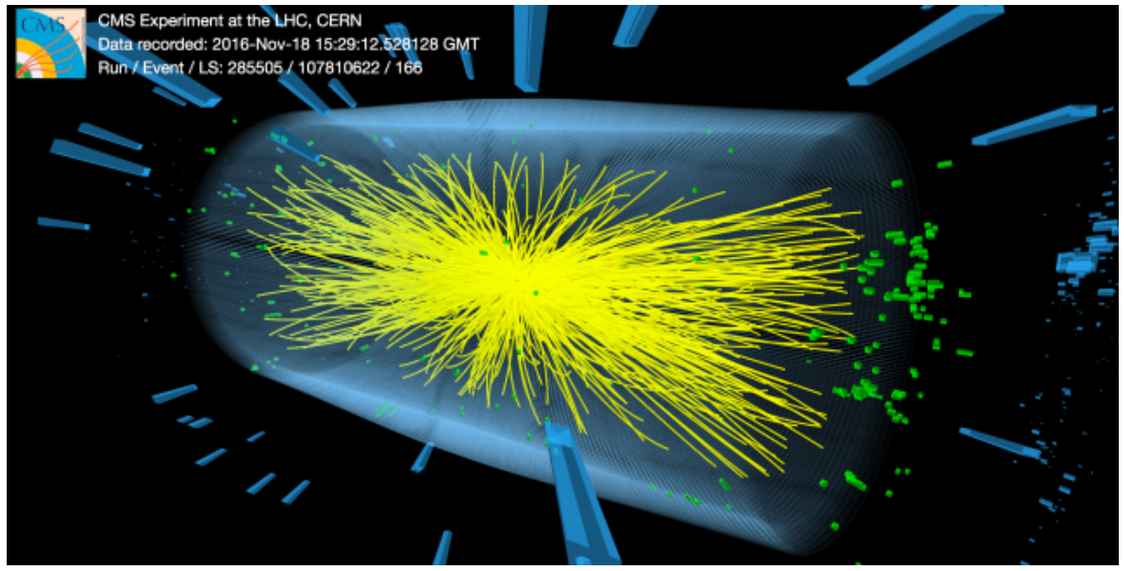

From protons to ions

proton-lead collisions

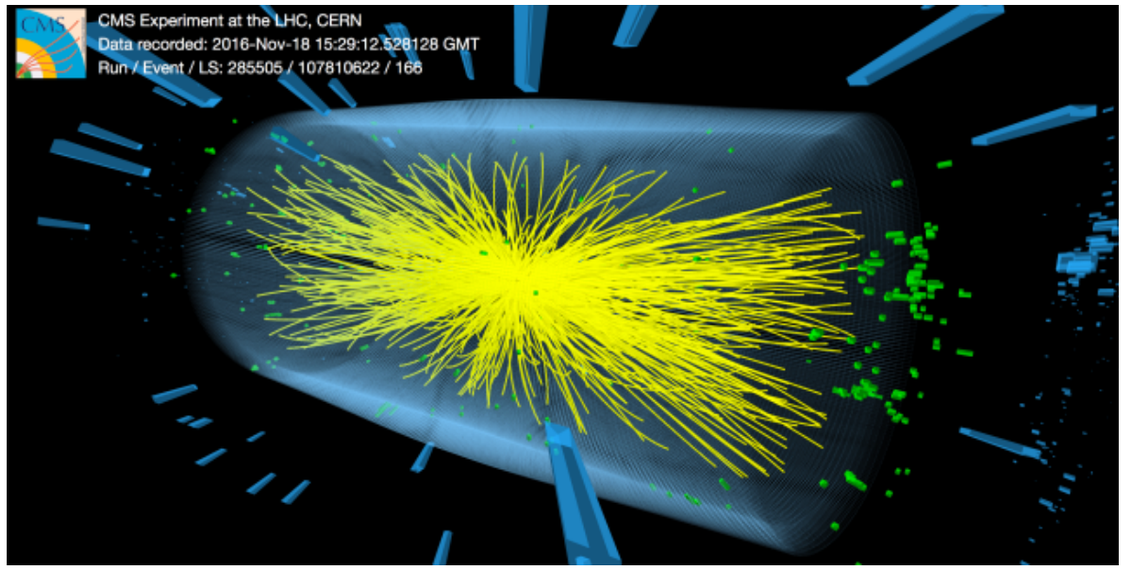

lead-lead collisions

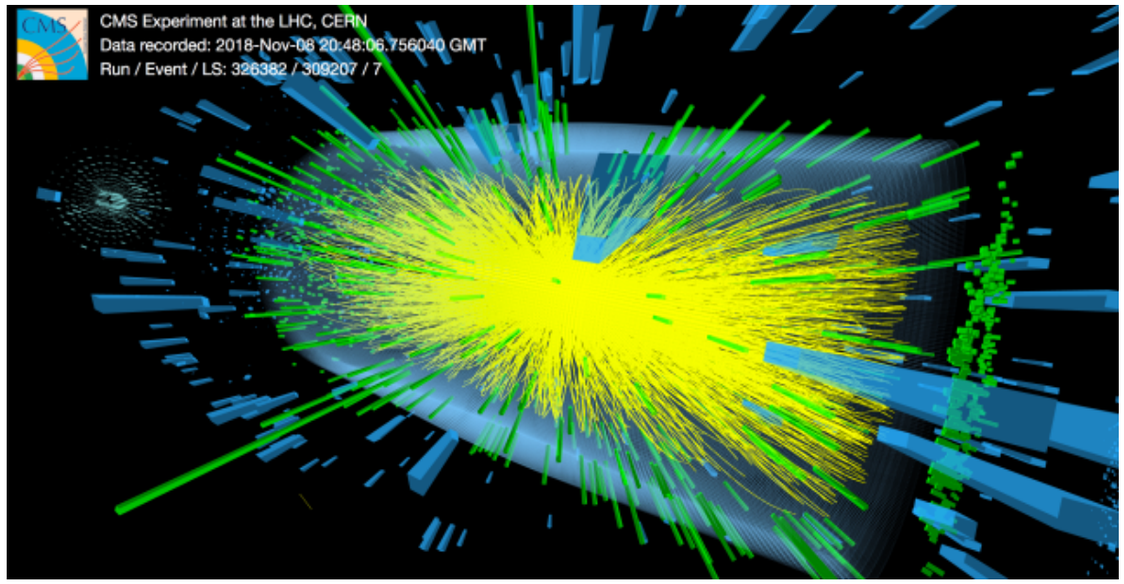

From protons to ions

proton-lead collisions

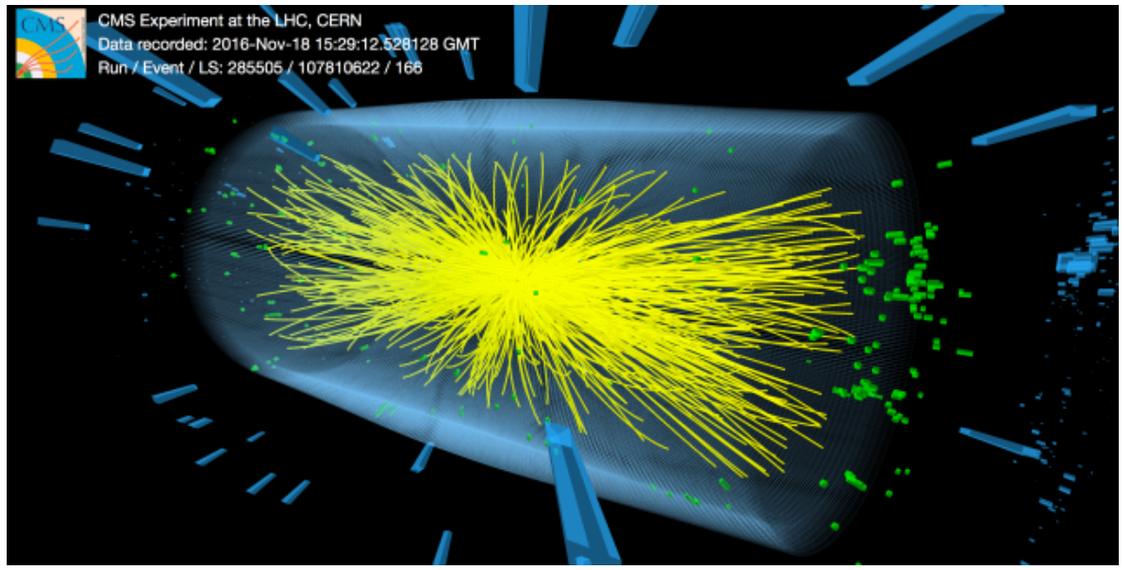

lead-lead collisions

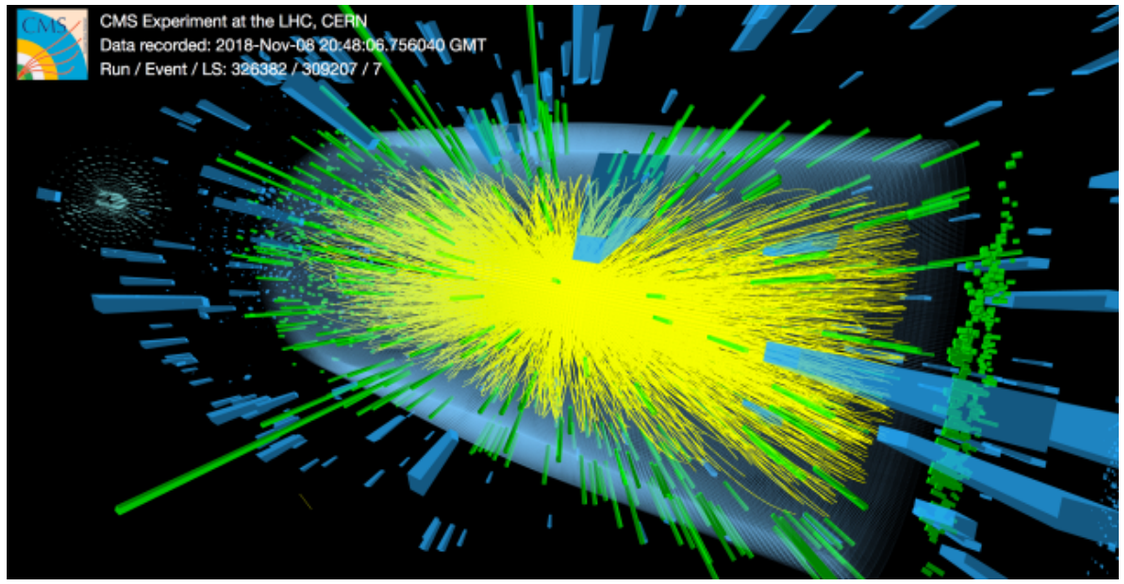

Increasing complexity of the interactions and events

It is very difficult to learn about nuclear structure from heavy ion collisions

Why electron-proton/ion?

proton-proton

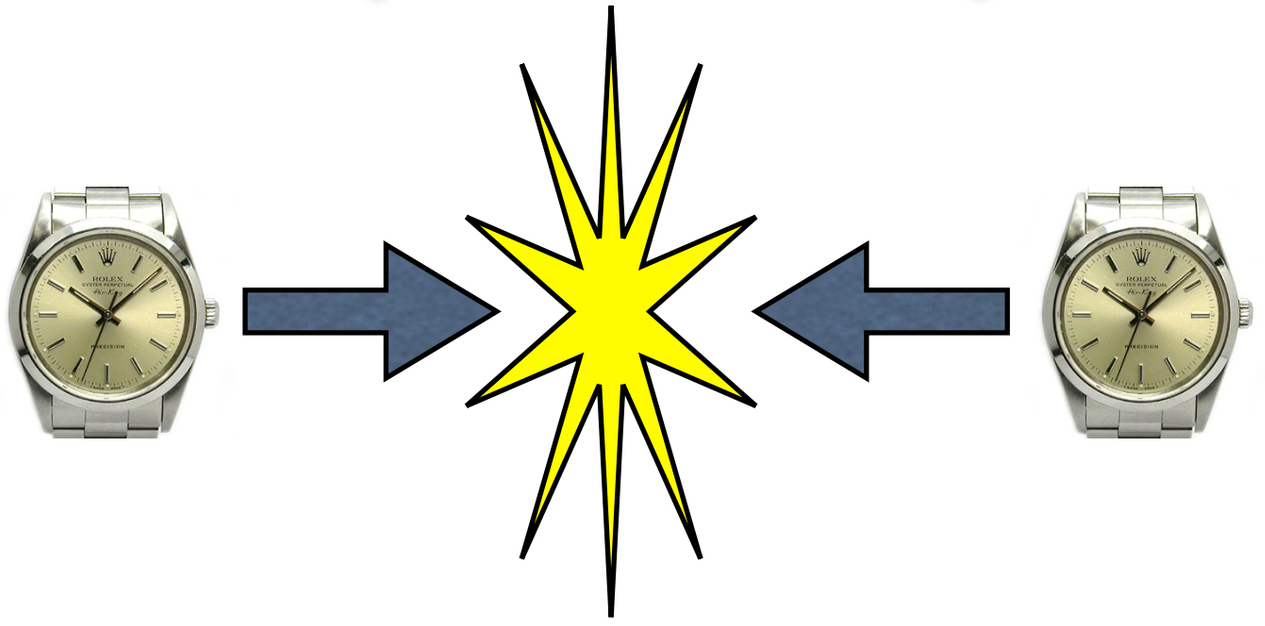

trying to find out how the watches work by investigating the debris may be difficult...

Why electron-proton/ion?

proton-proton

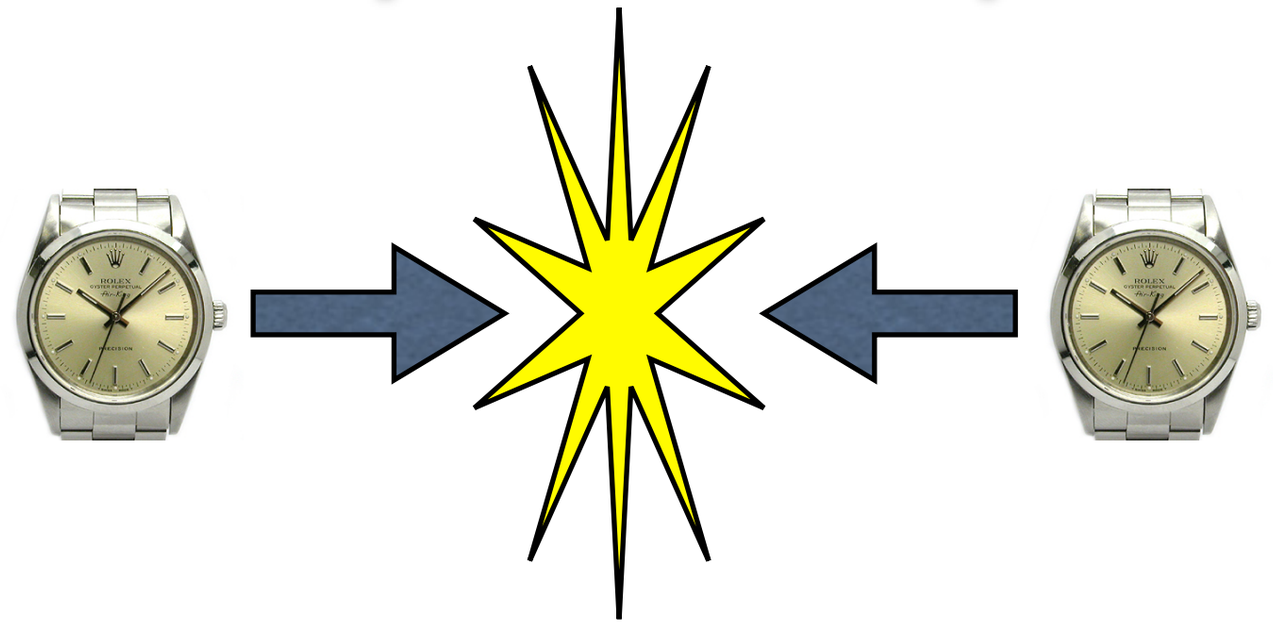

trying to find out how the watches work by investigating the debris may be difficult...

electron-proton

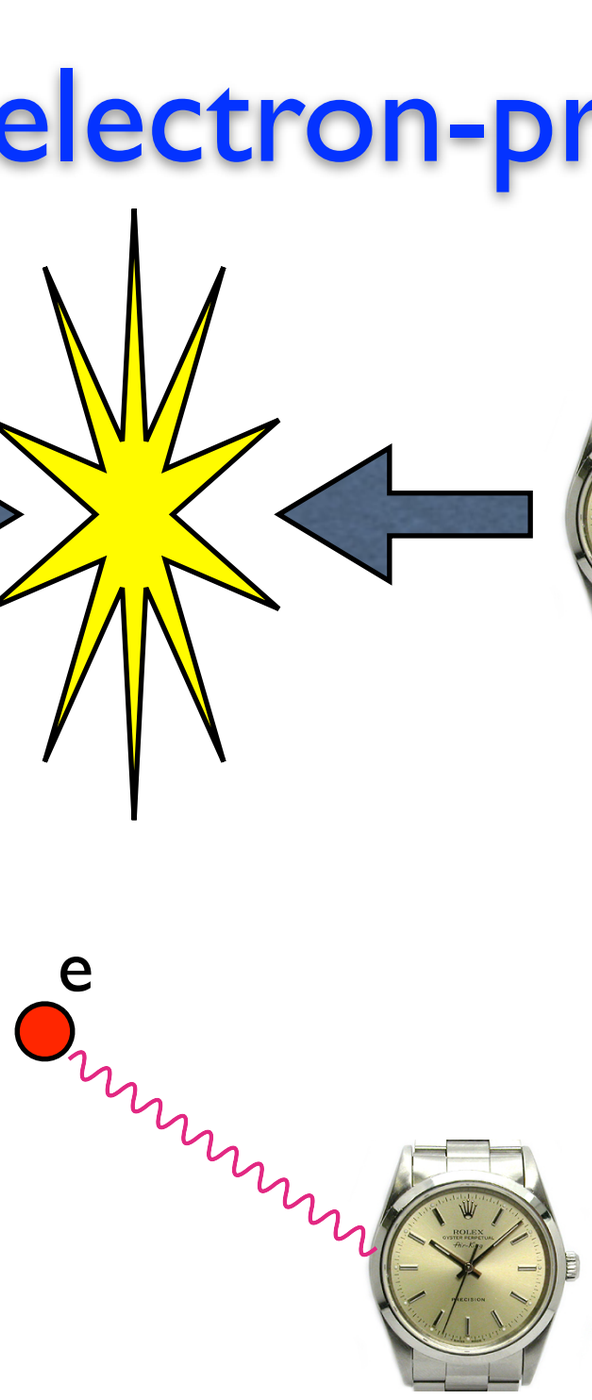

scattering with electron is like putting the watch under microscope...

Why electron-proton/ion?

proton-proton

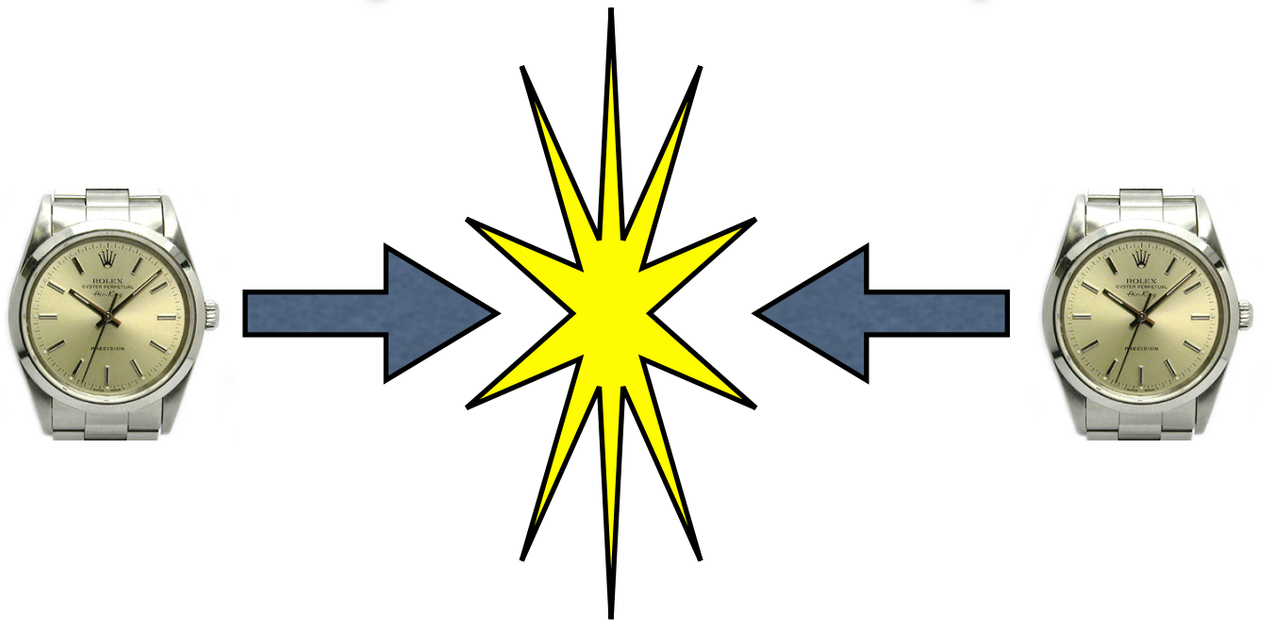

trying to find out how the watches work by investigating the debris may be difficult...

electron-proton

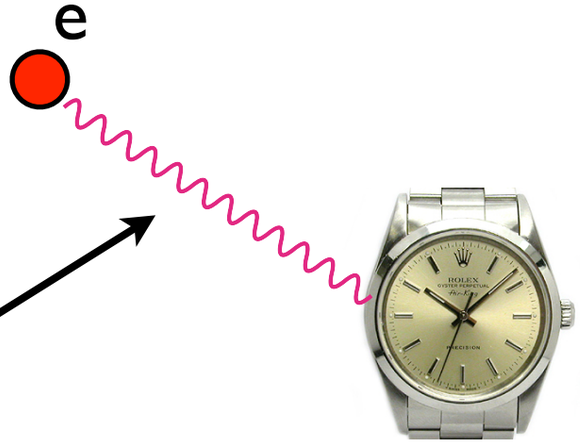

by controlling the virtuality Q^2 of the photon you can ...

scattering with electron is like putting the watch under microscope...

Why electron-proton/ion?

proton-proton

trying to find out how the watches work by investigating the debris may be difficult...

electron-proton

by controlling the virtuali Q^2 of the photon you can ..

scattering with electron is like putting the watch under microscope...

...zoom in... (note: photon is energetic enough that it can destroy the watch)

Atomic structure revealed

Geiger-Marsden experiment 1909

Scattering of alpha particles off the gold foil.
Observation of large angle scattering.

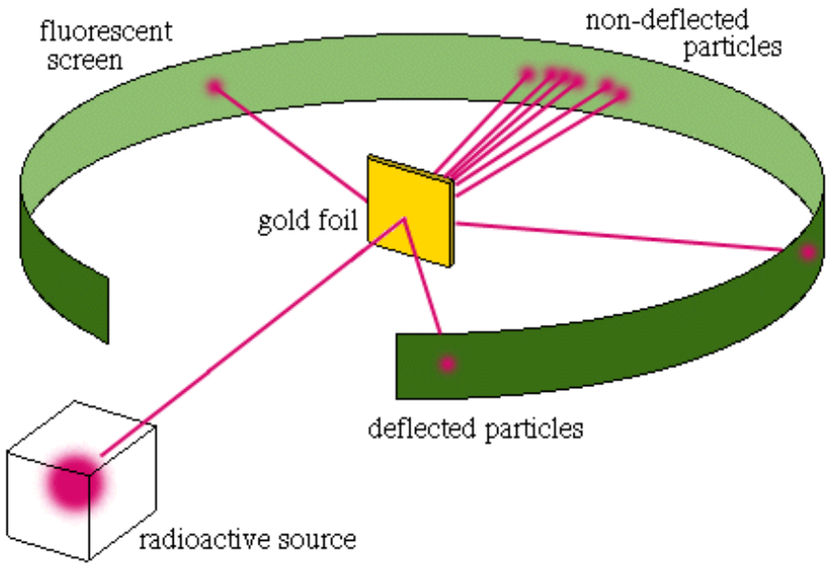

Rutherford model 1911

Atomic structure: positively charged small nucleus

LXXIX. *The Scattering of α and β Particles by Matter and the Structure of the Atom.* *By* Professor E. RUTHERFORD, *F.R.S., University of Manchester* *.

traversed. The observations, however, of Geiger and Marsden † on the scattering of α rays indicate that some of the α particles must suffer a deflexion of more than a right angle at a single encounter. They found, for example, that

It seems reasonable to suppose that the deflexion through a large angle is due to a single atomic encounter, for the chance of a second encounter of a kind to produce a large deflexion must in most cases be exceedingly small. A simple calculation shows that the atom must be a seat of an intense electric field in order to produce such a large deflexion at a single encounter.

Atomic structure revealed

Geiger-Marsden experiment 1909

Scattering of alpha particles off the gold foil.
Observation of large angle scattering.

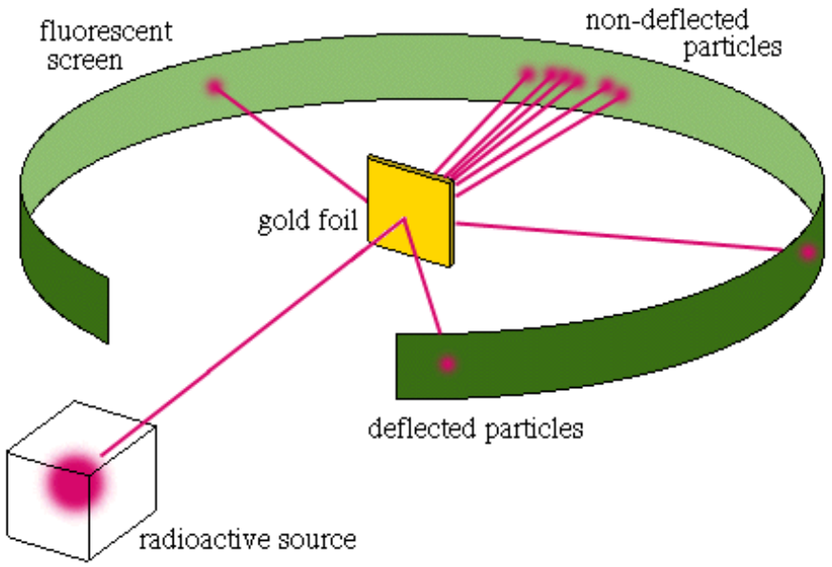

Rutherford model 1911

Atomic structure: positively charged small nucleus

LXXIX. *The Scattering of α and β Particles by Matter and the Structure of the Atom.* *By* Professor E. RUTHERFORD, *F.R.S., University of Manchester* *.

traversed. The observations, however, of Geiger and Marsden † on the scattering of α rays indicate that some of the α particles must suffer a deflexion of more than a right angle at a single encounter. They found, for example, that

It seems reasonable to suppose that the deflexion through a large angle is due to a single atomic encounter, for the chance of a second encounter of a kind to produce a large deflexion must in most cases be exceedingly small. A simple calculation shows that the atom must be a seat of an intense electric field in order to produce such a large deflexion at a single encounter.

Later on addressing a Royal Society anniversary meeting as its President, Rutherford commented prophetically, "It would be of great scientific interest if it were possible in experiments to have a supply of electrons... of which the individual energy of motion is greater even than that of the α particle".

Nucleon size

Hofstadter experiments in 1950-1957

Electron scattering off nuclei, determining the charge and shape of nuclei, and measuring the finite size of protons.

Energy of electrons 188 MeV

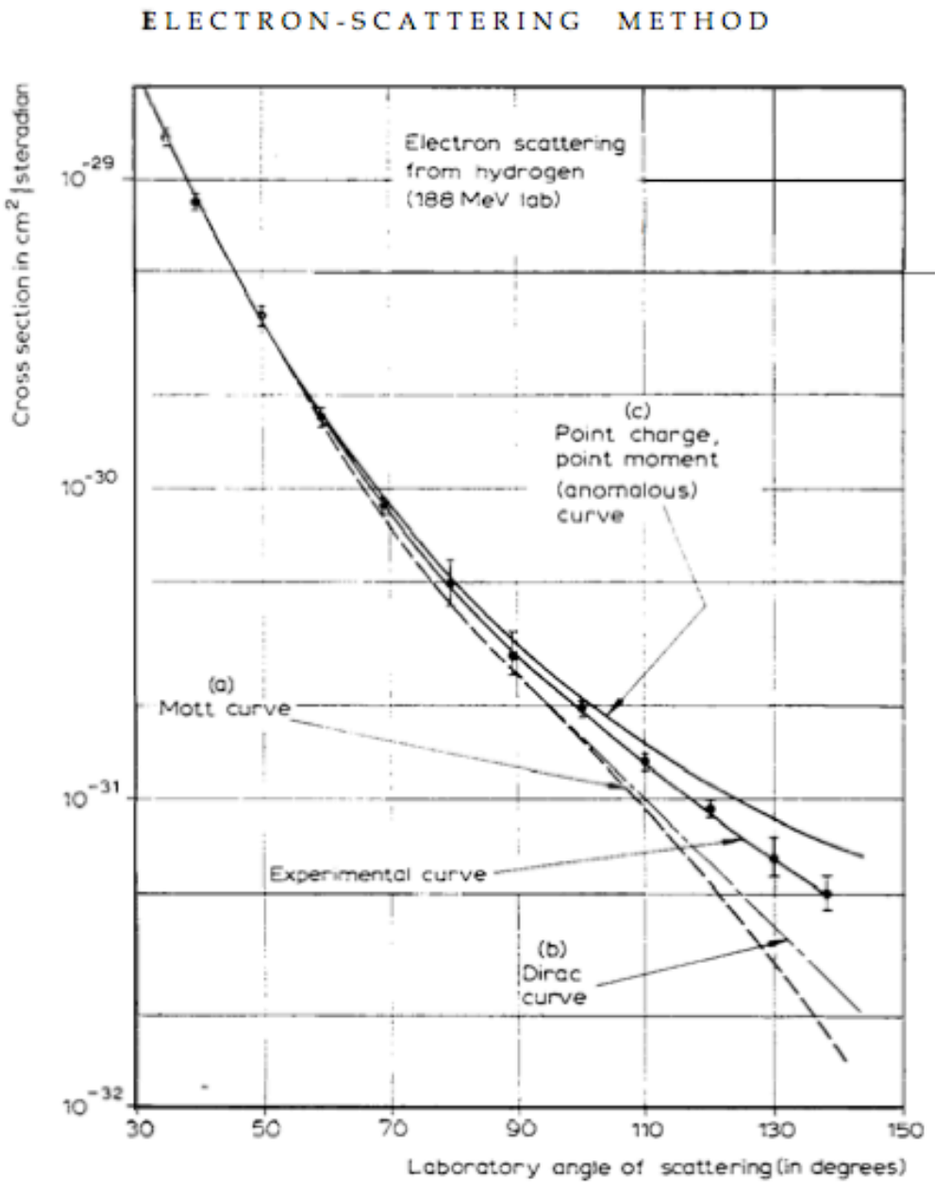

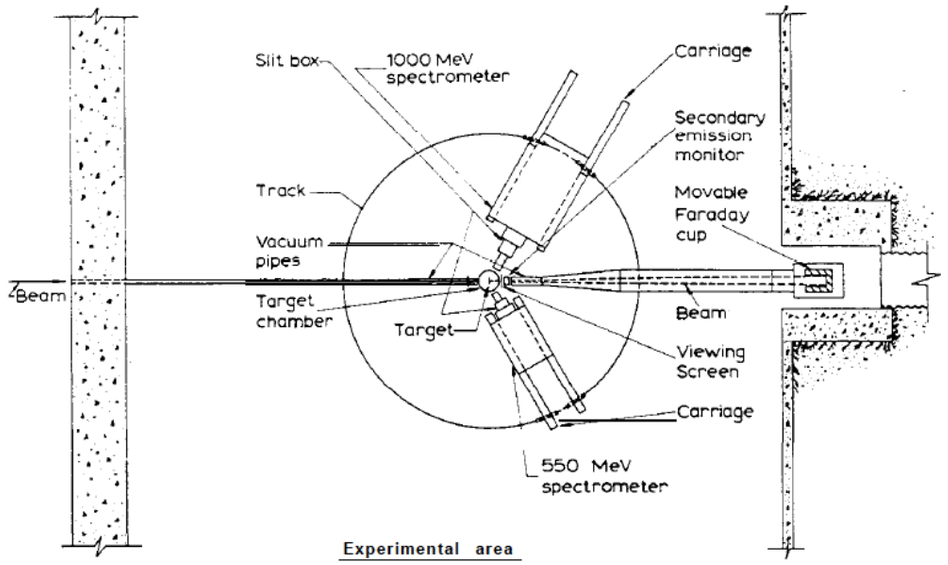

Fig. 2. This figure shows a schematic diagram of a modern electron-scattering experimental area. The track on which the spectrometers roll has an approximate radius of 13.5 feet.

Hofstadter: $(0.74 \pm 0.24) \cdot 10^{-13}$ cm

Current experimental value (measured with electrons):

$$R_p = 0.87 \text{ fm}$$

$$1 \text{ fm} = 10^{-13} \text{ cm}$$

Nuclei sizes

Nuclear form factor - measured

Nuclear density - extracted

$$F = \frac{4\pi}{q}\int_0^\infty \varrho\,(\mathrm{r})\,(\sin\ \mathrm{qr})\ r\,\mathrm{d}r$$

Momentum transfer

$$q = \frac{(2E/\hbar c)\,\sin\theta/2}{\sqrt{1+(2E/Mc^2)\,\sin^2\theta/2}}$$

θ Scattering angle

E Incident electron energy

Cross section: Au

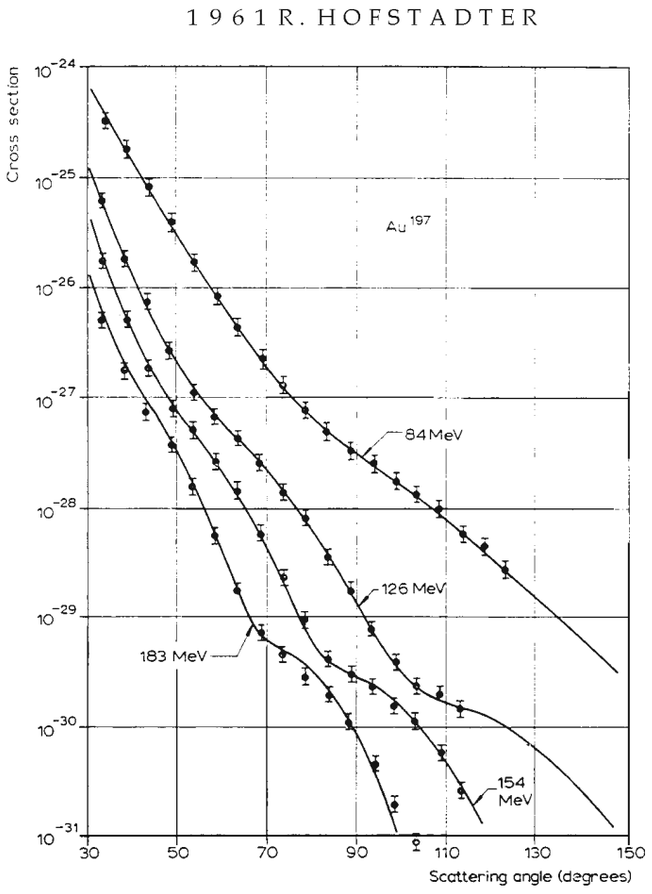

Extracted charge density for Au

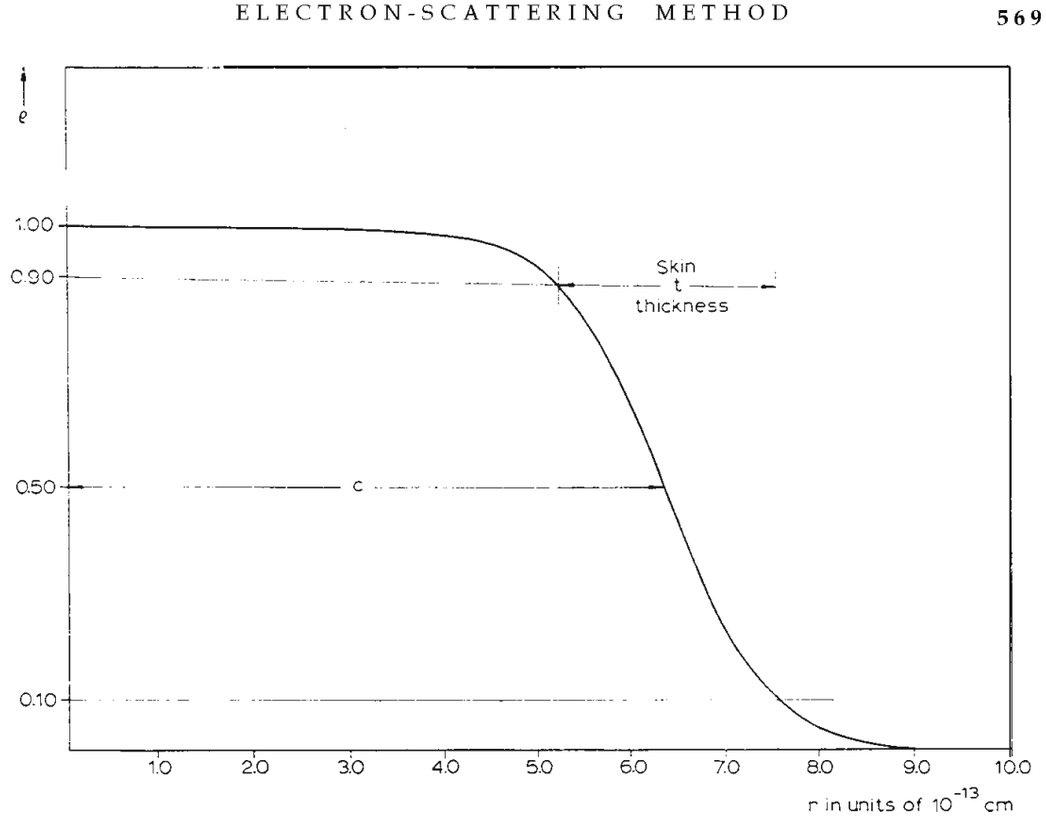

Nuclei sizes

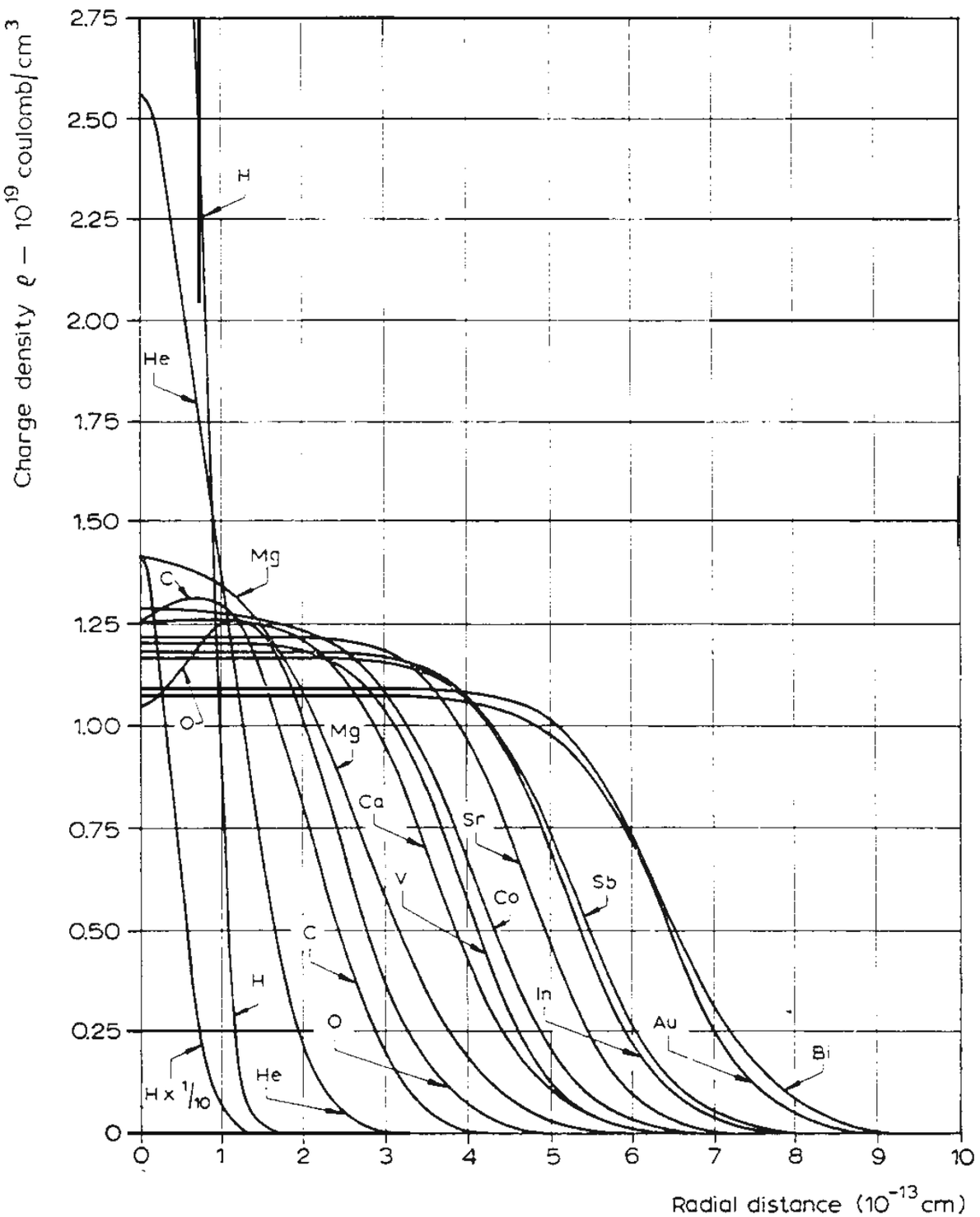

Nuclear charge density
can be described by Fermi distribution.

Fermi: $\rho(r) = \rho_1 / \{\exp[(r-c)/z_1] + 1\}$; (1)

Modified Gaussian:[22] $\rho(r) = \rho_2 / \{\exp[(r^2-c^2)/z_2^2] + 1\}$; (2)

Trapezoidal: $\rho(r) = \rho_3, \quad 0 < r < c-z_3,$

$= \rho_3(c+z_3-r)/2z_3, \quad c-z_3 < r < c+z_3,$ (3)

$= 0, \quad r > c+z_3.$

$$c = (1.07 \pm 0.02) \cdot 10^{-13} A^{\frac{1}{3}} \text{ cm}$$

$$t = (2.4 \pm 0.3) \cdot 10^{-13} \text{ cm} = \text{constant}$$

c - mean nuclear radius
t - thickness

Charge density constant in the center (except for lightest nuclei)
Thickness is the same for all nuclei - universal feature

Hofstadter experiments

Over a period of time lasting at least two thousand years, Man has puzzled over and sought an understanding of the composition of matter. It is no wonder that his interest has been aroused in this deep question because all objects he experiences, including even his own body, are in a most basic sense special configurations of matter. The history of physics shows that whenever experimental techniques advance to an extent that matter, as then known, can be analyzed by reliable and proved methods into its «elemental» parts, newer and more powerful studies subsequently show that the «elementary particles» have a structure themselves. Indeed this structure may be quite complex, so that the elegant idea of elementarity must be abandoned.

From Nobel prize lecture 1961

First observation of proton structure

VOLUME 23, NUMBER 16 PHYSICAL REVIEW LETTERS 20 OCTOBER 1969

OBSERVED BEHAVIOR OF HIGHLY INELASTIC ELECTRON-PROTON SCATTERING

M. Breidenbach, J. I. Friedman, and H. W. Kendall
Department of Physics and Laboratory for Nuclear Science,*
Massachusetts Institute of Technology, Cambridge, Massachusetts 02139

and

E. D. Bloom, D. H. Coward, H. DeStaebler, J. Drees, L. W. Mo, and R. E. Taylor
Stanford Linear Accelerator Center,† Stanford, California 94305
(Received 22 August 1969)

20 GeV electron beam scattering off protons

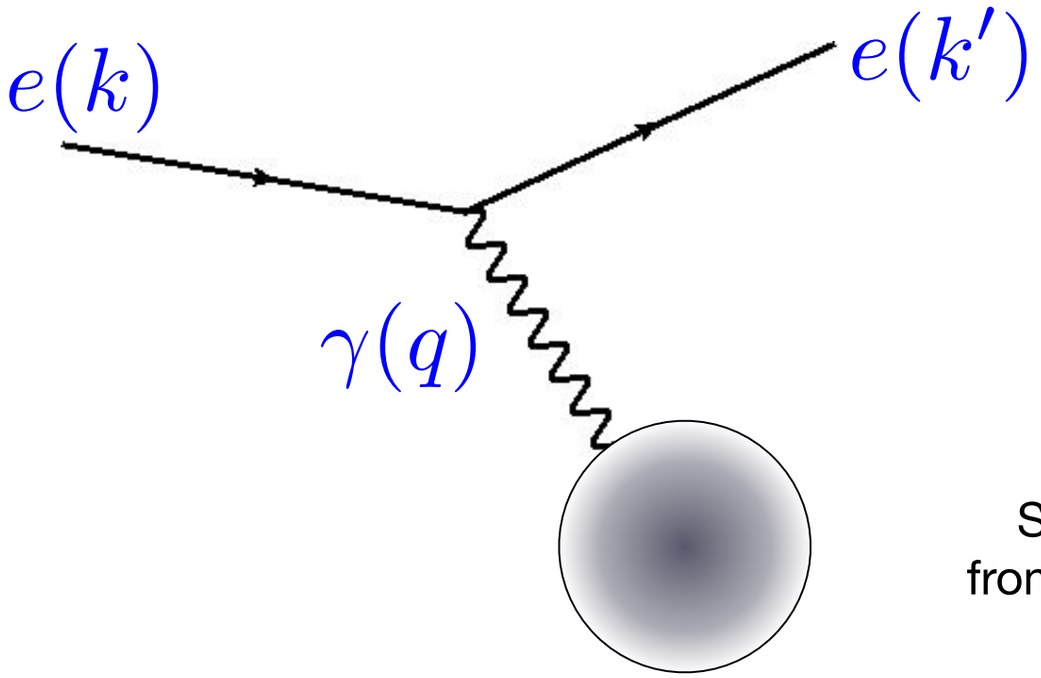

$$\left(\frac{d\sigma}{d\Omega}\right)_{MOTT} = \frac{e^4}{4E^2}\,\frac{\cos^2\theta/2}{\sin^4\theta/2}$$

Spectacular deviation from theoretical prediction

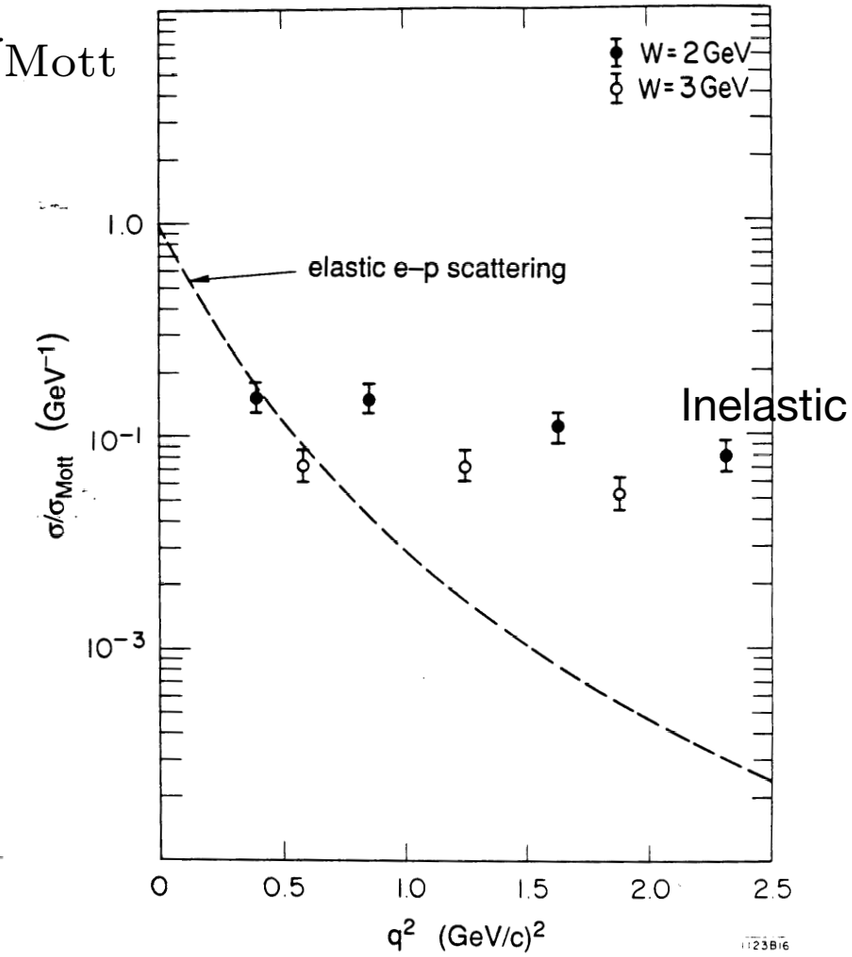

$Q^2 = -q^2$:resolving power of interaction

First observation of proton structure

VOLUME 23, NUMBER 16 PHYSICAL REVIEW LETTERS 20 OCTOBER 1969

OBSERVED BEHAVIOR OF HIGHLY INELASTIC ELECTRON-PROTON SCATTERING

M. Breidenbach, J. I. Friedman, and H. W. Kendall
Department of Physics and Laboratory for Nuclear Science,*
Massachusetts Institute of Technology, Cambridge, Massachusetts 02139

and

E. D. Bloom, D. H. Coward, H. DeStaebler, J. Drees, L. W. Mo, and R. E. Taylor
Stanford Linear Accelerator Center,† Stanford, California 94305
(Received 22 August 1969)

20 GeV electron beam scattering off protons

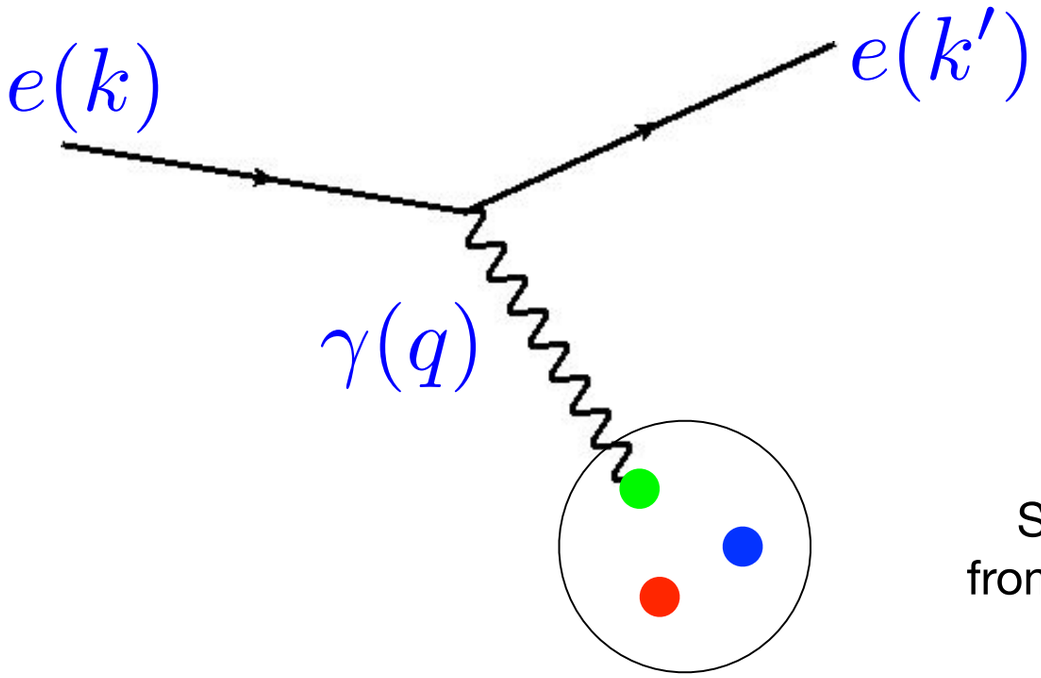

$$\left(\frac{d\sigma}{d\Omega}\right)_{MOTT} = \frac{e^4}{4E^2}\,\frac{\cos^2\theta/2}{\sin^4\theta/2}$$

Spectacular deviation from theoretical prediction

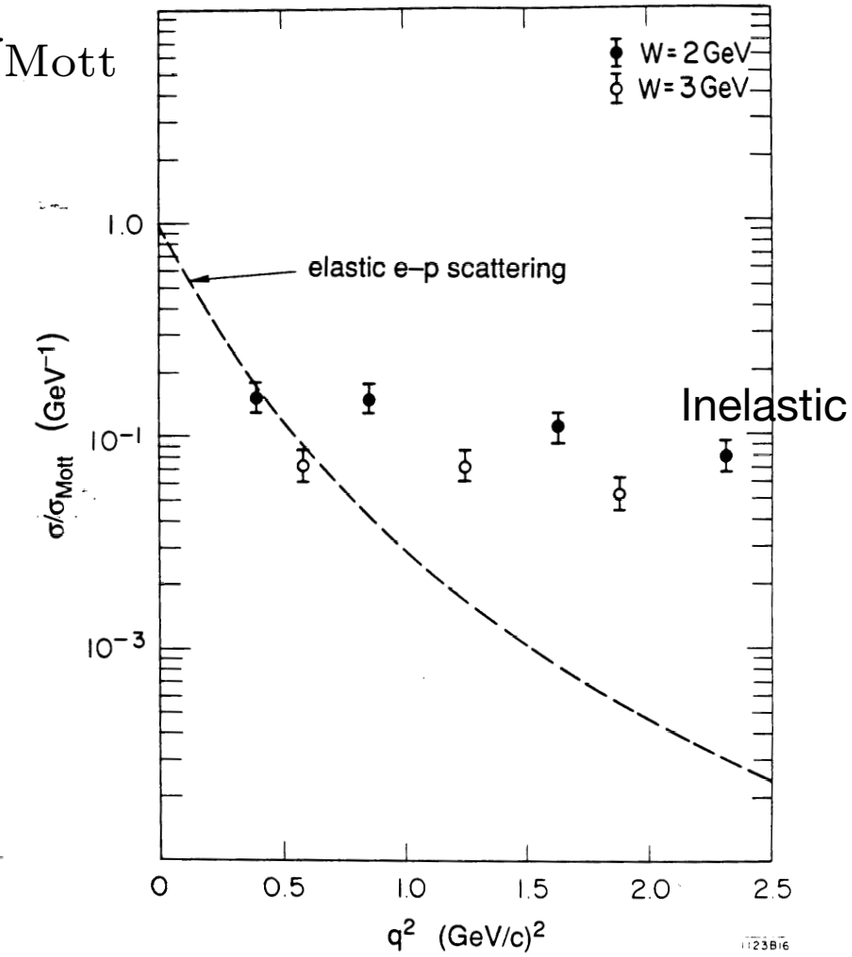

$Q^2 = -q^2$:resolving power of interaction

lepton-hadron/nucleus DIS

electron-proton

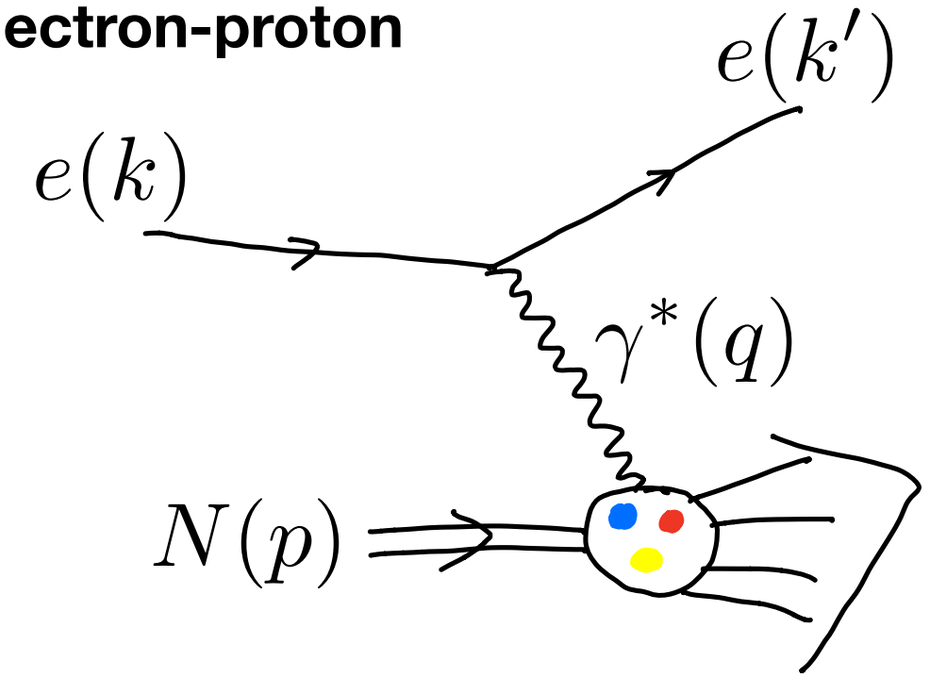

electron-ion

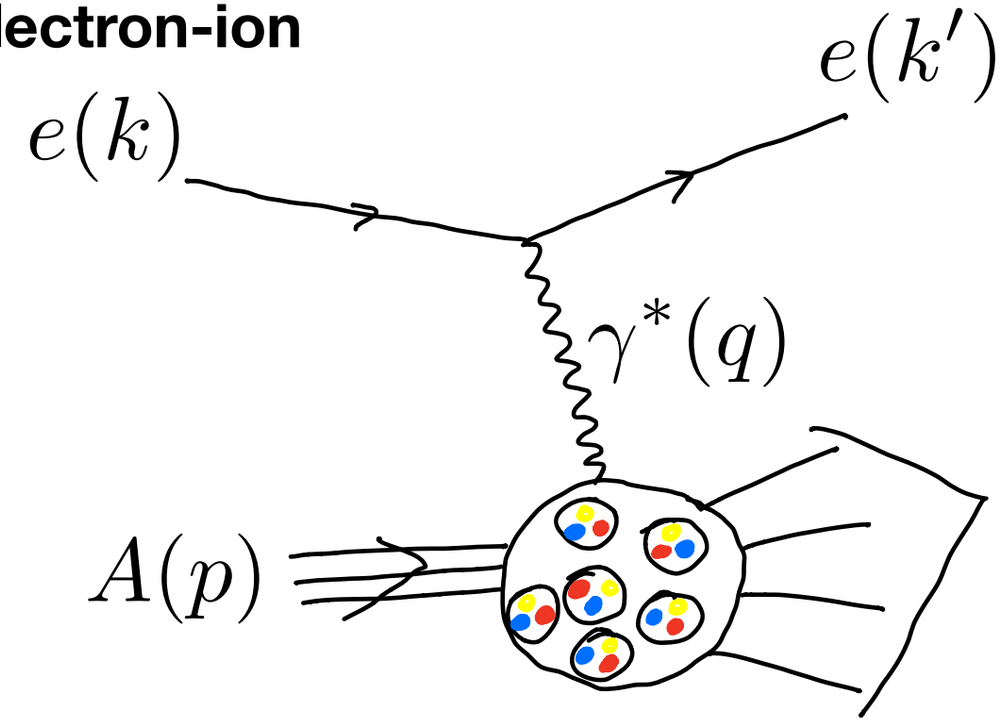

lepton-hadron/nucleus DIS

electron-proton

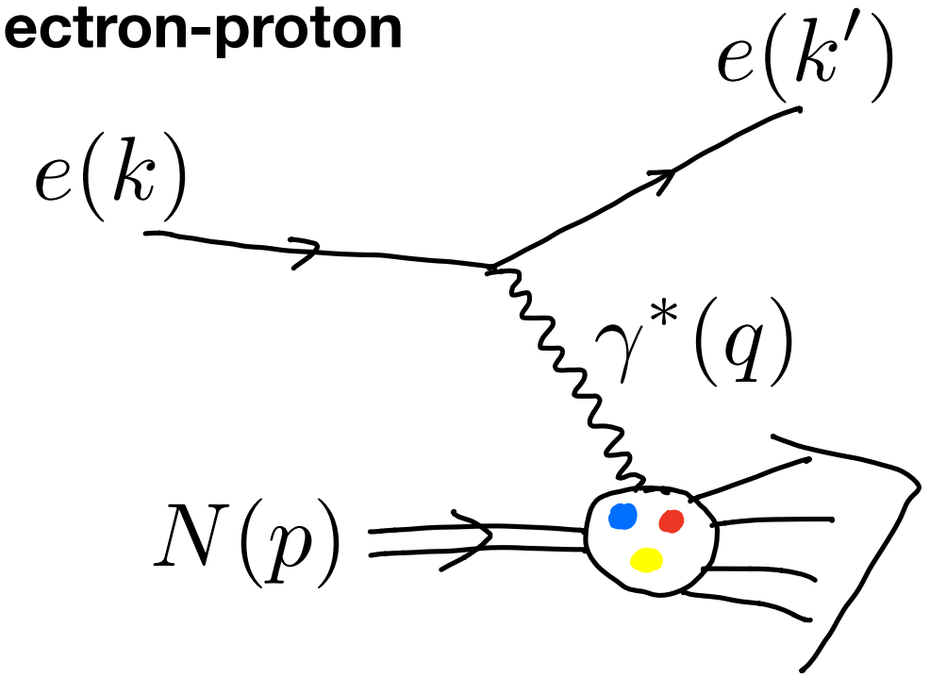

electron-ion

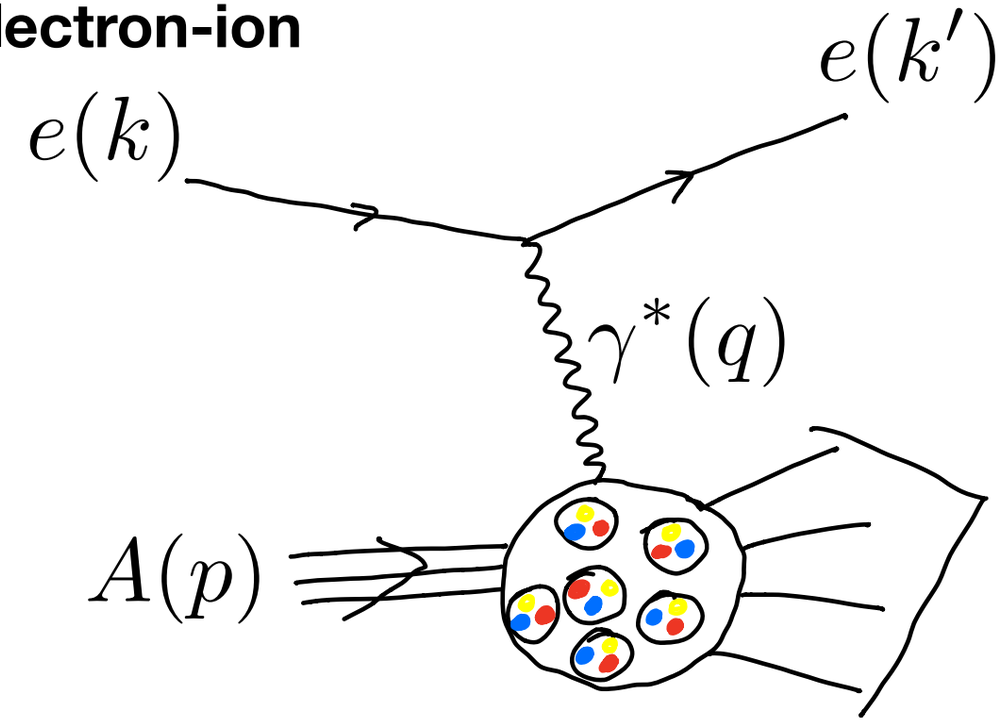

Deep inelastic electron-hadron/nucleus scattering : elastic scattering off a quark

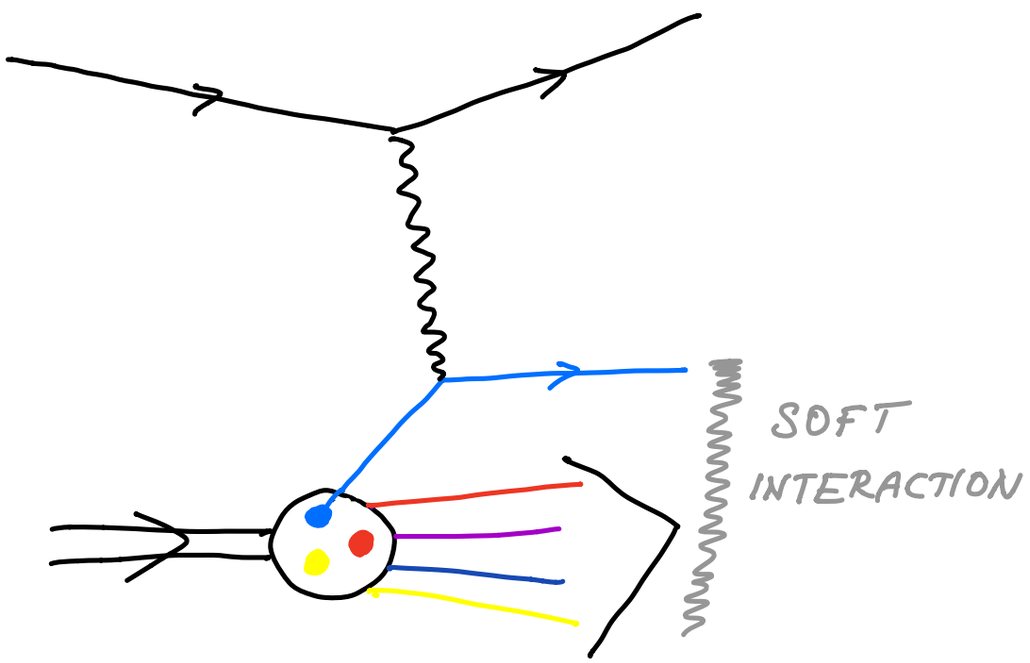

- Virtual photon probes the structure of the target: proton or nucleus
- Photon interacts with individual quarks
- Assumption: the color recombination (soft interaction) occurs on different scales than the hard interaction of photon with the quark - **factorization**

DIS kinematics

Inelastic scattering off proton

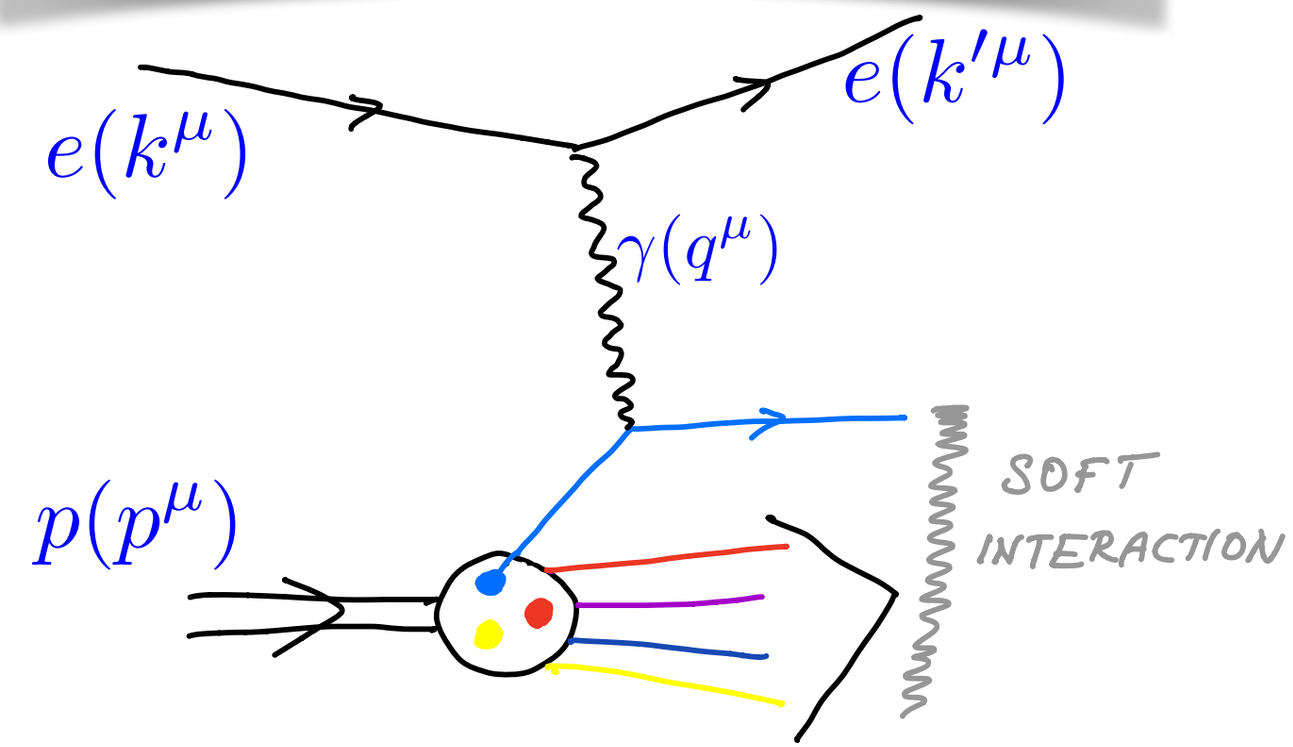

Elastic scattering off parton (quark)

$$Q^2 = -q^2$$ Photon virtuality : resolving power

$$x = \frac{Q^2}{2p \cdot q} \simeq \frac{Q^2}{Q^2 + W^2}$$ Bjorken x

$$W^2 = (p+q)^2$$ total energy of photon-proton system

$$s = (p+k)^2$$ total cms energy

$$k^\mu = (E, 0, 0, E)_{LAB}$$

$$k'^\mu = (E', 0, 0, E')_{LAB}$$

$$\nu = \frac{q \cdot p}{M} = E - E'$$

Lepton energy loss in nucleon rest frame

$$y = \frac{p \cdot q}{p \cdot k} = \frac{\nu}{E}$$ Inelasticity: fraction of lepton energy loss in the nucleon rest frame

DIS preliminaries

Scattering amplitude:

$$\mathcal{M} = e^2 \bar{u}(k', \lambda') \gamma^\mu u(k, \lambda) \frac{1}{q^2} < X | J_\mu^{em}(0) | N, \sigma >$$

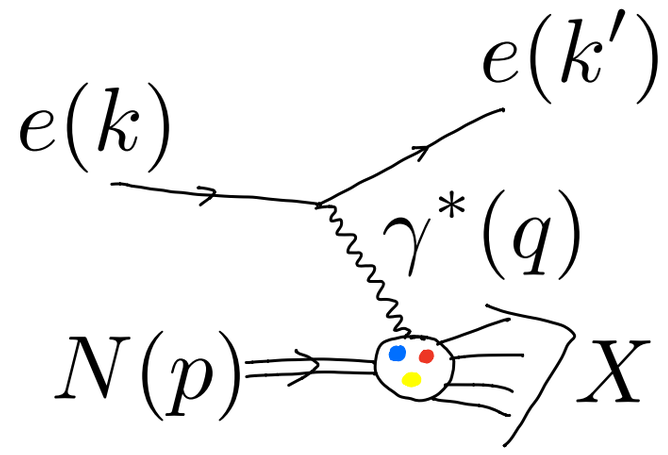

$\langle X|$ Hadronic final state

$|N, \sigma\rangle$ Nucleon/nucleus initial state

$J_\mu^{\rm em}(0)$ Electromagnetic current

Cross section:

$$d\sigma = \frac{1}{F} \frac{d^3 k'}{2E'(2\pi)^3} \frac{1}{4} \sum_{\sigma \lambda \lambda'} |\mathcal{M}|^2$$

Flux factor:

$$F = 4p \cdot k$$

Sum performed over the polarization states

DIS preliminaries

DIS cross section can be written in the factorized way:

$$\frac{d^2\sigma}{dE'd\Omega} = \frac{\alpha^2}{Q^4}\frac{E'}{E}L^{em}_{\mu\nu}W^{\mu\nu}$$

Leptonic tensor, can be evaluated straightforwardly

$$L^{\mu\nu}_{\rm em} = \frac{1}{2}\sum_{s'}\bar{u}^{(s')}_{\alpha}(k')\gamma^{\mu}_{\alpha\beta}\sum_{s}u^{(s)}_{\beta}(k)\bar{u}^{(s)}_{\gamma}(k)\gamma^{\nu}_{\gamma\delta}u^{(s')}_{\delta}(k')$$

And the final result is :

$$L^{\mu\nu}_{\rm em} = \frac{1}{2}Tr(\not{k}'\gamma^{\mu}\not{k}\gamma^{\nu}) = 2(k^{\mu}k'^{\nu} + k'^{\mu}k^{\nu} - \frac{1}{2}Q^2g^{\mu\nu})$$

Note that it only depends on 4-momenta of initial, final leptons and photon 4-momentum

DIS preliminaries

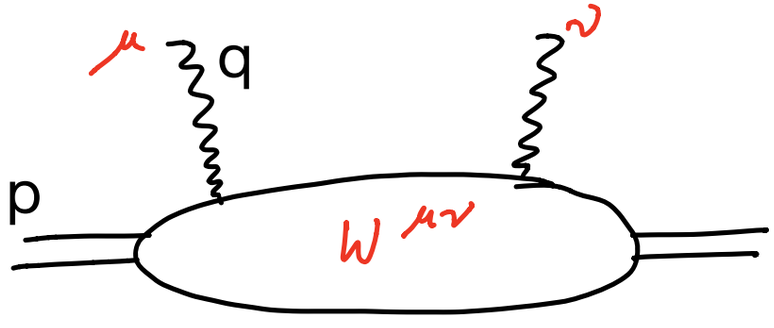

Hadronic tensor contains all the information about the hadron involved in the process.

Depends on the 4-momenta of the incoming nucleon and the photon

Definition of the hadronic tensor:

$$W_{\mu\nu}(p,q) = \frac{1}{4M}\sum_{\sigma}\int \frac{d^4x}{2\pi}e^{iqx} < N\sigma|[J^{em}_{\mu}(x), J^{em}_{\nu}(0)]|N\sigma >$$

Decomposition of the hadronic tensor:

$$W_{\mu\nu}(p,q) = -W_1(g_{\mu\nu} - \frac{q_\mu q_\nu}{q^2}) + \frac{W_2}{M^2}(p_\mu - \frac{p\cdot q}{q^2}q_\mu)\cdot(p_\nu - \frac{p\cdot q}{q^2}q_\nu)$$

Two independent structure functions (unpolarized, only photon exchange):

$$MW_1 = F_1 \qquad \frac{Q^2}{2Mx}W_2 = F_2$$

Dimensionless

Parton model - Bjorken scaling

If proton consists of pointlike constituents which do not interact, then the scattering off proton will be just an **incoherent scattering** off the pointlike constituents.

DIS cross section

$$\frac{d^2\sigma}{d\Omega dE'} = \frac{\alpha^2}{4E^2 \sin^4 \frac{\Theta}{2}}(2W_1 \sin^2 \frac{\Theta}{2} + W_2 \cos^2 \frac{\Theta}{2})$$

Θ Lepton scattering angle in the hadron rest frame

Compare with **electron-muon** cross section

$$\frac{d^2\sigma^{e\mu\to e\mu}}{d\Omega dE'} = \frac{\alpha^2}{4E^2 \sin^4 \frac{\Theta}{2}}[\cos^2 \frac{\Theta}{2} - \frac{q^2}{2M^2} \sin^2 \frac{\Theta}{2}]\delta(\nu + \frac{q^2}{2M})$$

Can read off structure functions in this case immediately

$$2MW_1^p(\nu, Q^2) = 2F_1 = \frac{Q^2}{2M\nu}\delta(1 - \frac{Q^2}{2M\nu})$$

$$\nu W_2^p(\nu, Q^2) = F_2 = \delta(1 - \frac{Q^2}{2M\nu})$$

Parton model - Bjorken scaling

The structure functions for scattering on **pointlike parton**
have the property that they depend only on one dimensionless variable:

$$x = \frac{Q^2}{2M\nu} = \frac{Q^2}{2p \cdot q}$$

$$F_1(x, Q^2) \to F_1(x) \qquad F_2(x, Q^2) \to F_2(x)$$

No dependence on Q^2: **Bjorken scaling**

$$\omega = \frac{1}{x}$$

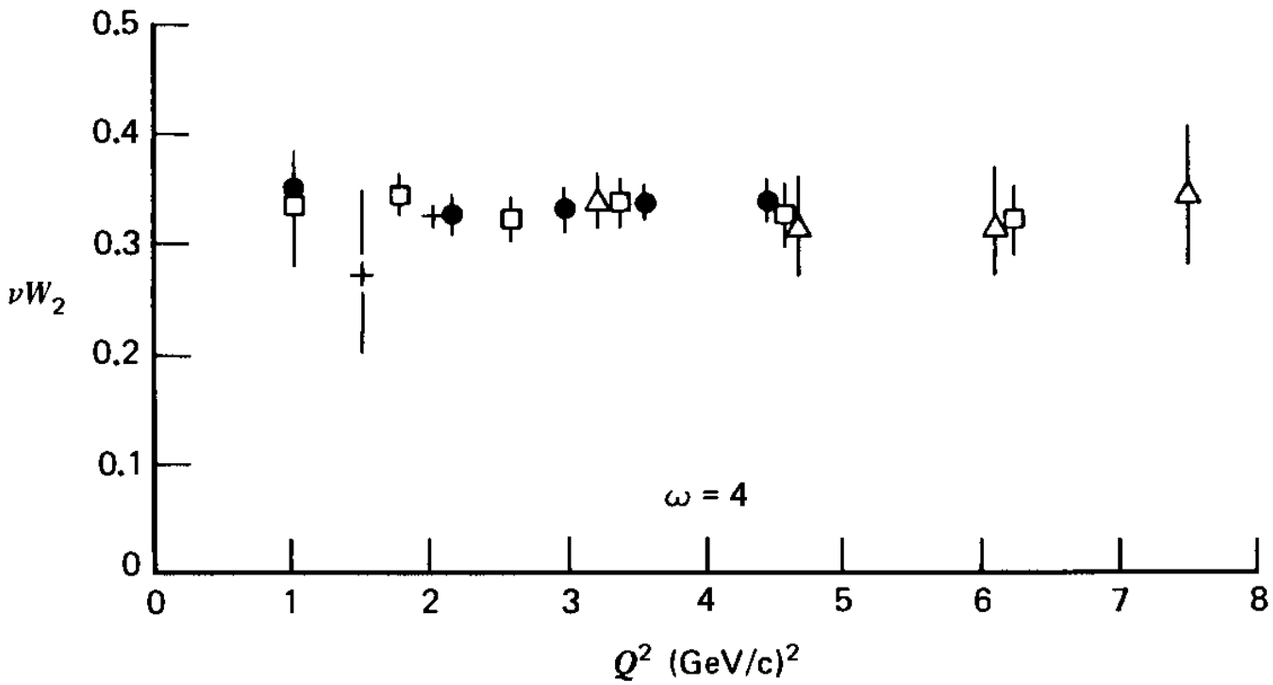

Fig. 9.2 The structure function νW_2 determined by electron–proton scattering as a function of Q^2 for $\omega = 4$. Data are from the Stanford Linear Accelerator.

Parton model

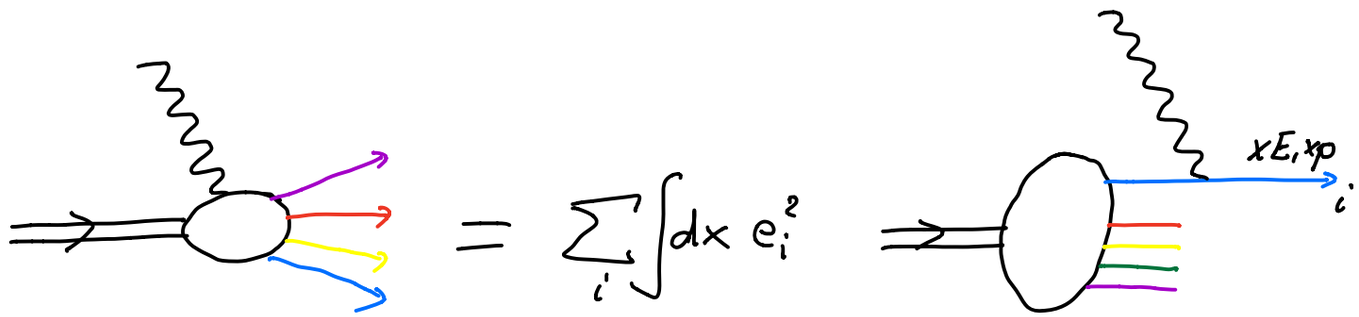

x: longitudinal momentum fraction of the proton carried by the struck parton

Parton distribution function

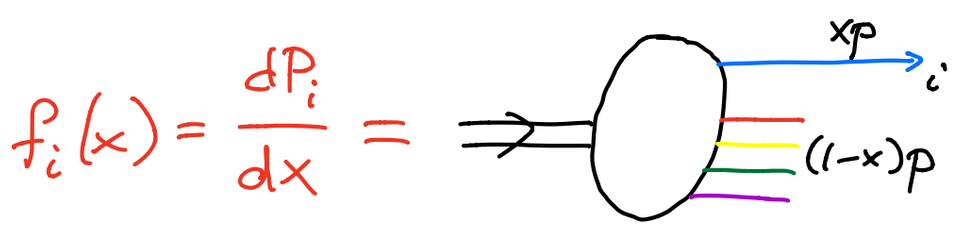

Momentum sum rule

$$\sum_k \int_0^1 dx\, x f_k(x) = 1$$

Structure functions:

$$\nu W_2^p(\nu, Q^2) = F_2 = \sum_i \int_0^1 dx e_i^2 f_i(x) x \delta(x - \frac{1}{\omega}) = \sum_i e_i^2 x f_i(x)$$

$$MW_1^p(\nu, Q^2) = F_1 = \frac{\omega}{2} F_2$$

$$x = \frac{Q^2}{2M\nu} = \frac{Q^2}{2p \cdot q} = \frac{1}{\omega}$$

$$F_2(x) = \sum_i e_i^2 x f_i(x) \qquad F_1(x) = \frac{1}{2x} F_2(x)$$

Callan-Gross relation

$$F_1(x) = \frac{1}{2x} F_2(x)$$

Consequence of parton model and spin 1/2 quarks

Longitudinal structure function has to vanish in the scaling limit

$$F_L(x) = F_2(x) - 2xF_1(x)$$

Callan-Gross relation

$$F_1(x) = \frac{1}{2x} F_2(x)$$

Consequence of parton model and spin 1/2 quarks

Longitudinal structure function has to vanish in the scaling limit

$$F_L(x) = F_2(x) - 2xF_1(x)$$

Helicity is conserved in the high energy limit. Imagine the scattering of a photon on a quark.

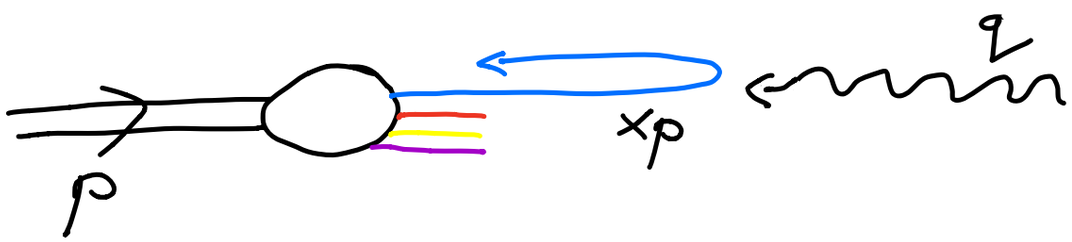

Spin 1/2 quark can only absorb photon with

$$\lambda = \pm 1$$

Therefore

$$\sigma_L \sim F_L \to 0$$

Callan-Gross relation

$$F_1(x) = \frac{1}{2x} F_2(x)$$

Consequence of parton model and spin 1/2 quarks

Longitudinal structure function has to vanish in the scaling limit

$$F_L(x) = F_2(x) - 2xF_1(x)$$

Helicity is conserved in the high energy limit. Imagine the scattering of a photon on a quark.

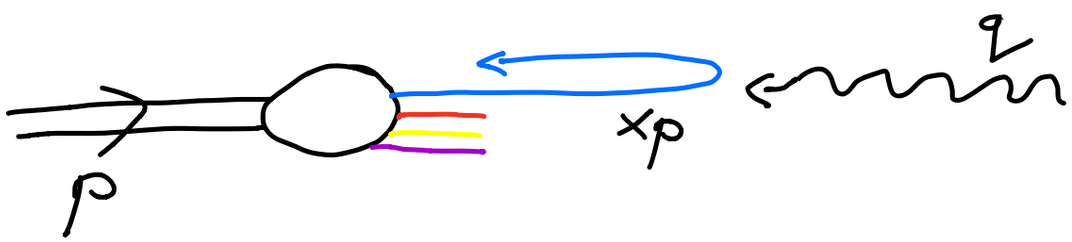

Spin 1/2 quark can only absorb photon with

$$\lambda = \pm 1$$

Therefore $\sigma_L \sim F_L \to 0$

Parton model assumptions:

Callan-Gross relation

$$F_1(x) = \frac{1}{2x} F_2(x)$$

Consequence of parton model and spin 1/2 quarks

Longitudinal structure function has to vanish in the scaling limit

$$F_L(x) = F_2(x) - 2xF_1(x)$$

Helicity is conserved in the high energy limit. Imagine the scattering of a photon on a quark.

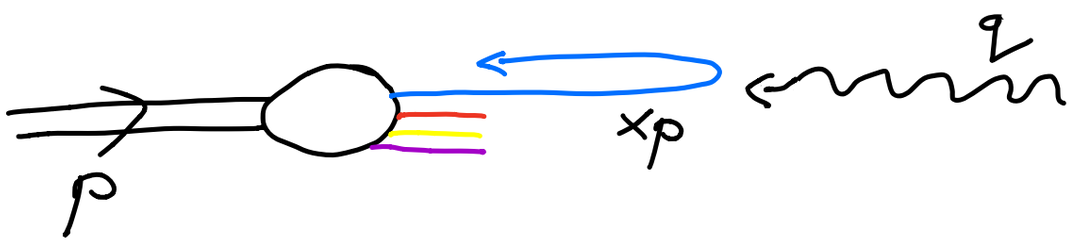

Spin 1/2 quark can only absorb photon with

$$\lambda = \pm 1$$

Therefore $\sigma_L \sim F_L \to 0$

Parton model assumptions:

- **Incoherent** scattering on **pointlike** constituents

Callan-Gross relation

$$F_1(x) = \frac{1}{2x} F_2(x)$$

Consequence of parton model and spin 1/2 quarks

Longitudinal structure function has to vanish in the scaling limit

$$F_L(x) = F_2(x) - 2xF_1(x)$$

Helicity is conserved in the high energy limit. Imagine the scattering of a photon on a quark.

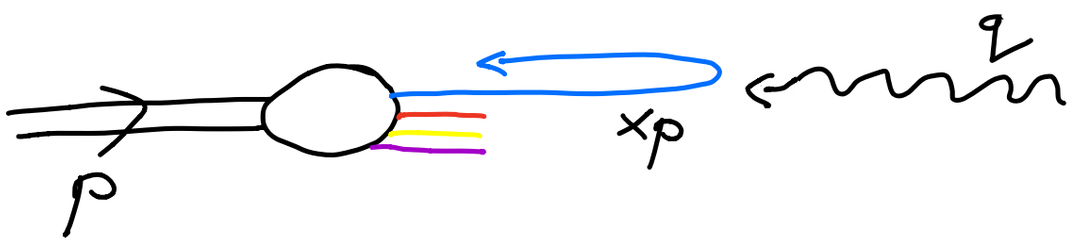

Spin 1/2 quark can only absorb photon with

$$\lambda = \pm 1$$

Therefore

$$\sigma_L \sim F_L \to 0$$

Parton model assumptions:

- **Incoherent** scattering on **pointlike** constituents
- **Transverse** momenta of the partons are **limited** (i.e. do not grow with Q^2)

Parton model

$$\nu W_2^p(\nu, Q^2) = F_2 = \sum_i \int_0^1 dx e_i^2 f_i(x) x \delta(x - \frac{1}{\omega}) = \sum_i e_i^2 x f_i(x)$$

How the structure function shape reflects the parton distribution inside the proton:

Parton model

$$\nu W_2^p(\nu, Q^2) = F_2 = \sum_i \int_0^1 dx e_i^2 f_i(x) x \delta(x - \frac{1}{\omega}) = \sum_i e_i^2 x f_i(x)$$

How the structure function shape reflects the parton distribution inside the proton:

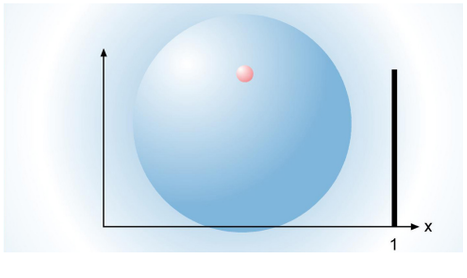

- One valence quark

Parton model

$$\nu W_2^p(\nu, Q^2) = F_2 = \sum_i \int_0^1 dx e_i^2 f_i(x) x \delta(x - \frac{1}{\omega}) = \sum_i e_i^2 x f_i(x)$$

How the structure function shape reflects the parton distribution inside the proton:

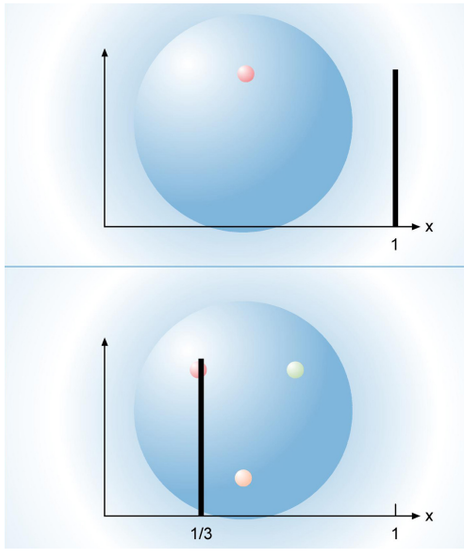

✦ One valence quark

✦Three, non-interacting valence quarks, sharing equal momentum

Parton model

$$\nu W_2^p(\nu, Q^2) = F_2 = \sum_i \int_0^1 dx e_i^2 f_i(x) x \delta(x - \frac{1}{\omega}) = \sum_i e_i^2 x f_i(x)$$

How the structure function shape reflects the parton distribution inside the proton:

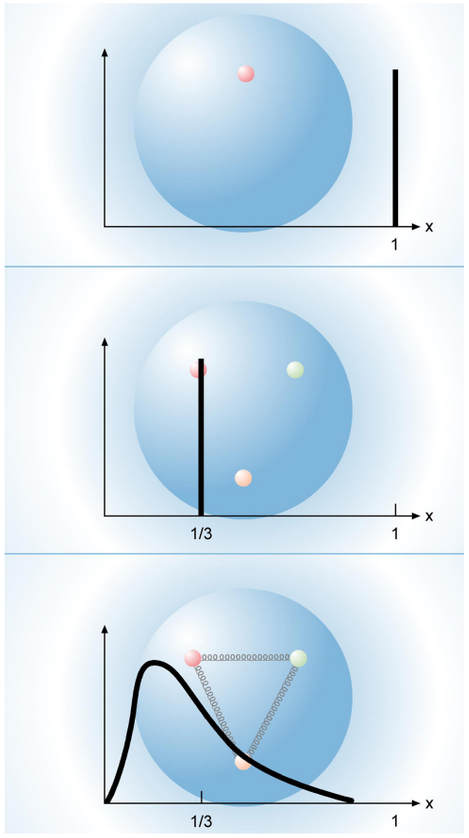

✦ One valence quark

✦Three, non-interacting valence quarks, sharing equal momentum

✦ Three quarks interacting, changing the momentum

Parton model

$$\nu W_2^p(\nu, Q^2) = F_2 = \sum_i \int_0^1 dx e_i^2 f_i(x) x \delta(x - \frac{1}{\omega}) = \sum_i e_i^2 x f_i(x)$$

How the structure function shape reflects the parton distribution inside the proton:

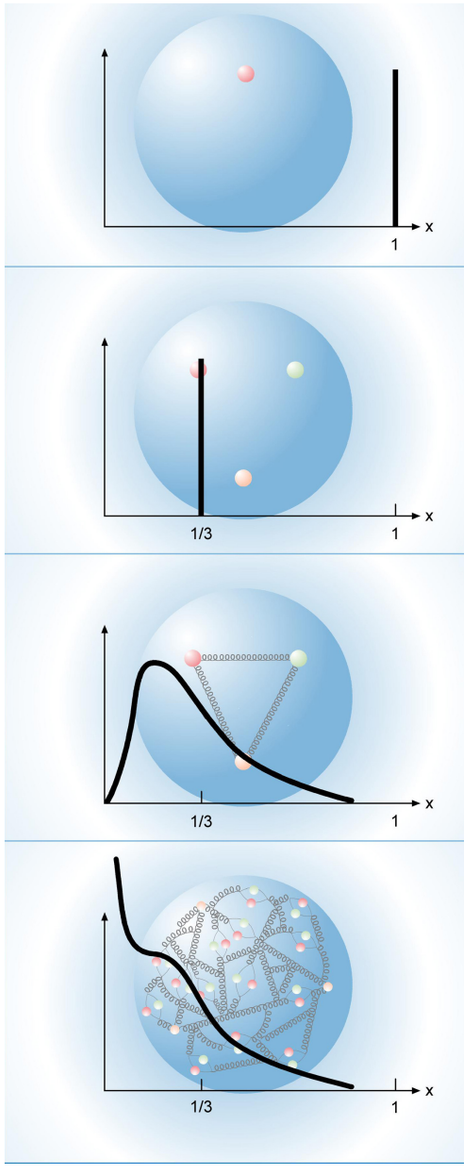

- One valence quark
- Three, non-interacting valence quarks, sharing equal momentum
- Three quarks interacting, changing the momentum
- Many sea quarks

Proton structure function: data

low energy:

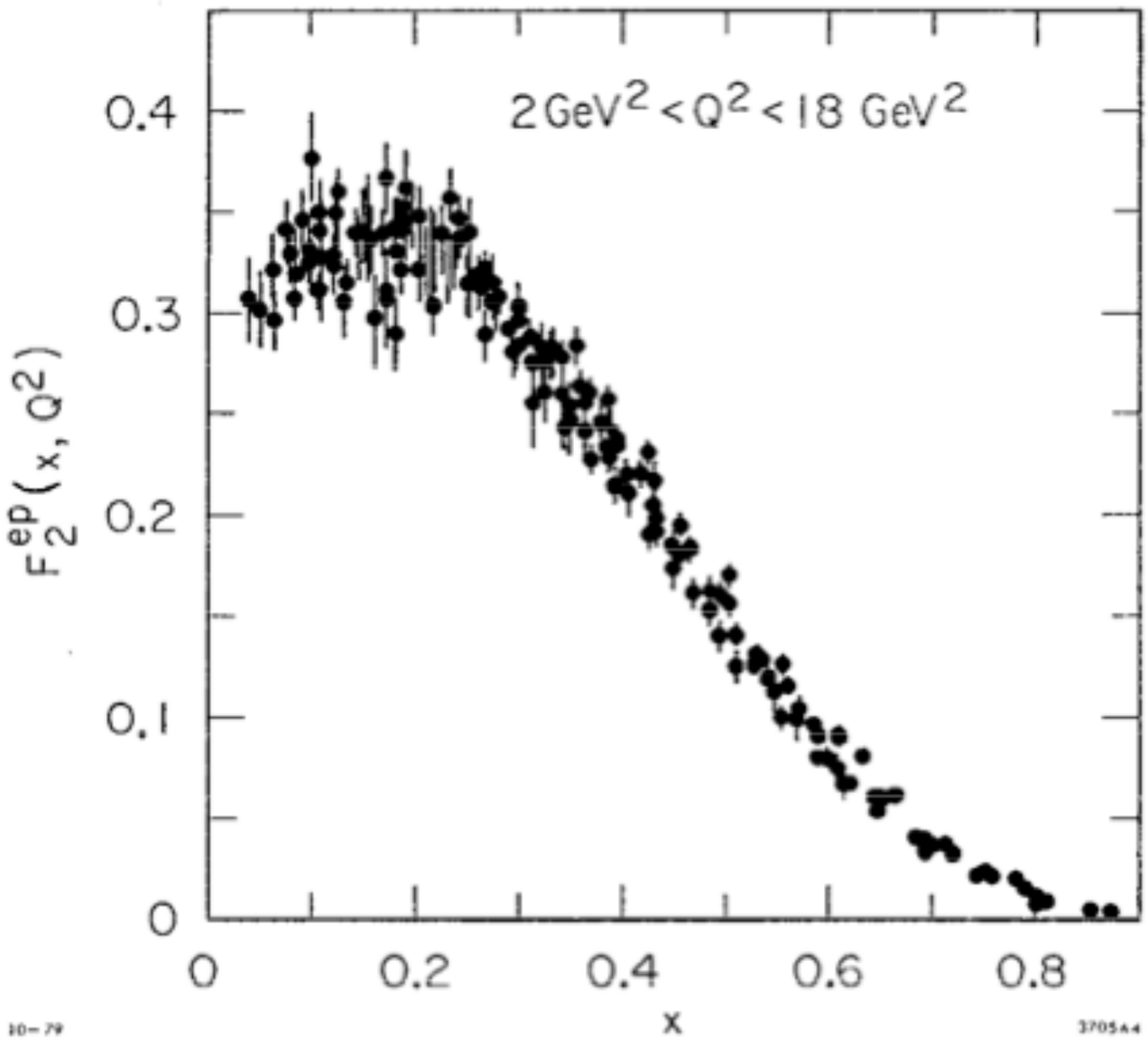

Exploring proton structure at high energy

DESY - Hamburg
HERA Collider
1992-2007

The only electron(positron)-proton collider ever built

Center of mass energy:

$$E_{\rm cm} = 320\ {\rm GeV}$$

equivalent to 50 TeV electron beam on a fixed proton target...about 2500 times more than at SLAC

Measurements of proton structure function

low energy: SLAC

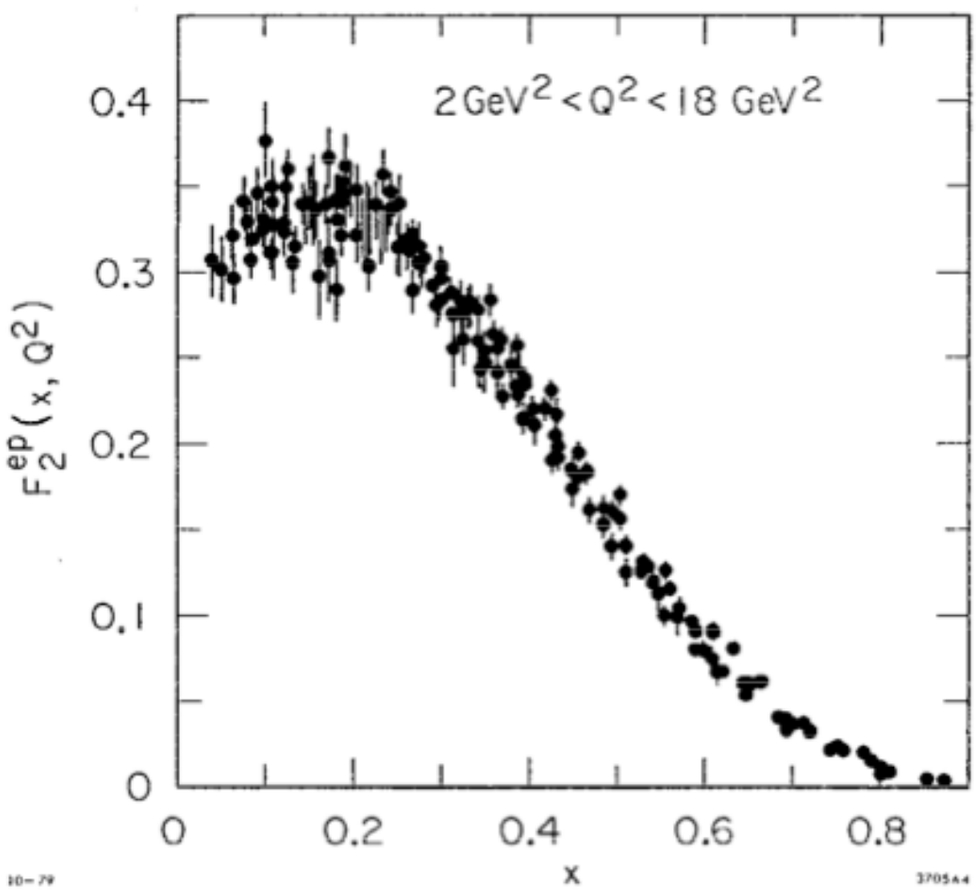

high energy: HERA ep collider

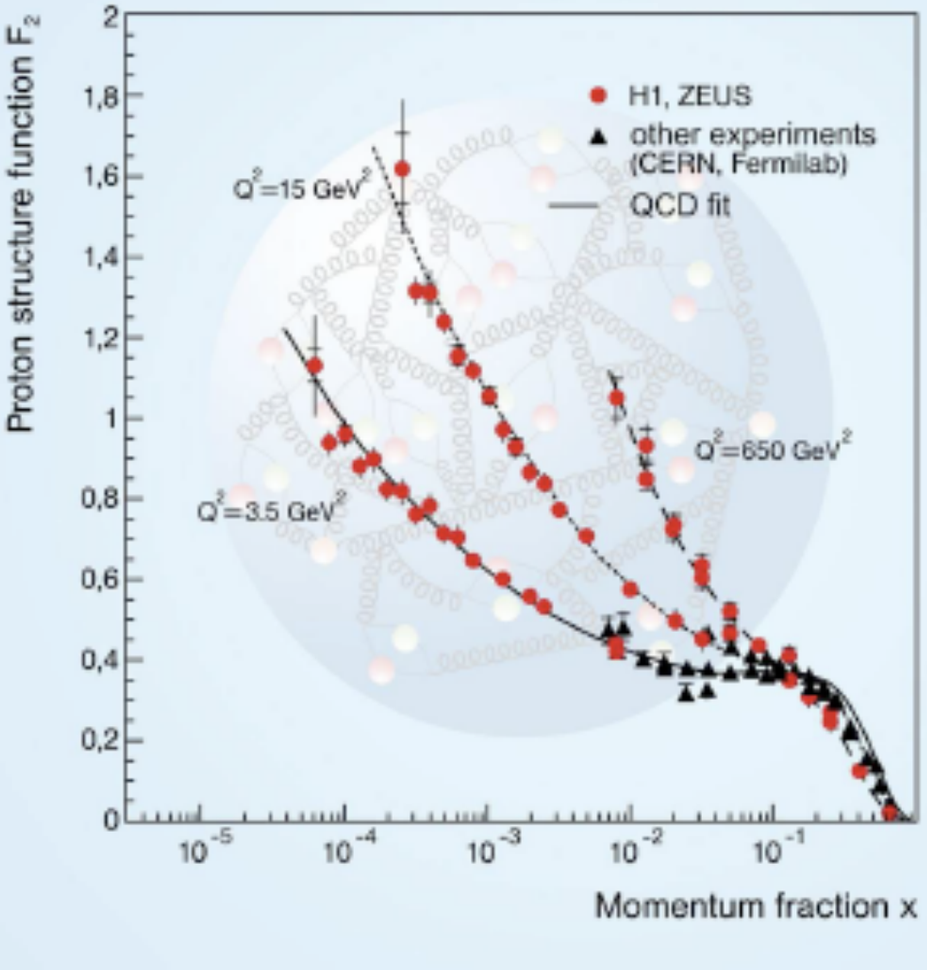

Measurements of proton structure function

low energy: SLAC

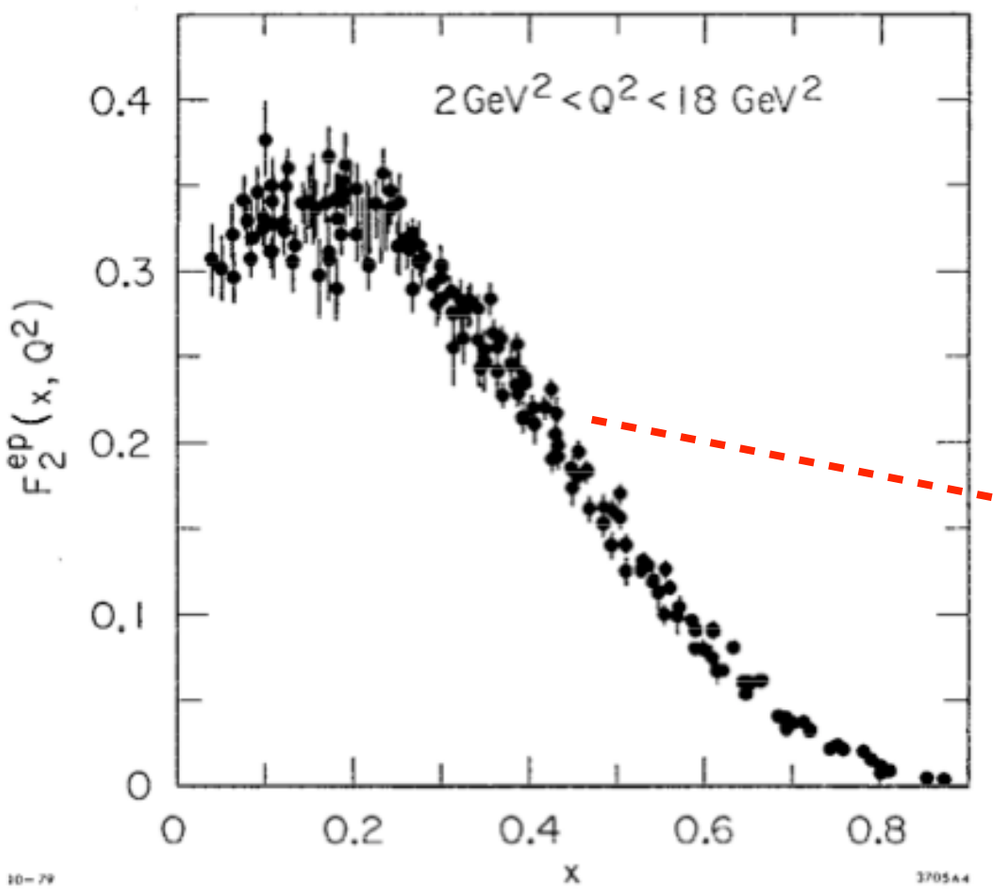

high energy: HERA ep collider

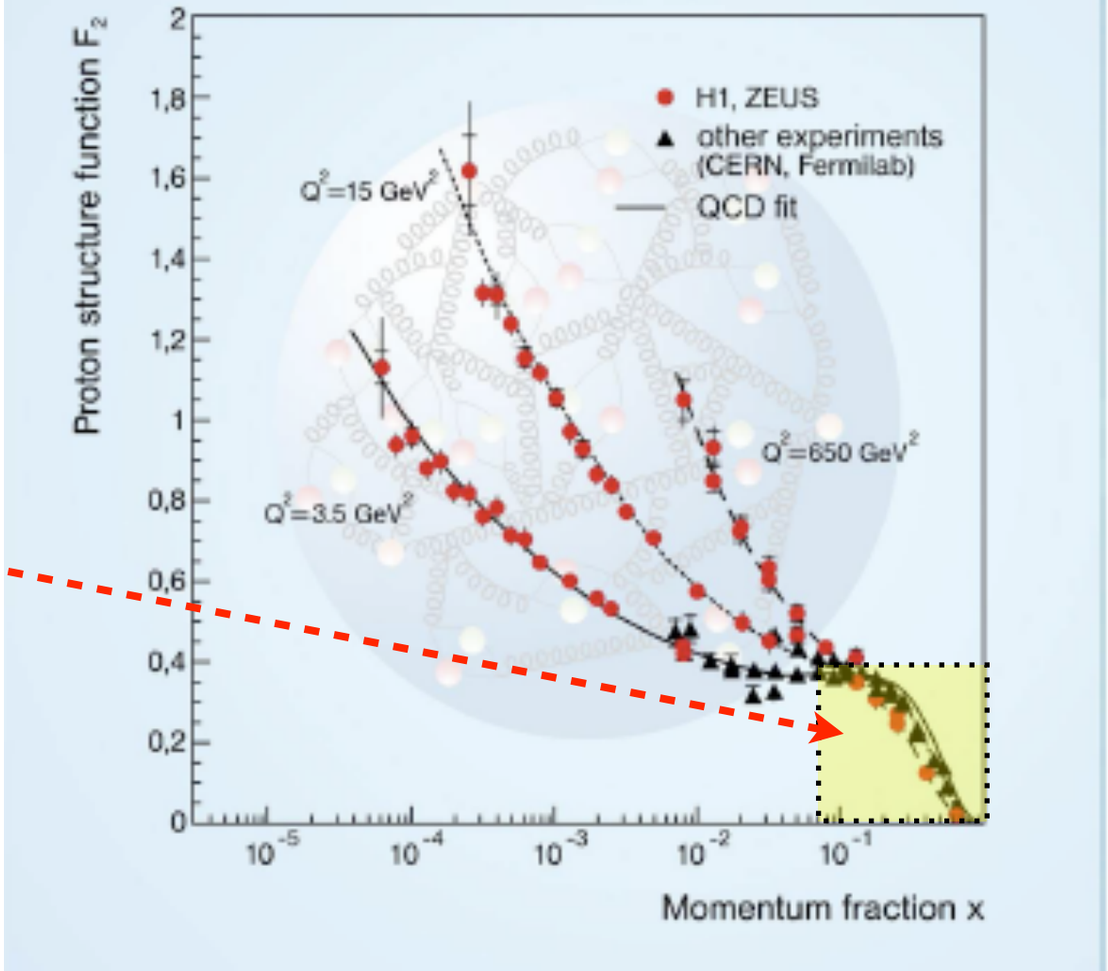

Measurements of proton structure function

low energy: SLAC

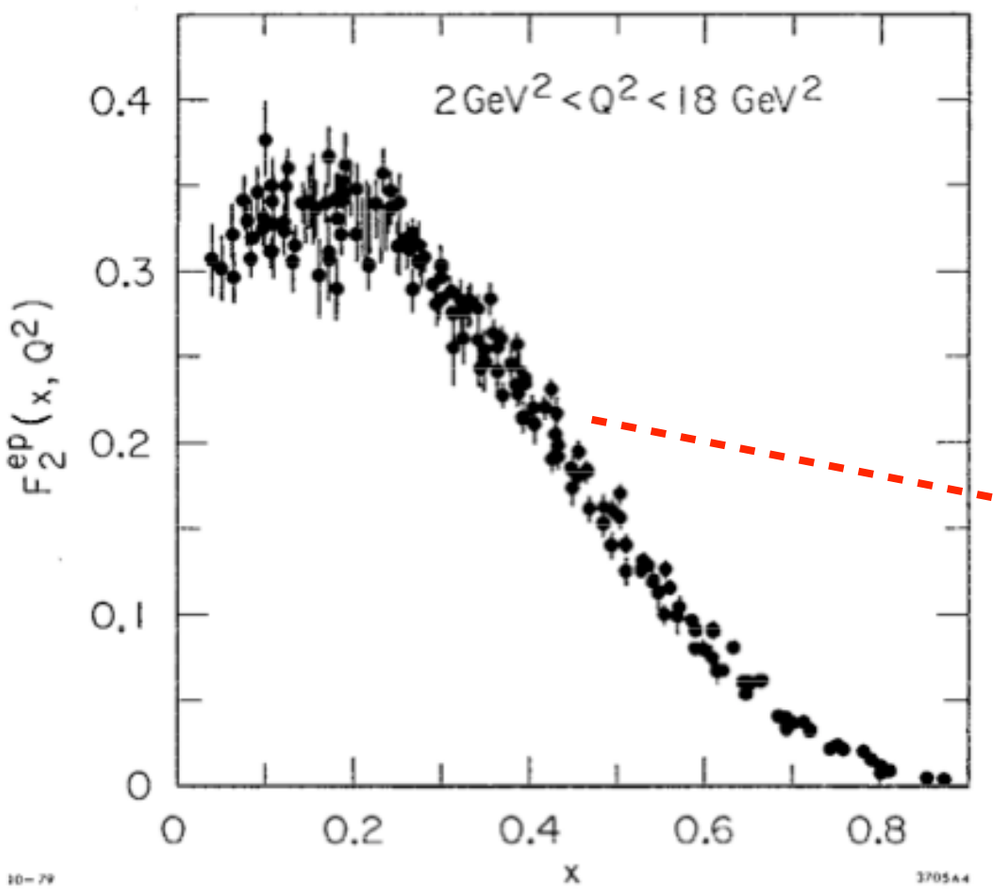

high energy: HERA ep collider

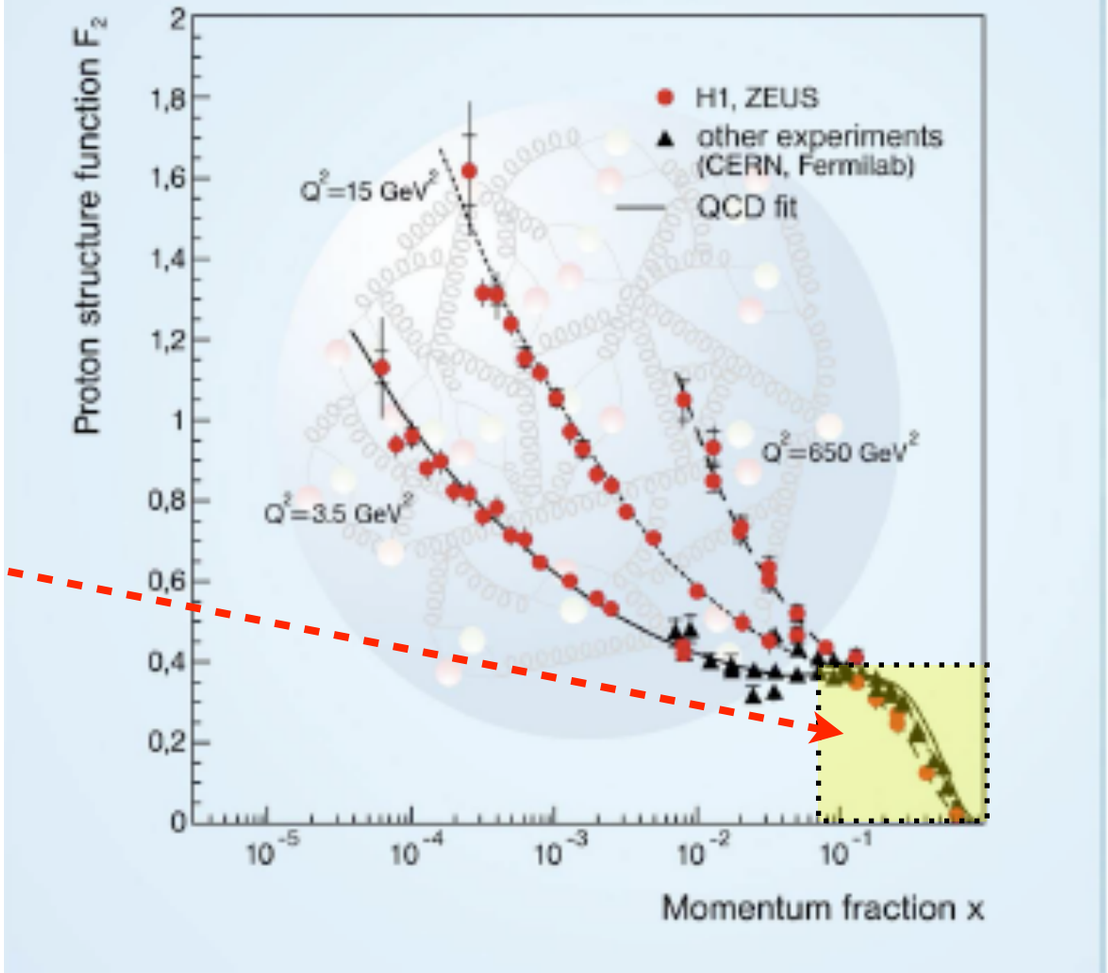

Cross section and that means parton density increases:

- with decreasing x
- with increasing scale Q

Measurements of proton structure function

low energy: SLAC

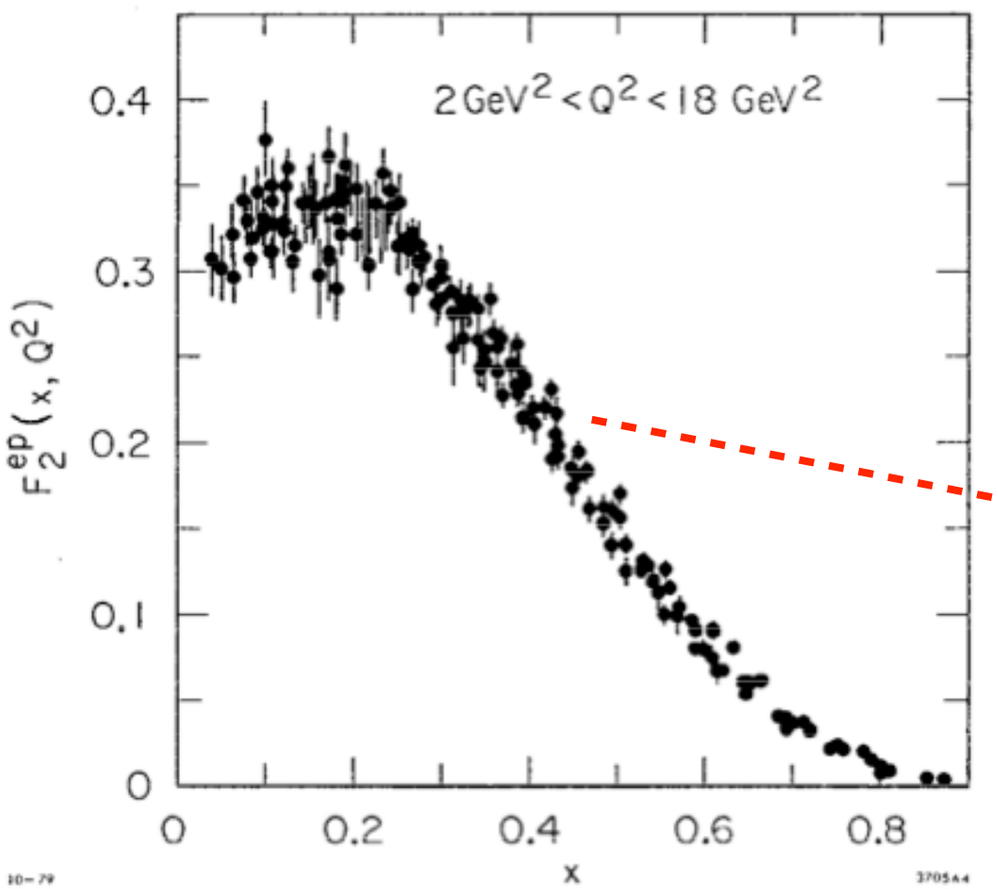

high energy: HERA ep collider

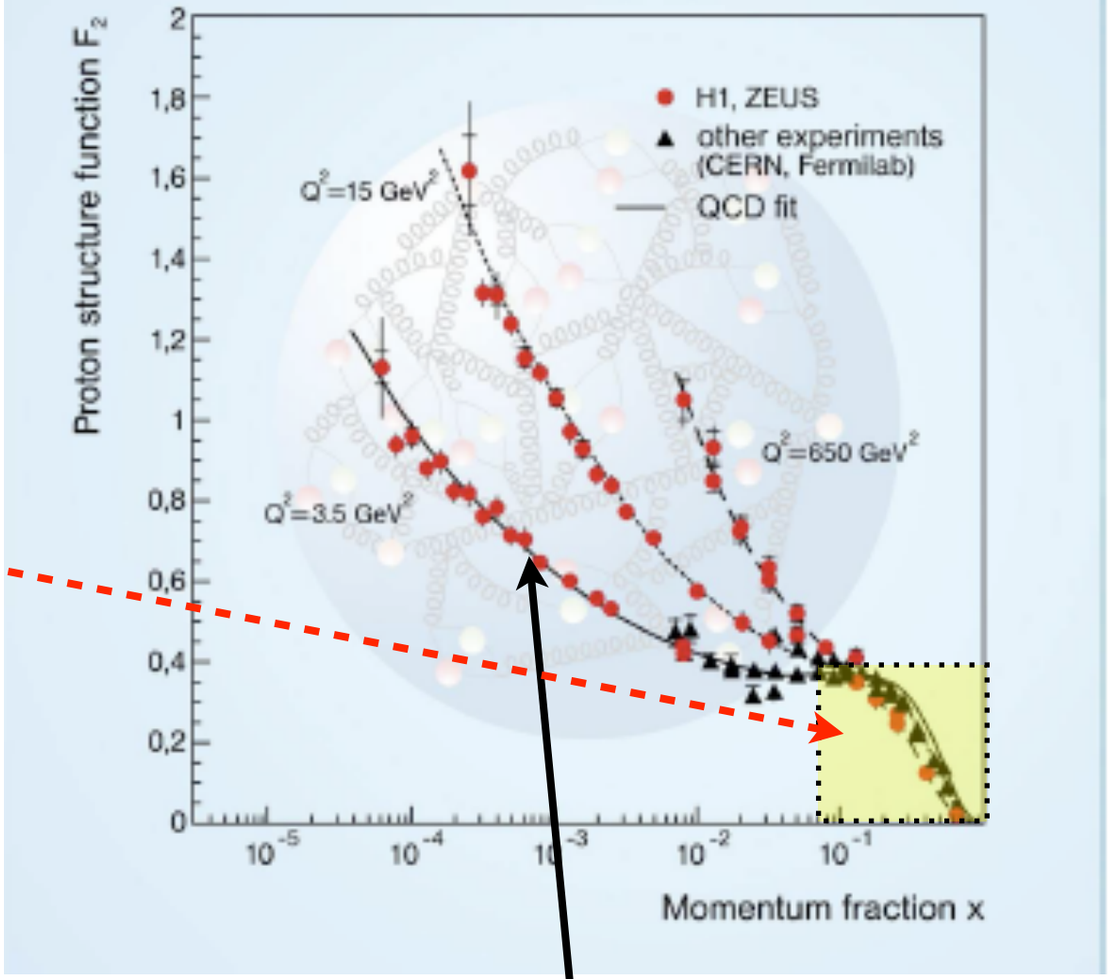

Cross section and that means parton density increases:

- with decreasing x
- with increasing scale Q

Where does this rise come from?

Answer: QCD radiation

Parton model

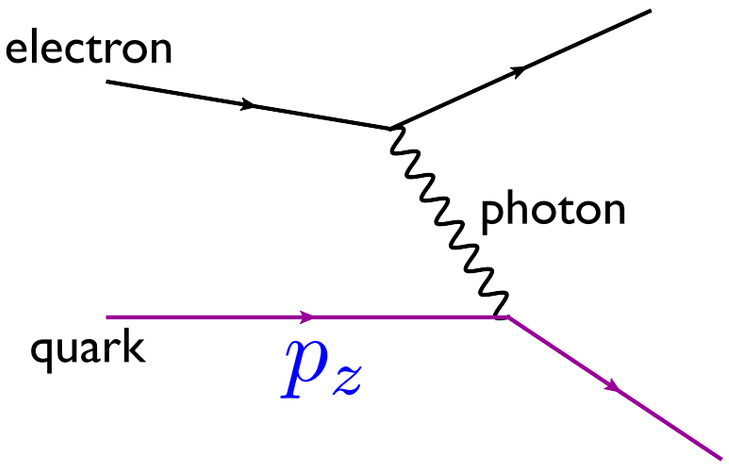

Parton model

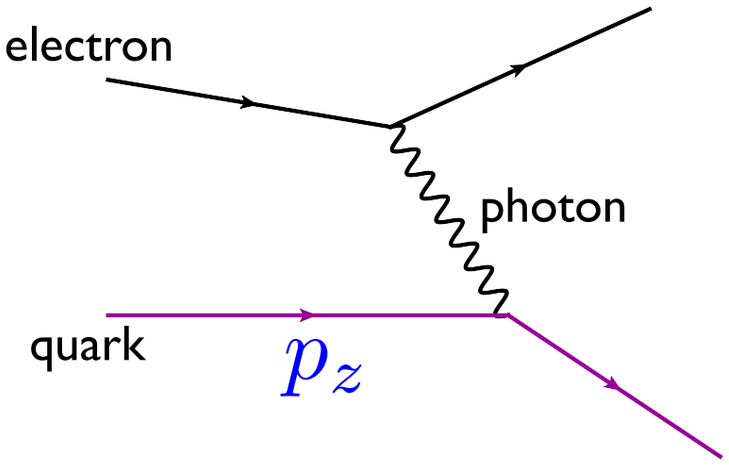

QCD radiation

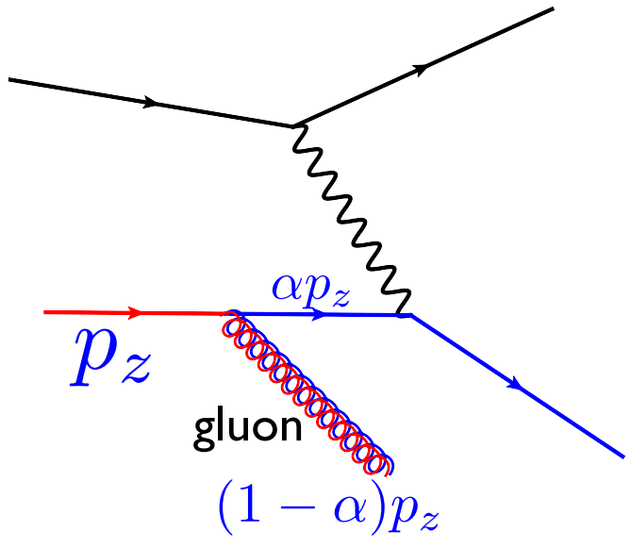

Parton model

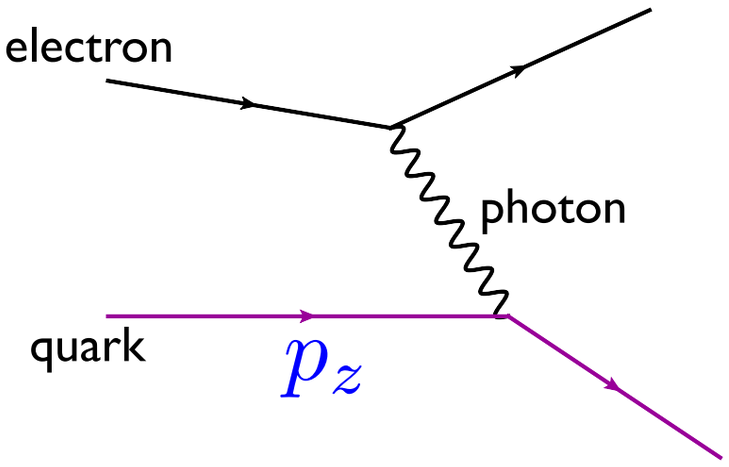

QCD radiation

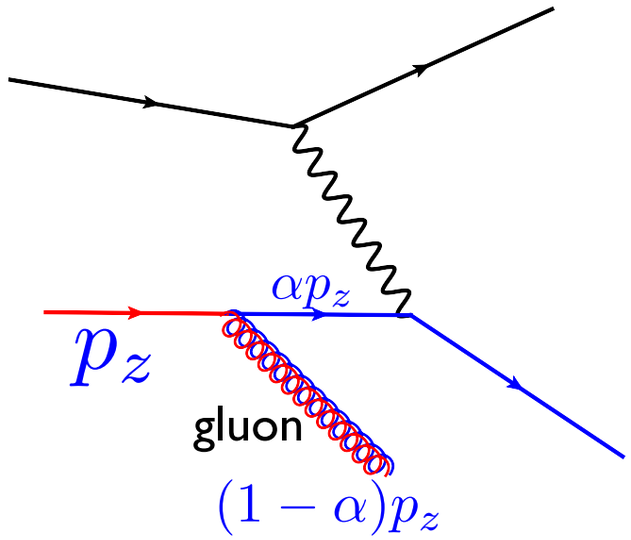

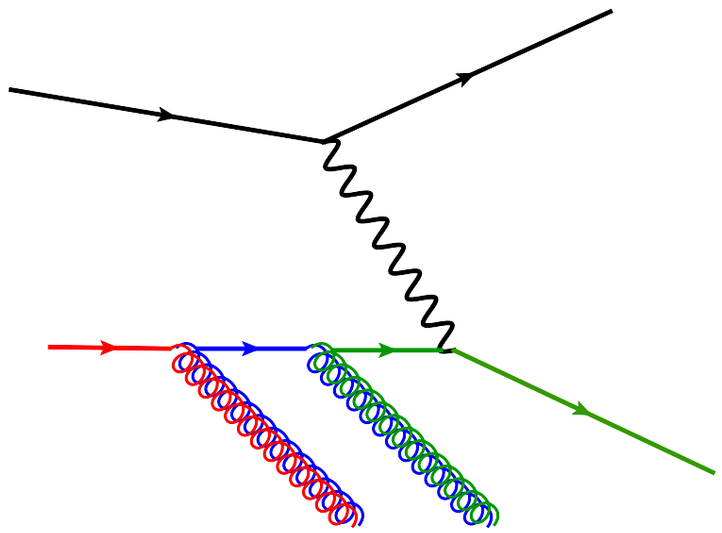

Parton model

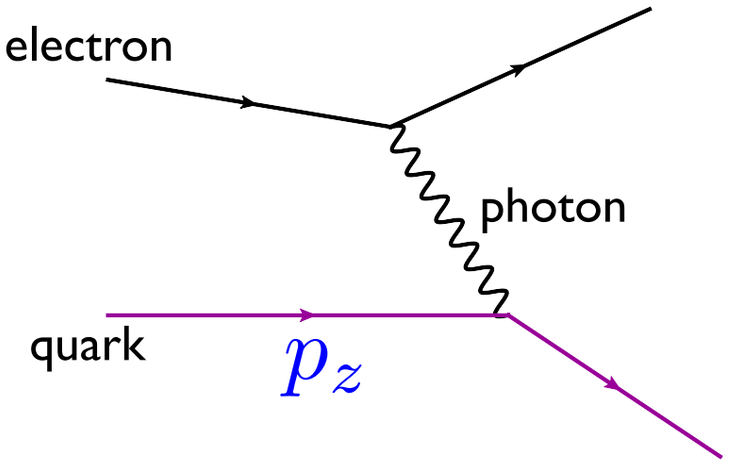

QCD radiation

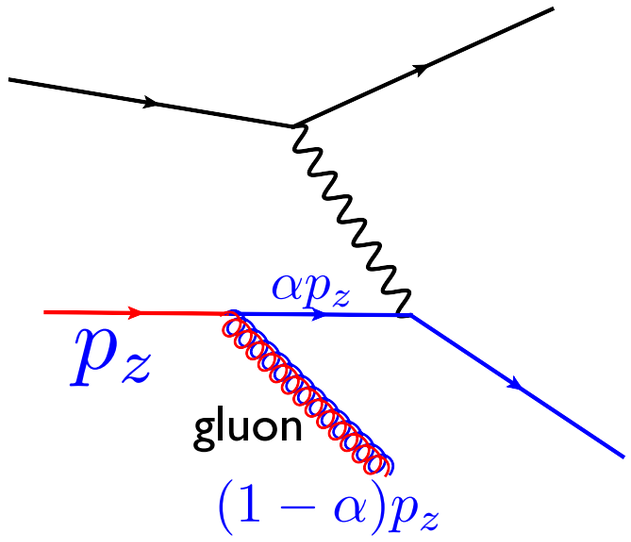

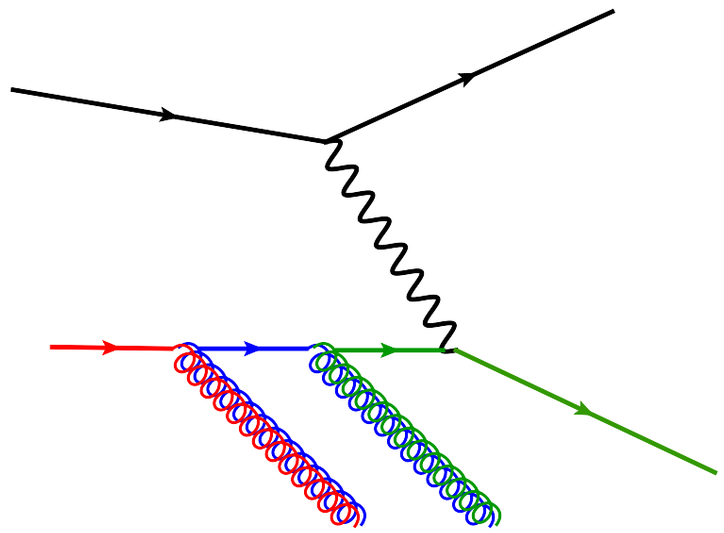

Pair production of sea quarks

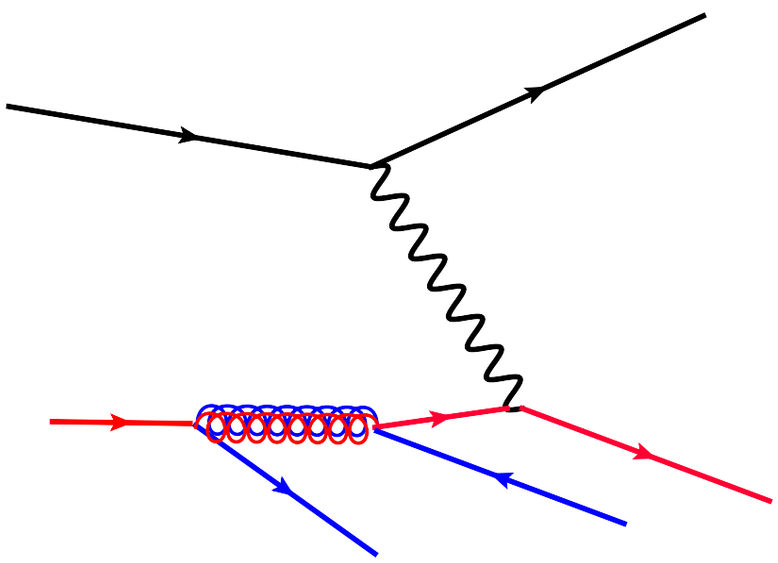

Parton model

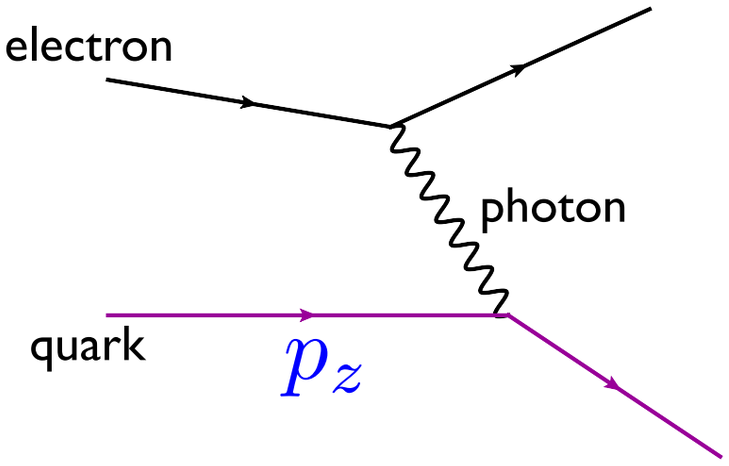

QCD radiation

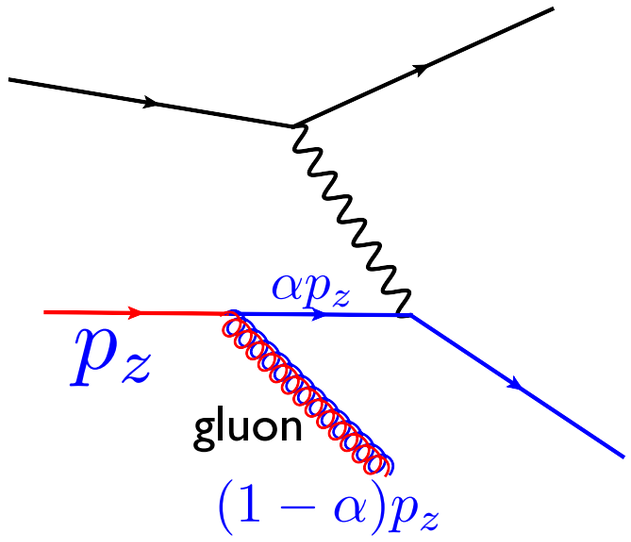

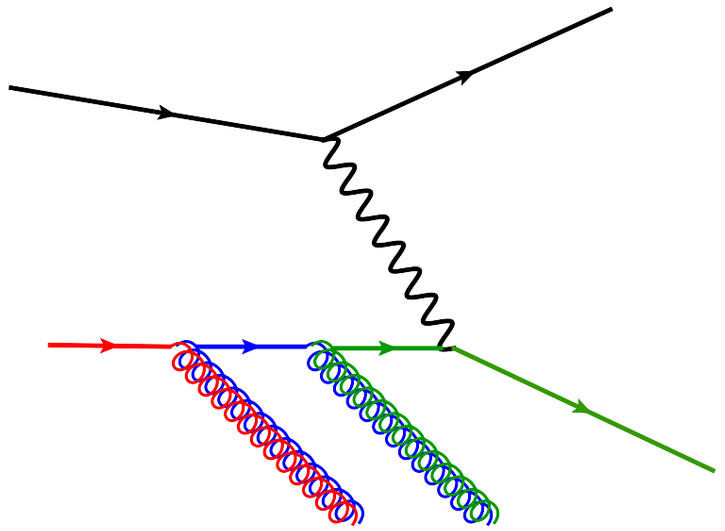

Pair production of sea quarks

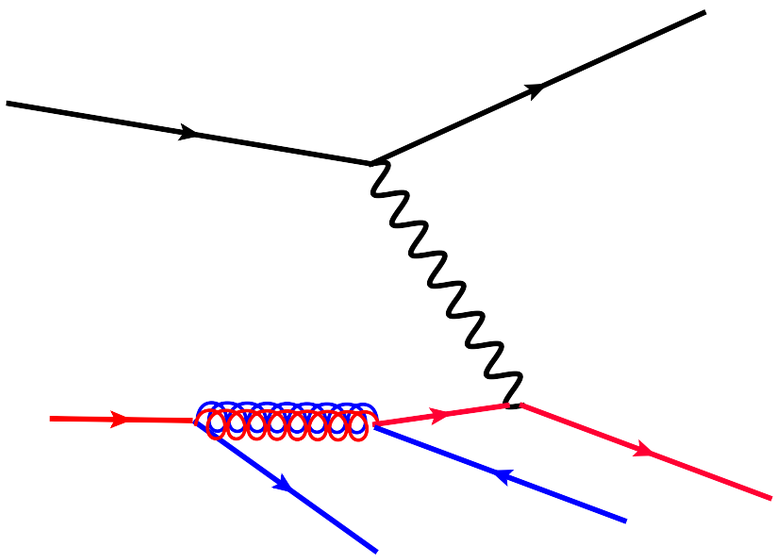

Gluon splitting

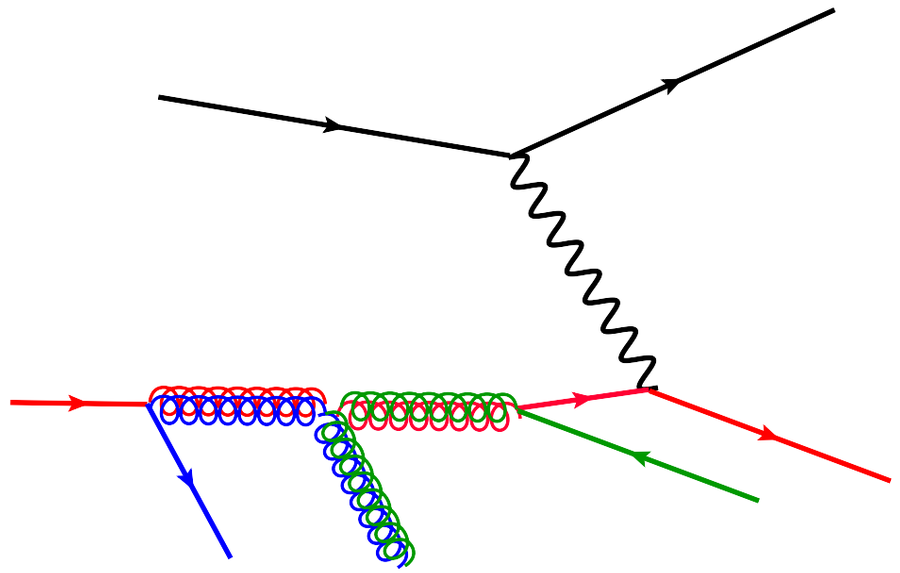

Parton model

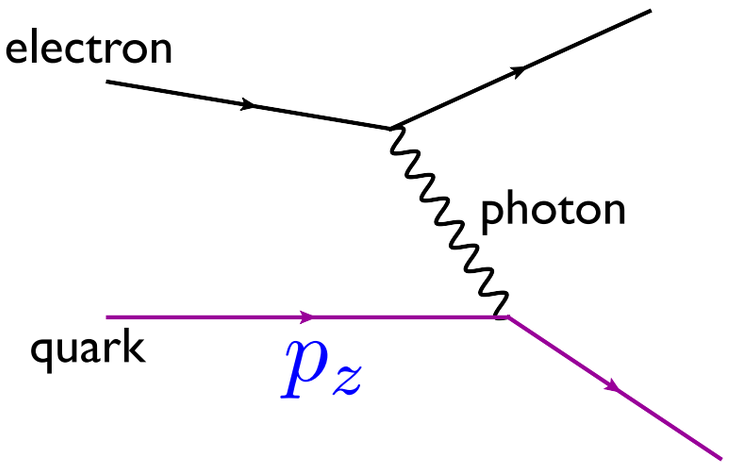

QCD radiation

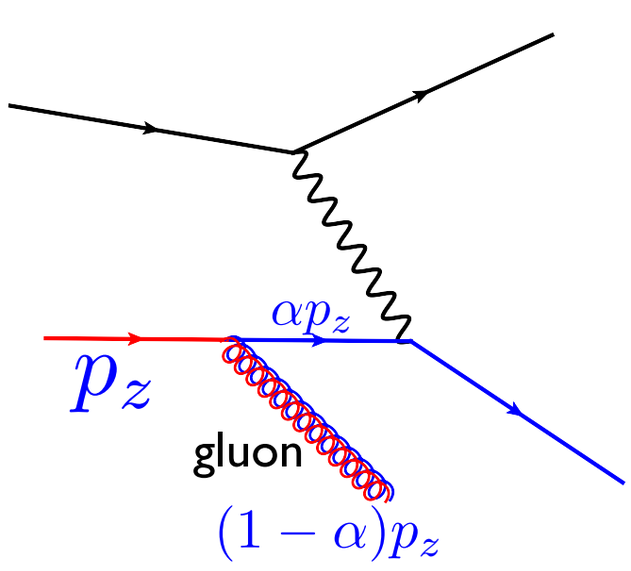

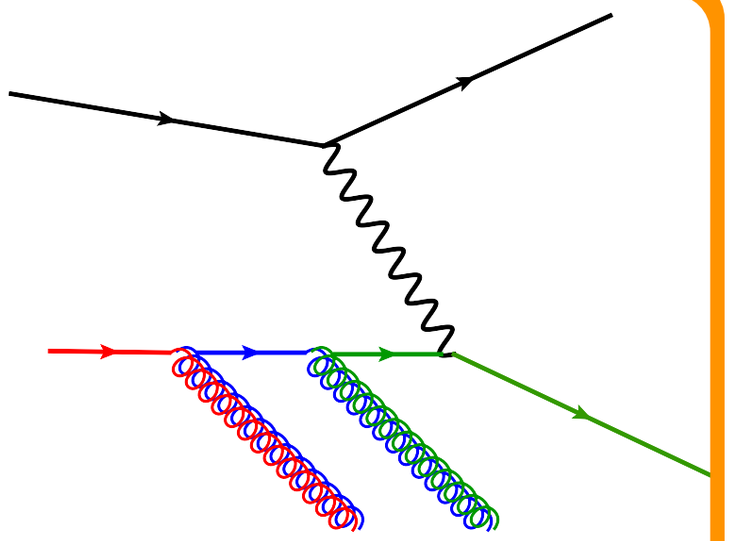

QED like

Pair production of sea quarks

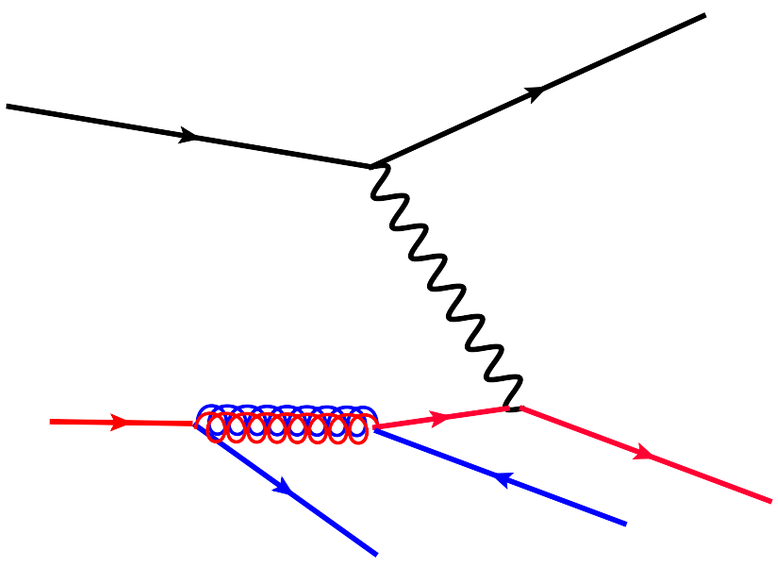

QED like

Gluon splitting

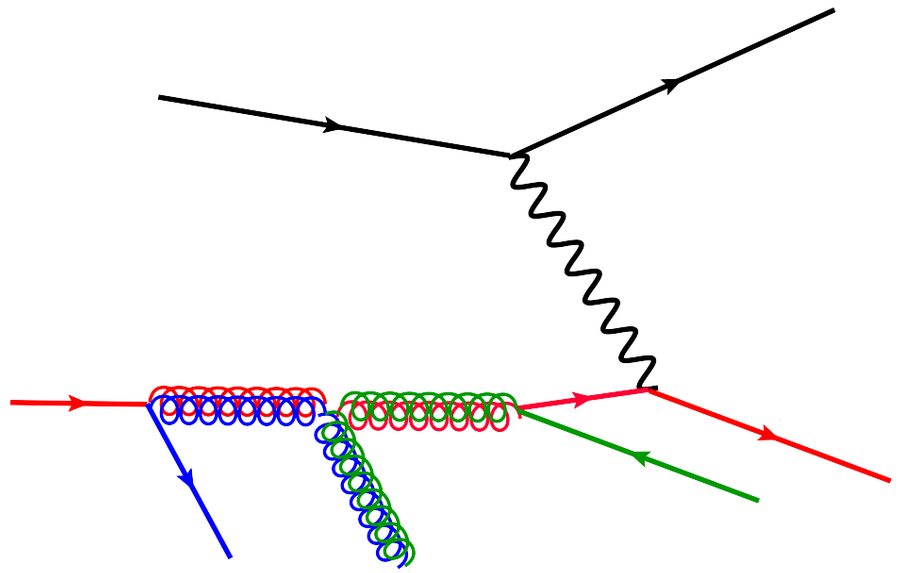

Parton model

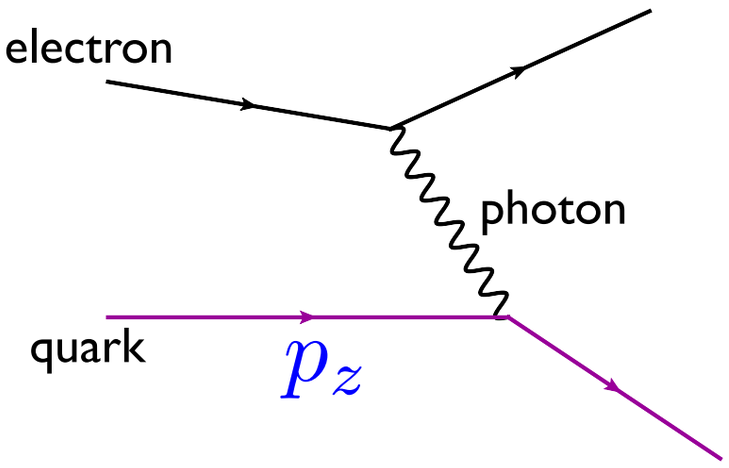

QCD radiation

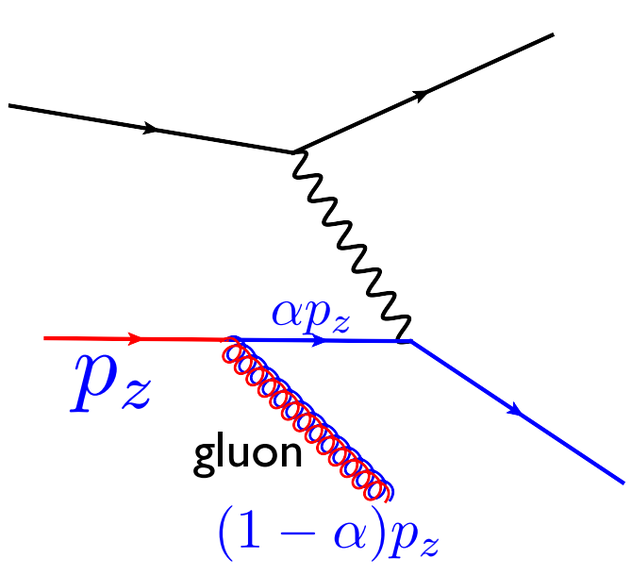

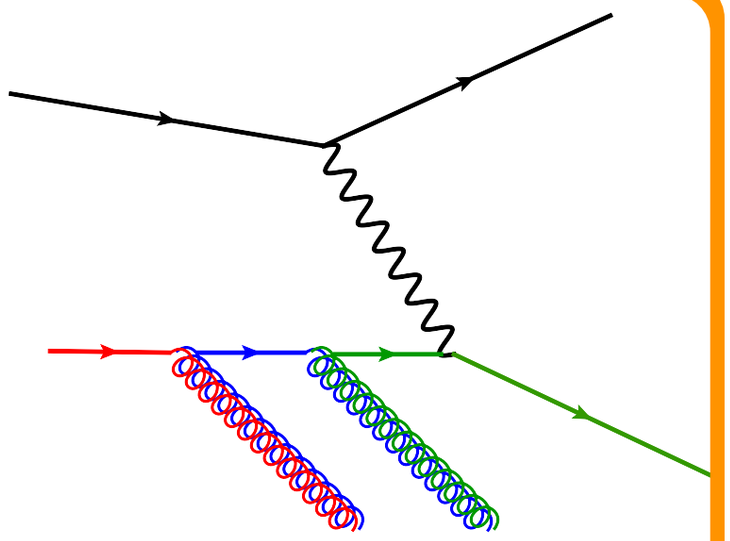

QED like

Pair production of sea quarks

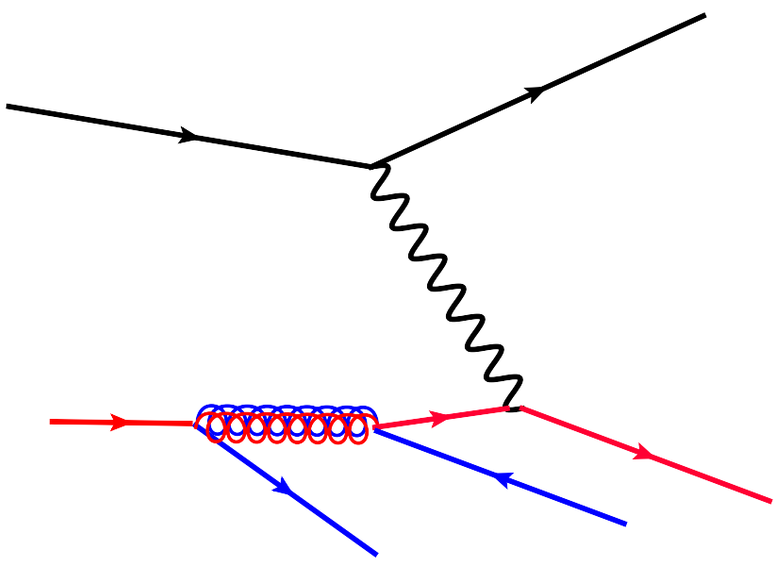

QED like

Gluon splitting

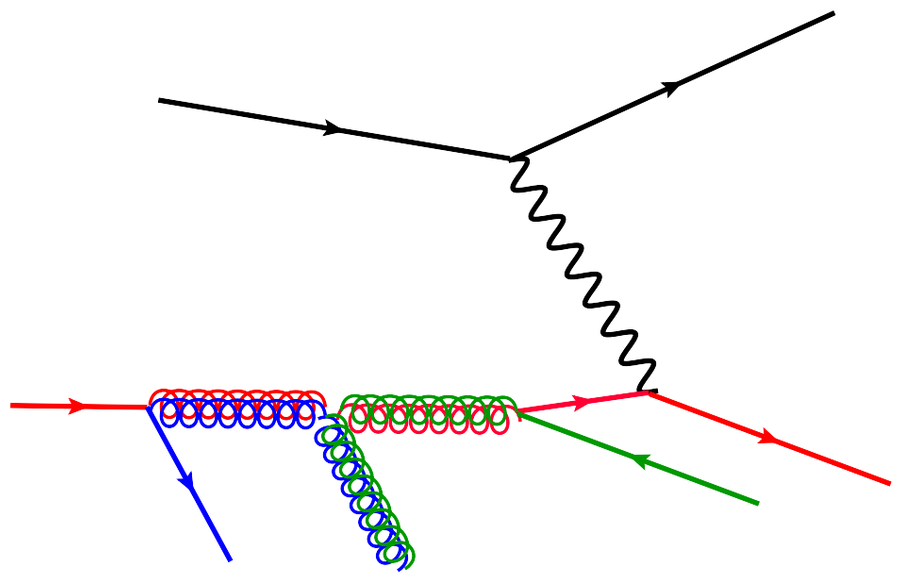

Unique to non-abelian theory

Structure functions in QCD

Formalizm in QCD - Collinear factorization:

$$F_i(x,Q^2) = \sum_j \int_x^1 dy\, C_i^j(x/y, Q^2, \alpha_s)\, f_j(y,Q^2) + \mathcal{O}(\frac{\Lambda^2}{Q^2})$$

$C_i^j(x/y, Q^2, \alpha_s)$

Coefficient functions, perturbatively calculable

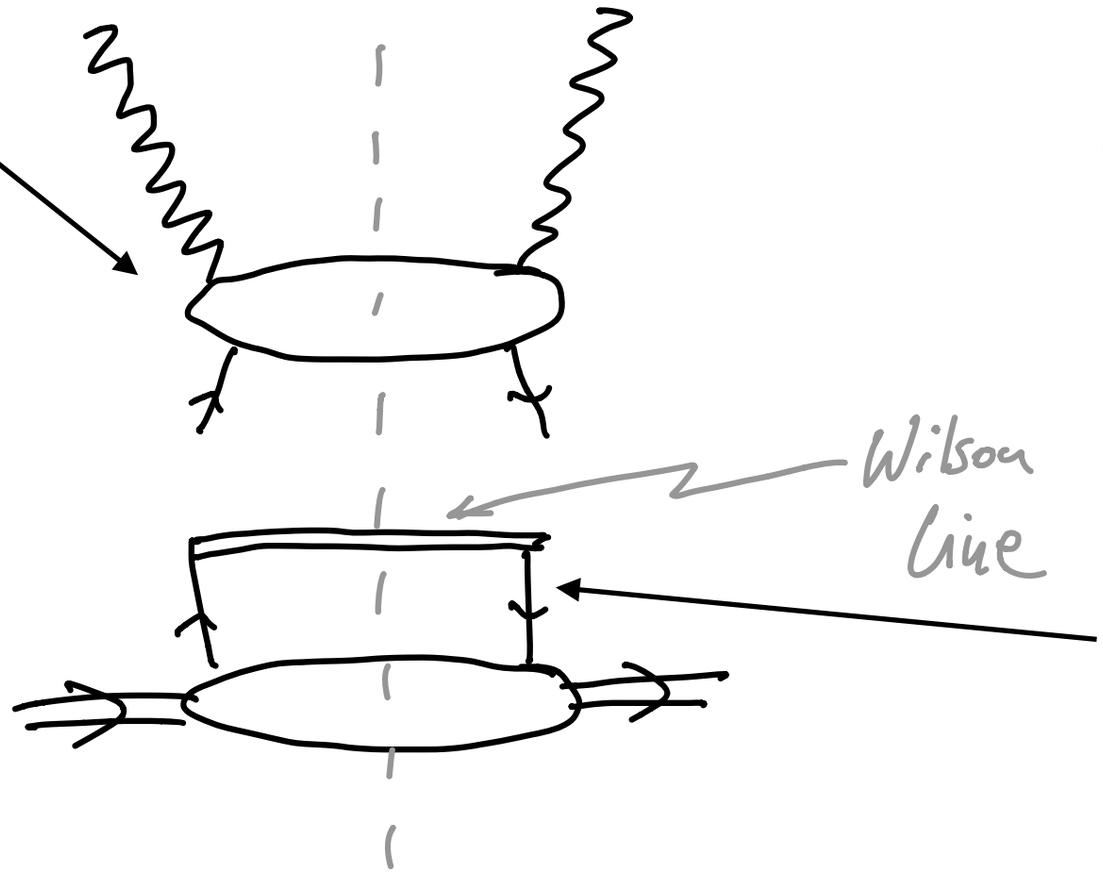

Parton distributions with scaling violations, cannot be perturbatively calculated. Their scale dependence can be predicted through the perturbative evolution

$f_j(y, \mu^2)$

$\mathcal{O}(\frac{\Lambda^2}{Q^2})$

Power corrections.
Control the onset of the regime where the factorization in violated
The scale could be determined experimentally, can depend on energy (saturation scale) and target type

DGLAP evolution equations

$t = \ln Q^2/Q_0^2$

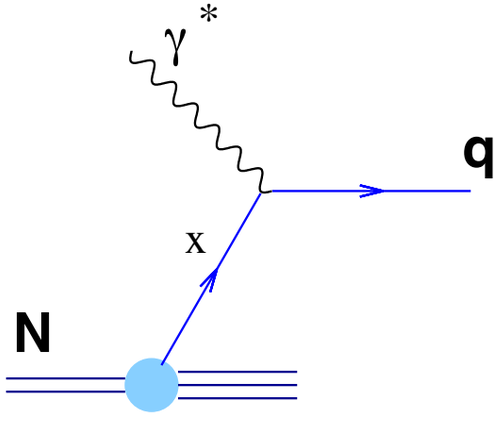

$q(x,t)$

$t + \delta t$

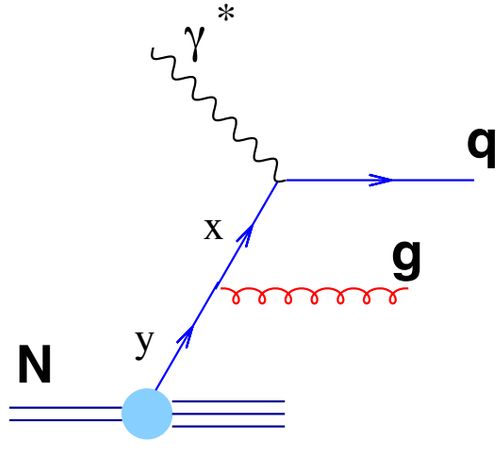

$q(x,t) + \delta q(x,t)$

quarks with fraction $x = \frac{Q^2}{s}$ of target momentum .

DGLAP evolution equations

$t = \ln Q^2/Q_0^2$

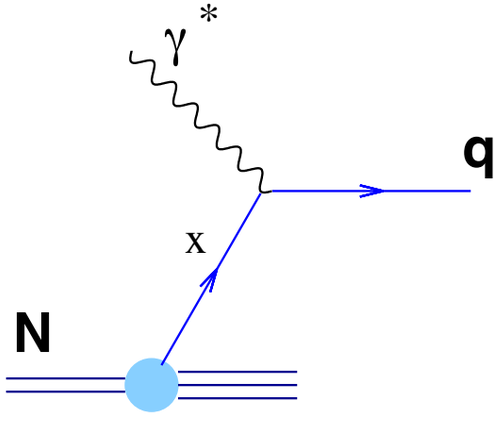

$q(x,t)$

$t + \delta t$

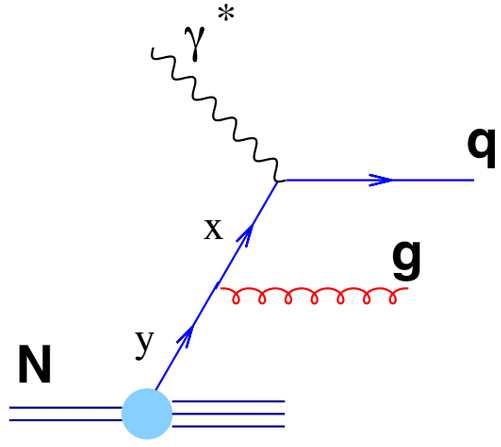

$q(x,t) + \delta q(x,t)$

quarks with fraction $x = \frac{Q^2}{s}$ of target momentum .

Evolution equation:

$$\frac{dq(x,t)}{dt} = \frac{\alpha_s(t)}{2\pi} \int_x^1 \frac{dy}{y} P_{qq}(x/y)\, q(y,t)$$

$P_{qq}(z,\alpha_s)$ is the probablity of finding quark in the quark with $z(=x/y)$ fraction of its momentum

DGLAP evolution equations

Apart from $q(x,t)$ one has to include $g(x,t)$

$t = \ln Q^2/Q_0^2$ $\quad\quad$ $t+\delta t$

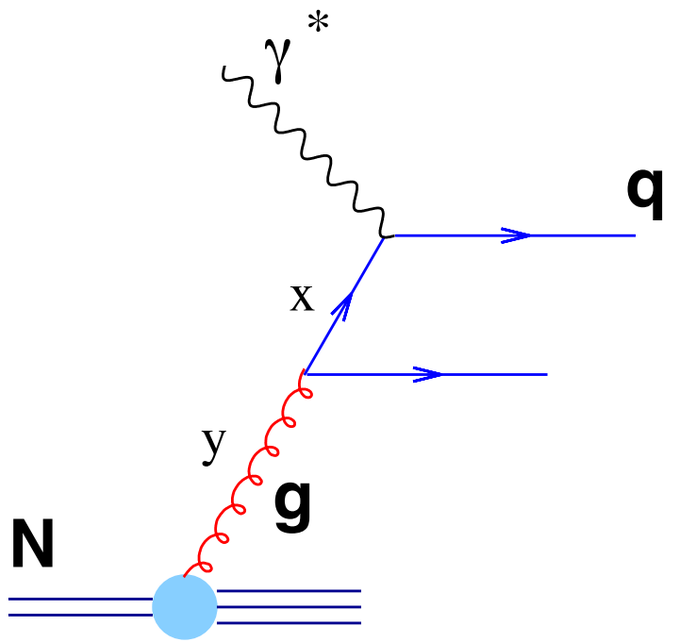

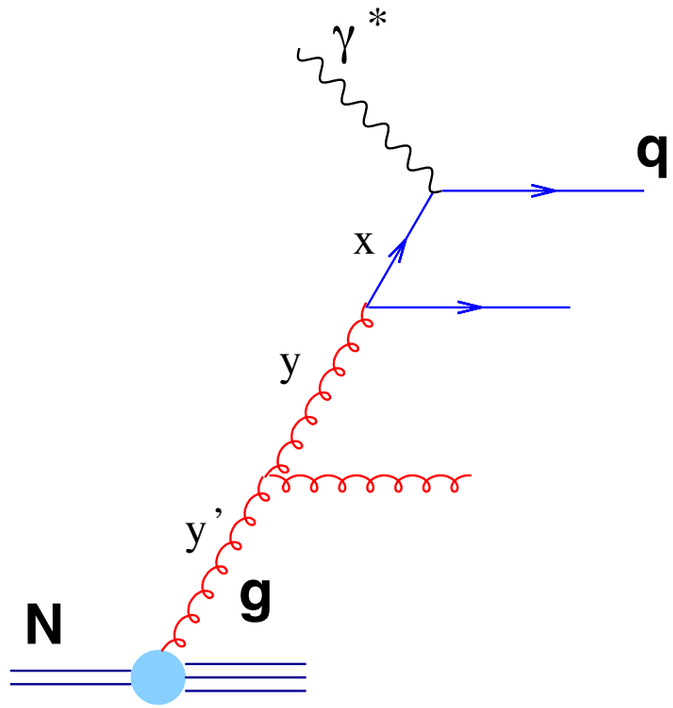

DGLAP evolution equations

Apart from $q(x,t)$ one has to include $g(x,t)$

$t = \ln Q^2/Q_0^2$ $\qquad$ $t+\delta t$

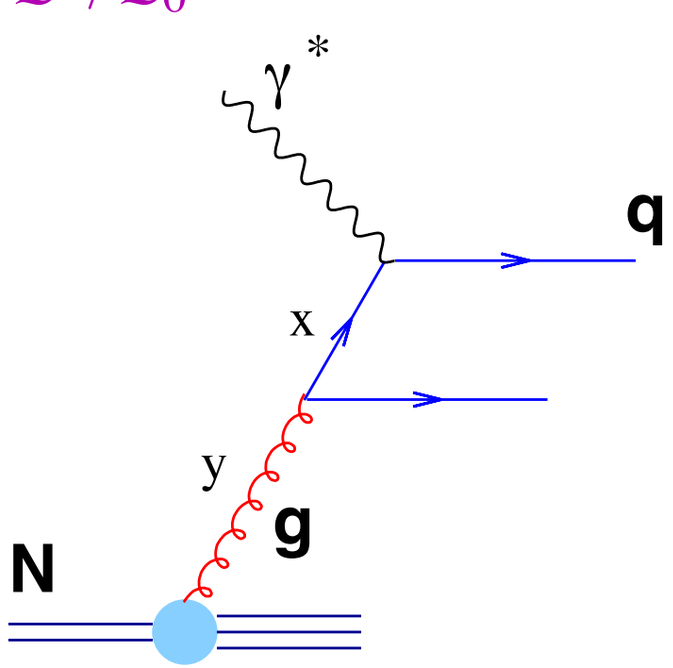

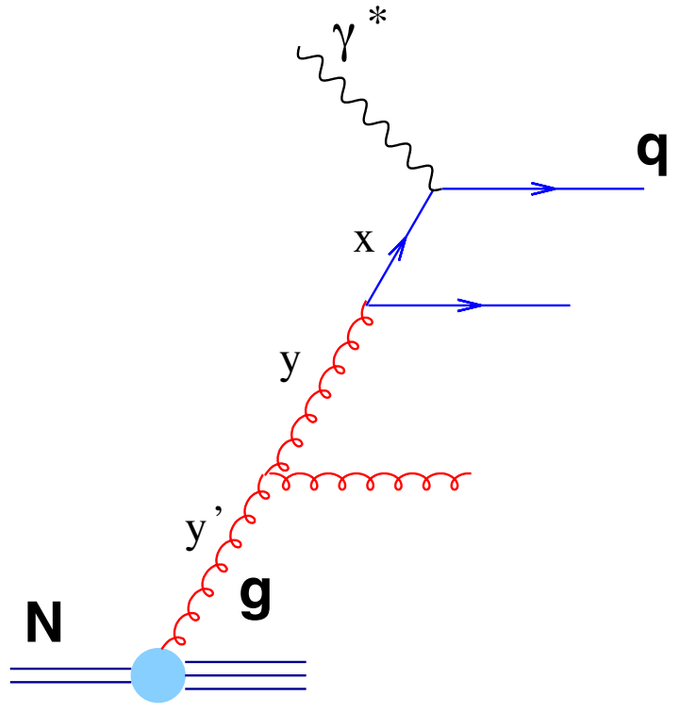

Set of evolution equations (flavour singlet case):

$$\frac{\partial}{\partial t}\begin{bmatrix}\Sigma(x,t)\\ g(x,t)\end{bmatrix} = \frac{\alpha_s(t)}{2\pi}\begin{bmatrix}P_{qq} & 2N_f P_{qg}\\ P_{gq} & P_{gg}\end{bmatrix} \overset{x}{\otimes} \begin{bmatrix}\Sigma(x,t)\\ g(x,t)\end{bmatrix}$$

where $\Sigma(x,t) = \sum_i [q_i(x,t) + \bar{q}_i(x,t)]$

DGLAP evolution

DGLAP evolution: PDFs

Evolution is predicted perturbatively. Currently known orders LO, NLO, NNLO

Splitting functions: $$P_i(z) = \alpha_s P_i^{(0)} + \alpha_s^2 P_i^{(1)} + \alpha_s^3 P_i^{(2)}$$

Ongoing efforts to compute the splitting functions at N³LO *Moch,Vermaseren,Vogt et al*

DGLAP evolution: PDFs

Evolution is predicted perturbatively. Currently known orders LO, NLO, NNLO

Splitting functions: $P_i(z) = \alpha_s P_i^{(0)} + \alpha_s^2 P_i^{(1)} + \alpha_s^3 P_i^{(2)}$

Ongoing efforts to compute the splitting functions at N³LO *Moch,Vermaseren,Vogt et al*

Initial conditions must be parametrized at some scale
Example of HERAPDF2.0 parametrization, generic form for the parton density:

$$xf(x) = Ax^B(1-x)^C(1+Dx+Ex^2)$$

$$\begin{aligned}
xg(x) &= A_g x^{B_g}(1-x)^{C_g} - A'_g x^{B'_g}(1-x)^{C'_g}, \\
xu_v(x) &= A_{u_v} x^{B_{u_v}}(1-x)^{C_{u_v}}\left(1+E_{u_v}x^2\right), \\
xd_v(x) &= A_{d_v} x^{B_{d_v}}(1-x)^{C_{d_v}}, \\
x\bar{U}(x) &= A_{\bar{U}} x^{B_{\bar{U}}}(1-x)^{C_{\bar{U}}}(1+D_{\bar{U}}x), \\
x\bar{D}(x) &= A_{\bar{D}} x^{B_{\bar{D}}}(1-x)^{C_{\bar{D}}}.
\end{aligned}$$

$$\begin{aligned}
xU &= xu + xc \\
x\bar{U} &= x\bar{u} + x\bar{c} \\
xD &= xd + xs \\
x\bar{D} &= x\bar{d} + x\bar{s} \\
xu_v &= xU - x\bar{U} \\
xd_v &= xD - x\bar{D}
\end{aligned}$$

15 parameter fit at NLO
14 parameter fit at NNLO

Proton PDFs

Parametrization

$$xf(x) = Ax^B(1-x)^C(1+Dx+Ex^2)$$

- There is no particular reason to limit the analysis to this form, but pragmatically this is what works
- The power on (1-x) terms is positive and ensures that the distribution vanishes for x=1
- The power at x term can be positive or negative, depending on whether the distribution is valence like or sea
- Note that gluons at this order are initially valence-like
- They can become negative. Formally this is not a problem since this is not observable quantity. Practically this is a problem since the cross section can turn negative and this is then unphysical

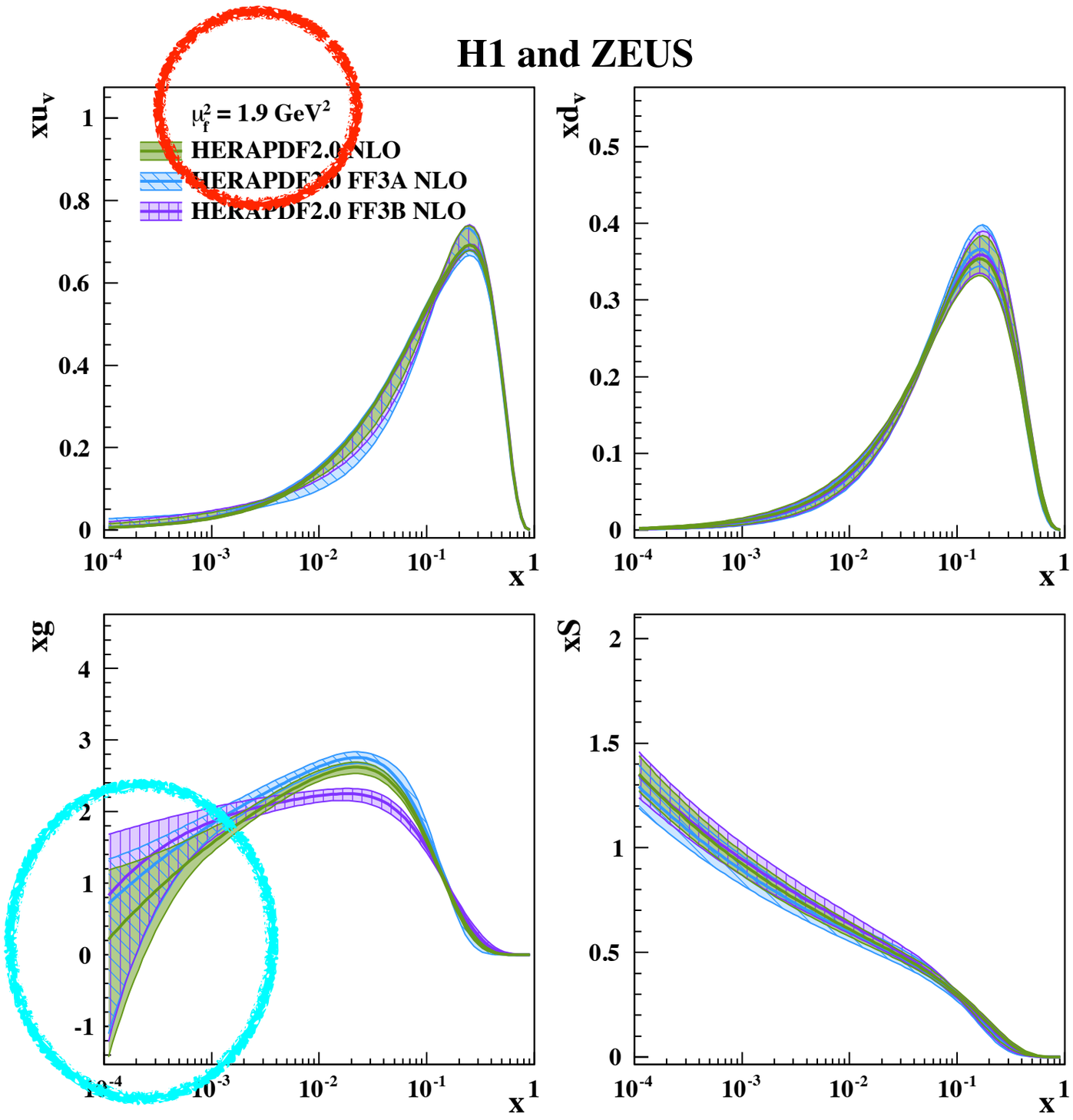

Proton PDFs

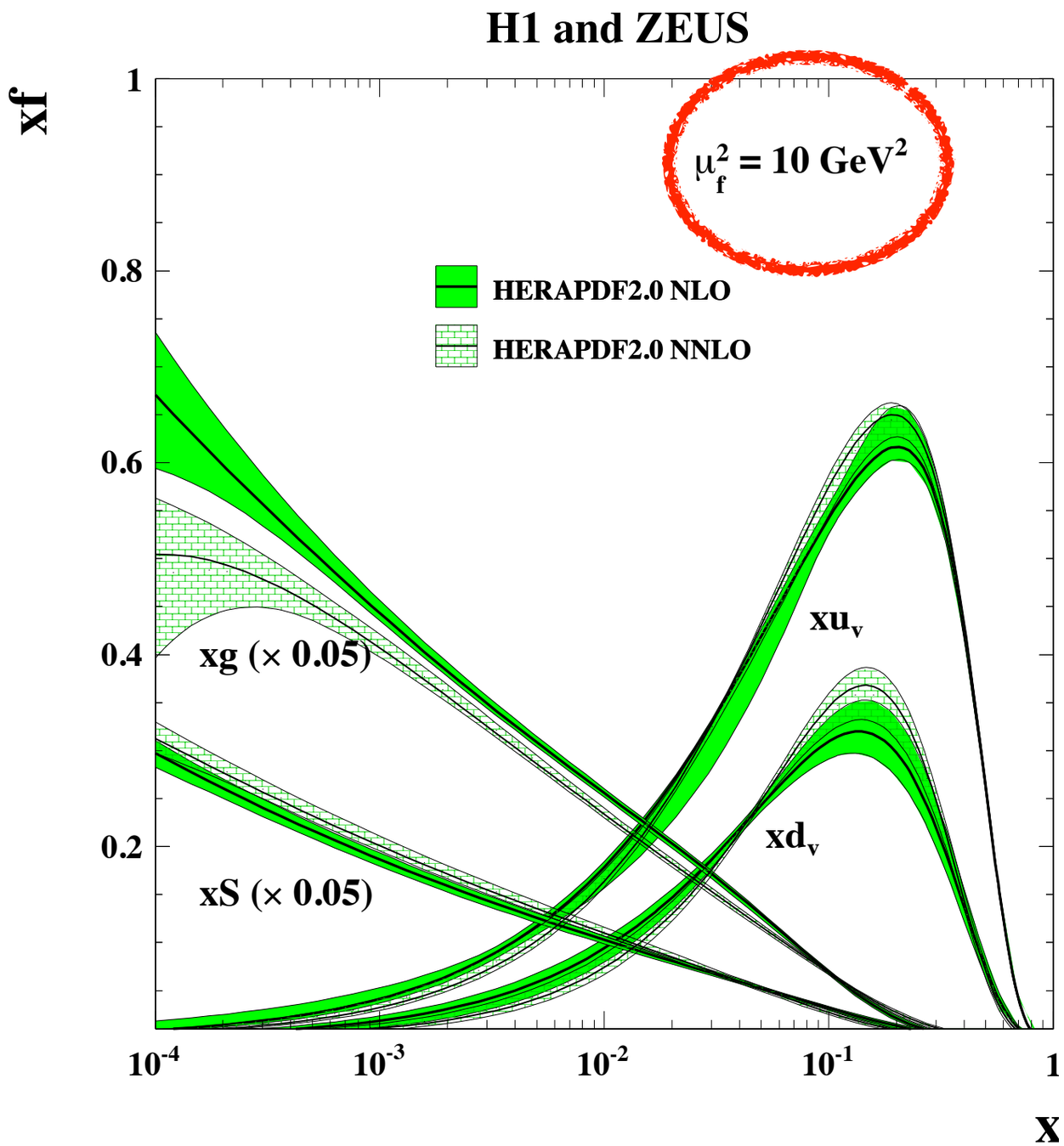

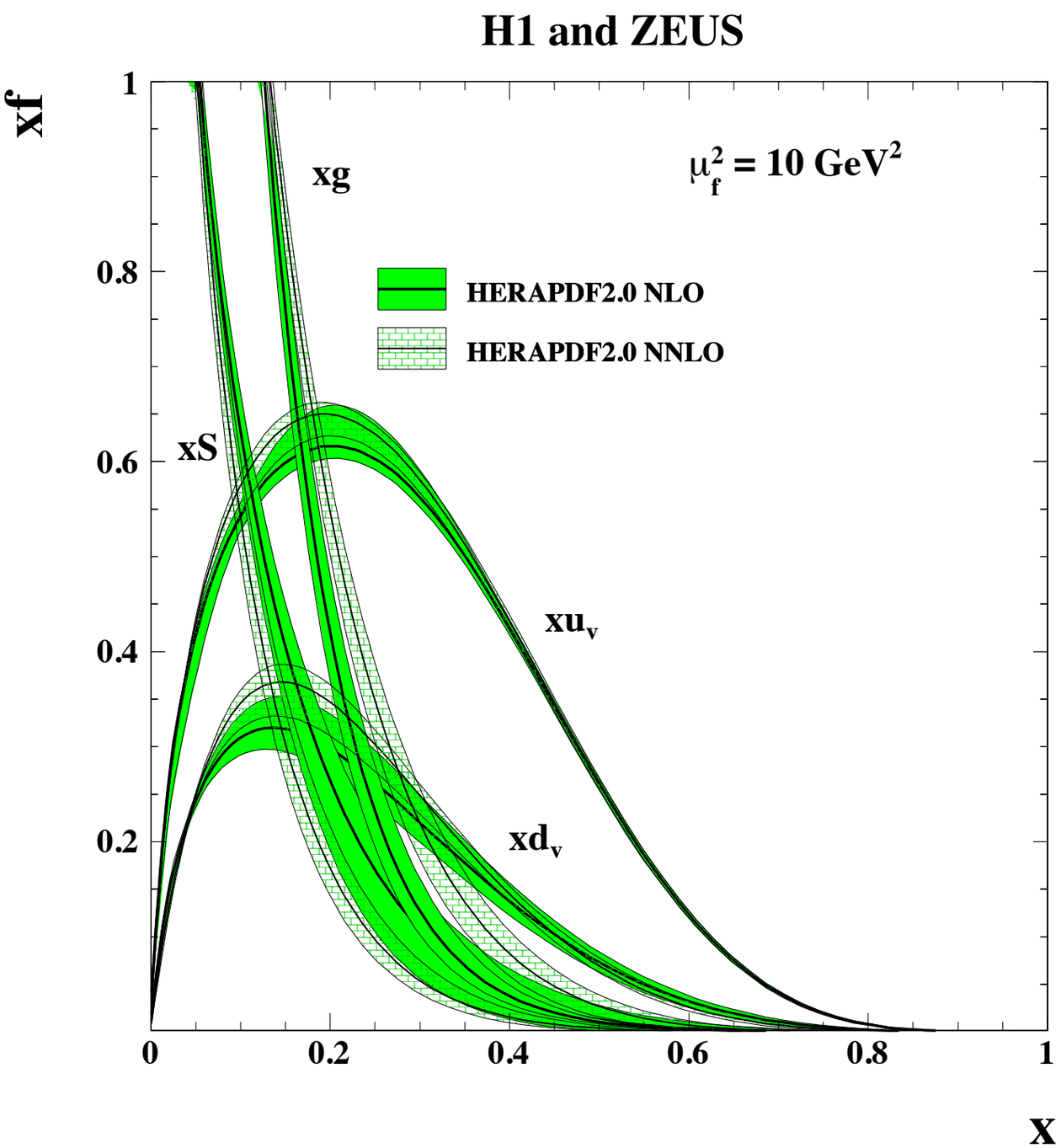

Dominance of the gluon density at small x.
Valence distributions have a peak at around x= 0.1.

DGLAP fits of F_2 for proton

DGLAP based fits of the structure function for proton work very well

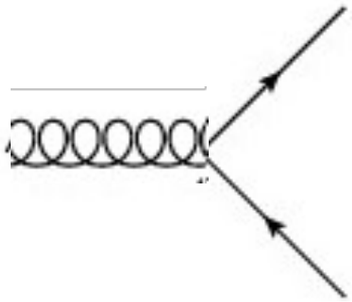

@ low x

QCD scaling violations

Bjorken scaling region

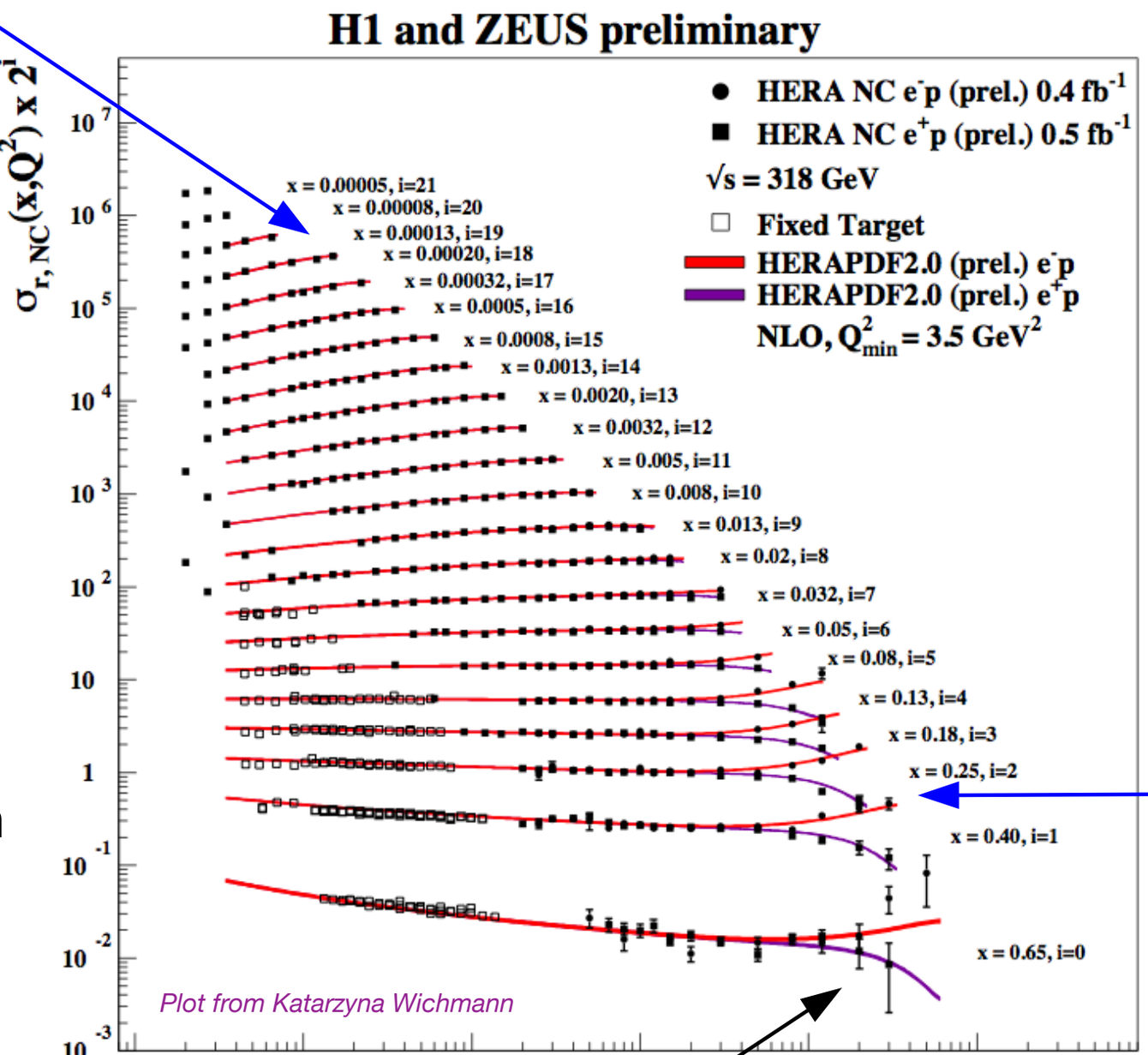

Plot from Katarzyna Wichmann

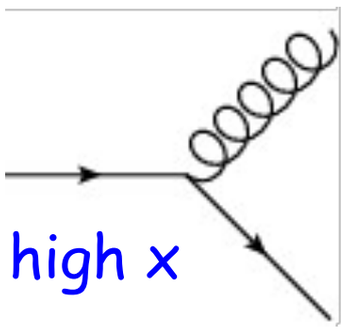

@ high x

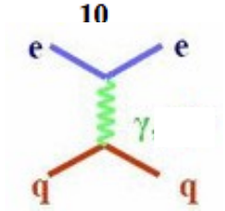

@ high Q^2

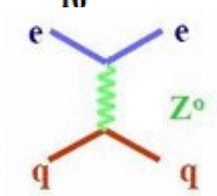

Reduced cross section

$$\sigma_{r,NC} = F_2 - \frac{y^2}{Y+} F_L$$

$$Q^2 \ll M_Z^2$$

DIS with nuclei

What happens when the lepton scatters off a nucleus instead of nucleon?
How the presence of a nuclear target modifies cross sections and structure functions?

Typical distance between nucleons $d \simeq 1.9\,\mathrm{fm}$

Baryon density $\rho_0 \simeq 0.15\,\mathrm{fm}^{-3}$

Fermi momentum $p_F \simeq 0.26\,\mathrm{GeV}$

Incoherent scattering from A nucleons but with their structure modified by the presence of nuclear medium. For example, mean field that nucleon experiences in the presence of other nucleons, Fermi motion of nucleons in the nucleus.

Coherent scattering which involve more than one nucleon at a time. Such effects arise when the hadronic fluctuations produced by the photon propagate over the distance (in laboratory frame) which are longer than the characteristic length scale between nucleons, d=2 fm. An example of such effect is shadowing.

DIS with nuclei

Similarly to the DIS on nucleons the information about the nuclear structure is encoded in the hadronic tensor.

$$W_{\mu\nu}(p,q) = -W_1(g_{\mu\nu} - \frac{q_\mu q_\nu}{q^2}) + \frac{W_2}{M^2}(p_\mu - \frac{p\cdot q}{q^2}q_\mu)\cdot(p_\nu - \frac{p\cdot q}{q^2}q_\nu)$$

Number of independent structure functions depend on the spin of nucleus, which can be measured in the polarized DIS. Here we focus on the unpolarized case.

DIS with nuclei

Similarly to the DIS on nucleons the information about the nuclear structure is encoded in the hadronic tensor.

$$W_{\mu\nu}(p,q) = -W_1(g_{\mu\nu} - \frac{q_\mu q_\nu}{q^2}) + \frac{W_2}{M^2}(p_\mu - \frac{p\cdot q}{q^2}q_\mu)\cdot(p_\nu - \frac{p\cdot q}{q^2}q_\nu)$$

Number of independent structure functions depend on the spin of nucleus, which can be measured in the polarized DIS. Here we focus on the unpolarized case.

Nuclear structure functions:

$$F_{1,2}^A(x_A, Q^2)$$

P 4-mom of nucleus
p 4-mom of nucleon

$$x_A = \frac{Q^2}{2P\cdot q} \qquad 0 < x_A \leq 1$$

DIS with nuclei

Similarly to the DIS on nucleons the information about the nuclear structure is encoded in the hadronic tensor.

$$W_{\mu\nu}(p,q) = -W_1(g_{\mu\nu} - \frac{q_\mu q_\nu}{q^2}) + \frac{W_2}{M^2}(p_\mu - \frac{p\cdot q}{q^2}q_\mu)\cdot(p_\nu - \frac{p\cdot q}{q^2}q_\nu)$$

Number of independent structure functions depend on the spin of nucleus, which can be measured in the polarized DIS. Here we focus on the unpolarized case.

Nuclear structure functions:

$$F_{1,2}^A(x_A, Q^2)$$

P 4-mom of nucleus
p 4-mom of nucleon

$$x_A = \frac{Q^2}{2P\cdot q} \qquad\qquad 0 < x_A \leq 1$$

Typically the dependence is on Bjorken x on a single nucleon:

$$F_{1,2}^A(x, Q^2)$$

$$x = \frac{Q^2}{2p\cdot q} = x_A A$$

Note that: $0 < x \leq A$

DIS kinematics: proton vs nuclei

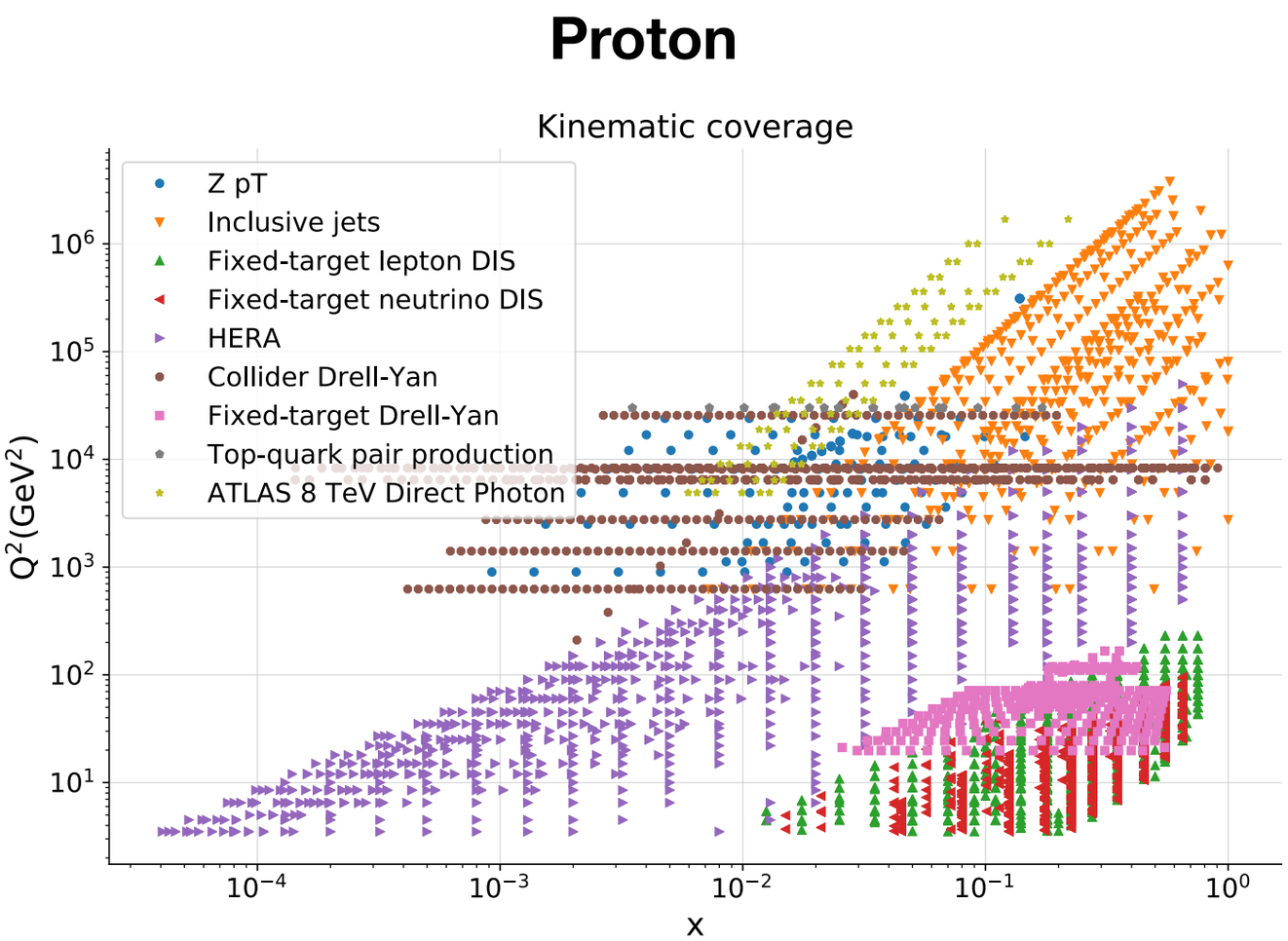

DIS kinematics: proton vs nuclei

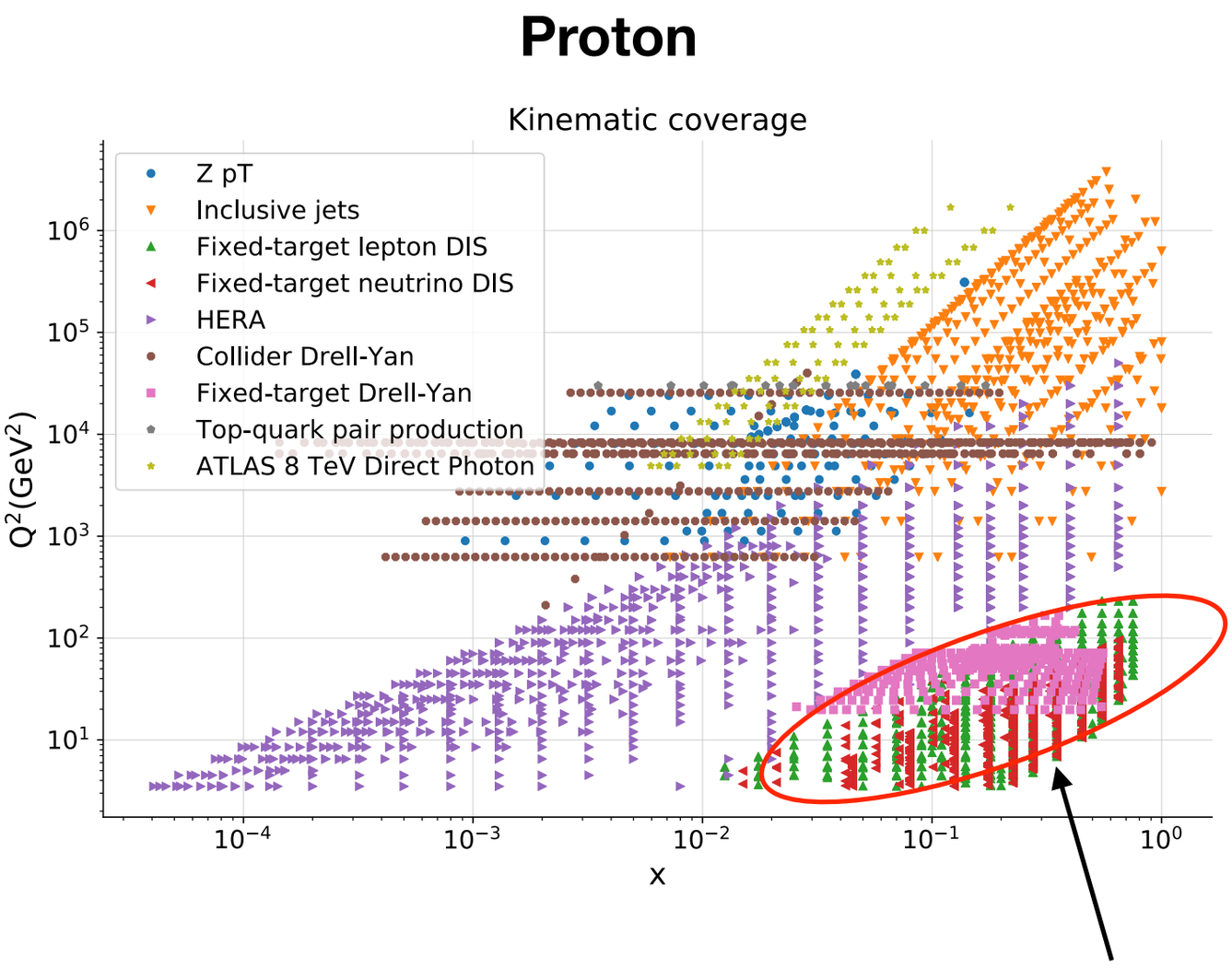

Fixed target

DIS kinematics: proton vs nuclei

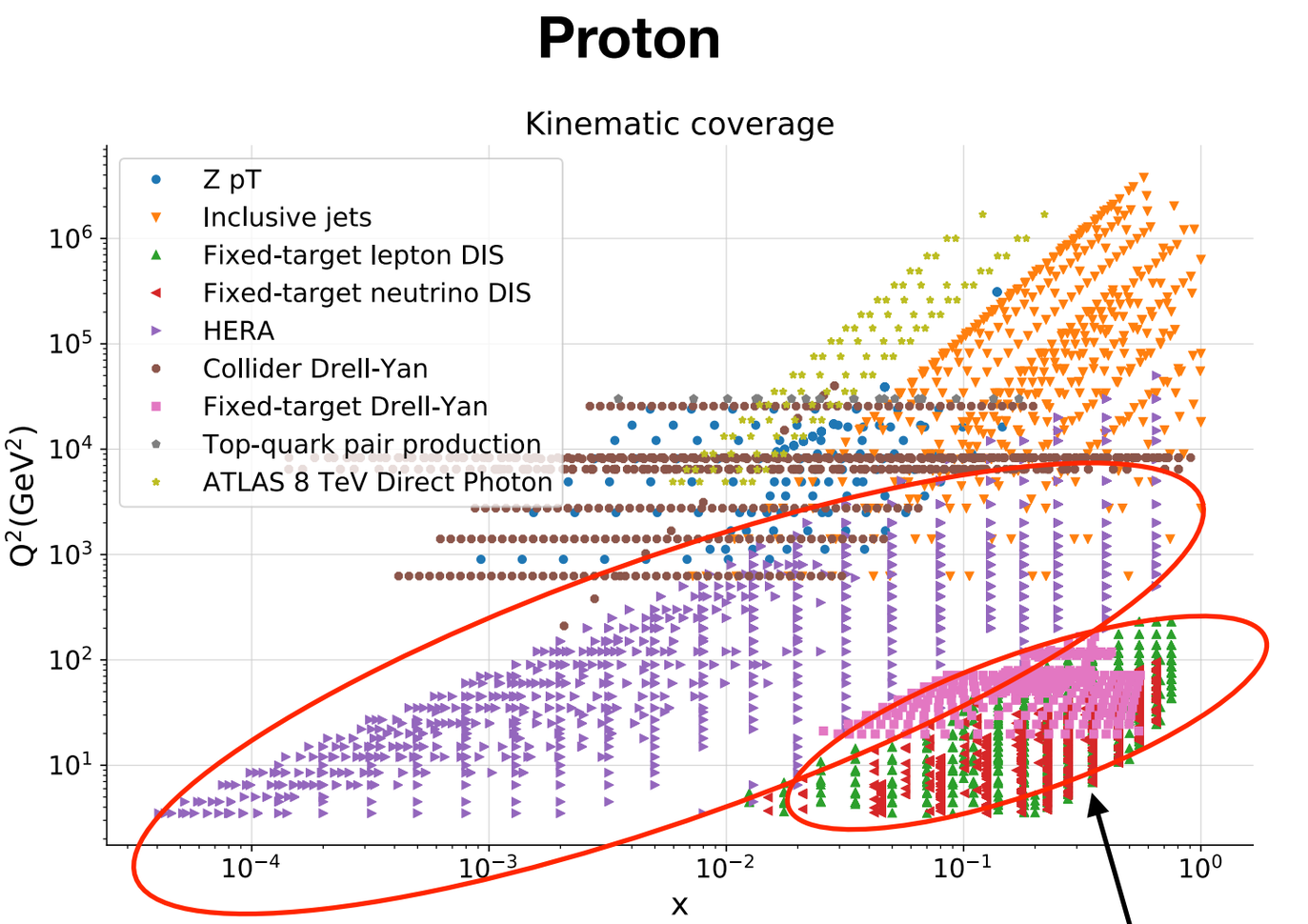

HERA collider

Fixed target

DIS kinematics: proton vs nuclei

Proton

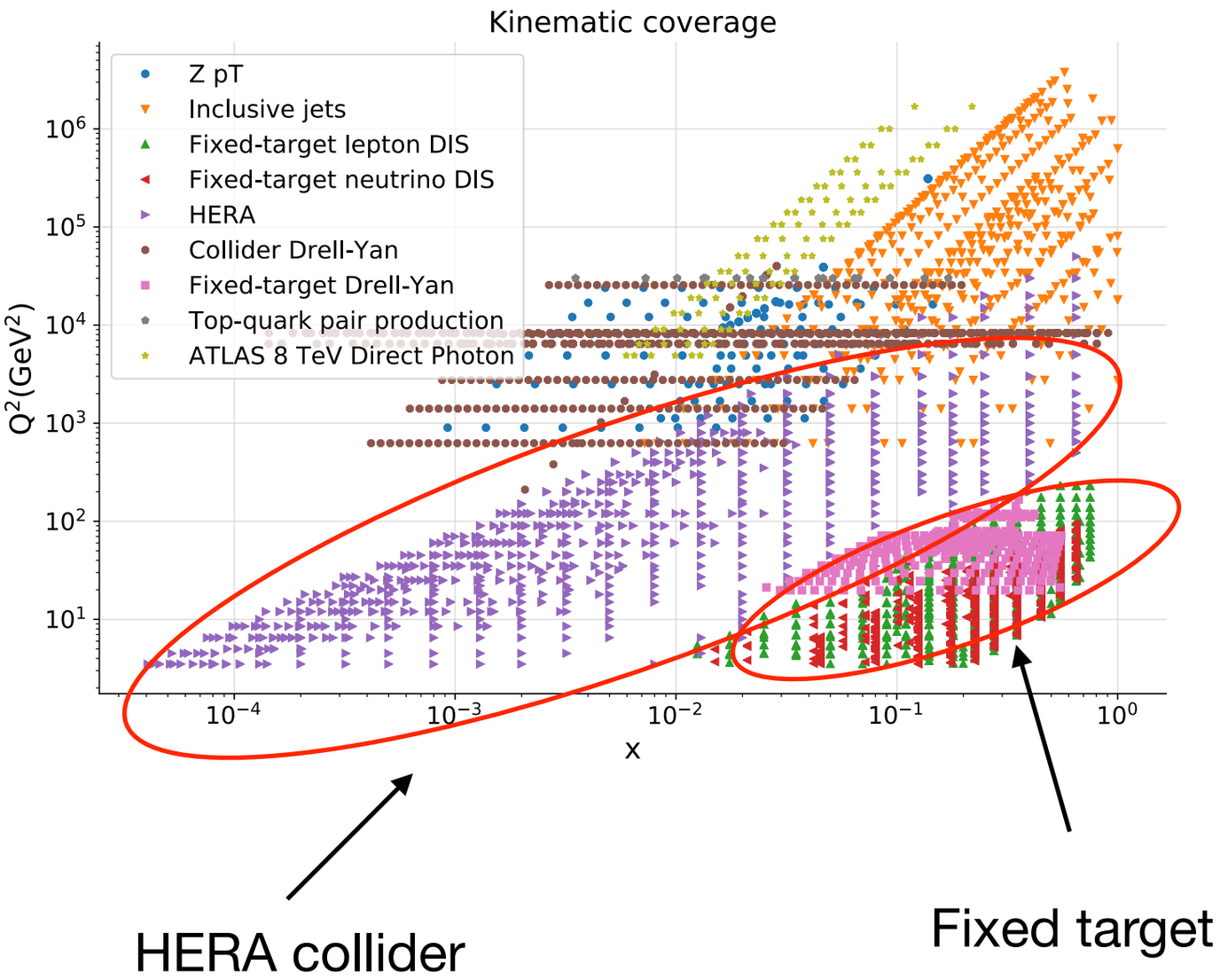

Nucleus

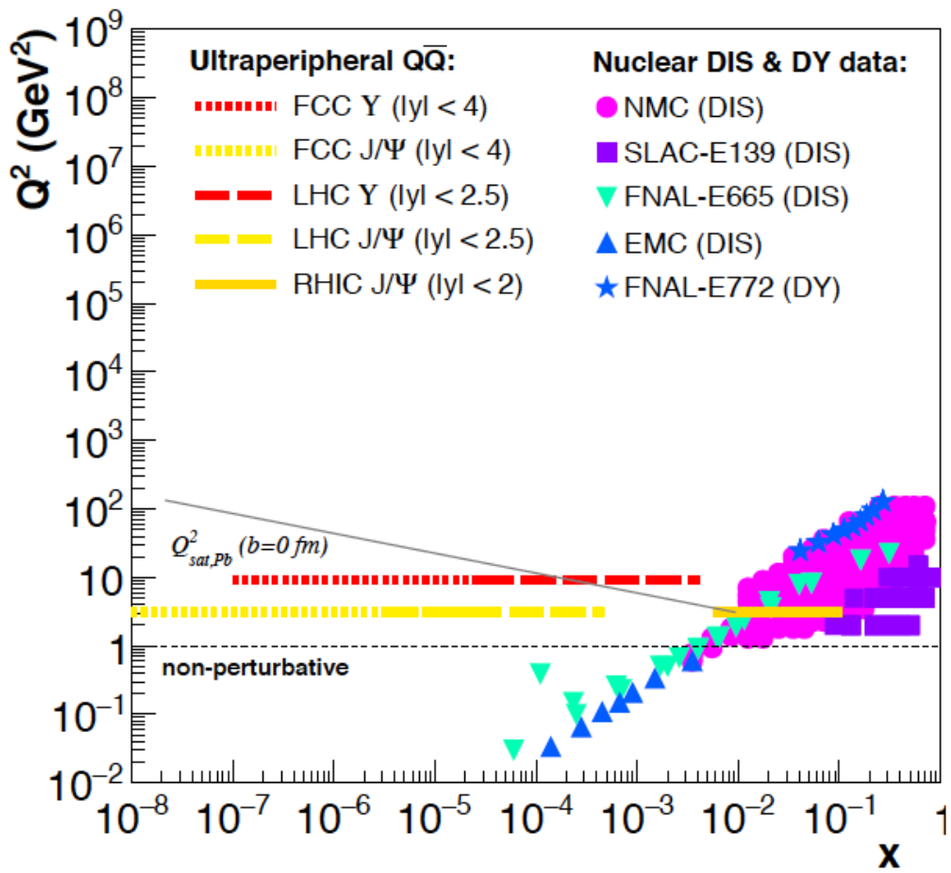

DIS kinematics: proton vs nuclei

Proton

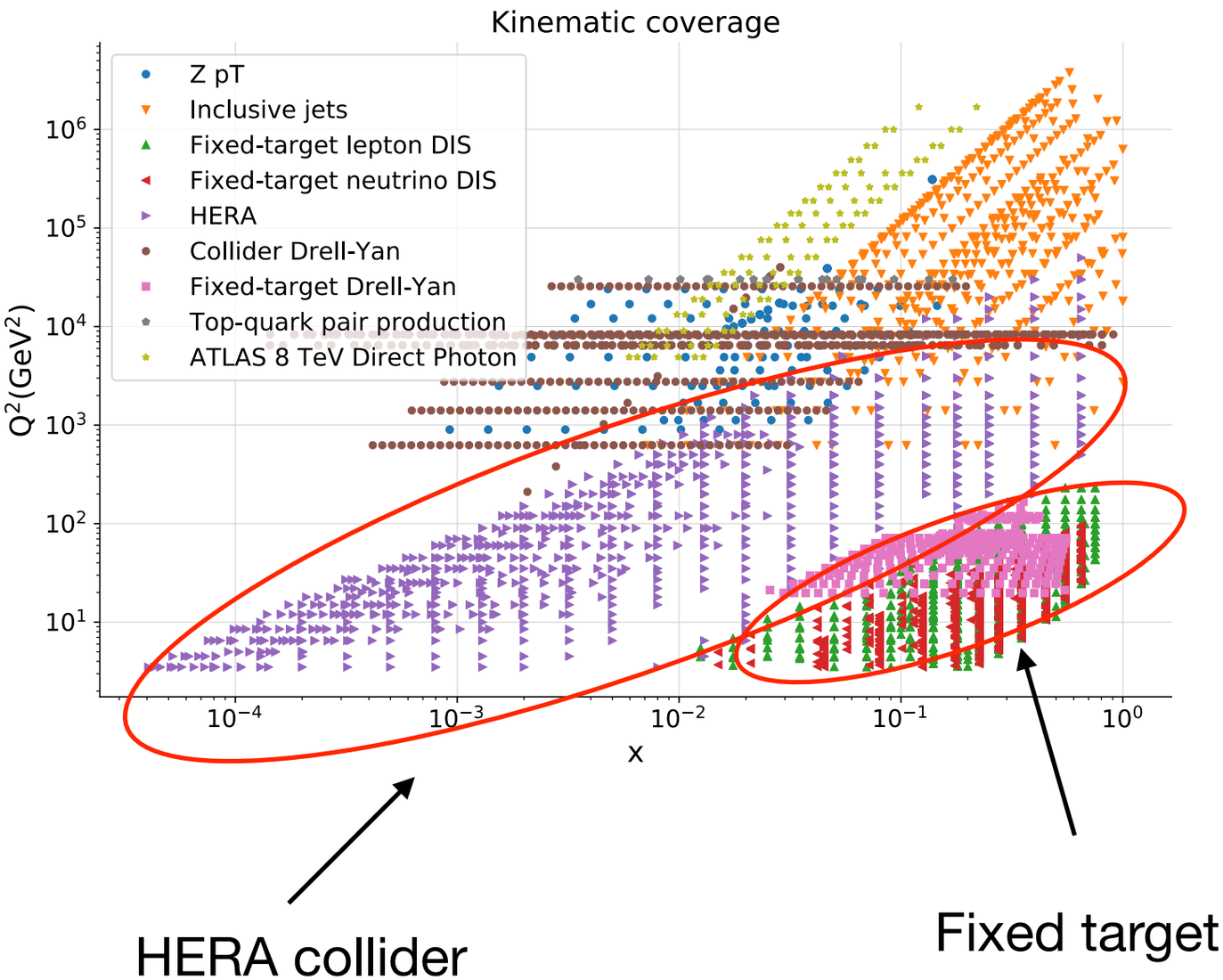

Nucleus

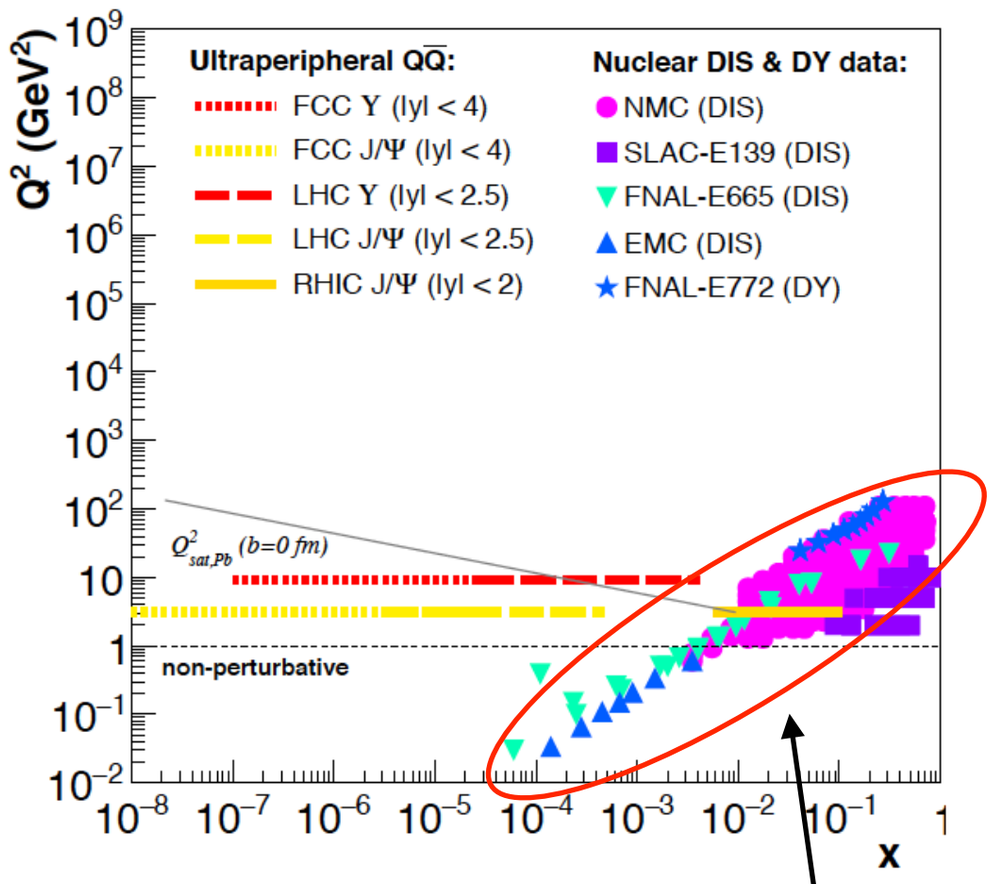

DIS kinematics: proton vs nuclei

Proton

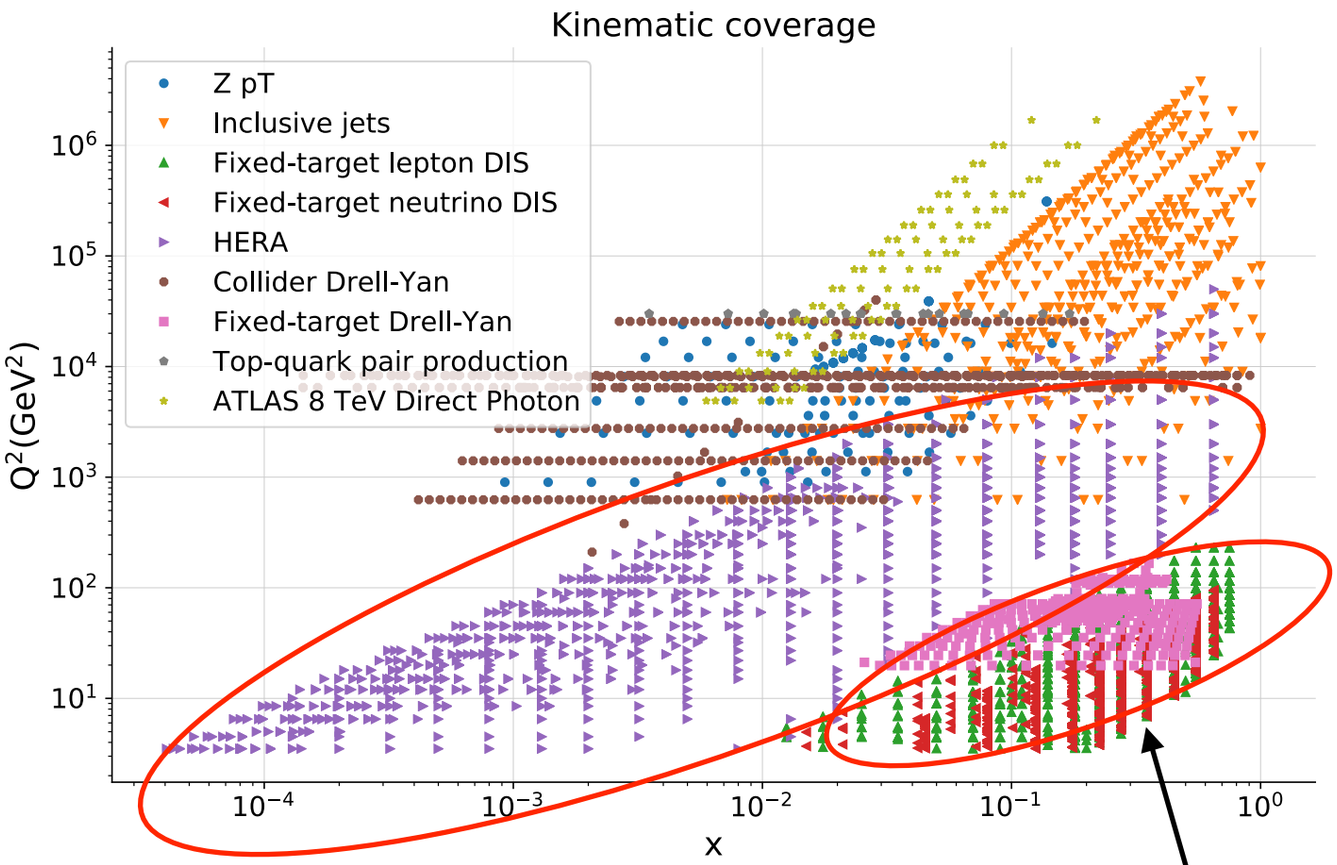

HERA collider

Fixed target

Nucleus

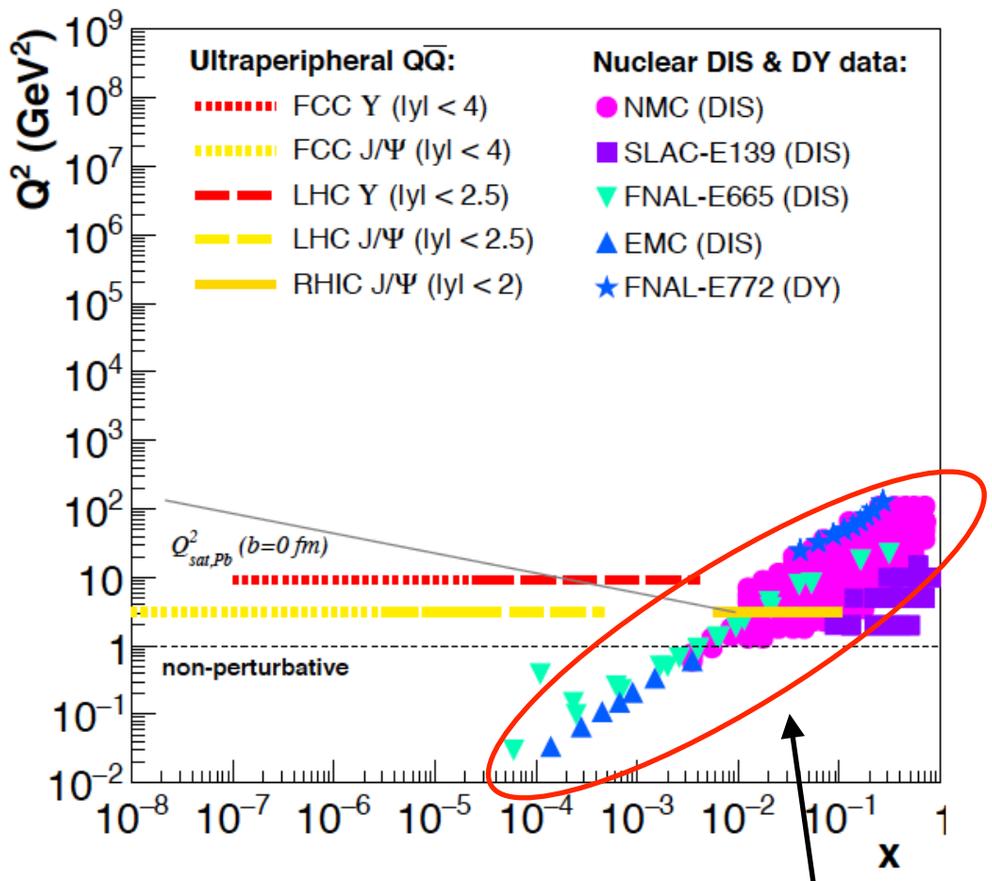

Fixed target

Very restricted kinematics covered by the experimental data for nuclear DIS
(some information may be provided by proton-nucleus and UPCs - ultraperipheral collisions)

Nuclear structure

Deep Inelastic Scattering :

$$\frac{d^2\sigma^{ep\to eX}}{dxdQ^2} = \frac{4\pi\alpha^2_{e.m.}}{xQ^4}\left[\left(1-y+\frac{y^2}{2}\right)F_2(x,Q^2)-\frac{y^2}{2}F_L(x,Q^2)\right]$$

Nuclear ratio for structure function

$$R^A_{F_2}(x,Q^2) = \frac{F_2^A(x,Q^2)}{A\,F_2^{\text{nucleon}}(x,Q^2)}$$

Nuclear structure

Deep Inelastic Scattering :

$$\frac{d^2\sigma^{ep\to eX}}{dxdQ^2} = \frac{4\pi\alpha^2_{e.m.}}{xQ^4}\left[\left(1-y+\frac{y^2}{2}\right)F_2(x,Q^2)-\frac{y^2}{2}F_L(x,Q^2)\right]$$

Nuclear ratio for structure function

$$R^A_{F_2}(x,Q^2) = \frac{F_2^A(x,Q^2)}{A\,F_2^{\text{nucleon}}(x,Q^2)}$$

Nuclear effects $R^A \neq 1$

Nuclear structure

Deep Inelastic Scattering :

$$\frac{d^2\sigma^{ep\to eX}}{dxdQ^2} = \frac{4\pi\alpha^2_{e.m.}}{xQ^4}\left[\left(1-y+\frac{y^2}{2}\right)F_2(x,Q^2)-\frac{y^2}{2}F_L(x,Q^2)\right]$$

Nuclear ratio for structure function

$$R^A_{F_2}(x,Q^2) = \frac{F_2^A(x,Q^2)}{A\,F_2^{\text{nucleon}}(x,Q^2)}$$

Nuclear effects $R^A \neq 1$

Schematic picture

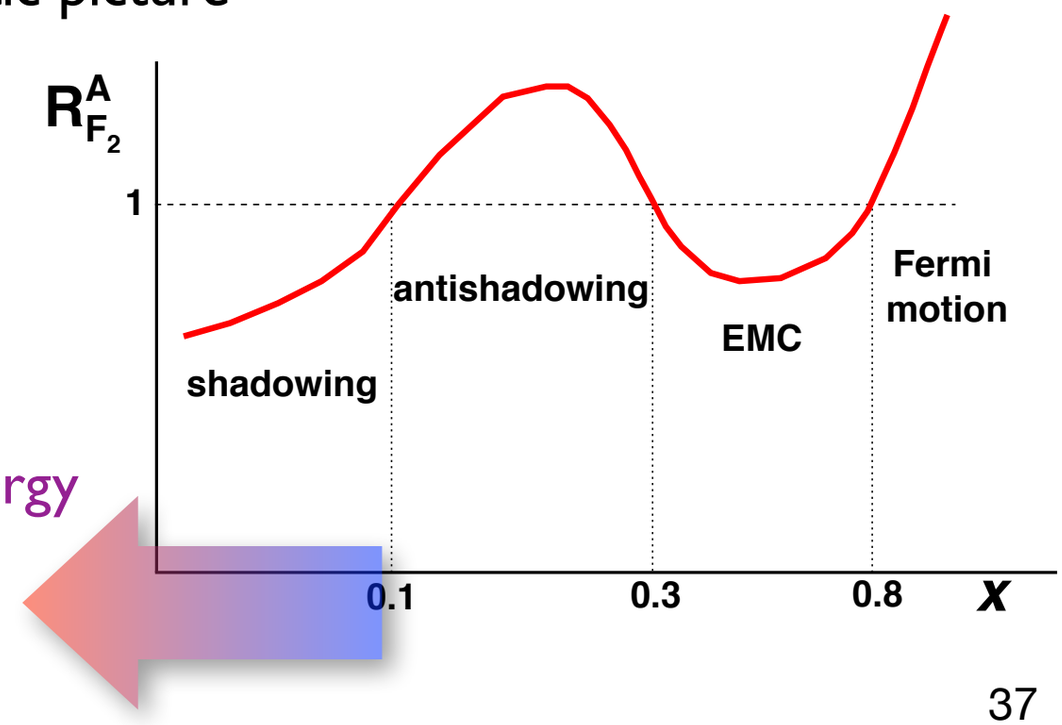

Nuclear structure

Deep Inelastic Scattering :

$$\frac{d^2\sigma^{ep\to eX}}{dxdQ^2} = \frac{4\pi\alpha^2_{e.m.}}{xQ^4}\left[\left(1-y+\frac{y^2}{2}\right)F_2(x,Q^2)-\frac{y^2}{2}F_L(x,Q^2)\right]$$

Nuclear ratio for structure function

$$R^A_{F_2}(x,Q^2) = \frac{F_2^A(x,Q^2)}{A\,F_2^{\text{nucleon}}(x,Q^2)}$$

Nuclear effects $R^A \neq 1$

Schematic picture

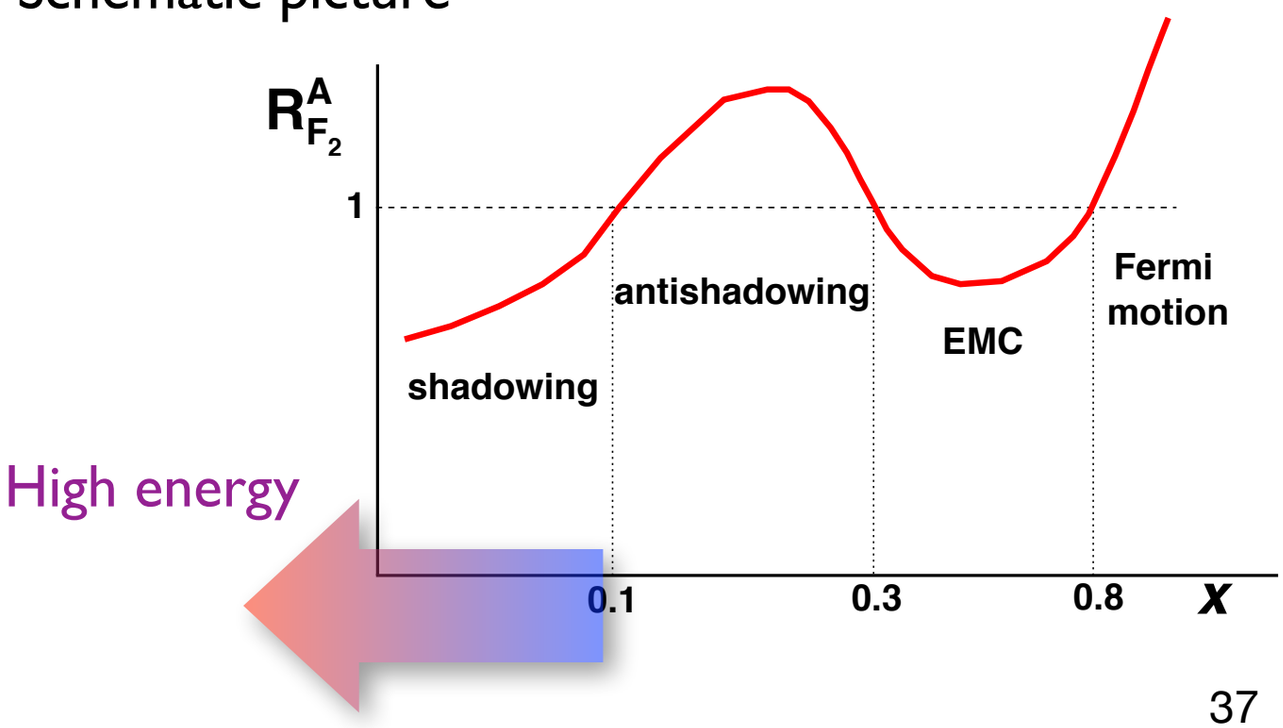

- Fermi motion
  $x \geq 0.8$
- EMC region
  $0.25 - 0.3 \leq x \leq 0.8$
- Antishadowing region
  $0.1 \leq x \leq 0.25 - 0.3$
- Shadowing region
  $x \leq 0.1$

Nuclear structure function

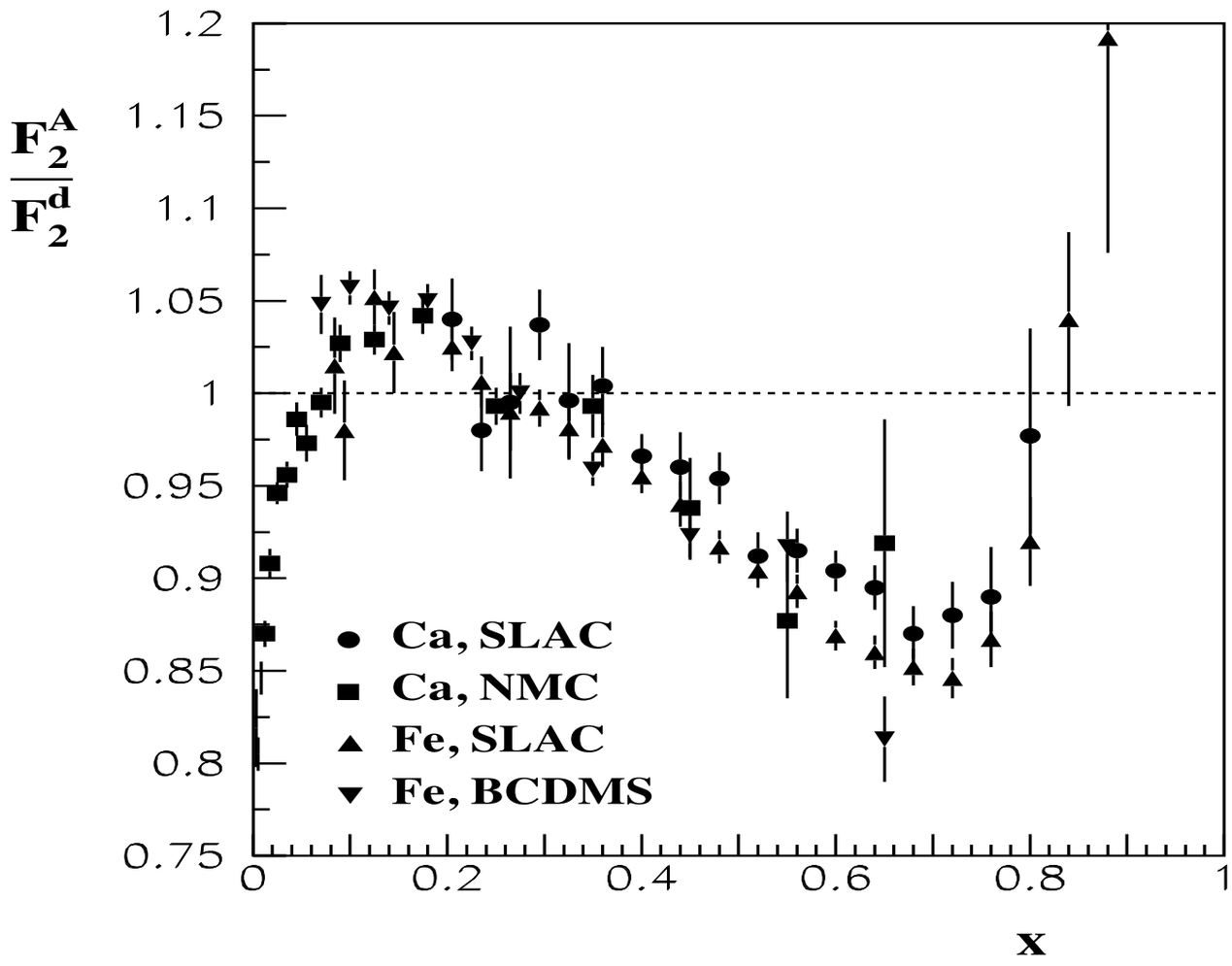

Nuclear structure function

- Fermi motion: ratio >1 for x>0.8.
  Due to motion of bound nucleons inside the nucleus.

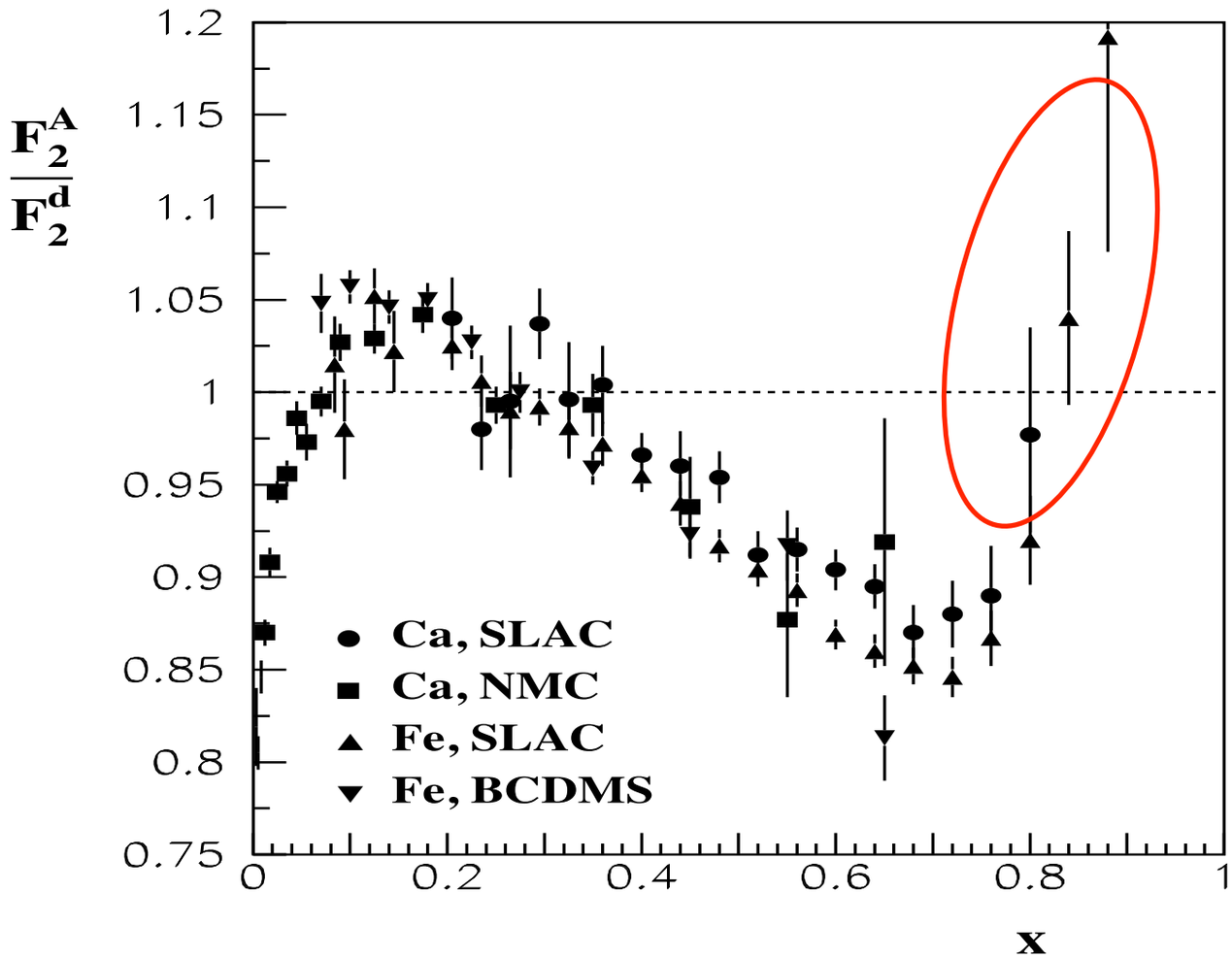

Nuclear structure function

- Fermi motion: ratio >1 for x>0.8. Due to motion of bound nucleons inside the nucleus.

- EMC region: EMC collaboration discovered large deviation of the ratio from 1 in the region of 0.3<x<0.8. Usually referred as the EMC effect. There exist several explanations. Mean field modification: nucleon structure is modified by presence of nuclear matter. Short range correlations between nucleons, most nucleons are not modified but some experiencing SRC are modified (about 20%).

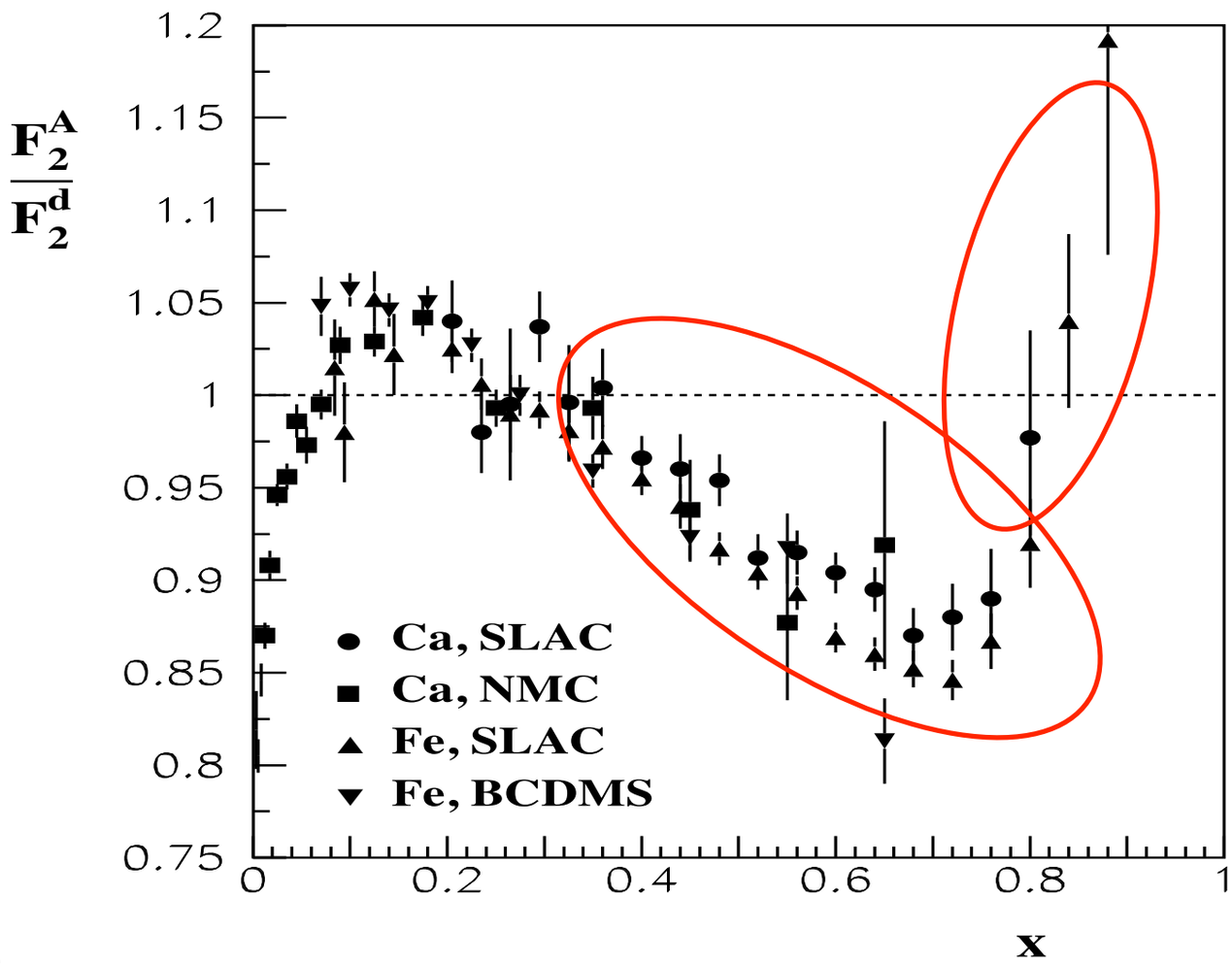

Nuclear structure function

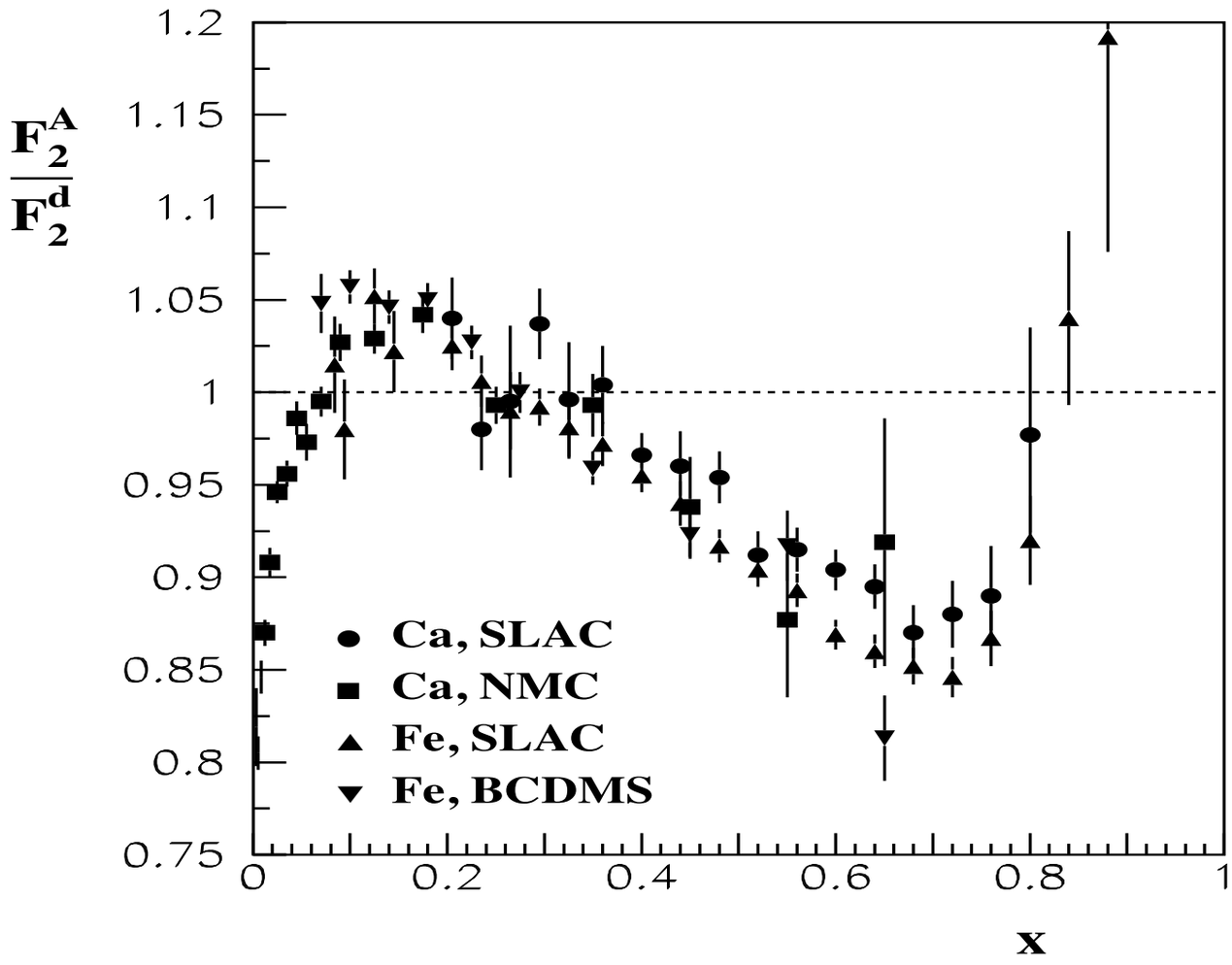

Nuclear structure function

- Antishadowing: Ratio > 1 for 0.1<x<0.3. Momentum sum rule (?)

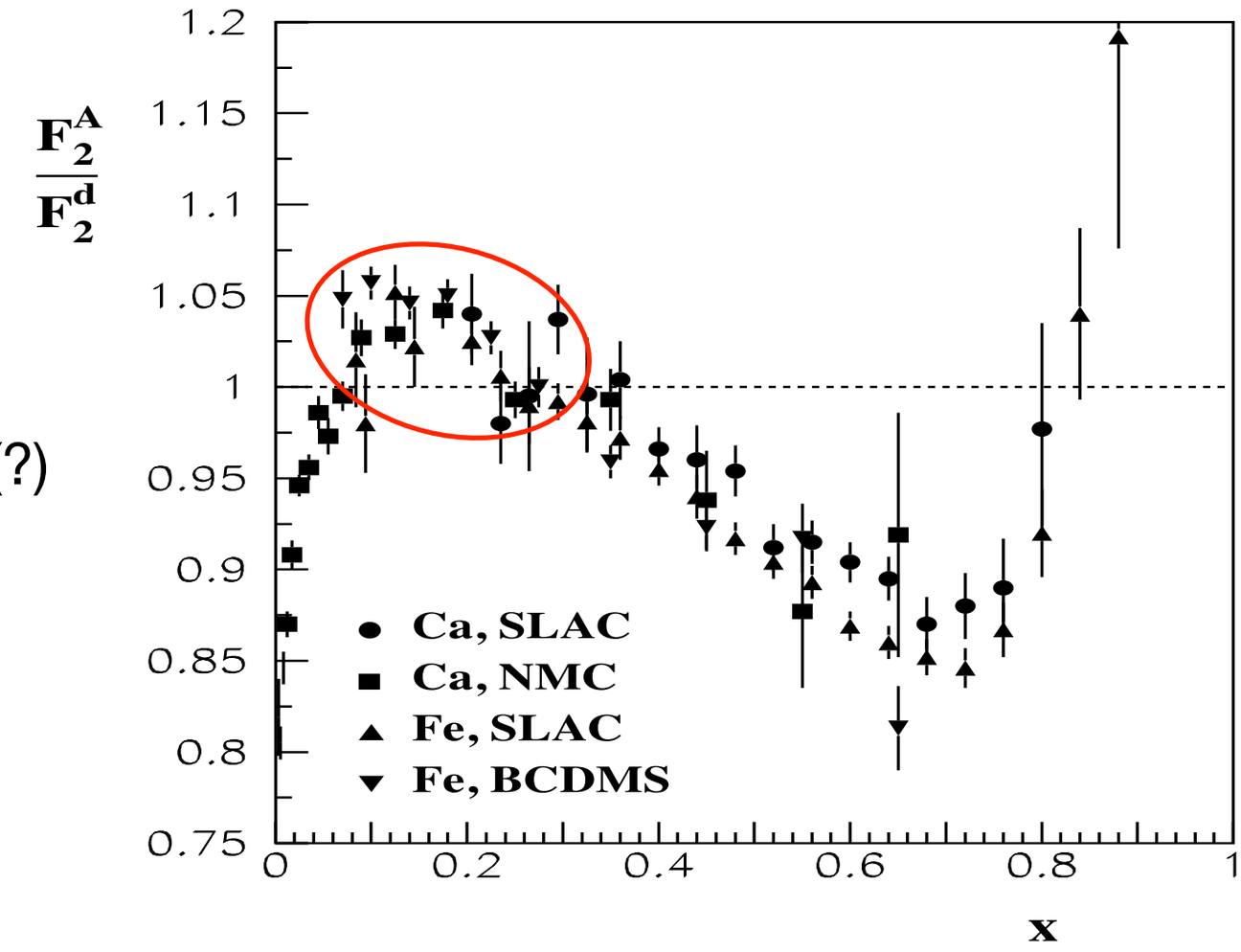

Nuclear structure function

- Antishadowing: Ratio > 1 for 0.1<x<0.3. Momentum sum rule (?)
- Shadowing: ratio < 1 for small x, x<0.1.

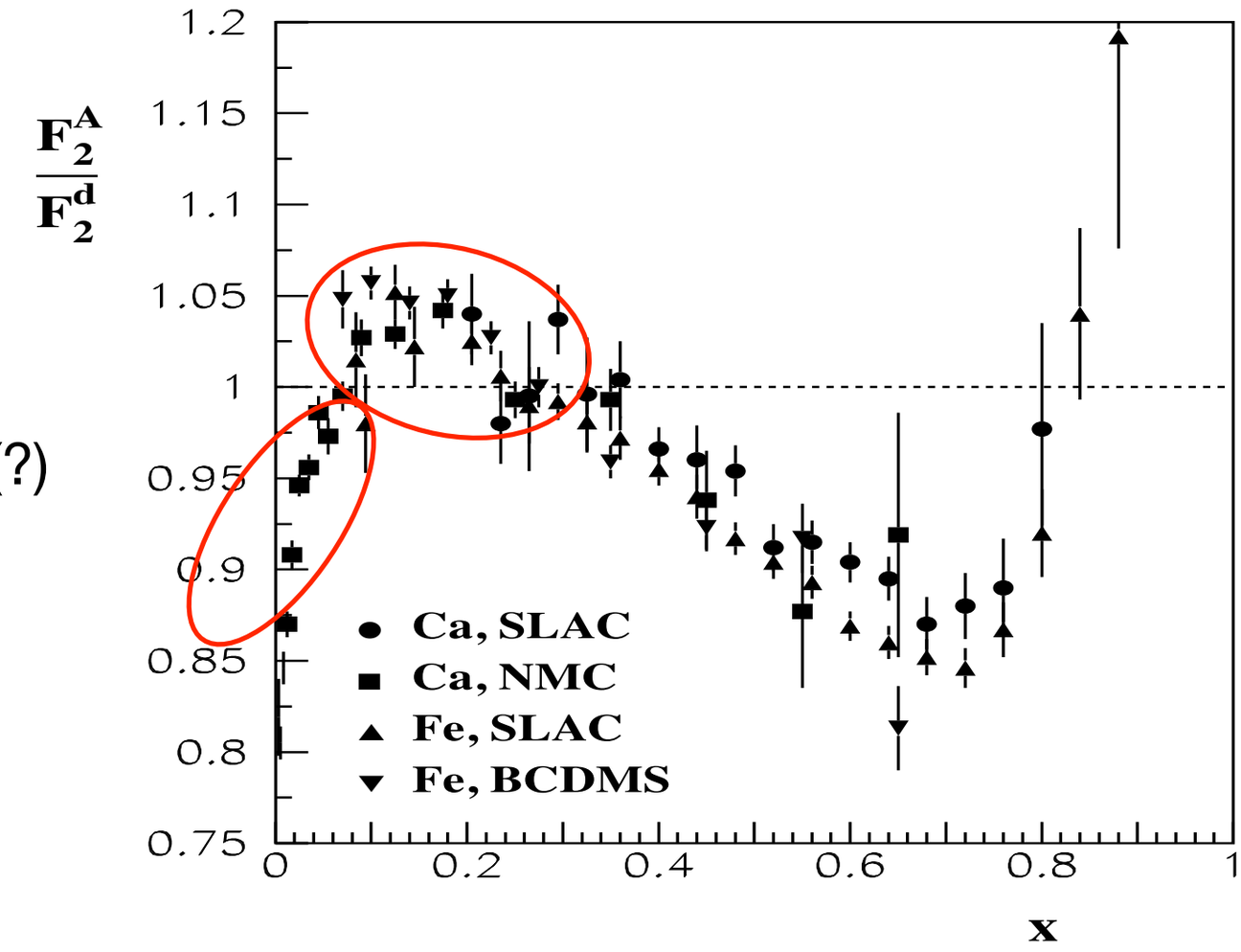

Nuclear structure function

- Antishadowing: Ratio > 1 for 0.1<x<0.3. Momentum sum rule (?)
- Shadowing: ratio < 1 for small x, x<0.1.

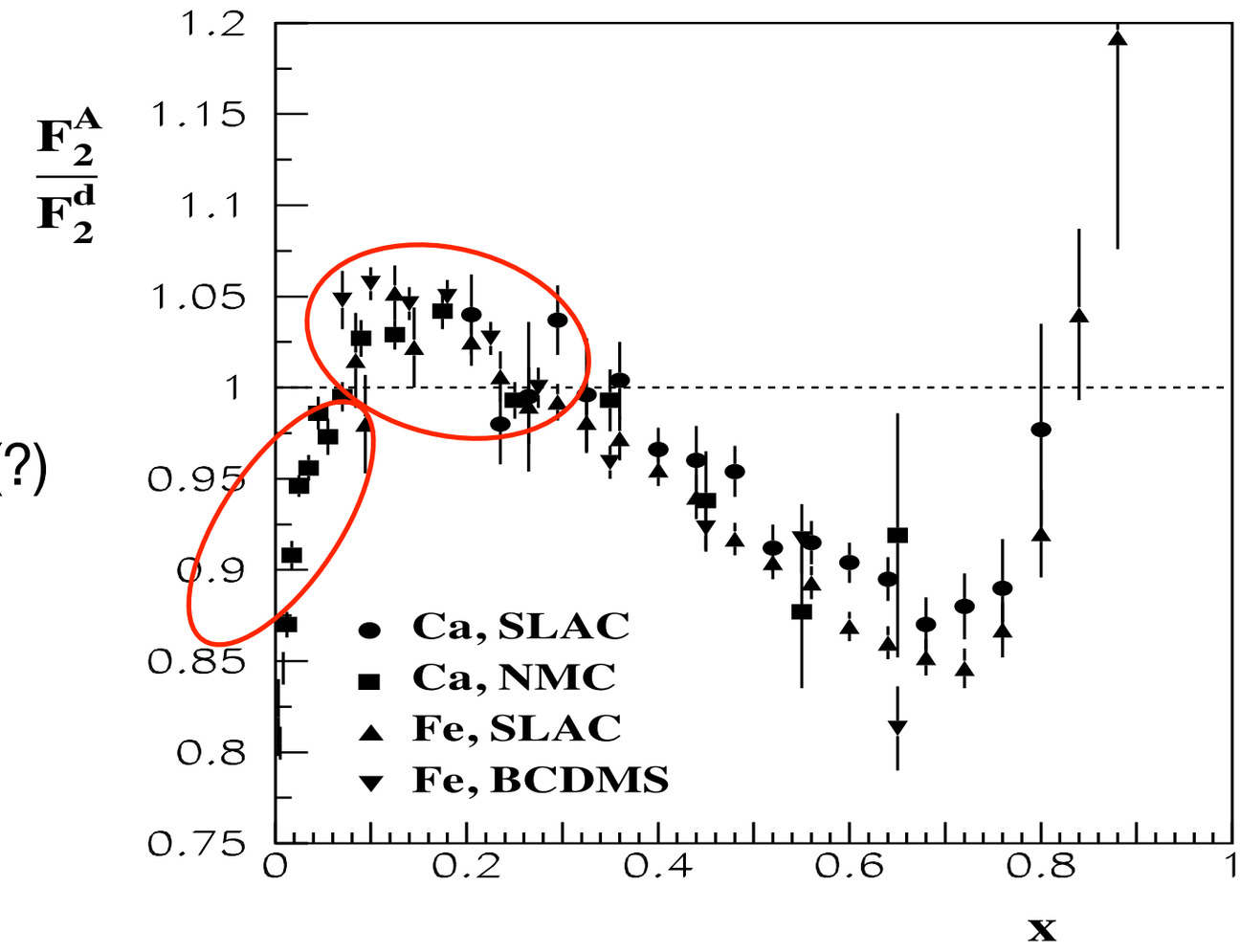

We shall focus here on the physics of shadowing since it is small x phenomenon

What the nuclear data tell us about shadowing?

Shadowing increases with A and increases with decreasing x

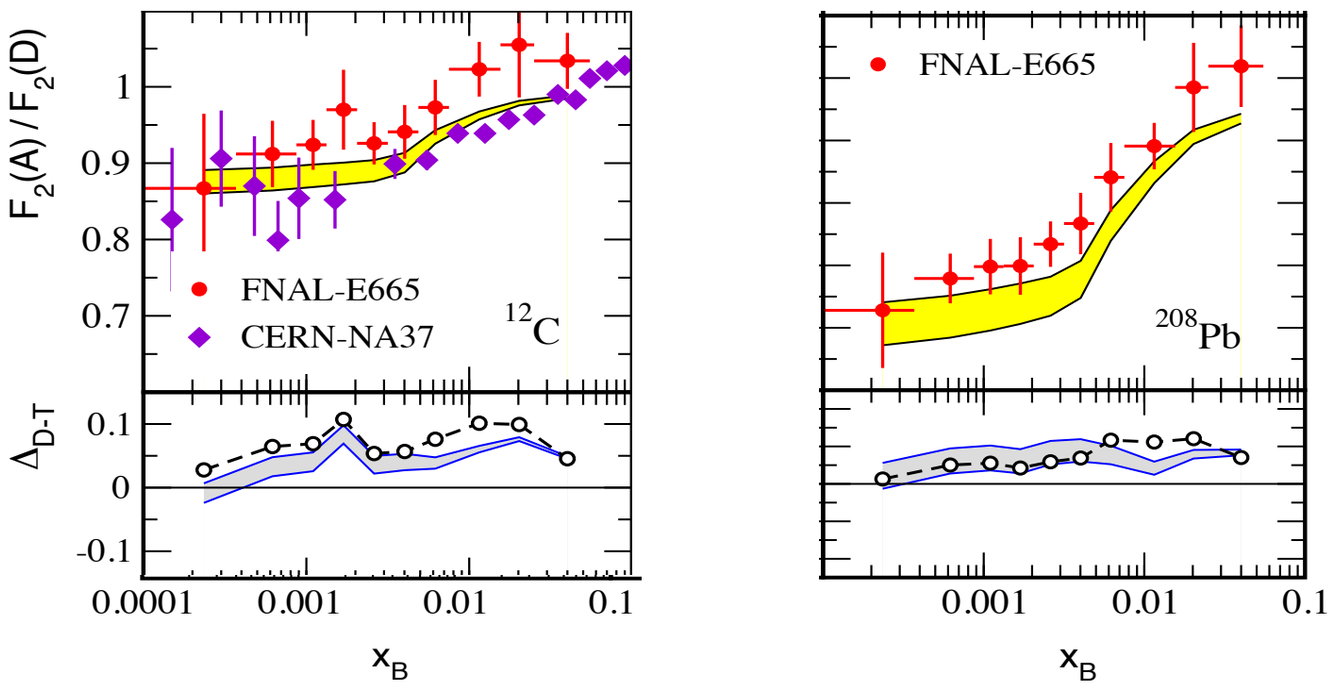

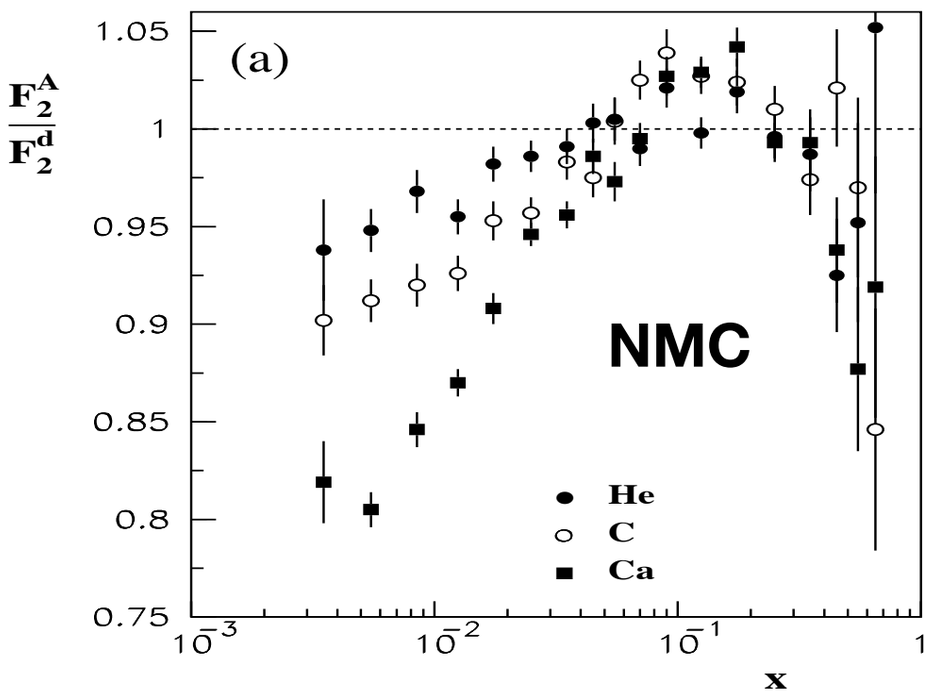

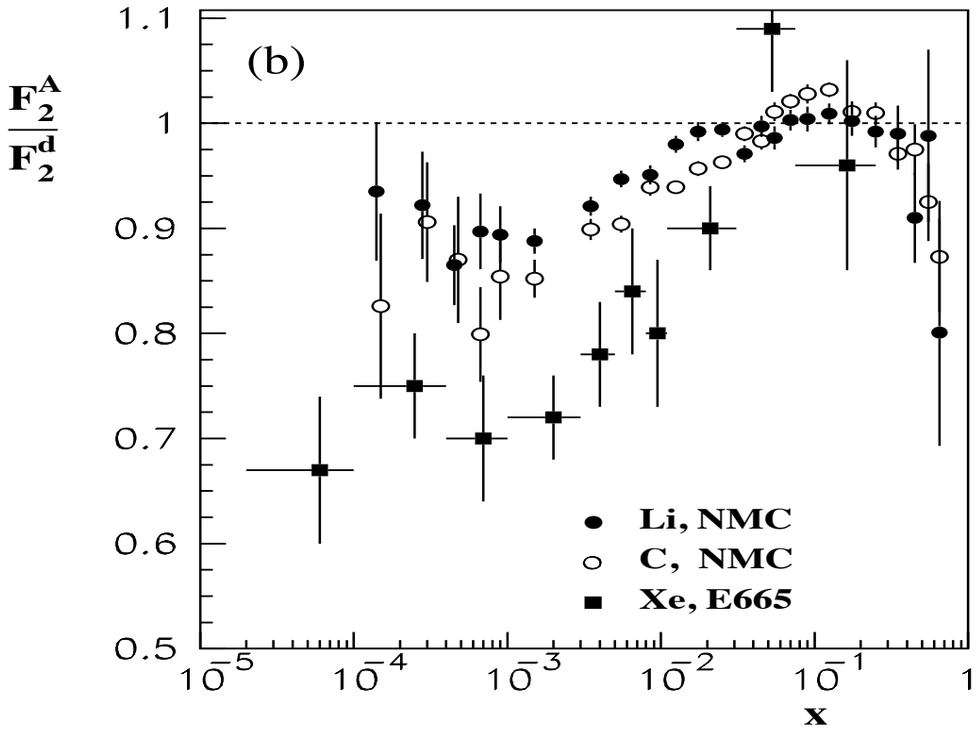

Shadowing decreases with increasing Q

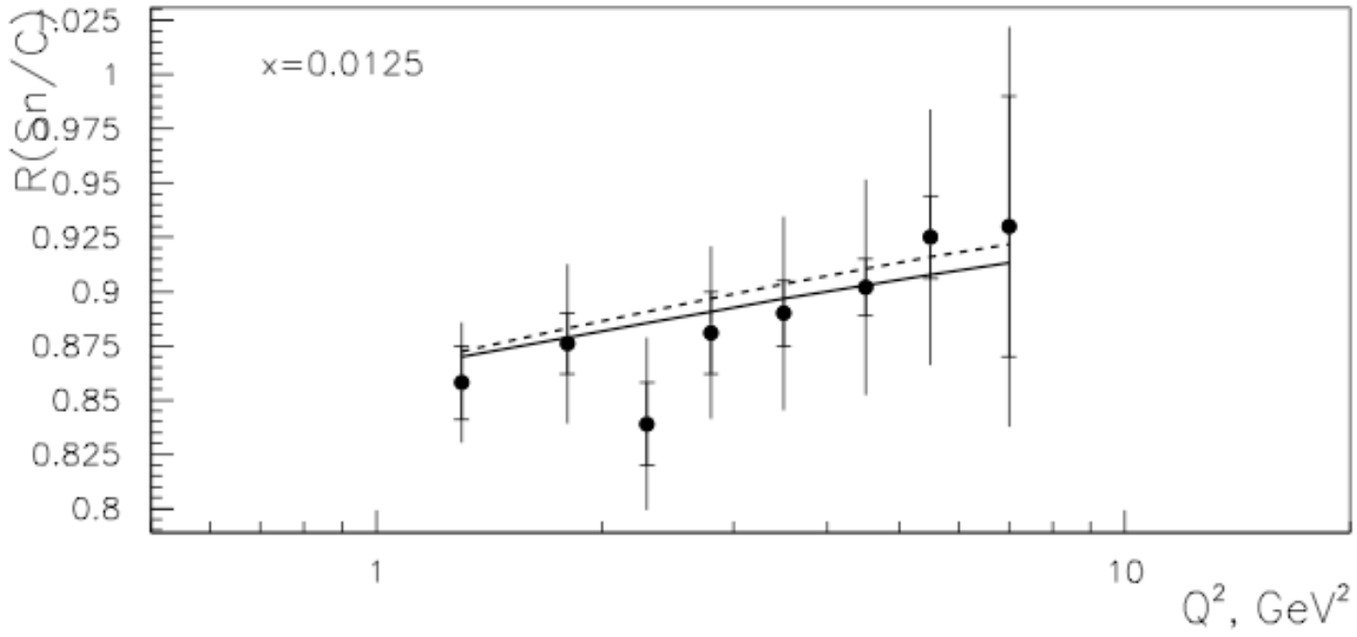

Approaches to nuclear shadowing

The usual approach to nuclear shadowing is based on multiple scattering.
Models differ significantly.

Glauber rescattering.

Gribov shadowing: relation to **diffraction**.

High energy approaches: parton **saturation**.

- ✦There are also approaches which do not try to provide physical explanation of shadowing but rather are based on parametrization.
- ✦**DGLAP** fits to nuclear structure functions resulting in **nuclear PDFs** similar in spirit to the parametrization of proton PDFs.
- ✦The idea behind is that nuclear effects are of **non-perturbative** origin which needs to be parametrized but at high Q^2 the DIS on nuclei is fundamentally the same as the DIS on a proton.

$$F_i(x,Q^2) = \sum_j \int_x^1 dy\, C_i^j(x/y, Q^2, \alpha_s)\, f_j(y,Q^2) + \mathcal{O}(\frac{\Lambda^2}{Q^2})$$

$f_j(y,\mu^2)$ Obeys DGLAP evolution

Available sets nuclear PDFs

SET		**EPS09** JHEP 0904 (2009) 065	**DSSZ** PRD85 (2012) 074028	**nCTEQ15** PRD93 (2016) 085037	**KA15** PRD93 (2016) 014036	**EPPS16** EPJC C77 (2017)163	**nNNPDF1.0** 1904.00018
data	eDIS	✔	✔	✔	✔	✔	✔
	DY	✔	✔	✔	✔	✔	✘
	π^0	✔	✔	✔	✘	✔	✘
	νDIS	✘	✔	✘	✘	✔	✘
	pPb	✘	✘	✘	✘	✔	✘
# data		929	1579	740	1479	1811	451
order		NLO	NLO	NLO	NNLO	NLO	NNLO
proton PDF		CTEQ6.1	MSTW2008	~CTEQ6.1	JR09	CT14NLO	NNPDF3.1
mass scheme		ZM-VFNS	GM-VFNS	GM-VFNS	ZM-VFNS	GM-VFNS	FONLL-B
comments		$\Delta\chi^2$=50, ratios, huge shadowing-antishadowing	$\Delta\chi^2$=30, ratios, medium-modified FFs for π^0	$\Delta\chi^2$=35, PDFs, valence flavour sep., not enough sensitivity	PDFs, deuteron data included	$\Delta\chi^2$=52, flavour sep., ratios, LHC pPb data	NNPDF methodology, isoscalarity assumed

EPPS16

Bound proton PDF for species i and nucleus with mass number A: $f_i^{\mathrm{p}/A}(x, Q^2)$

Defined relative to the free proton PDF:

$$f_i^{\mathrm{p}/A}(x, Q^2) = R_i^A(x, Q^2) f_i^{\mathrm{p}}(x, Q^2)$$

Nuclear modification factor $R_i^A(x, Q^2)$

Free proton PDF baseline CT14NLO

EPPS16

Bound proton PDF for species i and nucleus with mass number A: $f_i^{\mathrm{p}/A}(x, Q^2)$

Defined relative to the free proton PDF:

$$f_i^{\mathrm{p}/A}(x, Q^2) = R_i^A(x, Q^2) f_i^{\mathrm{p}}(x, Q^2)$$

Nuclear modification factor $R_i^A(x, Q^2)$

Free proton PDF baseline CT14NLO

$$R_i^A(x, Q_0^2) = \begin{cases} a_0 + a_1(x - x_a)^2 & x \le x_a \\ b_0 + b_1 x^\alpha + b_2 x^{2\alpha} + b_3 x^{3\alpha} & x_a \le x \le x_e \\ c_0 + (c_1 - c_2 x)(1 - x)^{-\beta} & x_e \le x \le 1, \end{cases}$$

Parameters a,b,c fixed by the requirement of continuity of function and derivative and the following constraints:

$y_0 = R_i^A(x \to 0, Q_0^2)$ **Small x shadowing**

$y_a = R_i^A(x_a, Q_0^2)$ **Antishadowing max.**

$y_e = R_i^A(x_e, Q_0^2)$ **EMC min.**

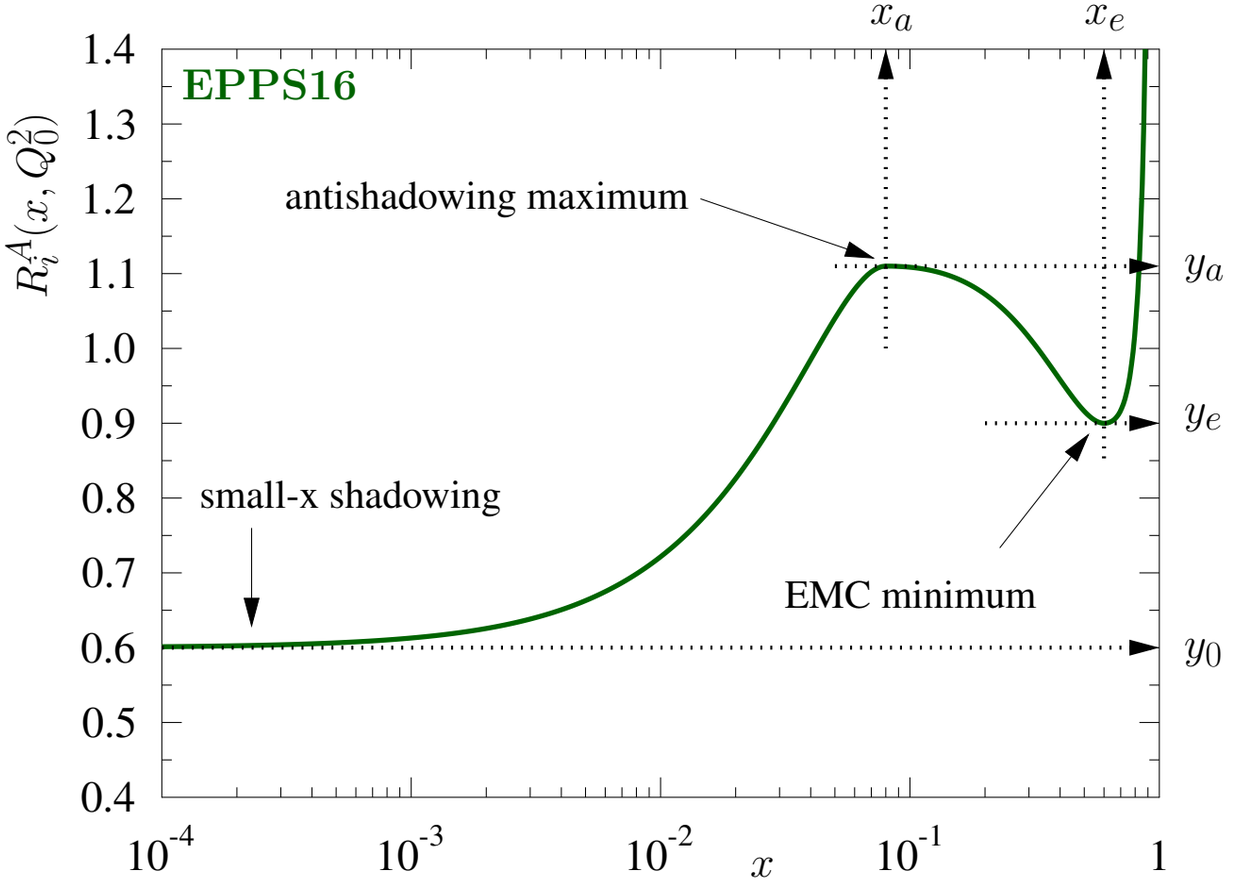

EPPS16

A dependence of the parameters:

$$y_i(A) = y_i(A_{\rm ref}) \left(\frac{A}{A_{\rm ref}} \right)^{\gamma_i [y_i(A_{\rm ref})-1]} \qquad \gamma_i \geq 0 \qquad A_{\rm ref} = 12$$

$$\int_0^1 dx f_{u_{\rm V}}^{{\rm p}/A}(x, Q_0^2) = 2,$$

$$\int_0^1 dx f_{d_{\rm V}}^{{\rm p}/A}(x, Q_0^2) = 1,$$

Valence quark sum rules

$$\int_0^1 dx x \sum_i f_i^{{\rm p}/A}(x, Q_0^2) = 1,$$

Momentum sum rule

Deuteron A=2 is assumed to be free from nuclear effects

Bound neutron PDFs are determined from bound proton PDFs through isospin symmetry.

$$f_{u,\overline{u}}^{{\rm n}/A}(x, Q^2) = f_{d,\overline{d}}^{{\rm p}/A}(x, Q^2),$$

$$f_{d,\overline{d}}^{{\rm n}/A}(x, Q^2) = f_{u,\overline{u}}^{{\rm p}/A}(x, Q^2),$$

$$f_i^{{\rm n}/A}(x, Q^2) = f_i^{{\rm p}/A}(x, Q^2) \quad \text{for other flavours.}$$

Data used in EPPS16

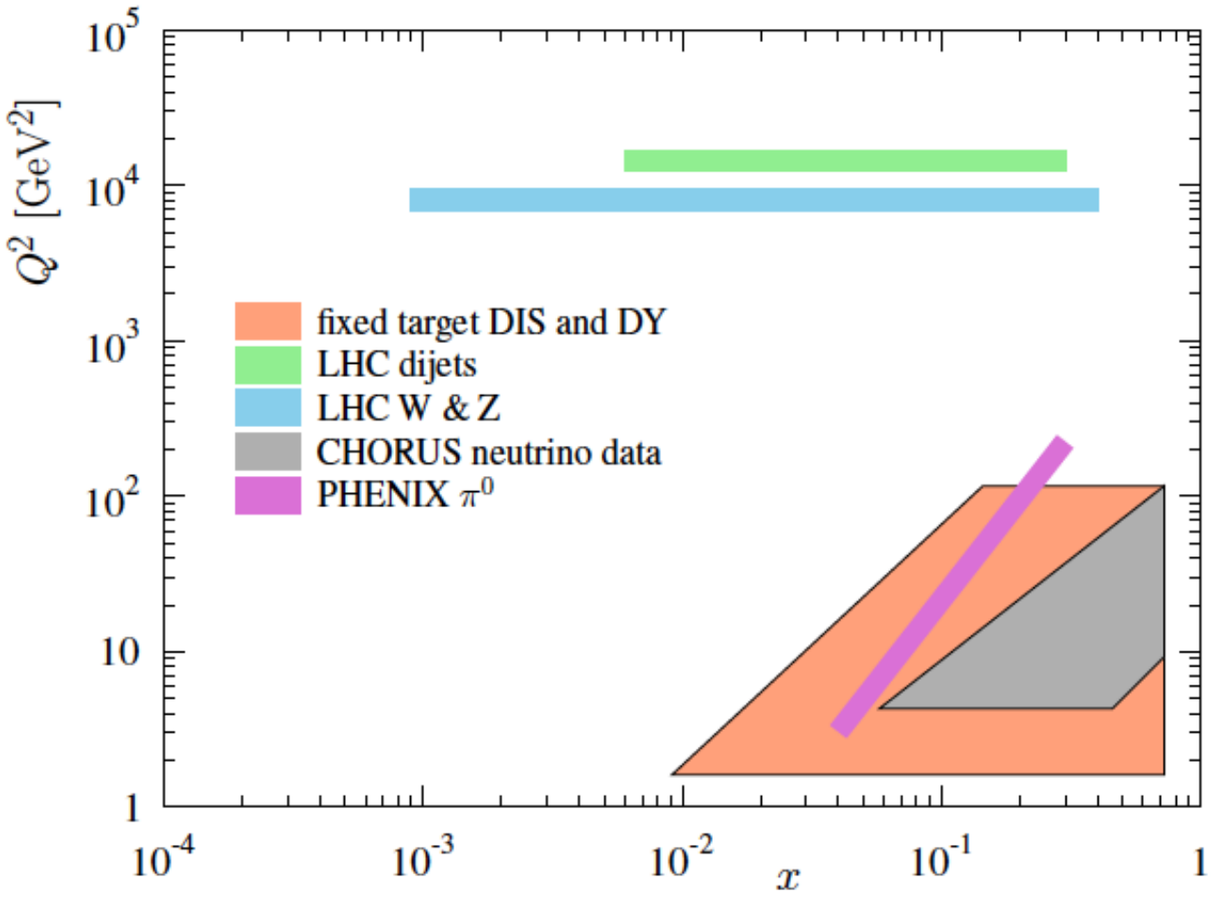

- Fixed target eA DIS and pA Drell-Yan
- Neutrino data
- Pion data from dA
- LHC data from dijets and electroweak W,Z boson production: high scales, low x

Experiment	Observable	Collisions	Data points	χ^2	Ref.
SLAC E139	DIS	e^-He(4), e^-D	21	12.2	[69]
CERN NMC 95, re.	DIS	μ^-He(4), μ^-D	16	18.0	[70]
CERN NMC 95	DIS	μ^-Li(6), μ^-D	15	18.4	[71]
CERN NMC 95, Q^2 dep.	DIS	μ^-Li(6), μ^-D	153	161.2	[71]
SLAC E139	DIS	e^-Be(9), e^-D	20	12.9	[69]
CERN NMC 96	DIS	μ^-Be(9), μ^-C	15	4.4	[72]
SLAC E139	DIS	e^-C(12), e^-D	7	6.4	[69]
CERN NMC 95	DIS	μ^-C(12), μ^-D	15	9.0	[71]
CERN NMC 95, Q^2 dep.	DIS	μ^-C(12), μ^-D	165	133.6	[71]
CERN NMC 95, re.	DIS	μ^-C(12), μ^-D	16	16.7	[70]
CERN NMC 95, re.	DIS	μ^-C(12), μ^-Li(6)	20	27.9	[70]
FNAL E772	DY	pC(12), pD	9	11.3	[73]
SLAC E139	DIS	e^-Al(27), e^-D	20	13.7	[69]
CERN NMC 96	DIS	μ^-Al(27), μ^-C(12)	15	5.6	[72]
SLAC E139	DIS	e^-Ca(40), e^-D	7	4.8	[69]
FNAL E772	DY	pCa(40), pD	9	3.33	[73]
CERN NMC 95, re.	DIS	μ^-Ca(40), μ^-D	15	27.6	[70]
CERN NMC 95, re.	DIS	μ^-Ca(40), μ^-Li(6)	20	19.5	[70]
CERN NMC 96	DIS	μ^-Ca(40), μ^-C(12)	15	6.4	[72]
SLAC E139	DIS	e^-Fe(56), e^-D	26	22.6	[69]
FNAL E772	DY	e^-Fe(56), e^-D	9	3.0	[73]
CERN NMC 96	DIS	μ^-Fe(56), μ^-C(12)	15	10.8	[72]
FNAL E866	DY	pFe(56), pBe(9)	28	20.1	[74]
CERN EMC	DIS	μ^-Cu(64), μ^-D	19	15.4	[75]
SLAC E139	DIS	e^-Ag(108), e^-D	7	8.0	[69]
CERN NMC 96	DIS	μ^-Sn(117), μ^-C(12)	15	12.5	[72]
CERN NMC 96, Q^2 dep.	DIS	μ^-Sn(117), μ^-C(12)	144	87.6	[76]
FNAL E772	DY	pW(184), pD	9	7.2	[73]
FNAL E866	DY	pW(184), pBe(9)	28	26.1	[74]
CERN NA10★	DY	π^-W(184), π^-D	10	11.6	[49]
FNAL E615★	DY	π^+W(184), π^-W(184)	11	10.2	[50]
CERN NA3★	DY	π^-Pt(195), π^-H	7	4.6	[48]
SLAC E139	DIS	e^-Au(197), e^-D	21	8.4	[69]
RHIC PHENIX	π^0	dAu(197), pp	20	6.9	[28]
CERN NMC 96	DIS	μ^-Pb(207), μ^-C(12)	15	4.1	[72]
CERN CMS★	$W^\pm$	pPb(208)	10	8.8	[43]
CERN CMS★	Z	pPb(208)	6	5.8	[45]
CERN ATLAS★	Z	pPb(208)	7	9.6	[46]
CERN CMS★	dijet	pPb(208)	7	5.5	[34]
CERN CHORUS★	DIS	νPb(208), $\bar{\nu}$Pb(208)	824	998.6	[47]
Total			1811	1789	

EPPS16 nuclear PDFs

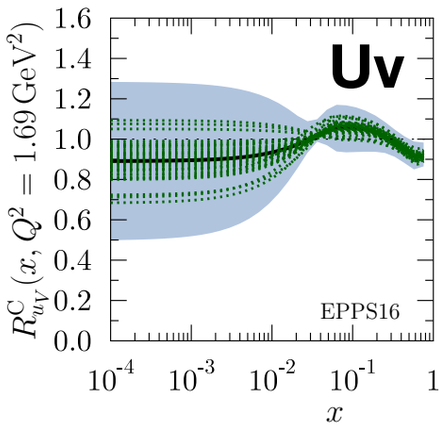

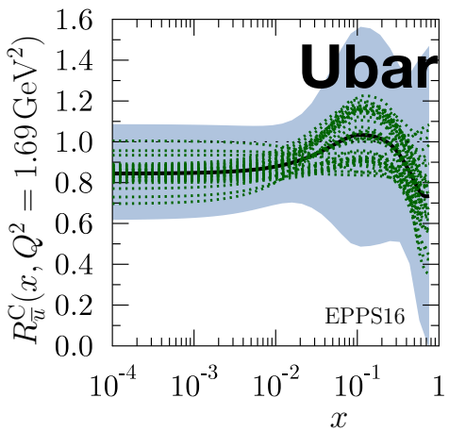

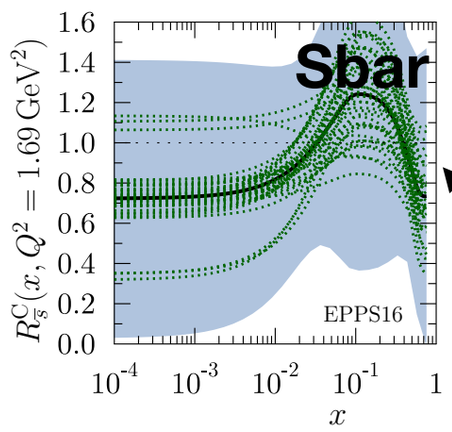

Carbon

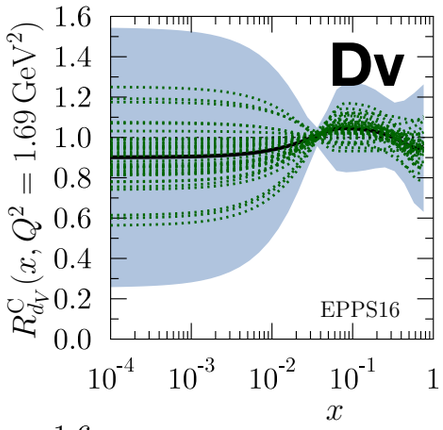

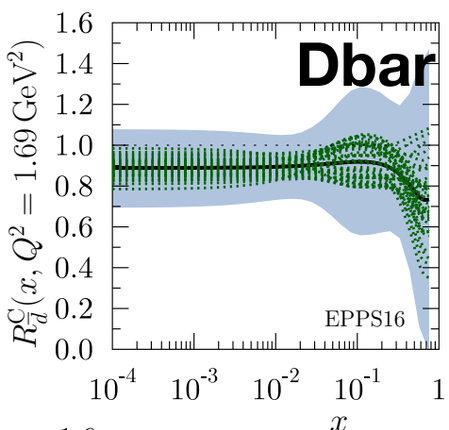

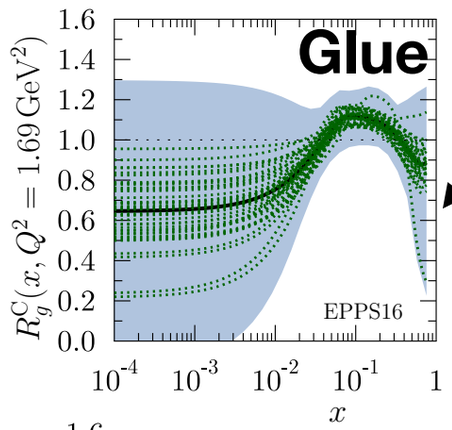

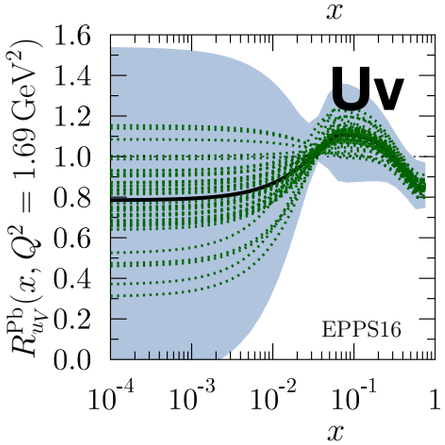

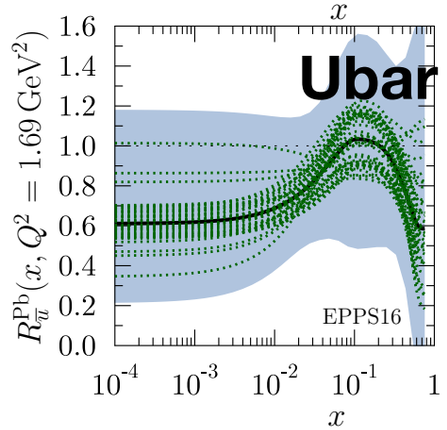

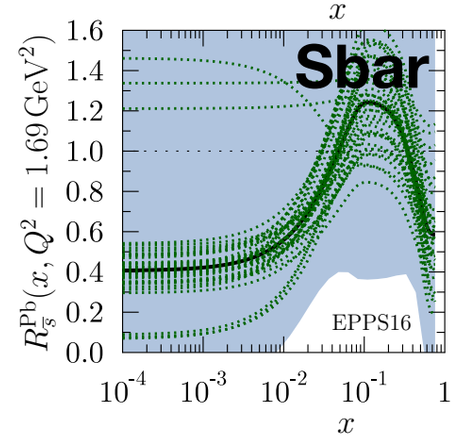

Lead

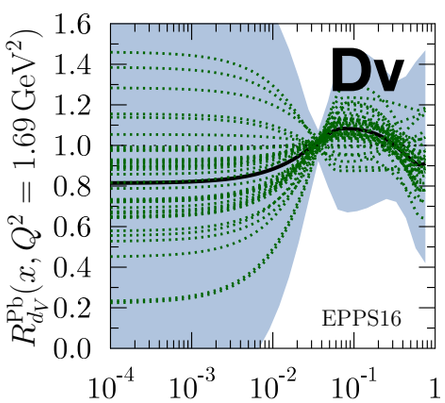

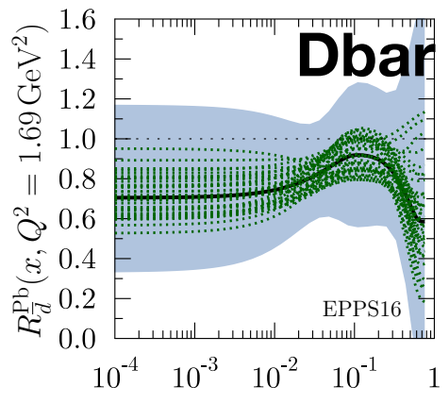

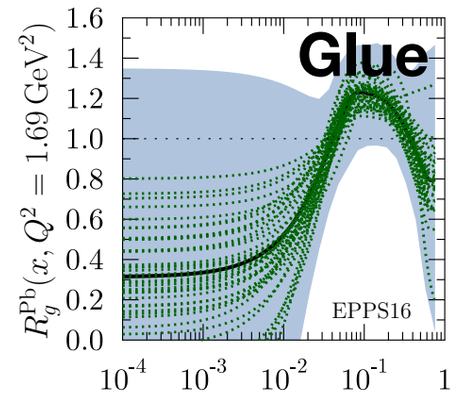

EPPS16 nuclear PDFs

✦Huge uncertainties, especially for low x

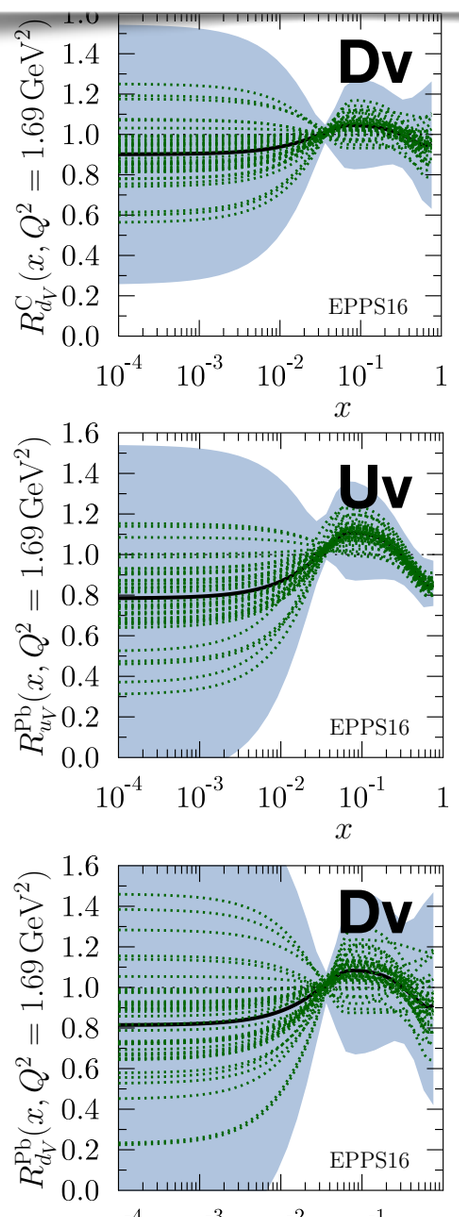

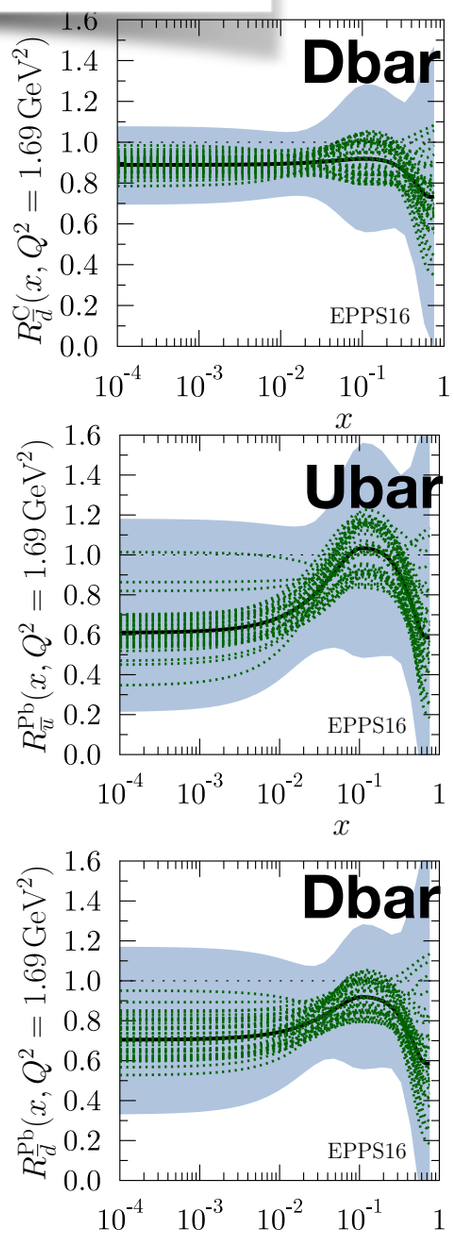

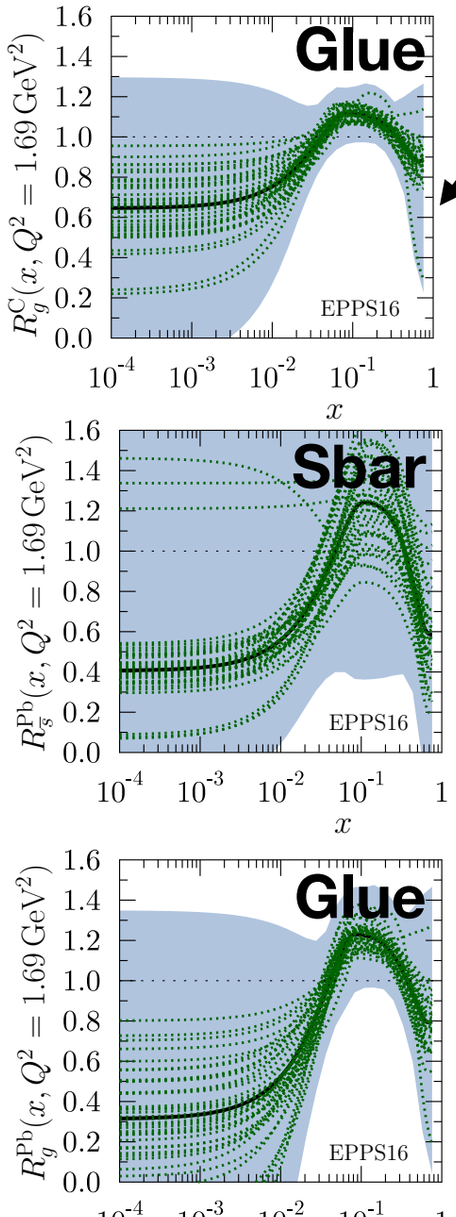

Carbon

Lead

EPPS16 nuclear PDFs

- ✦Huge uncertainties, especially for low x
- ✦Larger shadowing for lead than carbon

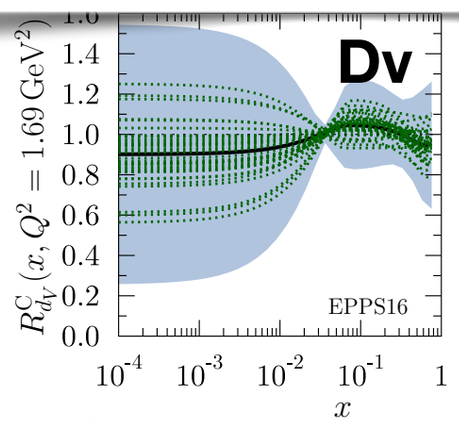

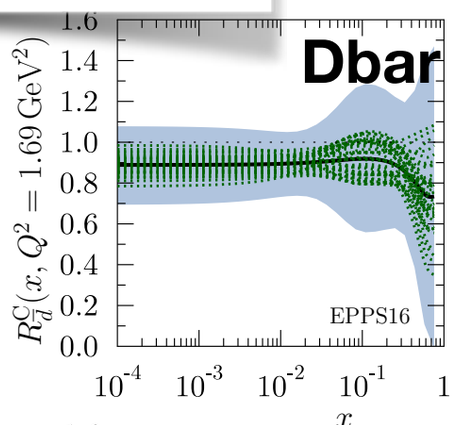

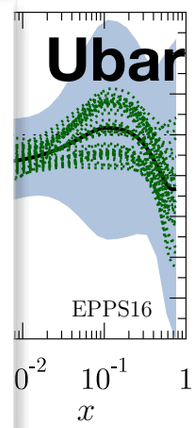

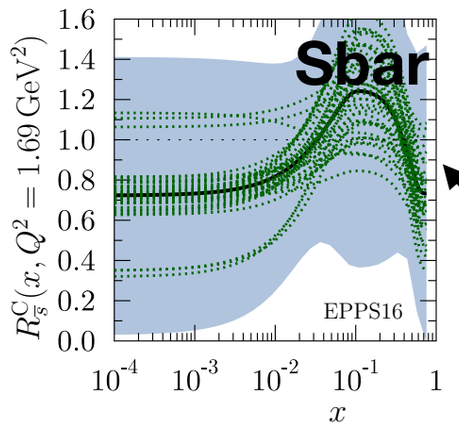

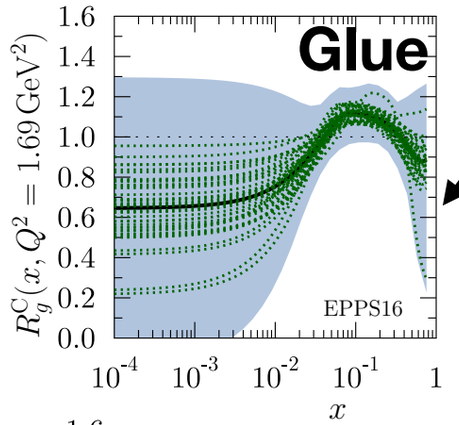

Carbon

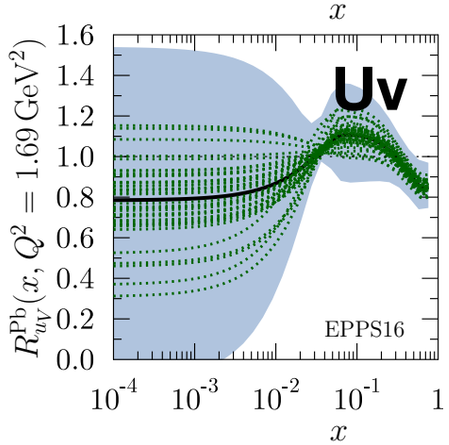

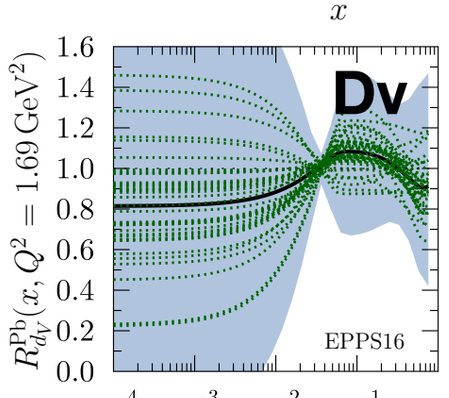

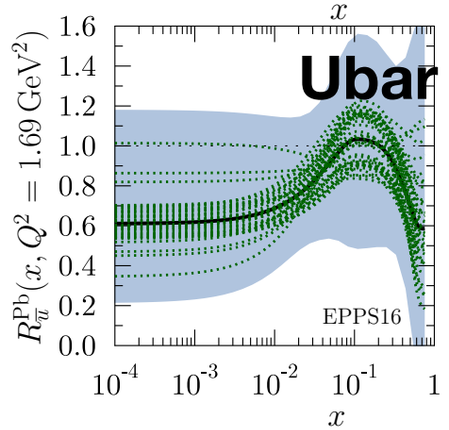

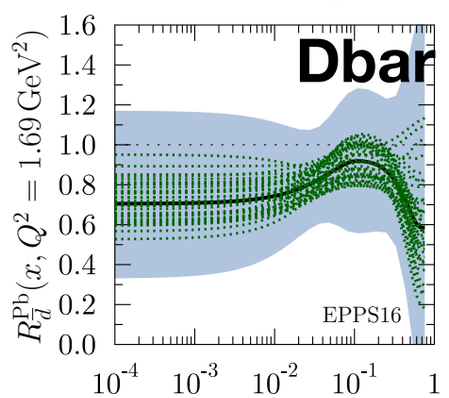

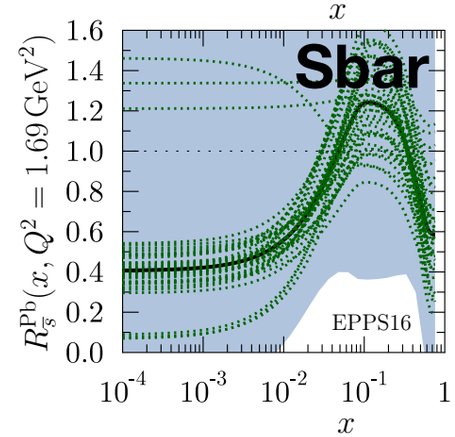

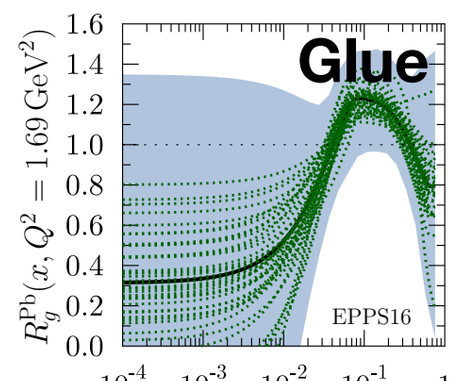

Lead

EPPS16 nuclear PDFs

- ✦Huge uncertainties, especially for low x
- ✦Larger shadowing for lead than carbon
- ✦Data are consistent even with enhancement at low x which is unphysical

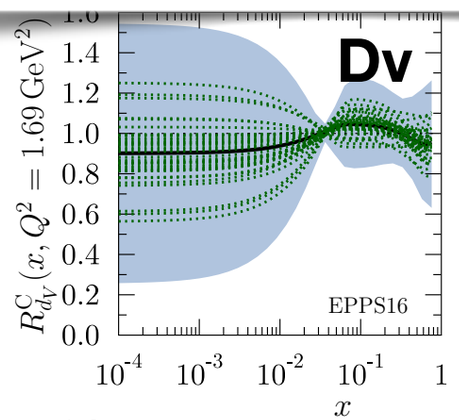

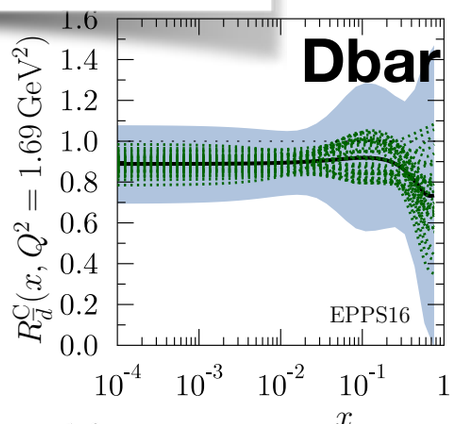

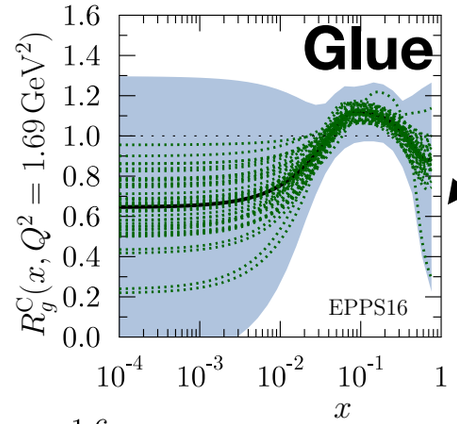

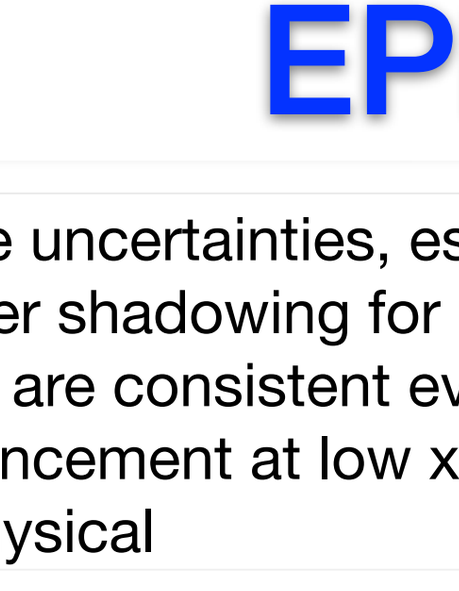

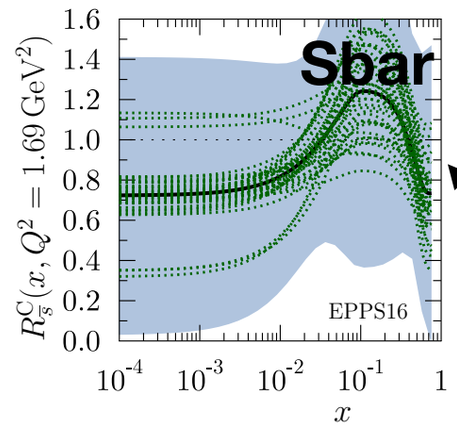

Carbon

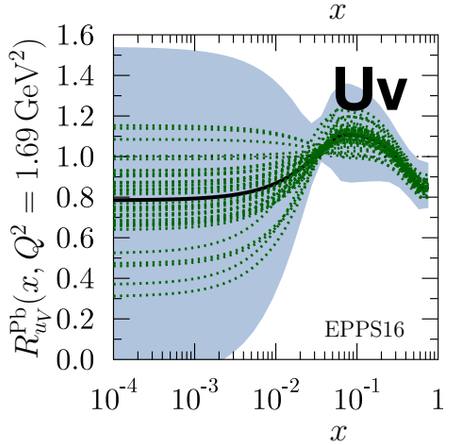

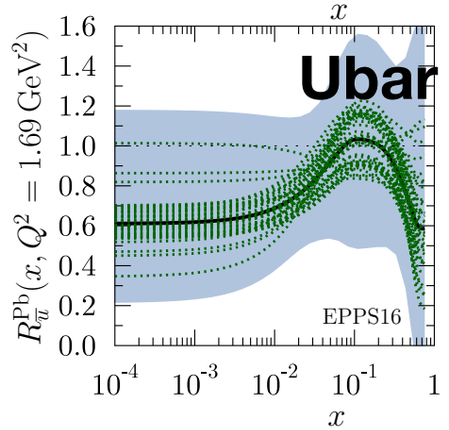

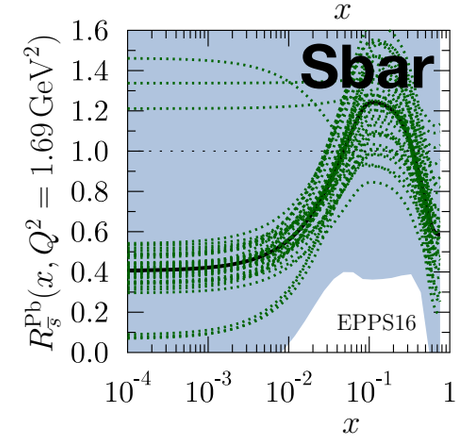

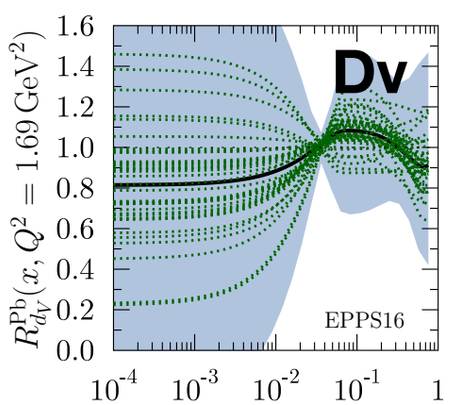

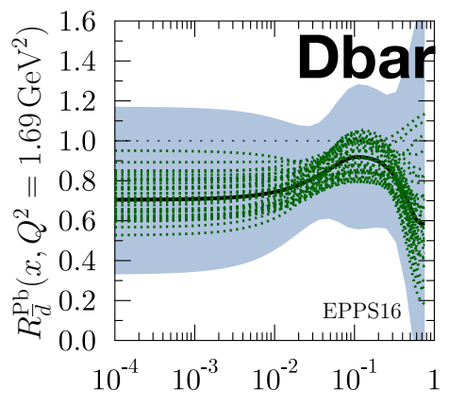

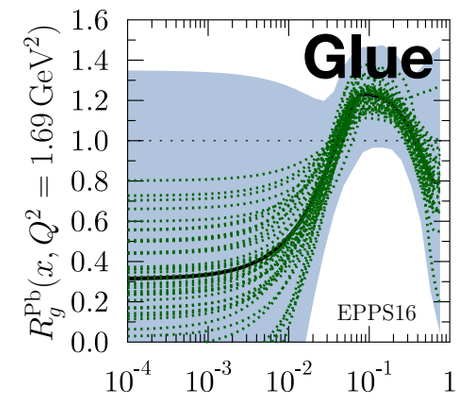

Lead

Nuclear PDFs at Electron-Ion Collider

We saw that nuclear PDFs are poorly constrained by the current data.
Need more precise data, ideally from clean eA DIS process to constrain better the PDFs and to determine whether the DGLAP based approach is applicable, and in what region, to nuclear data.

Nuclear PDFs at Electron-Ion Collider

We saw that nuclear PDFs are poorly constrained by the current data.
Need more precise data, ideally from clean eA DIS process to constrain better the PDFs and to determine whether the DGLAP based approach is applicable, and in what region, to nuclear data.

Answer: build a high luminosity electron-ion collider!

Nuclear PDFs at Electron-Ion Collider

We saw that nuclear PDFs are poorly constrained by the current data.
Need more precise data, ideally from clean eA DIS process to constrain better the PDFs and to determine whether the DGLAP based approach is applicable, and in what region, to nuclear data.

Answer: build a high luminosity electron-ion collider!

US-proposal

EIC: 5-20 GeV electrons
20-140 GeV CoM energy
Lumi: 10^{34} cm^{-2} s^{-1}
Polarized e,p,d,^{3}He
Wide range of nuclei

Nuclear PDFs at Electron-Ion Collider

We saw that nuclear PDFs are poorly constrained by the current data.
Need more precise data, ideally from clean eA DIS process to constrain better the PDFs and to determine whether the DGLAP based approach is applicable, and in what region, to nuclear data.

Answer: build a high luminosity electron-ion collider!

US-proposal

EIC: 5-20 GeV electrons
20-140 GeV CoM energy
Lumi: 10^{34} cm^{-2} s^{-1}
Polarized e,p,d,^{3}He
Wide range of nuclei

CERN-based

LHeC: 60 GeV electrons x LHC protons and ions.
1.3 TeV CoM energy in ep, 812 GeV CoM energy in eA per nucleon
Lumi: 10^{34} cm^{-2} s^{-1}
Simultaneous running with ATLAS and CMS in HL-LHC period

Nuclear PDFs at Electron-Ion Collider

We saw that nuclear PDFs are poorly constrained by the current data.
Need more precise data, ideally from clean eA DIS process to constrain better the PDFs and to determine whether the DGLAP based approach is applicable, and in what region, to nuclear data.

Answer: build a high luminosity electron-ion collider!

US-proposal

EIC: 5-20 GeV electrons
20-140 GeV CoM energy
Lumi: 10^{34} cm^{-2} s^{-1}
Polarized e,p,d,^{3}He
Wide range of nuclei

CERN-based

LHeC: 60 GeV electrons x LHC protons and ions.
1.3 TeV CoM energy in ep, 812 GeV CoM energy in eA per nucleon
Lumi: 10^{34} cm^{-2} s^{-1}
Simultaneous running with ATLAS and CMS in HL-LHC period

CERN-based

FCC-ep: 60 GeV electrons x 50 TeV protons from FCC, lead beams 19.7 TeV/per nucleon
3.5 TeV CoM in ep
2.2 TeV CoM in eA per nucleon
Lumi: 10^{34} cm^{-2} s^{-1}

Summary of machines:

Lepton-proton/nucleus scattering facilities

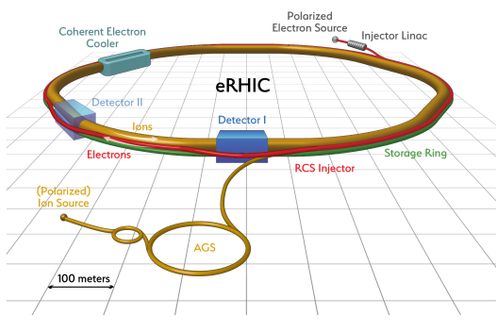

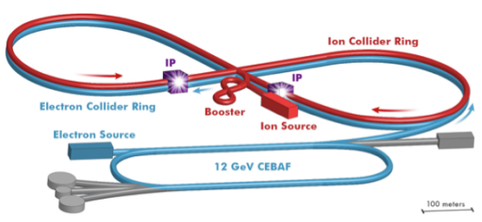

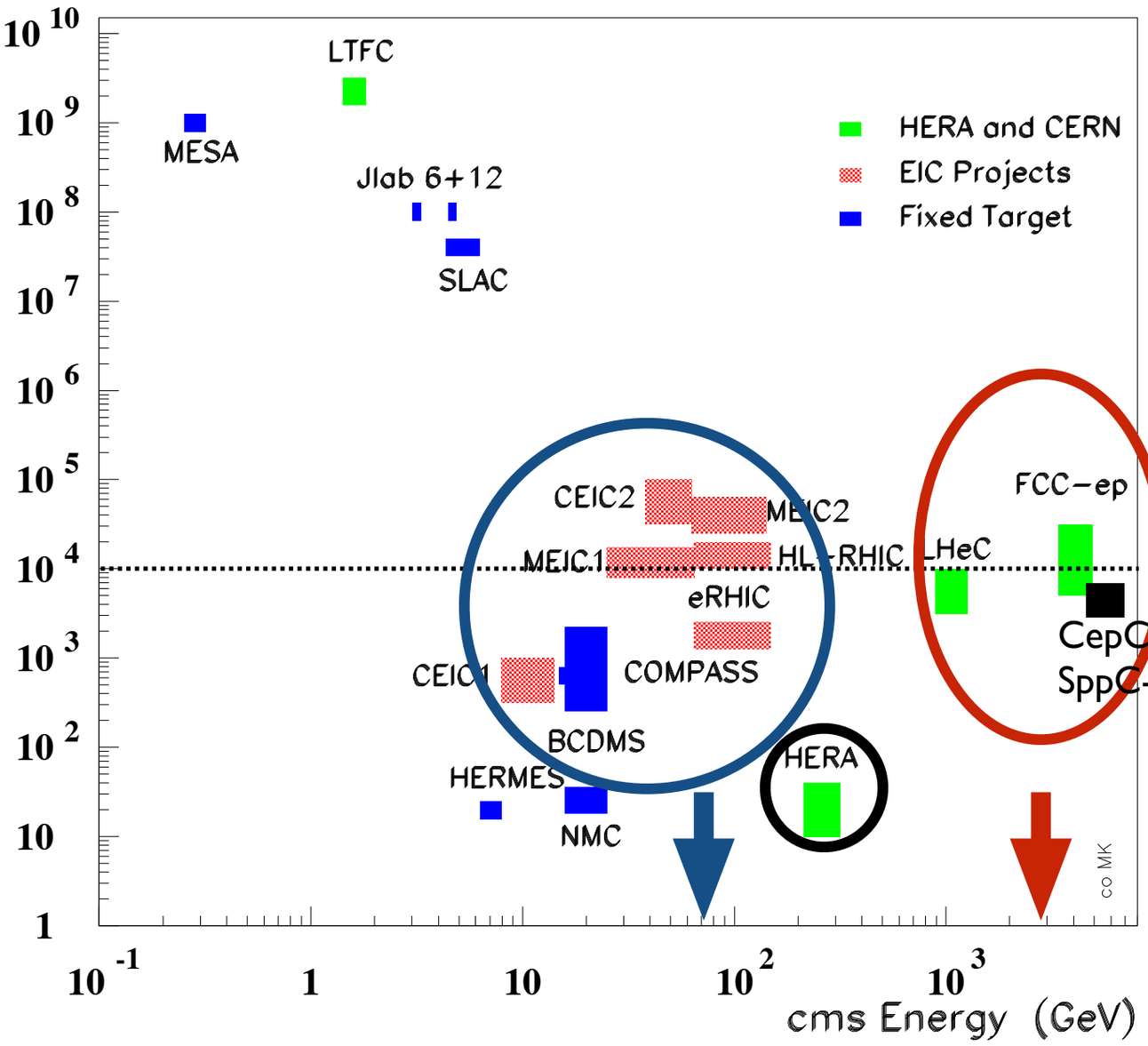

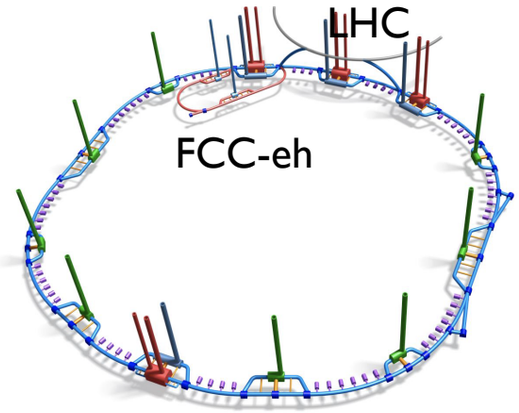

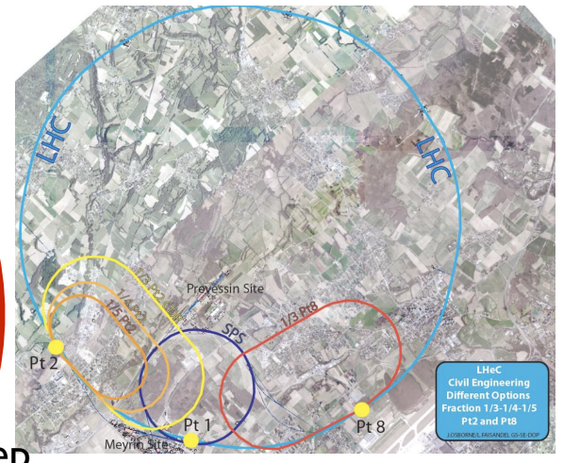

DIS machines at CERN

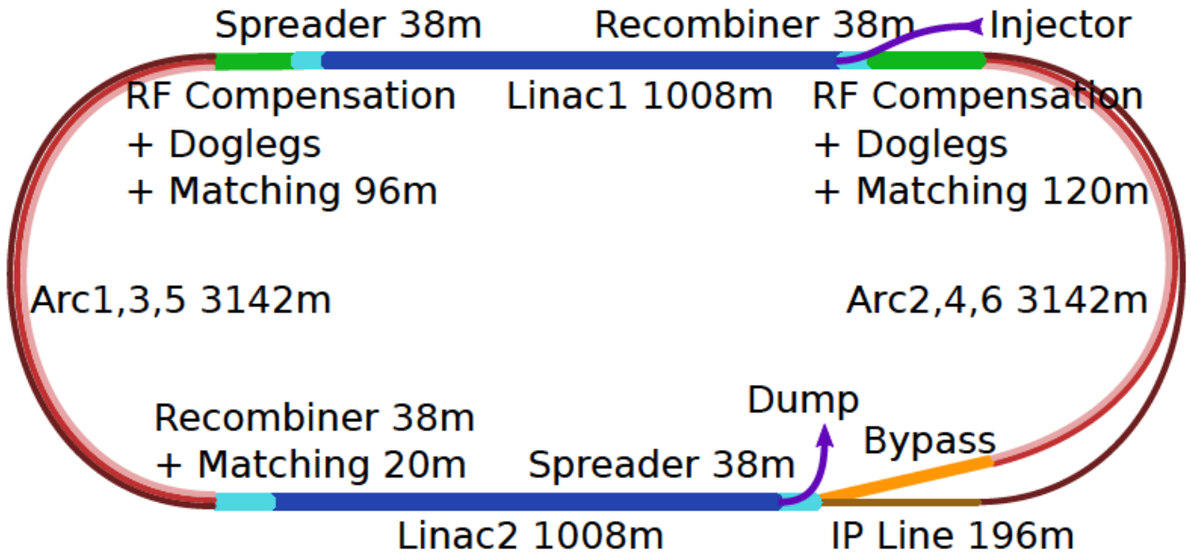

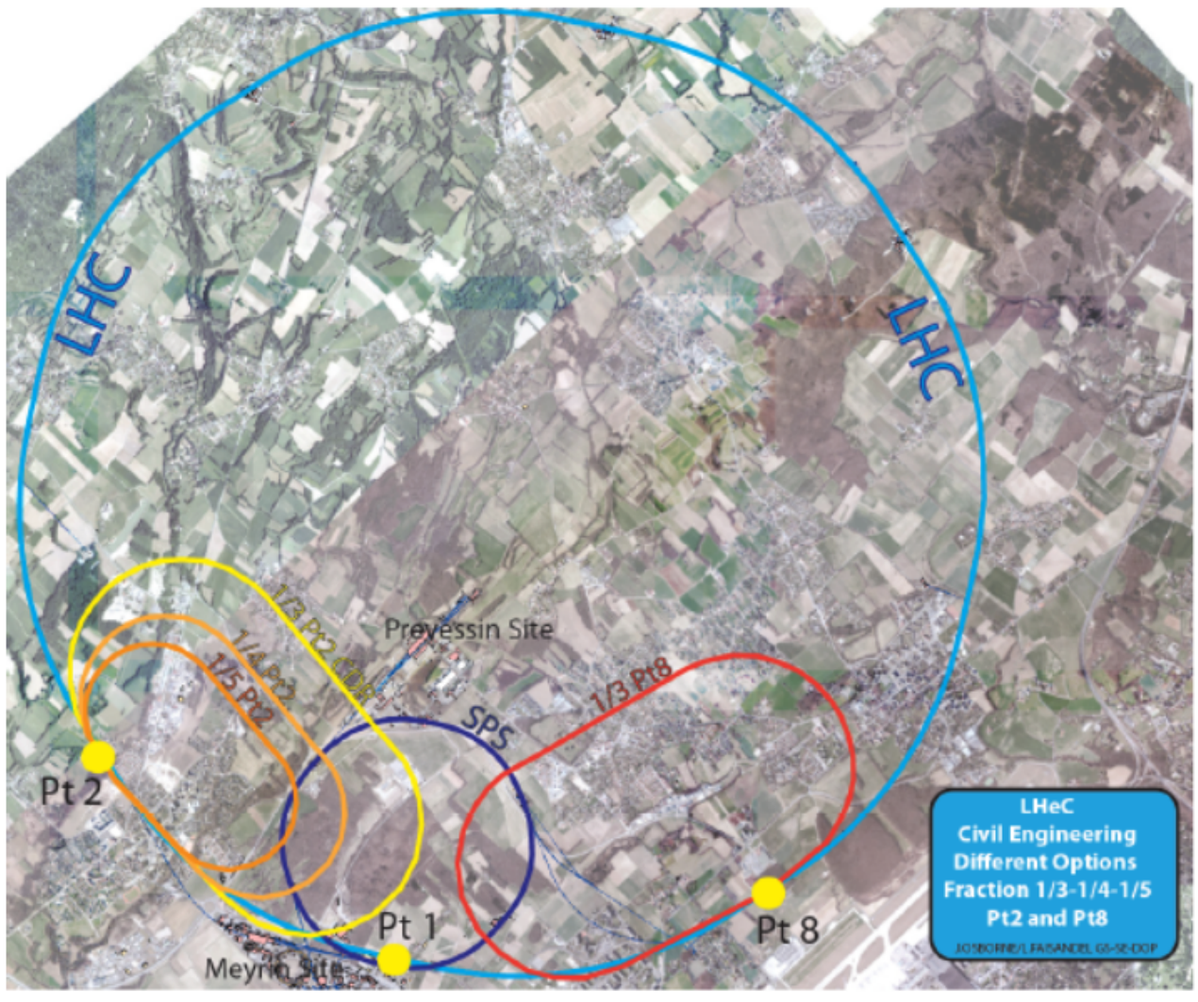

- 60 GeV e^- (ERL) against the (HL/HE-)LHC/FCC hadron beams: eA to run either concurrently with pA/AA or in dedicated mode.

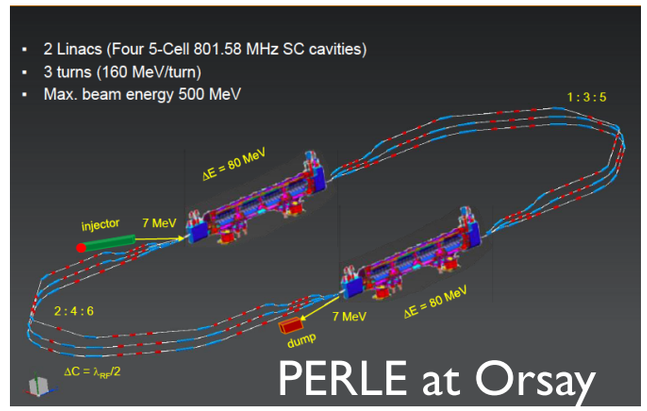

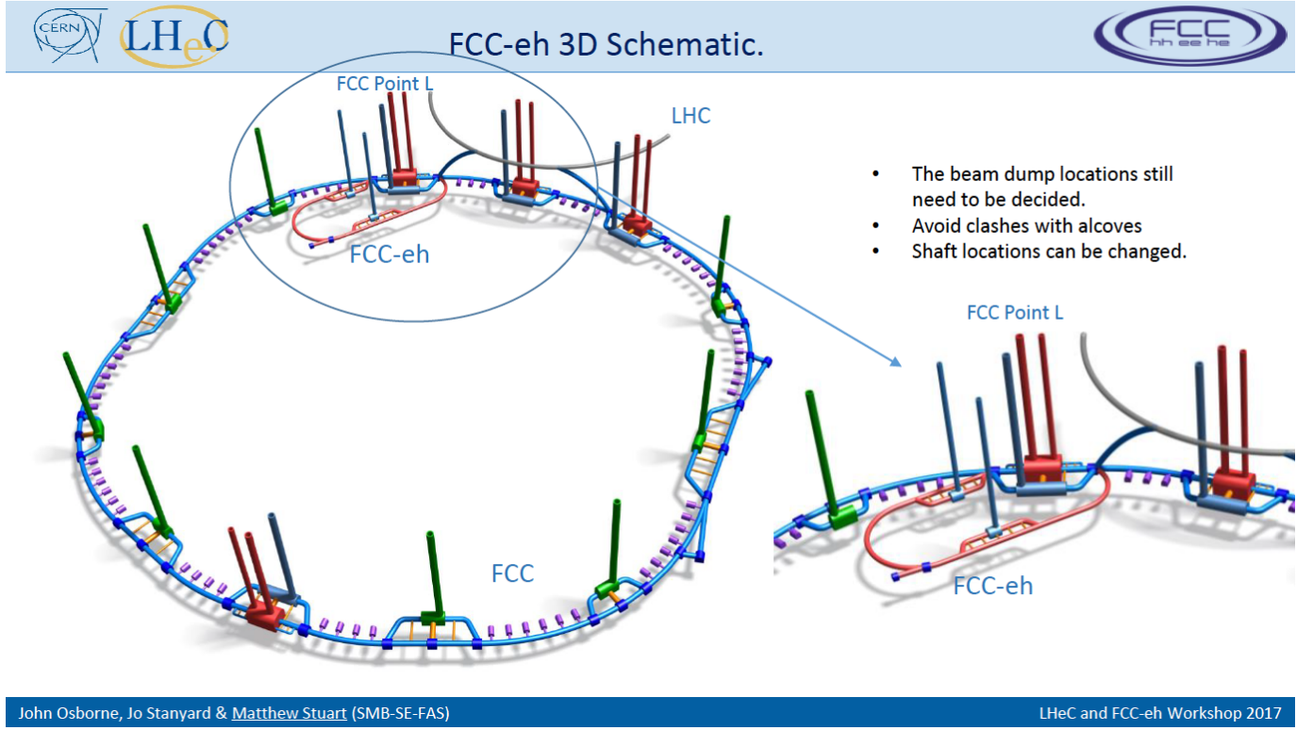

DIS machines at CERN

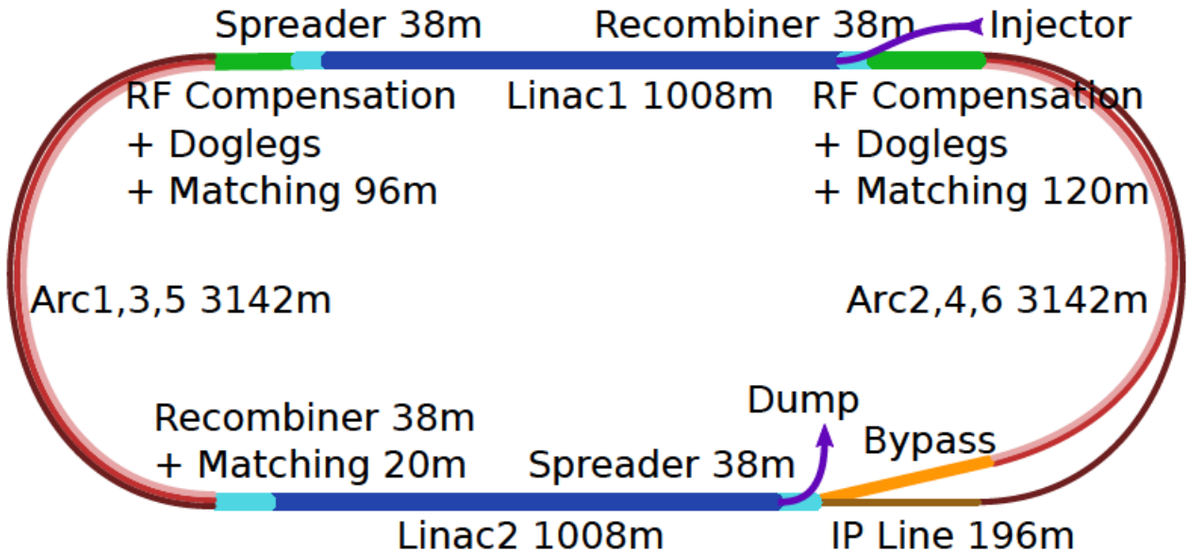

- 60 GeV e^- (ERL) against the (HL/HE-)LHC/FCC hadron beams: eA to run either concurrently with pA/AA or in dedicated mode.

CERN-ACC-2017-0019

parameter [unit]	LHeC (HL-LHC)	eA at HE-LHC	FCC-he
E_{Pb} [PeV]	0.574	1.03	4.1
E_e [GeV]	60	60	60
$\sqrt{s_{eN}}$ electron-nucleon [TeV]	0.8	1.1	2.2
bunch spacing [ns]	50	50	100
no. of bunches	1200	1200	2072
ions per bunch [10^8]	1.8	1.8	1.8
$\gamma\epsilon_A$ [μm]	1.5	1.0	0.9
electrons per bunch [10^9]	4.67	6.2	12.5
electron current [mA]	15	20	20
IP beta function β^*_A [cm]	7	10	15
hourglass factor H_{geom}	0.9	0.9	0.9
pinch factor H_{b-b}	1.3	1.3	1.3
bunch filling H_{coll}	0.8	0.8	0.8
luminosity [$10^{32}\mathrm{cm}^{-2}\mathrm{s}^{-1}$]	7	18	54
Integrated lumi. in 10 y. (fb^{-1}) ~~	6	15	45

- 100 times larger luminosity than HERA, full HERA integrated luminosity in less than a month.

EIC vs LHeC vs FCC-eh kinematics

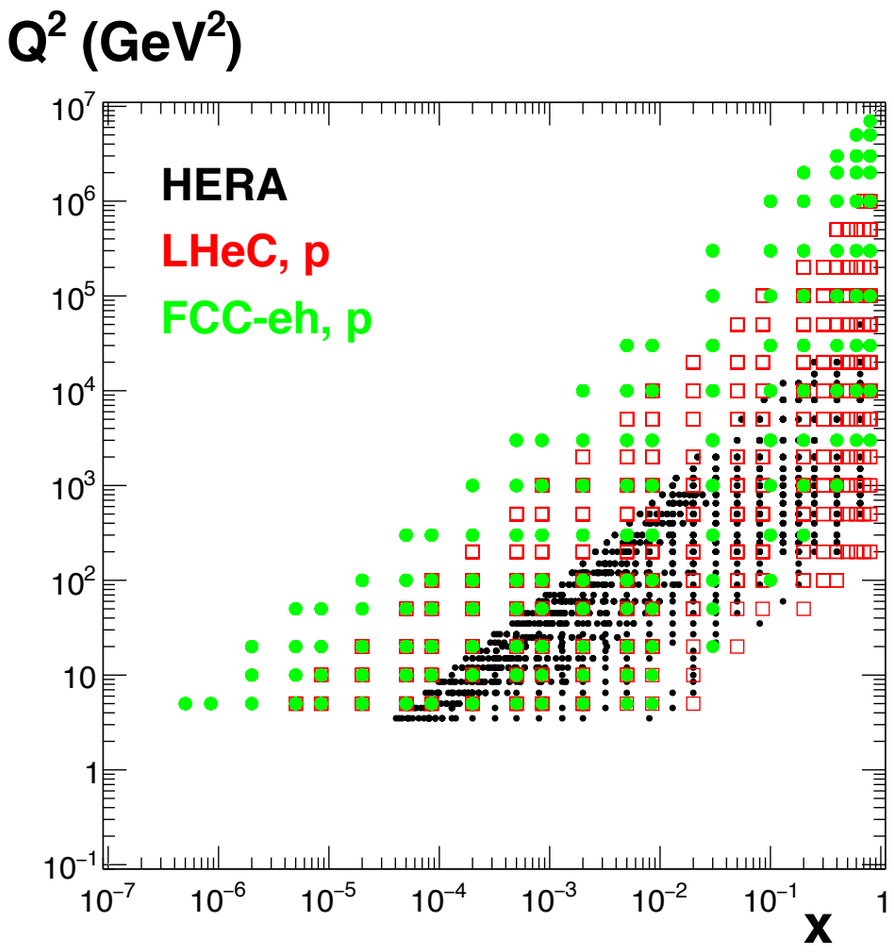

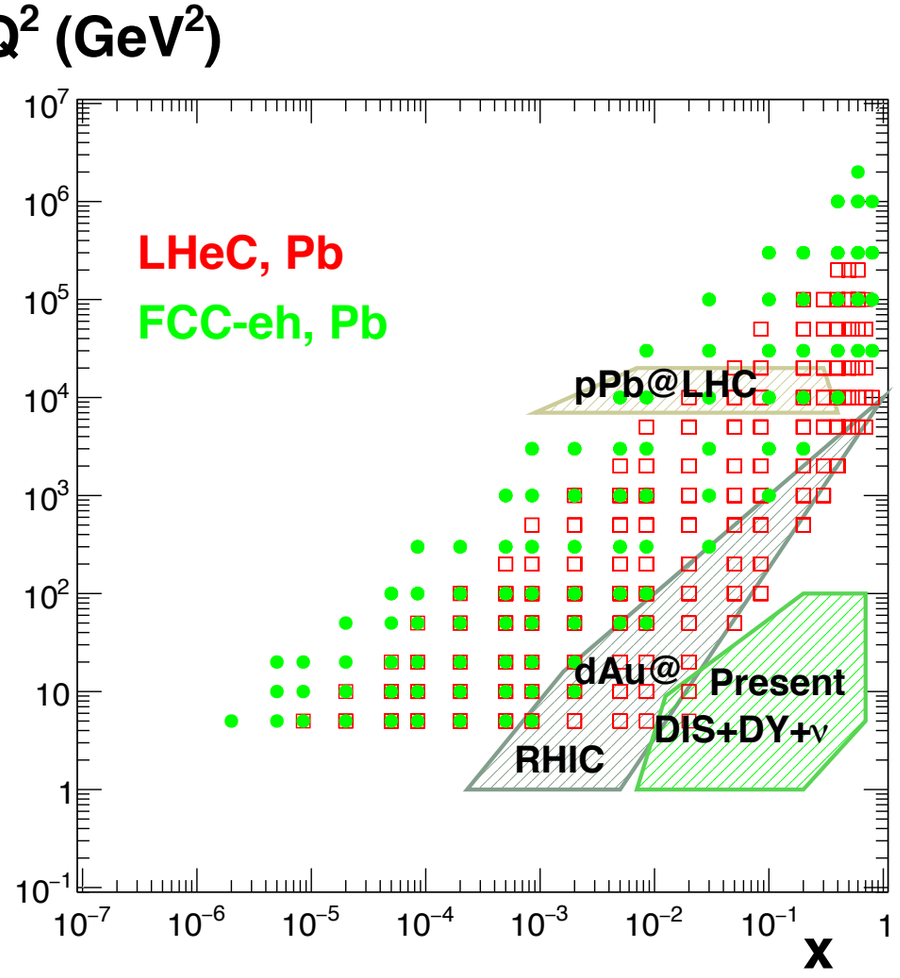

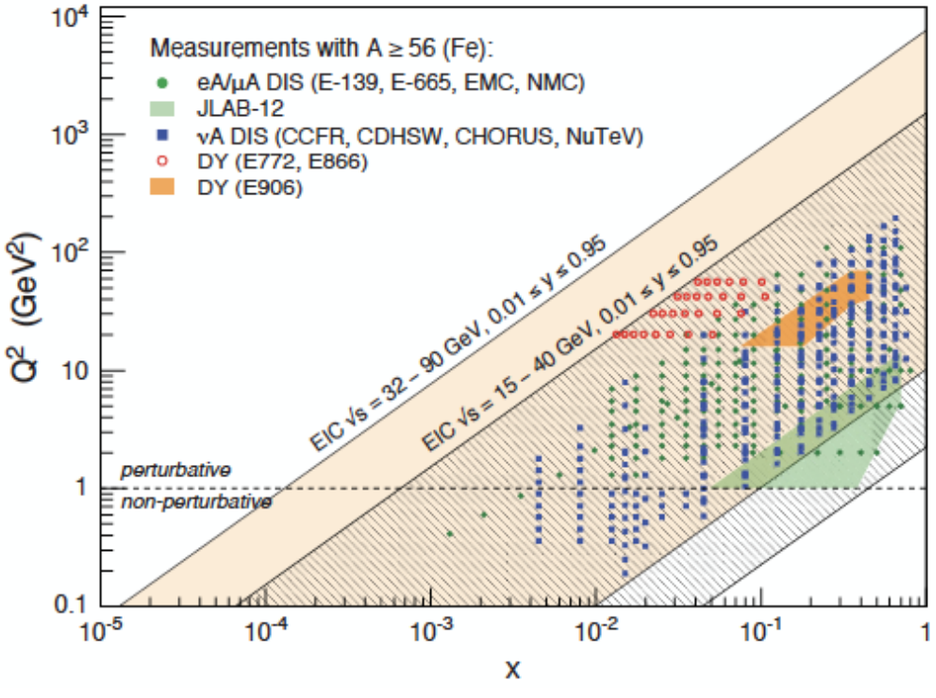

Huge extension of the kinematics in (x,Q) in eA scattering in all machines
High luminosity would allow for very precise measurements

Impact of EIC pseudodata on nPDFs

- EIC pseudodata generated with EPS09, uncertainties as achieved at HERA
- Very good prospects for longitudinal structure function measurement and for charm

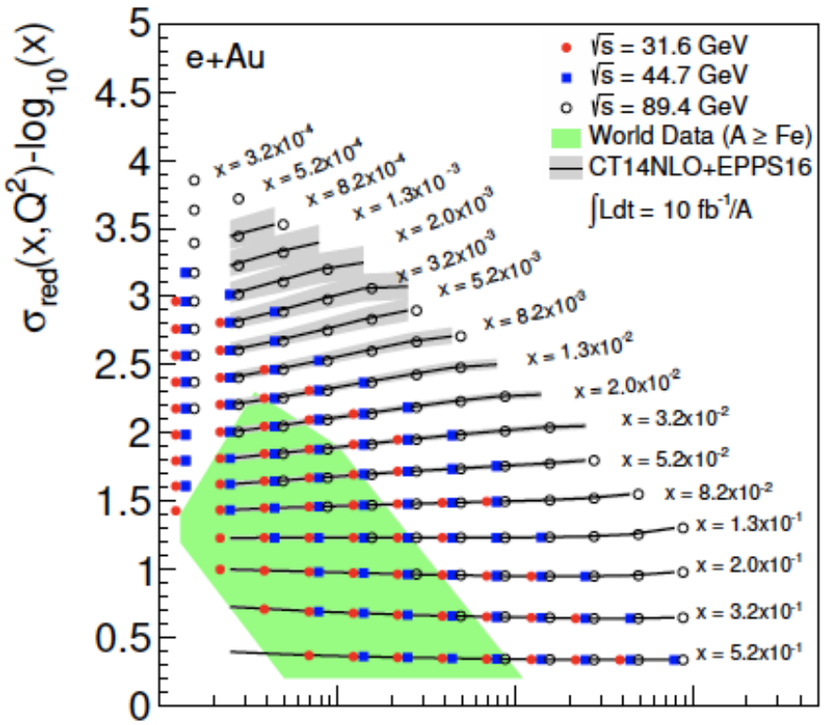

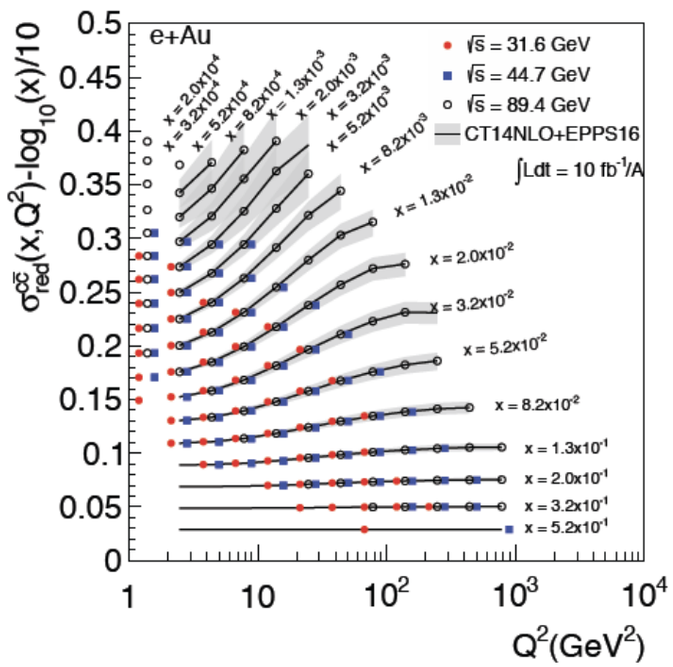

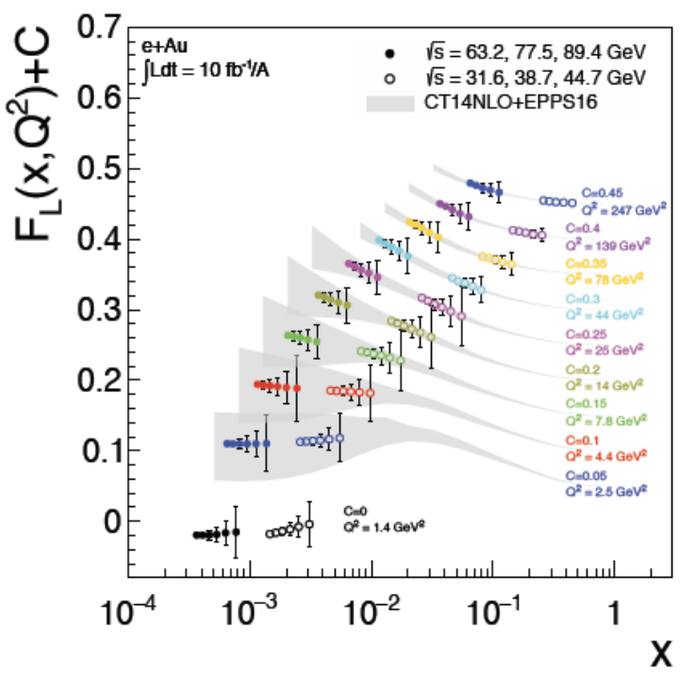

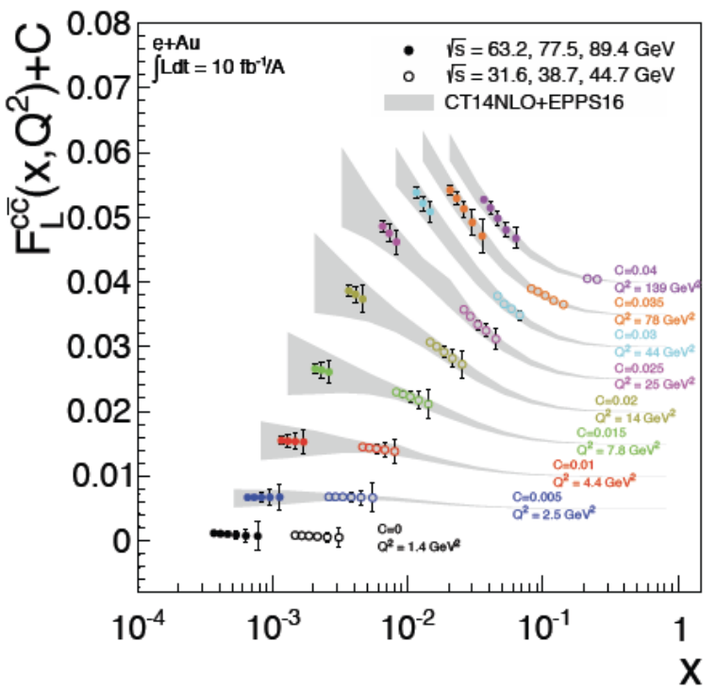

Impact of EIC pseudodata on nPDFs

Study of impact of charm in the data
Significant reduction of uncertainties, for gluon and u,d valence and sea

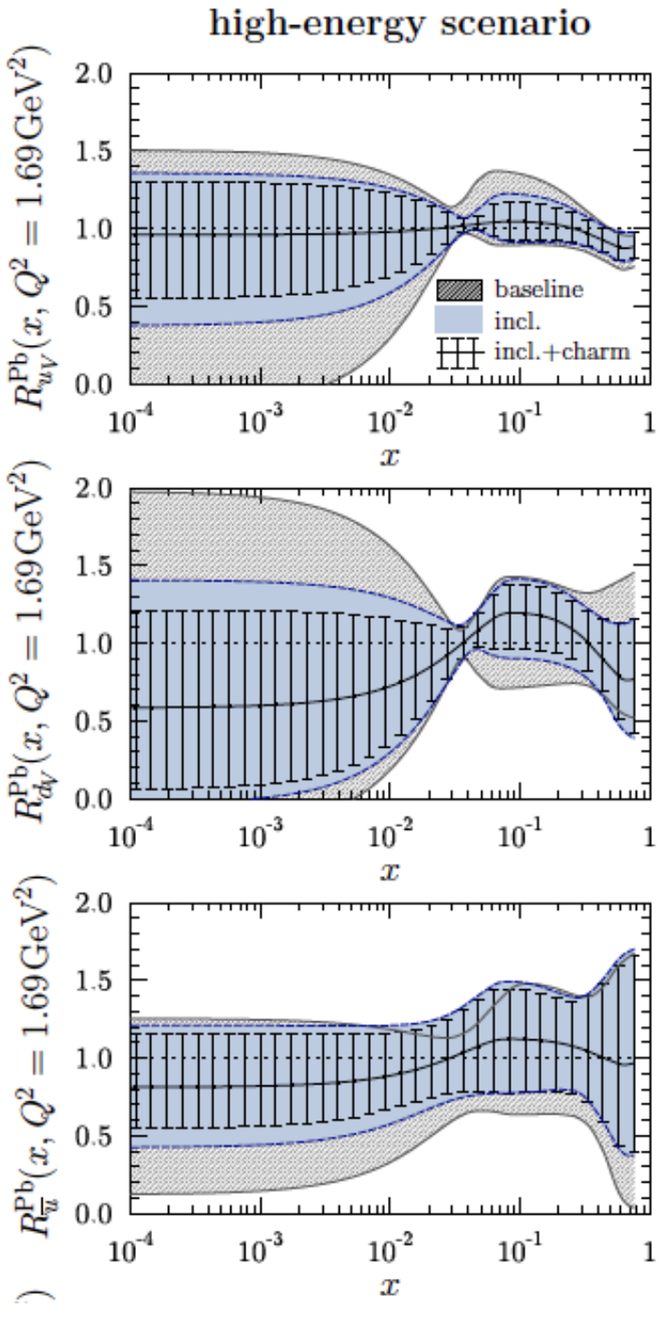

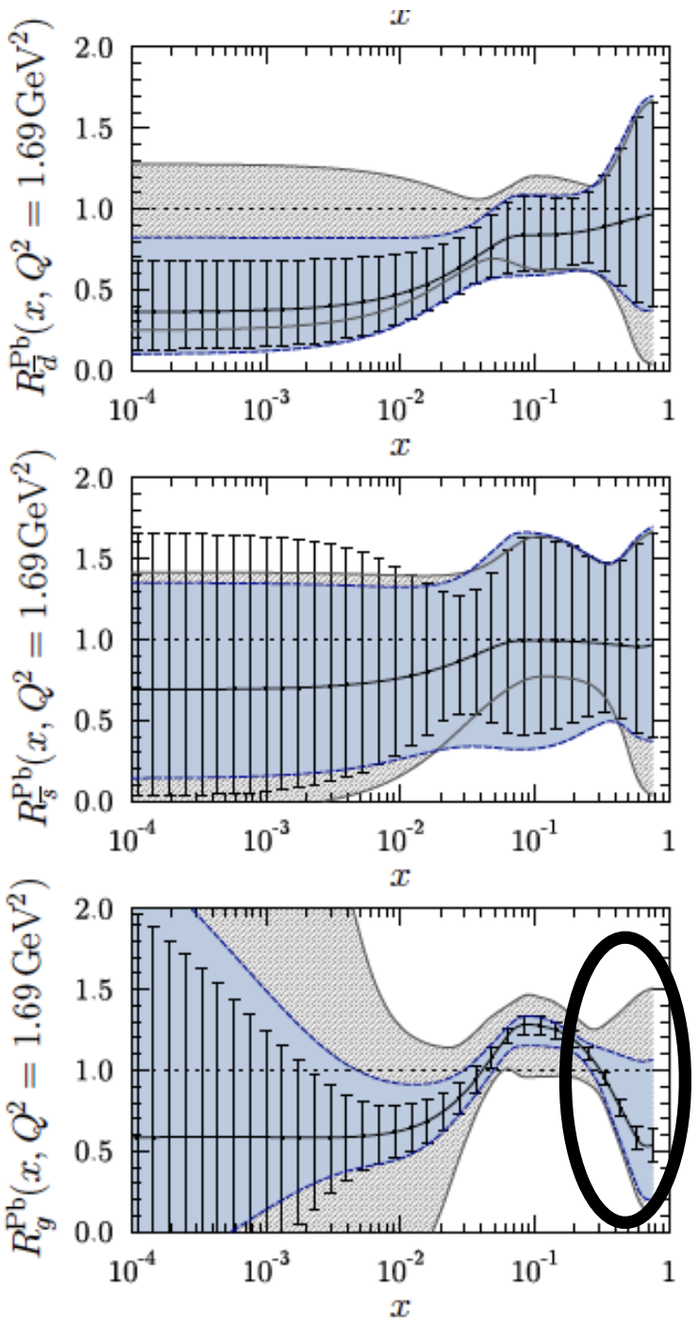

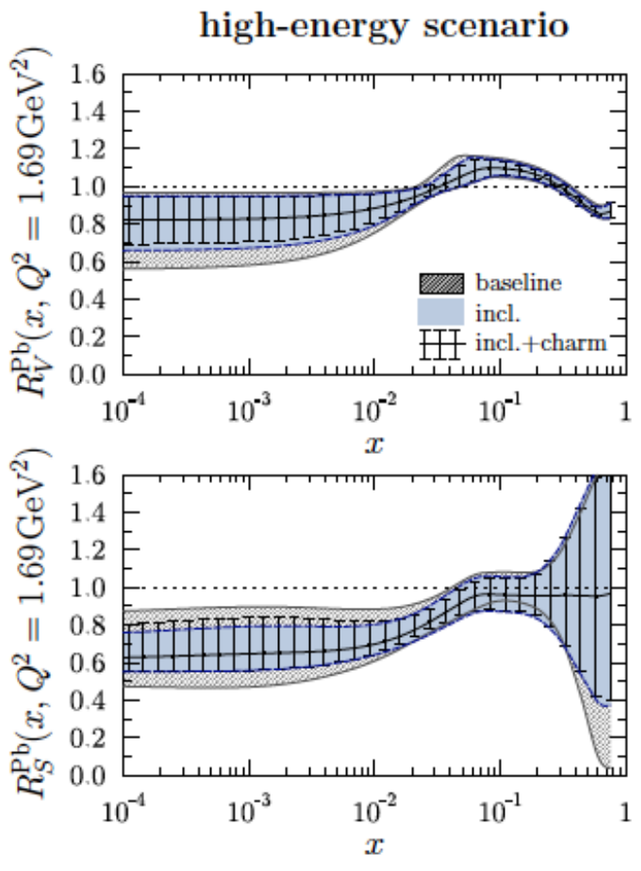

- Charm has a large impact for the large x glue.

Pseudodata:

	E_e (GeV)	E_h (TeV/nucleon)	Polarisation	Luminosity (fb^{-1})	NC/CC	# data
ep@LHeC, 1005 data points for $Q^2 \geq 3.5$ GeV^2	60 (e^-)	1 (p)	0	100	CC	93
	60 (e^-)	1 (p)	0	100	NC	136
	60 (e^-)	7 (p)	-0.8	1000	CC	114
	60 (e^-)	7 (p)	0.8	300	CC	113
	60 (e^+)	7 (p)	0	100	CC	109
	60 (e^-)	7 (p)	-0.8	1000	NC	159
	60 (e^-)	7 (p)	0.8	300	NC	159
	60 (e^+)	7 (p)	0	100	NC	157
ePb@LHeC, 484 data points for $Q^2 \geq 3.5$ GeV^2	20 (e^-)	2.75 (Pb)	-0.8	0.03	CC	51
	20 (e^-)	2.75 (Pb)	-0.8	0.03	NC	93
	26.9 (e^-)	2.75 (Pb)	-0.8	0.02	CC	55
	26.9 (e^-)	2.75 (Pb)	-0.8	0.02	NC	98
	60 (e^-)	2.75 (Pb)	-0.8	1	CC	85
	60 (e^-)	2.75 (Pb)	-0.8	1	NC	129
ep@FCC-eh, 619 data points for $Q^2 \geq 3.5$ GeV^2	20 (e^-)	7 (p)	0	100	CC	46
	20 (e^-)	7 (p)	0	100	NC	89
	60 (e^-)	50 (p)	-0.8	1000	CC	67
	60 (e^-)	50 (p)	0.8	300	CC	65
	60 (e^+)	50 (p)	0	100	CC	60
	60 (e^-)	50 (p)	-0.8	1000	NC	111
	60 (e^-)	50 (p)	0.8	300	NC	110
	60 (e^+)	50 (p)	0	100	NC	107
ePb@FCC-eh, 150 data points for $Q^2 \geq 3.5$ GeV^2	60 (e^-)	20 (Pb)	-0.8	10	CC	58
	60 (e^-)	20 (Pb)	-0.8	10	NC	101

Pseudodata:

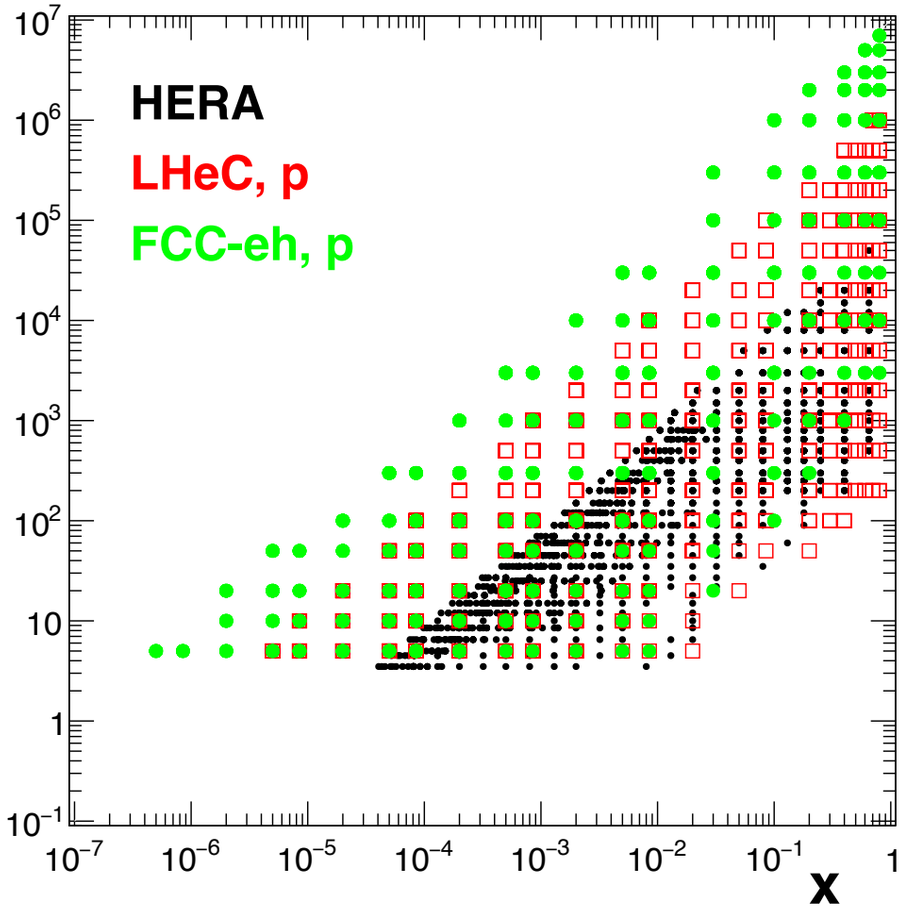

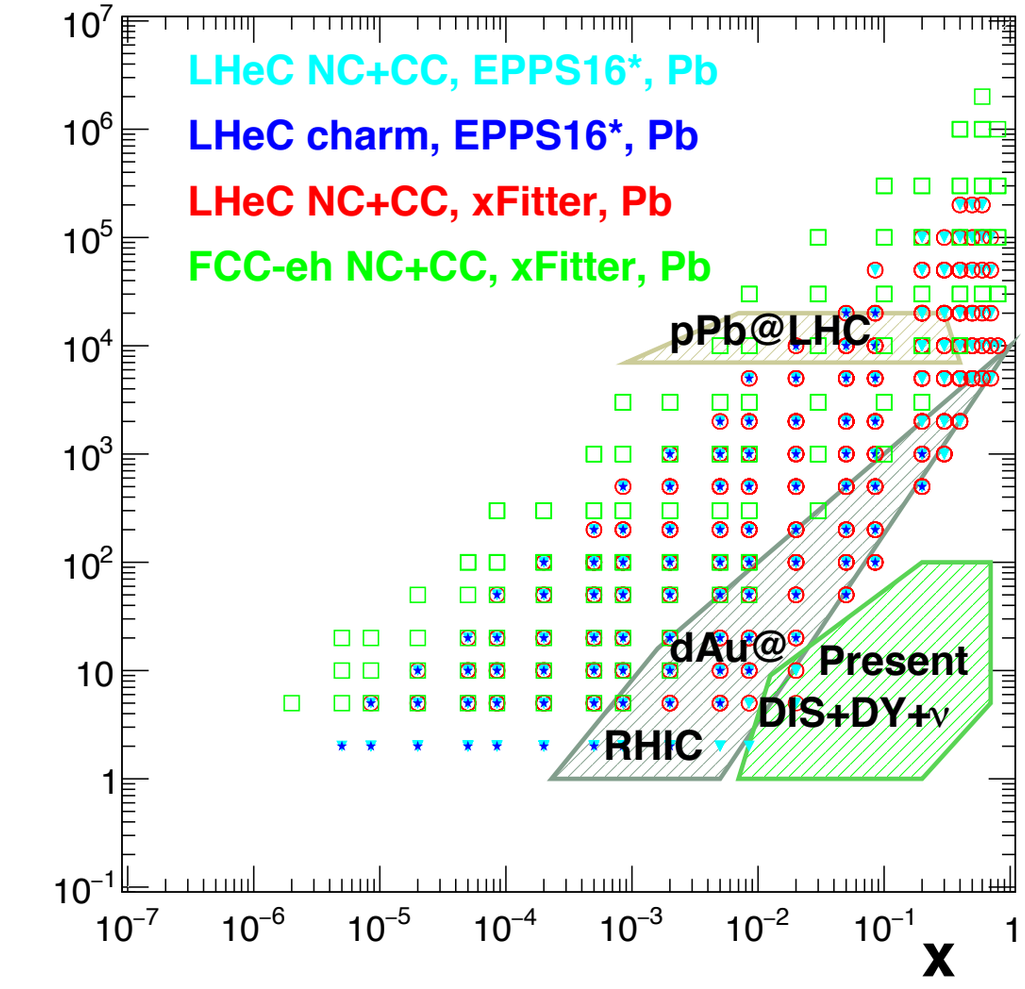

- Pseudodata generated using a code (Max Klein) validated with the H1 MC.
- Cuts: $|\eta_{max}|=5$, $0.95 < y < 0.001$.
- Error assumptions ~ factor 2 better than at HERA (luminosity uncertainty kept aside).

Source of uncertainty	Error on the source or cross section
scattered electron energy scale	0.1 %
scattered electron polar angle	0.1 mrad
hadronic energy scale	0.5 %
calorimeter noise ($y < 0.01$)	1-3 %
radiative corrections	1-2 %
photoproduction background	1 %
global efficiency error	0.7 %

Pseudodata:

Q^2 (GeV^2)

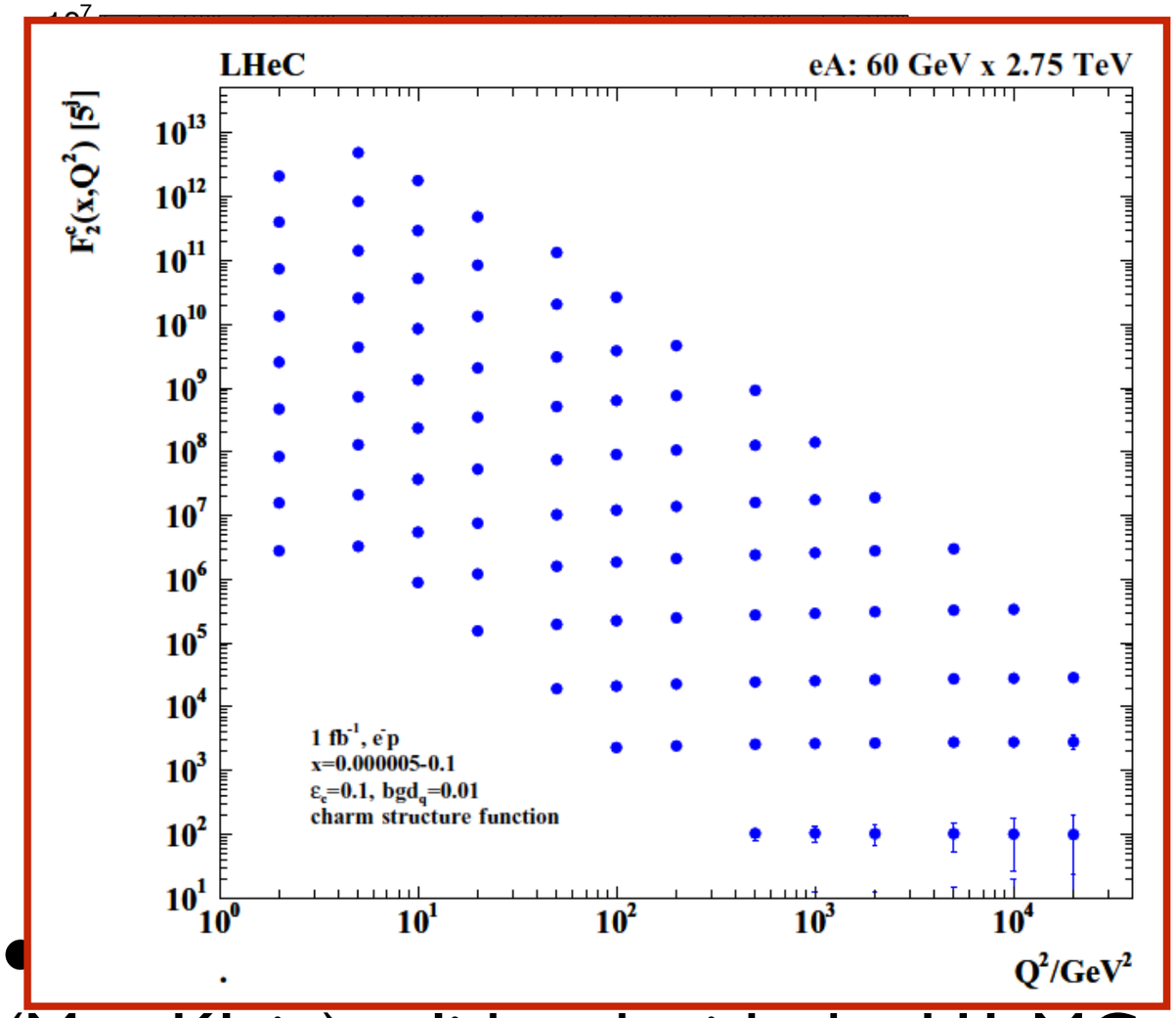

Q^2 (GeV^2)

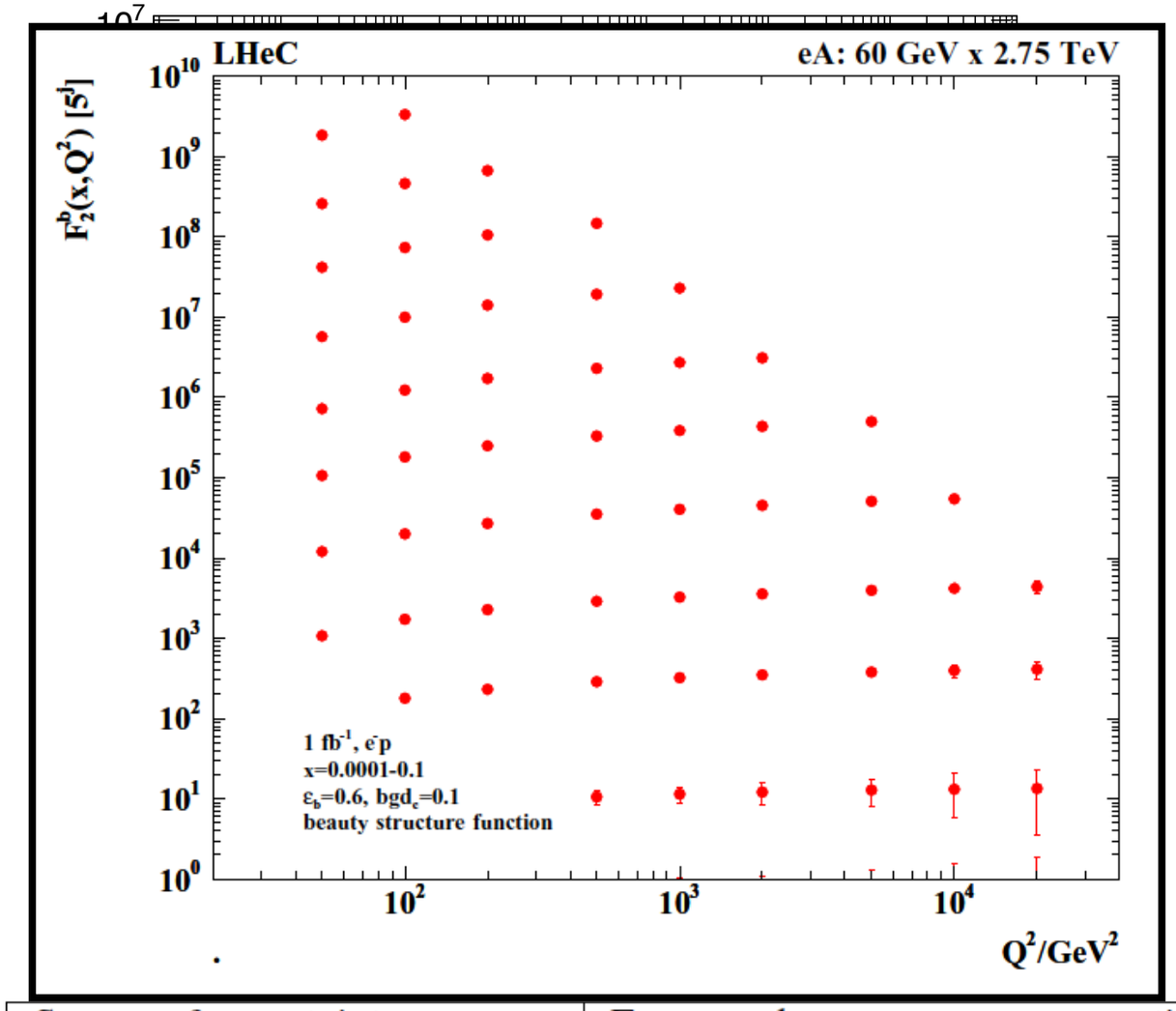

- (Max Klein) validated with the H1 MC.
- Cuts: $|\eta_{max}|$=5, 0.95< y< 0.001.
- Error assumptions ~ factor 2 better than at HERA (luminosity uncertainty kept aside).

Source of uncertainty	Error on the source or cross section
scattered electron energy scale	0.1 %
scattered electron polar angle	0.1 mrad
hadronic energy scale	0.5 %
calorimeter noise ($y < 0.01$)	1-3 %
radiative corrections	1-2 %
photoproduction background	1 %
global efficiency error	0.7 %

Pseudodata:

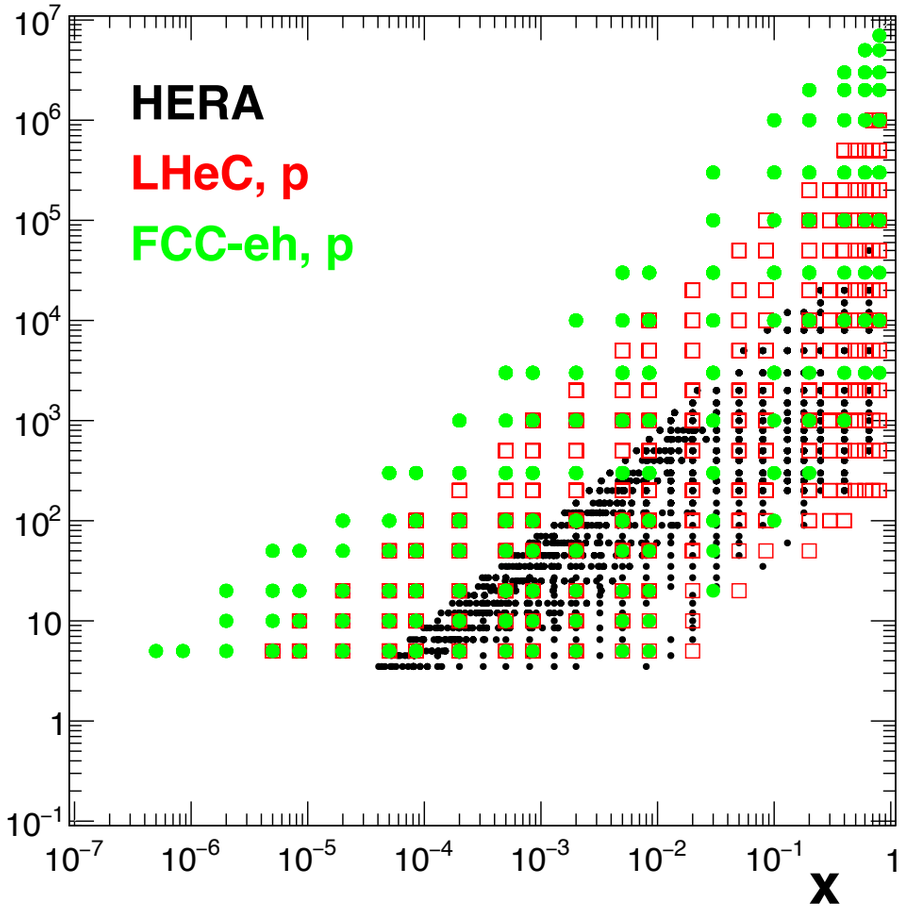

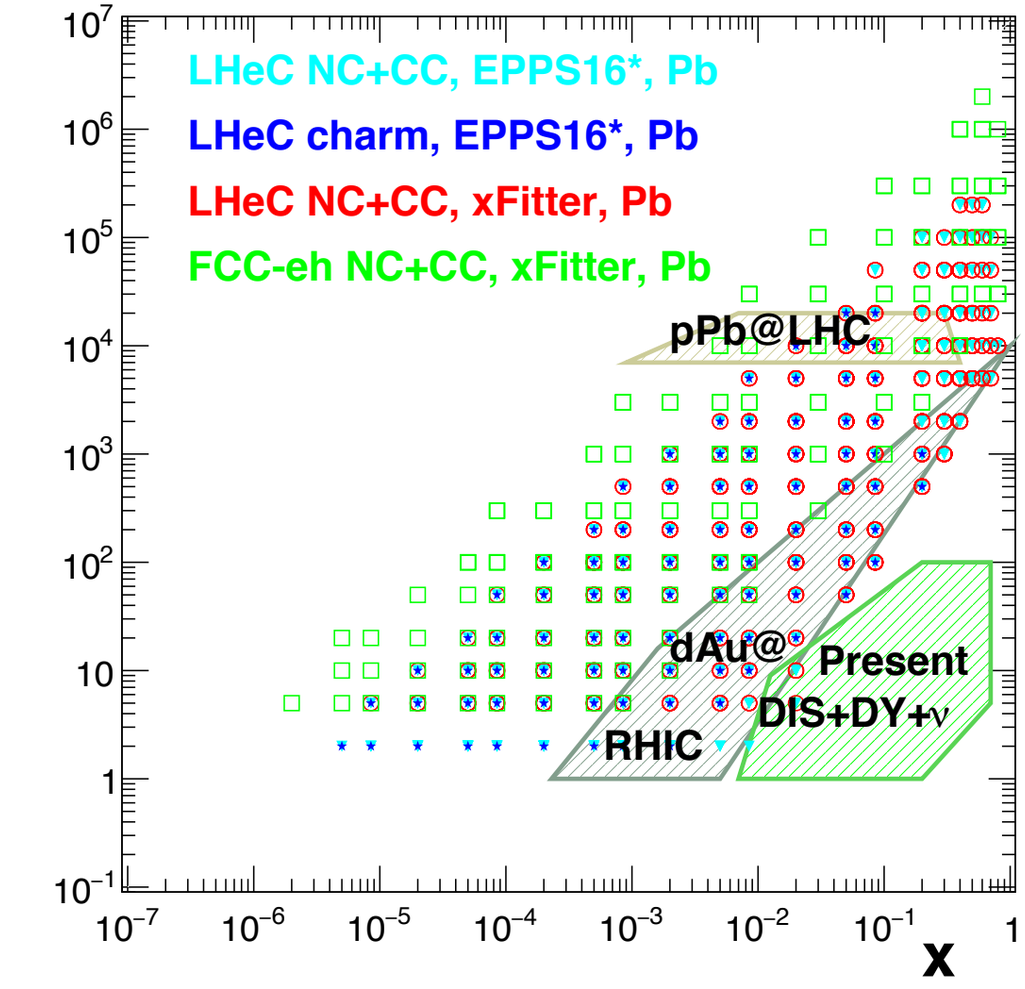

- Pseudodata generated using a code (Max Klein) validated with the H1 MC.
- Cuts: $|\eta_{max}|=5$, $0.95 < y < 0.001$.
- Error assumptions ~ factor 2 better than at HERA (luminosity uncertainty kept aside).

Source of uncertainty	Error on the source or cross section
scattered electron energy scale	0.1 %
scattered electron polar angle	0.1 mrad
hadronic energy scale	0.5 %
calorimeter noise ($y < 0.01$)	1-3 %
radiative corrections	1-2 %
photoproduction background	1 %
global efficiency error	0.7 %

EPPS16*: results

- Large effect of NC+CC LHeC pseudodata, and of charm on the glue at small x.
- Limitation on u/d decomposition inherent to almost isospin symmetric nuclei (u/d difference suppressed by 2Z/A-1).

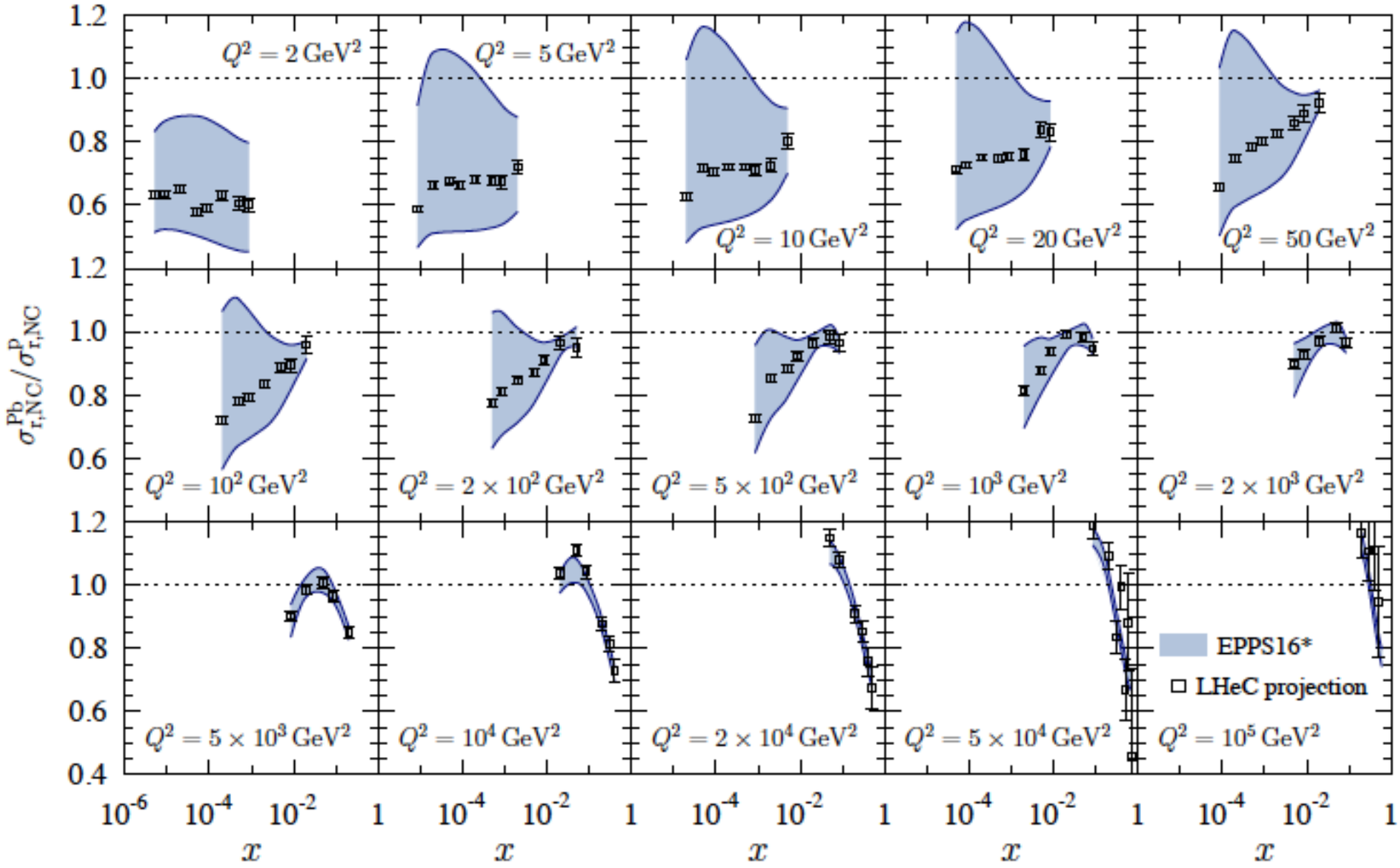

EPPS16*: results

- Large effect of NC+CC LHeC pseudodata, and of charm on the glue at small x.
- Limitation on u/d decomposition inherent to almost isospin symmetric nuclei (u/d difference suppressed by 2Z/A-1).

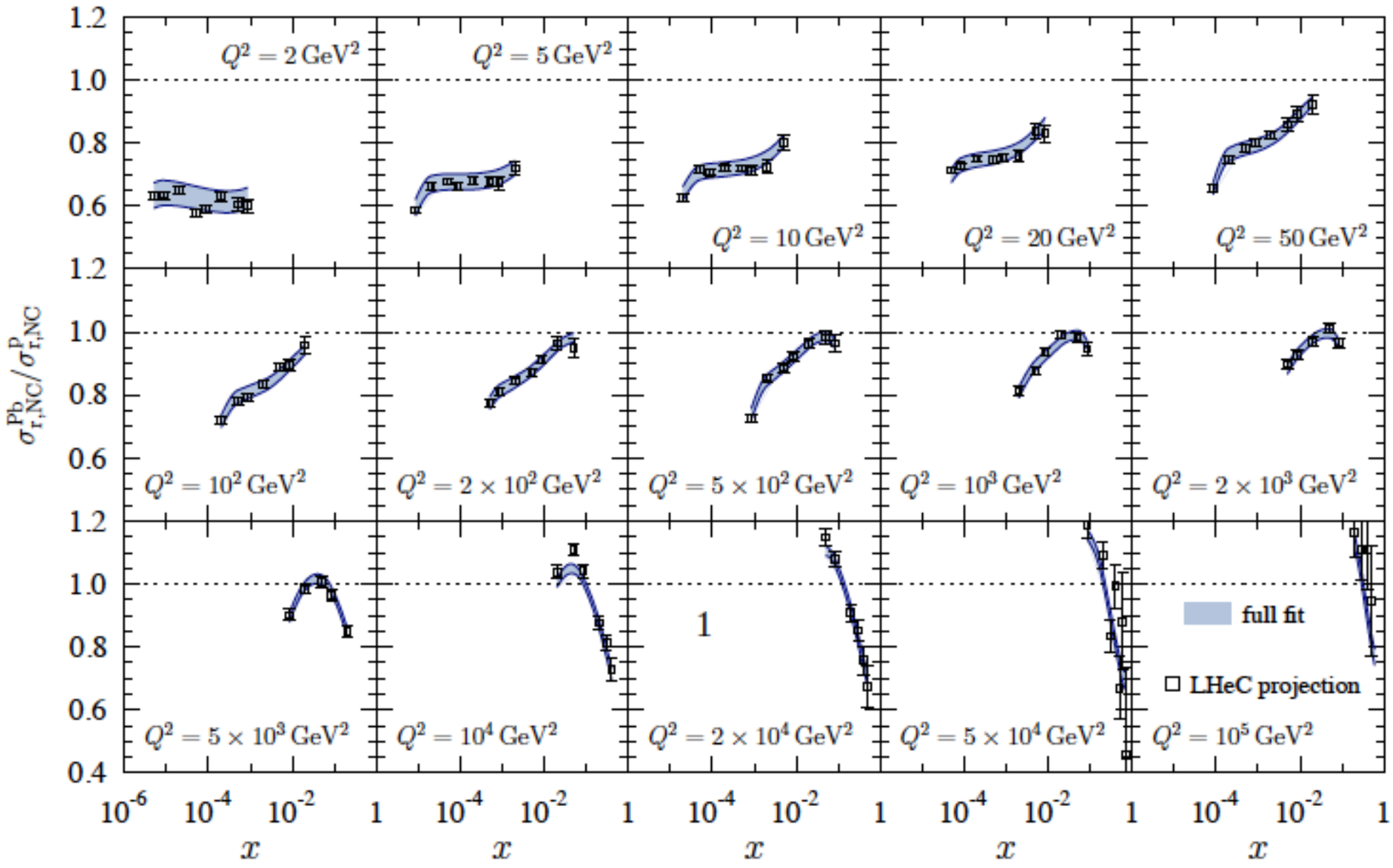

EPPS16*: results

- Large effect of NC+CC LHeC pseudodata, and of charm on the glue at small x.
- Limitation on u/d decomposition inherent to almost isospin symmetric nuclei (u/d difference suppressed by 2Z/A-1).

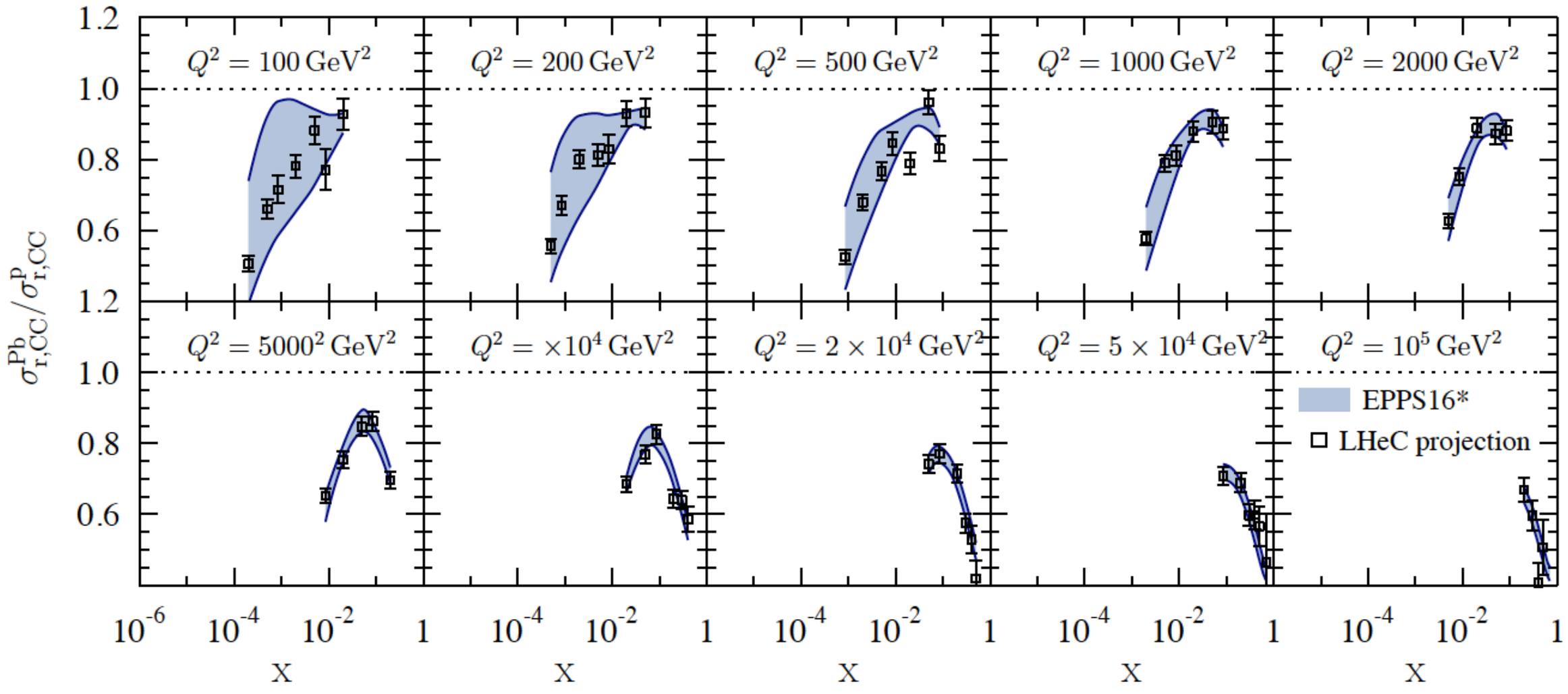

EPPS16*: results

- Large effect of NC+CC LHeC pseudodata, and of charm on the glue at small x.
- Limitation on u/d decomposition inherent to almost isospin symmetric nuclei (u/d difference suppressed by 2Z/A-1).

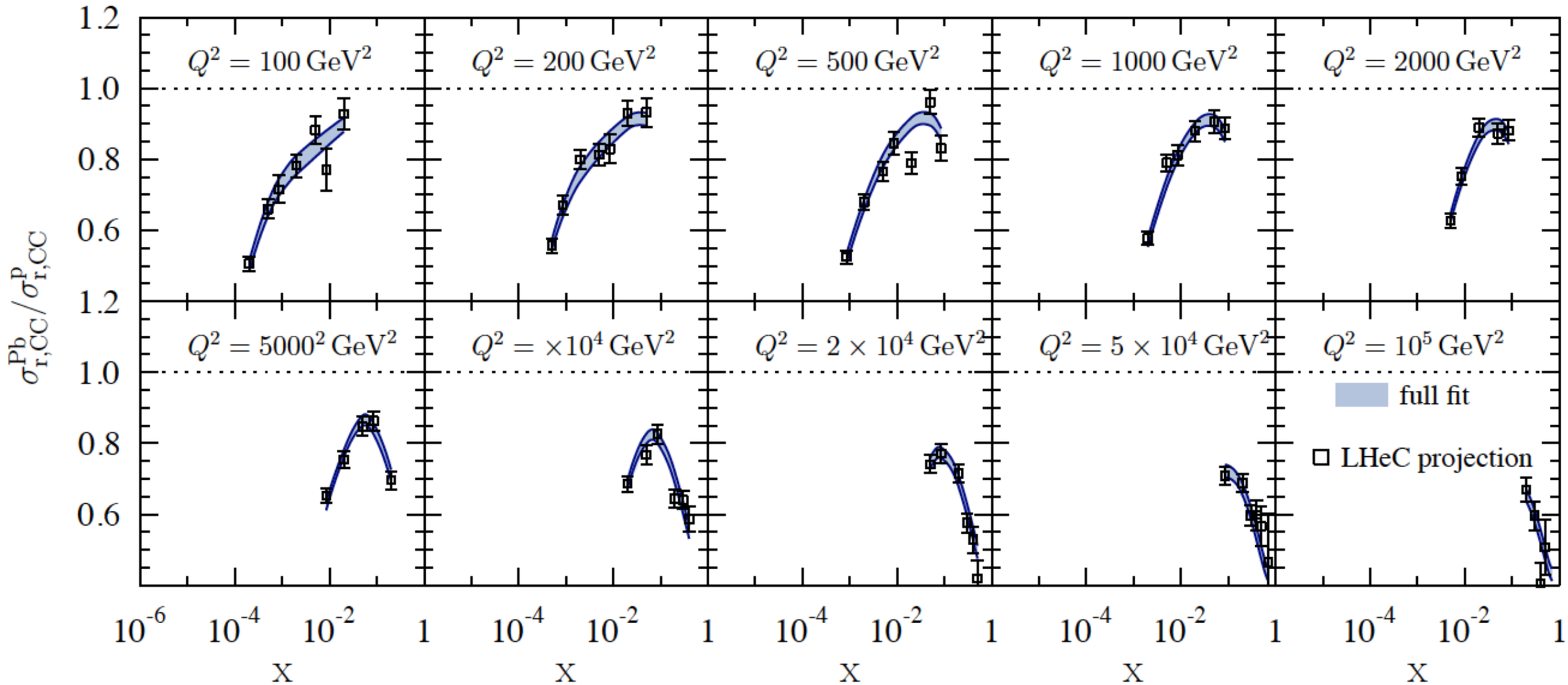

EPPS16*: results

- Large effect of NC+CC LHeC pseudodata, and of charm on the glue at small x.
- Limitation on u/d decomposition inherent to almost isospin symmetric nuclei (u/d difference suppressed by 2Z/A-1).

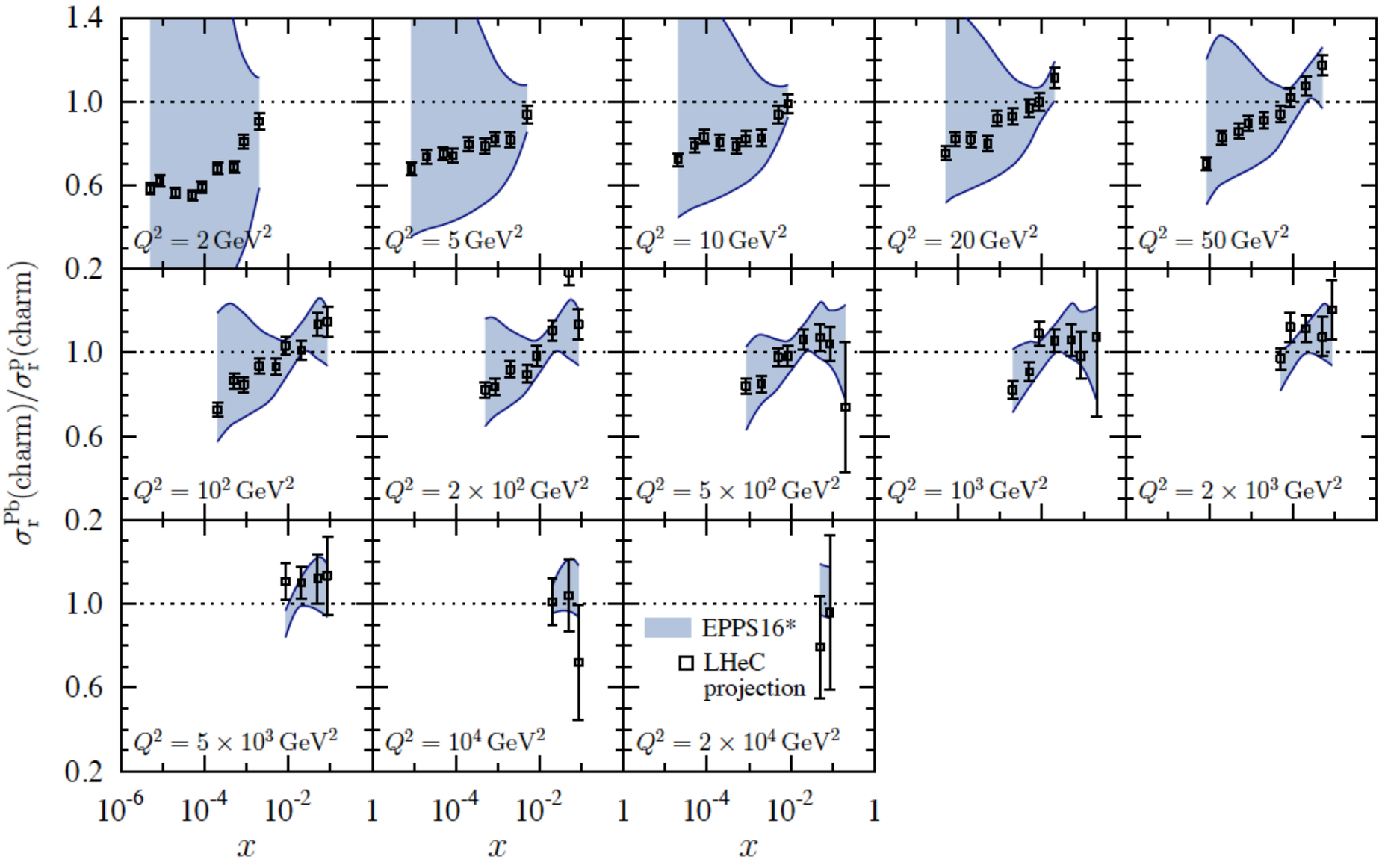

EPPS16*: results

- Large effect of NC+CC LHeC pseudodata, and of charm on the glue at small x.
- Limitation on u/d decomposition inherent to almost isospin symmetric nuclei (u/d difference suppressed by 2Z/A-1).

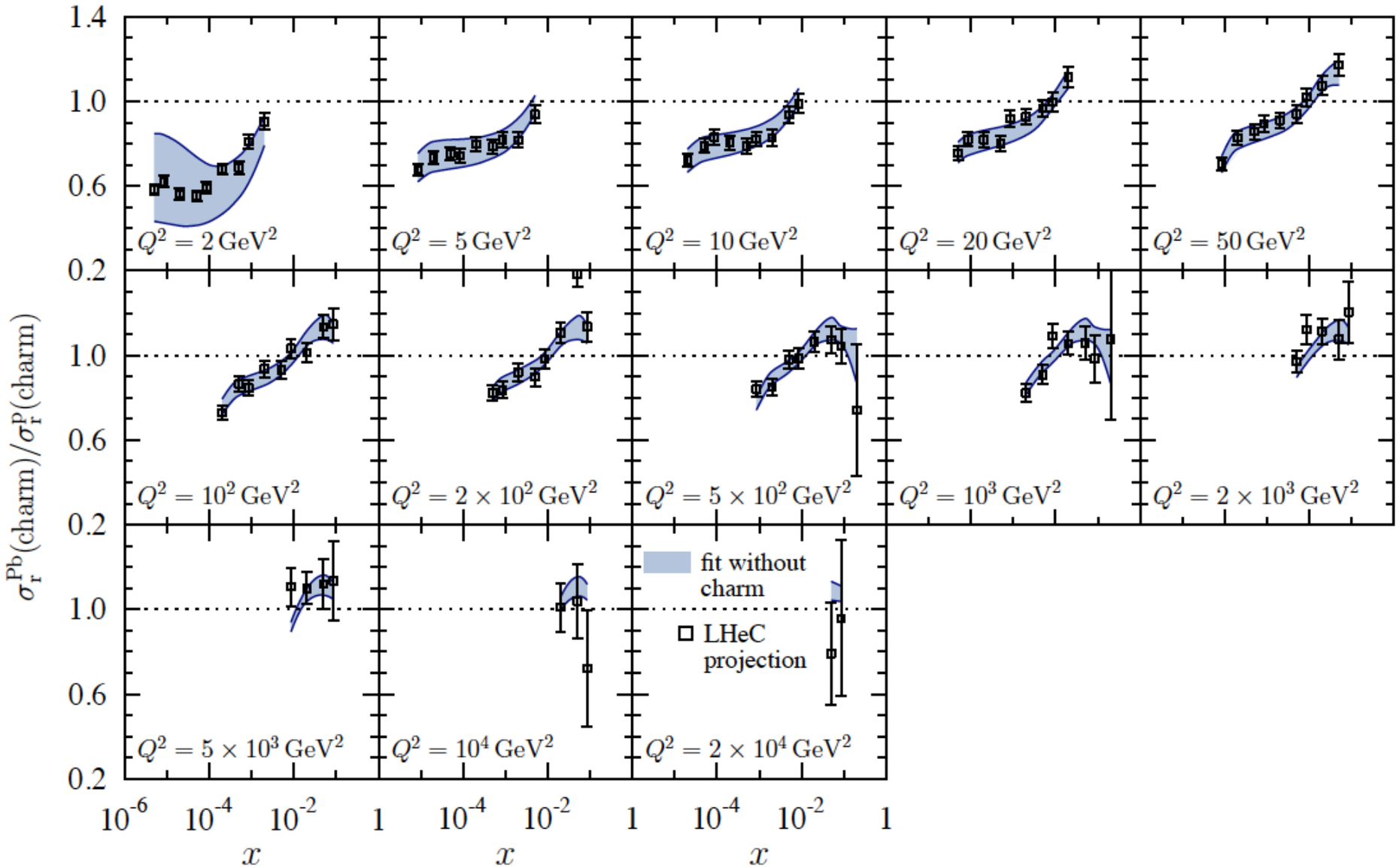

EPPS16*: results

- Large effect of NC+CC LHeC pseudodata, and of charm on the glue at small x.
- Limitation on u/d decomposition inherent to almost isospin symmetric nuclei (u/d difference suppressed by 2Z/A-1).

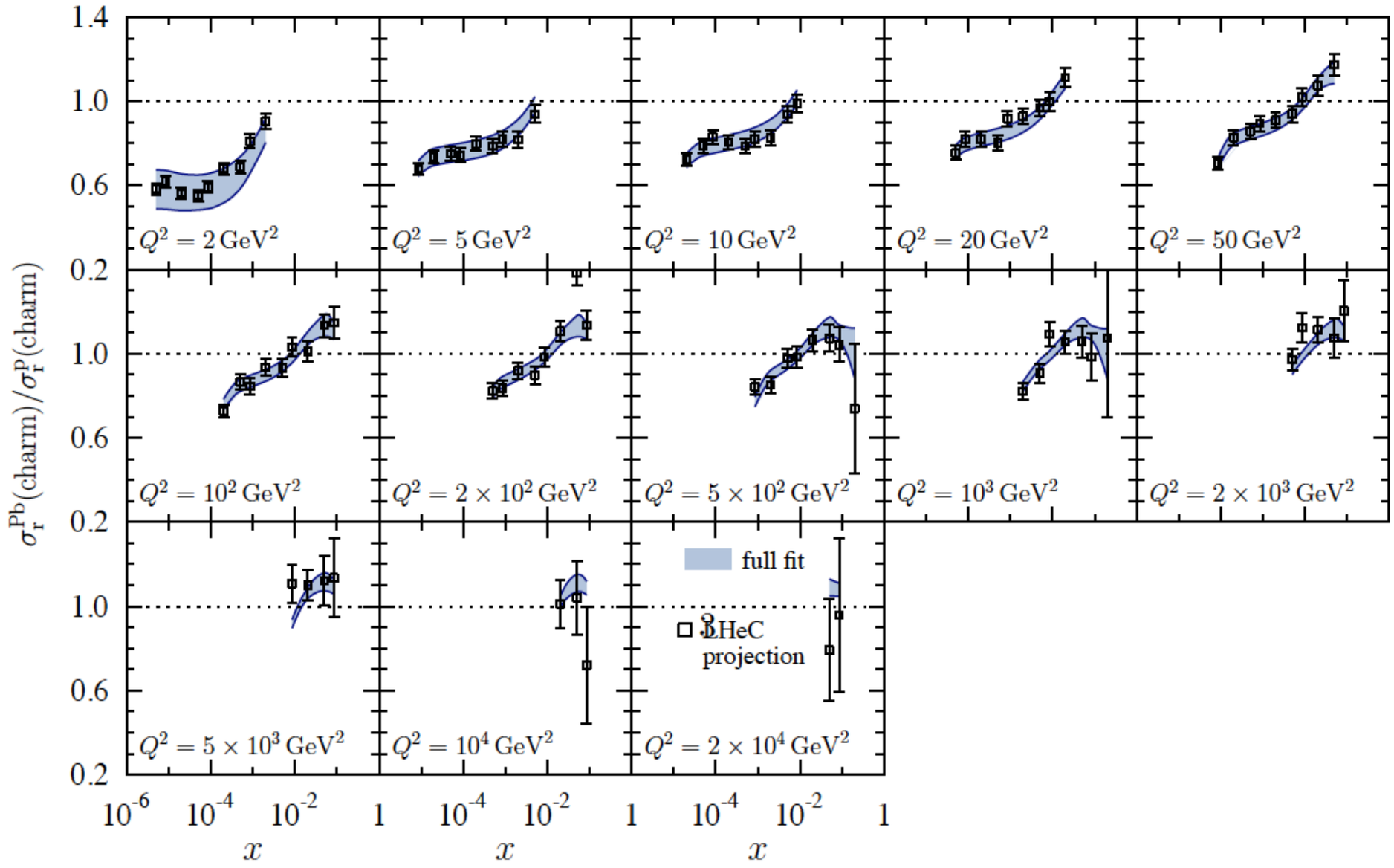

Impact of LHeC pseudodata

- Large effect of NC+CC LHeC pseudodata, and of charm on the glue at small x.
- Limitation on u/d decomposition inherent to almost isospin symmetric nuclei (u/d difference suppressed by 2Z/A-1).

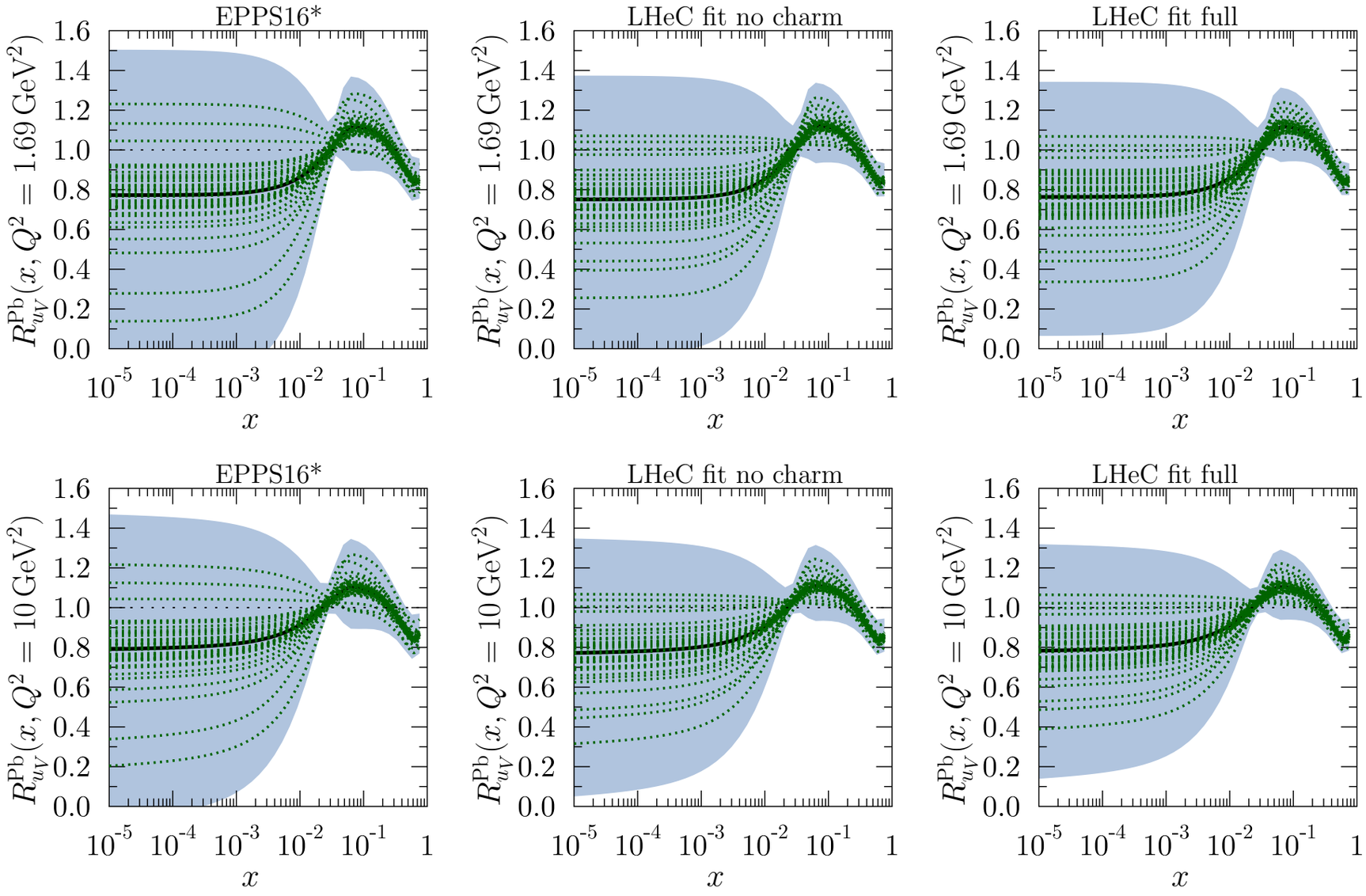

Impact of LHeC pseudodata

- Large effect of NC+CC LHeC pseudodata, and of charm on the glue at small x.
- Limitation on u/d decomposition inherent to almost isospin symmetric nuclei (u/d difference suppressed by 2Z/A-1).

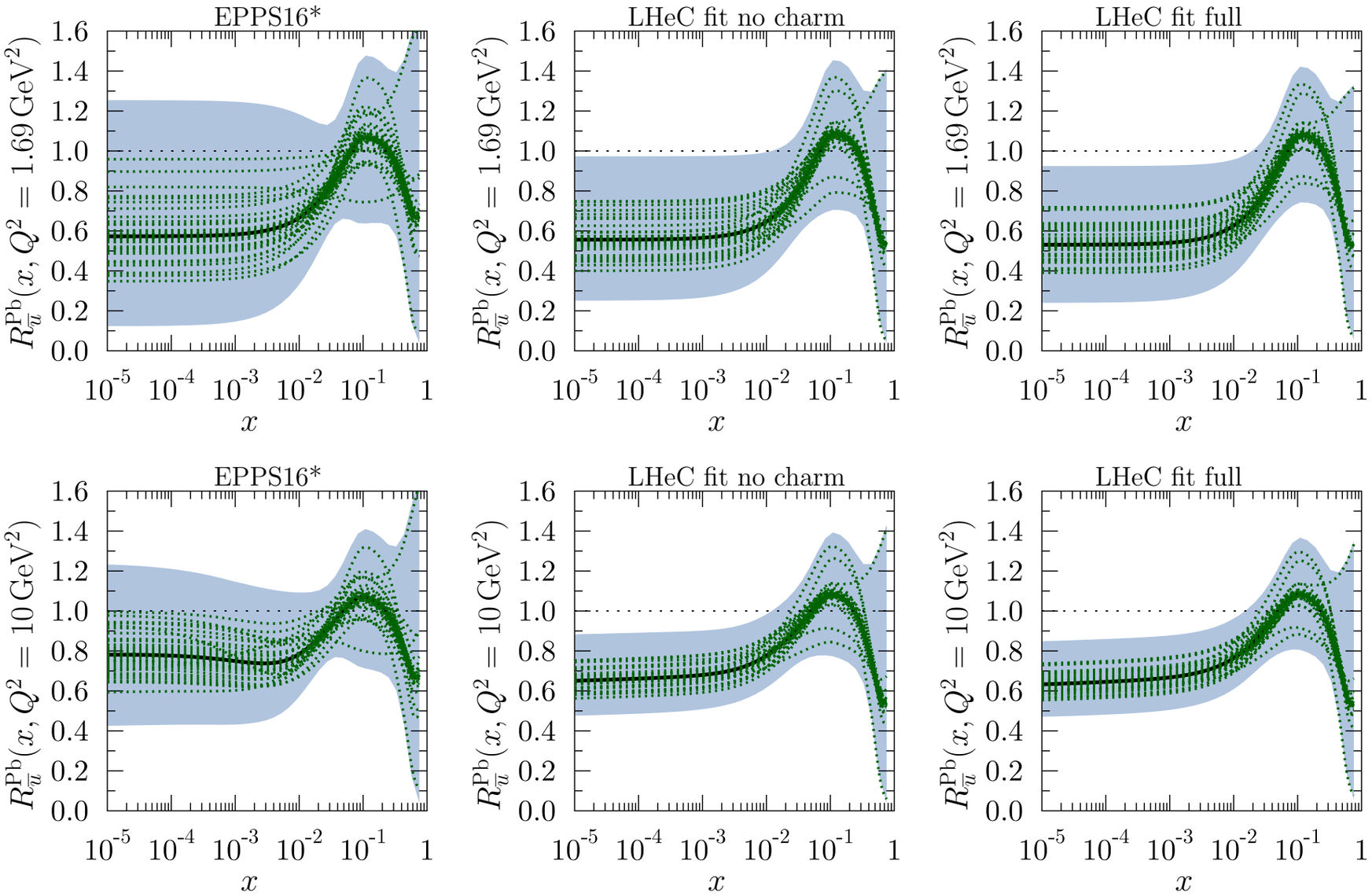

Impact of LHeC pseudodata

- Large effect of NC+CC LHeC pseudodata, and of charm on the glue at small x.
- Limitation on u/d decomposition inherent to almost isospin symmetric nuclei (u/d difference suppressed by 2Z/A-1).

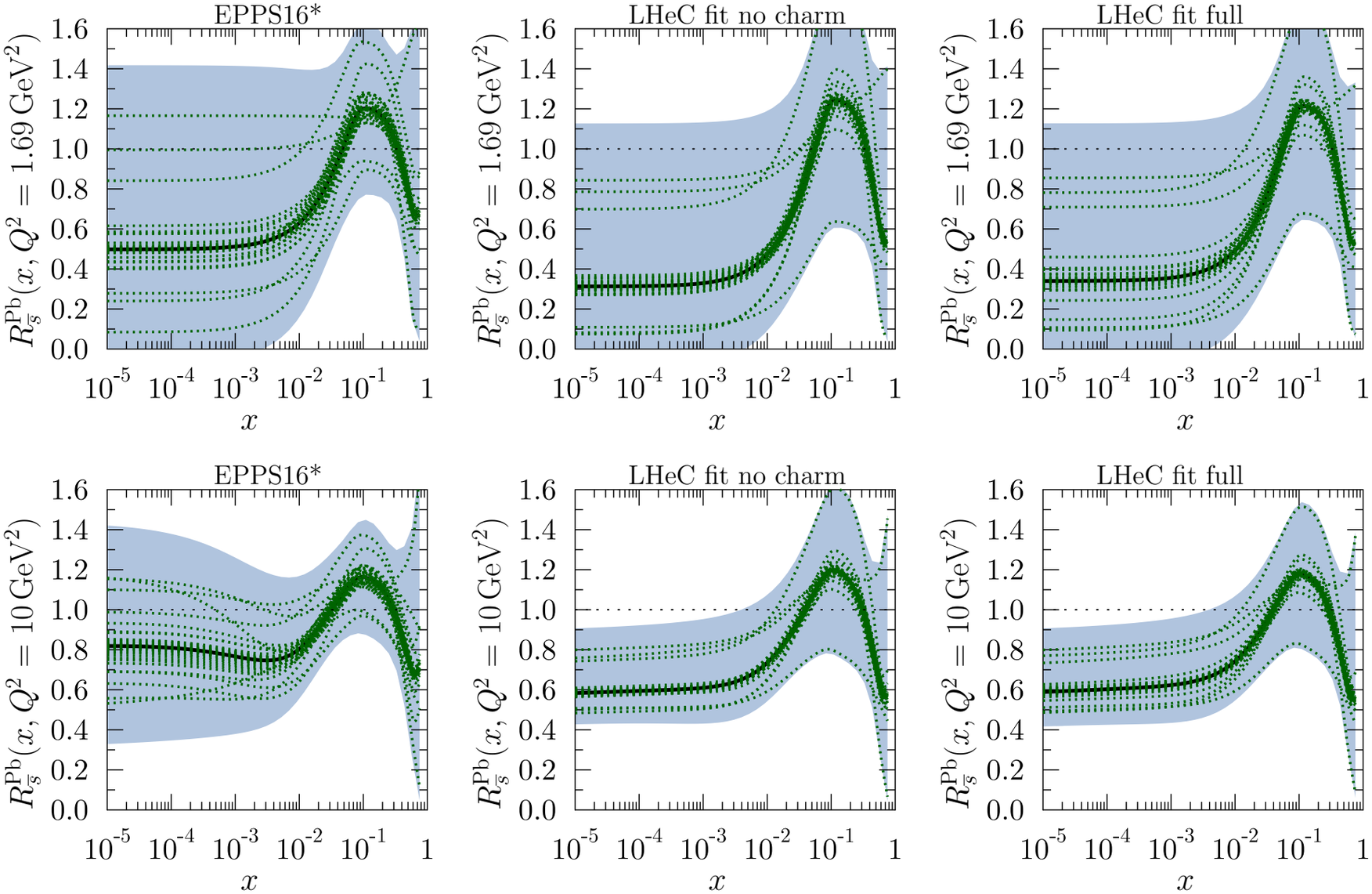

Impact of LHeC pseudodata

- Large effect of NC+CC LHeC pseudodata, and of charm on the glue at small x.
- Limitation on u/d decomposition inherent to almost isospin symmetric nuclei (u/d difference suppressed by 2Z/A-1).

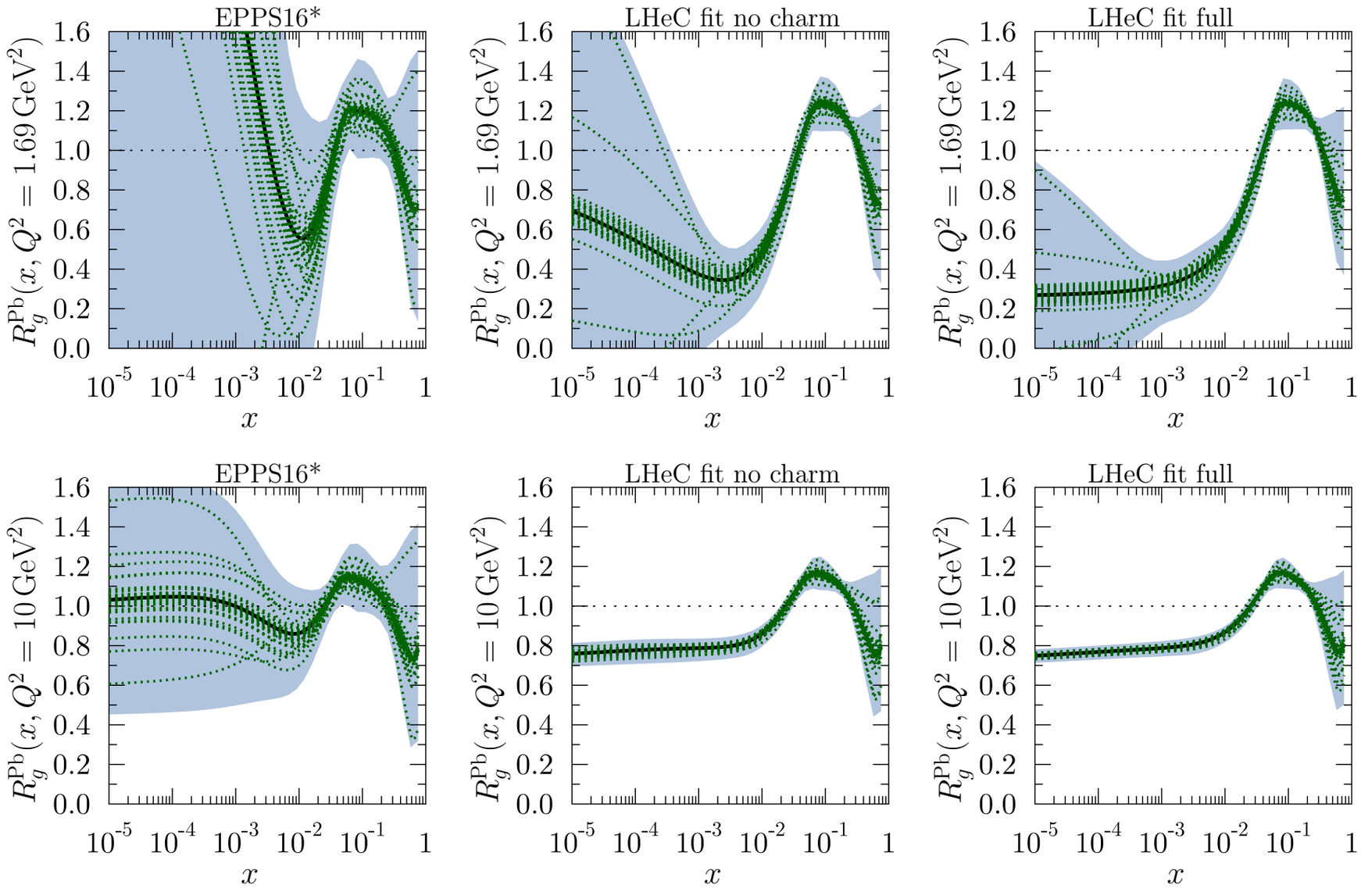

Impact of LHeC pseudodata

- Large effect of NC+CC LHeC pseudodata, and of charm on the glue at small x.
- Limitation on u/d decomposition inherent to almost isospin symmetric nuclei (u/d difference suppressed by 2Z/A-1).

- Possible further improvements: beauty, c-tagged CC for strange.

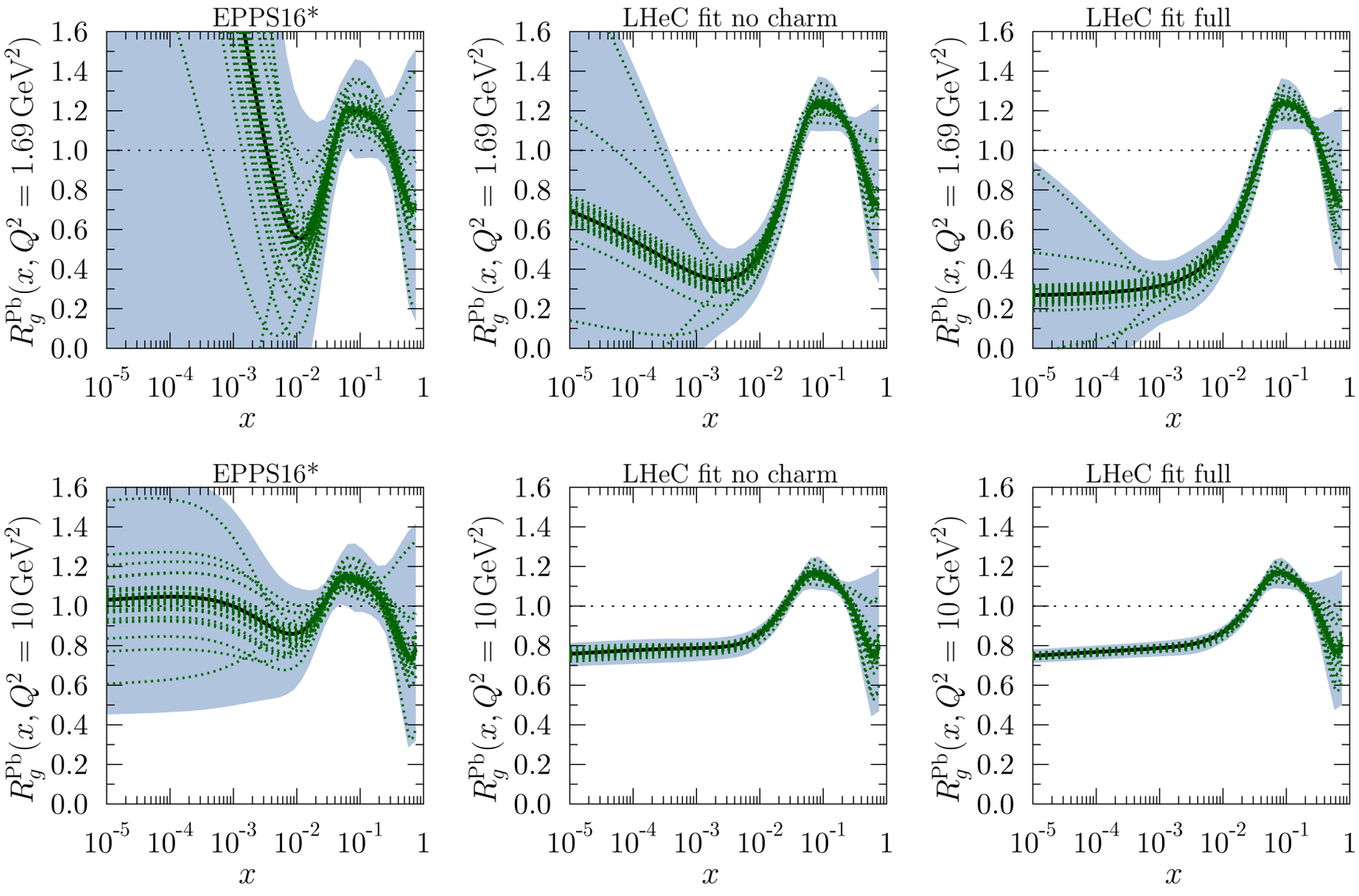

Physics of nuclear shadowing

- So far we have discussed the DGLAP fits to nuclear data on structure functions
- Nuclear effects are **parametrized** at low scales, assumed to be non-perturbative
- Structure functions calculated from **collinear** factorization
- Nuclear pdfs evolved using **linear DGLAP** evolution
- This does not have to be true, may be violated by **power corrections**
- Linear DGLAP evolution may also be insufficient: **nonlinear evolution**

Physics of nuclear shadowing

- So far we have discussed the DGLAP fits to nuclear data on structure functions
- Nuclear effects are **parametrized** at low scales, assumed to be non-perturbative
- Structure functions calculated from **collinear** factorization
- Nuclear pdfs evolved using **linear DGLAP** evolution
- This does not have to be true, may be violated by **power corrections**
- Linear DGLAP evolution may also be insufficient: **nonlinear evolution**

$$F_i(x,Q^2) = \sum_j \int_x^1 dy\, C_i^j(x/y, Q^2, \alpha_s)\, f_j(y,Q^2) + \mathcal{O}(\frac{\Lambda^2}{Q^2})$$

These questions could be answered by EIC or LHeC/FCC-eh, when more, very precise data are available.

Physics of nuclear shadowing

- So far we have discussed the DGLAP fits to nuclear data on structure functions
- Nuclear effects are **parametrized** at low scales, assumed to be non-perturbative
- Structure functions calculated from **collinear** factorization
- Nuclear pdfs evolved using **linear DGLAP** evolution
- This does not have to be true, may be violated by **power corrections**
- Linear DGLAP evolution may also be insufficient: **nonlinear evolution**

$$F_i(x,Q^2) = \sum_j \int_x^1 dy\, C_i^j(x/y, Q^2, \alpha_s)\, f_j(y,Q^2) + \mathcal{O}(\frac{\Lambda^2}{Q^2})$$

These questions could be answered by EIC or LHeC/FCC-eh, when more, very precise data are available.

Physics of the nuclear shadowing:

- **Glauber rescattering**.
- Gribov shadowing: relation to **diffraction**.
- High energy approaches: parton **saturation**.

Multiple scattering: generalities

Consider scattering of a scalar particle off a nucleus with mass number A
The scattering center plus the interaction vertex is given by the forward scattering amplitude on a nucleon times the nuclear density.

Light-cone coordinates $v_\pm = v_0 \pm v_z$ $v = (v_+, v_-, v_T)$

Projectile propagates along the '+' direction.

Single scattering

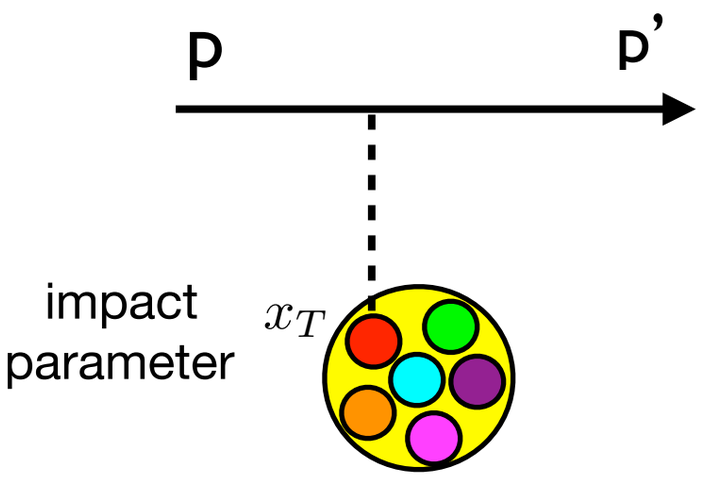

Define momentum transfer $q = p - p'$

Projectile-nucleon $it(q=0) = it_{\rm forw} = -\sigma$

n-scattering projectile-nucleus $i\mathcal{T}_n(q=0) = -\sigma_A^n$

Single scattering

Amplitude for single scattering

$$c(p_+,p'_+)i\mathcal{T}_1(q) = it_{\rm forw}\ A(p_+ + p'_+)\int d^4x\,\rho_A(x_+,x_T)e^{ix\cdot(p'-p)} \quad = it_{\rm forw}\ c(p_+,p'_+)A\int d^2x_T\,T_A(x_T)e^{-ix_T\cdot(p'_T-p_T)}$$

Nuclear profile

$$T_A(x_T) = \int_{-\infty}^{+\infty} dx_+\,\rho_A(x_+,x_T) \qquad \int d^2b\,T_A(b) = 1$$

Normalization

$$c(p_+,p'_+) = (2\pi)2p_+\delta(p'_+ - p_+)$$

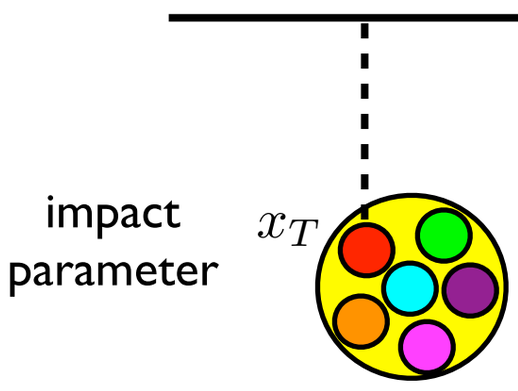

Forward limit: $q \to 0$

$$c(p_+,p'_+)i\mathcal{T}_1(q) \quad = it_{\rm forw}\ c(p_+,p'_+)A\int d^2x_T\,T_A(x_T)e^{-ix_T\cdot(p'_T-p_T)}$$

Cross section: $\sigma_A^{(1)} = \sigma A$

Particle-nucleon cross section: $\sigma = iT_N(q=0)$

Scattering cross section on a nucleus is a superposition of cross sections on individual nucleons.

Double scattering

Double scattering

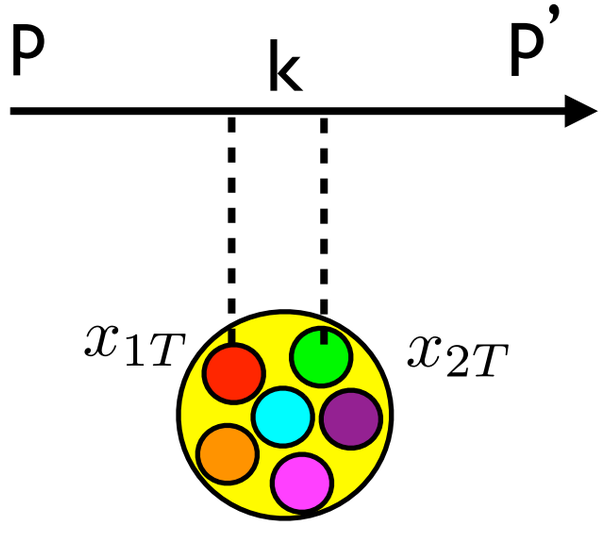

$$c(p_+,p'_+)i\mathcal{T}_2(q) = iA(A-1)(it_{\rm forw})^2\int\frac{d^4k}{(2\pi)^4}d^4x_1d^4x_2\,e^{ix_1\cdot(k-p)}$$
$$\times\, e^{ix_2\cdot(p'-k)}\frac{(p_+ + k_+)(k_+ + p'_+)}{k^2+i\epsilon}\rho_A(x_{1+},x_{1T})\rho_A(x_{2+},x_{2T})$$
$$= c(p_+,p'_+)A(A-1)(it_{\rm forw})^2$$
$$\times\int\frac{d^2k_T}{(2\pi)^2}dx_{1+}dx_{2+}d^2x_{1T}d^2x_{2T}\,e^{-ik_T^2(x_{2+}-x_{1+})/(2p_+)}$$
$$\times\, e^{-i[x_{1T}\cdot(k_T-p_T)+x_{2T}\cdot(p'_T-k_T)]}\rho_A(x_{1+},x_{1T})\rho_A(x_{2+},x_{2T})\theta(x_{2+}-x_{1+}),$$

Amplitude contains the phase, depending on the coherence length $l_c = 2p^+/k_T^2$

Low energy, incoherent limit: $p_+ \to 0$

Coherence length vanishes and $i\mathcal{T}_2(0)\to 0$ $\sigma_A^{(2)}\to 0$

All higher order scatterings also vanish, only single scattering survives

High energy, coherent limit: $p_+\to\infty$

Double scattering is a *negative* term $\sigma_A^{(2)} = -\frac{A(A-1)}{2}\int d^2b\,[T_A(b)\sigma]^2$

Double scattering

Double scattering

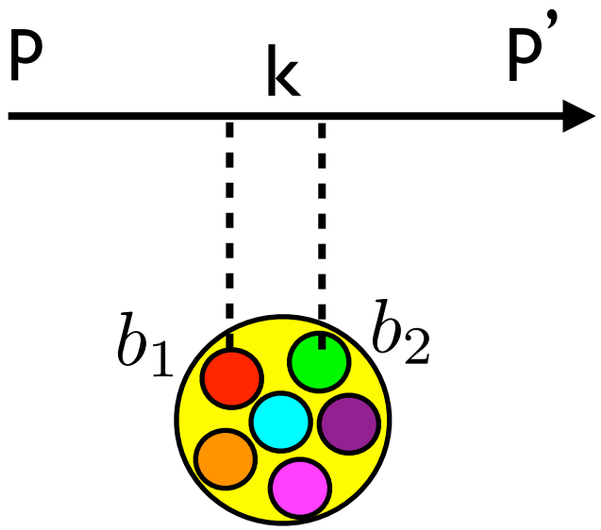

High energy, coherent limit: $p_+ \to \infty$

Coherence length: $l_c \to \infty$

Contribution from double scattering:

$$\sigma_A^{(2)} = -\frac{A(A-1)}{2}\int d^2b\,[T_A(b)\sigma]^2$$

- ✦Double scattering is a *negative* term
- ✦The cross section is smaller than the incoherent superposition of individual scatterings
- ✦Shadowing **increases** with **increasing** mass number **A**
- ✦Shadowing **increases** with **increasing single-nucleon cross section**. This in turn becomes larger for **smaller** values of **x** and **smaller** values of **Q^2**
- ✦If not integrated over impact parameter, it increased with the increasing density which is largest for smallest values of impact parameter, i.e. most central collisions.
- ✦**All these features are seen in experimental data**

Coherent scattering

In the laboratory frame where nuclear target is at rest the lifetime of a hadronic fluctuation of a photon with a given virtuality Q^2 can be estimated from uncertainty principle and the Lorentz dilation in this frame

$$\tau \simeq \frac{1}{2mx}$$

Lifetime **increases** when x **decreases**

For the hadronic fluctuation to interact with the nucleus as a whole the lifetime must be such that the length exceeds the nuclear radius R

$$\tau > R_A$$

$$x \leq \frac{1}{2mR_A}$$

$$R_A \sim A^{1/3}\ \mathrm{fm}$$

Roughly it gives the result that coherent scattering takes place when x is smaller than

$$x < 0.1A^{-1/3}$$

Glauber-Gribov scattering - dipole picture

Usually realized in the ‘dipole picture’ of deep inelastic high - energy scattering

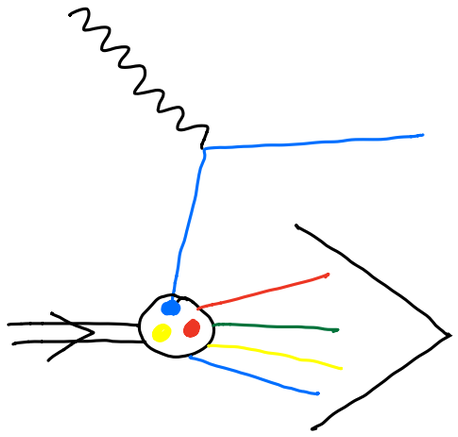

Standard DIS picture: virtual photon ‘probes’ the structure of the target - proton or a nucleus

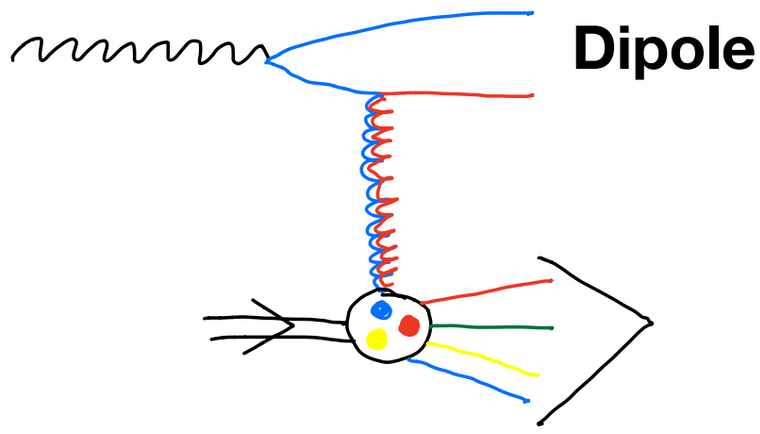

Dipole picture: virtual photon fluctuates into a quark-antiquark pair-a dipole-of a given size which subsequently interacts with a target (nucleon or nucleus). **High - energy or low x limit.**

Glauber-Gribov scattering - dipole picture

Usually realized in the ‘dipole picture’ of deep inelastic high - energy scattering

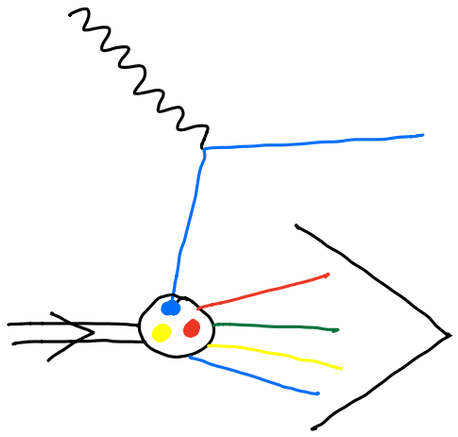

Standard DIS picture: virtual photon ‘probes’ the structure of the target - proton or a nucleus

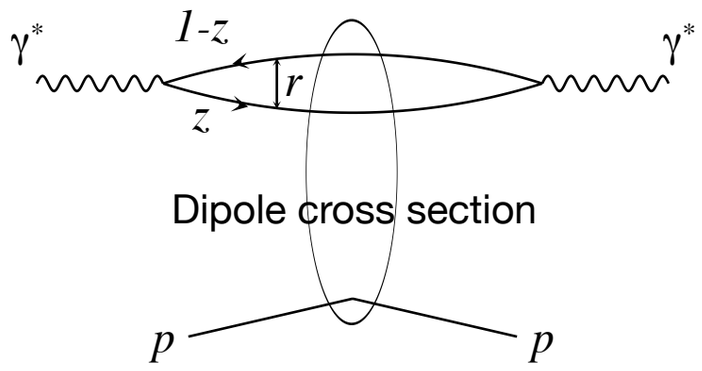

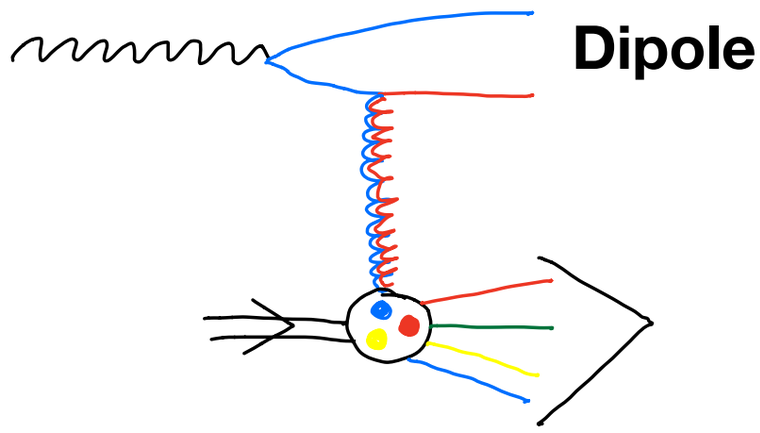

Dipole picture: virtual photon fluctuates into a quark-antiquark pair-a dipole-of a given size which subsequently interacts with a target (nucleon or nucleus). **High - energy or low x limit.**

Eikonal approximation: the dipole size is unchanged after the interaction.

Glauber-Gribov scattering - dipole picture

Usually realized in the ‘dipole picture’ of deep inelastic high - energy scattering

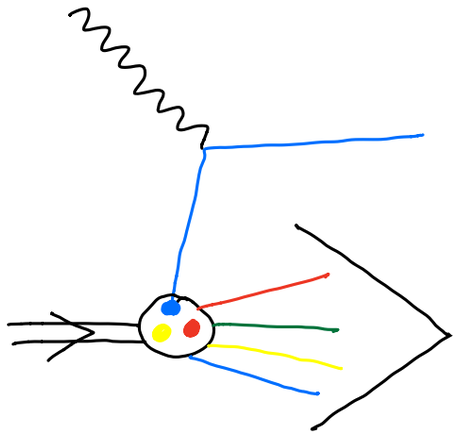

Standard DIS picture: virtual photon ‘probes’ the structure of the target - proton or a nucleus

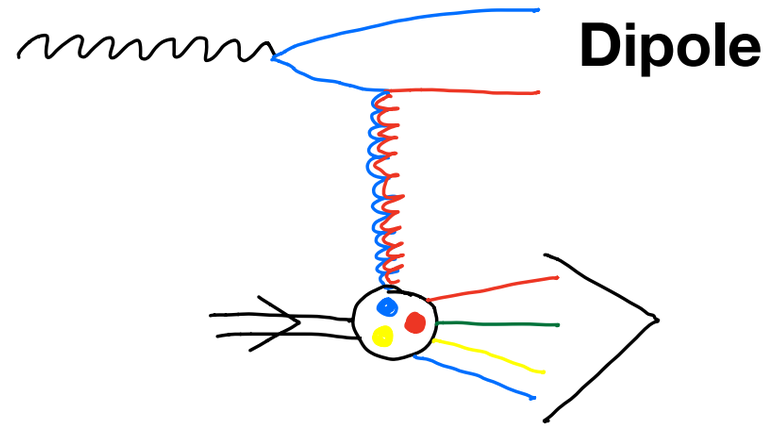

Dipole picture: virtual photon fluctuates into a quark-antiquark pair-a dipole-of a given size which subsequently interacts with a target (nucleon or nucleus). **High - energy or low x limit.**

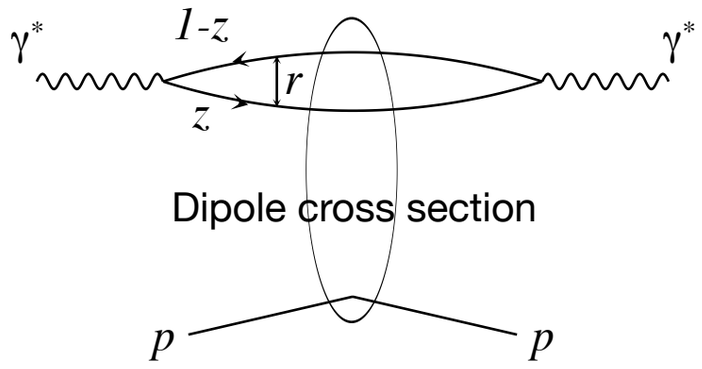

Eikonal approximation: the dipole size is unchanged after the interaction.

$$\sigma_{T,L}^{\gamma^* p}(x,Q) = \sum_f \int \mathrm{d}^2\boldsymbol{r} \int_0^1 \frac{\mathrm{d}z}{4\pi} (\Psi^*\Psi)_{T,L}^f \, \sigma_{q\bar{q}}(x,r)$$

Dipole factorization

Glauber-Gribov scattering - dipole picture

Usually realized in the ‘dipole picture’ of deep inelastic high - energy scattering

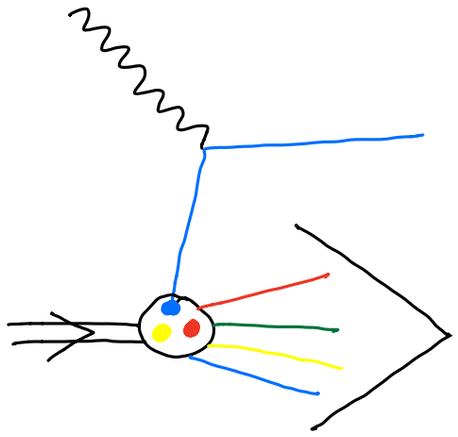

Standard DIS picture: virtual photon ‘probes’ the structure of the target - proton or a nucleus

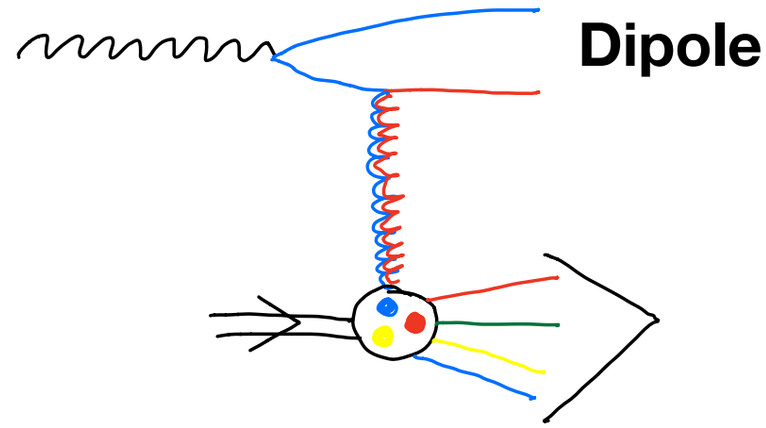

Dipole picture: virtual photon fluctuates into a quark-antiquark pair-a dipole-of a given size which subsequently interacts with a target (nucleon or nucleus). **High - energy or low x limit.**

Eikonal approximation: the dipole size is unchanged after the interaction.

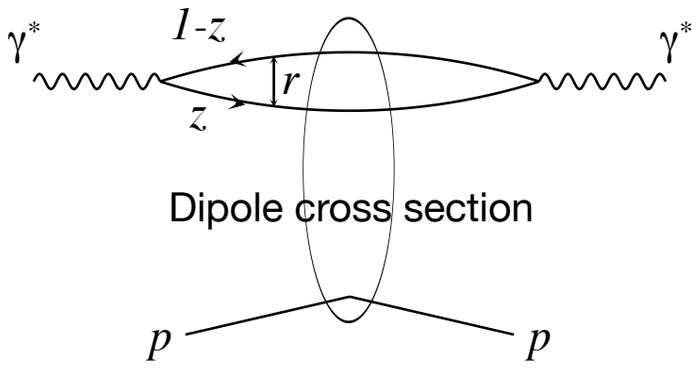

$$\sigma_{T,L}^{\gamma^* p}(x,Q) = \sum_f \int \mathrm{d}^2\boldsymbol{r} \int_0^1 \frac{\mathrm{d}z}{4\pi} (\Psi^*\Psi)_{T,L}^f \, \sigma_{q\bar{q}}(x,r)$$

Dipole factorization

Dipole cross section

Glauber-Gribov scattering - dipole picture

Usually realized in the ‘dipole picture’ of deep inelastic high - energy scattering

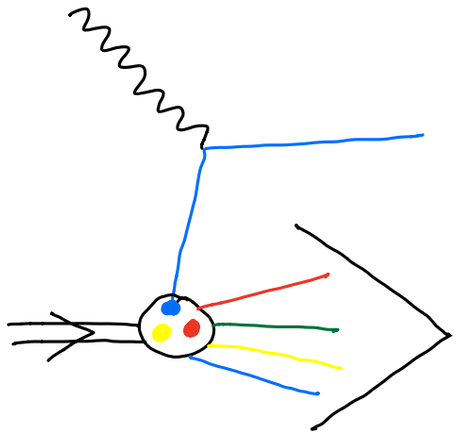

Standard DIS picture: virtual photon ‘probes’ the structure of the target - proton or a nucleus

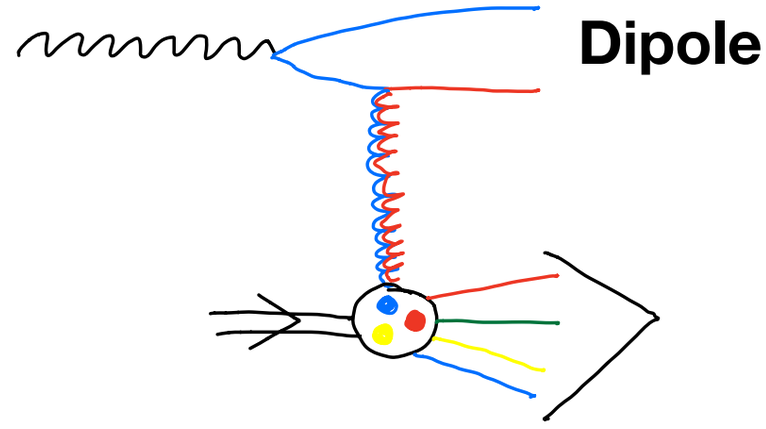

Dipole picture: virtual photon fluctuates into a quark-antiquark pair-a dipole-of a given size which subsequently interacts with a target (nucleon or nucleus). **High - energy or low x limit.**

Eikonal approximation: the dipole size is unchanged after the interaction.

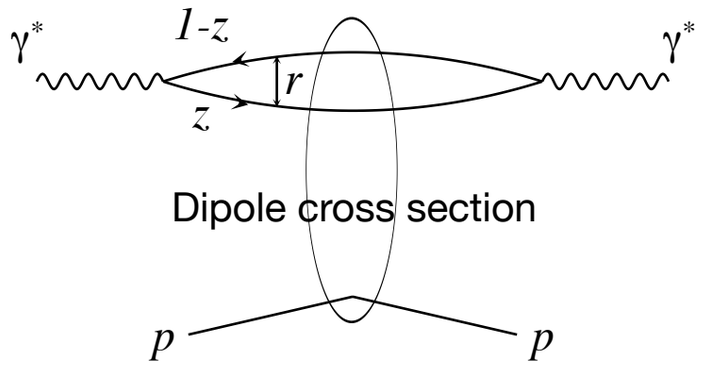

$$\sigma_{T,L}^{\gamma^* p}(x,Q) = \sum_f \int \mathrm{d}^2\boldsymbol{r} \int_0^1 \frac{\mathrm{d}z}{4\pi} (\Psi^*\Psi)_{T,L}^f \, \sigma_{q\bar{q}}(x,r)$$

Dipole factorization

Photon wave function

Dipole cross section

Dipole picture in high energy limit

Photon wave function: can be calculated in perturbative QCD in given orders of perturbation theory

Transverse photon polarization

$$(\Psi^*\Psi)^f_T \equiv \frac{1}{2}\sum_{\substack{h,\bar{h}=\pm\frac{1}{2}\\ \lambda=\pm 1}} \Psi^*_{h\bar{h},\lambda}\Psi_{h\bar{h},\lambda} = \frac{2N_c}{\pi}\alpha_{\rm em}e_f^2\left\{\left[z^2+(1-z)^2\right]\epsilon^2 K_1^2(\epsilon r)+m_f^2K_0^2(\epsilon r)\right\}$$

Longitudinal photon polarization

$$(\Psi^*\Psi)^f_L \equiv \sum_{h,\bar{h}=\pm\frac{1}{2}} \Psi^*_{h\bar{h},\lambda=0}\Psi_{h\bar{h},\lambda=0} = \frac{8N_c}{\pi}\alpha_{\rm em}e_f^2Q^2z^2(1-z)^2K_0^2(\epsilon r)$$

$$\epsilon^2 \equiv z(1-z)Q^2+m_f^2$$

Dipole cross section: includes the information about the hadronic interaction of the quark-antiquark pair with the target. It is non-perturbative, cannot be calculated from first principles (lattice?). It can be parametrized, or its evolution can be calculated perturbatively (BFKL-BK equations).

Relation to the standard gluon density in perturbative region

$$\sigma_{q\bar{q}}(x,r) \sim r^2\alpha_s(C/r^2)xg(x,C/r^2)$$

Dipole cross section can be extended to the large dipole size region: parametrization of the non-perturbative effects.

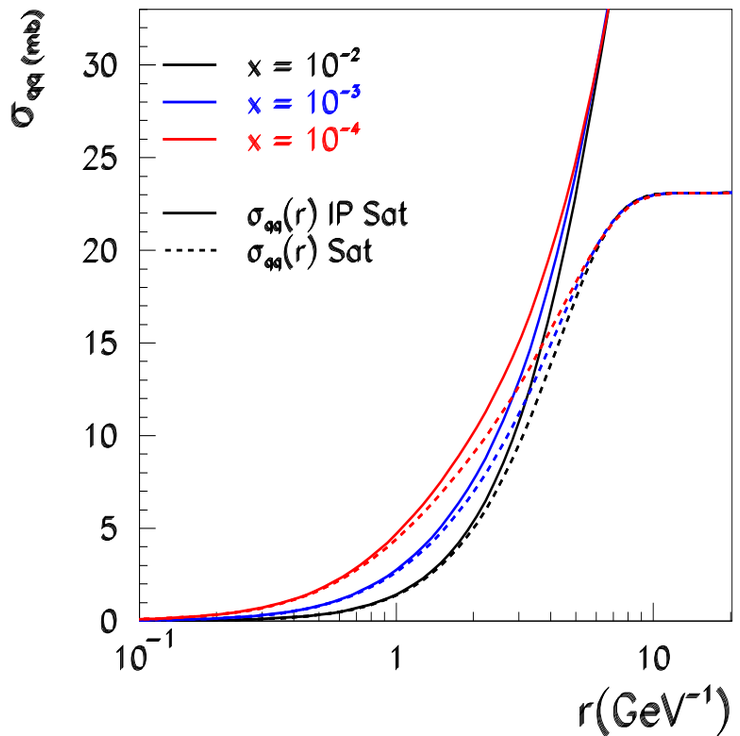

Glauber-Gribov scattering

Generalized to the dipole-nucleus scattering, by resummation of multiple scatterings in the eikonal approximation:

$$\sigma_{\text{dipole}-A}(x,r) = \int d^2b \;\; 2\left[1 - \exp\left(-\frac{1}{2}AT_A(b)\sigma_{\text{dipole}-\text{nucleon}}(x,r)\right)\right]$$

r: dipole size

b: impact parameter of the center of dipole relative to the center of nucleus

Glauber-Gribov scattering

Generalized to the dipole-nucleus scattering, by resummation of multiple scatterings in the eikonal approximation:

$$\sigma_{\text{dipole}-A}(x,r) = \int d^2b \;\; 2\left[1 - \exp\left(-\frac{1}{2}AT_A(b)\sigma_{\text{dipole}-\text{nucleon}}(x,r)\right)\right]$$

r: dipole size

b: impact parameter of the center of dipole relative to the center of nucleus

Expansion:

$$\sigma_{\text{dip}-\text{A}} = A\sigma_{\text{dip}-\text{N}} \int d^2b\, T_A(b) - \frac{1}{4}A^2\, \sigma^2_{\text{dip}-\text{N}} \int d^2b\, T_A^2(b) \; + \mathcal{O}(\sigma^3_{\text{dip}-\text{N}})$$

Single scattering Double scattering

Such model provides with unitarization of the dipole cross section for fixed impact parameter.

Unitarity limit: the scattering amplitude for fixed impact parameter is less than unity.
Conservation of probability.

Glauber-Gribov scattering

Generalized to the dipole-nucleus scattering, by resummation of multiple scatterings in the eikonal approximation:

$$\sigma_{\text{dipole}-A}(x,r) = \int d^2b \;\; 2\left[1 - \exp\left(-\frac{1}{2}AT_A(b)\sigma_{\text{dipole}-\text{nucleon}}(x,r)\right)\right]$$

r: dipole size

b: impact parameter of the center of dipole relative to the center of nucleus

Expansion:

$$\sigma_{\text{dip}-\text{A}} = A\sigma_{\text{dip}-\text{N}} \int d^2b\, T_A(b) - \frac{1}{4}A^2\, \sigma^2_{\text{dip}-\text{N}} \int d^2b\, T_A^2(b) \; + \mathcal{O}(\sigma^3_{\text{dip}-\text{N}})$$

Single scattering Double scattering

Such model provides with unitarization of the dipole cross section for fixed impact parameter.

Unitarity limit: the scattering amplitude for fixed impact parameter is less than unity.
Conservation of probability.

$$\sigma(x,r) = 2\int d^2b\, \mathcal{A}(x,r,b)$$

$$\mathcal{A}(x,r,b) \leq 1$$

Glauber-Gribov scattering

Generalized to the dipole-nucleus scattering, by resummation of multiple scatterings in the eikonal approximation:

$$\sigma_{\text{dipole}-A}(x,r) = \int d^2b \;\; 2\left[1-\exp\left(-\frac{1}{2}AT_A(b)\sigma_{\text{dipole}-\text{nucleon}}(x,r)\right)\right]$$

r: dipole size

b: impact parameter of the center of dipole relative to the center of nucleus

Expansion:

$$\sigma_{\text{dip}-\text{A}} = A\sigma_{\text{dip}-\text{N}}\int d^2b\, T_A(b) - \frac{1}{4}A^2\,\sigma^2_{\text{dip}-\text{N}}\int d^2b\, T_A^2(b) + \mathcal{O}(\sigma^3_{\text{dip}-\text{N}})$$

Single scattering Double scattering

Such model provides with unitarization of the dipole cross section for fixed impact parameter.

Unitarity limit: the scattering amplitude for fixed impact parameter is less than unity.

Conservation of probability.

$$\sigma(x,r) = 2\int d^2b\,\mathcal{A}(x,r,b)$$

$$\mathcal{A}(x,r,b) \leq 1$$

Unitarization in IPsat model with impact parameter

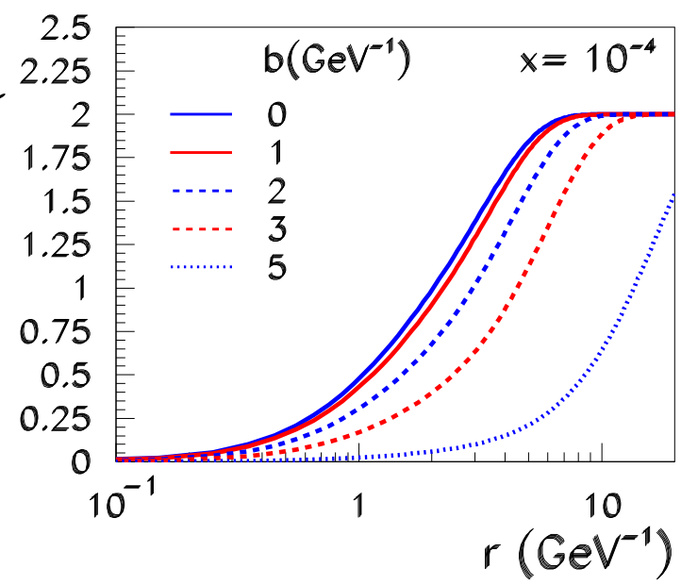

Glauber-Gribov scattering

$$\sigma_{\mathrm{dipole}-A}(x,r) = \int d^2b \;\; 2\left[1-\exp\left(-\frac{1}{2}AT_A(b)\sigma_{\mathrm{dipole}-\mathrm{nucleon}}(x,r)\right)\right]$$

Once the dipole-nucleon cross section is fixed through the fit to the proton data, the description of the nuclear data requires only the fit of the nuclear profile.

$$\sigma_{T,L}^{\gamma^* A}(x,Q) = \sum_f \int d^2r \int \frac{dz}{4\pi} \, (\Psi^*\Psi)_{T,L}^f \, \sigma_{\mathrm{dipole}-\mathrm{A}}(x,r)$$

Kowalski, Lappi, Venugopalan

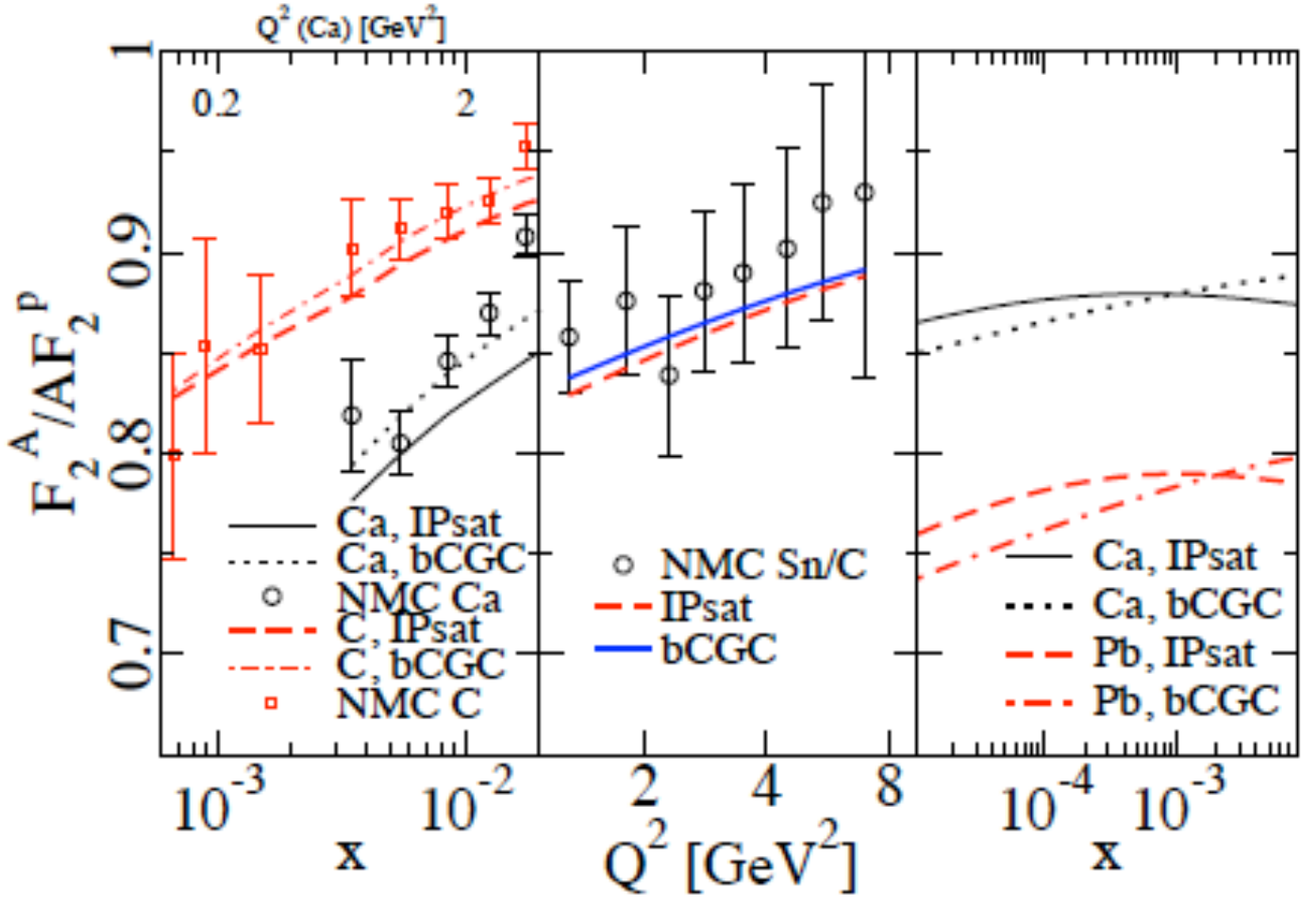

IPsat model: Gribov-Glauber model with DGLAP evolution

Good description of the Q,x and A dependence

Parton saturation

Gluon density at high energies

DIS in protons:
Observation of large scaling violations.

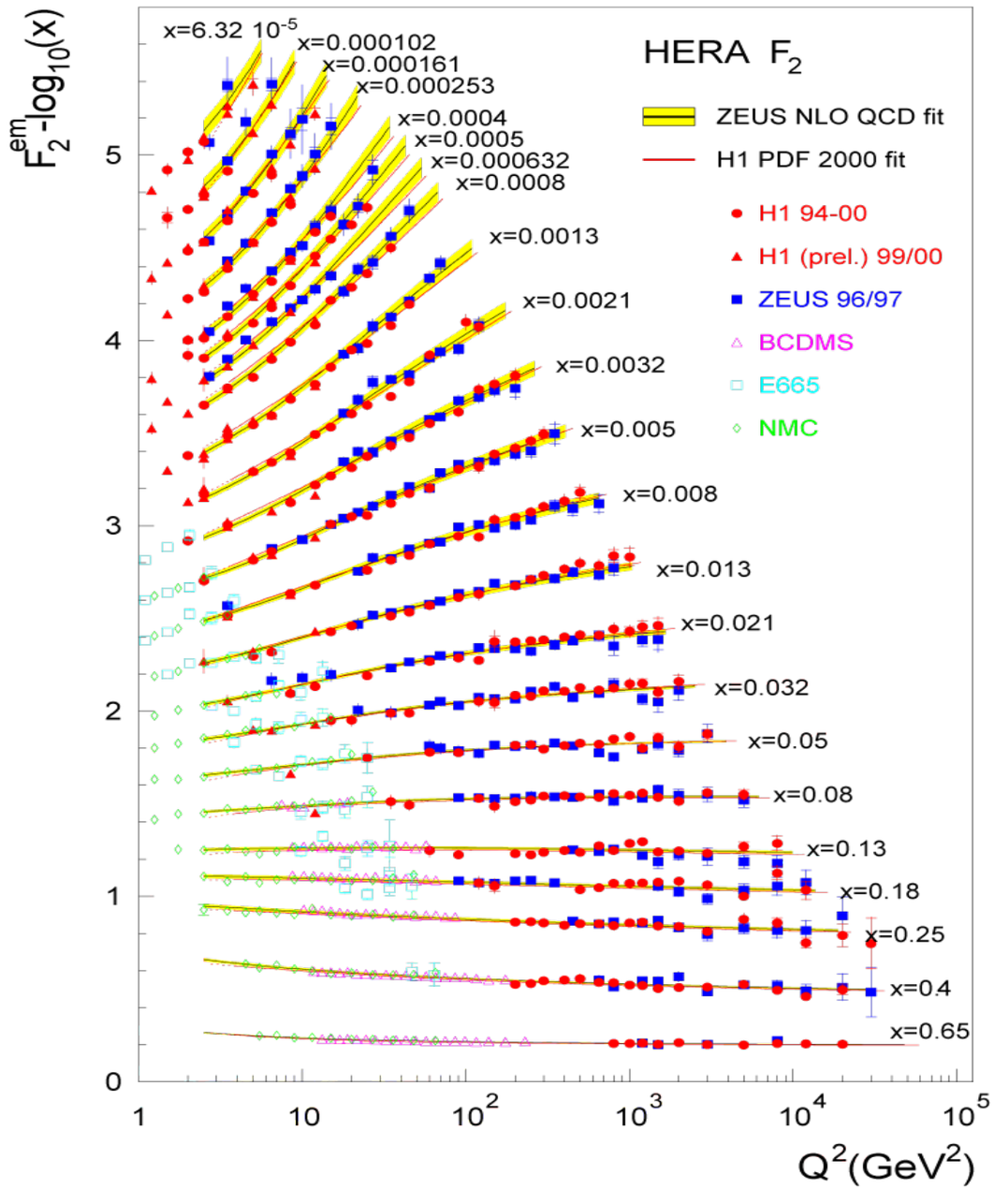

Gluon density dominates at small x!

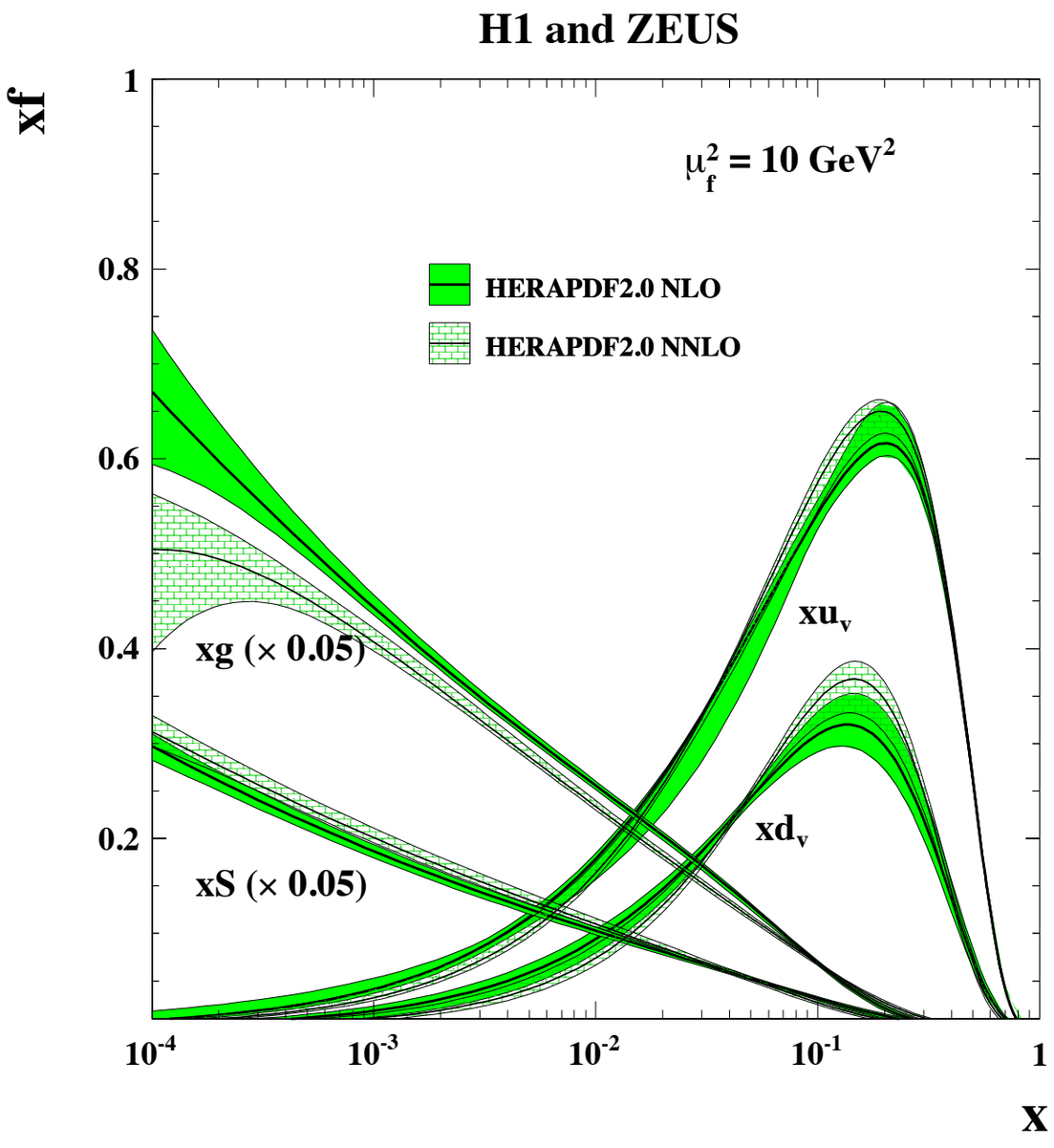

Can the gluon density rise forever?
How fast?

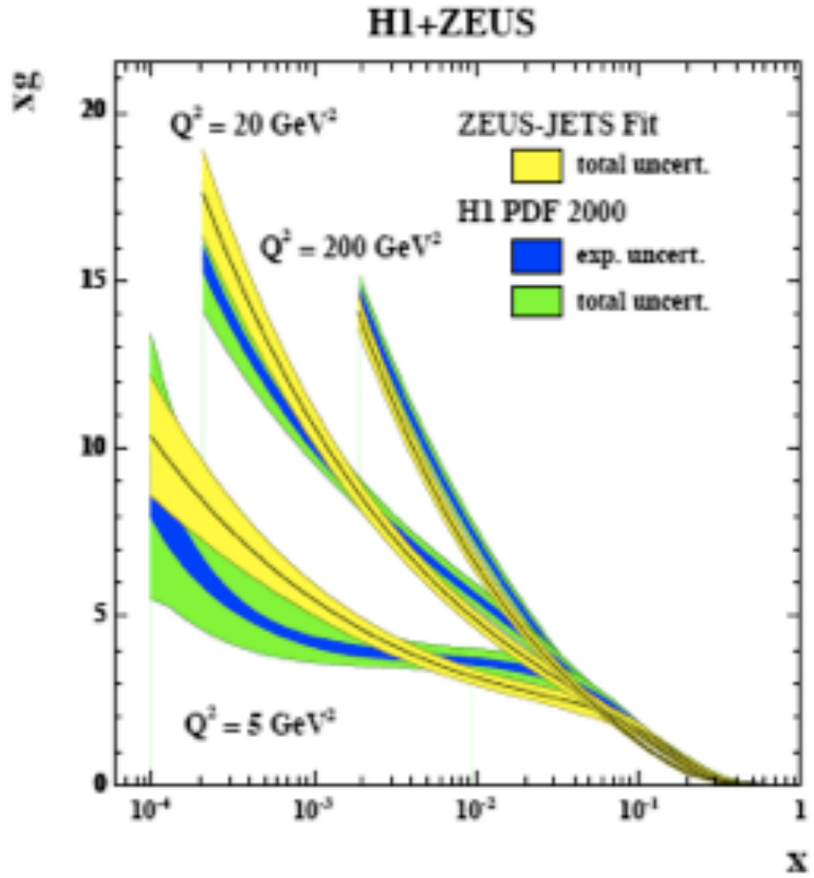

Can the gluon density rise forever?
How fast?

very large density of gluons

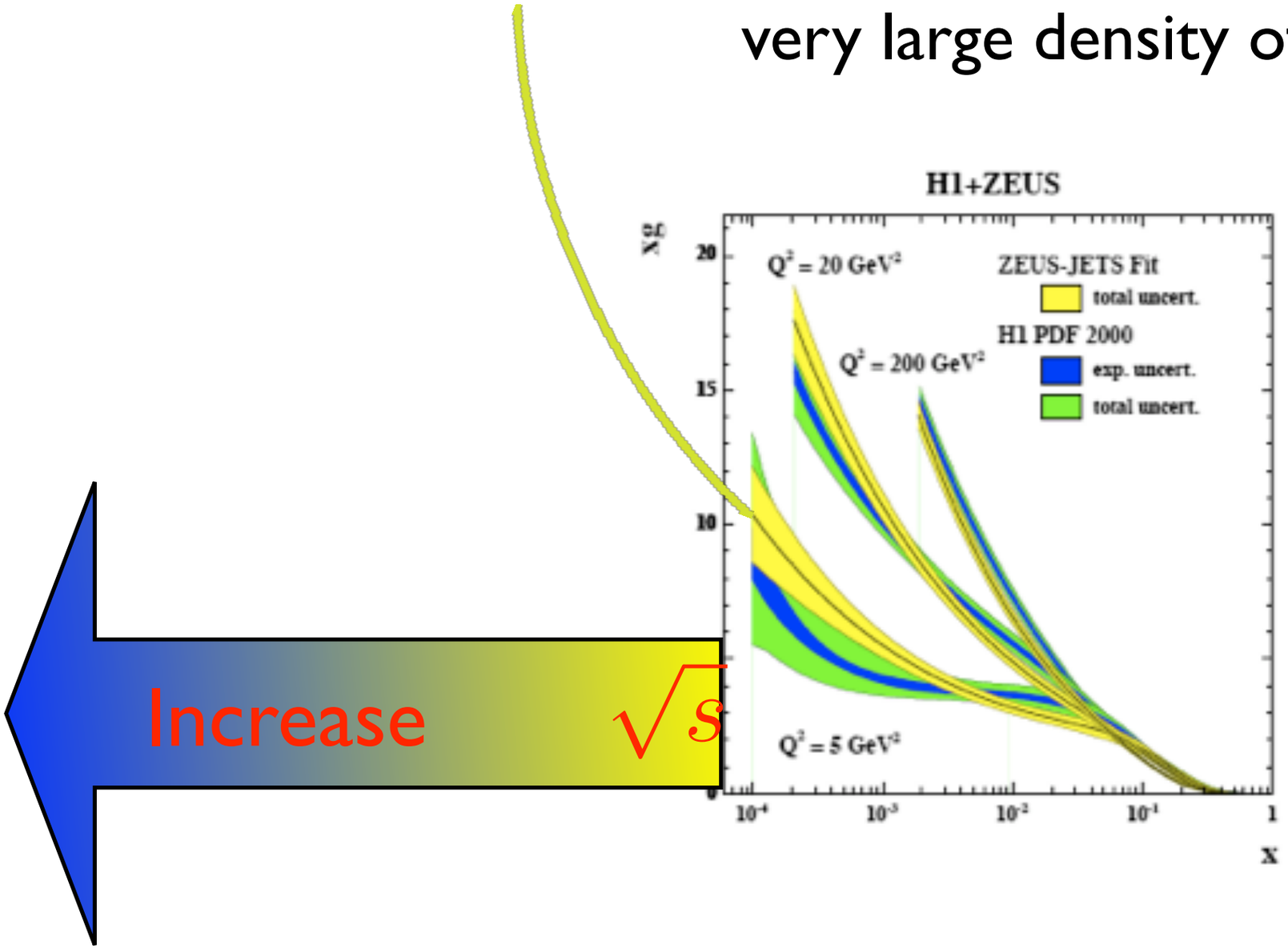

Can the gluon density rise forever?
How fast?

very large density of gluons

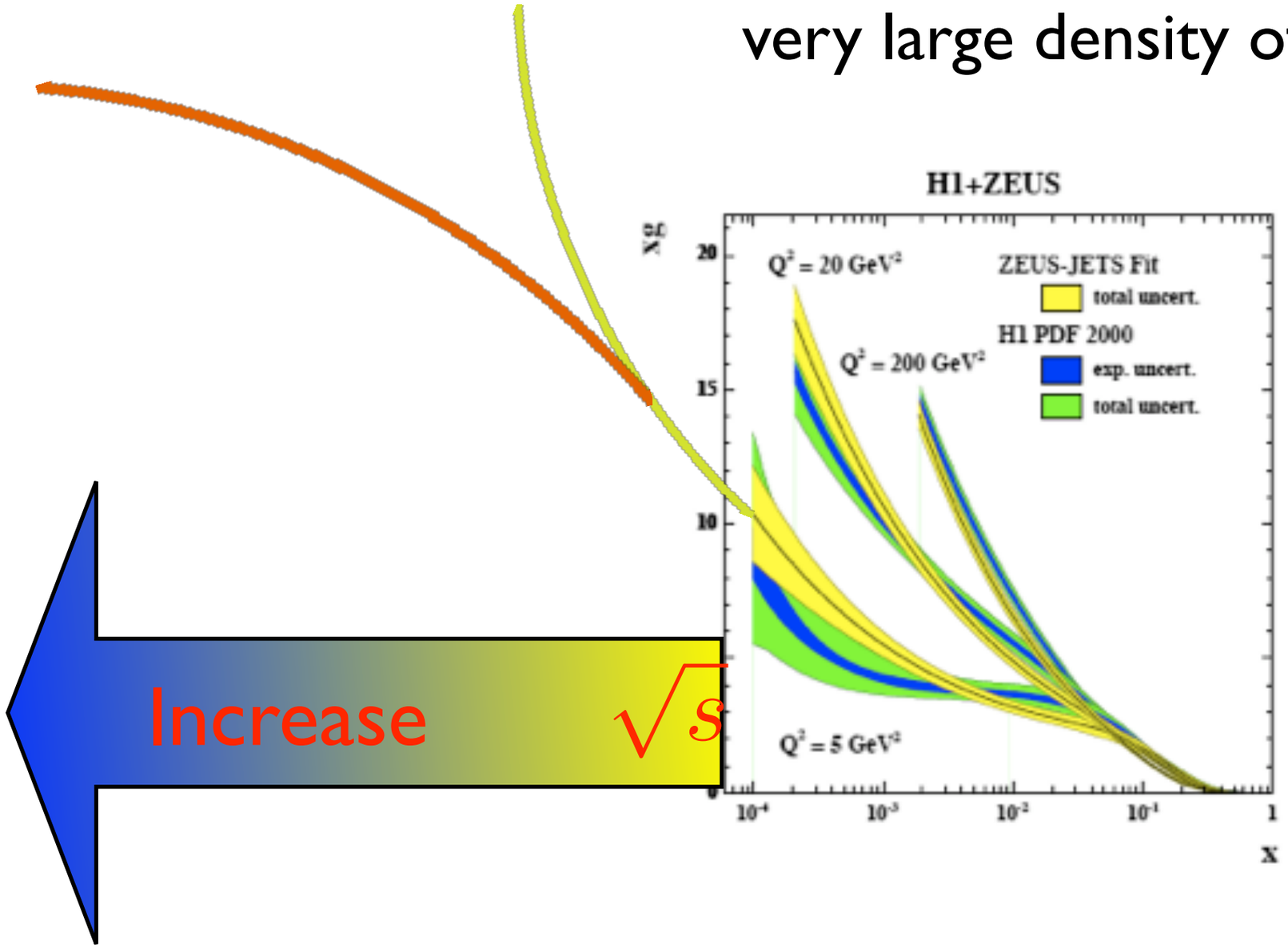

Gluon density at high energies

Gluon density at high energies

- Gluon recombination need to be taken into account in addition to the radiation of gluons at small x.

Gluon density at high energies

- Gluon recombination need to be taken into account in addition to the radiation of gluons at small x.

- On a more fundamental level it is related to the requirement of the unitarity of the strong interactions.

Gluon density at high energies

- Gluon recombination need to be taken into account in addition to the radiation of gluons at small x.
- On a more fundamental level it is related to the requirement of the unitarity of the strong interactions.
- Different approaches:

Gluon density at high energies

- Gluon recombination need to be taken into account in addition to the radiation of gluons at small x.
- On a more fundamental level it is related to the requirement of the unitarity of the strong interactions.
- Different approaches:
  - Dipole splitting, evolution and multiple scattering.(Mueller,Kovchegov)

Gluon density at high energies

- Gluon recombination need to be taken into account in addition to the radiation of gluons at small x.
- On a more fundamental level it is related to the requirement of the unitarity of the strong interactions.
- Different approaches:
  - Dipole splitting, evolution and multiple scattering.(Mueller,Kovchegov)
  - Operator product expansion for high energy scattering.(Balitsky)

Gluon density at high energies

- Gluon recombination need to be taken into account in addition to the radiation of gluons at small x.
- On a more fundamental level it is related to the requirement of the unitarity of the strong interactions.
- Different approaches:
  - Dipole splitting, evolution and multiple scattering.(Mueller,Kovchegov)
  - Operator product expansion for high energy scattering.(Balitsky)
  - Effective theory with renormalization group equation for the hadron wave function (Color Glass Condensate, McLerran, Venugopalan,Kovner,Leonidov,Iancu,Jalilian-Marian,Weigert...).

Gluon density at high energies

- Gluon recombination need to be taken into account in addition to the radiation of gluons at small x.
- On a more fundamental level it is related to the requirement of the unitarity of the strong interactions.
- Different approaches:
  - Dipole splitting, evolution and multiple scattering.(Mueller,Kovchegov)
  - Operator product expansion for high energy scattering.(Balitsky)
  - Effective theory with renormalization group equation for the hadron wave function (Color Glass Condensate, McLerran, Venugopalan,Kovner,Leonidov,Iancu,Jalilian-Marian,Weigert...).
- All these approaches have a common limit (after several simplifications): **Balitsky-Kovchegov** equation.

Gluon density at high energies

- Gluon recombination need to be taken into account in addition to the radiation of gluons at small x.
- On a more fundamental level it is related to the requirement of the unitarity of the strong interactions.
- Different approaches:
  - Dipole splitting, evolution and multiple scattering.(Mueller,Kovchegov)
  - Operator product expansion for high energy scattering.(Balitsky)
  - Effective theory with renormalization group equation for the hadron wave function (Color Glass Condensate, McLerran, Venugopalan,Kovner,Leonidov,Iancu,Jalilian-Marian,Weigert...).
- All these approaches have a common limit (after several simplifications): **Balitsky-Kovchegov** equation.
- Both small x and large A (nuclear effects) can be in principle addressed in this formalism.

fast quark

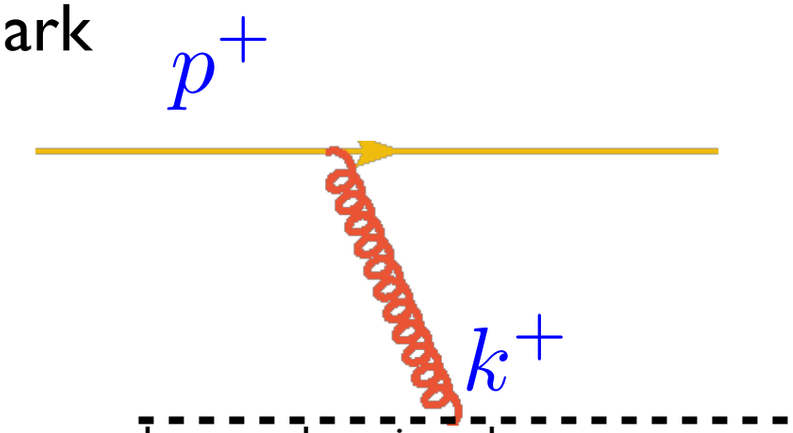

probe(for example a quark-antiquark pair from the virtual photon in DIS)

$p^+ \gg k^+$

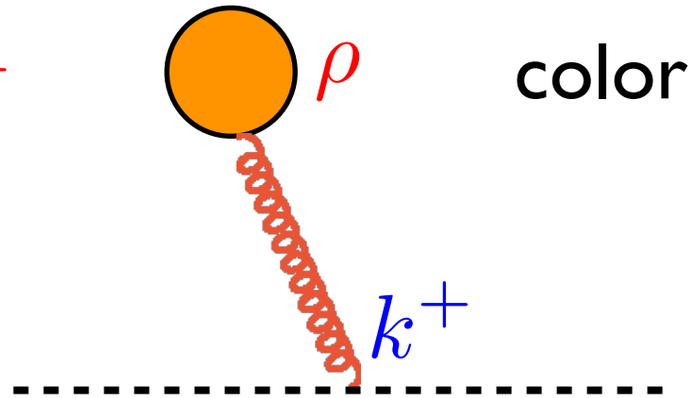

color charge

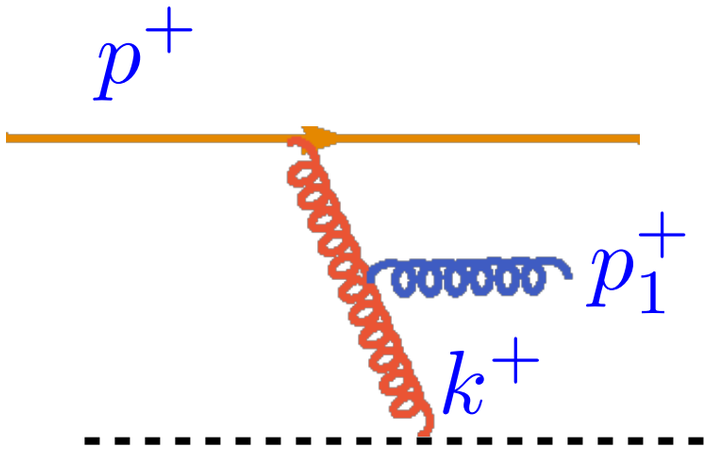

One gluon emission

$p^+ \gg p_1^+ \gg k^+$

Separation of scales (ordering in energies)

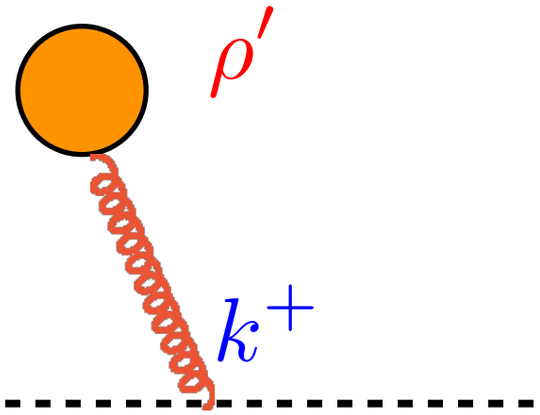

Radiation of gluons: Bremsstrahlung

Renormalized charge

The effect of the additional gluon emission is to renormalize the effective color charge.

Single charge(source)

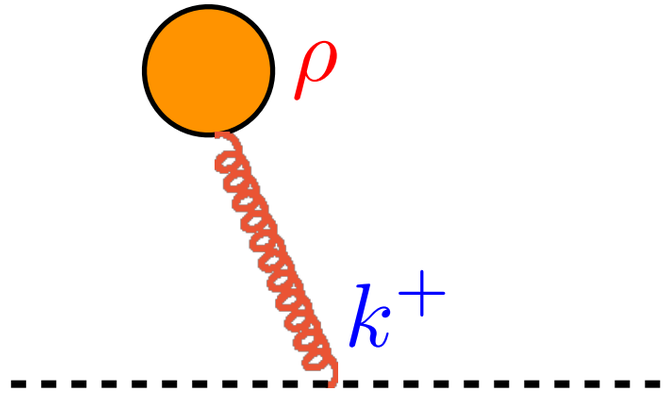

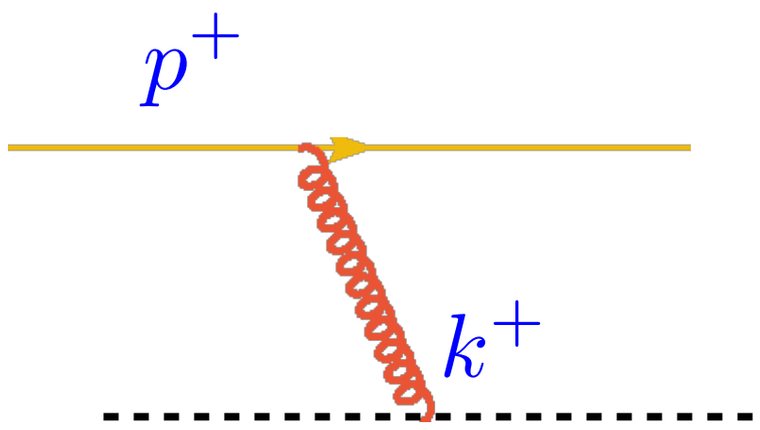

Fast nucleus

Many charges (sources)

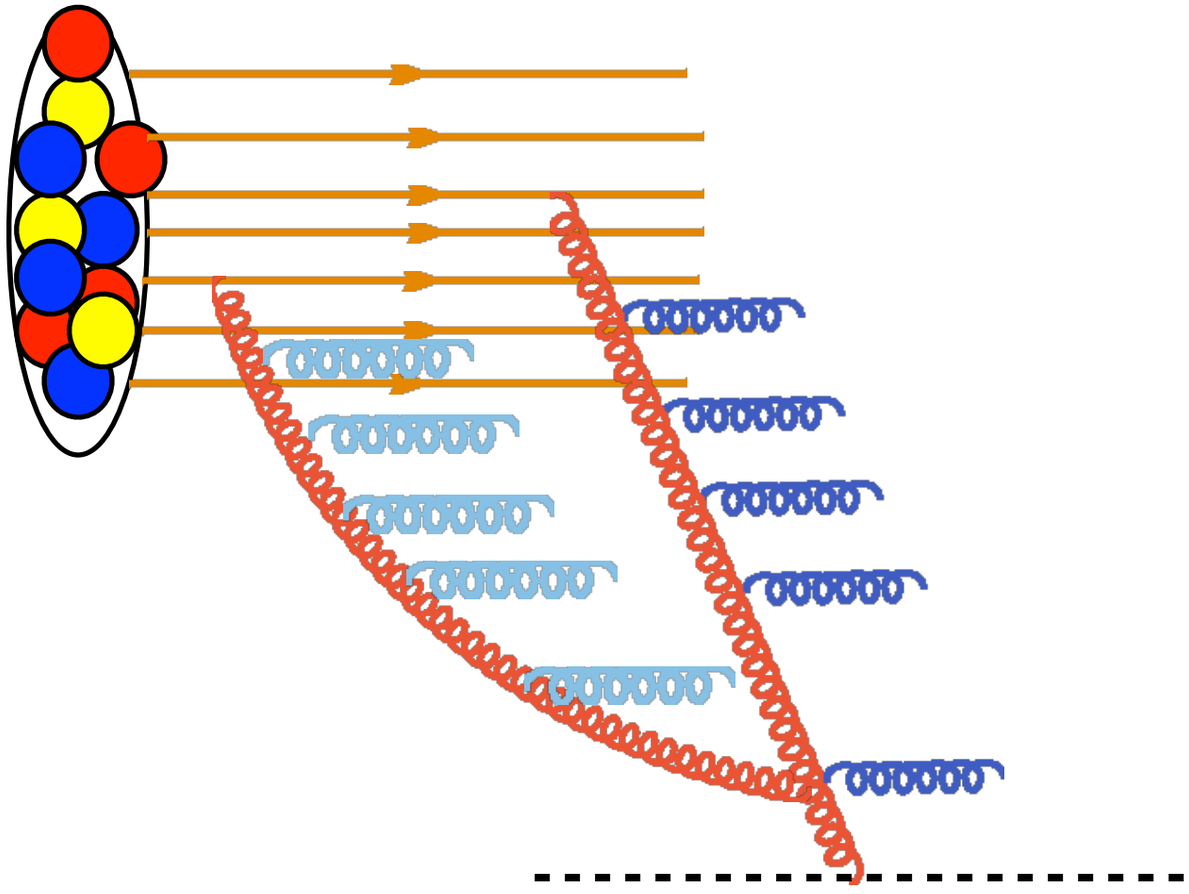

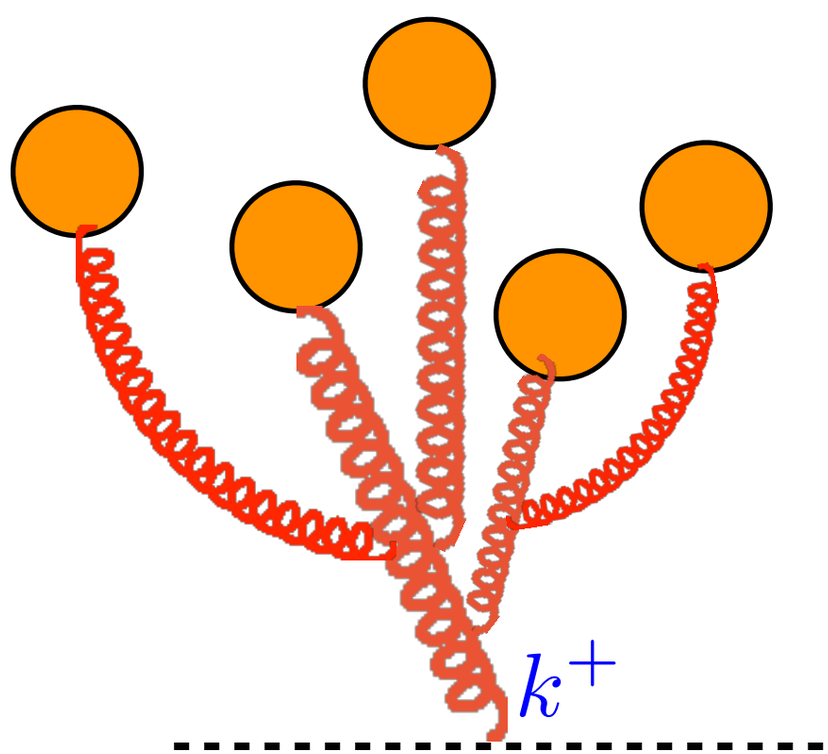

The same process in the dipole language

Now the nucleus is at rest. The photon develops a small x wave function in terms of many quark-antiquark dipoles

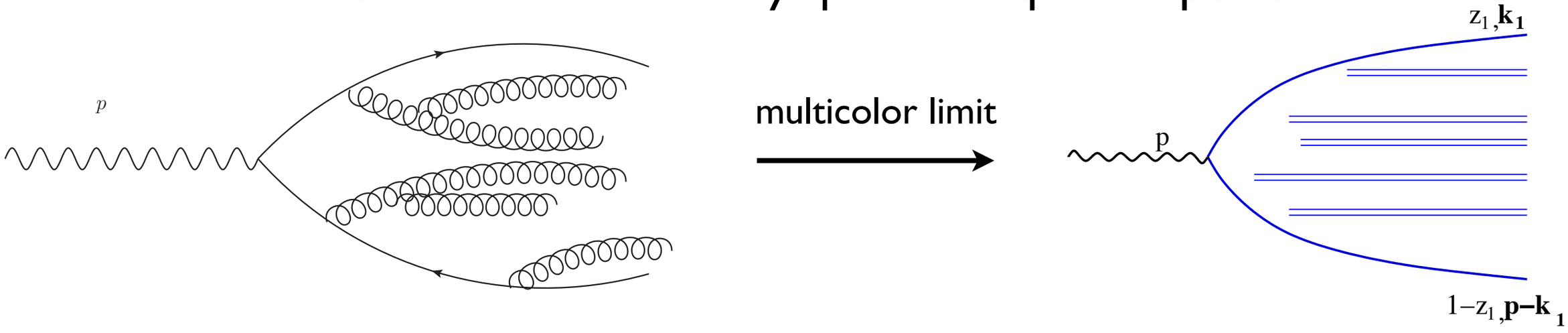

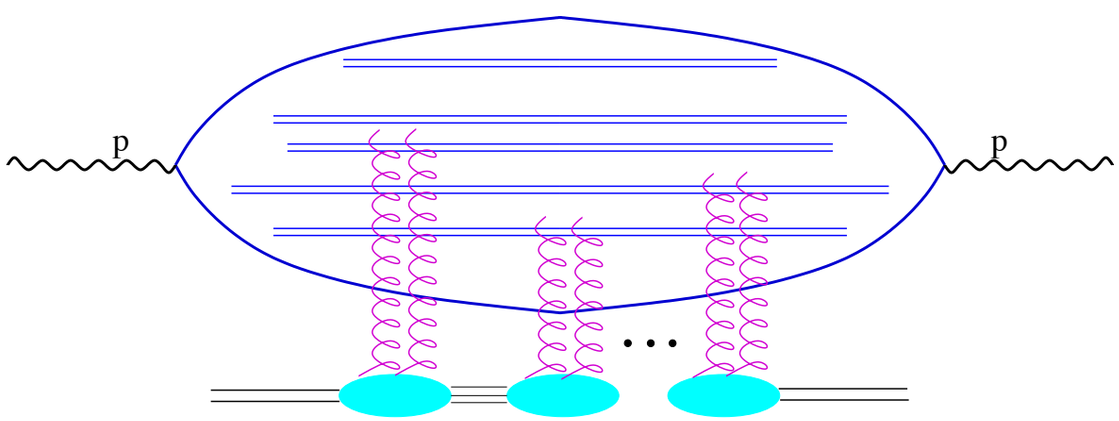

Multiple scatterings of different components of the small x photon wave function on the nucleus.

Multiple scattering in rest frame of the nucleus is viewed as recombination of gluons in the frame in which the nucleus moves very fast.

Gluon density at high energies

The evolution equation for the gluon density becomes nonlinear.

Evolution equation for the dipole-hadron(nucleus) scattering amplitude.

$$\frac{dN(\mathbf{b}_{01},\mathbf{x}_{01},Y)}{dY} = \bar{\alpha}_s \int \frac{d^2\mathbf{x}_2\,\mathbf{x}_{01}^2}{\mathbf{x}_{20}^2\,\mathbf{x}_{12}^2}\Big[N(\mathbf{b}_{01}+\frac{\mathbf{x}_{12}}{2},\mathbf{x}_{20},Y)+N(\mathbf{b}_{01}-\frac{\mathbf{x}_{20}}{2},\mathbf{x}_{12},Y) - N(\mathbf{b}_{01},\mathbf{x}_{01},Y) - N(\mathbf{b}_{01}+\frac{\mathbf{x}_{12}}{2},\mathbf{x}_{20},Y)\,N(\mathbf{b}_{01}-\frac{\mathbf{x}_{20}}{2},\mathbf{x}_{12},Y)\Big]$$

Dipole amplitude is related to the unintegrated gluon density (impact parameter neglected)

$$N(b,r,Y=\ln 1/x) \longleftrightarrow f(x,k_T)$$

$$\frac{df_g(x,k_T^2)}{d\ln 1/x} = \frac{\alpha_s N_c}{\pi}\int d^2k_T' \mathcal{K}(k_T,k_T')\; f_g(x,k_T') \; - \frac{\alpha_s N_c}{\pi}(f_g(x,k_T^2))^2$$

Gluon density at high energies

The evolution equation for the gluon density becomes nonlinear.

Evolution equation for the dipole-hadron(nucleus) scattering amplitude.

$$\frac{dN(\mathbf{b}_{01},\mathbf{x}_{01},Y)}{dY} = \bar{\alpha}_s \int \frac{d^2\mathbf{x}_2\,\mathbf{x}_{01}^2}{\mathbf{x}_{20}^2\,\mathbf{x}_{12}^2}\Big[N(\mathbf{b}_{01}+\frac{\mathbf{x}_{12}}{2},\mathbf{x}_{20},Y)+N(\mathbf{b}_{01}-\frac{\mathbf{x}_{20}}{2},\mathbf{x}_{12},Y) - N(\mathbf{b}_{01},\mathbf{x}_{01},Y) - N(\mathbf{b}_{01}+\frac{\mathbf{x}_{12}}{2},\mathbf{x}_{20},Y)\,N(\mathbf{b}_{01}-\frac{\mathbf{x}_{20}}{2},\mathbf{x}_{12},Y)\Big]$$

Dipole amplitude is related to the unintegrated gluon density (impact parameter neglected)

$$N(b,r,Y=\ln 1/x) \longleftrightarrow f(x,k_T)$$

$$\frac{df_g(x,k_T^2)}{d\ln 1/x} = \frac{\alpha_s N_c}{\pi}\int d^2k_T' \mathcal{K}(k_T,k_T')\; f_g(x,k_T') - \frac{\alpha_s N_c}{\pi}(f_g(x,k_T^2))^2$$

L.V.Gribov, E. Levin, M. Ryskin;
I.Balitsky,Y.Kovchegov; J.Jalilian-Marian, E.Iancu,L.McLerran,H.Weigert, Leonidov

Gluon density at high energies

The evolution equation for the gluon density becomes nonlinear.

Evolution equation for the dipole-hadron(nucleus) scattering amplitude.

$$\frac{dN(\mathbf{b}_{01},\mathbf{x}_{01},Y)}{dY} = \bar{\alpha}_s \int \frac{d^2\mathbf{x}_2\,\mathbf{x}_{01}^2}{\mathbf{x}_{20}^2\,\mathbf{x}_{12}^2}\Big[N(\mathbf{b}_{01}+\frac{\mathbf{x}_{12}}{2},\mathbf{x}_{20},Y)+N(\mathbf{b}_{01}-\frac{\mathbf{x}_{20}}{2},\mathbf{x}_{12},Y) - N(\mathbf{b}_{01},\mathbf{x}_{01},Y) - N(\mathbf{b}_{01}+\frac{\mathbf{x}_{12}}{2},\mathbf{x}_{20},Y)\,N(\mathbf{b}_{01}-\frac{\mathbf{x}_{20}}{2},\mathbf{x}_{12},Y)\Big]$$

Dipole amplitude is related to the unintegrated gluon density (impact parameter neglected)

$$N(b,r,Y=\ln 1/x) \longleftrightarrow f(x,k_T)$$

$$\frac{df_g(x,k_T^2)}{d\ln 1/x} = \frac{\alpha_s N_c}{\pi}\int d^2k_T' \mathcal{K}(k_T,k_T')\; f_g(x,k_T') - \frac{\alpha_s N_c}{\pi}(f_g(x,k_T^2))^2$$

L.V.Gribov, E. Levin, M. Ryskin;
I.Balitsky, Y.Kovchegov; J.Jalilian-Marian, E.Iancu, L.McLerran, H.Weigert, Leonidov

Linear term: gluon splitting, increase of the density

Gluon density at high energies

The evolution equation for the gluon density becomes nonlinear.

Evolution equation for the dipole-hadron(nucleus) scattering amplitude.

$$\frac{dN(\mathbf{b}_{01},\mathbf{x}_{01},Y)}{dY} = \bar{\alpha}_s \int \frac{d^2\mathbf{x}_2\,\mathbf{x}_{01}^2}{\mathbf{x}_{20}^2\,\mathbf{x}_{12}^2}\Big[N(\mathbf{b}_{01}+\frac{\mathbf{x}_{12}}{2},\mathbf{x}_{20},Y)+N(\mathbf{b}_{01}-\frac{\mathbf{x}_{20}}{2},\mathbf{x}_{12},Y) - N(\mathbf{b}_{01},\mathbf{x}_{01},Y) - N(\mathbf{b}_{01}+\frac{\mathbf{x}_{12}}{2},\mathbf{x}_{20},Y)\,N(\mathbf{b}_{01}-\frac{\mathbf{x}_{20}}{2},\mathbf{x}_{12},Y)\Big]$$

Dipole amplitude is related to the unintegrated gluon density (impact parameter neglected)

$$N(b,r,Y=\ln 1/x) \longleftrightarrow f(x,k_T)$$

$$\frac{df_g(x,k_T^2)}{d\ln 1/x} = \frac{\alpha_s N_c}{\pi}\int d^2k_T' \mathcal{K}(k_T,k_T')\; f_g(x,k_T') - \frac{\alpha_s N_c}{\pi}(f_g(x,k_T^2))^2$$

L.V.Gribov, E. Levin, M. Ryskin;
I.Balitsky, Y.Kovchegov; J.Jalilian-Marian, E.Iancu, L.McLerran, H.Weigert, Leonidov

Linear term: gluon splitting, increase of the density

Nonlinear term: gluon merging, slow down the growth of the density with the energy

Gluon density at high energies

The evolution equation for the gluon density becomes nonlinear.

Evolution equation for the dipole-hadron(nucleus) scattering amplitude.

$$\frac{dN(\mathbf{b}_{01},\mathbf{x}_{01},Y)}{dY} = \bar{\alpha}_s \int \frac{d^2\mathbf{x}_2\,\mathbf{x}_{01}^2}{\mathbf{x}_{20}^2\,\mathbf{x}_{12}^2}\Big[N(\mathbf{b}_{01}+\frac{\mathbf{x}_{12}}{2},\mathbf{x}_{20},Y)+N(\mathbf{b}_{01}-\frac{\mathbf{x}_{20}}{2},\mathbf{x}_{12},Y) - N(\mathbf{b}_{01},\mathbf{x}_{01},Y) - N(\mathbf{b}_{01}+\frac{\mathbf{x}_{12}}{2},\mathbf{x}_{20},Y)\,N(\mathbf{b}_{01}-\frac{\mathbf{x}_{20}}{2},\mathbf{x}_{12},Y)\Big]$$

Dipole amplitude is related to the unintegrated gluon density (impact parameter neglected)

$$N(b,r,Y=\ln 1/x) \longleftrightarrow f(x,k_T)$$

$$\frac{df_g(x,k_T^2)}{d\ln 1/x} = \frac{\alpha_s N_c}{\pi}\int d^2k_T' \mathcal{K}(k_T,k_T')\; f_g(x,k_T') - \frac{\alpha_s N_c}{\pi}(f_g(x,k_T^2))^2$$

L.V.Gribov, E. Levin, M. Ryskin;
I.Balitsky, Y.Kovchegov; J.Jalilian-Marian, E.Iancu, L.McLerran, H.Weigert, Leonidov

Linear term: gluon splitting, increase of the density

Nonlinear term: gluon merging, slow down the growth of the density with the energy

Equilibrium: nonlinear term compensates the linear term.

Gluon density at high energies

The evolution equation for the gluon density becomes nonlinear.

Evolution equation for the dipole-hadron(nucleus) scattering amplitude.

$$\frac{dN(\mathbf{b}_{01},\mathbf{x}_{01},Y)}{dY} = \bar{\alpha}_s \int \frac{d^2\mathbf{x}_2\,\mathbf{x}_{01}^2}{\mathbf{x}_{20}^2\,\mathbf{x}_{12}^2}\Big[N(\mathbf{b}_{01}+\frac{\mathbf{x}_{12}}{2},\mathbf{x}_{20},Y)+N(\mathbf{b}_{01}-\frac{\mathbf{x}_{20}}{2},\mathbf{x}_{12},Y) - N(\mathbf{b}_{01},\mathbf{x}_{01},Y) - N(\mathbf{b}_{01}+\frac{\mathbf{x}_{12}}{2},\mathbf{x}_{20},Y)\,N(\mathbf{b}_{01}-\frac{\mathbf{x}_{20}}{2},\mathbf{x}_{12},Y)\Big]$$

Dipole amplitude is related to the unintegrated gluon density (impact parameter neglected)

$$N(b,r,Y=\ln 1/x) \longleftrightarrow f(x,k_T)$$

$$\frac{df_g(x,k_T^2)}{d\ln 1/x} = \frac{\alpha_s N_c}{\pi}\int d^2k_T' \mathcal{K}(k_T,k_T')\; f_g(x,k_T') \; - \frac{\alpha_s N_c}{\pi}(f_g(x,k_T^2))^2$$

L.V.Gribov, E. Levin, M. Ryskin;
I.Balitsky, Y.Kovchegov; J.Jalilian-Marian, E.Iancu, L.McLerran, H.Weigert, Leonidov

Linear term: gluon splitting, increase of the density

Nonlinear term: gluon merging, slow down the growth of the density with the energy

Equilibrium: nonlinear term compensates the linear term.

Gluon density saturates: ***parton saturation***

Saturation scale

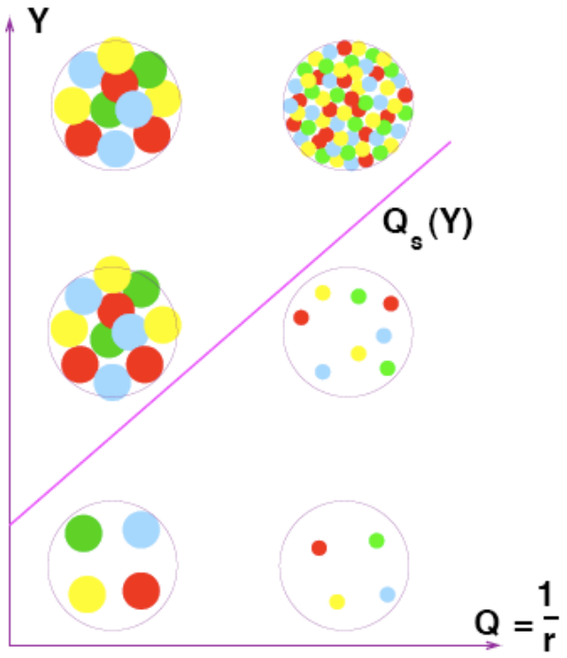

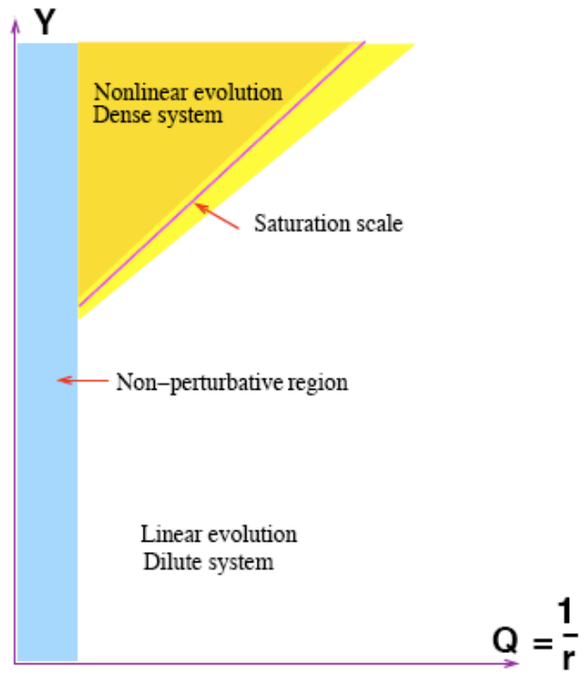

Dynamically generated saturation scale

For a nucleus there is an enhancement factor related to the nuclear size. The dense region is approached either by selecting larger nucleus and probing smaller impact parameters or by decreasing value of x.

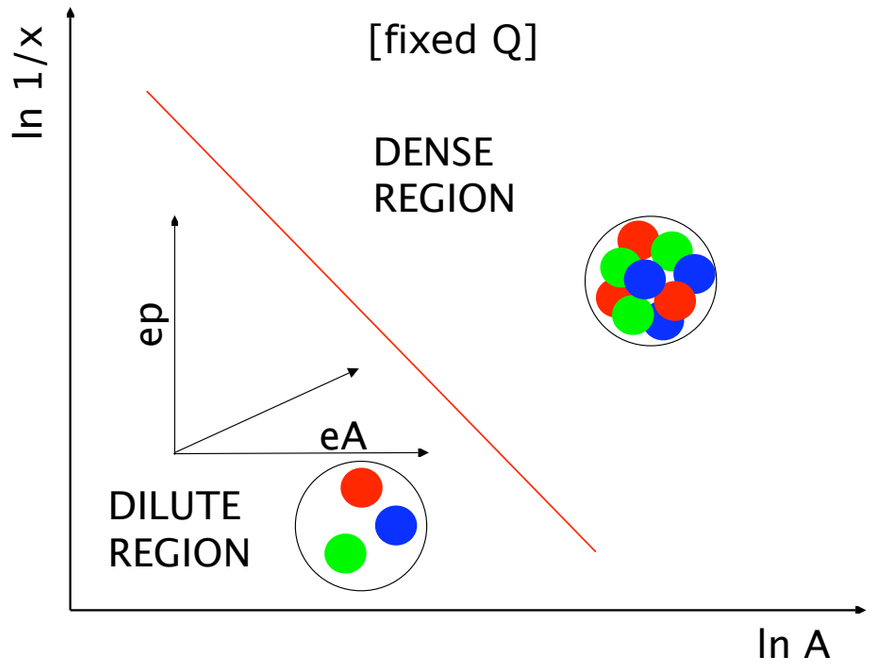

Saturation scale

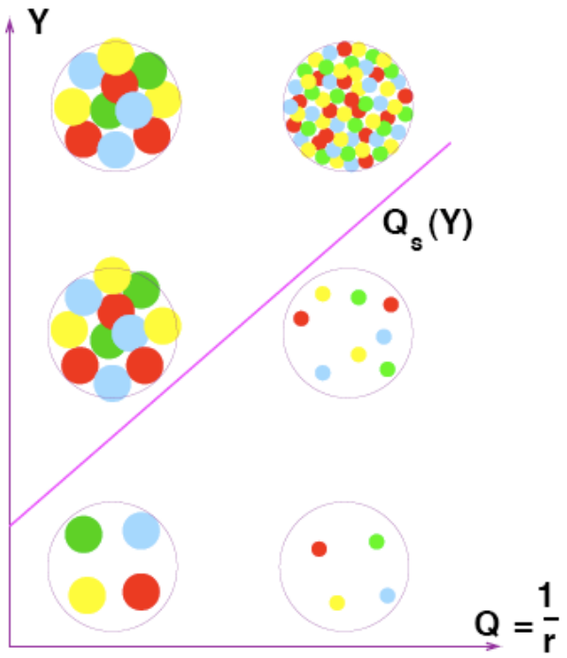

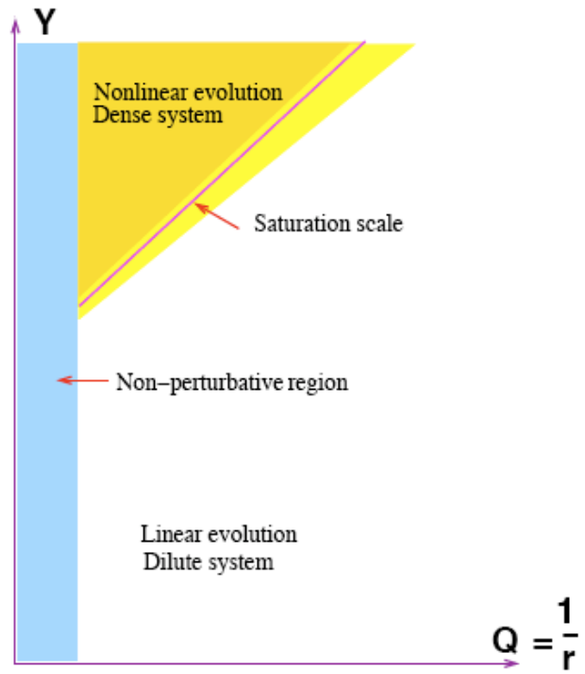

Dynamically generated saturation scale

$$\frac{A \times xg(x,Q_s^2)}{\pi A^{2/3}} \times \frac{\alpha_s(Q_s^2)}{Q_s^2} \sim 1 \qquad Q_s^2 \sim A^{1/3} Q_0^2 \left(\frac{1}{x}\right)^{\lambda}$$

For a nucleus there is an enhancement factor related to the nuclear size. The dense region is approached either by selecting larger nucleus and probing smaller impact parameters or by decreasing value of x.

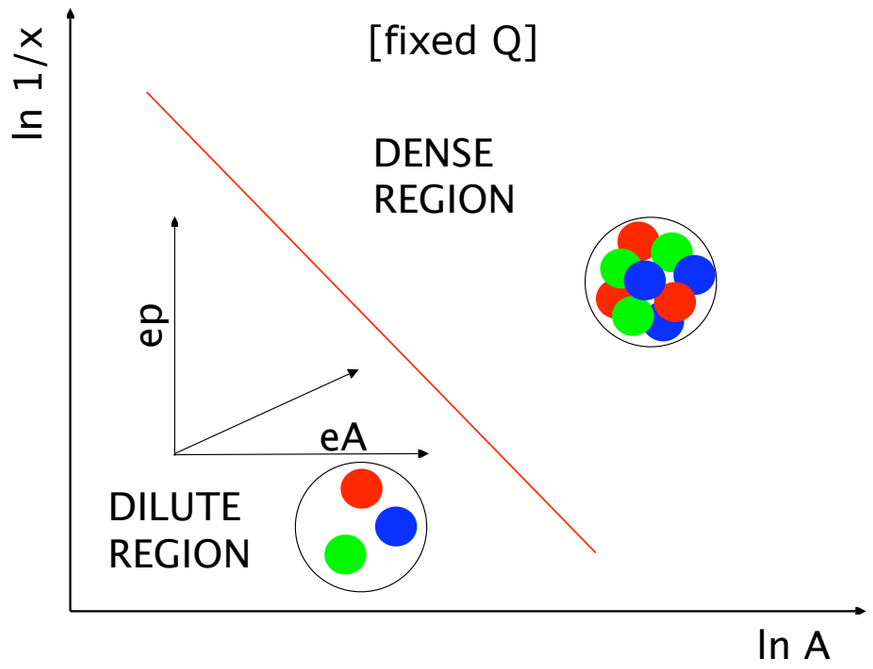

BK equation: solution (no impact parameter dependence)

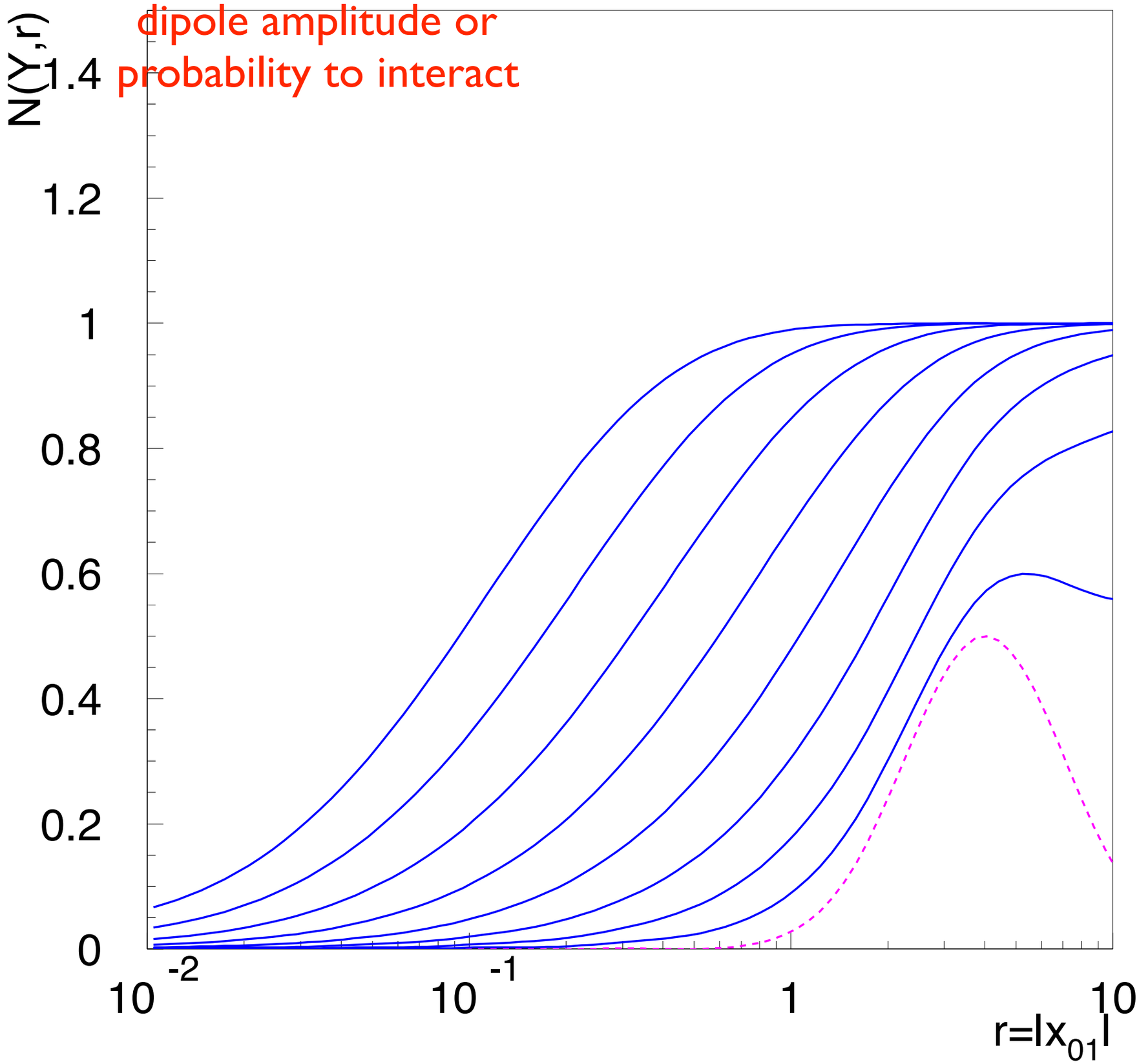

BK equation: solution (no impact parameter dependence)

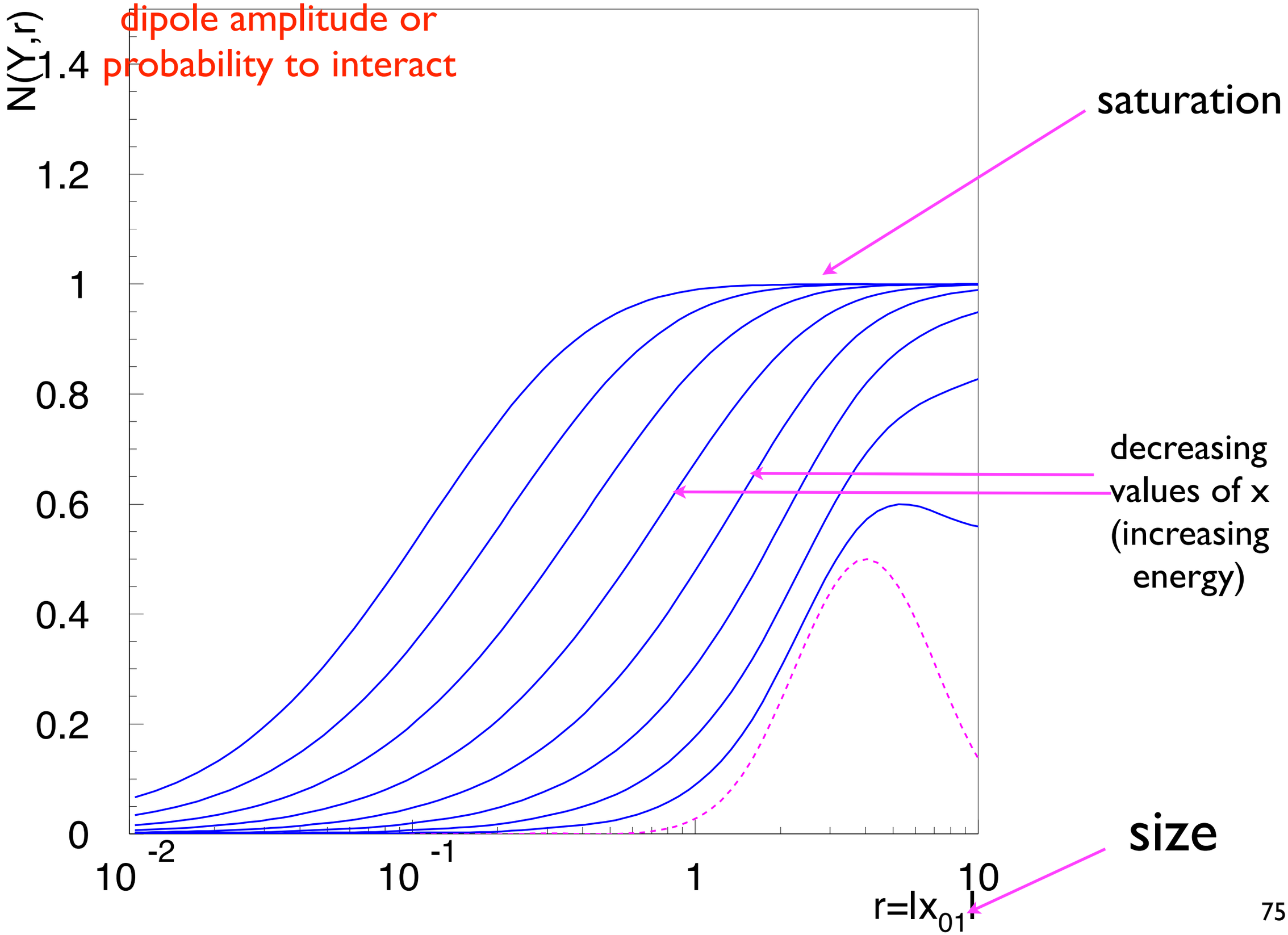

BK equation: solution (no impact parameter dependence)

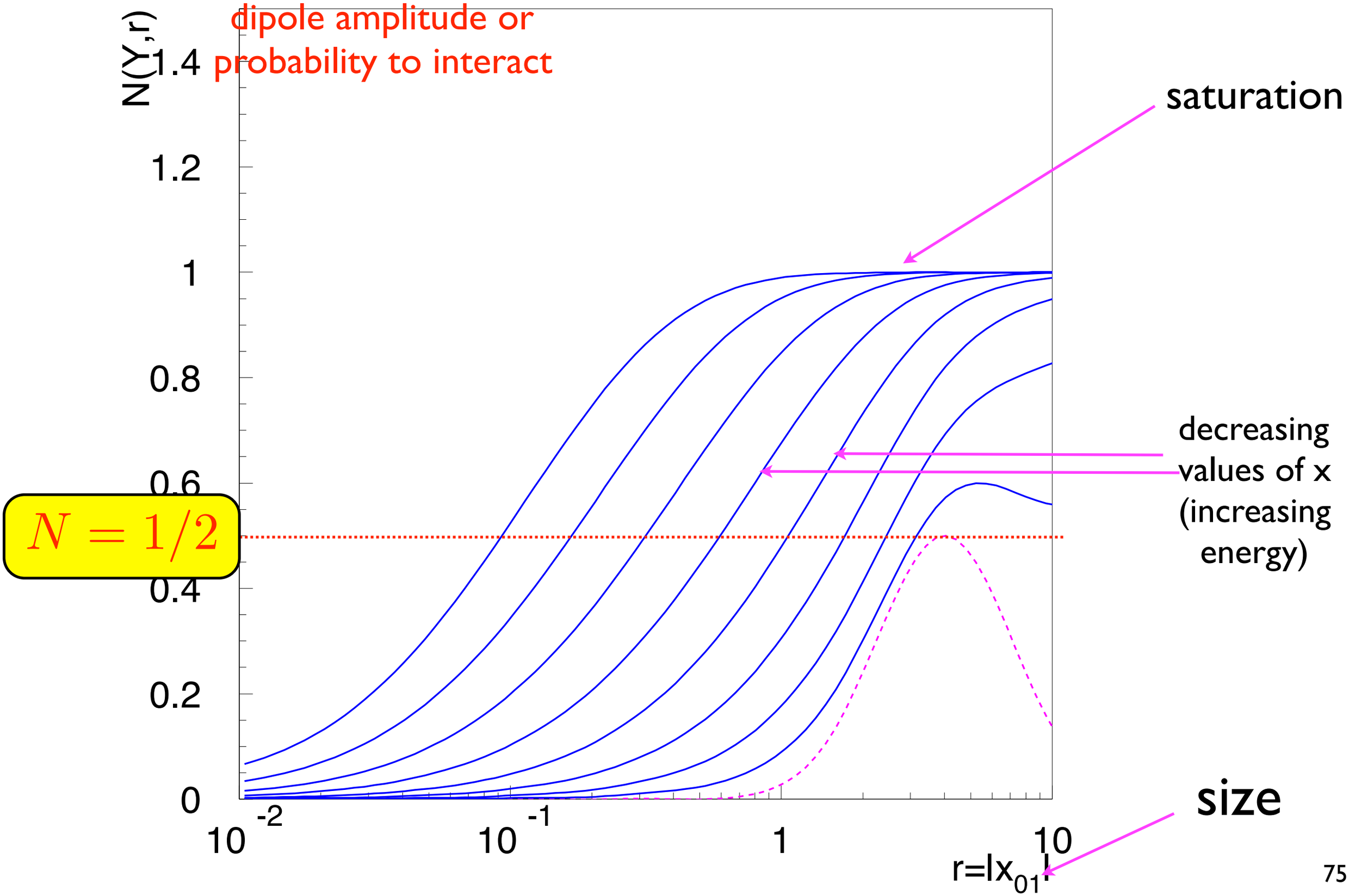

BK equation: solution (no impact parameter dependence)

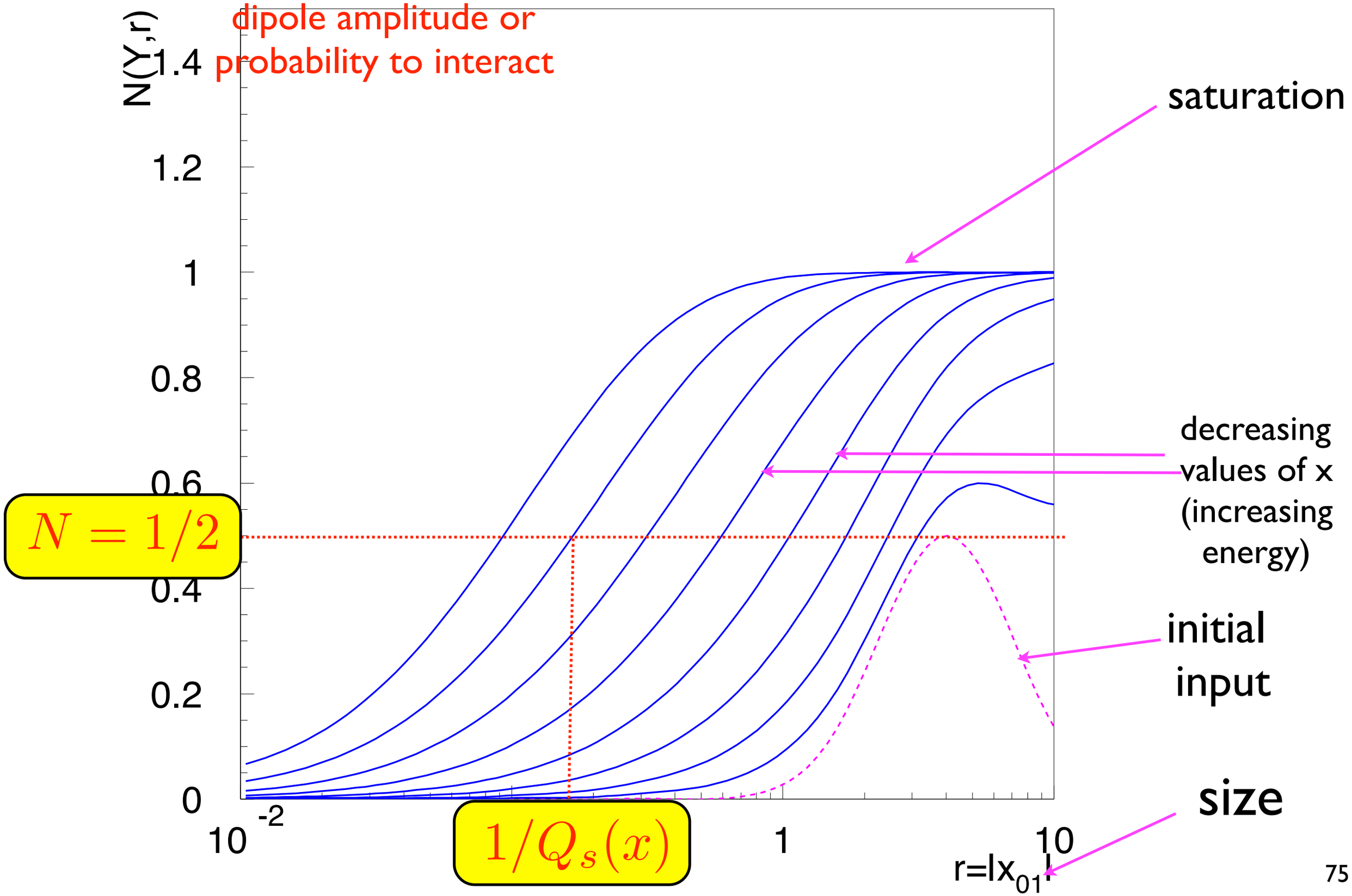

Nuclear shadowing from BK equation

Armesto, Braun

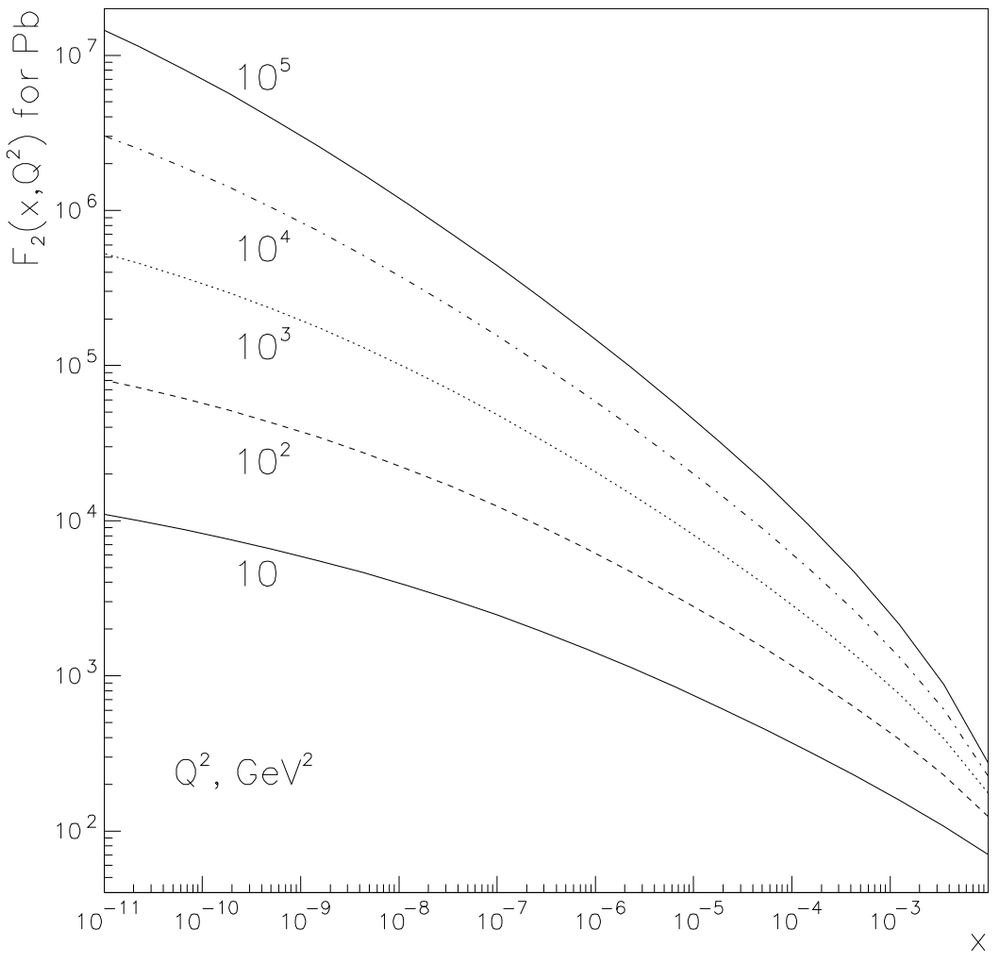

Structure function for Pb

$$F_2^{Pb} \sim \ln^2 1/x$$

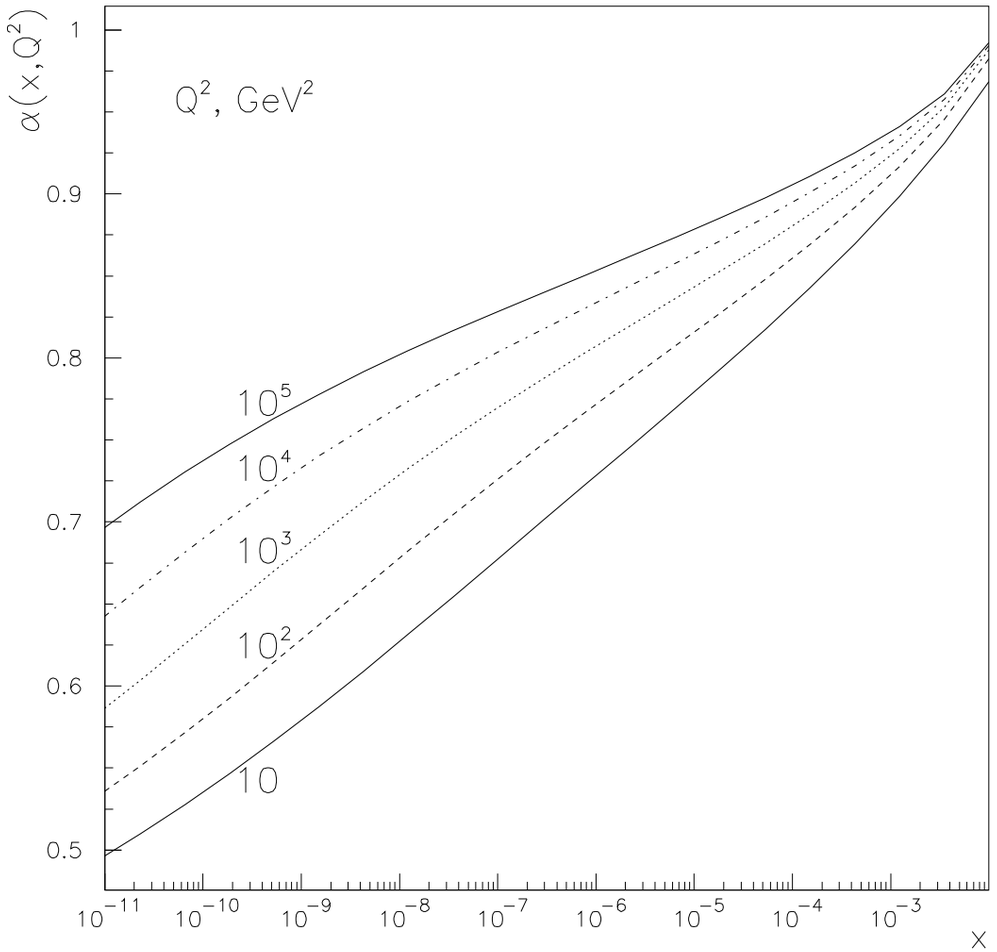

Power α as a function of x

$$F_{2A}(x,Q^2) = A^{\alpha(x,Q^2)} F(x,Q^2).$$

At large x close to 1 and independent of Q.
At small x goes significantly below 1, strong saturation which leads to the suppression of the structure function for Pb with respect to the proton case

Diffraction

Diffraction in ep and eA

Term **diffraction** is derived from optics where it means the phenomena related to the passage of light when it encounters a slit or an obstacle and its decomposition into the components with different frequencies.

Diffraction in ep and eA

Term **diffraction** is derived from optics where it means the phenomena related to the passage of light when it encounters a slit or an obstacle and its decomposition into the components with different frequencies.

In high energy physics the term originally referred to the small-angle elastic scattering of hadrons.

Diffraction in ep and eA

Term **diffraction** is derived from optics where it means the phenomena related to the passage of light when it encounters a slit or an obstacle and its decomposition into the components with different frequencies.

In high energy physics the term originally referred to the small-angle elastic scattering of hadrons.

However, more complicated phenomena can occur in hadronic (ep and pp) interactions: elastic,single diffractive, double diffractive, central exclusive….

Diffraction in ep and eA

Term **diffraction** is derived from optics where it means the phenomena related to the passage of light when it encounters a slit or an obstacle and its decomposition into the components with different frequencies.

In high energy physics the term originally referred to the small-angle elastic scattering of hadrons.

However, more complicated phenomena can occur in hadronic (ep and pp) interactions: elastic,single diffractive, double diffractive, central exclusive….

Diffractive processes are characterized by the **rapidity gap**:

absence of any activity in part of the detector

Diffraction in ep and eA

Term **diffraction** is derived from optics where it means the phenomena related to the passage of light when it encounters a slit or an obstacle and its decomposition into the components with different frequencies.

In high energy physics the term originally referred to the small-angle elastic scattering of hadrons.

However, more complicated phenomena can occur in hadronic (ep and pp) interactions: elastic,single diffractive, double diffractive, central exclusive….

Diffractive processes are characterized by the **rapidity gap**:
absence of any activity in part of the detector

At HERA in **electron-proton** collisions:
about 10% events diffractive

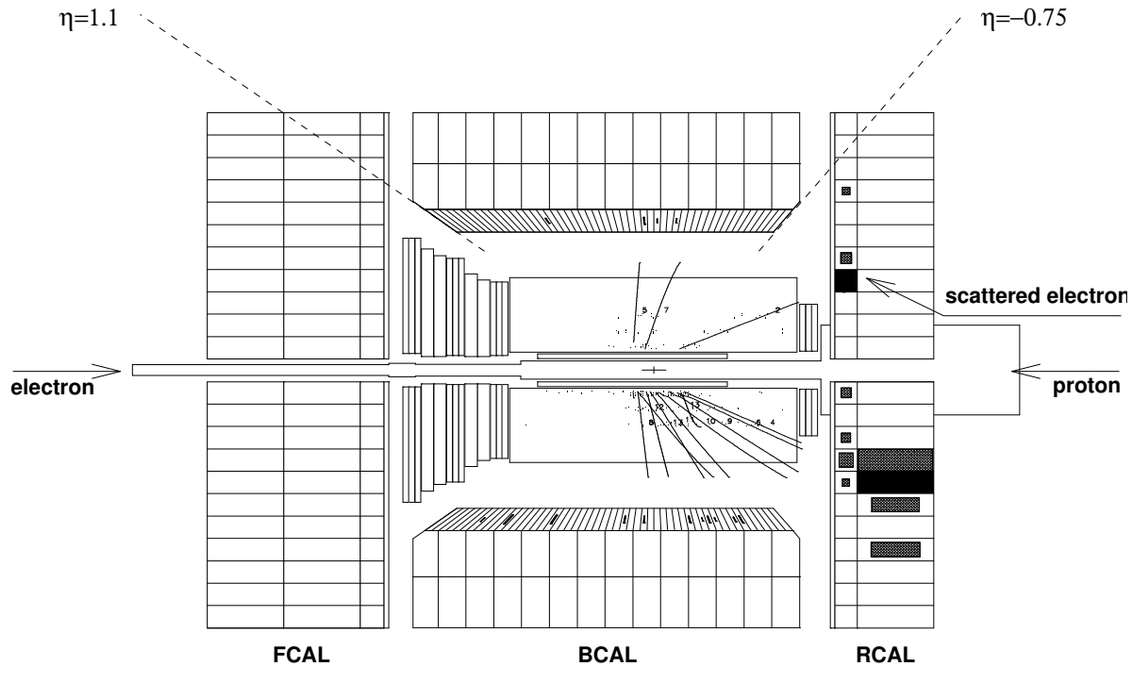

Diffractive event in ZEUS at HERA

Diffraction in ep and eA

Term **diffraction** is derived from optics where it means the phenomena related to the passage of light when it encounters a slit or an obstacle and its decomposition into the components with different frequencies.

In high energy physics the term originally referred to the small-angle elastic scattering of hadrons.

However, more complicated phenomena can occur in hadronic (ep and pp) interactions: elastic,single diffractive, double diffractive, central exclusive….

Diffractive processes are characterized by the **rapidity gap**:
absence of any activity in part of the detector

At HERA in **electron-proton** collisions:
about 10% events diffractive

Experimental methods:
Rapidity gap
Proton tagging

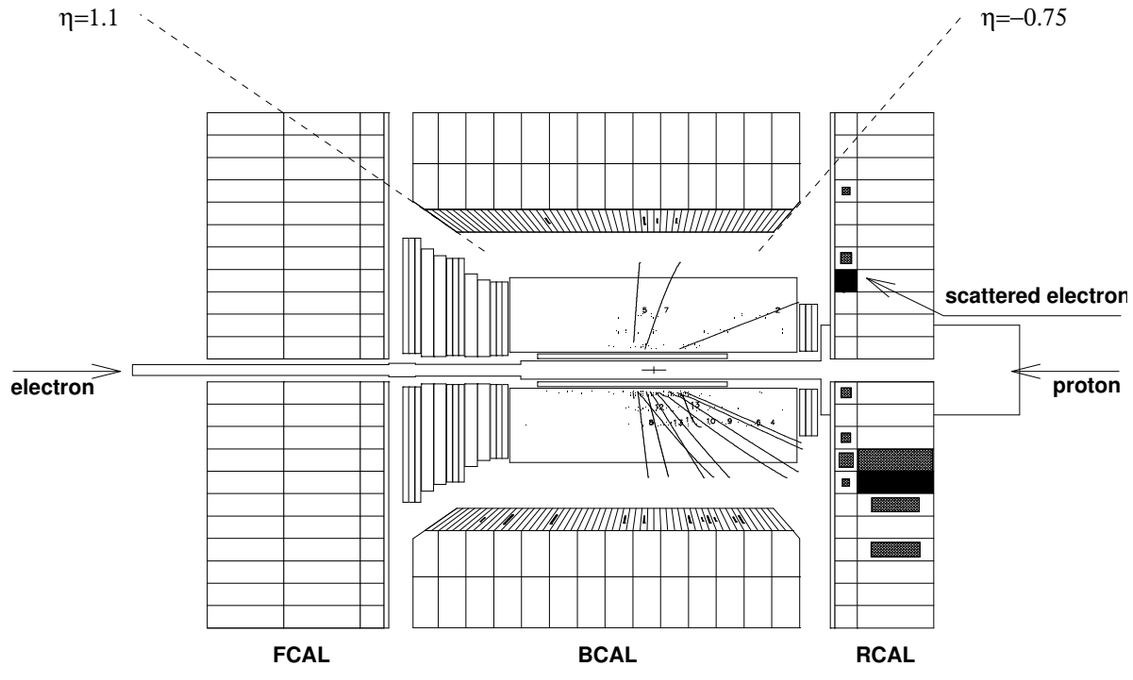

Diffractive event in ZEUS at HERA

Experimental evidence for diffraction in ep

Pseudorapidty

$$\eta = -\ln\tan(\theta/2)$$

- ✦Angle of the outgoing particle relative to the beam axis
- ✦Pseudorapidity=rapidity if particles are massless

$\eta_{\max}$

- ✦Defined as the maximum rapidity of calorimeter cluster in an event.
- ✦Cluster is defined as an isolated set of adjacent cells with deposited energy larger than 400 MeV

Monte Carlo shows exponential suppression of large rapidity gaps

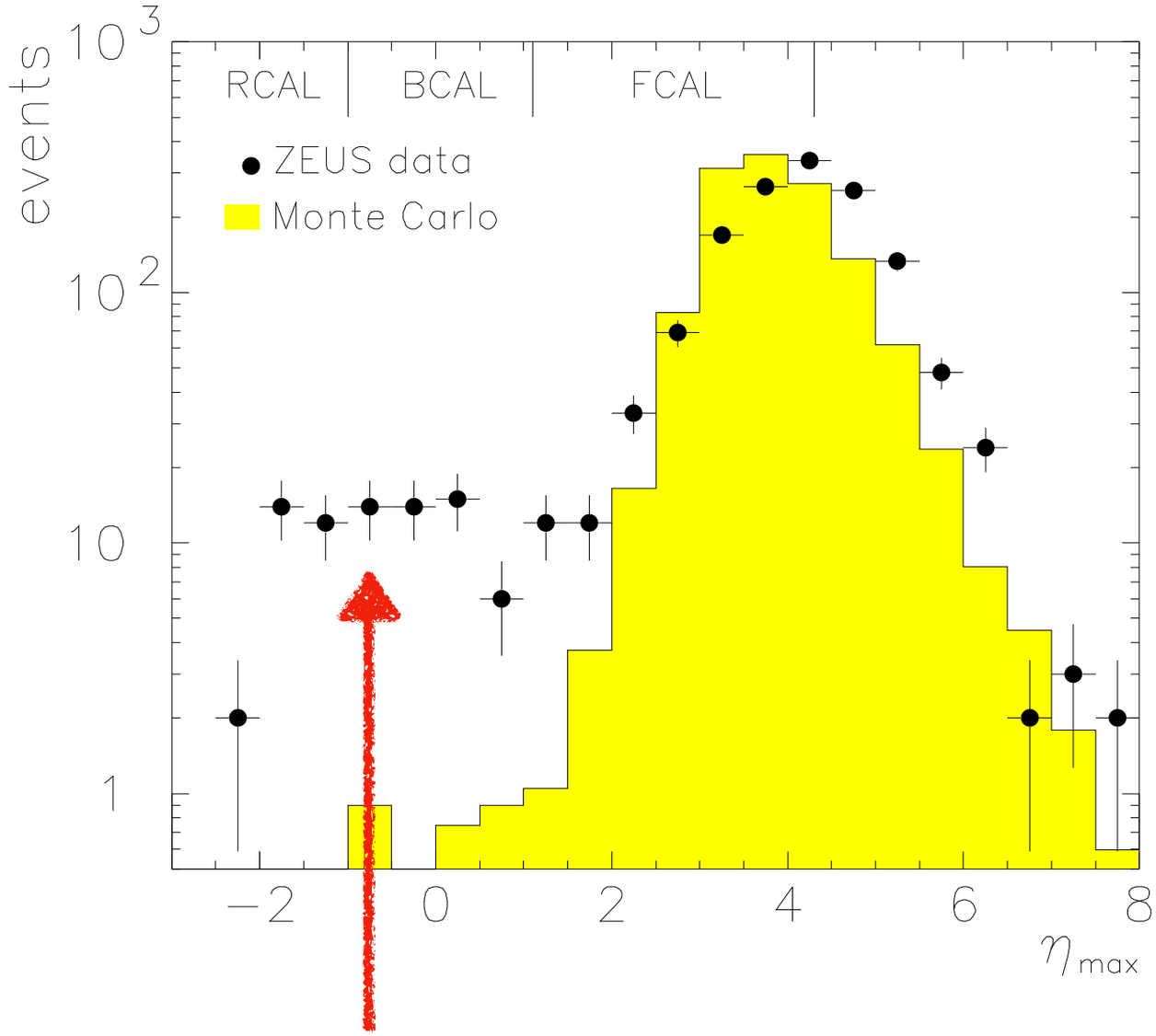

Data are in striking disagreement with the Monte Carlo : there are many events with large rapidity gaps!

Diffraction in DIS

Elastic: proton stays intact

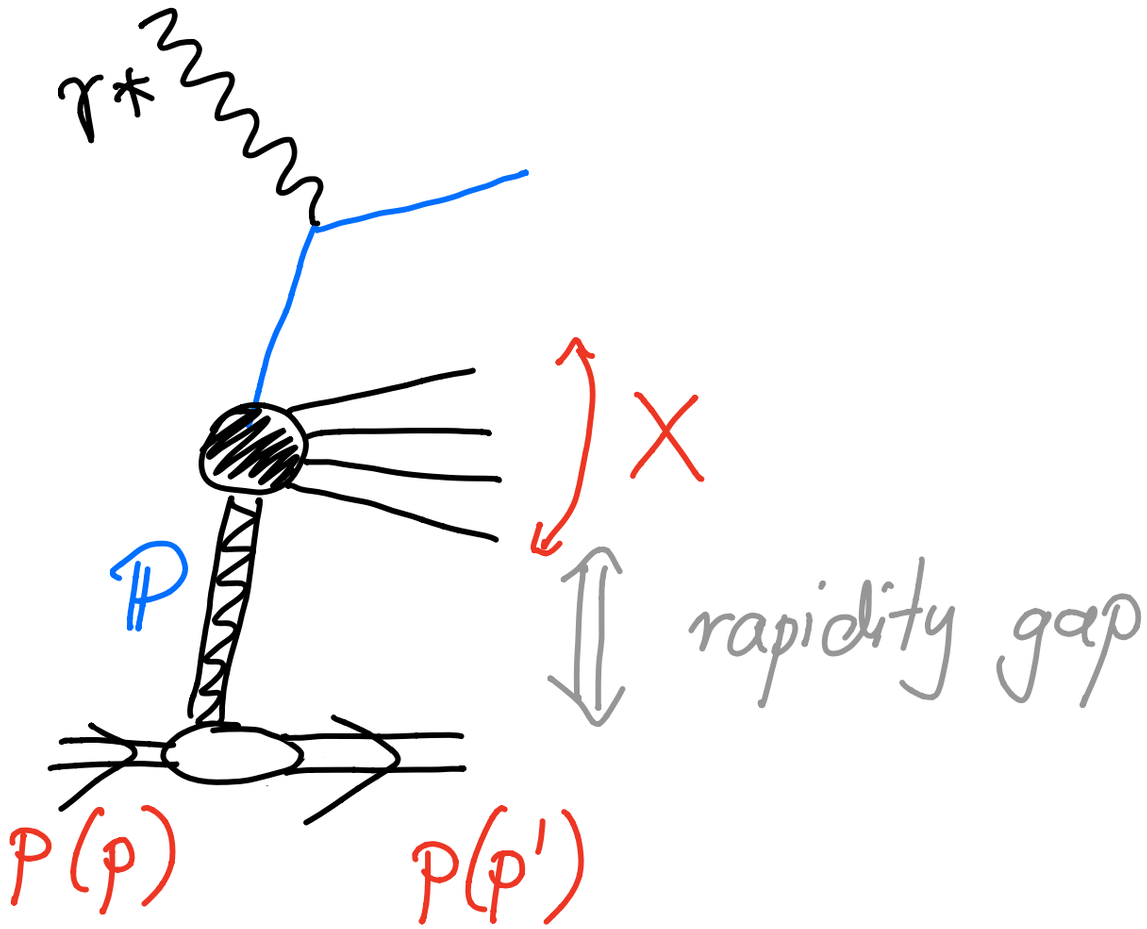

Diffraction in DIS

Elastic: proton stays intact

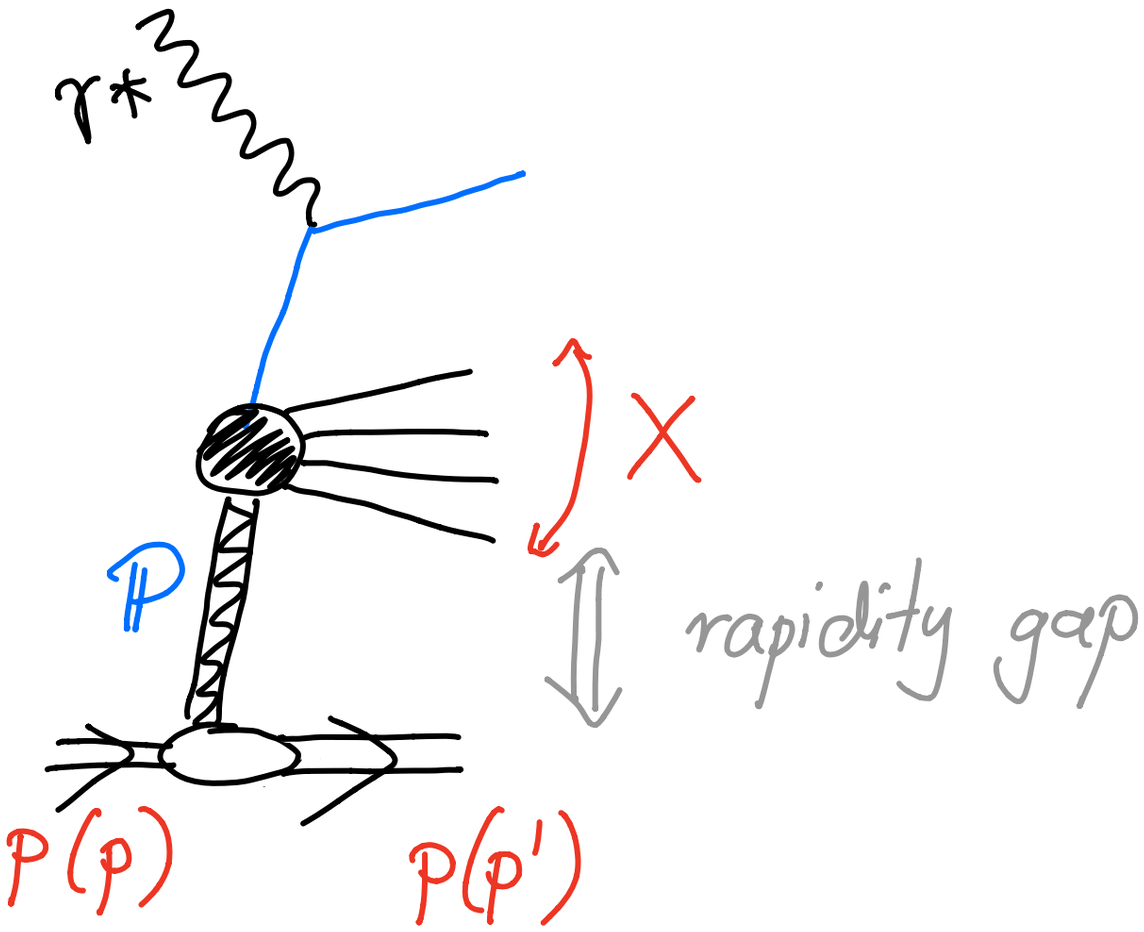

Diffractive dissociation: proton breaks up into system Y

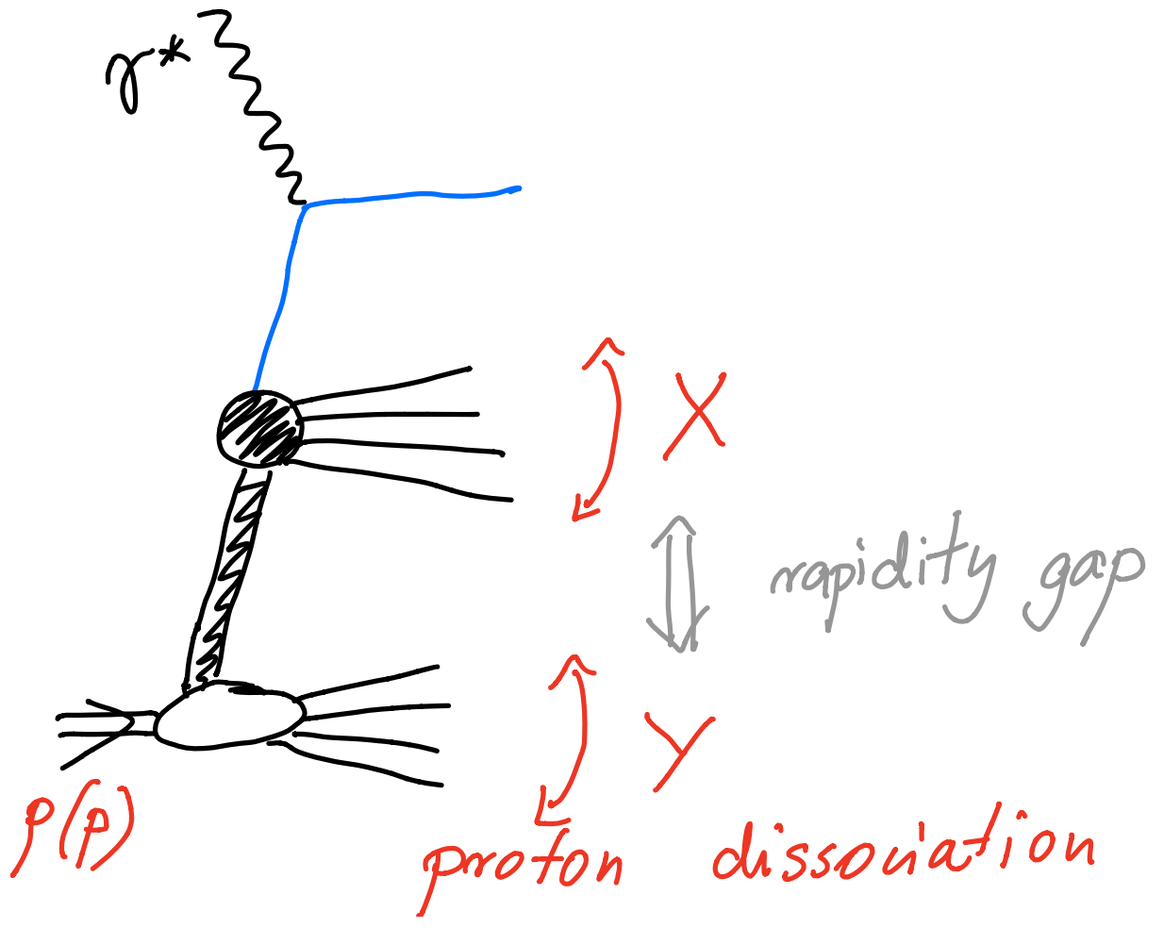

Diffraction in DIS

Elastic: proton stays intact

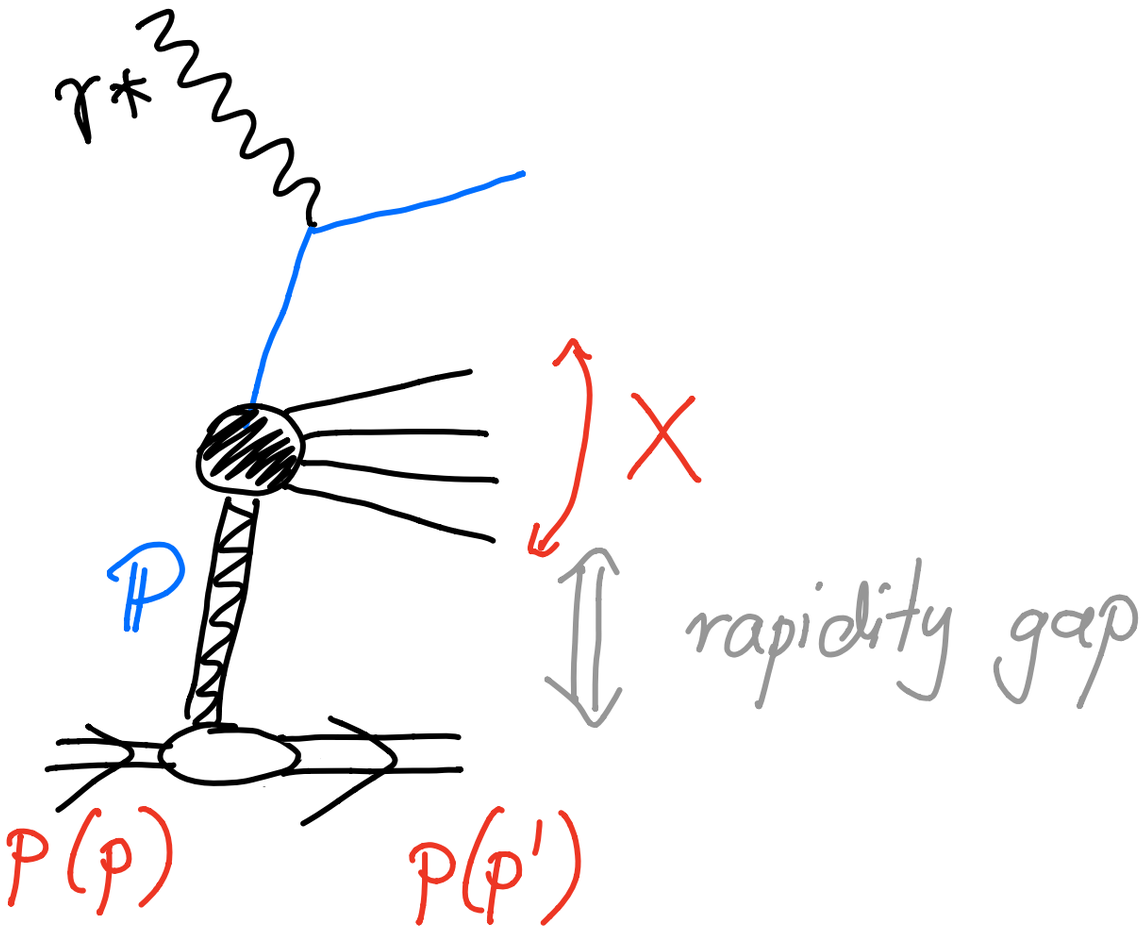

Diffractive dissociation: proton breaks up into system Y

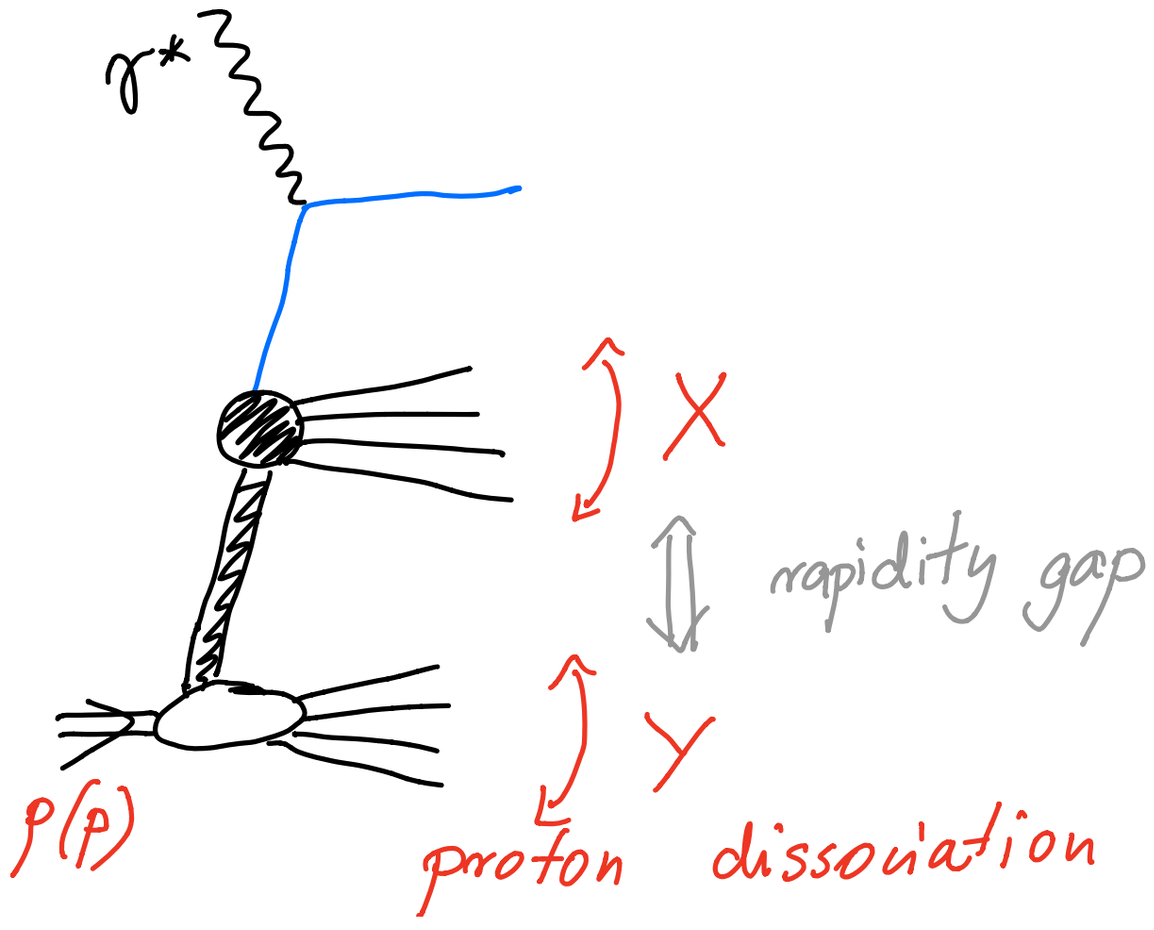

Diffraction interpretation: usually explained in terms of the exchange of a colorless object with the quantum numbers of a vacuum - **the Pomeron**

Diffraction in DIS

Elastic: proton stays intact

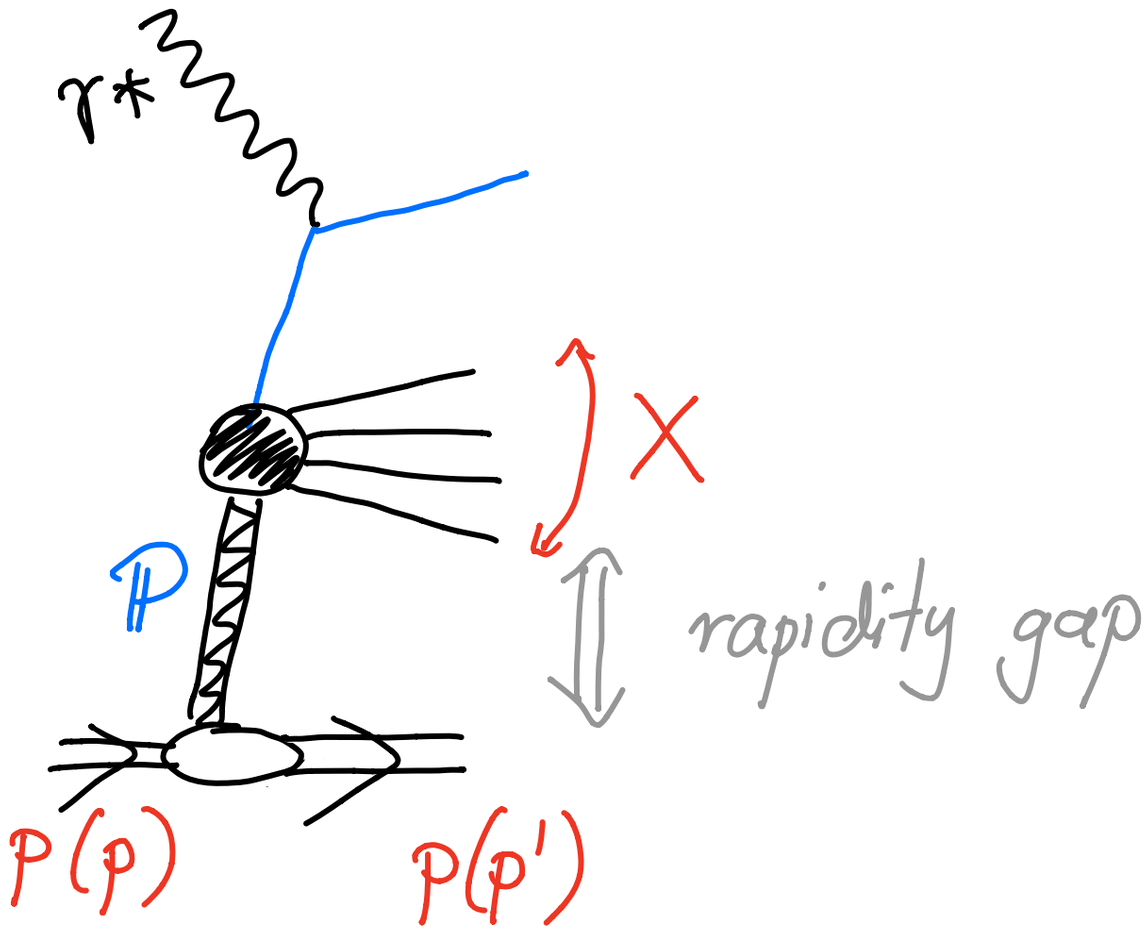

Diffractive dissociation: proton breaks up into system Y

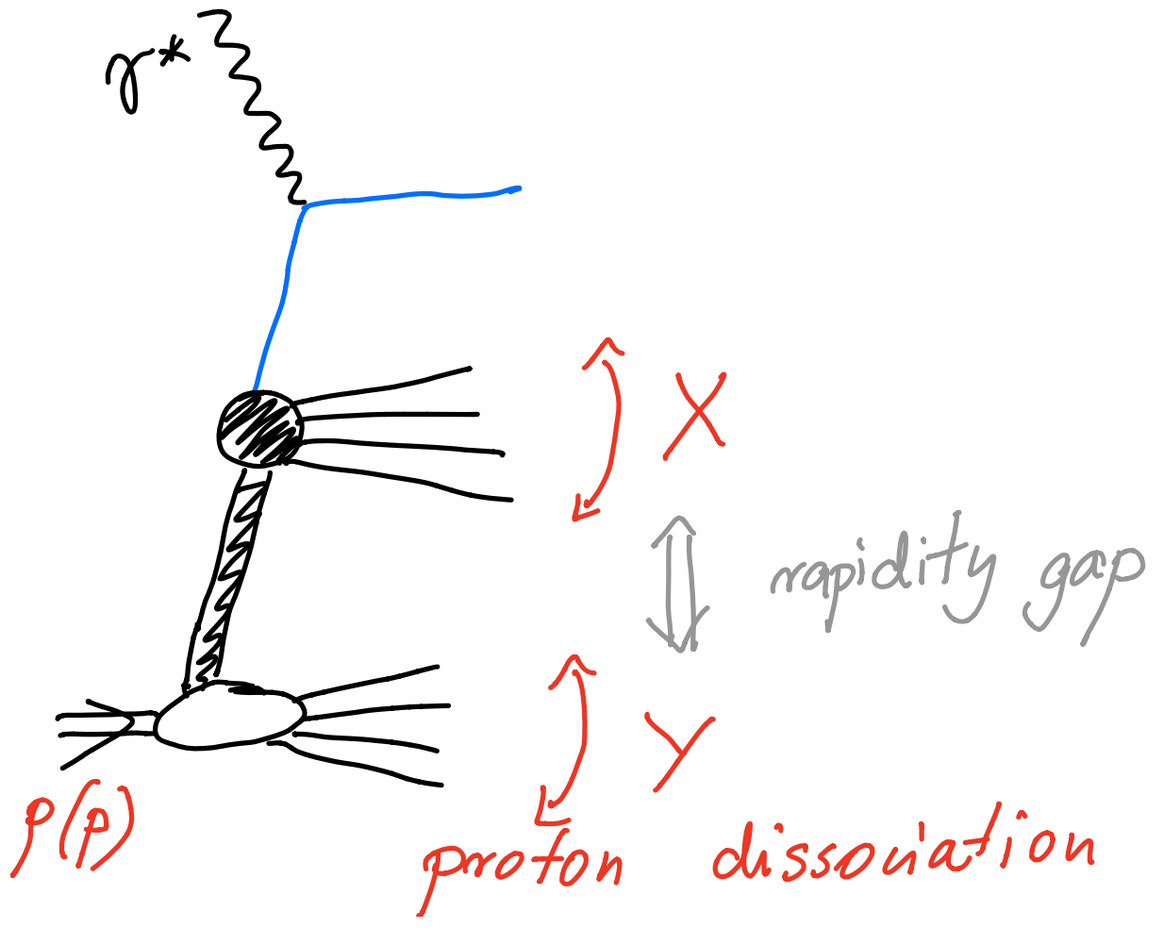

Diffraction interpretation: usually explained in terms of the exchange of a colorless object with the quantum numbers of a vacuum - **the Pomeron**

Other explanations: **soft color interaction** model - color neutralization through the soft exchanges in the final state

Diffractive kinematics in DIS

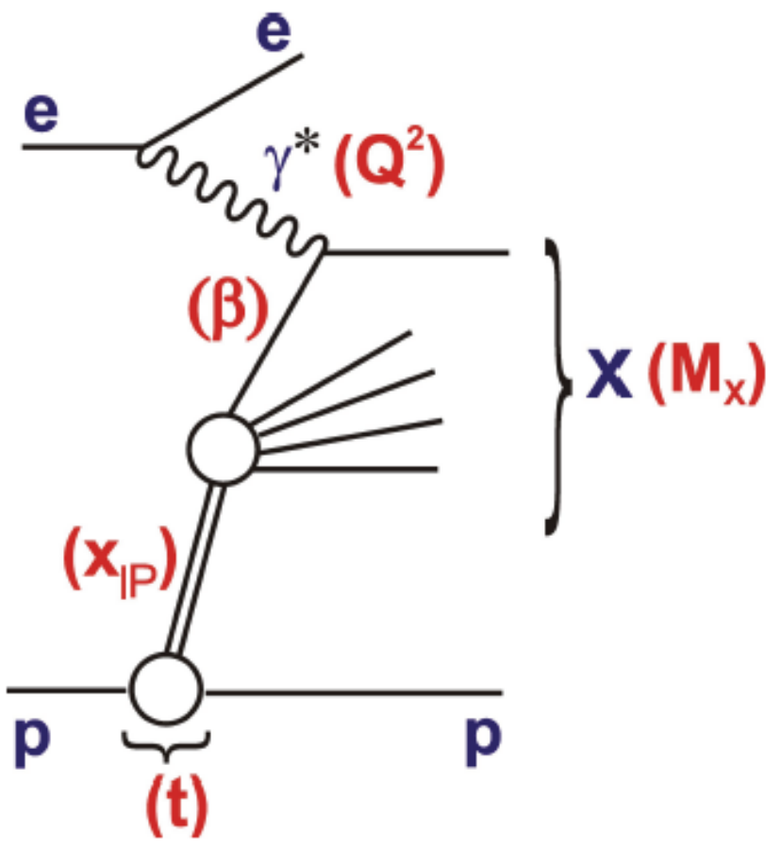

Standard DIS variables:

electron-proton cms energy squared:

$$s = (k+p)^2$$

photon-proton cms energy squared:

$$W^2 = (q+p)^2$$

inelasticity

$$y = \frac{p \cdot q}{p \cdot k}$$

Bjorken x

$$x = \frac{-q^2}{2p \cdot q}$$

(minus) photon virtuality

$$Q^2 = -q^2$$

Diffractive kinematics in DIS

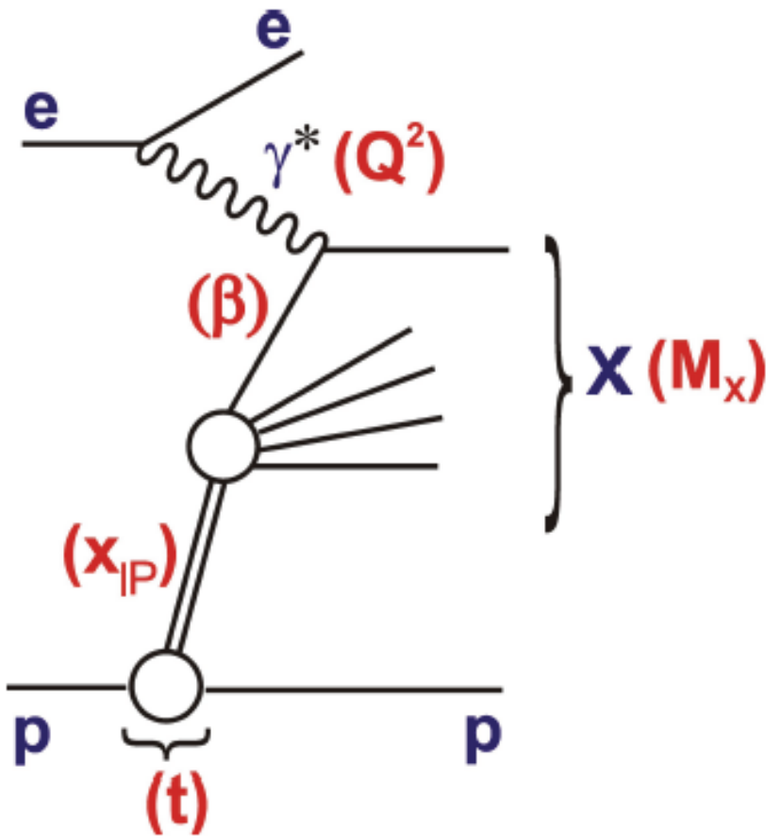

Standard DIS variables:

electron-proton cms energy squared:

$$s = (k+p)^2$$

photon-proton cms energy squared:

$$W^2 = (q+p)^2$$

inelasticity

$$y = \frac{p \cdot q}{p \cdot k}$$

Bjorken x

$$x = \frac{-q^2}{2p \cdot q}$$

(minus) photon virtuality

$$Q^2 = -q^2$$

Diffractive DIS variables:

$$x_{IP} = \frac{Q^2 + M_X^2 - t}{Q^2 + W^2}$$

momentum fraction of the Pomeron w.r.t hadron

$$\beta = \frac{Q^2}{Q^2 + M_X^2 - t}$$

momentum fraction of parton w.r.t Pomeron

$$x_{Bj} = x_{IP}\beta$$

$$t = (p - p')^2$$

4-momentum transfer squared

Diffractive kinematics in DIS

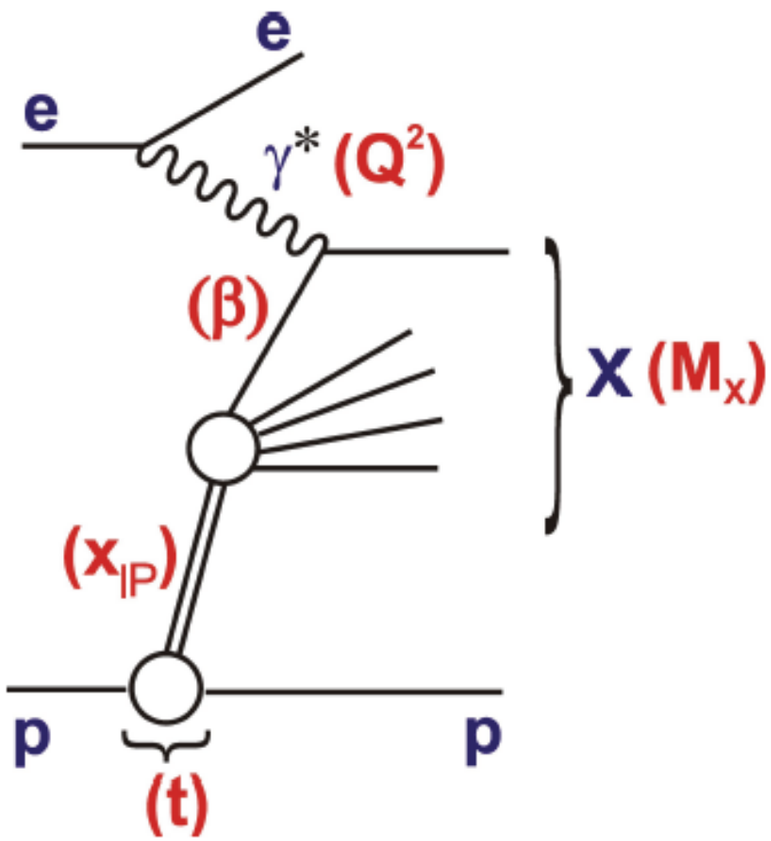

Standard DIS variables:

electron-proton cms energy squared:

$$s = (k+p)^2$$

photon-proton cms energy squared:

$$W^2 = (q+p)^2$$

inelasticity

$$y = \frac{p \cdot q}{p \cdot k}$$

Bjorken x

$$x = \frac{-q^2}{2p \cdot q}$$

(minus) photon virtuality

$$Q^2 = -q^2$$

Diffractive DIS variables:

$$x_{IP} = \frac{Q^2 + M_X^2 - t}{Q^2 + W^2}$$

momentum fraction of the Pomeron w.r.t hadron

$$\beta = \frac{Q^2}{Q^2 + M_X^2 - t}$$

momentum fraction of parton w.r.t Pomeron

$$x_{Bj} = x_{IP}\beta$$

$$t = (p - p')^2$$

4-momentum transfer squared

Two classes of diffractive events in DIS:

$Q^2 \sim 0$ photoproduction

$Q^2 \gg 0$ deep inelastic scattering

Diffractive structure functions

$$\frac{d^3\sigma^D}{dx_{IP}\,dx\,dQ^2} = \frac{2\pi\alpha_{\rm em}^2}{xQ^4}\,Y_+\,\sigma_r^{D(3)}(x_{IP},x,Q^2)$$

$$Y_+ = 1+(1-y)^2$$

Reduced diffractive cross section depends on two structure functions

$$\sigma_r^{D(3)} = F_2^{D(3)} - \frac{y^2}{Y_+}F_L^{D(3)}$$

For y not to close to unity we have: $\sigma_r^{D(3)} \simeq F_2^{D(3)}$

Integrated vs unintegrated structure functions over t

$$F_{T,L}^{D(3)}(x,Q^2,x_{IP}) = \int_{-\infty}^{0} dt F_{T,L}^{D(4)}(x,Q^2,x_{IP},t)$$

$$F_2^{D(4)} = F_T^{D(4)} + F_L^{D(4)}$$

Collinear factorization in diffraction

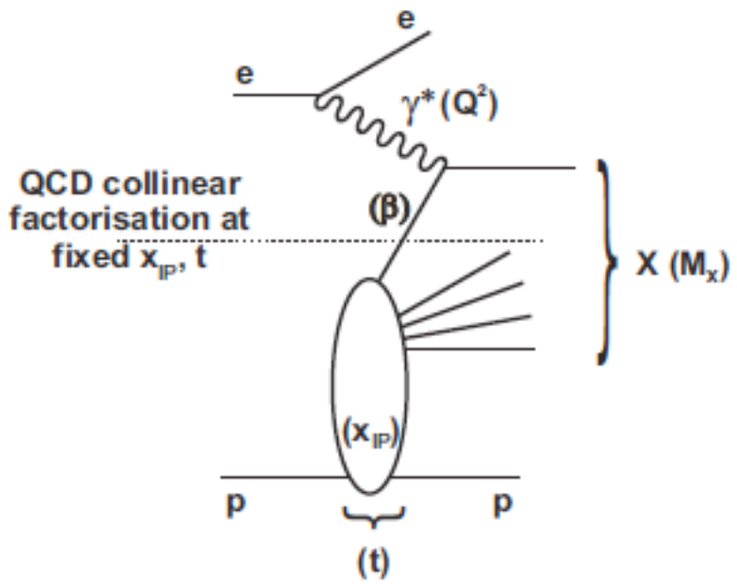

Collins

Collinear factorization in diffractive DIS

$$d\sigma^{ep\to eXY}(x,Q^2,x_{IP},t) = \sum_i f_i^D(x,Q^2,x_{IP},t) \otimes d\hat{\sigma}^{ei}(x,Q^2) + \mathcal{O}(\Lambda^2/Q^2)$$

- Diffractive cross section can be factorized into the convolution of the perturbatively calculable partonic cross sections and diffractive parton distributions (DPDFs).
- Partonic cross sections are the same as for the inclusive DIS.
- The DPDFs represent the conditional probability distributions for partons i in the proton under the constraint that the proton is scattered into the system Y with a specified 4-momentum.
- Factorization should be valid for sufficiently(?) large Q^2 (and fixed t and x_{IP}).
- Another way of asking the same question: what is value of Λ? Is it the same as for the inclusive case?

Regge factorization

Ingelman-Schlein model:

$$f_i^D(x, Q^2, x_{IP}, t) = f_{IP/p}(x_{IP}, t)\, f_i(\beta = x/x_{IP}, Q^2)$$

pomeron flux

parton distributions in the pomeron

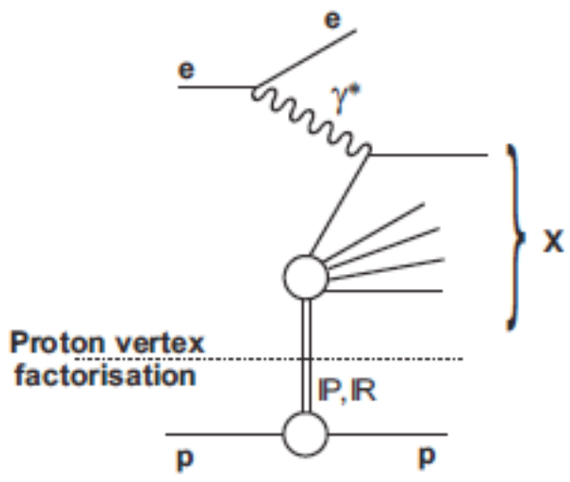

- It is usually assumed that Regge vertex factorization occurs.
- This is in addition to collinear factorization. It is a different assumption.
- The diffractive scattering occurs through the exchange of the Pomeron with the longitudinal momentum fraction x_{IP} of the proton.
- The Pomeron couples to the proton through the 'pomeron flux factor' that determines probability of the coupling with particular value of x_{IP} and t .
- Subsequent hard scattering of the photon on a partonic constituents of the Pomeron. The struck parton carries fraction β of the longitudinal momentum of the Pomeron.

DPDF parametrization

Example of parametrization by H1 and ZEUS:

Standard choice of parametrization similar to the inclusive PDFs:

$$f_k(z) = A_k x^{B_k}(1-x)^{C_k}$$

where k=g,d. Light quarks assumed to be equal u=d=s.

Pomeron flux is parametrized as

$$f_{IP/p}(x_{IP},t) = A_{IP}\frac{e^{B_{IP}t}}{x^{2\alpha_{IP}(t)-1}}$$

Pomeron trajectory assumed to be linear:

$$\alpha_{IP}(t) = \alpha_{IP}(0) + \alpha'_{IP}t$$

For good description of the data usually subleading Reggeons are included

$$f_i^D(x,Q^2,x_{IP},t) = f_{IP/p}(x_{IP},t)\, f_i(\beta,Q^2) + n_{IR} f_{IR/p}(x_{IP},t)\, f_i^{IR}(\beta,Q^2)$$

Subleading contributions important for large values of x_{IP}>0.01

Reggeon parton distributions are constrained by the data on the pion structure functions.

Diffractive fits

Example of the DGLAP fit to the diffractive data

$\xi = x_{IP}$

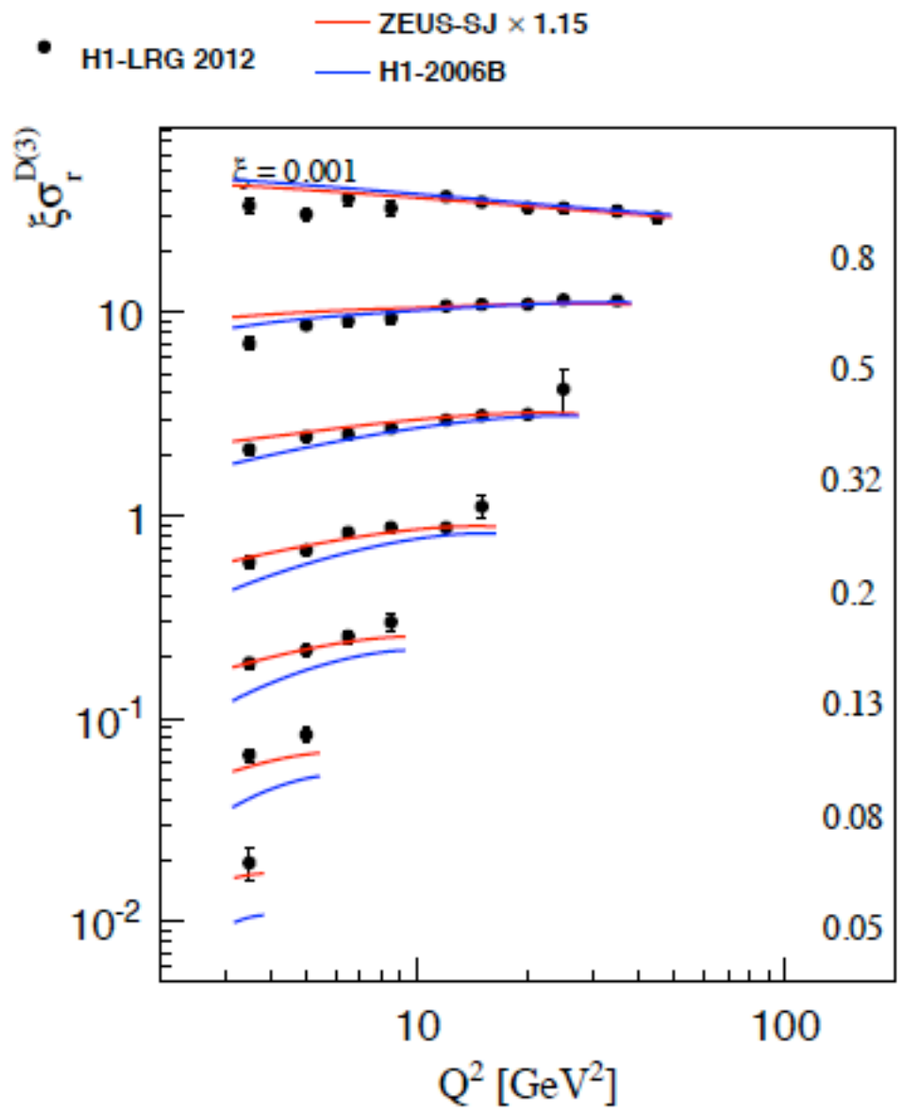

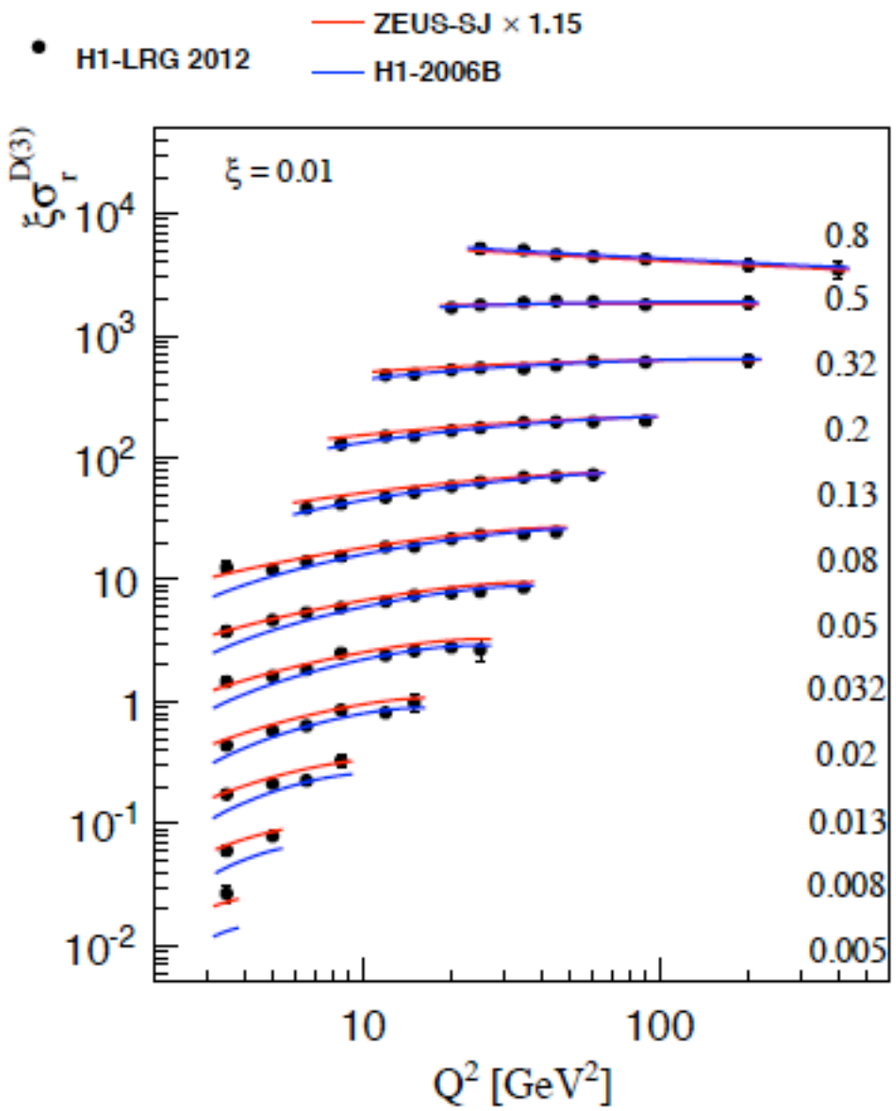

Comparison of H1-2006B and ZEUS-SJ fits to the H1-LRG 2012 data
ZEUS-SJ fit seems to better describe the data in the low β region

Diffraction in new machines

Prospects for diffractive phenomena measurements at EIC/LHeC/FCC-eh

Diffraction in new machines

Prospects for diffractive phenomena measurements at EIC/LHeC/FCC-eh

- Higher luminosity - > better statistics for rare processes like exclusive diffraction of vector mesons

Diffraction in new machines

Prospects for diffractive phenomena measurements at EIC/LHeC/FCC-eh

- ✦ Higher luminosity - > better statistics for rare processes like exclusive diffraction of vector mesons
- ✦ Extended kinematics (LHeC/FCC-eh) probing the diffraction in a new regime

Diffraction in new machines

Prospects for diffractive phenomena measurements at EIC/LHeC/FCC-eh

- ✦ Higher luminosity - > better statistics for rare processes like exclusive diffraction of vector mesons
- ✦ Extended kinematics (LHeC/FCC-eh) probing the diffraction in a new regime
- ✦ New diffractive final states involving EW bosons, top

Diffraction in new machines

Prospects for diffractive phenomena measurements at EIC/LHeC/FCC-eh

- ✦ Higher luminosity - > better statistics for rare processes like exclusive diffraction of vector mesons
- ✦ Extended kinematics (LHeC/FCC-eh) probing the diffraction in a new regime
- ✦ New diffractive final states involving EW bosons, top
- ✦ Extended lever arm and higher precision allows for the more constraints on the diffractive parton distribution functions

Diffraction in new machines

Prospects for diffractive phenomena measurements at EIC/LHeC/FCC-eh

- ✦ Higher luminosity - > better statistics for rare processes like exclusive diffraction of vector mesons
- ✦ Extended kinematics (LHeC/FCC-eh) probing the diffraction in a new regime
- ✦ New diffractive final states involving EW bosons, top
- ✦ Extended lever arm and higher precision allows for the more constraints on the diffractive parton distribution functions
- ✦ Test the limits of factorization in diffraction

Diffraction in new machines

Prospects for diffractive phenomena measurements at EIC/LHeC/FCC-eh

- ✦ Higher luminosity - > better statistics for rare processes like exclusive diffraction of vector mesons
- ✦ Extended kinematics (LHeC/FCC-eh) probing the diffraction in a new regime
- ✦ New diffractive final states involving EW bosons, top
- ✦ Extended lever arm and higher precision allows for the more constraints on the diffractive parton distribution functions
- ✦ Test the limits of factorization in diffraction
- ✦ Explore the relation between the diffraction and shadowing

Diffraction in new machines

Prospects for diffractive phenomena measurements at EIC/LHeC/FCC-eh

- ✦ Higher luminosity - > better statistics for rare processes like exclusive diffraction of vector mesons
- ✦ Extended kinematics (LHeC/FCC-eh) probing the diffraction in a new regime
- ✦ New diffractive final states involving EW bosons, top
- ✦ Extended lever arm and higher precision allows for the more constraints on the diffractive parton distribution functions
- ✦ Test the limits of factorization in diffraction
- ✦ Explore the relation between the diffraction and shadowing
- ✦ Possibility of precise diffractive measurements in nuclei

Diffraction in new machines

Prospects for diffractive phenomena measurements at EIC/LHeC/FCC-eh

- ✦ Higher luminosity - > better statistics for rare processes like exclusive diffraction of vector mesons
- ✦ Extended kinematics (LHeC/FCC-eh) probing the diffraction in a new regime
- ✦ New diffractive final states involving EW bosons, top
- ✦ Extended lever arm and higher precision allows for the more constraints on the diffractive parton distribution functions
- ✦ Test the limits of factorization in diffraction
- ✦ Explore the relation between the diffraction and shadowing
- ✦ Possibility of precise diffractive measurements in nuclei
- ✦ First extraction of the diffractive parton distributions in nuclei

Diffraction in new machines

Prospects for diffractive phenomena measurements at EIC/LHeC/FCC-eh

- ✦ Higher luminosity - > better statistics for rare processes like exclusive diffraction of vector mesons
- ✦ Extended kinematics (LHeC/FCC-eh) probing the diffraction in a new regime
- ✦ New diffractive final states involving EW bosons, top
- ✦ Extended lever arm and higher precision allows for the more constraints on the diffractive parton distribution functions
- ✦ Test the limits of factorization in diffraction
- ✦ Explore the relation between the diffraction and shadowing
- ✦ Possibility of precise diffractive measurements in nuclei
- ✦ First extraction of the diffractive parton distributions in nuclei
- ✦ Possibility of nuclei tomography using the elastic diffractive vector meson production and virtual Compton scattering on nuclei

Phase space: HERA to LHeC to FCC-eh

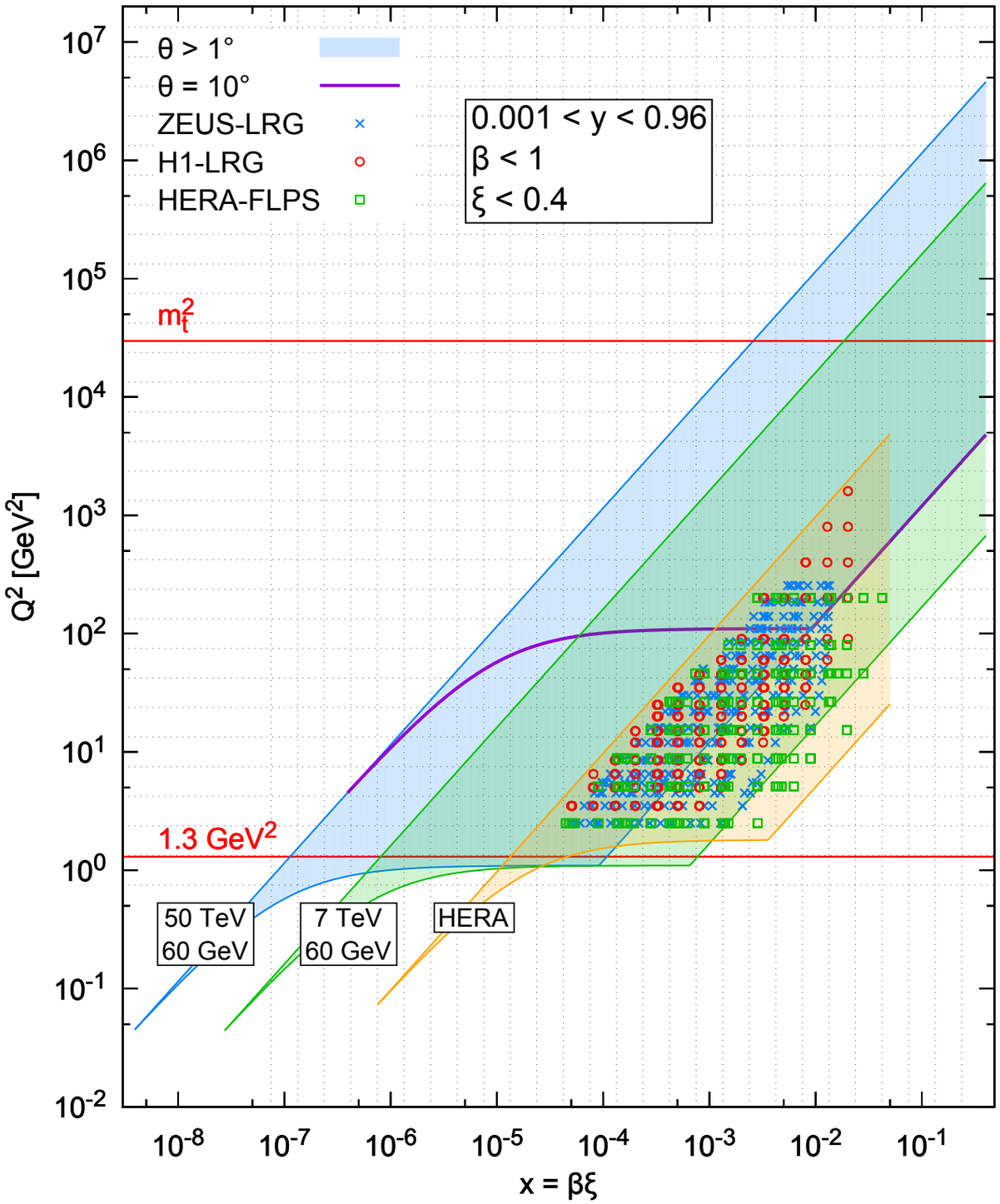

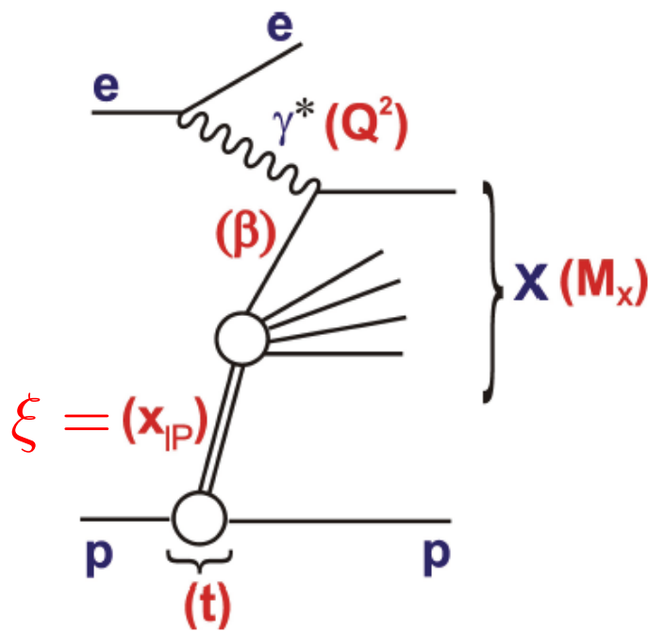

$E_e = 60\ GeV$

- $E_p = 7$ TeV vs. HERA
  - $x_{\min}$ down by factor ~20
  - $Q^2_{\max}$ up by factor ~100
- $E_p = 50$ TeV vs. 7 TeV
  - $x_{\min}$ down by factor ~10
  - $Q^2_{\max}$ up by factor ~10

LHeC phase space: (β,Q^2) fixed ξ

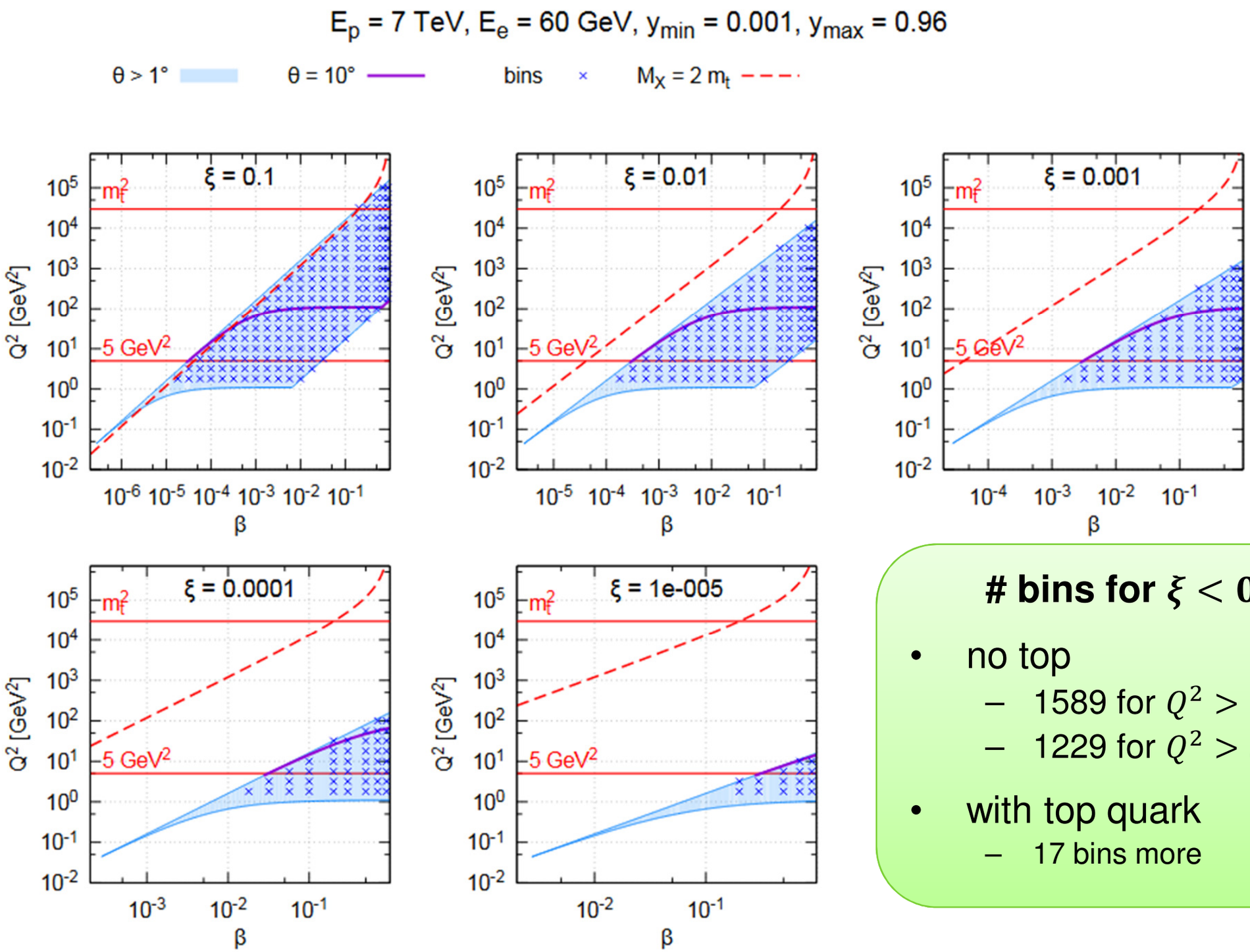

 # bins for $\xi < 0.15$

- no top
  - 1589 for $Q^2 > 1.3\ \mathrm{GeV}^2$
  - 1229 for $Q^2 > 5\ \mathrm{GeV}^2$
- with top quark
  - 17 bins more

FCC-eh phase space: (β,Q^2) fixed ξ

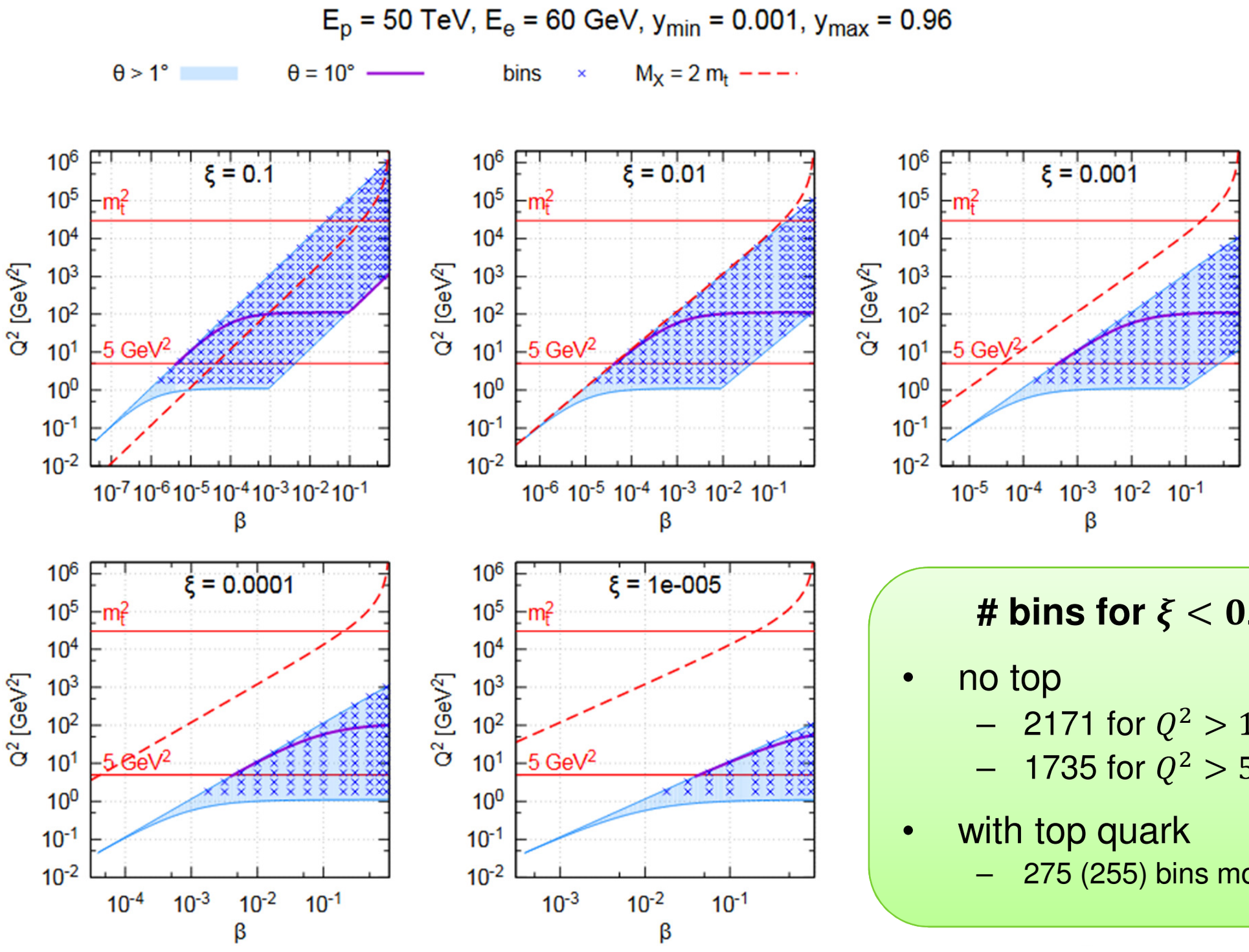

 # bins for $\xi < 0.15$

- no top
  - 2171 for $Q^2 > 1.3\ \mathrm{GeV}^2$
  - 1735 for $Q^2 > 5\ \mathrm{GeV}^2$
- with top quark
  - 275 (255) bins more

Data simulations

- Simulations based on extrapolation from ZEUS-SJ DPDFs
- VFNS scheme but no top at HERA so top contribution neglected in the simulation
- Errors simulated with 5% Gaussian noise
- Reggeon contribution is included but hard to constrain at HERA, could lead to large uncertainty in the extrapolation at $\xi > 0.01$
- Binning to assume negligible statistical errors

Example of data: large ξ, LHeC

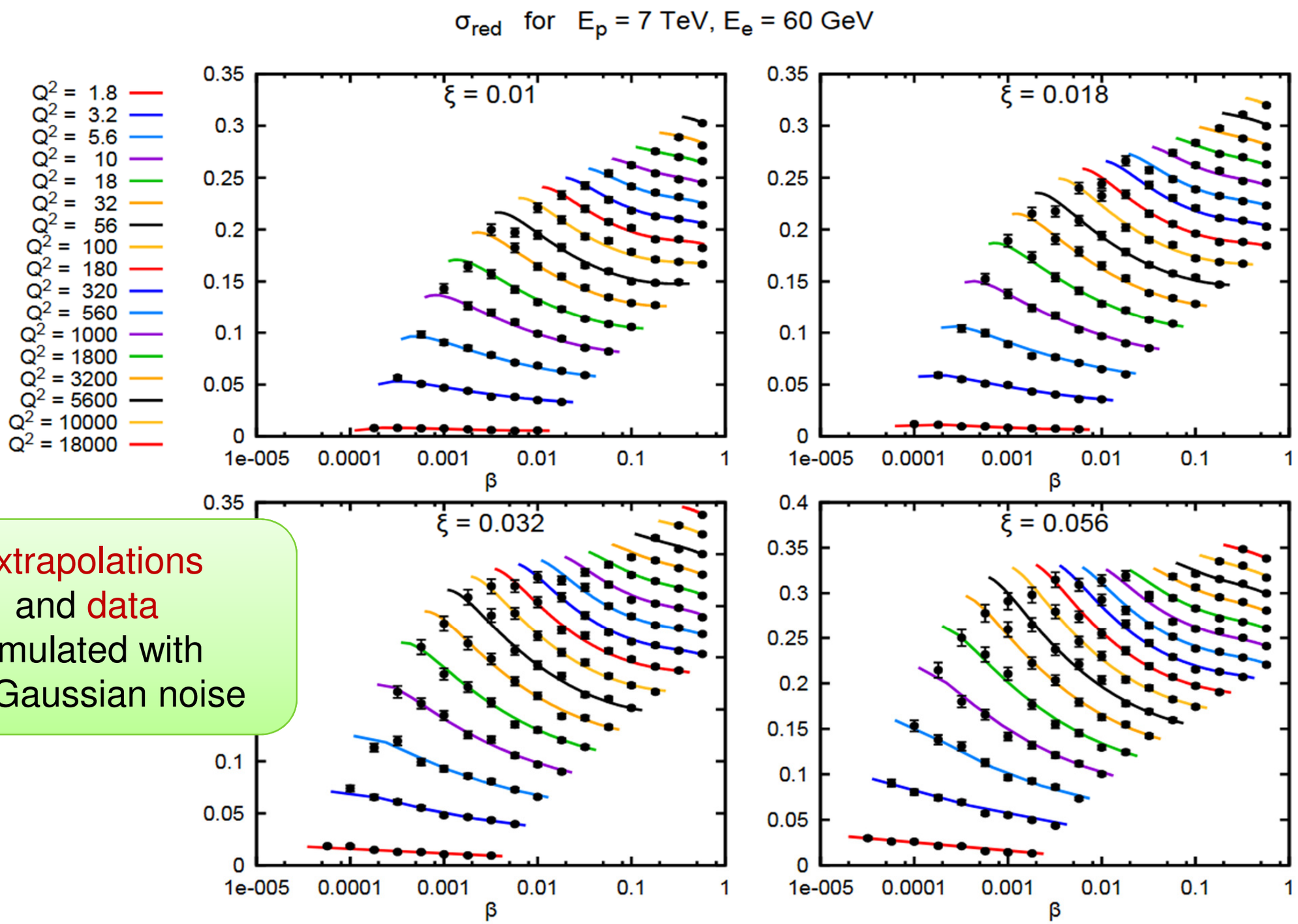

Extrapolations
and data
simulated with
5% Gaussian noise

Example of data: large ξ, FCC-eh

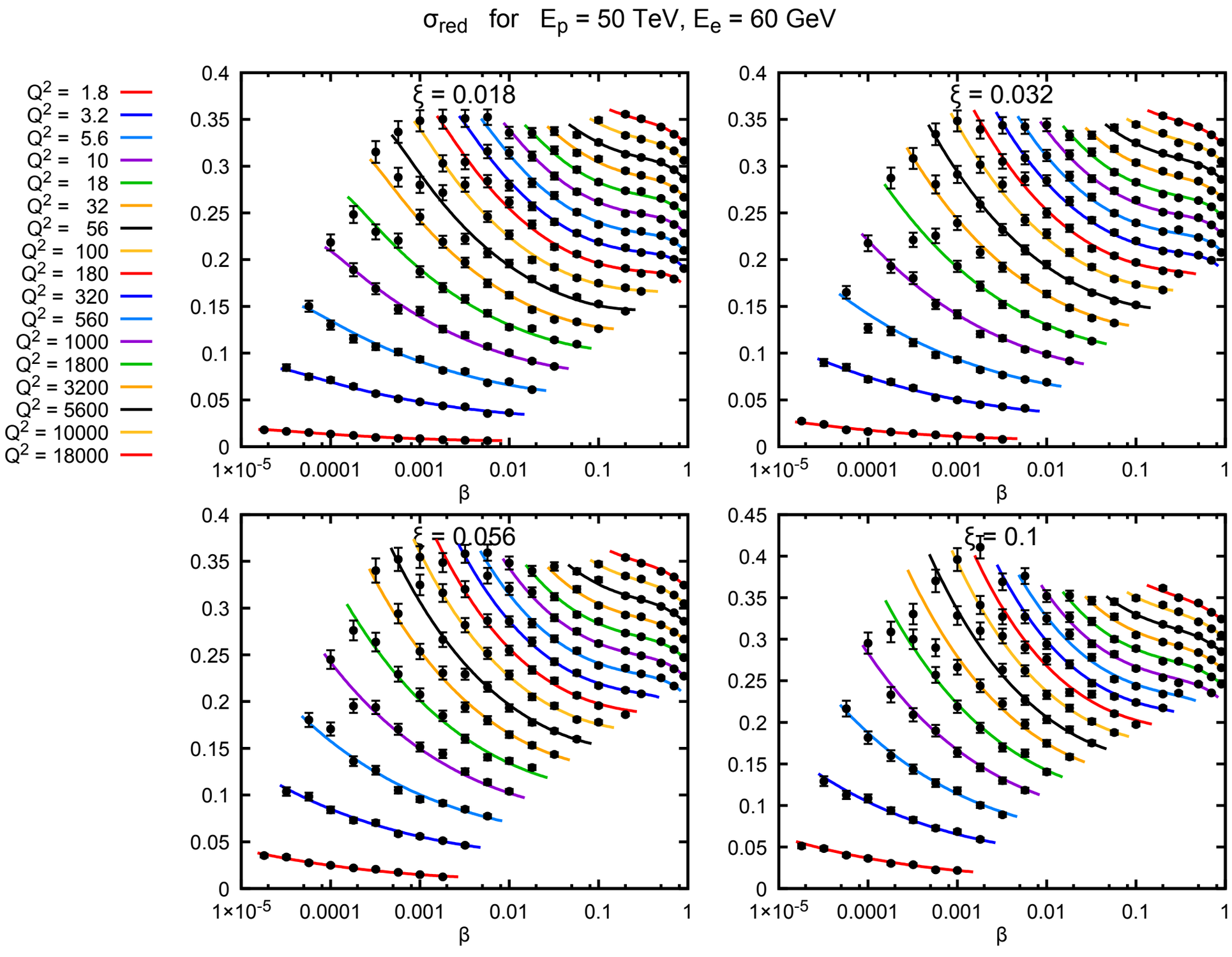

DPDFs from simulations

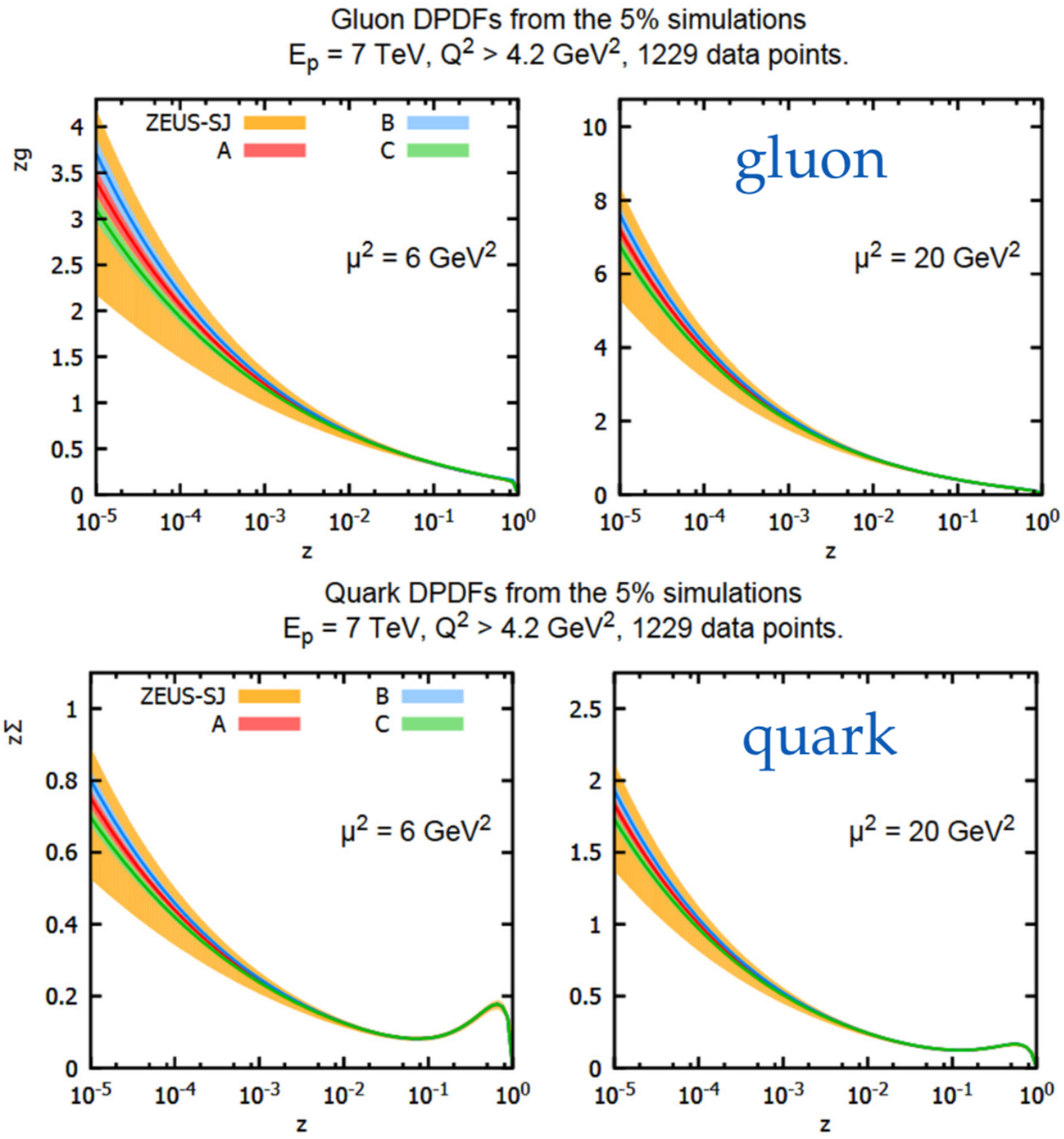

$$Q^2_{\min} \approx 5\ \mathrm{GeV}^2$$

$$E_p = 7\ \mathrm{TeV}$$

- Substantially improved accuracy wrt. HERA
- Statistical spread ~ 2 × error-band
- Statistical spreads well below error-bands for $Q^2_{\min} \approx 1.3\ \mathrm{GeV}^2$ or

DPDFs error bands

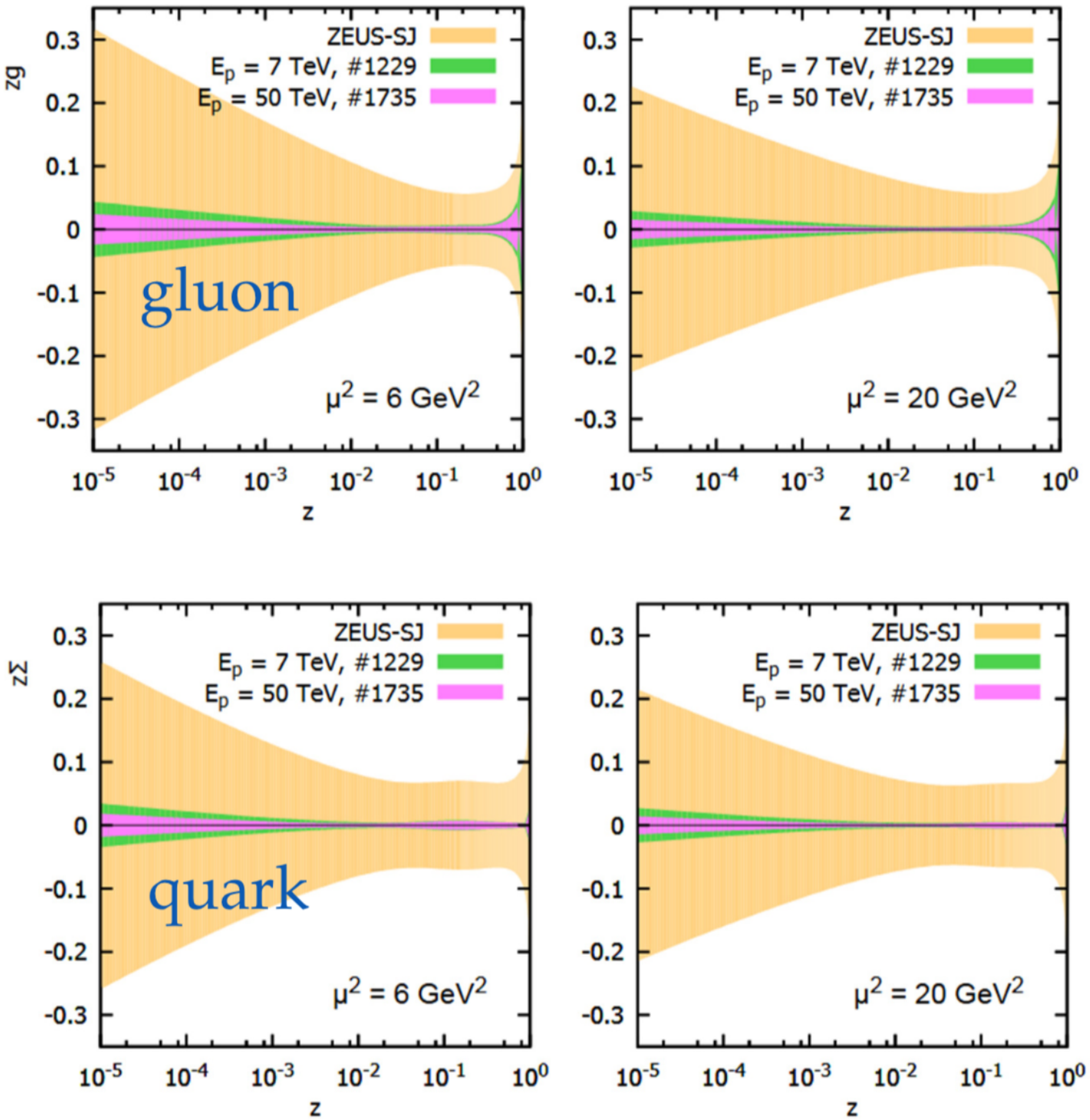

$$Q^2_{\min} \approx 5\ \mathrm{GeV}^2$$

Accuracy increased by

- ✓ factor ~10 for LHeC
- ✓ factor ~20 for FCC-he

Dependence on Q_{min}^2 and E_p

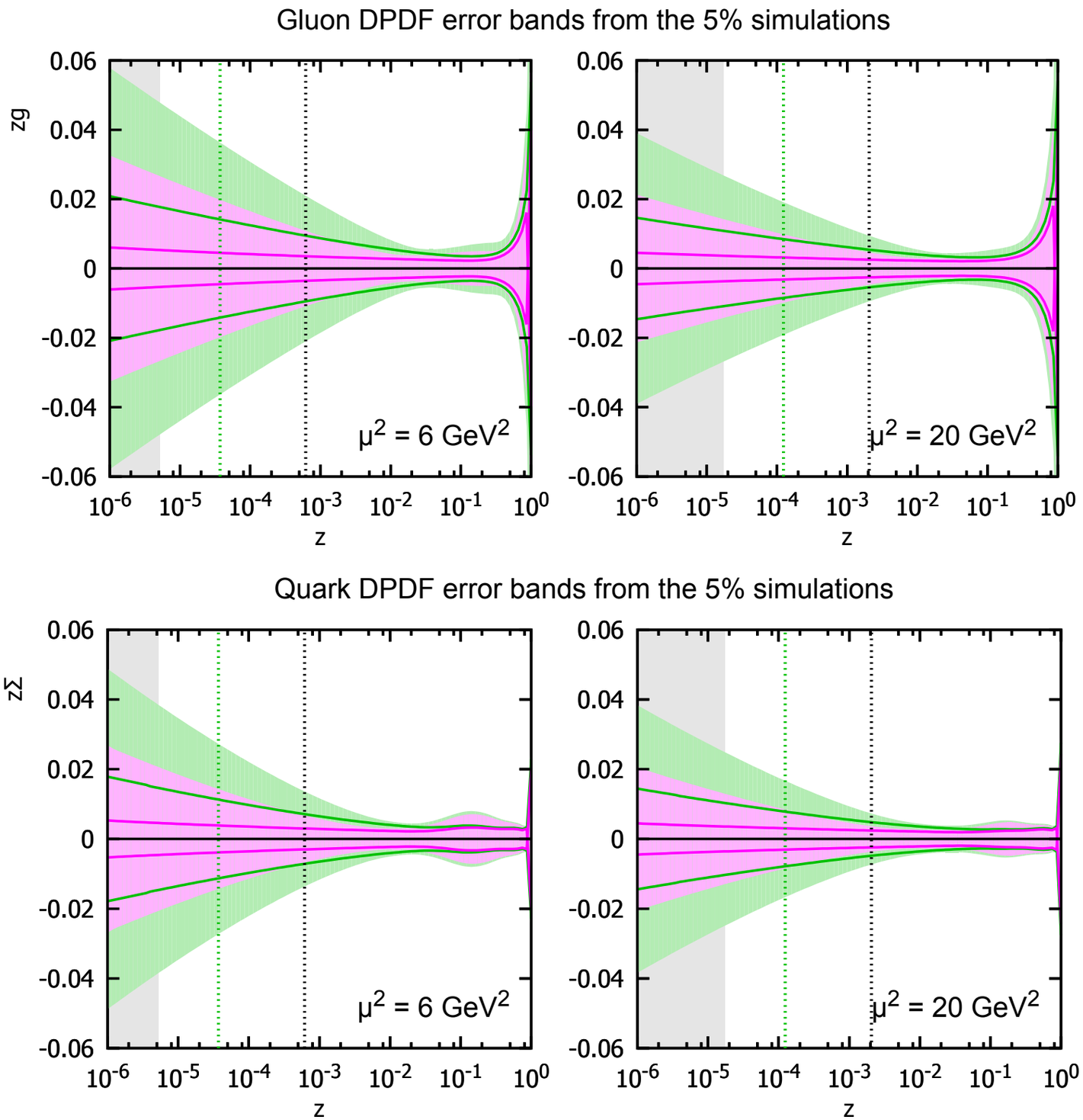

E_p = 7 TeV, #1229, Q^2_{min} = 4.2 GeV^2
E_p = 50 TeV, #1735, Q^2_{min} = 4.2 GeV^2

E_p = 7 TeV, #1589, Q^2_{min} = 1.3 GeV^2
E_p = 50 TeV, #2171, Q^2_{min} = 1.3 GeV^2

Improvement of accuracy of factor about 3 ÷ 5 for low Q_{min}^2

Low Q^2 region sensitive to higher twists, saturation etc especially in diffraction. DGLAP fits may not work/ be reliable in this region.

Nuclear diffractive structure functions

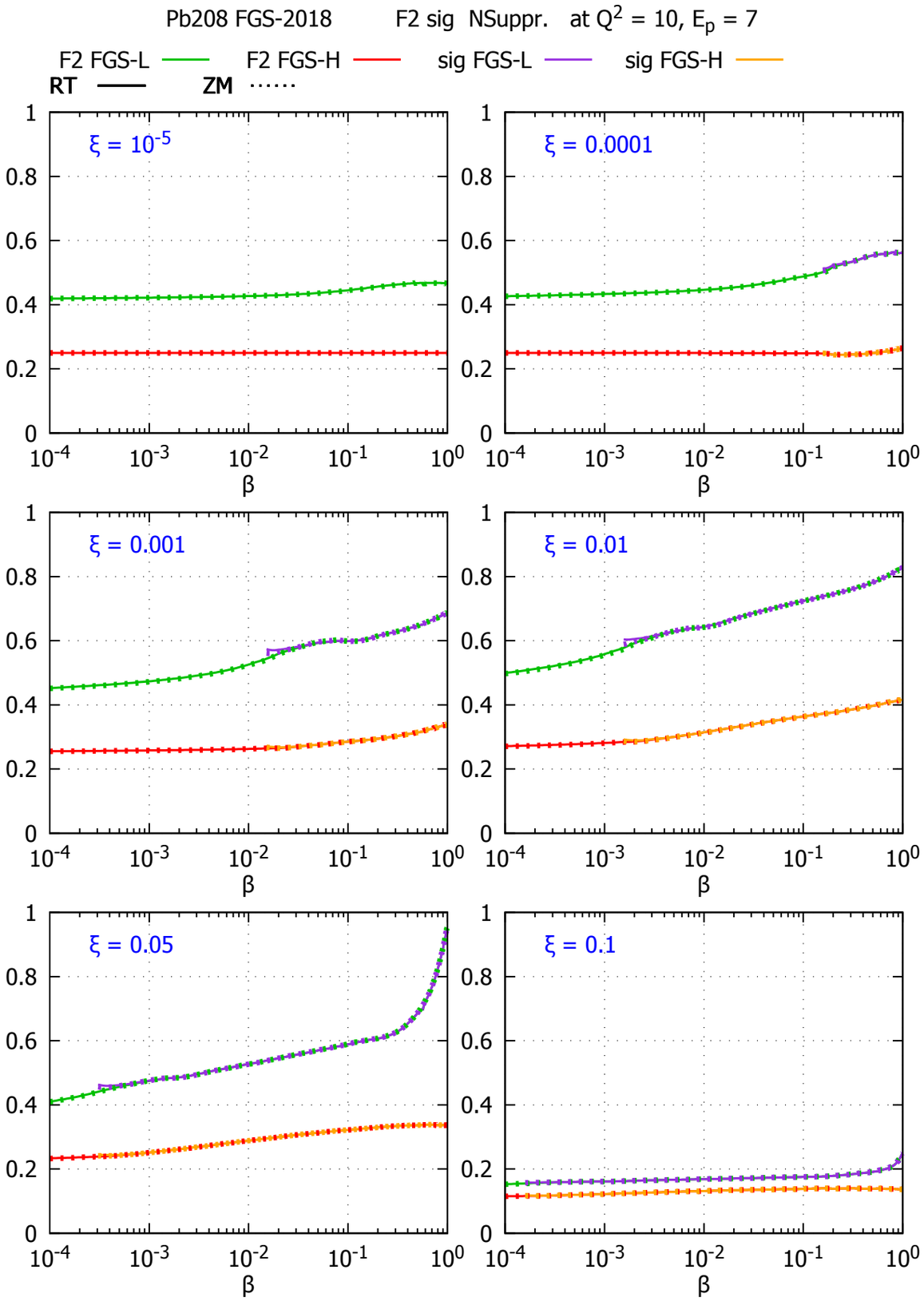

- Model for nuclear shadowing: Frankfurt,Guzey,Strikman
- Two models: high and low shadowing
- Large discrepancies between two models
- Results for nuclear ratio:

$$R_k(\beta, \xi, Q^2) = \frac{f_{k/A}^{D(3)}(\beta, \xi, Q^2)}{A\, f_{k/p}^{D(3)}(\beta, \xi, Q^2)}$$

Electron Ion Collider (EIC/LHeC/FCC-eh) will be able to quickly pin down the nuclear diffractive structure functions

Nuclear diffractive structure functions

e Pb $E_{Pb}/A = 2.76$ TeV, $E_e = 60$ GeV, $L = 2$ fb^{-1}

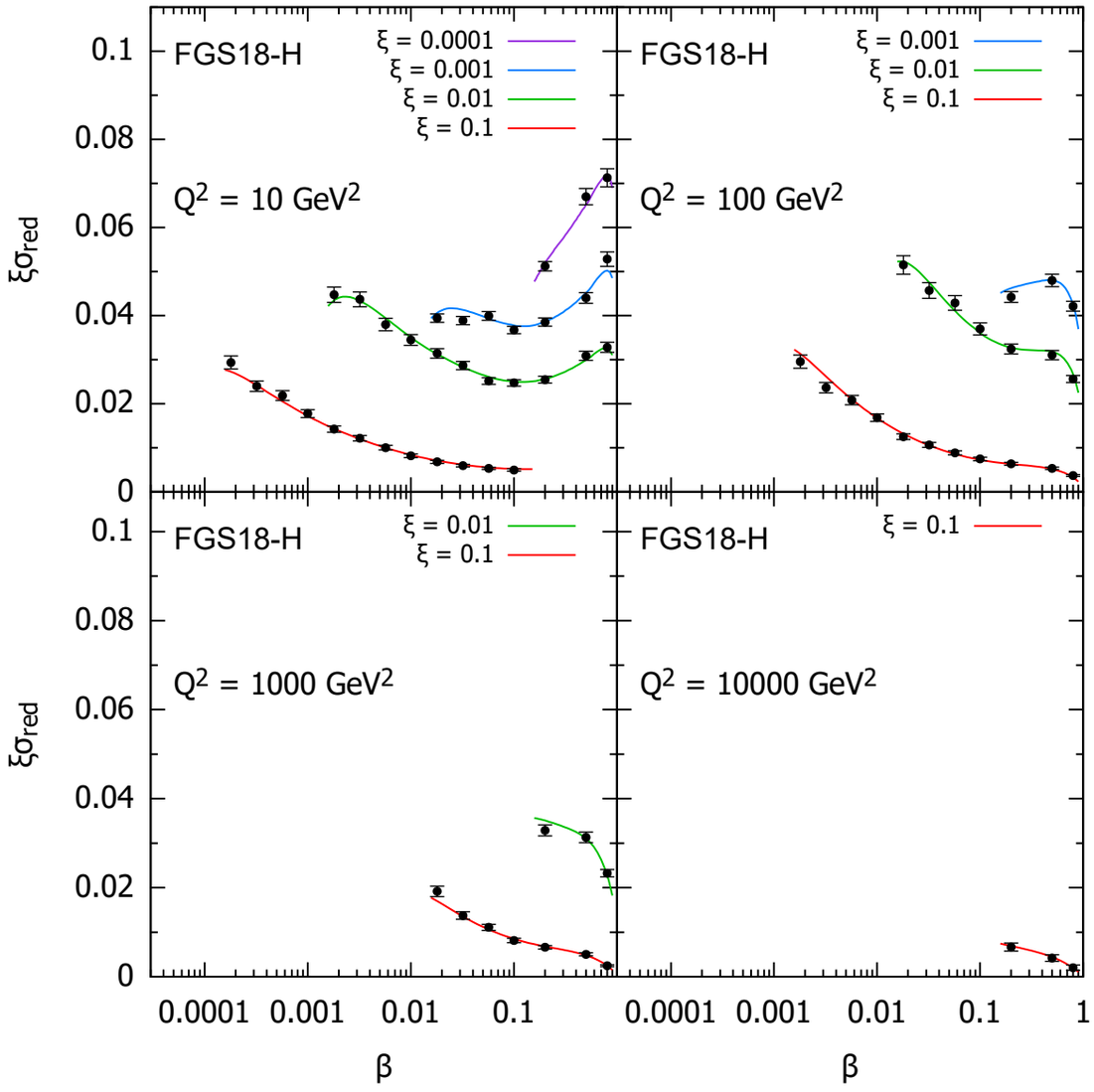

e Pb $E_{Pb}/A = 19.7$ TeV, $E_e = 60$ GeV, $L = 2$ fb^{-1}

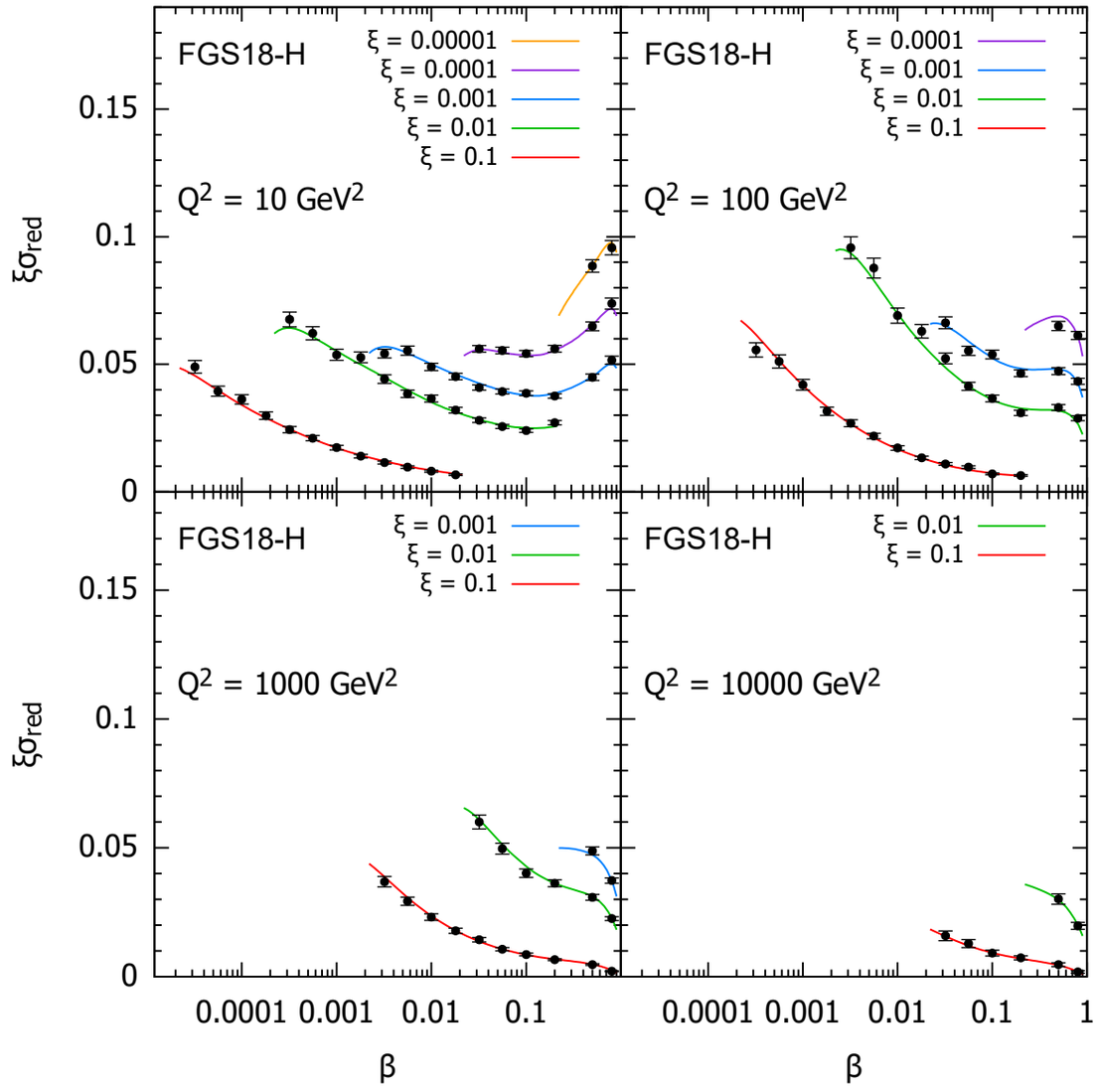

Precision of the data limited by systematics
5% error is conservative, could be as low as 2%
This would allow for the extraction of the nuclear diffractive PDFs with the same precision as the proton PDFs.

Exclusive diffraction

Elastic diffractive production of vector meson

$q\bar{q}$ valence component

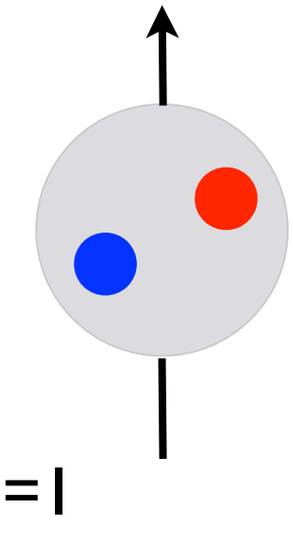

J/Ψ	3 GeV
ρ	0.77 GeV
ω	0.782 GeV

Elastic production of meson V in the interaction of photon-proton

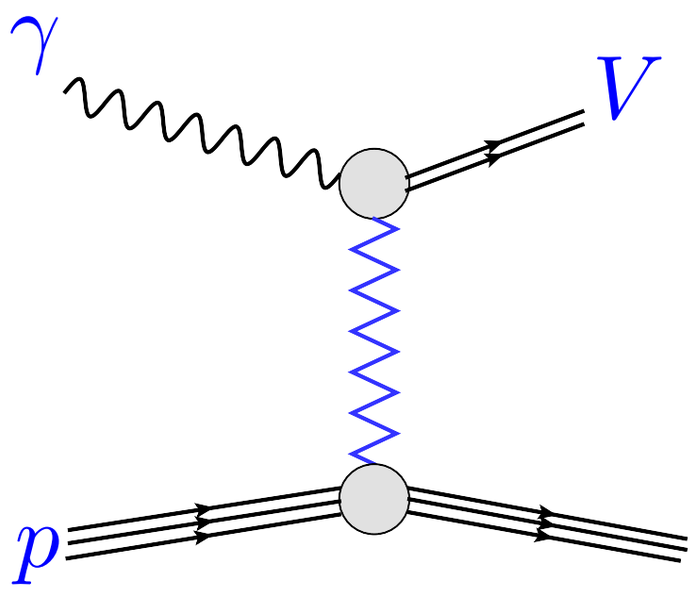

$\gamma p \to J/\psi\, p$ cross section from HERA and LHC

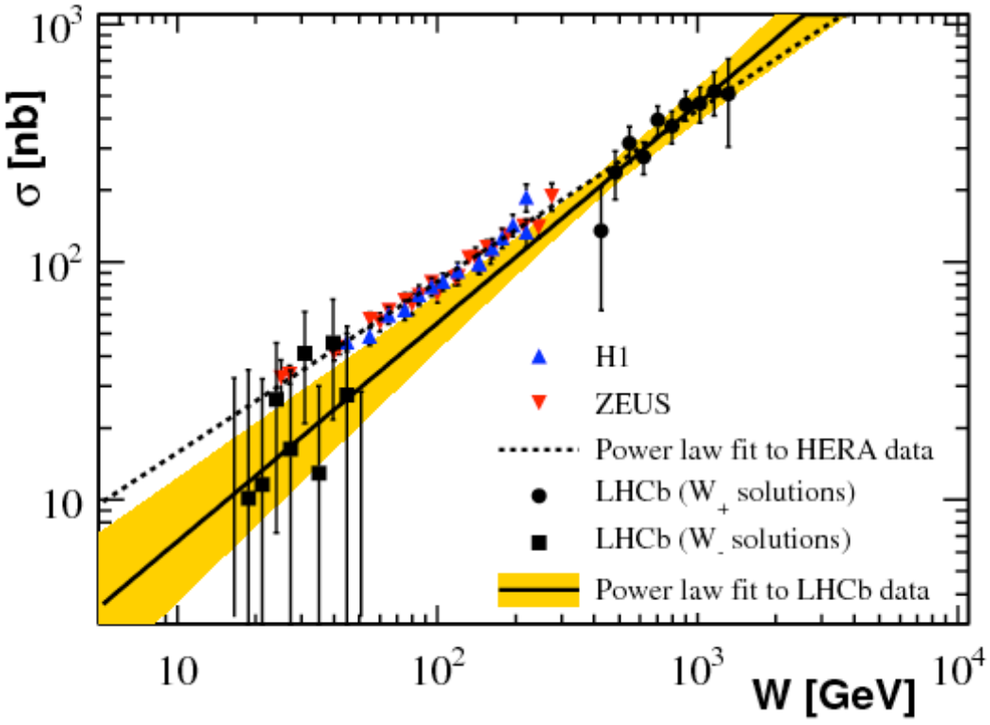

Diffraction in optics

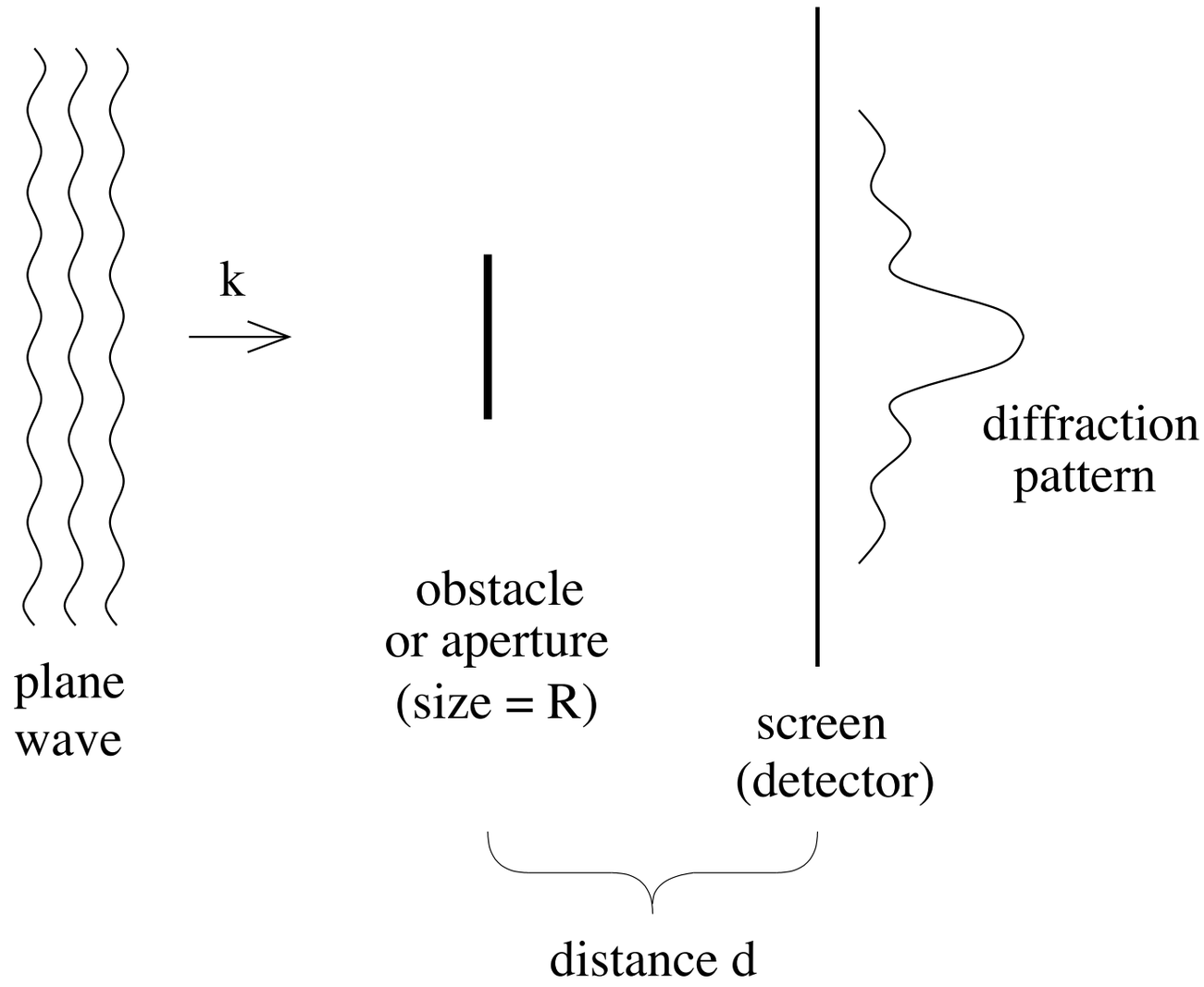

By studying diffraction pattern one can learn about the size of the obstacle and its density

Diffraction in optics and in hadron physics

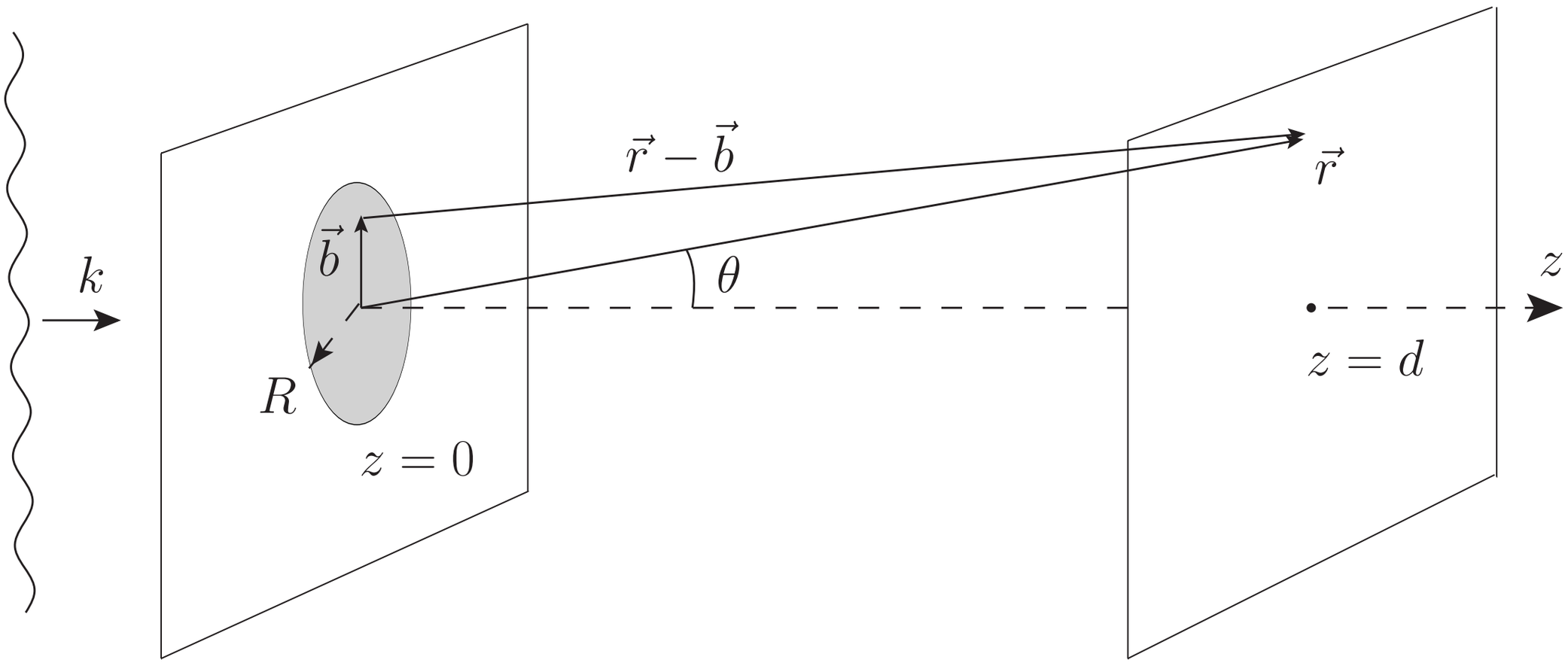

In optics: diffraction is analyzed in terms of angle θ

In particle physics: diffraction is analyzed in terms of Mandelstam invariant t : momentum transfer

Elastic diffractive production of vector meson

Dipole picture of VM production

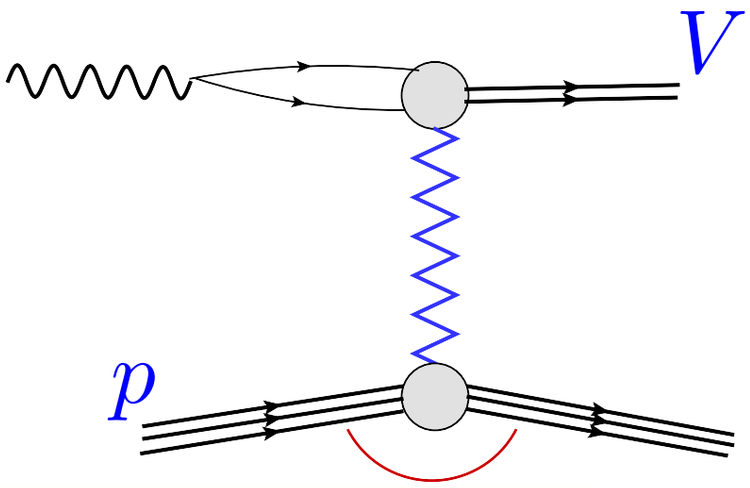

Momentum transfer $t = -\Delta^2$

Elastic diffractive production of vector meson

Dipole picture of VM production

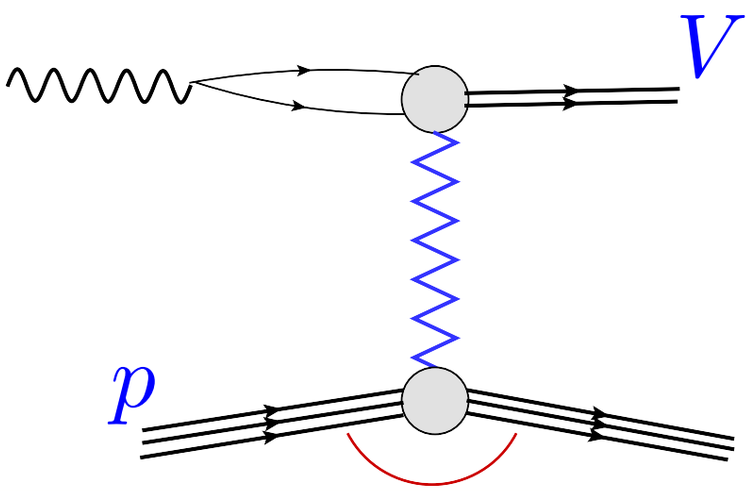

Differential cross section

$$\frac{\mathrm{d}\sigma_{T,L}^{\gamma^* p\to Ep}}{\mathrm{d}t} = \frac{1}{16\pi}\left|\mathcal{A}_{T,L}^{\gamma^* p\to Ep}\right|^2$$

Amplitude

$$\mathcal{A}_{T,L}^{\gamma^* p\to Ep}(x,Q,\Delta) = \mathrm{i}\int \mathrm{d}^2\boldsymbol{r}\int_0^1 \frac{\mathrm{d}z}{4\pi}\int \mathrm{d}^2\boldsymbol{b}\,(\Psi_E^*\Psi)_{T,L}\,\mathrm{e}^{-\mathrm{i}[\boldsymbol{b}-(1-z)\boldsymbol{r}]\cdot\boldsymbol{\Delta}}\,\frac{\mathrm{d}\sigma_{q\bar{q}}}{\mathrm{d}^2\boldsymbol{b}}.$$

Momentum transfer $t = -\Delta^2$

Elastic diffractive production of vector meson

Dipole picture of VM production

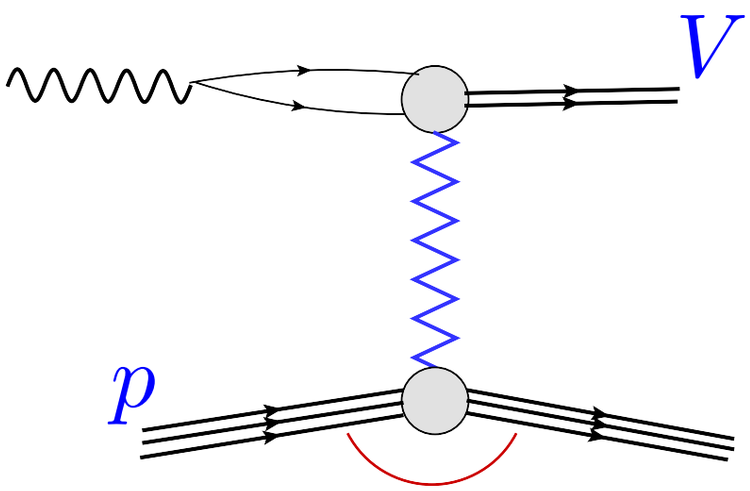

Momentum transfer $t = -\Delta^2$

Differential cross section

$$\frac{\mathrm{d}\sigma_{T,L}^{\gamma^* p\to Ep}}{\mathrm{d}t} = \frac{1}{16\pi}\left|\mathcal{A}_{T,L}^{\gamma^* p\to Ep}\right|^2$$

Amplitude

$$\mathcal{A}_{T,L}^{\gamma^* p\to Ep}(x,Q,\Delta) = \mathrm{i}\int \mathrm{d}^2\boldsymbol{r}\int_0^1 \frac{\mathrm{d}z}{4\pi}\int \mathrm{d}^2\boldsymbol{b}\,(\Psi_E^*\Psi)_{T,L}\,\mathrm{e}^{-\mathrm{i}[\boldsymbol{b}-(1-z)\boldsymbol{r}]\cdot\boldsymbol{\Delta}}\,\frac{\mathrm{d}\sigma_{q\bar{q}}}{\mathrm{d}^2\boldsymbol{b}}.$$

Dipole amplitude with impact parameter dependence

$$\frac{\mathrm{d}\sigma_{q\bar{q}}}{\mathrm{d}^2\boldsymbol{b}} = 2[1-\mathrm{Re}\,S(x,r,b)] = 2N(x,r,b)$$

Elastic diffractive production of vector meson

Dipole picture of VM production

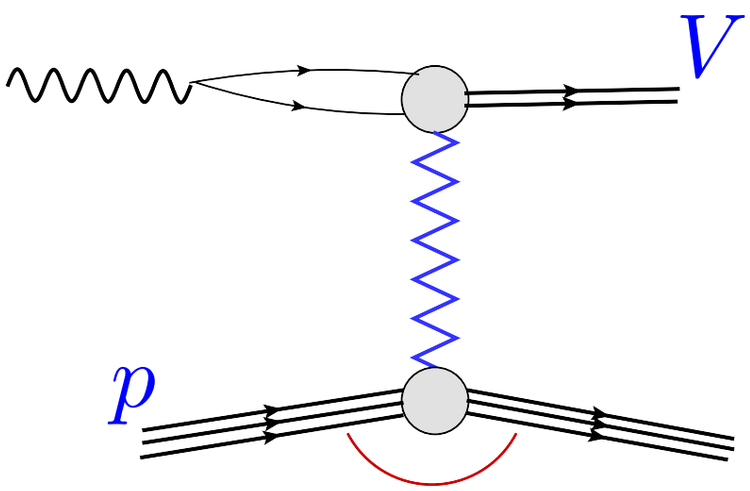

Momentum transfer $t = -\Delta^2$

Differential cross section

$$\frac{\mathrm{d}\sigma_{T,L}^{\gamma^* p \to Ep}}{\mathrm{d}t} = \frac{1}{16\pi} \left| \mathcal{A}_{T,L}^{\gamma^* p \to Ep} \right|^2$$

Amplitude

$$\mathcal{A}_{T,L}^{\gamma^* p \to Ep}(x, Q, \Delta) = \mathrm{i} \int \mathrm{d}^2\boldsymbol{r} \int_0^1 \frac{\mathrm{d}z}{4\pi} \int \mathrm{d}^2\boldsymbol{b}\, (\Psi_E^* \Psi)_{T,L}\, \mathrm{e}^{-\mathrm{i}[\boldsymbol{b}-(1-z)\boldsymbol{r}]\cdot\boldsymbol{\Delta}}\, \frac{\mathrm{d}\sigma_{q\bar{q}}}{\mathrm{d}^2\boldsymbol{b}}.$$

Dipole amplitude with impact parameter dependence

$$\frac{\mathrm{d}\sigma_{q\bar{q}}}{\mathrm{d}^2\boldsymbol{b}} = 2[1 - \mathrm{Re}\, S(x, r, b)] = 2N(x, r, b)$$

Dipole cross section

$$\sigma_{q\bar{q}}(x, r) = \int \mathrm{d}^2\boldsymbol{b}\, 2[1 - \mathrm{Re}\, S(x, r, b)]$$

Elastic diffractive production of vector meson

Dipole picture of VM production

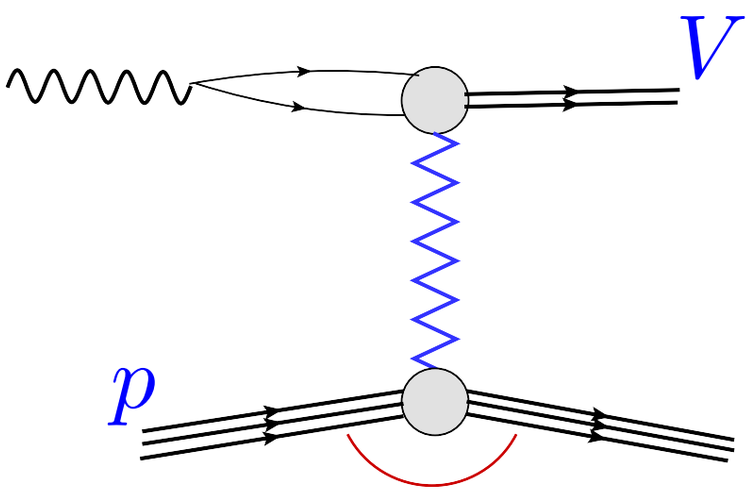

Momentum transfer $t = -\Delta^2$

Differential cross section

$$\frac{\mathrm{d}\sigma_{T,L}^{\gamma^* p \to Ep}}{\mathrm{d}t} = \frac{1}{16\pi} \left| \mathcal{A}_{T,L}^{\gamma^* p \to Ep} \right|^2$$

Amplitude

$$\mathcal{A}_{T,L}^{\gamma^* p \to Ep}(x, Q, \Delta) = \mathrm{i} \int \mathrm{d}^2\boldsymbol{r} \int_0^1 \frac{\mathrm{d}z}{4\pi} \int \mathrm{d}^2\boldsymbol{b}\, (\Psi_E^* \Psi)_{T,L}\, \mathrm{e}^{-\mathrm{i}[\boldsymbol{b}-(1-z)\boldsymbol{r}]\cdot\boldsymbol{\Delta}}\, \frac{\mathrm{d}\sigma_{q\bar{q}}}{\mathrm{d}^2\boldsymbol{b}}.$$

Dipole amplitude with impact parameter dependence

$$\frac{\mathrm{d}\sigma_{q\bar{q}}}{\mathrm{d}^2\boldsymbol{b}} = 2[1 - \mathrm{Re}\, S(x, r, b)] = 2N(x, r, b)$$

Dipole cross section

$$\sigma_{q\bar{q}}(x, r) = \int \mathrm{d}^2\boldsymbol{b}\, 2[1 - \mathrm{Re}\, S(x, r, b)]$$

Vector meson wave function Ψ_E

$(\Psi_E^* \Psi)_{T,L}$ Overlap between meson and photon wave functions

Exclusive diffraction

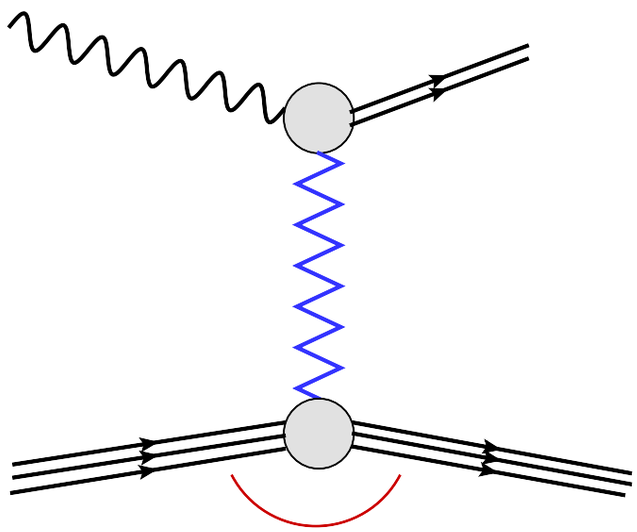

Momentum transfer $t = -\Delta^2$

- Exclusive diffractive production of VM is an excellent process for extracting the dipole amplitude and GPDs
- Suitable process for estimating the ‘blackness’ of the interaction.
- t-dependence provides an information about the impact parameter b-profile of the amplitude.

"b-Sat" dipole scattering amplitude with r = 1 GeV^{-1}

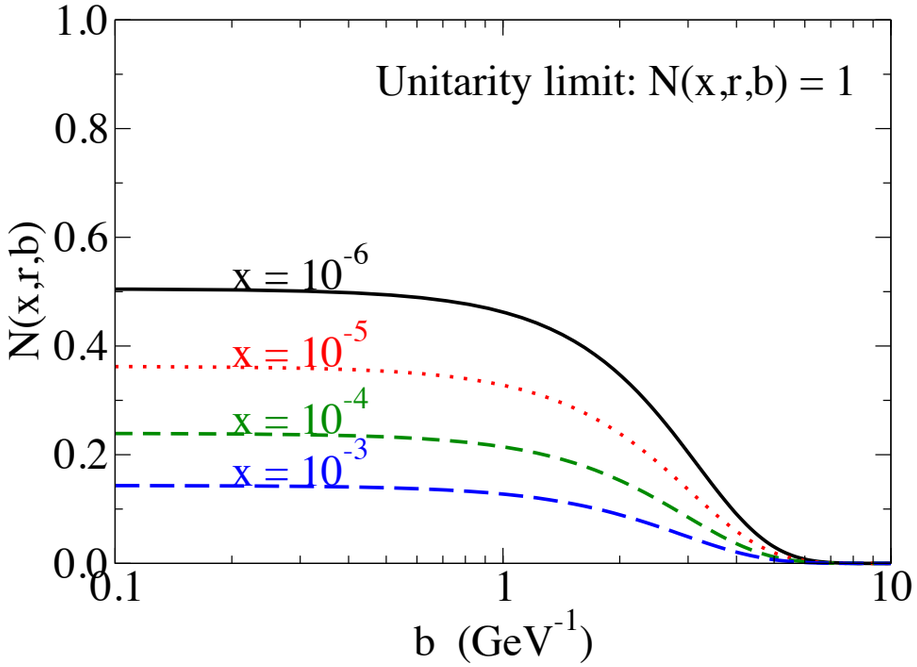

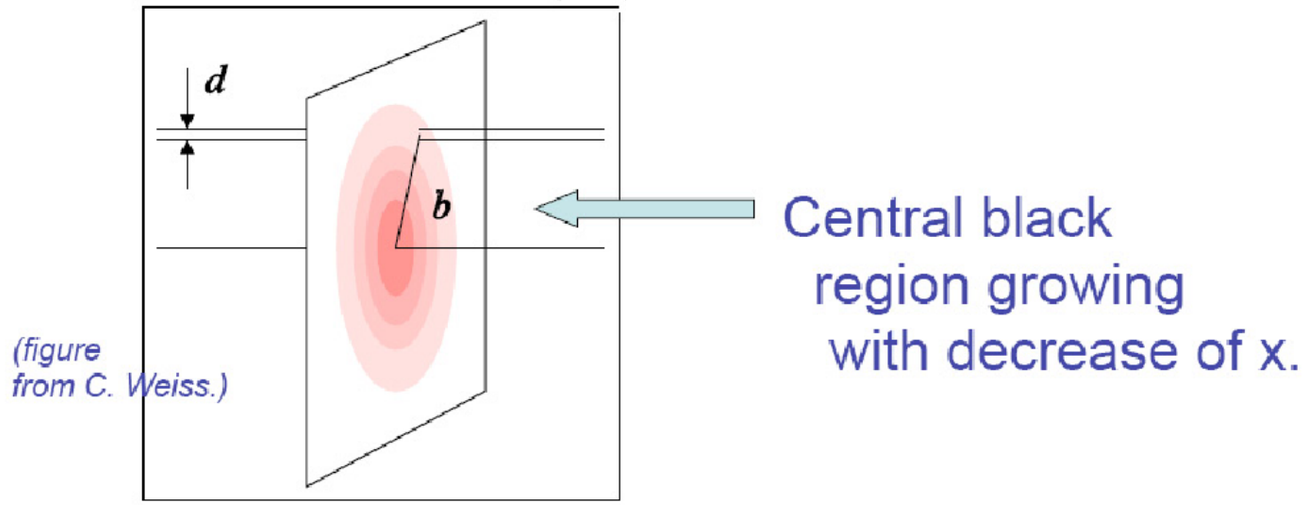

Large momentum transfer t probes small impact parameter where the density of interaction region is most dense.

Dipole amplitude with impact parameter dependence

BK equation in principle can provide with the solution that includes b-dependence.
But non-perturbative parameters are needed.
Dipole cross section with impact parameter parametrized in the literature.

$$\frac{\mathrm{d}\sigma_{q\bar{q}}}{\mathrm{d}^2\boldsymbol{b}} = 2[1 - \mathrm{Re}\, S(x, r, b)] = 2N(x, r, b)$$

Dipole amplitude depends on x, dipole size r and impact parameter b

Dipole amplitude with impact parameter dependence

BK equation in principle can provide with the solution that includes b-dependence.
But non-perturbative parameters are needed.
Dipole cross section with impact parameter parametrized in the literature.

$$\frac{\mathrm{d}\sigma_{q\bar{q}}}{\mathrm{d}^2\boldsymbol{b}} = 2[1 - \mathrm{Re}\, S(x, r, b)] = 2N(x, r, b)$$

Dipole amplitude depends on x, dipole size r and impact parameter b

Example of dipole amplitude parametrization with impact parameter dependence (IP-sat model)

$$\frac{d\sigma_{q\bar{q}}}{d^2b} = 2\left[1 - \exp\left(-\frac{\pi^2}{2\,N_C} r^2 \alpha_s(\mu^2) x g(x, \mu^2) T(b)\right)\right] .$$

Gluon density from DGLAP evolution: $xg(x, \mu^2)$ $\mu^2 = \frac{C}{r^2} + \mu_0^2$

Gaussian impact parameter profile:

$$T_G(b) = \frac{1}{2\pi B_G} \exp\left(-b^2/2B_G\right)$$

Dipole amplitude with impact parameter dependence

$$\frac{d\sigma_{q\bar{q}}}{d^2b} = 2\left[1 - \exp\left(-\frac{\pi^2}{2\,N_C} r^2 \alpha_s(\mu^2) x g(x,\mu^2) T(b)\right)\right] . \qquad T_G(b) \;=\; \frac{1}{2\pi B_G} \exp\left(-b^2/2B_G\right)$$

With decreasing x and/or increasing dipole size r the amplitude grows
The amplitude saturates at central impact parameters

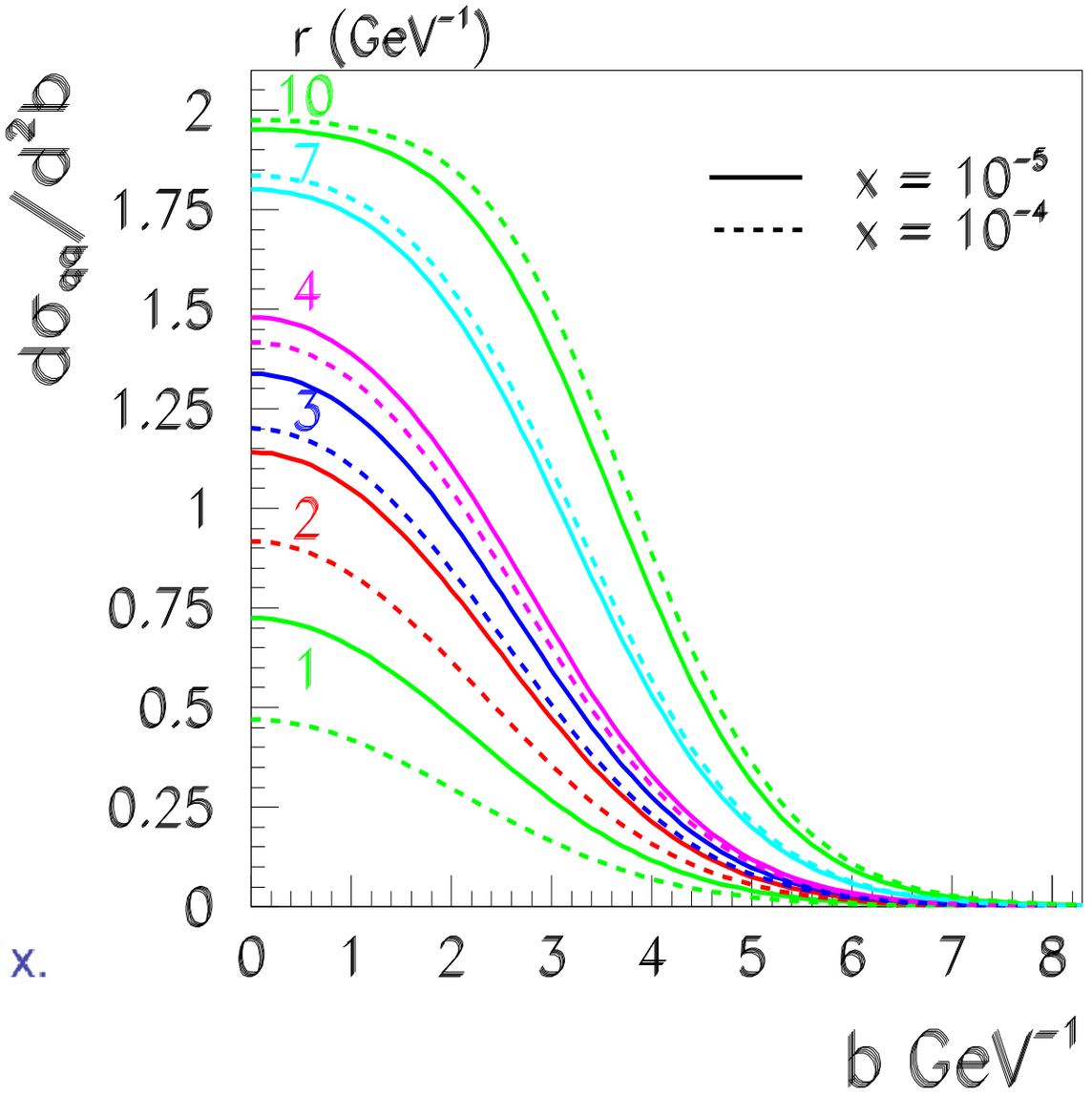

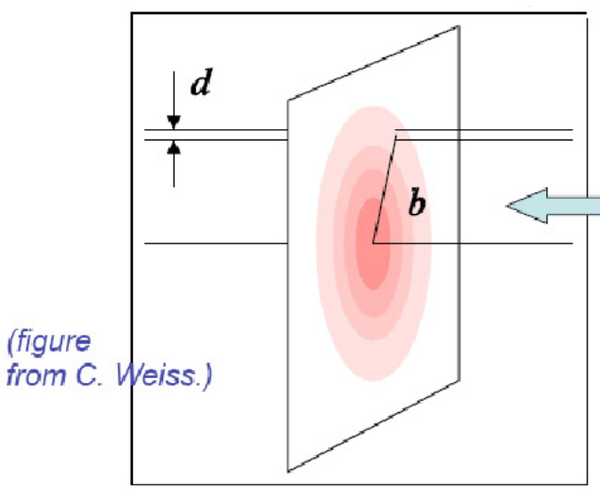

(figure from C. Weiss.)

Central black region growing with decrease of x.

Exclusive diffraction: predictions

$$\sigma^{\gamma p \to J/\Psi + p}(W)$$

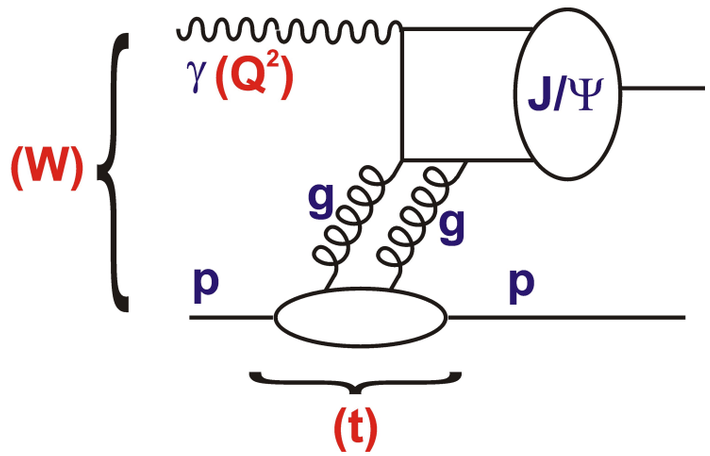

- b-Sat dipole model (Golec-Biernat, Wuesthoff, Bartels, Motyka, Kowalski, Watt)
- eikonalised: with saturation
- 1-Pomeron: no saturation

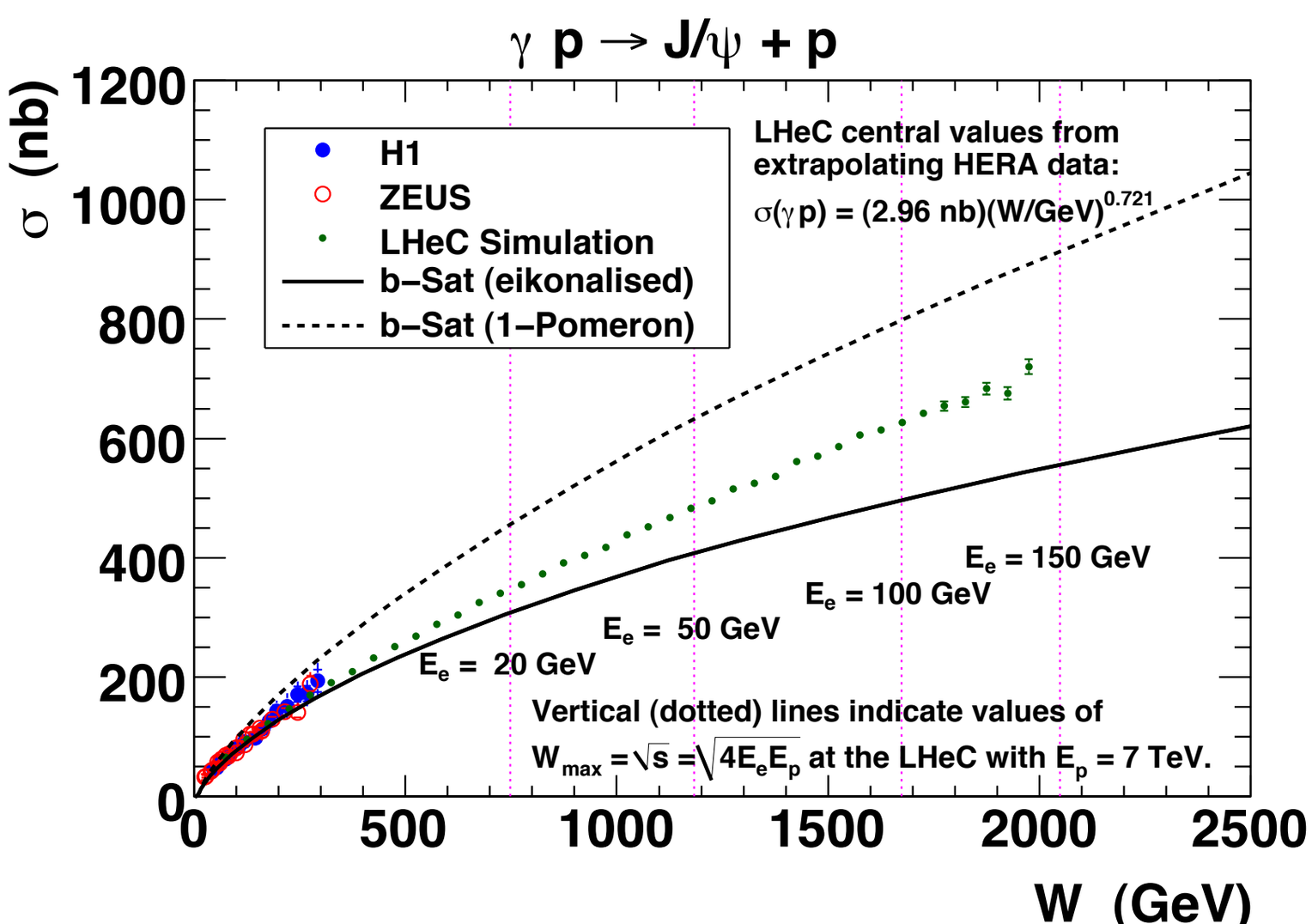

Large effects even for the t-integrated observable.

Different W behavior depending whether saturation is included or not.

Simulated data are from extrapolated fit to HERA data

Exclusive diffraction: predictions

$$\sigma^{\gamma p \to J/\Psi + p}(W)$$

- b-Sat dipole model (Golec-Biernat, Wuesthoff, Bartels, Motyka, Kowalski, Watt)
- eikonalised: with saturation
- 1-Pomeron: no saturation

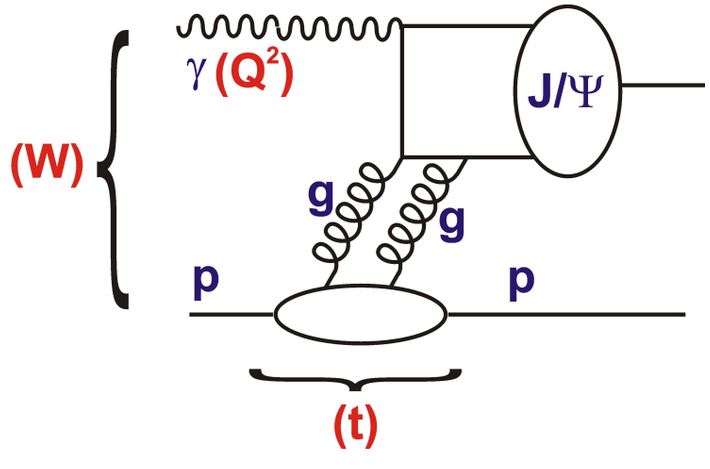

Large effects even for the t-integrated observable.

Different W behavior depending whether saturation is included or not.

Simulated data are from extrapolated fit to HERA data

Exclusive diffraction: predictions

$$\sigma^{\gamma p \to J/\Psi + p}(W)$$

- b-Sat dipole model (Golec-Biernat, Wuesthoff, Bartels, Motyka, Kowalski, Watt)
- eikonalised: with saturation
- 1-Pomeron: no saturation

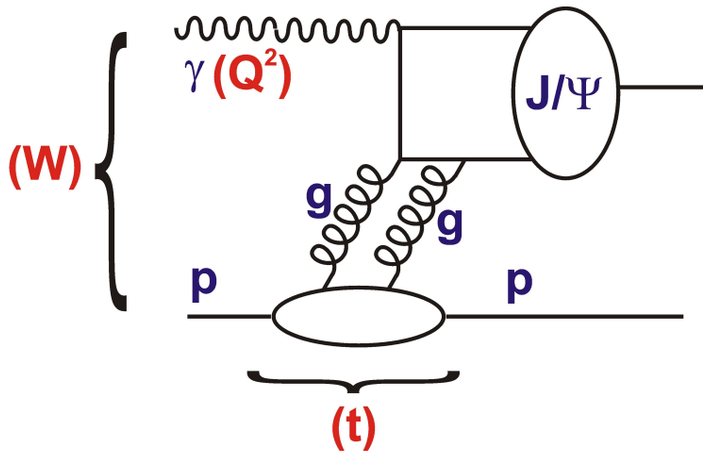

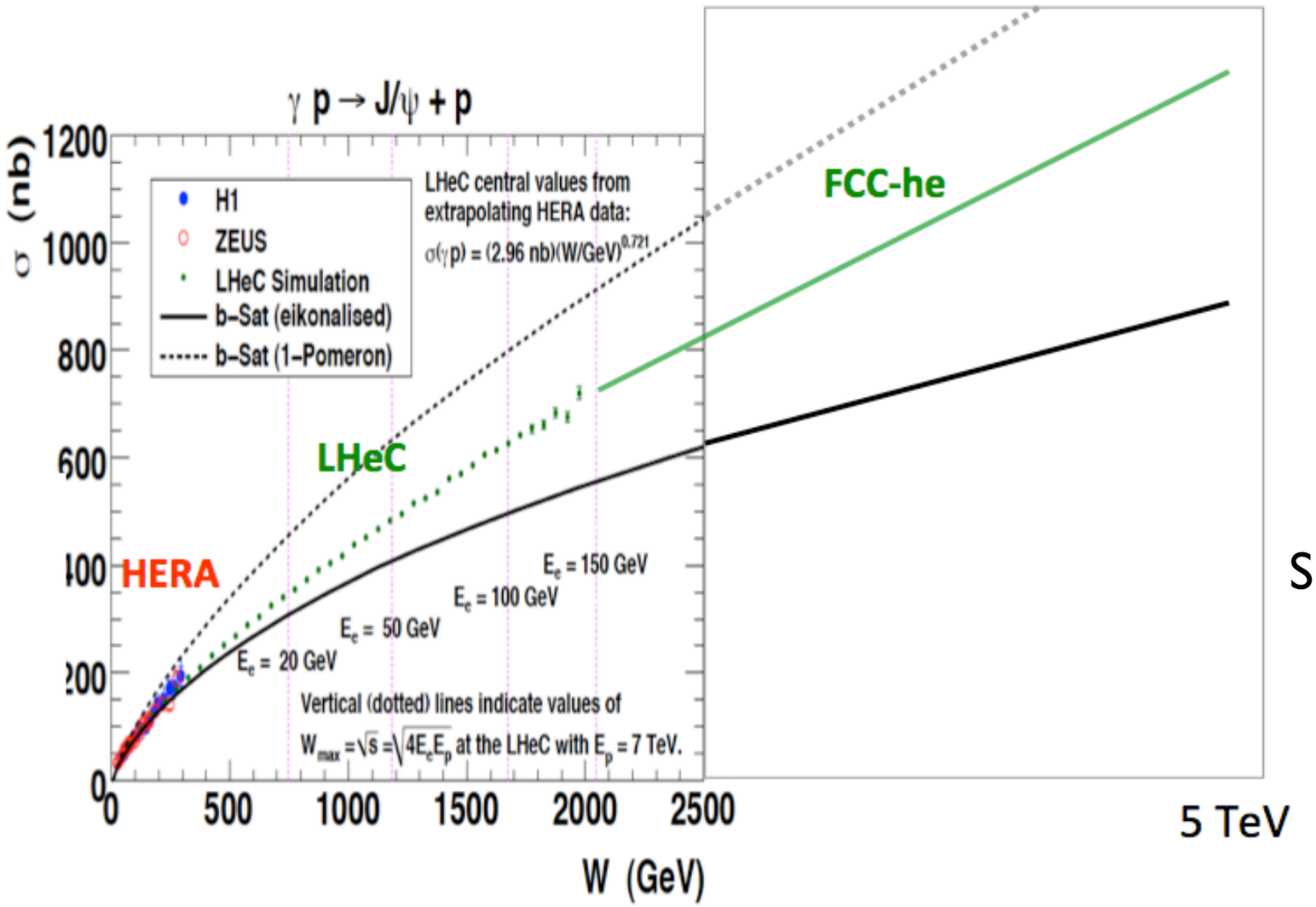

Large effects even for the t-integrated observable.

Different W behavior depending whether saturation is included or not.

Simulated data are from extrapolated fit to HERA data

t-dependence of the cross section for VM production

$$\frac{\mathrm{d}\sigma_{T,L}^{\gamma^* p\to Ep}}{\mathrm{d}t} = \frac{1}{16\pi}\left|\mathcal{A}_{T,L}^{\gamma^* p\to Ep}\right|^2$$

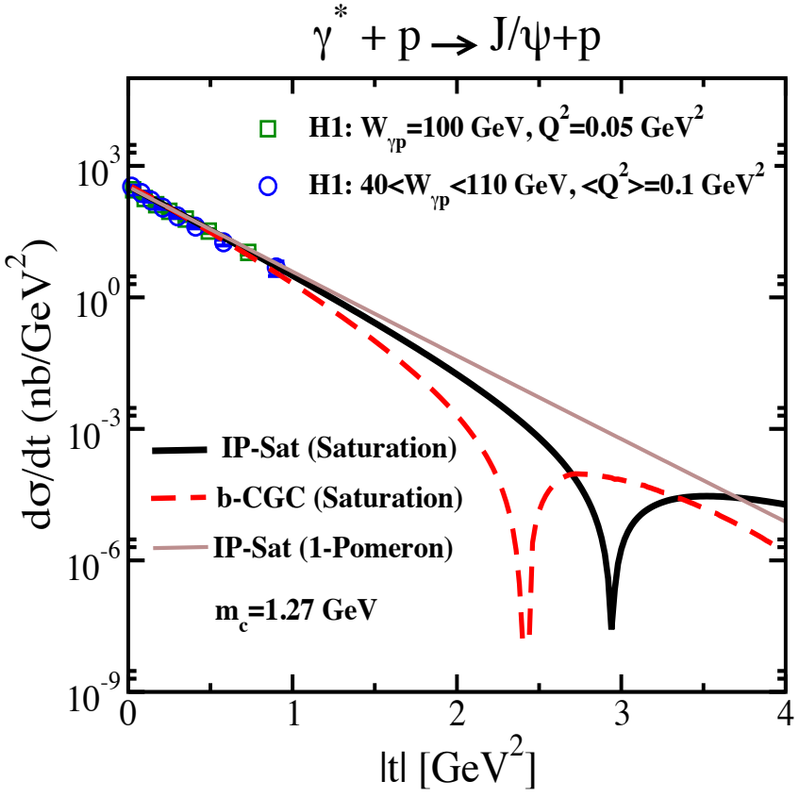

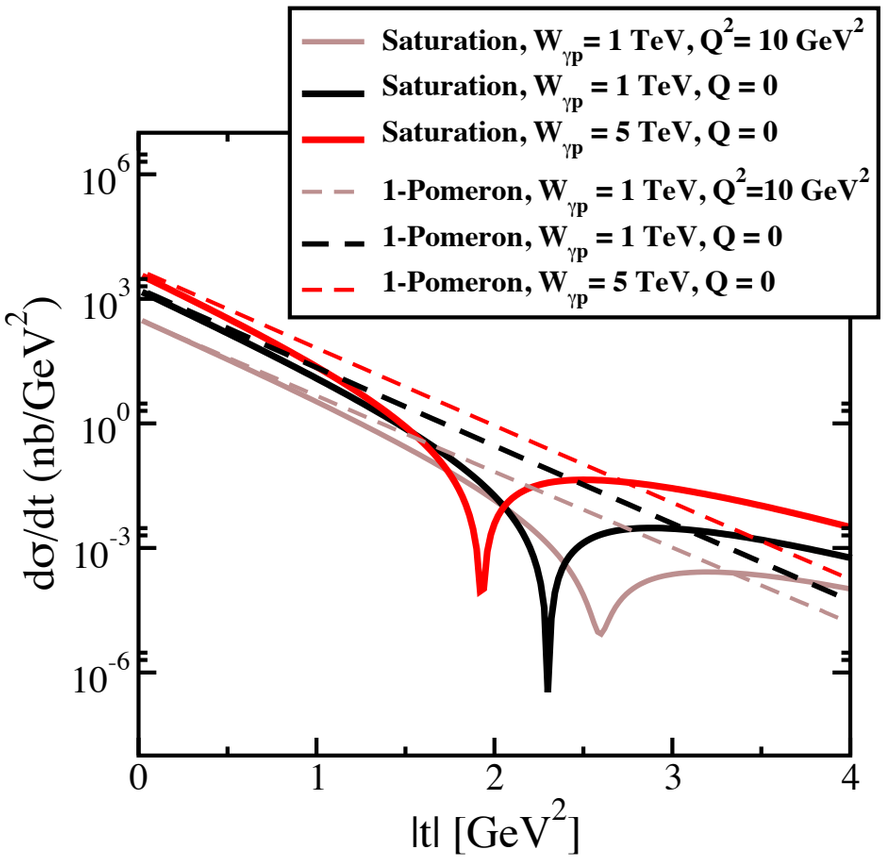

t-dependence of the cross section for VM production

$$\frac{\mathrm{d}\sigma_{T,L}^{\gamma^* p\to Ep}}{\mathrm{d}t} = \frac{1}{16\pi}\left|\mathcal{A}_{T,L}^{\gamma^* p\to Ep}\right|^2$$

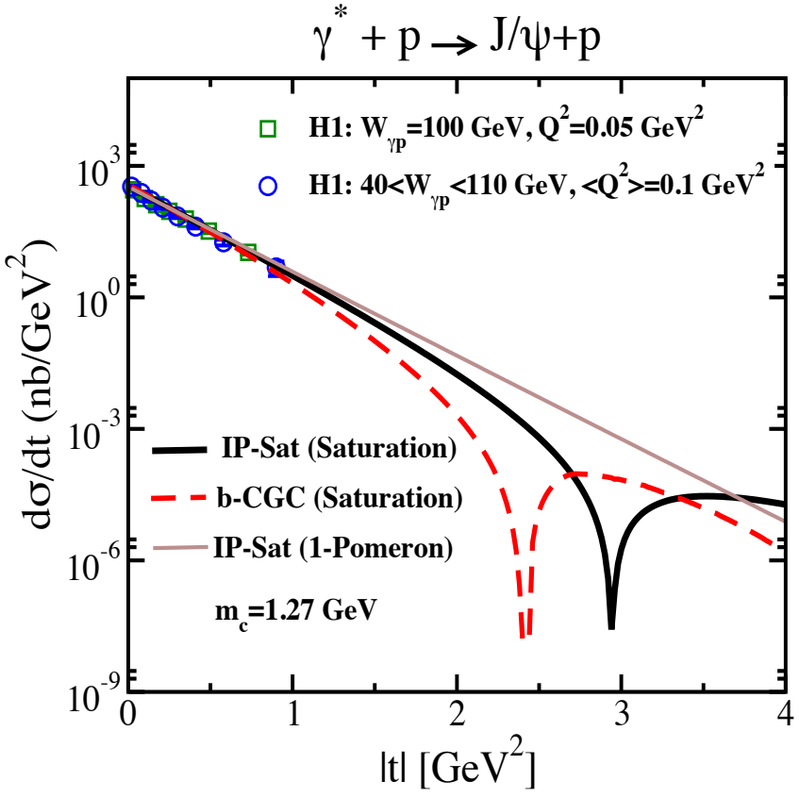

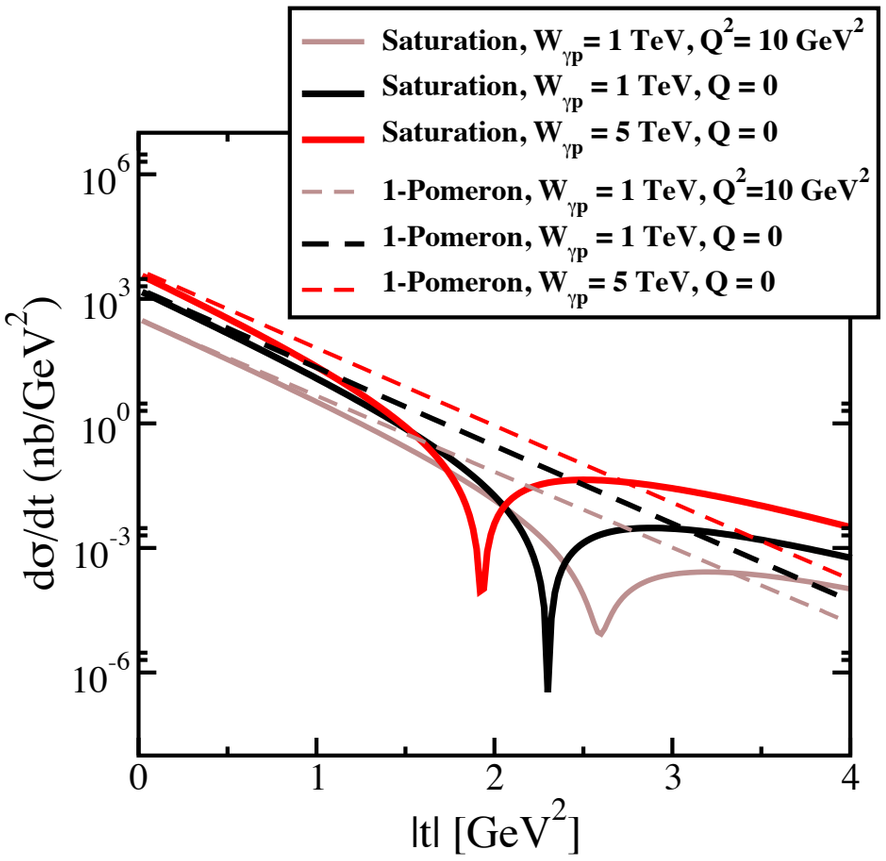

- Differential cross section steeply falls off with the momentum transfer t

t-dependence of the cross section for VM production

$$\frac{\mathrm{d}\sigma_{T,L}^{\gamma^* p\to Ep}}{\mathrm{d}t} = \frac{1}{16\pi}\left|\mathcal{A}_{T,L}^{\gamma^* p\to Ep}\right|^2$$

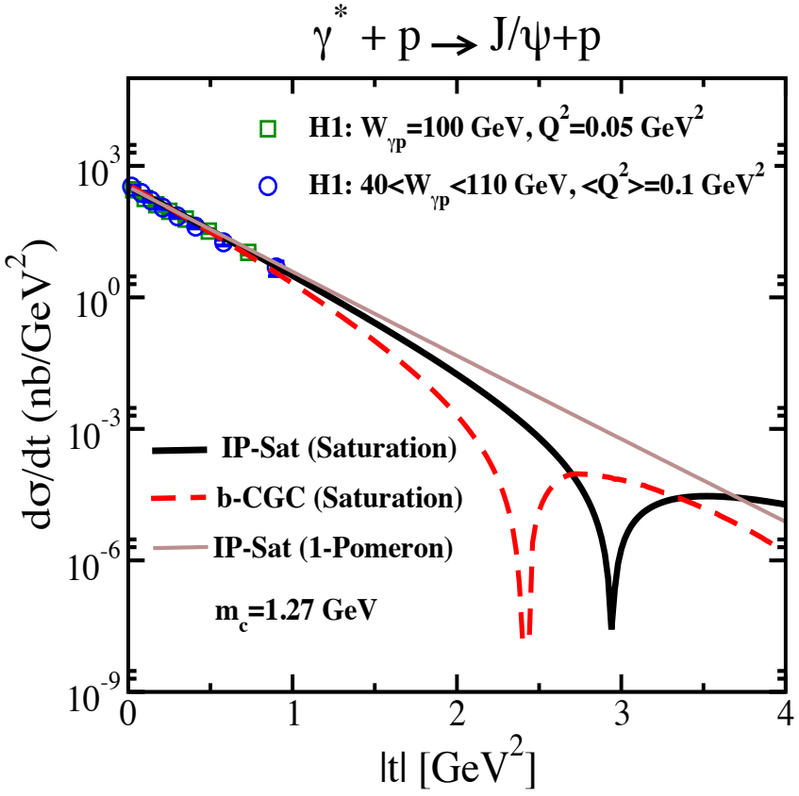

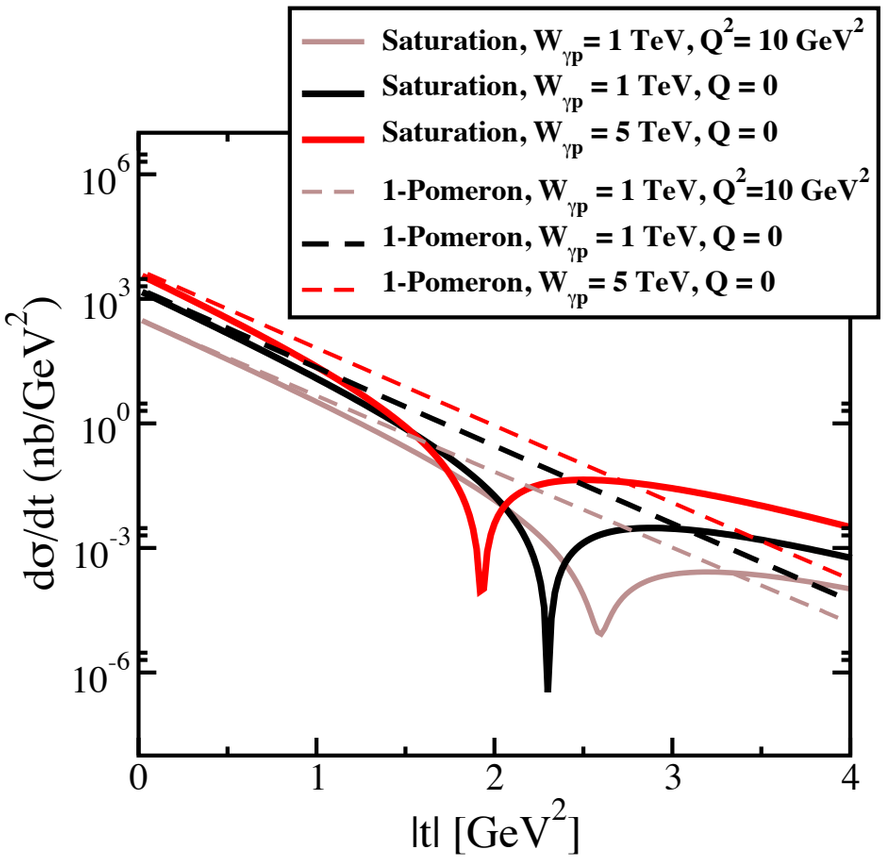

- Differential cross section steeply falls off with the momentum transfer t
- Different models coincide at small values of t: fit the data

t-dependence of the cross section for VM production

$$\frac{\mathrm{d}\sigma_{T,L}^{\gamma^* p\to Ep}}{\mathrm{d}t} = \frac{1}{16\pi}\left|\mathcal{A}_{T,L}^{\gamma^* p\to Ep}\right|^2$$

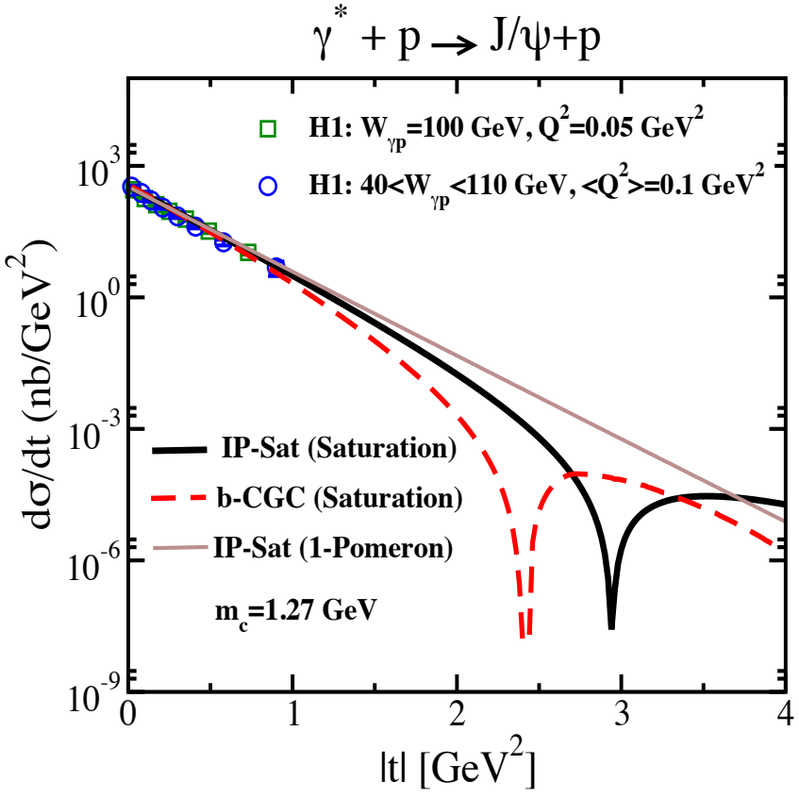

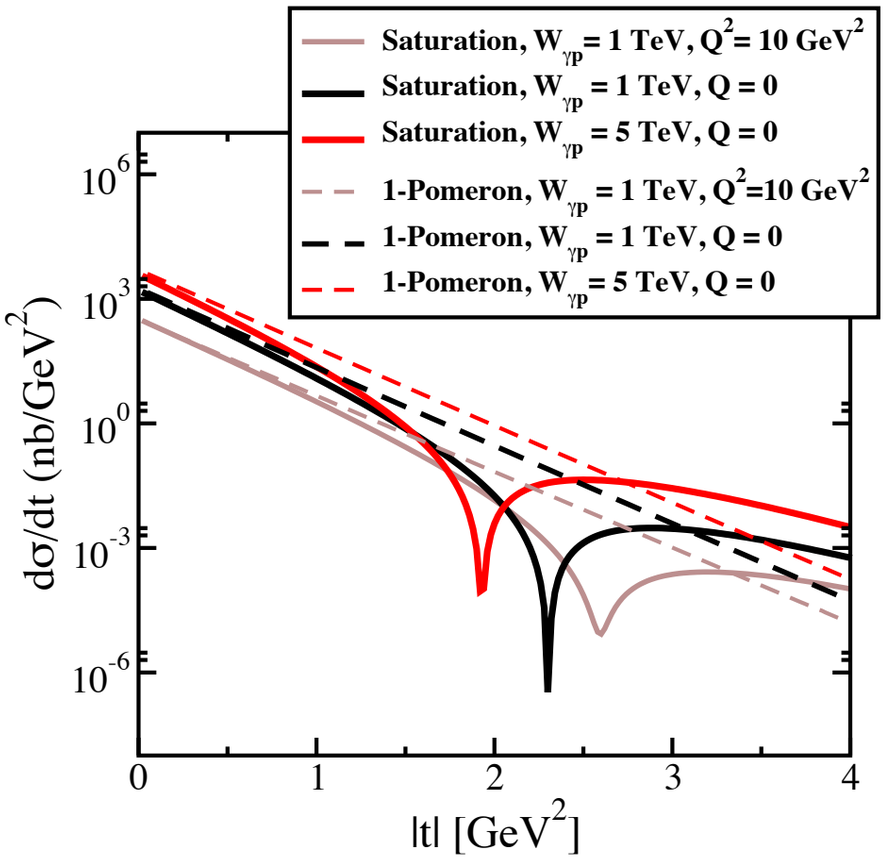

- Differential cross section steeply falls off with the momentum transfer t
- Different models coincide at small values of t: fit the data
- Differ greatly for larger values of t

t-dependence of the cross section for VM production

$$\frac{\mathrm{d}\sigma_{T,L}^{\gamma^* p\to Ep}}{\mathrm{d}t} = \frac{1}{16\pi}\left|\mathcal{A}_{T,L}^{\gamma^* p\to Ep}\right|^2$$

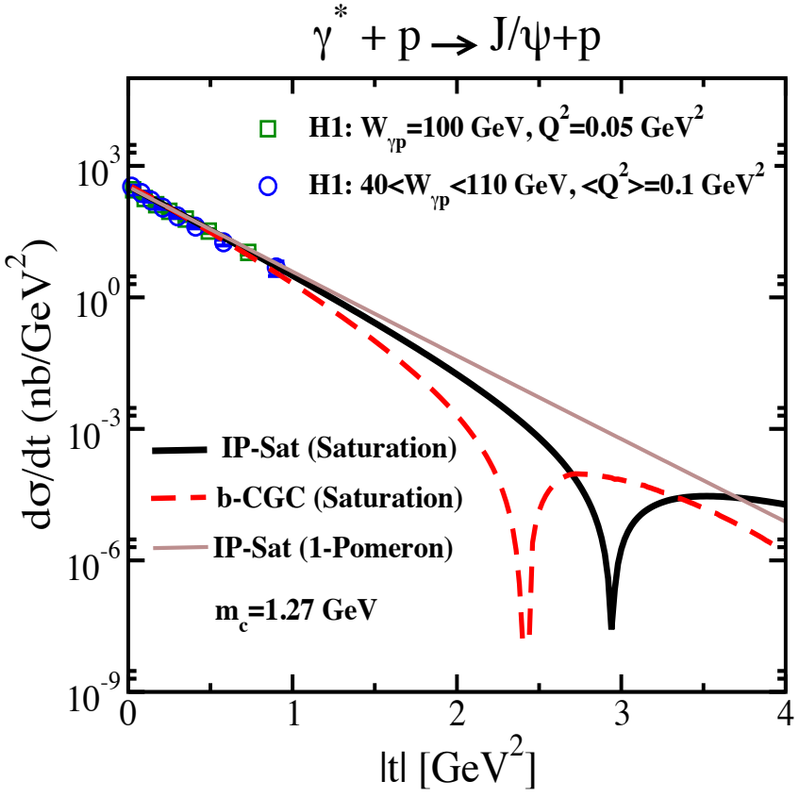

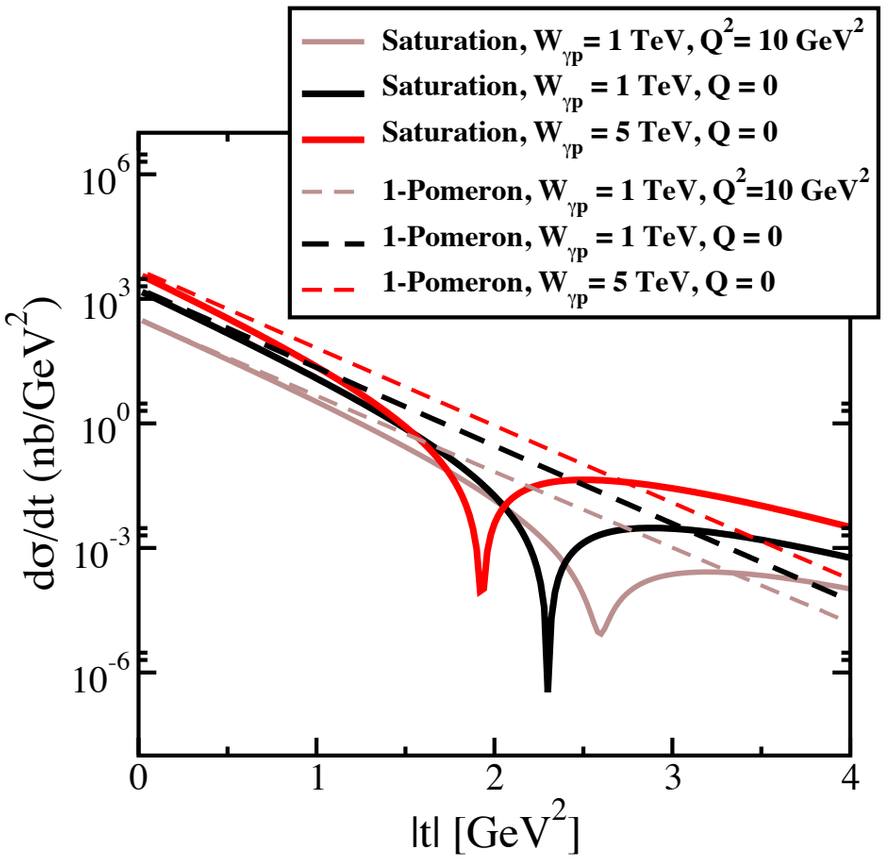

- Differential cross section steeply falls off with the momentum transfer t
- Different models coincide at small values of t: fit the data
- Differ greatly for larger values of t
- Appearance of dips in t, though some models lack them

t-dependence of the cross section for VM production

$$\frac{\mathrm{d}\sigma_{T,L}^{\gamma^* p\to Ep}}{\mathrm{d}t} = \frac{1}{16\pi}\left|\mathcal{A}_{T,L}^{\gamma^* p\to Ep}\right|^2$$

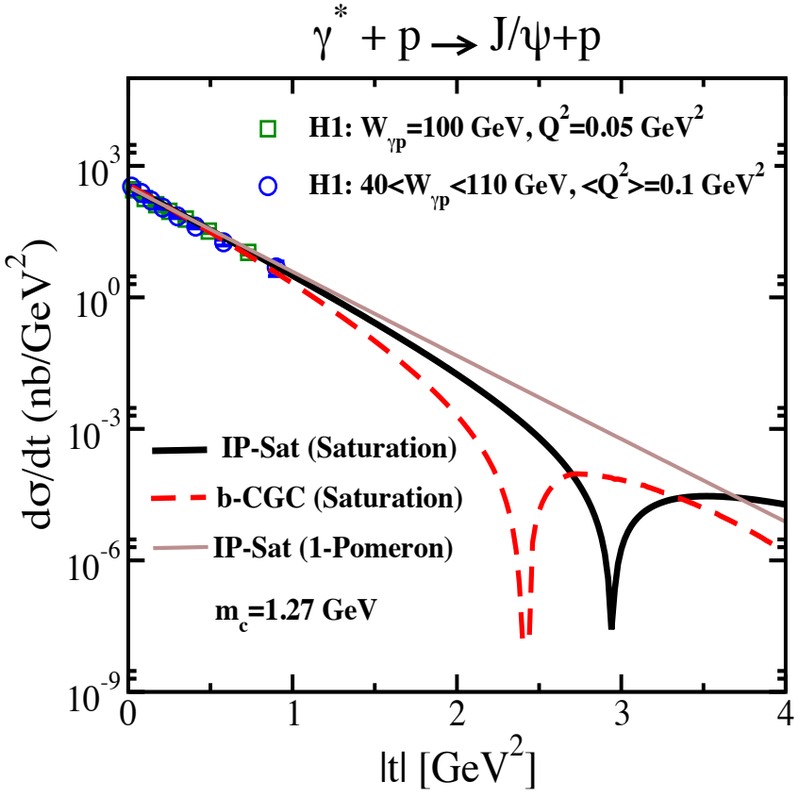

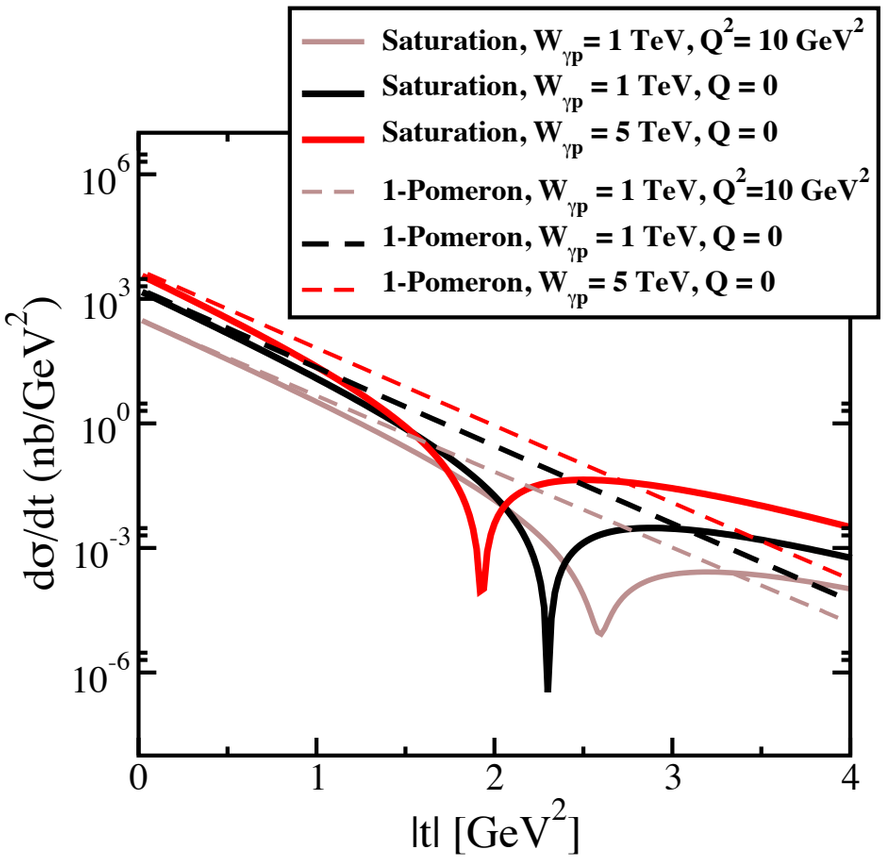

- Differential cross section steeply falls off with the momentum transfer t
- Different models coincide at small values of t: fit the data
- Differ greatly for larger values of t
- Appearance of dips in t, though some models lack them
- The position of the dips depend on the model, but within the single model they change with energy.

t-dependence of the cross section for VM production

$$\frac{\mathrm{d}\sigma_{T,L}^{\gamma^* p\to Ep}}{\mathrm{d}t} = \frac{1}{16\pi}\left|\mathcal{A}_{T,L}^{\gamma^* p\to Ep}\right|^2$$

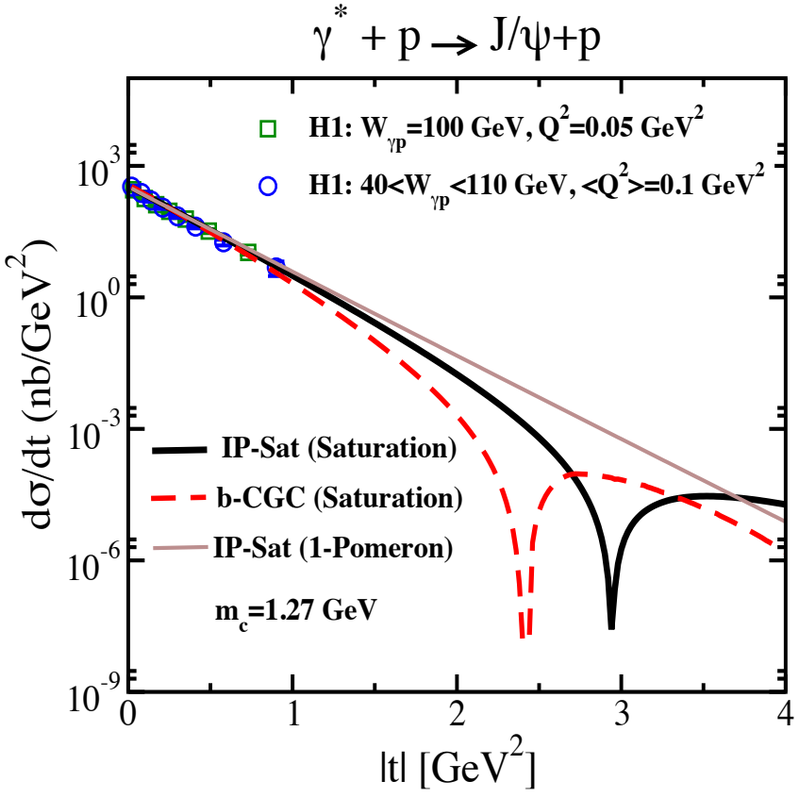

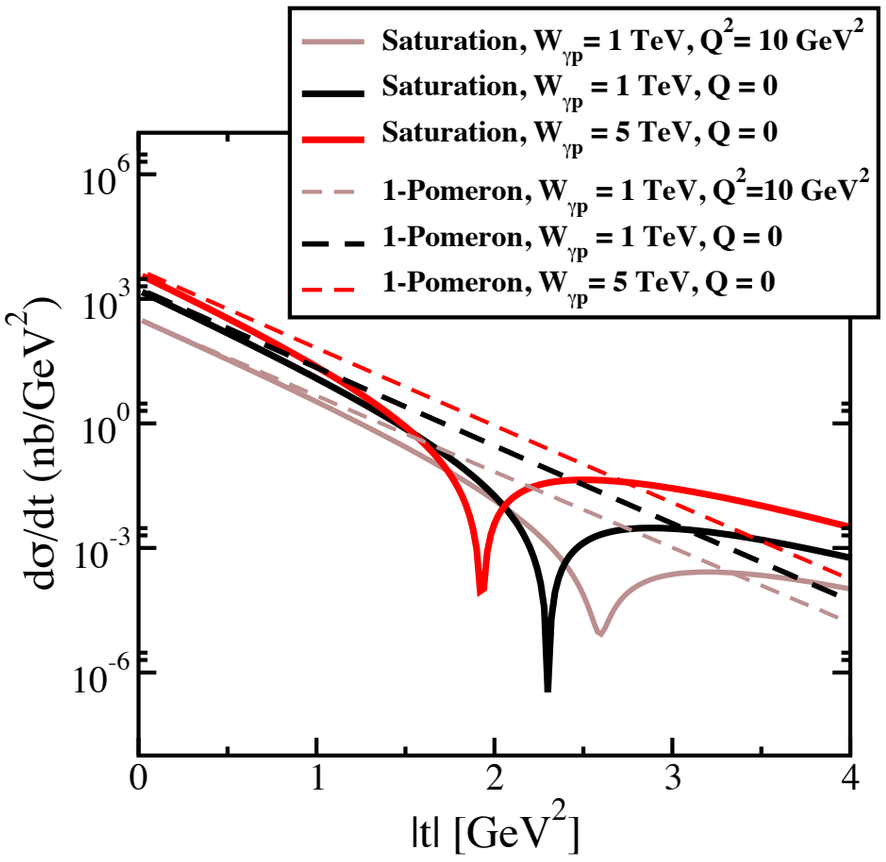

- Differential cross section steeply falls off with the momentum transfer t
- Different models coincide at small values of t: fit the data
- Differ greatly for larger values of t
- Appearance of dips in t, though some models lack them
- The position of the dips depend on the model, but within the single model they change with energy.
- The larger the energy the position of the dip moves to lower values of t

t-dependence of the cross section for VM production

$$\frac{\mathrm{d}\sigma_{T,L}^{\gamma^* p\to Ep}}{\mathrm{d}t} = \frac{1}{16\pi}\left|\mathcal{A}_{T,L}^{\gamma^* p\to Ep}\right|^2$$

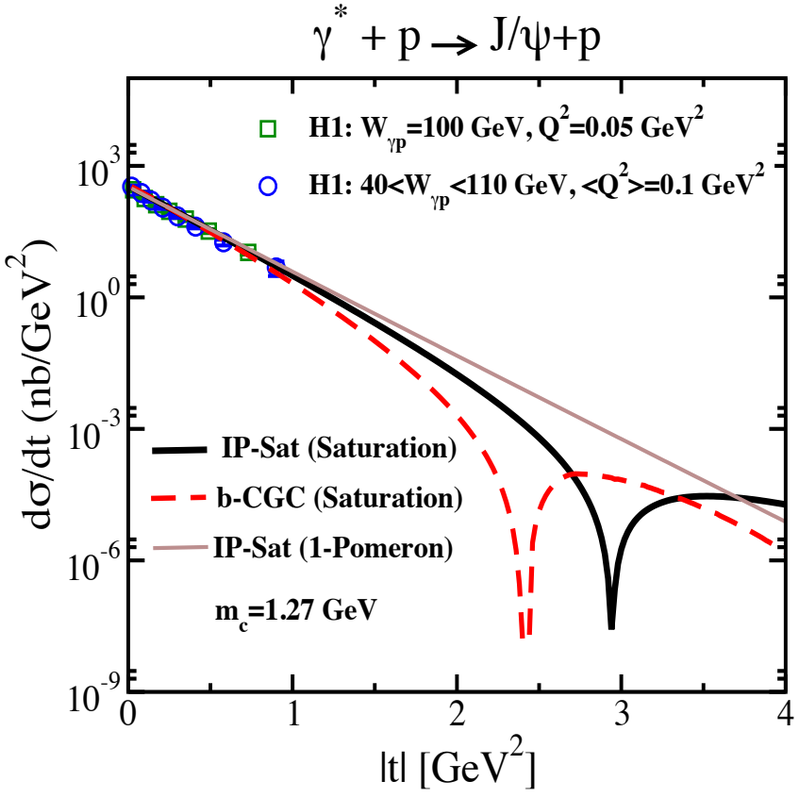

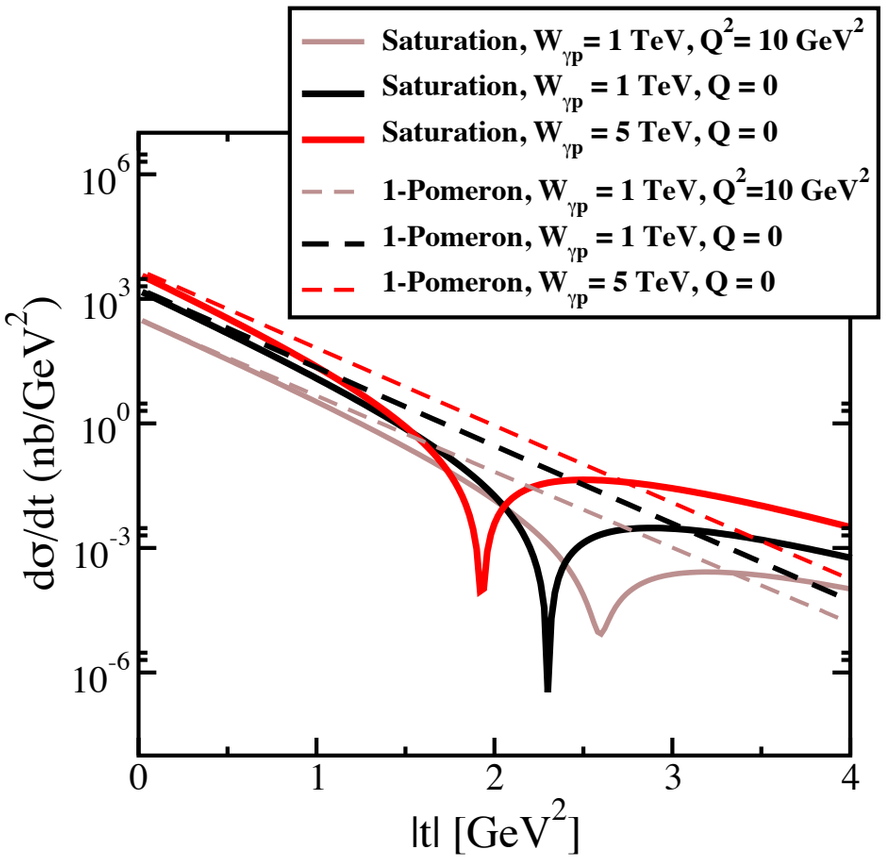

- Differential cross section steeply falls off with the momentum transfer t
- Different models coincide at small values of t: fit the data
- Differ greatly for larger values of t
- Appearance of dips in t, though some models lack them
- The position of the dips depend on the model, but within the single model they change with energy.
- The larger the energy the position of the dip moves to lower values of t
- The position of the dip depends on the photon virtuality: the lower the virtuality the lower t for the dip

t-dependence of the cross section for VM production

$$\frac{\mathrm{d}\sigma_{T,L}^{\gamma^* p\to Ep}}{\mathrm{d}t} = \frac{1}{16\pi}\left|\mathcal{A}_{T,L}^{\gamma^* p\to Ep}\right|^2$$

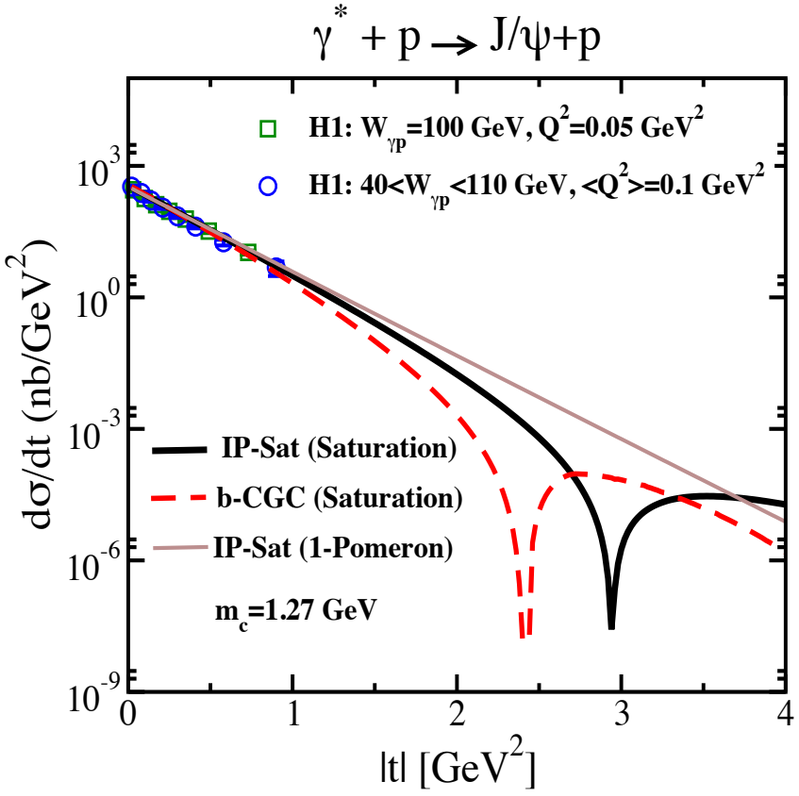

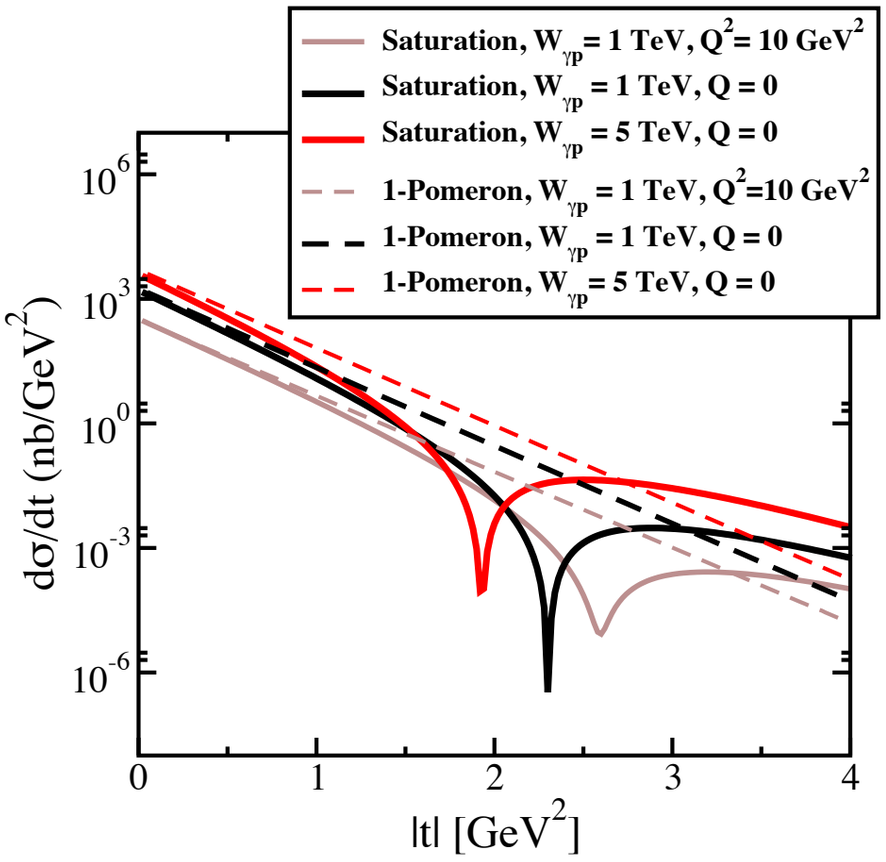

- Differential cross section steeply falls off with the momentum transfer t
- Different models coincide at small values of t: fit the data
- Differ greatly for larger values of t
- Appearance of dips in t, though some models lack them
- The position of the dips depend on the model, but within the single model they change with energy.
- The larger the energy the position of the dip moves to lower values of t
- The position of the dip depends on the photon virtuality: the lower the virtuality the lower t for the dip

Origin of dips in diffractive production of VM

Recall the cross section

$$\frac{\mathrm{d}\sigma_{T,L}^{\gamma^* p\to Ep}}{\mathrm{d}t} = \frac{1}{16\pi}\left|\mathcal{A}_{T,L}^{\gamma^* p\to Ep}\right|^2$$

$$\mathcal{A}_{T,L}^{\gamma^* p\to Ep}(x,Q,\Delta) = \mathrm{i}\int \mathrm{d}^2\boldsymbol{r}\int_0^1 \frac{\mathrm{d}z}{4\pi}\int \mathrm{d}^2\boldsymbol{b}\,(\Psi_E^*\Psi)_{T,L}\,\mathrm{e}^{-\mathrm{i}[\boldsymbol{b}-(1-z)\boldsymbol{r}]\cdot\boldsymbol{\Delta}}\,\frac{\mathrm{d}\sigma_{q\bar{q}}}{\mathrm{d}^2\boldsymbol{b}}.$$

$$t = -\Delta^2$$

Origin of dips in diffractive production of VM

Recall the cross section

$$\frac{\mathrm{d}\sigma_{T,L}^{\gamma^* p\to Ep}}{\mathrm{d}t} = \frac{1}{16\pi}\left|\mathcal{A}_{T,L}^{\gamma^* p\to Ep}\right|^2$$

$$\mathcal{A}_{T,L}^{\gamma^* p\to Ep}(x,Q,\Delta) = \mathrm{i}\int \mathrm{d}^2\boldsymbol{r}\int_0^1 \frac{\mathrm{d}z}{4\pi}\int \mathrm{d}^2\boldsymbol{b}\,(\Psi_E^*\Psi)_{T,L}\,\mathrm{e}^{-\mathrm{i}[\boldsymbol{b}-(1-z)\boldsymbol{r}]\cdot\boldsymbol{\Delta}}\,\frac{\mathrm{d}\sigma_{q\bar{q}}}{\mathrm{d}^2\boldsymbol{b}}.$$

Define the following integral:

$$\frac{d\sigma^{\mathrm{dipole}}}{dt} = 2\pi\left|\int_0^{\Lambda_r} rdr\int \mathrm{d}^2\boldsymbol{b}\,\mathrm{e}^{-\mathrm{i}\boldsymbol{b}\cdot\boldsymbol{\Delta}}\mathcal{N}(x,r,b)\right|^2, \qquad t=-\Delta^2$$

Λ_r is a cutoff on the integral. Such cutoff is provided by the overlap between the photon and vector meson wave function

Origin of dips in diffractive production of VM

Recall the cross section

$$\frac{\mathrm{d}\sigma_{T,L}^{\gamma^* p\to Ep}}{\mathrm{d}t} = \frac{1}{16\pi}\left|\mathcal{A}_{T,L}^{\gamma^* p\to Ep}\right|^2$$

$$\mathcal{A}_{T,L}^{\gamma^* p\to Ep}(x,Q,\Delta) = \mathrm{i}\int \mathrm{d}^2\boldsymbol{r}\int_0^1 \frac{\mathrm{d}z}{4\pi}\int \mathrm{d}^2\boldsymbol{b}\,(\Psi_E^*\Psi)_{T,L}\,\mathrm{e}^{-\mathrm{i}[\boldsymbol{b}-(1-z)\boldsymbol{r}]\cdot\boldsymbol{\Delta}}\,\frac{\mathrm{d}\sigma_{q\bar{q}}}{\mathrm{d}^2\boldsymbol{b}}.$$

Define the following integral:

$$\frac{d\sigma^{\mathrm{dipole}}}{dt} = 2\pi\left|\int_0^{\Lambda_r} rdr\int \mathrm{d}^2\boldsymbol{b}\,\mathrm{e}^{-\mathrm{i}\boldsymbol{b}\cdot\boldsymbol{\Delta}}\mathcal{N}(x,r,b)\right|^2, \qquad t=-\Delta^2$$

Λ_r is a cutoff on the integral. Such cutoff is provided by the overlap between the photon and vector meson wave function

The overlap gives the probability of finding the dipole with certain size r
The cutoff is larger for smaller photon virtualities and smaller masses

Origin of dips in diffractive production of VM

Recall the cross section

$$\frac{\mathrm{d}\sigma_{T,L}^{\gamma^* p\to Ep}}{\mathrm{d}t} = \frac{1}{16\pi}\left|\mathcal{A}_{T,L}^{\gamma^* p\to Ep}\right|^2$$

$$\mathcal{A}_{T,L}^{\gamma^* p\to Ep}(x,Q,\Delta) = \mathrm{i}\int \mathrm{d}^2\boldsymbol{r}\int_0^1 \frac{\mathrm{d}z}{4\pi}\int \mathrm{d}^2\boldsymbol{b}\,(\Psi_E^*\Psi)_{T,L}\,\mathrm{e}^{-\mathrm{i}[\boldsymbol{b}-(1-z)\boldsymbol{r}]\cdot\boldsymbol{\Delta}}\,\frac{\mathrm{d}\sigma_{q\bar{q}}}{\mathrm{d}^2\boldsymbol{b}}.$$

Define the following integral:

$$\frac{d\sigma^{\mathrm{dipole}}}{dt} = 2\pi\left|\int_0^{\Lambda_r} rdr\int \mathrm{d}^2\boldsymbol{b}\,\mathrm{e}^{-\mathrm{i}\boldsymbol{b}\cdot\boldsymbol{\Delta}}\mathcal{N}(x,r,b)\right|^2, \qquad t=-\Delta^2$$

Λ_r is a cutoff on the integral. Such cutoff is provided by the overlap between the photon and vector meson wave function

The overlap gives the probability of finding the dipole with certain size r
The cutoff is larger for smaller photon virtualities and smaller masses

Quantum evolution of the dipole amplitude leads to unitarity constraints for lower values of dipole sizes.
Depending on vector meson mass, virtuality, energy, different regions of the dipole amplitude are probed: color transparency or unitarity limit.

Understanding t-dependence

$$\mathcal{A}_{T,L}^{\gamma^* p \to Ep}(x, Q, \Delta) = \mathrm{i} \int \mathrm{d}^2\boldsymbol{r} \int_0^1 \frac{\mathrm{d}z}{4\pi} \int \mathrm{d}^2\boldsymbol{b}\, (\Psi_E^* \Psi)_{T,L}\, \mathrm{e}^{-\mathrm{i}[\boldsymbol{b}-(1-z)\boldsymbol{r}]\cdot\boldsymbol{\Delta}}\, \frac{\mathrm{d}\sigma_{q\bar{q}}}{\mathrm{d}^2\boldsymbol{b}}.$$

Large photon virtuality or large VM mass

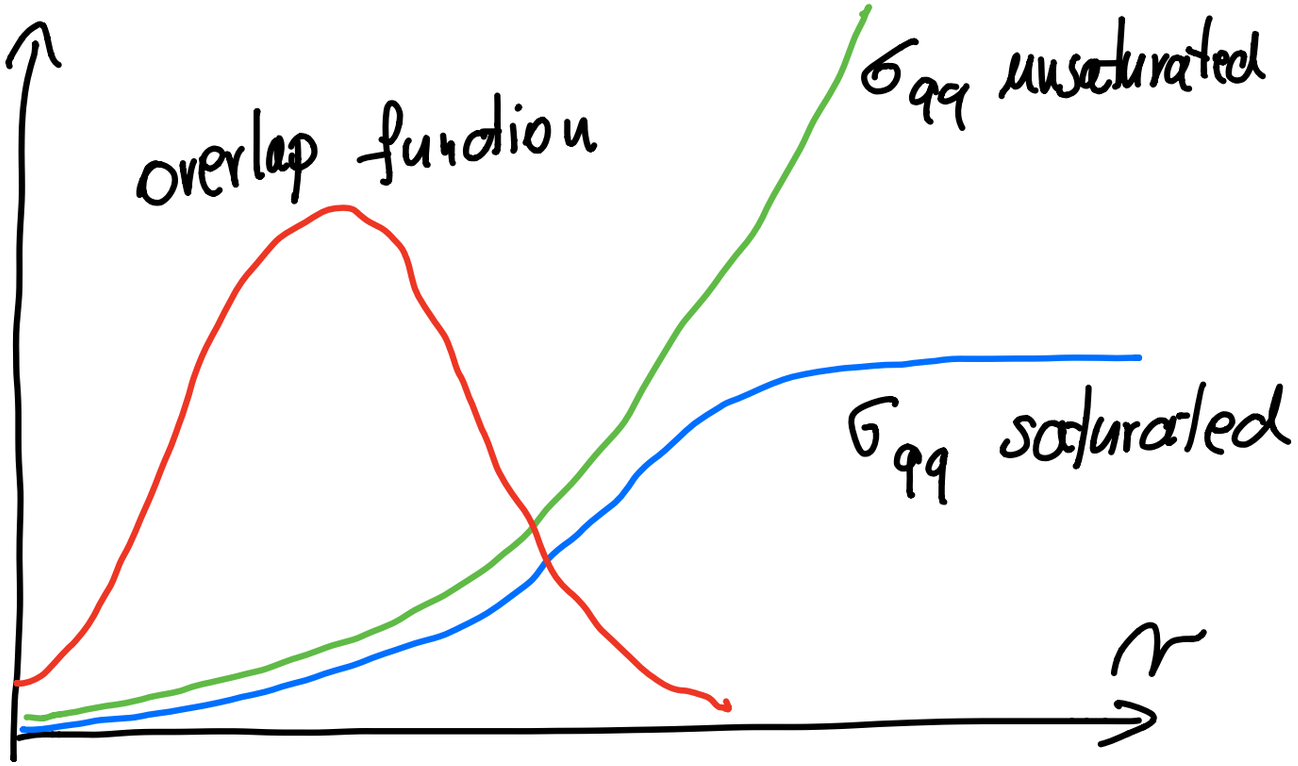

Smaller dipole sizes are probed

Smaller photon virtuality or smaller VM mass

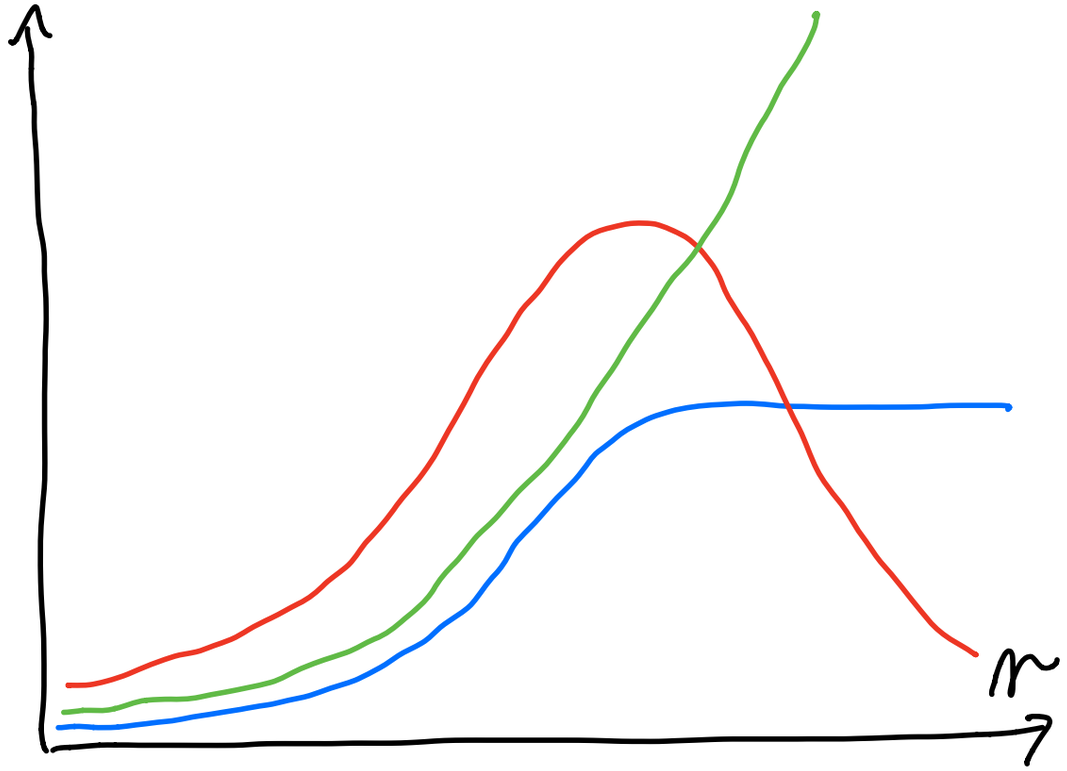

Larger dipole sizes are probed

Understanding t-dependence

IP-sat model (with saturation)

$$\frac{d\sigma_{q\bar{q}}}{d^2b} = 2\left[1 - \exp\left(-\frac{\pi^2}{2\,N_C} r^2 \alpha_s(\mu^2) x g(x,\mu^2) T(b)\right)\right] .$$

IP-sat model (1-Pomeron) : expand the exponent and keep the first term

$$\frac{d\sigma_{q\bar{q}}}{d^2b} = \frac{\pi^2}{N_c} r^2 \alpha_s(\mu^2) x g(x,\mu^2) T(b) \qquad T_G(b) = \frac{1}{2\pi B_G} \exp\left(-b^2/2B_G\right)$$

No unitarity constraints in such case

The Fourier transform of the Gaussian in b is exponential in t

There are no dips in this case

$\gamma^* + p \rightarrow J/\psi + p$

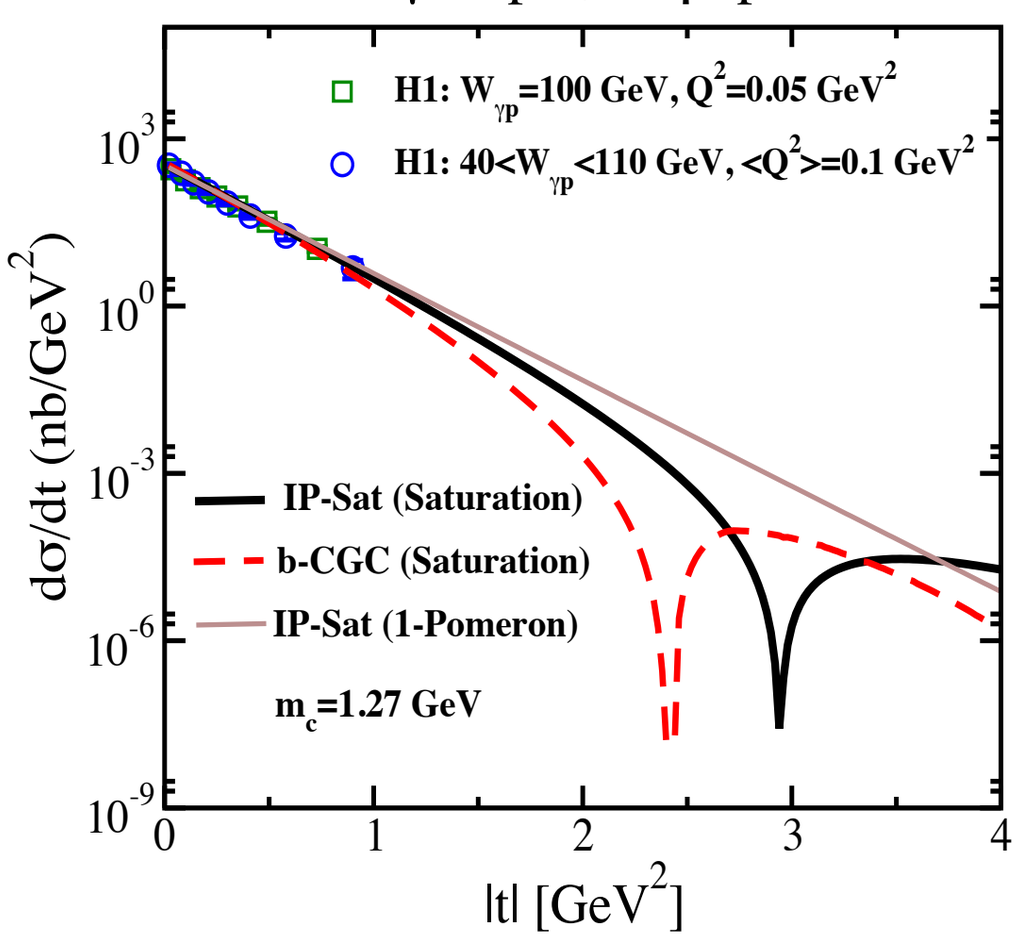

Understanding t-dependence

IP-sat model (with saturation)

$$\frac{d\sigma_{q\bar{q}}}{d^2b} = 2\left[1-\exp\left(-\frac{\pi^2}{2\,N_C}r^2\alpha_s(\mu^2)xg(x,\mu^2)T(b)\right)\right]. \qquad T_G(b) = \frac{1}{2\pi B_G}\exp\left(-b^2/2B_G\right)$$

For large b the exponent is small so the amplitude can be approximated by linear term and b-dependence is exponential. The result coincides with the IP-sat (1-Pomeron)

For small b the exponent is large and there is large deviation from the exponential, when large dipole sizes are probed. This happens when the effective cutoff is large as well: i.e. for small masses and/or small virtualities

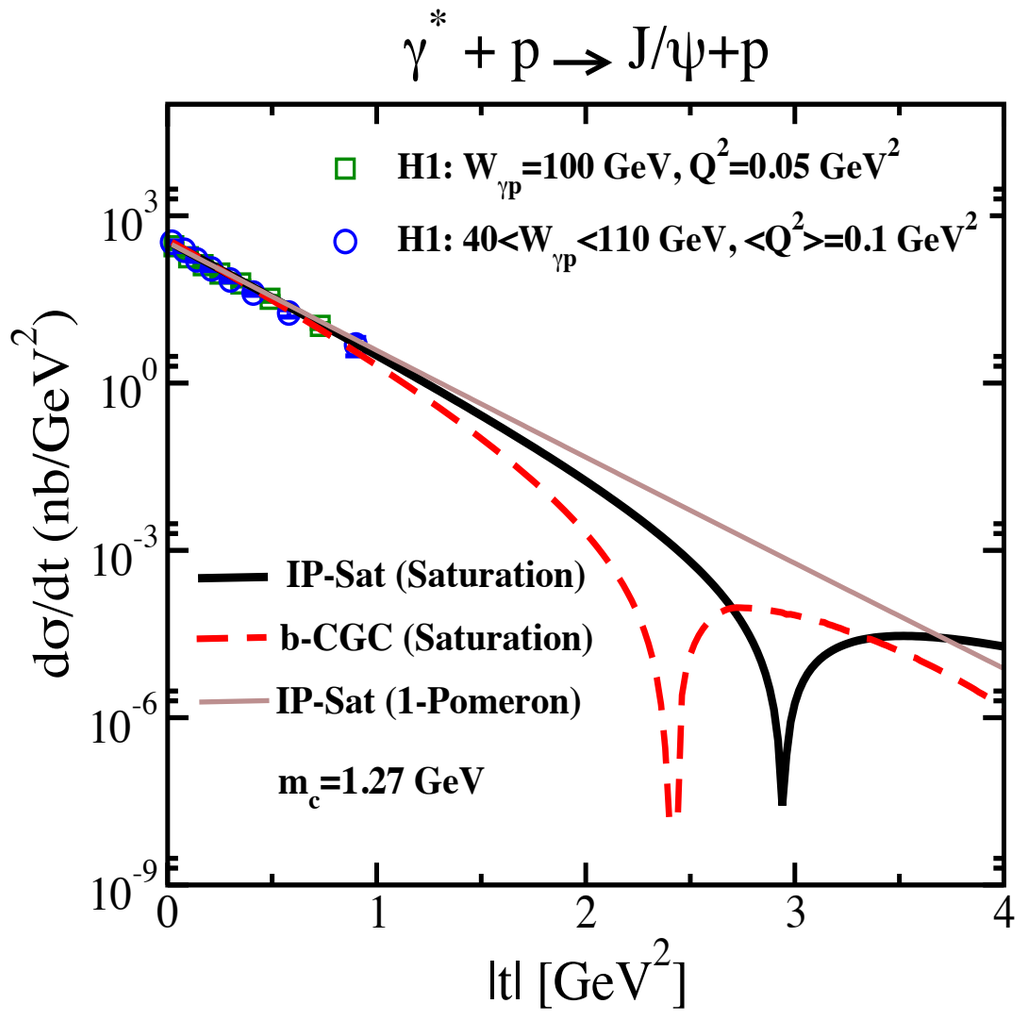

Dips in t-profile for VM production

Armesto-Rezaeian

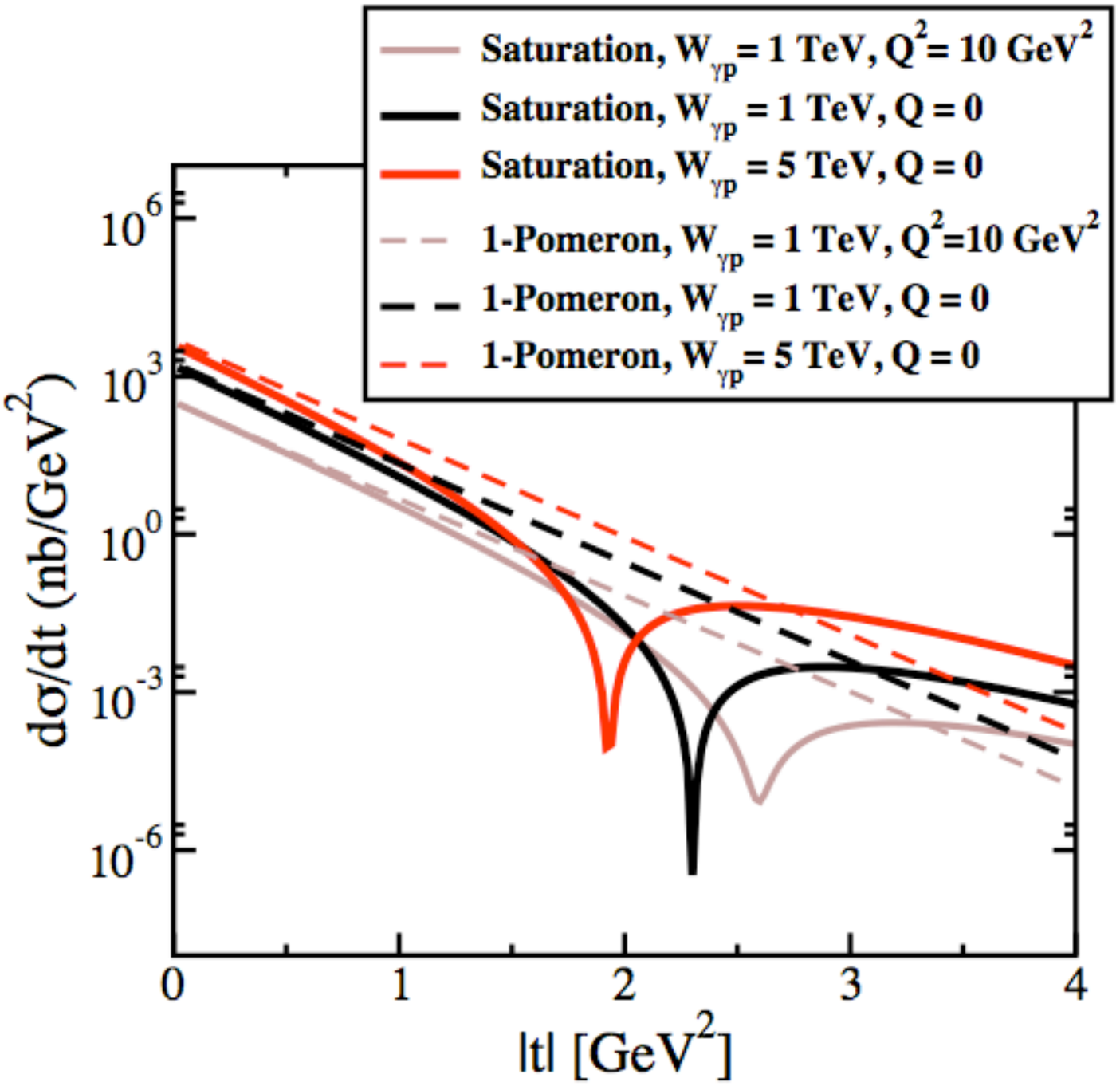

- position of dips depends on energy and scale
- within the LHeC/FCC-eh sensitive t-range

Dips in t-profile for VM production

Photoproduction of $J/\psi, \phi, \rho$

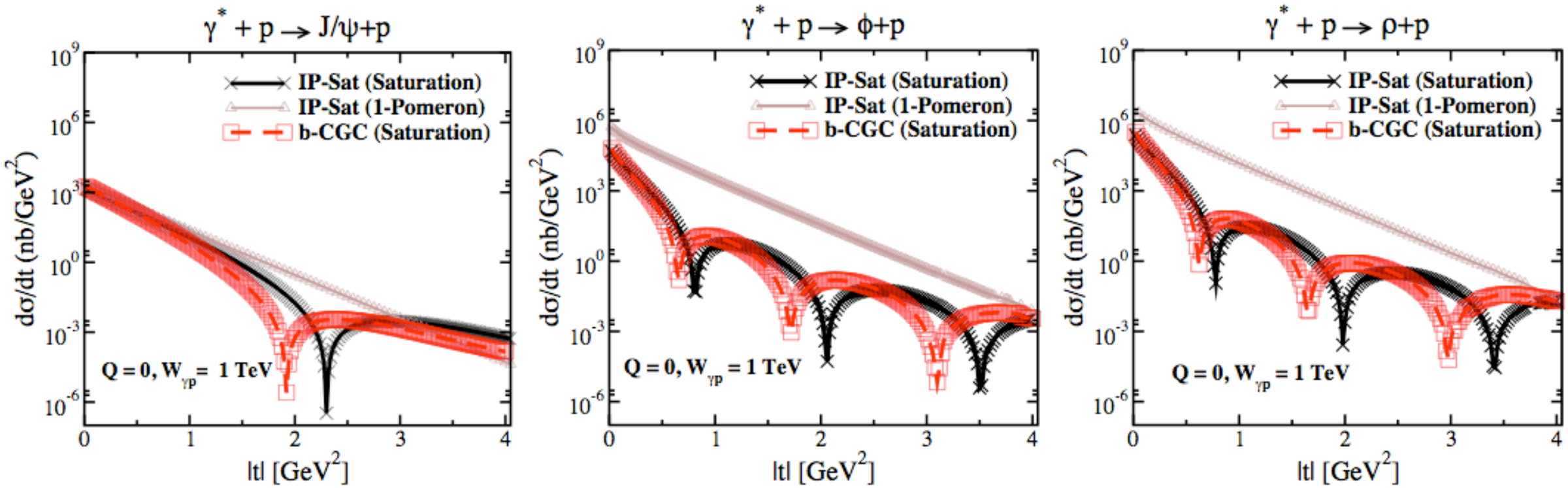

Dips in t move to lower values for lighter vector mesons.

Diffraction in eA

Diffraction on nuclei: possible coherent (nucleus stays intact) or incoherent (nucleus breaks but still rapidity gap present)

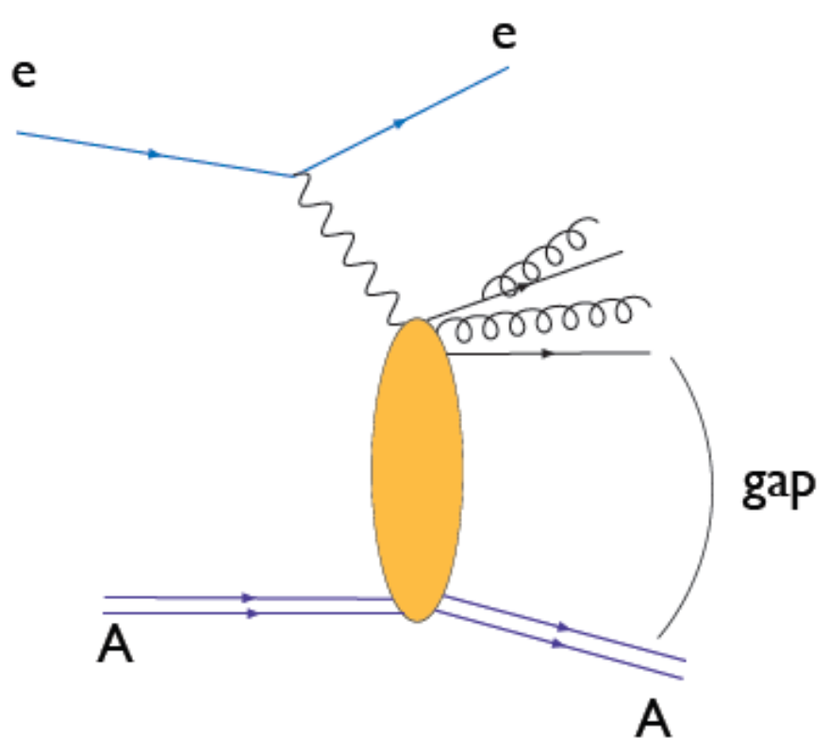

coherent

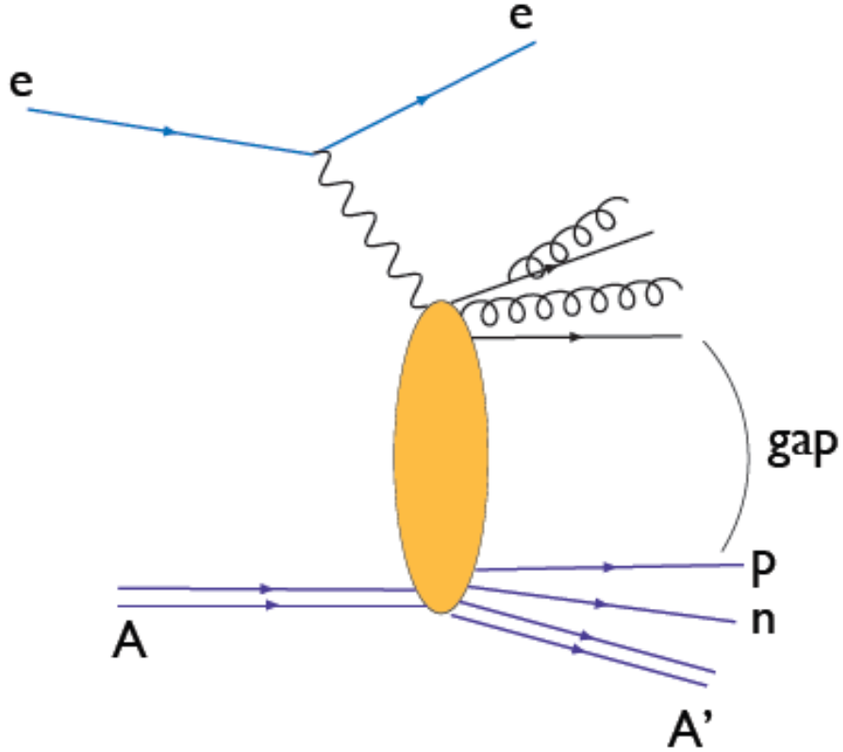

incoherent

Exclusive diffraction on nuclei

Possibility of using the same principle to learn about the gluon distribution in the nucleus.
Possible nuclear resonances at small t?

EIC: J/Ψ

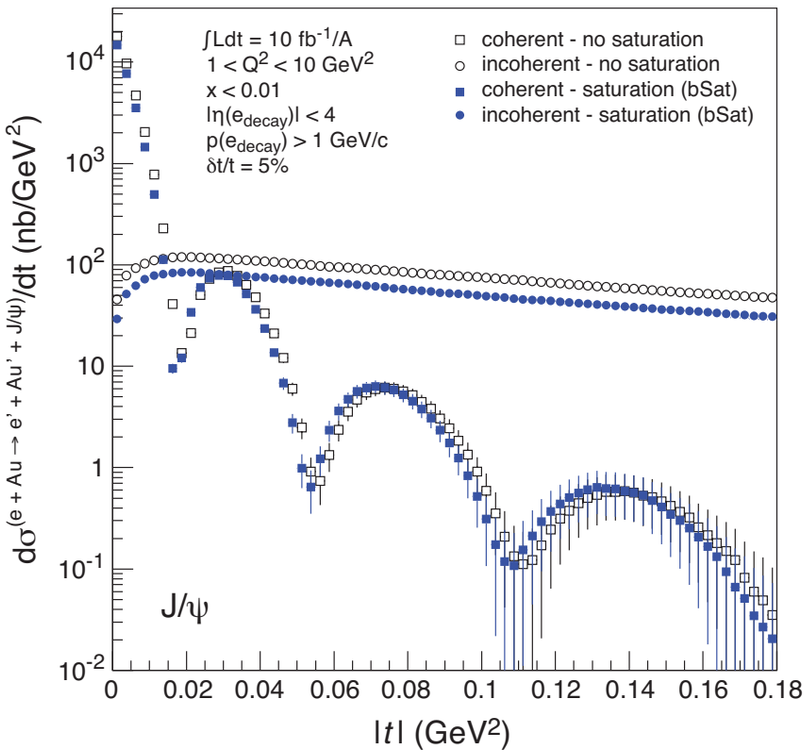

EIC: Φ

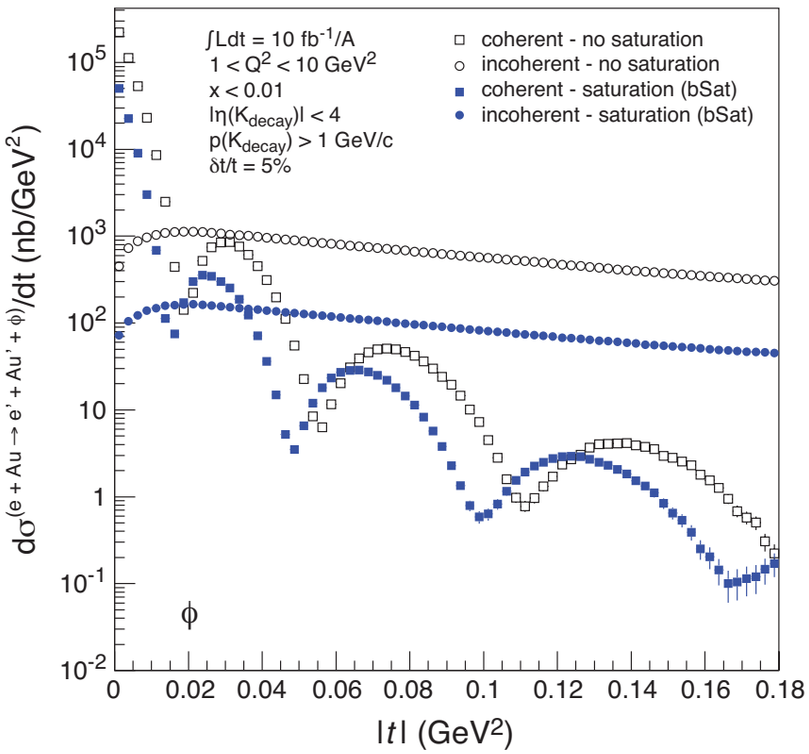

LHeC: J/Ψ

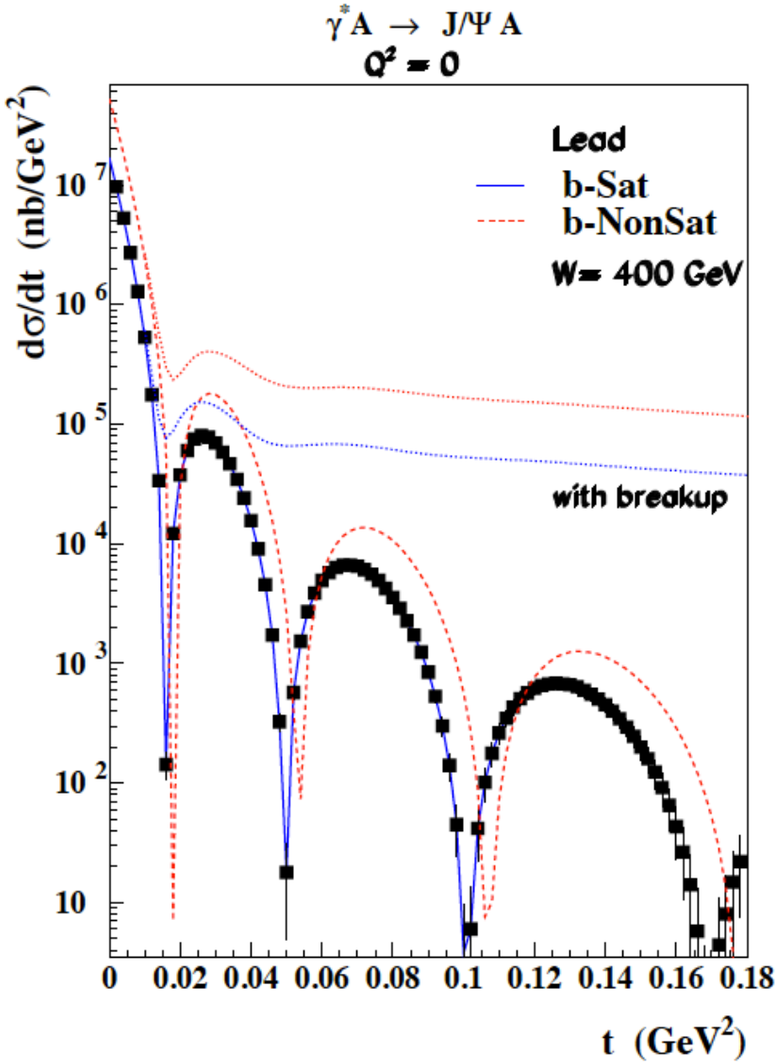

t-dependence: for nuclei dips. Position depends on model (sat no sat)
Challenges: need to distinguish between coherent and incoherent diffraction. Need dedicated instrumentation, zero degree calorimeter.

Exclusive diffraction on nuclei

Possibility of using the same principle to learn about the gluon distribution in the nucleus.
Possible nuclear resonances at small t?

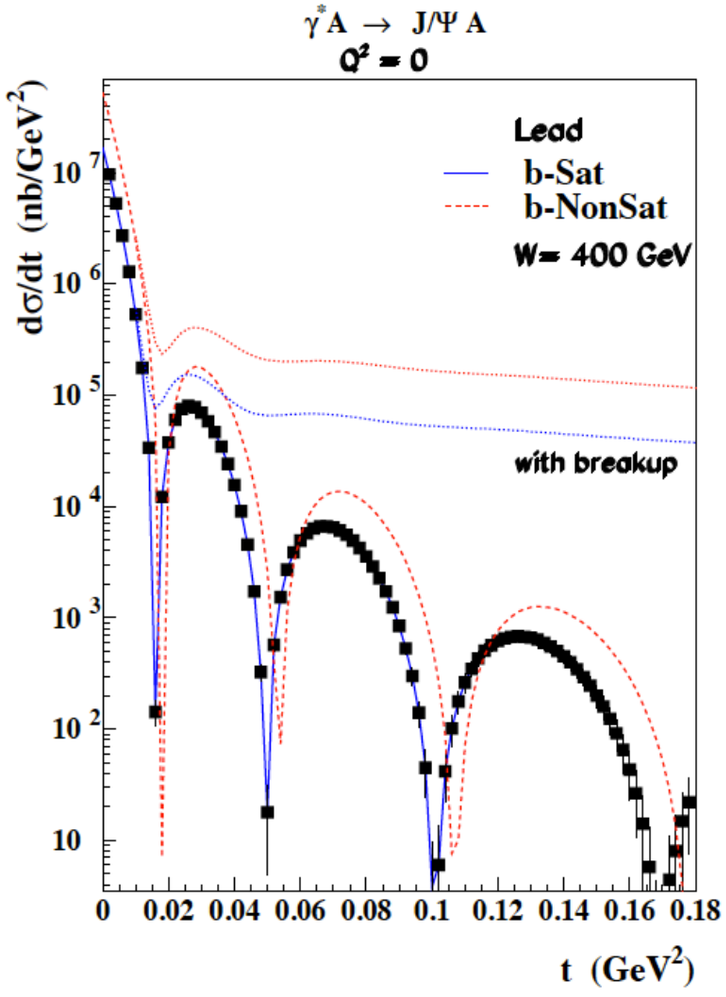

t-dependence: characteristic dips.
Challenges: need to distinguish between coherent and incoherent diffraction. Need dedicated instrumentation, zero degree calorimeter.

Energy dependence for different targets.

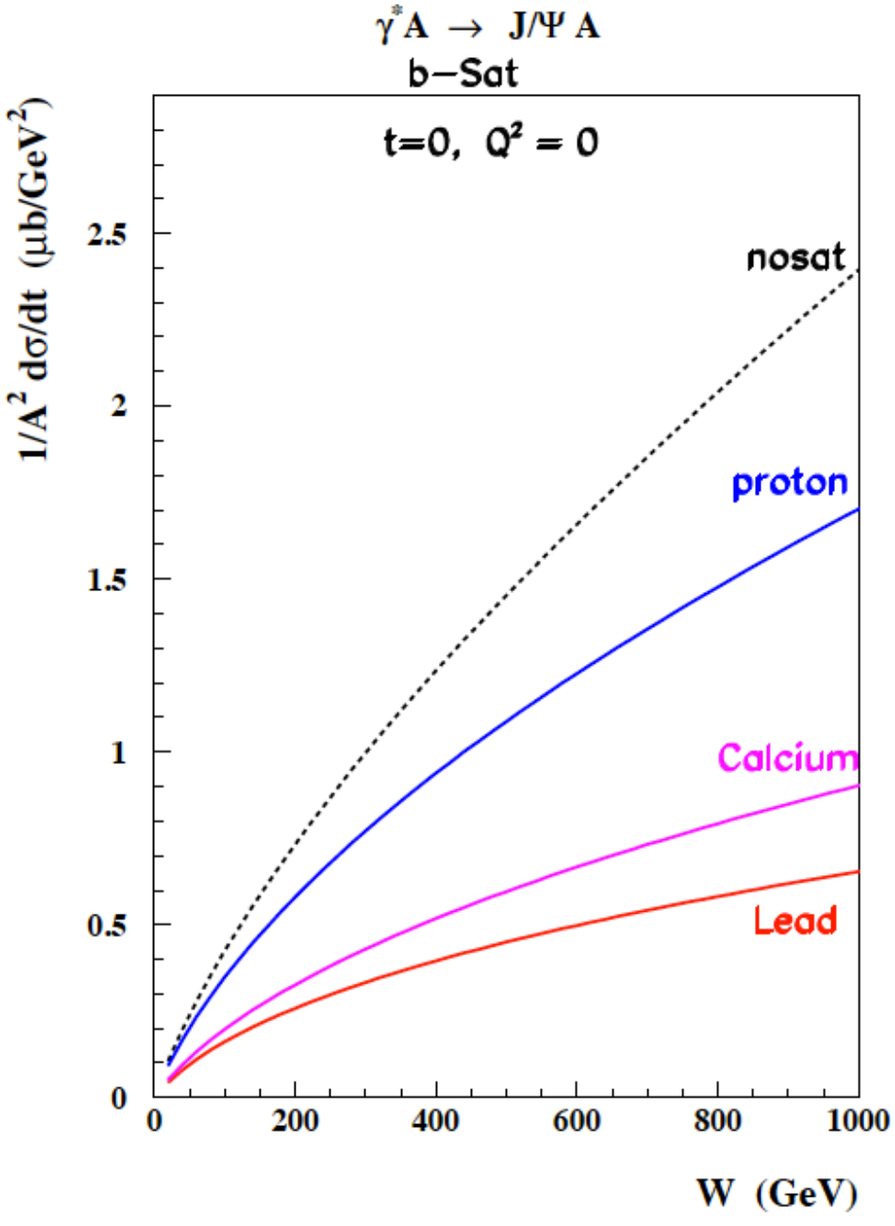

Exclusive diffraction on nuclei

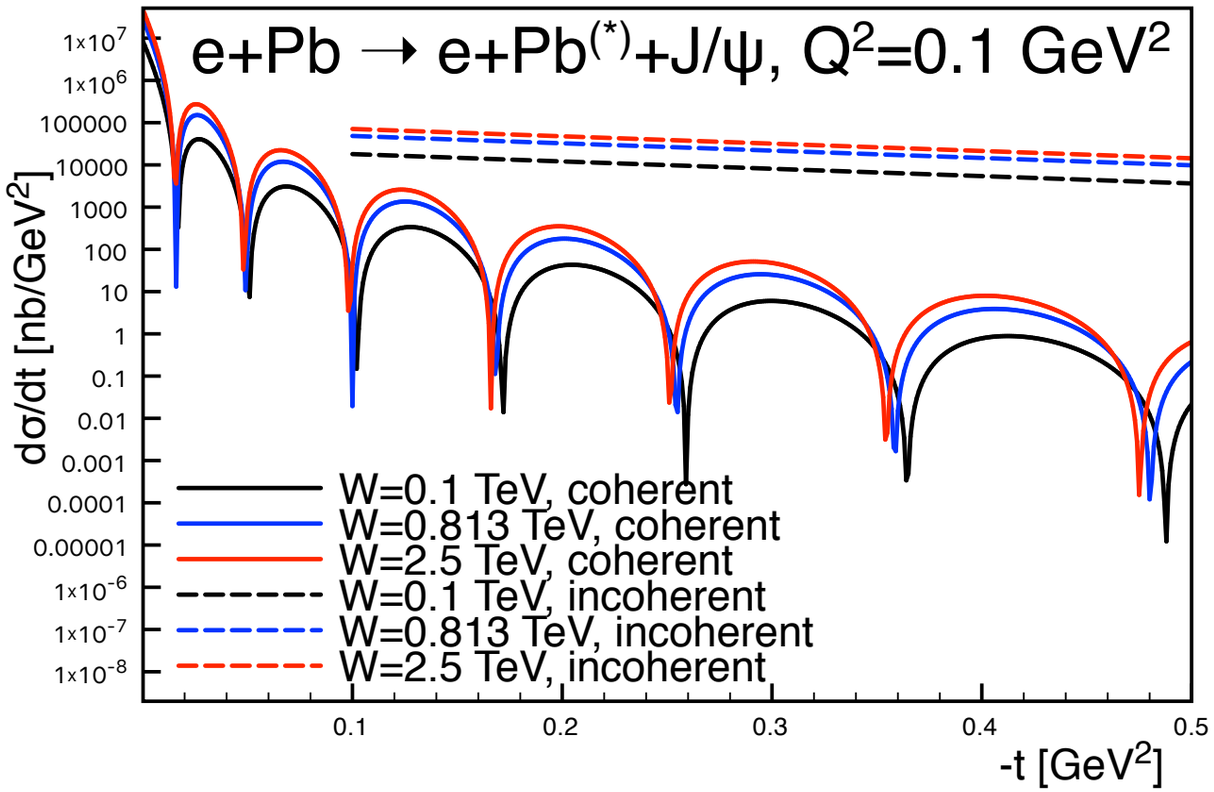

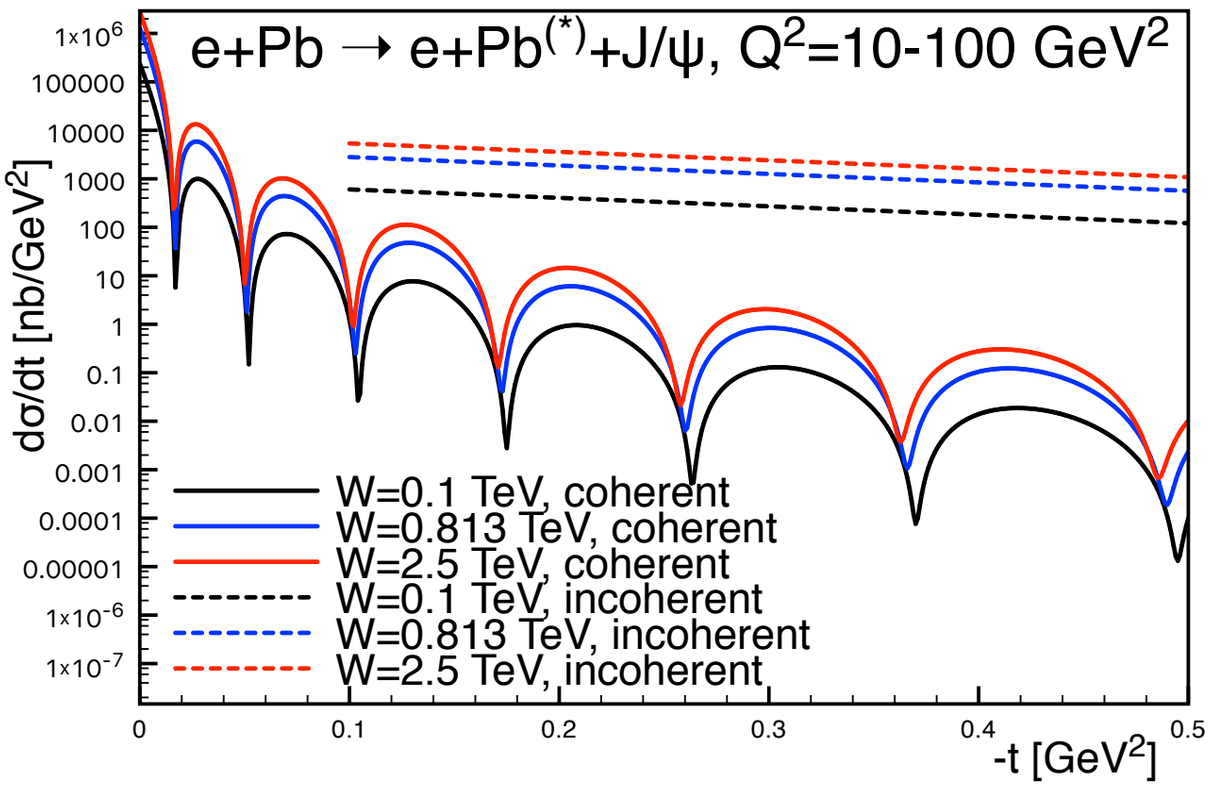

Mantysaari, 1011.1988, IPsat

Energy and scale dependence of the position of dips in |t|. Provides information about nuclear structure. Can perform similar measurements on proton target to estimate the saturation in proton vs nuclei. Challenging experimentally.

Gribov inelastic shadowing

Gribov's Reggeon calculus and AGK cutting rules.
Relation between diffraction and the nuclear shadowing with double scattering.
Direct manifestation of the unitarity in strong interactions.

Diffraction cross section related to the 'diffractive' cut of the double scattering diagram.

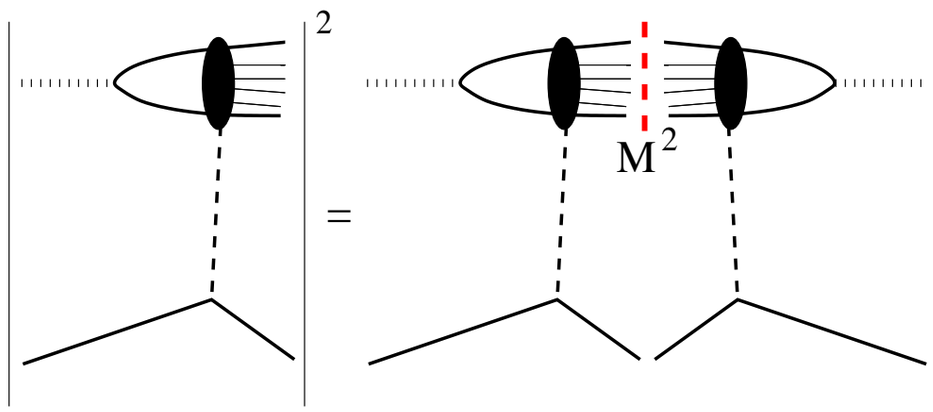

The contribution from the double cut which is responsible for the double scattering is related to the negative of the contribution of the diffractive cut.

$$\sigma_A^2 = -4\pi A(A-1)\int d^2b\, T_A^2(b) \int_{M_{min}^2}^{M_{max}^2} dM^2 \left.\frac{d\sigma^{\mathcal{D}}_{\gamma^*-\mathrm{p}}}{dM^2 dt}\right|_{t=0} F_A^2(t_{min}),$$

M^2 Mass of the diffractive system

$\frac{d\sigma^D_{\gamma^* p}}{dM^2 dt}$ Differential cross section for the diffractive dissociation of the virtual photon.

Gribov inelastic shadowing

- Close link between diffraction and shadowing.

- Once the diffractive part is known the shadowing in the nuclear case is parameter free (except for the higher order rescatterings, see below).

- Impact parameter dependence of the nuclear shadowing is provided in these models.

- Scatterings with N>2 need to be modeled:

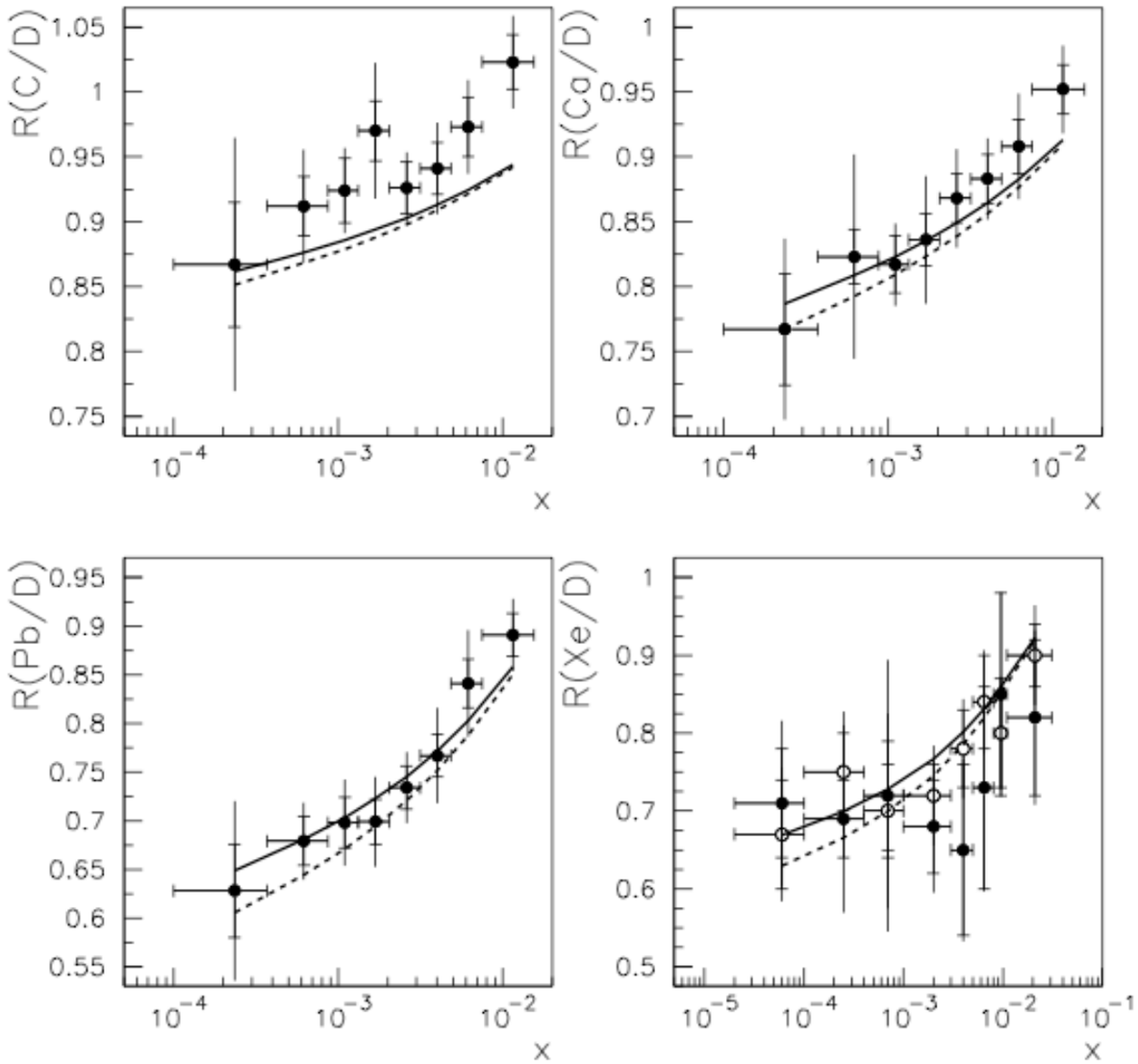

Armesto, Capella, Kaidalov, Albacete, Salgado

also used by Frankfurt, Guzey, Strikman

$$\sigma^{Sch}_{\gamma^*-A} = \sigma_{\gamma^*-\mathrm{nucleon}} \int d^2b \, \frac{AT_A(b)}{1+(A-1)f(x,Q^2)T_A(b)}$$

$$\sigma^{eik}_{\gamma^*-A} = \sigma_{\gamma^*-\mathrm{nucleon}} \int d^2b \, \frac{A\{1-\exp\left[-2(A-1)T_A(b)f(x,Q^2)\right]\}}{2(A-1)f(x,Q^2)}$$

Resummation at small x

DGLAP fits of F_2 for proton

DGLAP based fits of the structure function for proton work very well

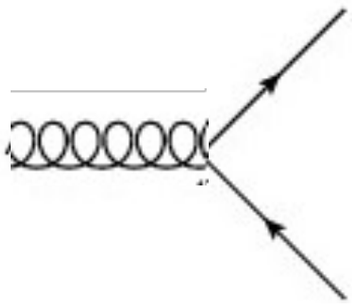

QCD scaling violations

@ low x

Reduced cross section

$$\sigma_{r,NC} = F_2 - \frac{y^2}{Y+} F_L$$

$$Q^2 \ll M_Z^2$$

Bjorken scaling region

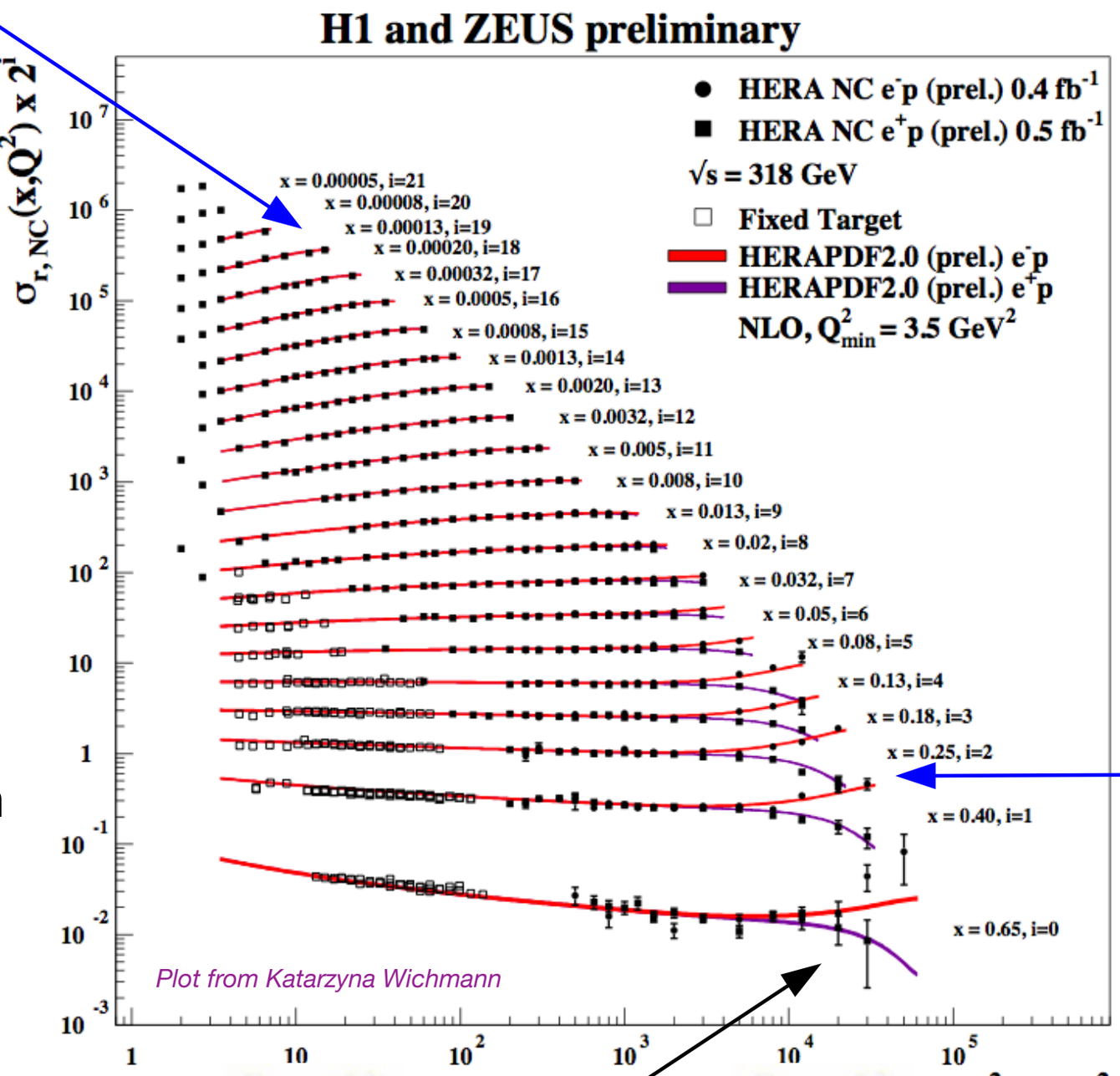

Plot from Katarzyna Wichmann

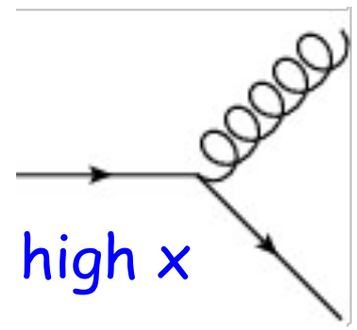

@ high x

@ high Q^2

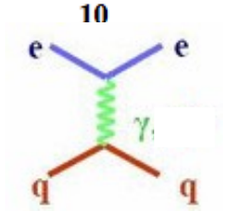

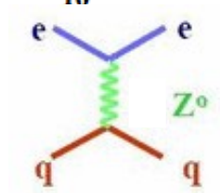

Question: *what is the range of applicability of standard collinear formalism with DGLAP evolution and the calculations with low x effects (including saturation)?*

Question: *what is the range of applicability of standard collinear formalism with DGLAP evolution and the calculations with low x effects (including saturation)?*

One possible answer: *it depends on the process*

Question: *what is the range of applicability of standard collinear formalism with DGLAP evolution and the calculations with low x effects (including saturation)?*

One possible answer: *it depends on the process*

Another possible answer: *it depends on the accuracy of calculation in both cases. More specifically, it is possible to extend the region of validity of any of these approaches through the resummation.*

Are structure function data compatible with DGLAP evolution?

NNPDF analysis

Ball,Bertoni,Bonvini,Marzani,Rojo,Rottoli

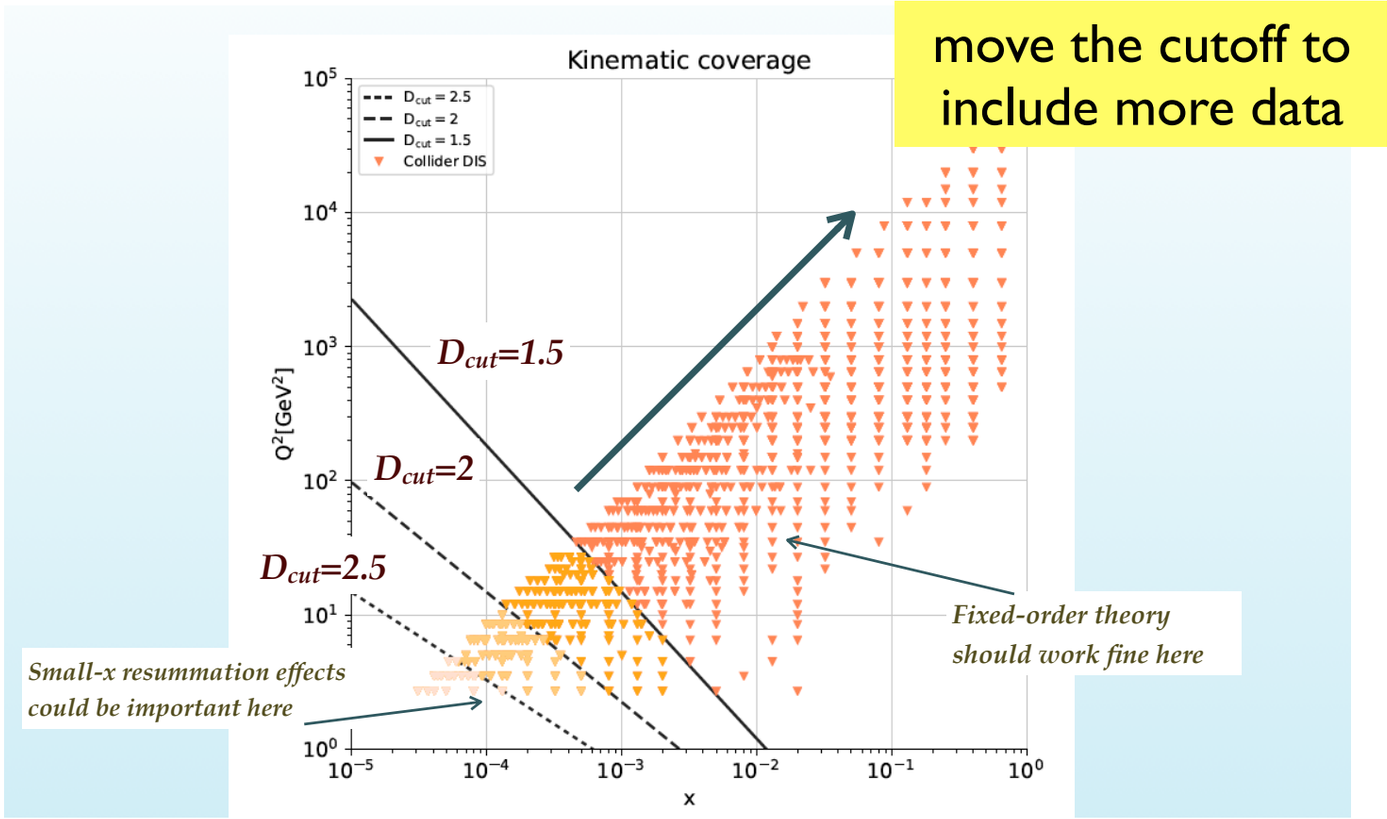

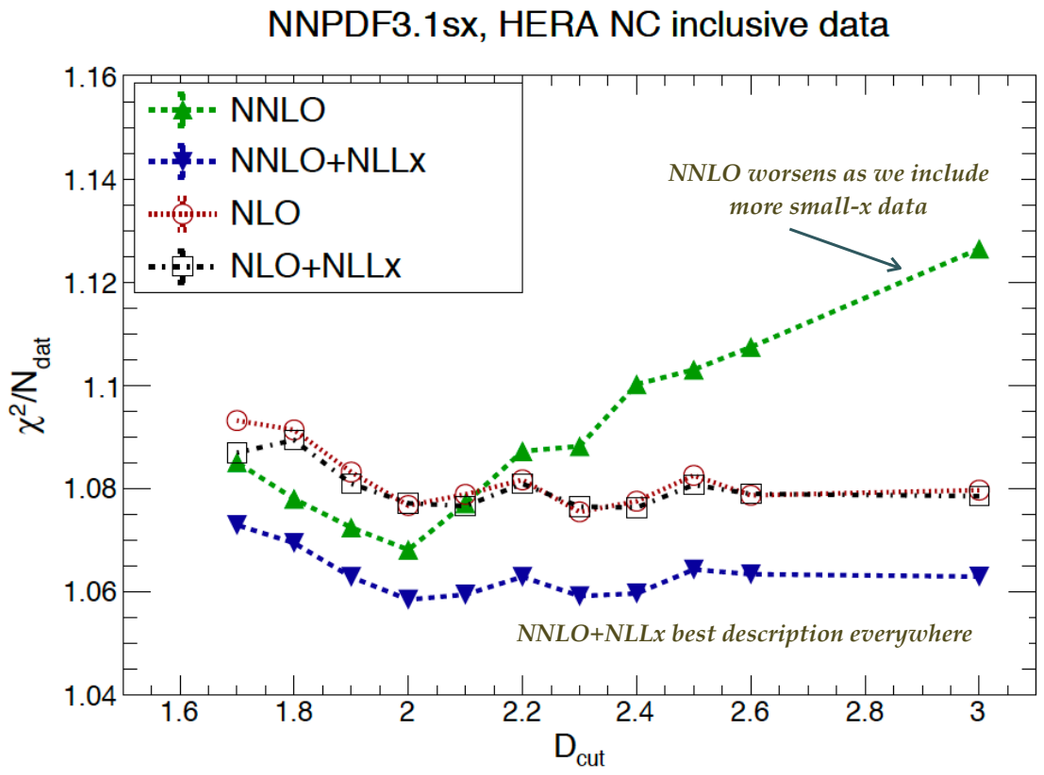

- The idea: introduce the cutoff and cut the small x - small Q^2 data
- Move the cutoff to exclude more data
- Observe variation of quality of fit
- Strong variation can indicate the problems with the fit
- Analysis indicated variation of the NNLO fit
- Resummation of small x effects improves the situation

DGLAP vs BFKL evolution

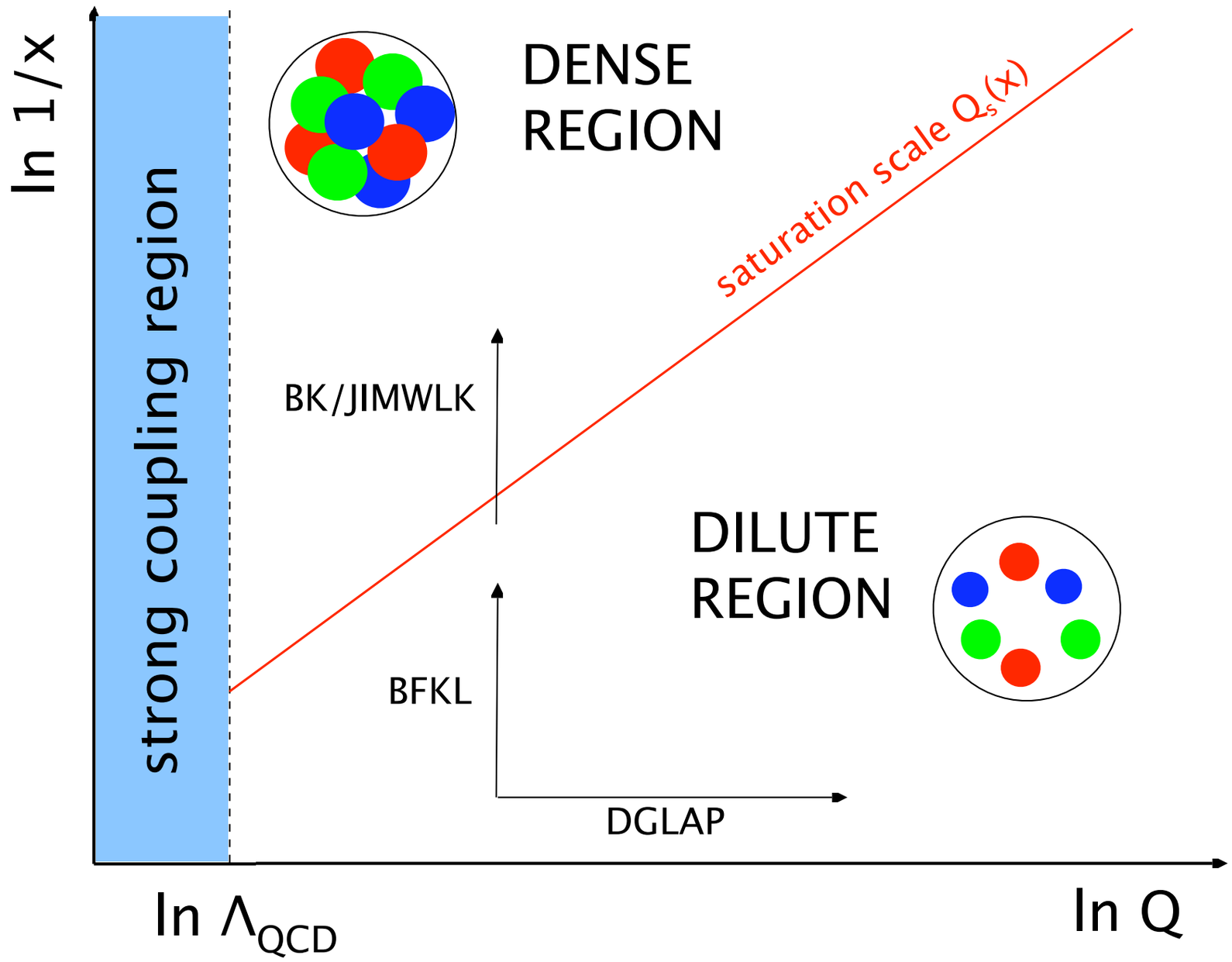

✦Schematically we know what should happen

✦But what are the exact regions of applicability and convergence of the both expansions?

✦How ‘small’ should ‘small x’ be for BFKL and BK to be applicable?

Collinear-DGLAP approach

$\gamma^* N$ as a template

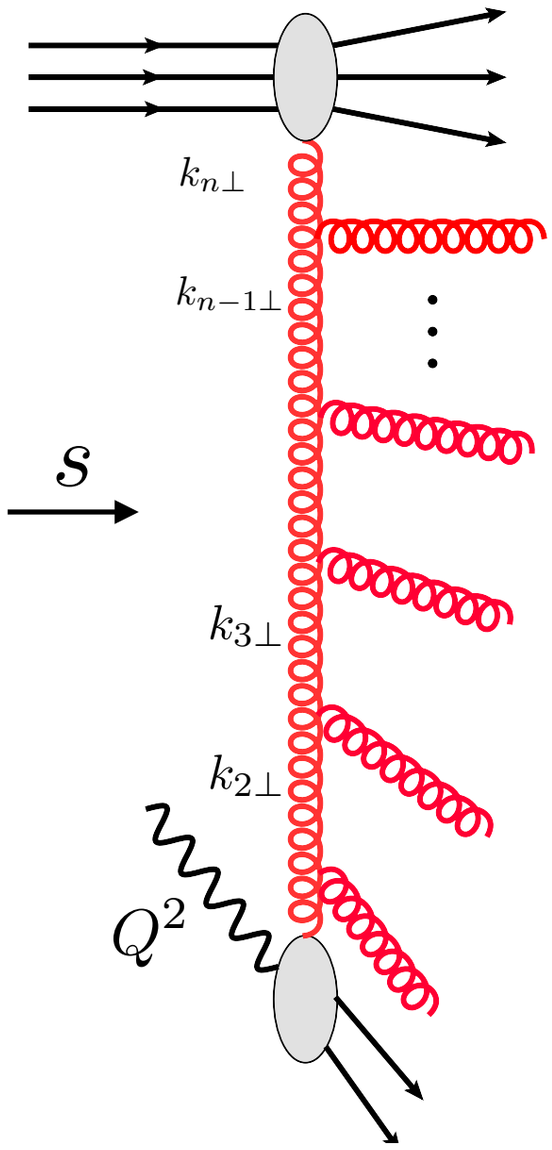

Large parameter

$$Q^2 \to \infty$$

s total energy is fixed

Probing small distances

Strong ordering in transverse momenta

$$Q^2 \gg k_{1\perp}^2 \gg k_{2\perp}^2 \gg k_{3\perp}^2 \cdots \gg k_{n\perp}^2$$

Resummation of large logarithms

$$\int_{\mu_0^2}^{Q^2} \frac{dk_{1\perp}^2}{k_{1\perp}^2} g^2 \int_{\mu_0^2}^{k_{1\perp}^2} \frac{dk_{2\perp}^2}{k_{2\perp}^2} g^2 \int_{\mu_0^2}^{k_{2\perp}^2} \frac{dk_{3\perp}^2}{k_{3\perp}^2} g^2 \cdots \int_{\mu_0^2}^{k_{n-1\perp}^2} \frac{dk_{n\perp}^2}{k_{n\perp}^2} g^2 \simeq \left(g^2 \log \frac{Q^2}{\mu_0^2} \right)^n$$

Collinear-DGLAP approach

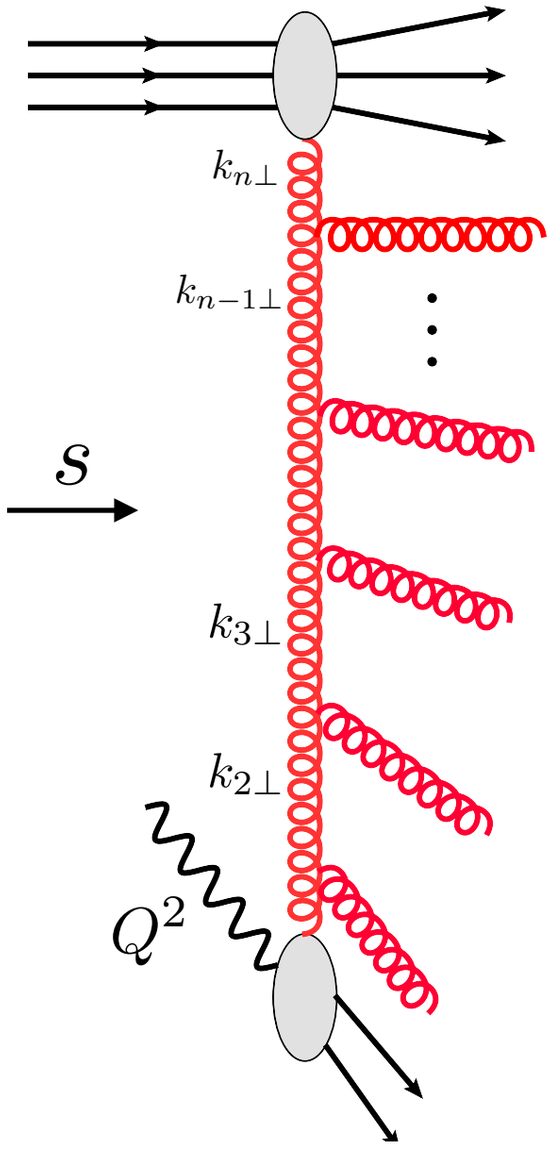

DGLAP evolution equation for parton densities

$$\frac{\partial f_i(x,Q^2)}{\partial \log(Q^2)} = \sum_j \int_x^1 \frac{dz}{z} P_{j\to i}(z) f_j(\frac{x}{z}, Q^2)$$

Splitting functions calculated perturbatively

$$P_{j\to i}(z) = \alpha_s P_{j\to i}^{(LO)}(z) + \alpha_s^2 P_{j\to i}^{(NLO)}(z) + \alpha_s^3 P_{j\to i}^{(NNLO)}(z) + \ldots$$

Parton densities: distributions in longitudinal momenta at a given scale

$$f_i(x, Q^2)$$

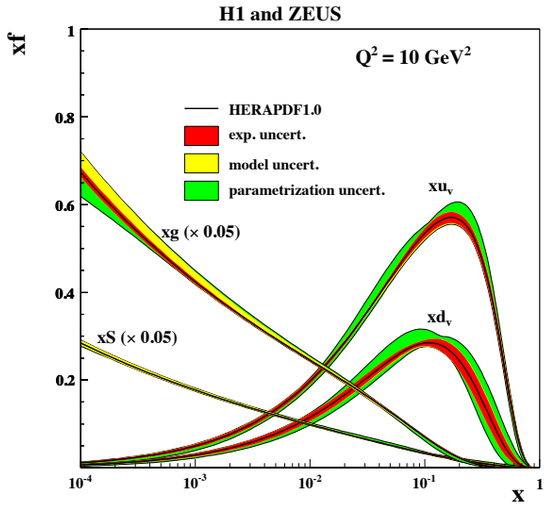

Collinear-DGLAP approach

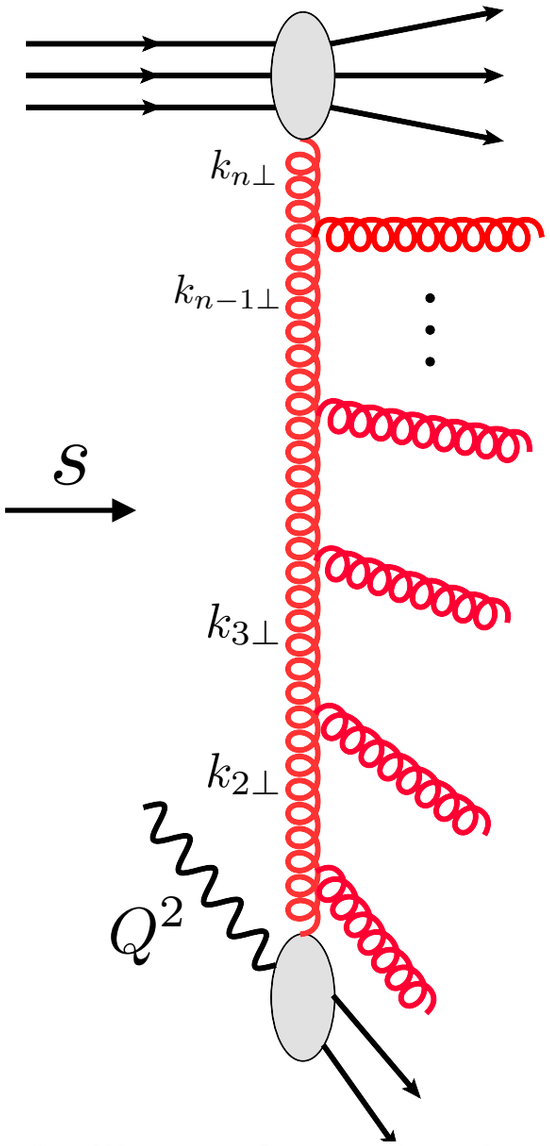

DGLAP evolution equation for parton densities

$$\frac{\partial f_i(x,Q^2)}{\partial \log(Q^2)} = \sum_j \int_x^1 \frac{dz}{z} P_{j\to i}(z) f_j(\frac{x}{z}, Q^2)$$

Splitting functions calculated perturbatively

$$P_{j\to i}(z) = \alpha_s P^{(LO)}_{j\to i}(z) + \alpha_s^2 P^{(NLO)}_{j\to i}(z) + \alpha_s^3 P^{(NNLO)}_{j\to i}(z) + \ldots$$

Parton densities: distributions in longitudinal momenta at a given scale

$$f_i(x,Q^2)$$

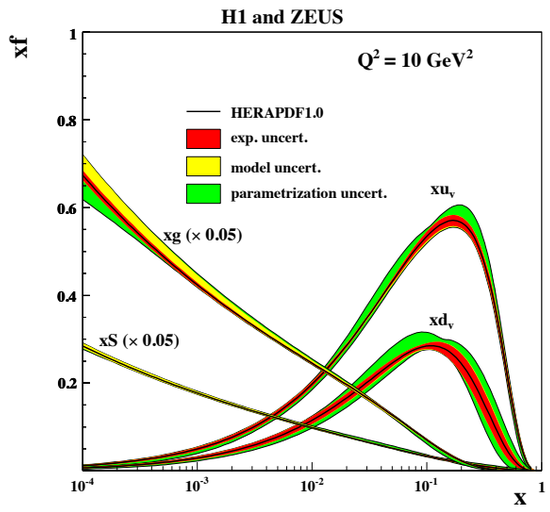

Collinear factorization of the cross section

$$d\sigma(x,Q^2) = \sum_i f_i \otimes d\hat{\sigma}^i + \mathcal{O}(\Lambda^2/Q^2)$$

$d\hat{\sigma}^i$ partonic cross section, calculable perturbatively

High energy limit-BFKL

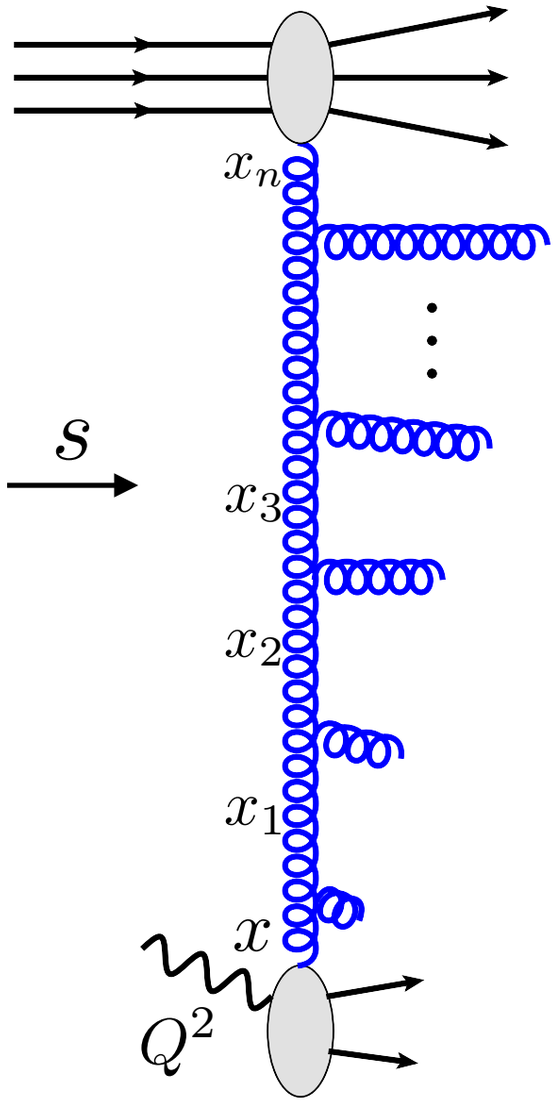

Large parameter

$$s \to \infty$$

High energy or Regge limit

$$s \gg Q^2 \gg \Lambda^2$$

Q^2 fixed, perturbative

Light cone proton momentum

$$p^+ = p^0 + p^z$$

$$k_i^+ = x_i p^+$$

Strong ordering in longitudinal momenta

$$x \ll x_1 \ll x_2 \ll \cdots \ll x_n$$

High energy limit-BFKL

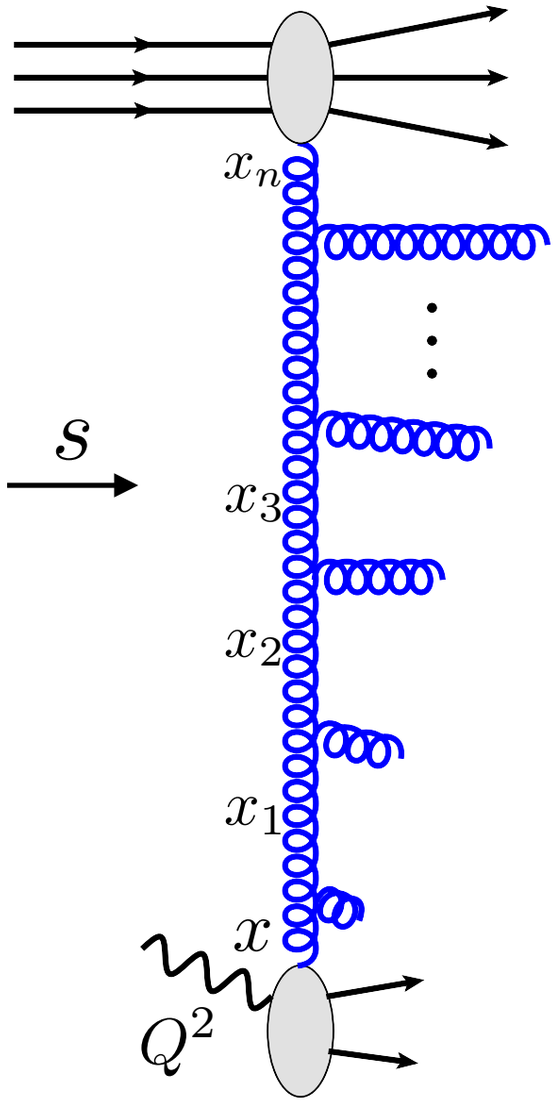

Large parameter

$$s \to \infty$$

High energy or Regge limit

$$s \gg Q^2 \gg \Lambda^2$$

Q^2 fixed, perturbative

Light cone proton momentum

$$p^+ = p^0 + p^z$$

$$k_i^+ = x_i p^+$$

Strong ordering in longitudinal momenta

$$x \ll x_1 \ll x_2 \ll \cdots \ll x_n$$

Perturbative coupling but large logarithm

$$\bar{\alpha}_s \ll 1$$

$$\ln \frac{1}{x} \simeq \ln \frac{s}{Q^2} \gg 1$$

High energy limit-BFKL

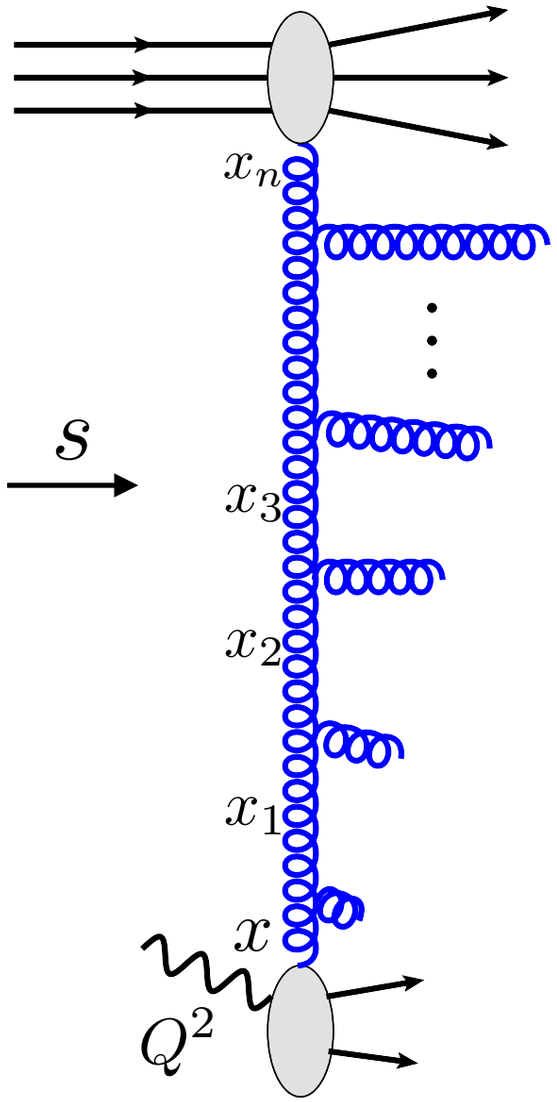

Large parameter

$$s \to \infty$$

High energy or Regge limit

$$s \gg Q^2 \gg \Lambda^2$$

Q^2 fixed, perturbative

Light cone proton momentum

$$p^+ = p^0 + p^z$$

$$k_i^+ = x_i p^+$$

Strong ordering in longitudinal momenta

$$x \ll x_1 \ll x_2 \ll \cdots \ll x_n$$

Perturbative coupling but large logarithm

$$\bar{\alpha}_s \ll 1$$

$$\ln \frac{1}{x} \simeq \ln \frac{s}{Q^2} \gg 1$$

Large logarithms

$$\frac{\alpha_s N_c}{\pi} \int_x^1 \frac{dz}{z} = \frac{\alpha_s N_c}{\pi} \ln \frac{1}{x} = \bar{\alpha}_s \ln \frac{1}{x}$$

Leading logarithmic resummation

$$\left(\bar{\alpha}_s \ln \frac{1}{x} \right)^n \qquad \left(\bar{\alpha}_s \ln \frac{s}{s_0} \right)^n$$

High energy limit-BFKL

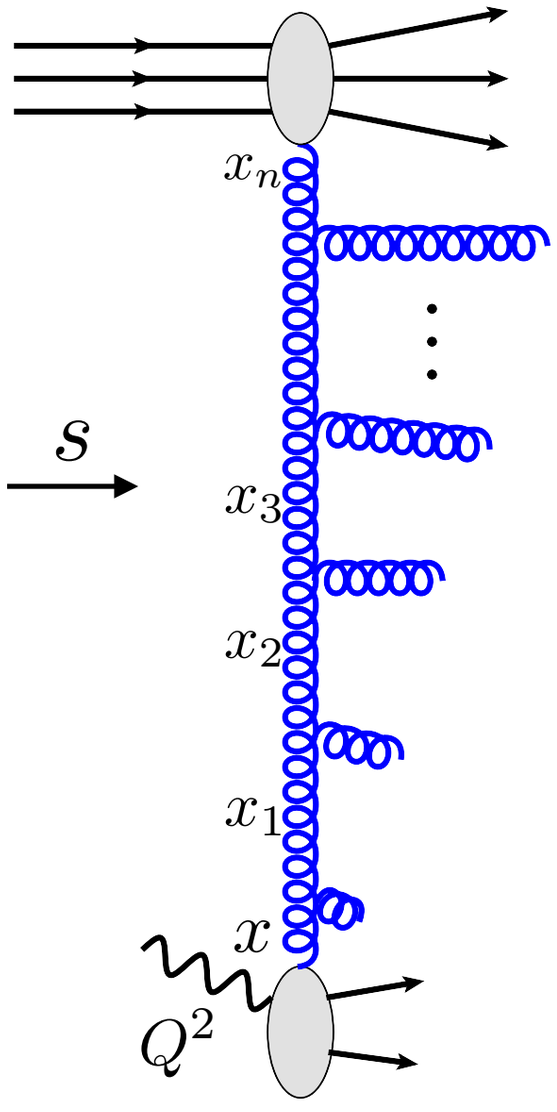

Resummation performed by Bethe-Salpeter type equation

BFKL evolution equation

$$\frac{\partial \mathcal{F}_g(x,k_T)}{\partial \ln 1/x} = \int d^2k'_T \, \mathcal{K}(k_T,k'_T)\, \mathcal{F}_g(x,k'_T)$$

High energy limit-BFKL

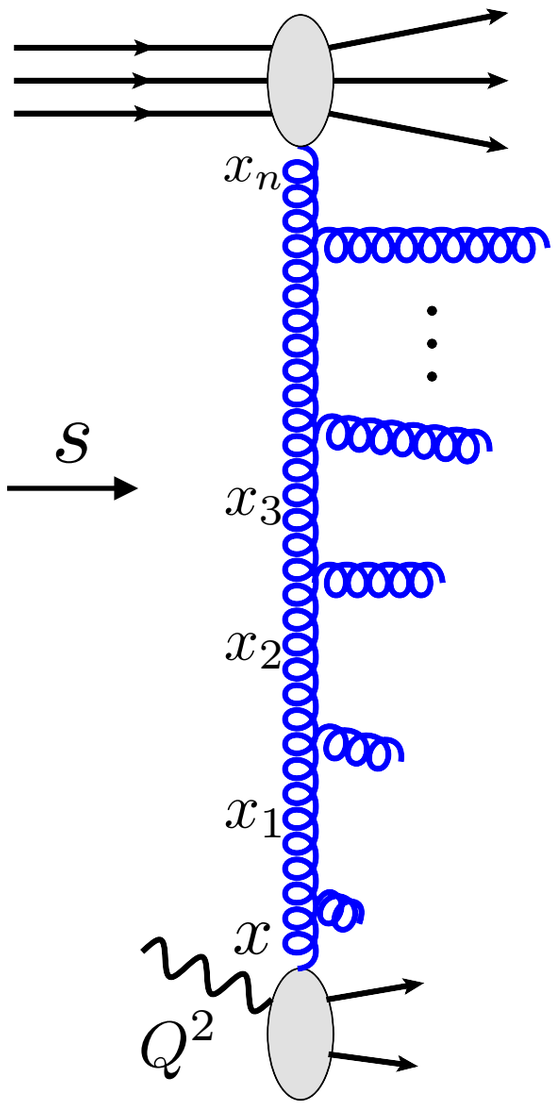

Resummation performed by Bethe-Salpeter type equation

BFKL evolution equation

$$\frac{\partial \mathcal{F}_g(x,k_T)}{\partial \ln 1/x} = \int d^2k'_T \, \mathcal{K}(k_T,k'_T)\, \mathcal{F}_g(x,k'_T)$$

Branching kernel (perturbative expansion)

$$\mathcal{K} = \bar{\alpha}_s \mathcal{K}^{LLx} + \bar{\alpha}_s^2 \mathcal{K}^{NLLx} + \bar{\alpha}_s^3 \mathcal{K}^{NNLLx} + \dots$$

QCD

N=4 SYM

High energy limit-BFKL

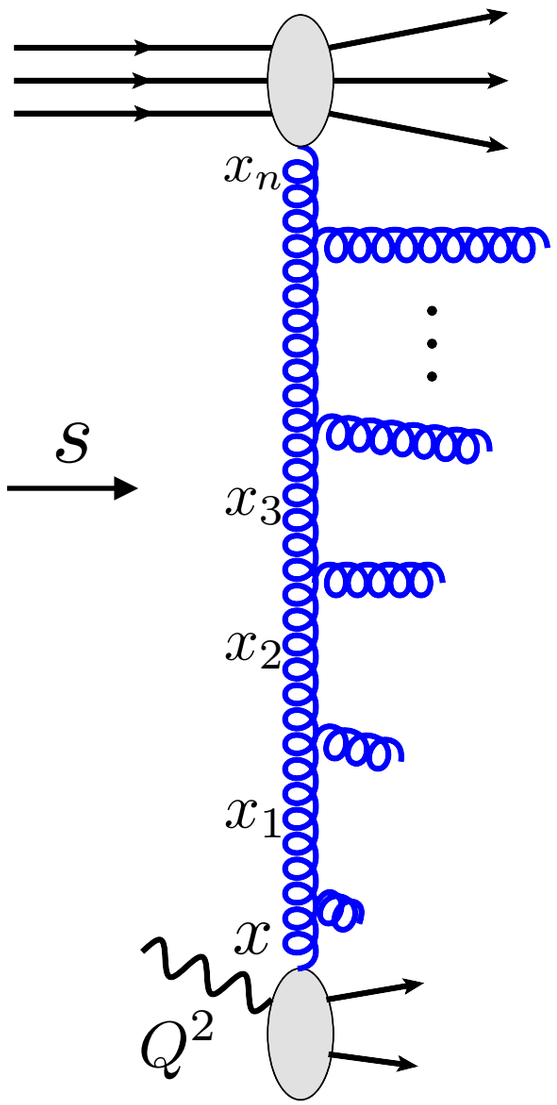

Resummation performed by Bethe-Salpeter type equation

BFKL evolution equation

$$\frac{\partial \mathcal{F}_g(x,k_T)}{\partial \ln 1/x} = \int d^2k'_T \, \mathcal{K}(k_T,k'_T)\, \mathcal{F}_g(x,k'_T)$$

Branching kernel (perturbative expansion)

$$\mathcal{K} = \bar{\alpha}_s \mathcal{K}^{LLx} + \bar{\alpha}_s^2 \mathcal{K}^{NLLx} + \bar{\alpha}_s^3 \mathcal{K}^{NNLLx} + \dots$$

QCD N=4 SYM

Unintegrated, (transverse momentum dependent) gluon density $\mathcal{F}_g(x,k_T)$

High energy limit-BFKL

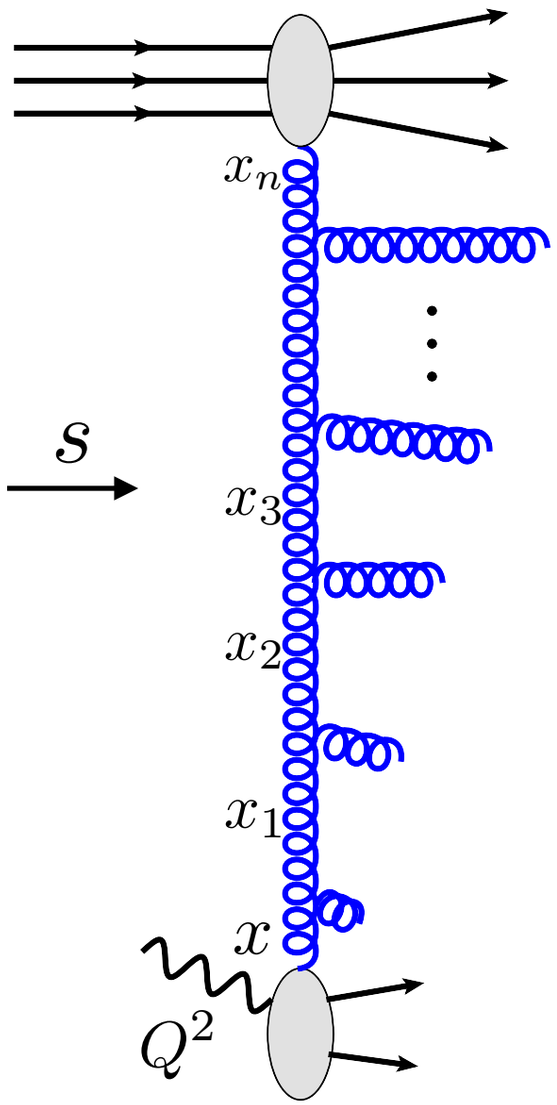

Resummation performed by Bethe-Salpeter type equation

BFKL evolution equation

$$\frac{\partial \mathcal{F}_g(x,k_T)}{\partial \ln 1/x} = \int d^2k'_T \, \mathcal{K}(k_T,k'_T)\, \mathcal{F}_g(x,k'_T)$$

Branching kernel (perturbative expansion)

$$\mathcal{K} = \bar{\alpha}_s \mathcal{K}^{LLx} + \bar{\alpha}_s^2 \mathcal{K}^{NLLx} + \bar{\alpha}_s^3 \mathcal{K}^{NNLLx} + \dots$$

QCD N=4 SYM

Unintegrated, (transverse momentum dependent) gluon density $\mathcal{F}_g(x,k_T)$

compare with DGLAP-collinear approach

$$\frac{\partial f_i(x,Q^2)}{\partial \log(Q^2)} = \sum_j \int_x^1 \frac{dz}{z} P_{j\to i}(z) f_j(\frac{x}{z},Q^2)$$

High energy limit

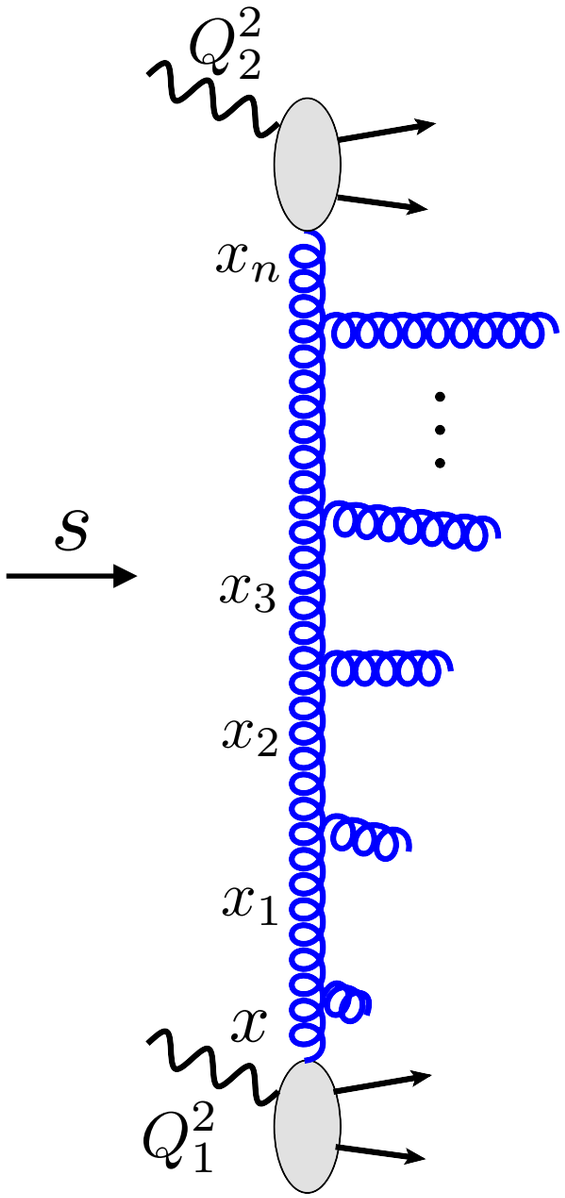

Random walk in transverse momenta

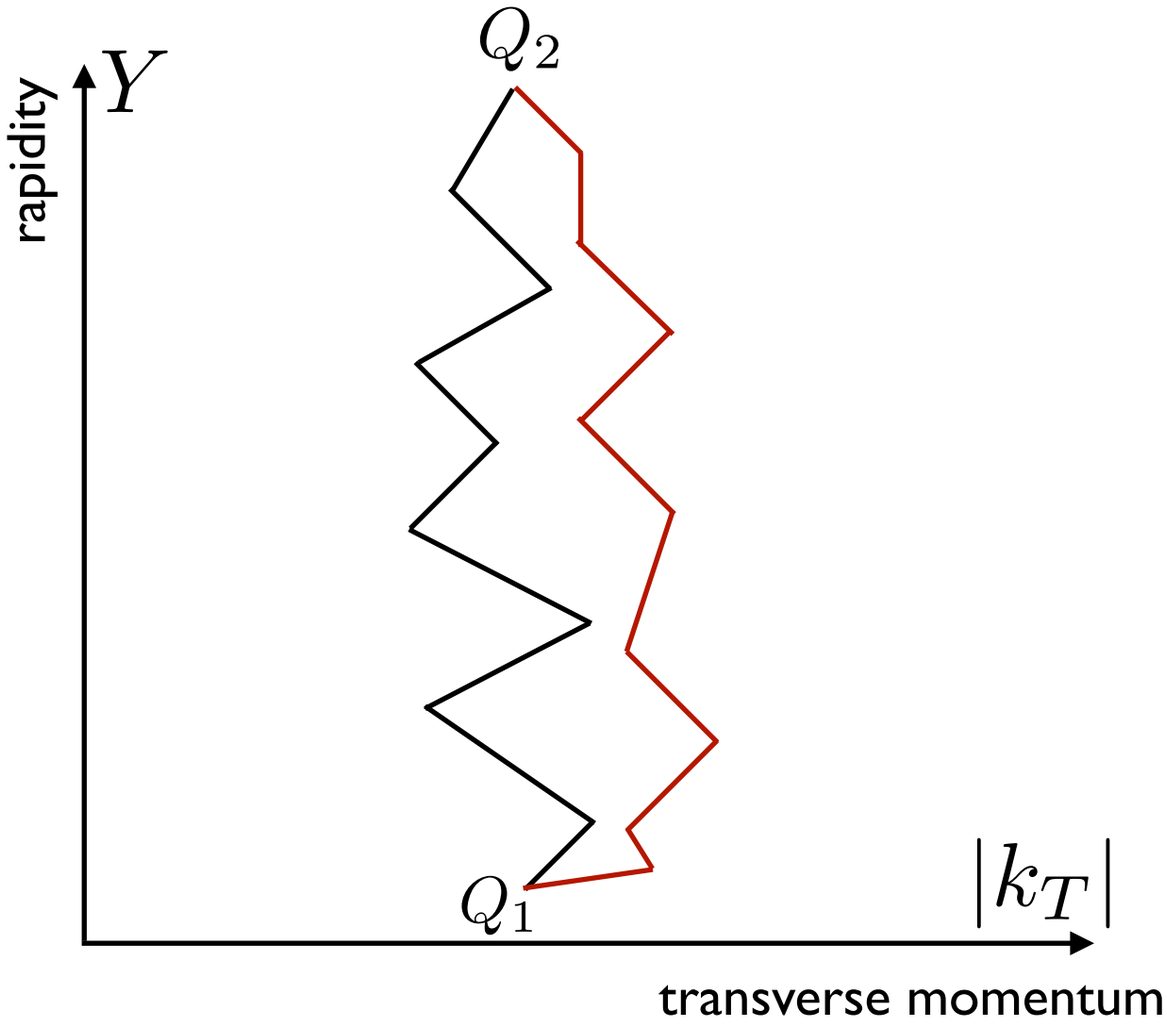

$$Y = \frac{1}{2} \ln \frac{p^+}{p^-}$$

Diffusion of transverse momenta towards IR and UV.
For large energies momenta can diffuse to low scales even when starting from large scales.

High energy limit

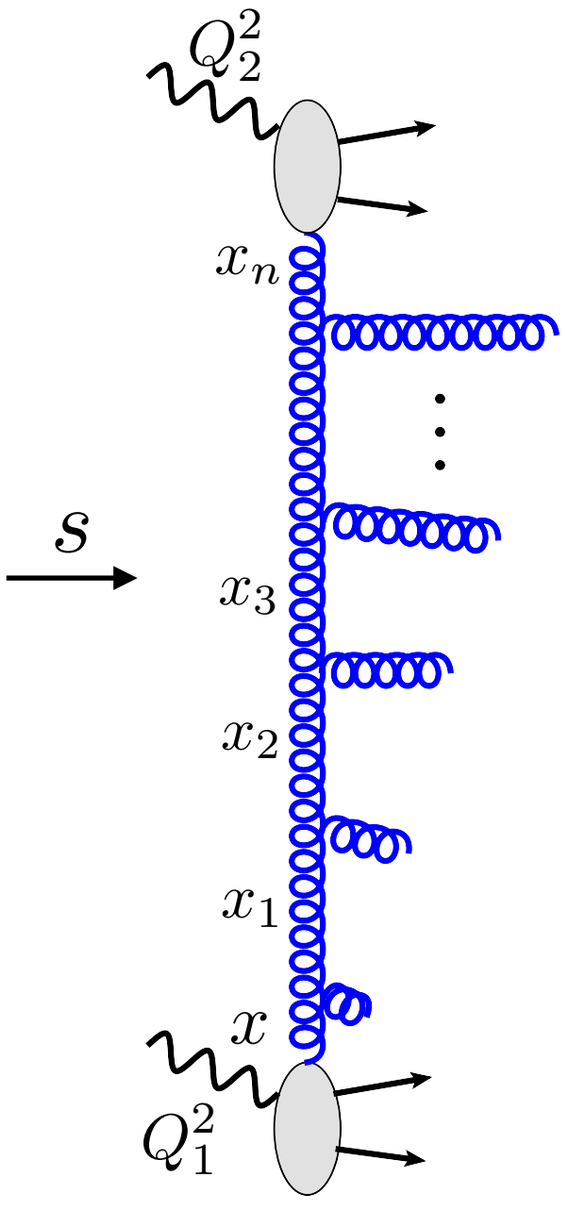

$$Y = \frac{1}{2} \ln \frac{p^+}{p^-}$$

Effects of running coupling:
'pull' towards the infrared region

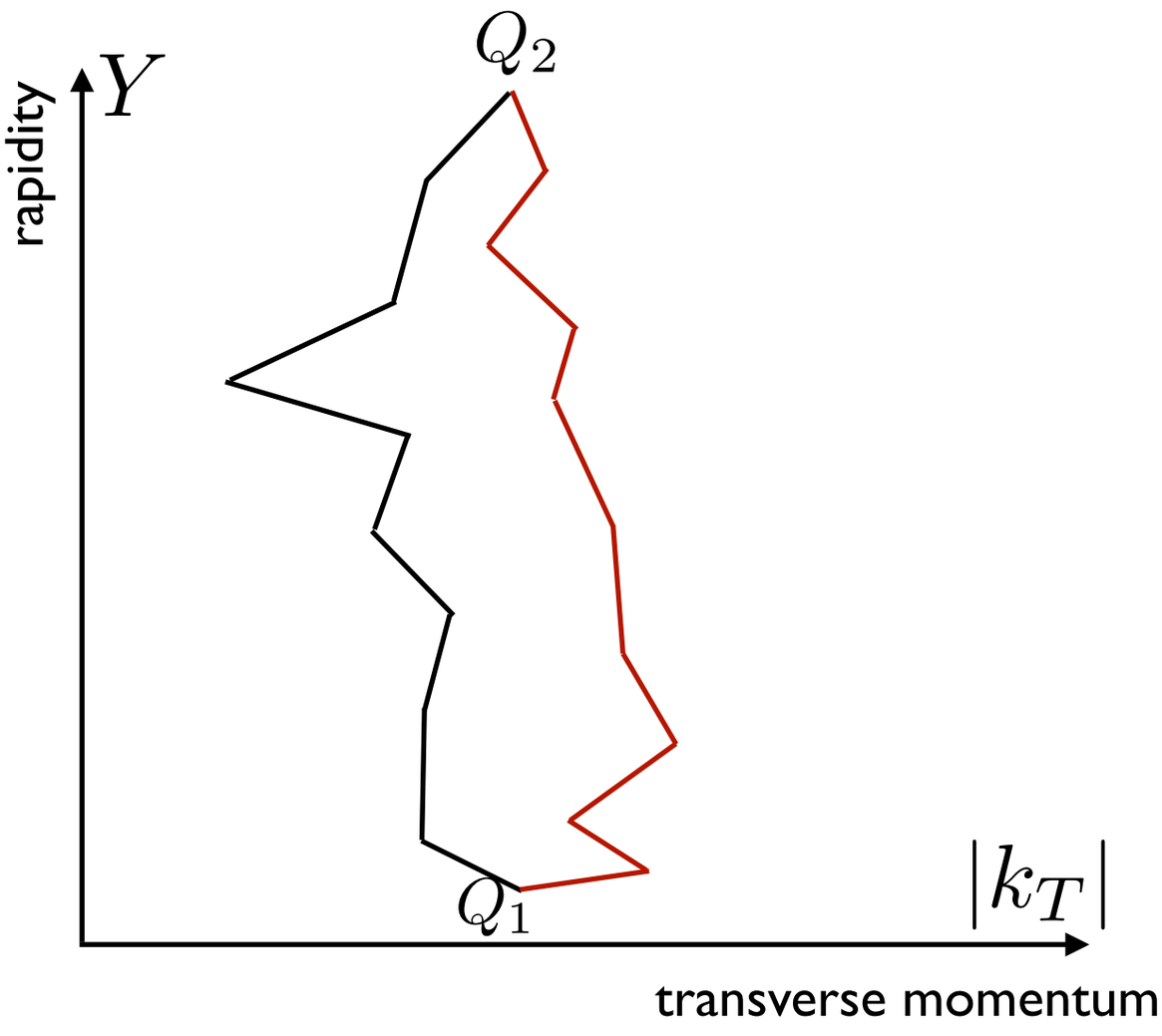

Large non-perturbative effects for large energies.

High energy limit

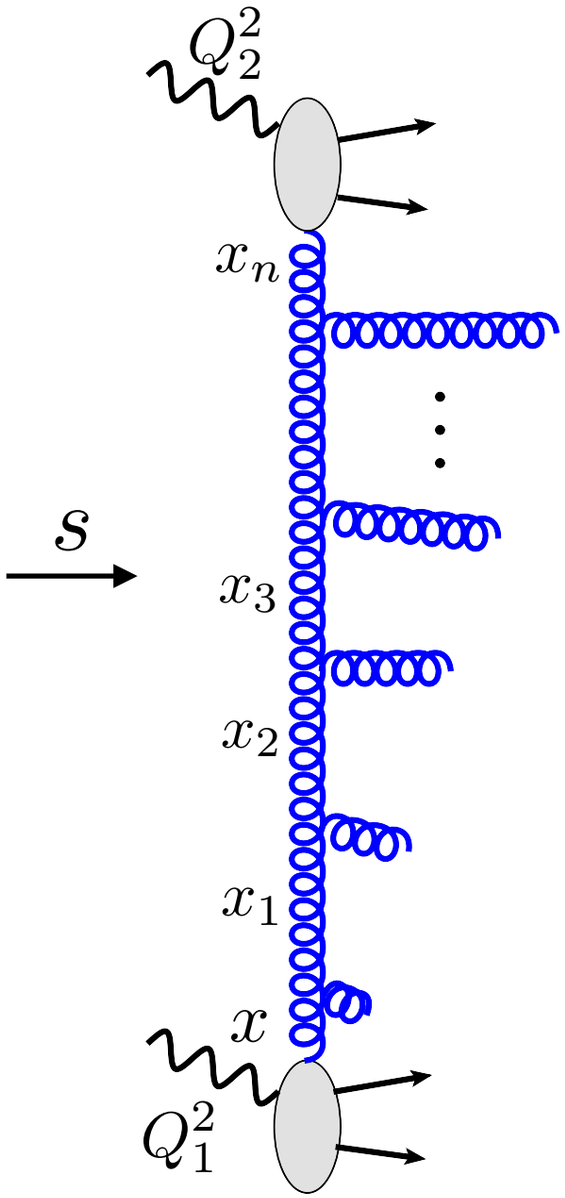

Effects of running coupling:
'pull' towards the infrared region

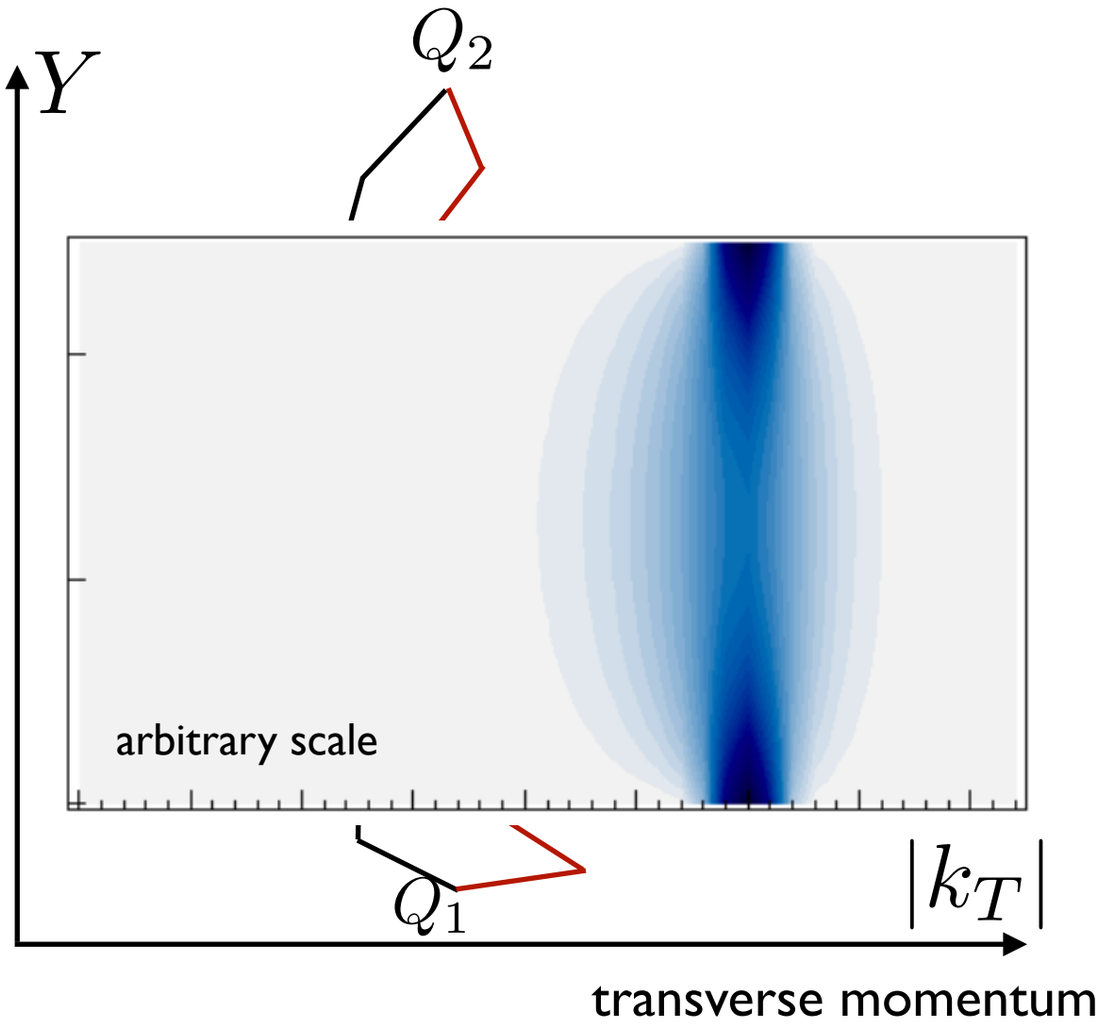

$$Y = \frac{1}{2} \ln \frac{p^+}{p^-}$$

Large non-perturbative effects for large energies.

BFKL solution

LL: *Balitsky,Fadin,Kuraev,Lipatov*
NLL: *Fadin, Lipatov; Camici,Ciafaloni*

BFKL solution

BFKL evolution equation

LL: *Balitsky,Fadin,Kuraev,Lipatov*
NLL: *Fadin, Lipatov; Camici,Ciafaloni*

$$\frac{\partial \mathcal{F}_g(x,k_T)}{\partial \ln 1/x} = \int d^2k'_T \, \mathcal{K}(k_T,k'_T)\, \mathcal{F}_g(x,k'_T)$$

Solution: $\mathcal{F}_g(x,k_T) \sim x^{-\omega_{IP}}$ Rise of cross sections: $\sigma^{\gamma^* p} \sim s^{\omega_{IP}}$

Pomeron intercept $\omega_{IP}^{LLx} = \bar{\alpha}_s 4 \ln 2$ leading logarithmic

BFKL solution

BFKL evolution equation

LL: *Balitsky,Fadin,Kuraev,Lipatov*
NLL: *Fadin, Lipatov; Camici,Ciafaloni*

$$\frac{\partial \mathcal{F}_g(x,k_T)}{\partial \ln 1/x} = \int d^2k'_T \, \mathcal{K}(k_T,k'_T)\, \mathcal{F}_g(x,k'_T)$$

Solution: $\mathcal{F}_g(x,k_T) \sim x^{-\omega_{IP}}$ Rise of cross sections: $\sigma^{\gamma^* p} \sim s^{\omega_{IP}}$

Pomeron intercept $\omega_{IP}^{LLx} = \bar{\alpha}_s 4 \ln 2$ leading logarithmic

$\omega_{IP}^{NLLx} \simeq \bar{\alpha}_s 4 \ln 2 (1 - 6.5\bar{\alpha}_s)$ next-to-leading logarithmic

BFKL solution

BFKL evolution equation

LL: *Balitsky,Fadin,Kuraev,Lipatov*
NLL: *Fadin, Lipatov; Camici,Ciafaloni*

$$\frac{\partial \mathcal{F}_g(x,k_T)}{\partial \ln 1/x} = \int d^2k'_T \, \mathcal{K}(k_T,k'_T)\, \mathcal{F}_g(x,k'_T)$$

Solution: $\mathcal{F}_g(x,k_T) \sim x^{-\omega_{IP}}$ Rise of cross sections: $\sigma^{\gamma^* p} \sim s^{\omega_{IP}}$

Pomeron intercept $\omega_{IP}^{LLx} = \bar{\alpha}_s 4 \ln 2$ leading logarithmic

$\omega_{IP}^{NLLx} \simeq \bar{\alpha}_s 4 \ln 2 (1 - 6.5\bar{\alpha}_s)$ next-to-leading logarithmic

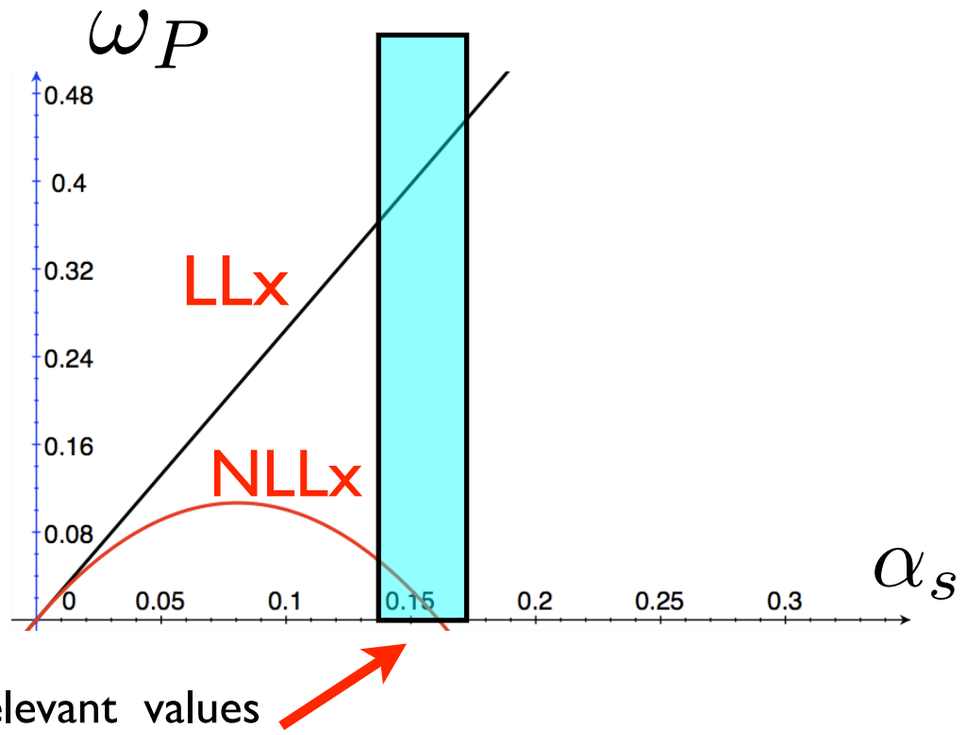

BFKL solution

BFKL evolution equation

LL: *Balitsky,Fadin,Kuraev,Lipatov*
NLL: *Fadin, Lipatov; Camici,Ciafaloni*

$$\frac{\partial \mathcal{F}_g(x,k_T)}{\partial \ln 1/x} = \int d^2k'_T \, \mathcal{K}(k_T,k'_T)\, \mathcal{F}_g(x,k'_T)$$

Solution: $\mathcal{F}_g(x,k_T) \sim x^{-\omega_{IP}}$ Rise of cross sections: $\sigma^{\gamma^* p} \sim s^{\omega_{IP}}$

Pomeron intercept $\omega_{IP}^{LLx} = \bar{\alpha}_s 4 \ln 2$ leading logarithmic

$\omega_{IP}^{NLLx} \simeq \bar{\alpha}_s 4 \ln 2 (1 - 6.5 \bar{\alpha}_s)$ next-to-leading logarithmic

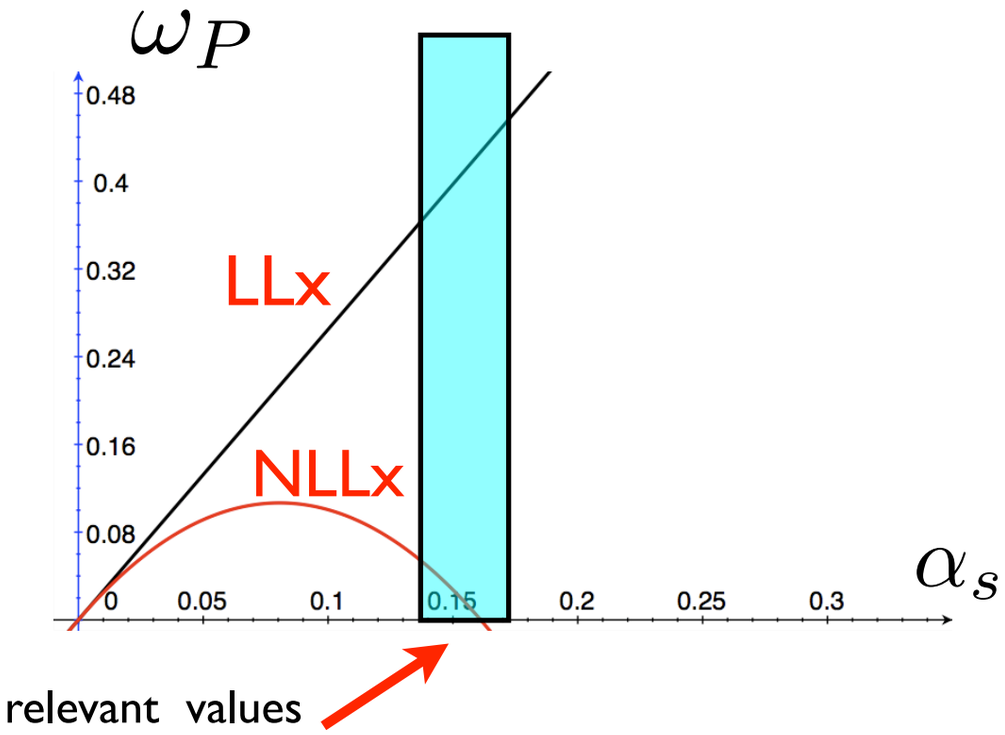

LLx vs NLLx BFKL solution for the gluon Green's function

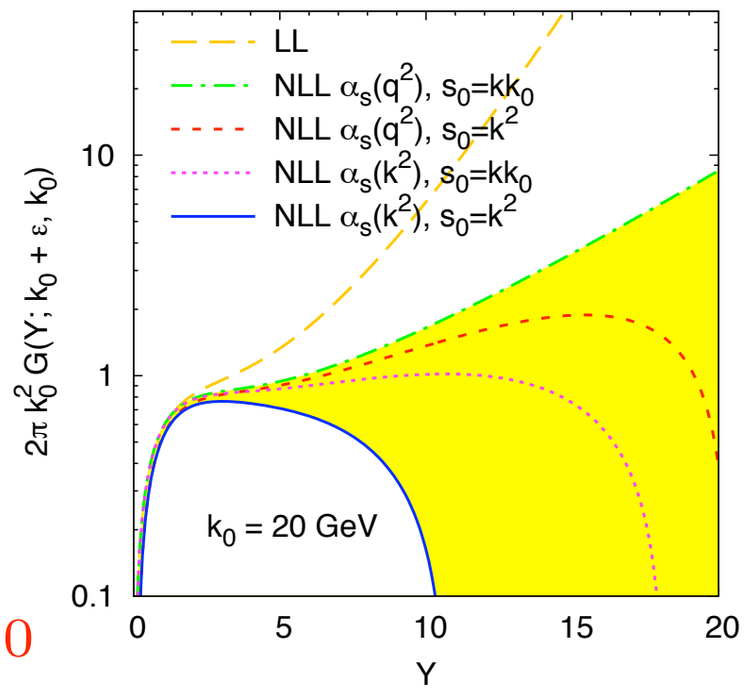

$Y = \ln s/s_0$

BFKL solution

BFKL evolution equation

LL: *Balitsky,Fadin,Kuraev,Lipatov*
NLL: *Fadin, Lipatov; Camici,Ciafaloni*

$$\frac{\partial \mathcal{F}_g(x,k_T)}{\partial \ln 1/x} = \int d^2k'_T \, \mathcal{K}(k_T,k'_T)\, \mathcal{F}_g(x,k'_T)$$

Solution: $\mathcal{F}_g(x,k_T) \sim x^{-\omega_{IP}}$ Rise of cross sections: $\sigma^{\gamma^* p} \sim s^{\omega_{IP}}$

Pomeron intercept $\omega_{IP}^{LLx} = \bar{\alpha}_s 4 \ln 2$ leading logarithmic

$\omega_{IP}^{NLLx} \simeq \bar{\alpha}_s 4 \ln 2 (1 - 6.5\bar{\alpha}_s)$ next-to-leading logarithmic

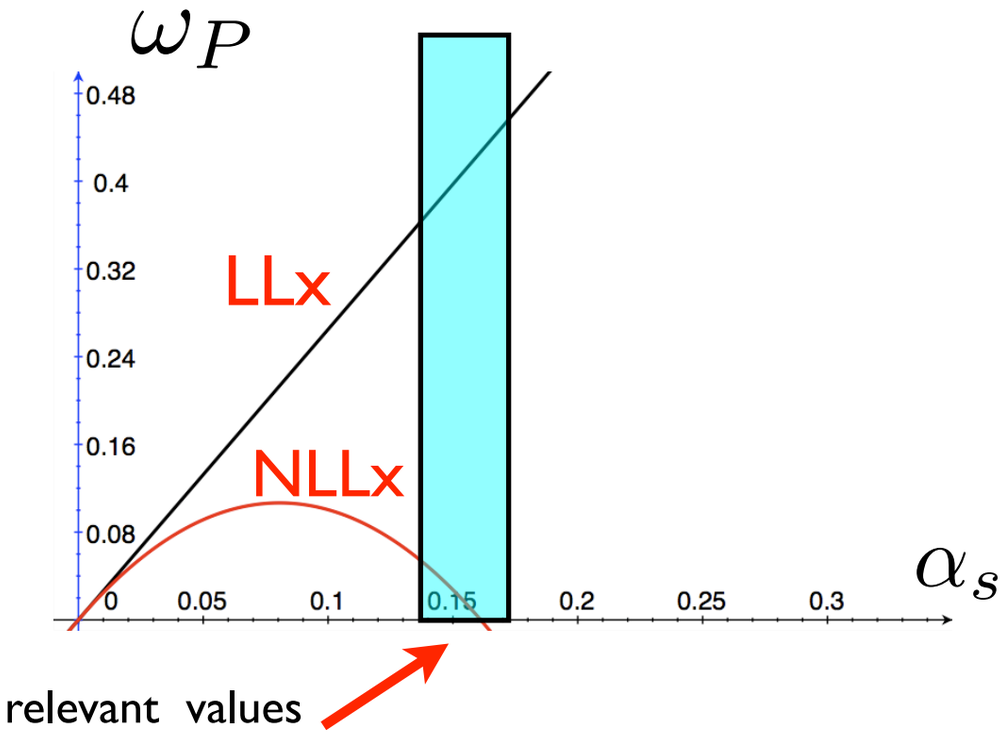

LLx vs NLLx BFKL solution for the gluon Green's function

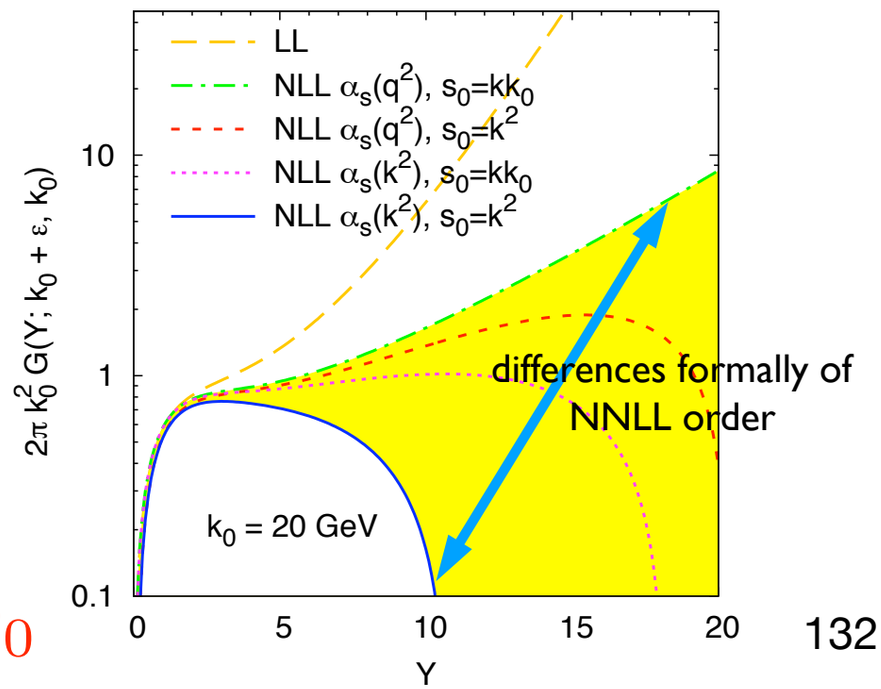

$Y = \ln s/s_0$

BFKL solution

BFKL evolution equation

LL: *Balitsky,Fadin,Kuraev,Lipatov*
NLL: *Fadin, Lipatov; Camici,Ciafaloni*

$$\frac{\partial \mathcal{F}_g(x,k_T)}{\partial \ln 1/x} = \int d^2k'_T \, \mathcal{K}(k_T,k'_T)\, \mathcal{F}_g(x,k'_T)$$

Solution: $\mathcal{F}_g(x,k_T) \sim x^{-\omega_{IP}}$ Rise of cross sections: $\sigma^{\gamma^* p} \sim s^{\omega_{IP}}$

Pomeron intercept $\omega_{IP}^{LLx} = \bar{\alpha}_s 4 \ln 2$ leading logarithmic

$\omega_{IP}^{NLLx} \simeq \bar{\alpha}_s 4 \ln 2 (1 - 6.5\bar{\alpha}_s)$ next-to-leading logarithmic

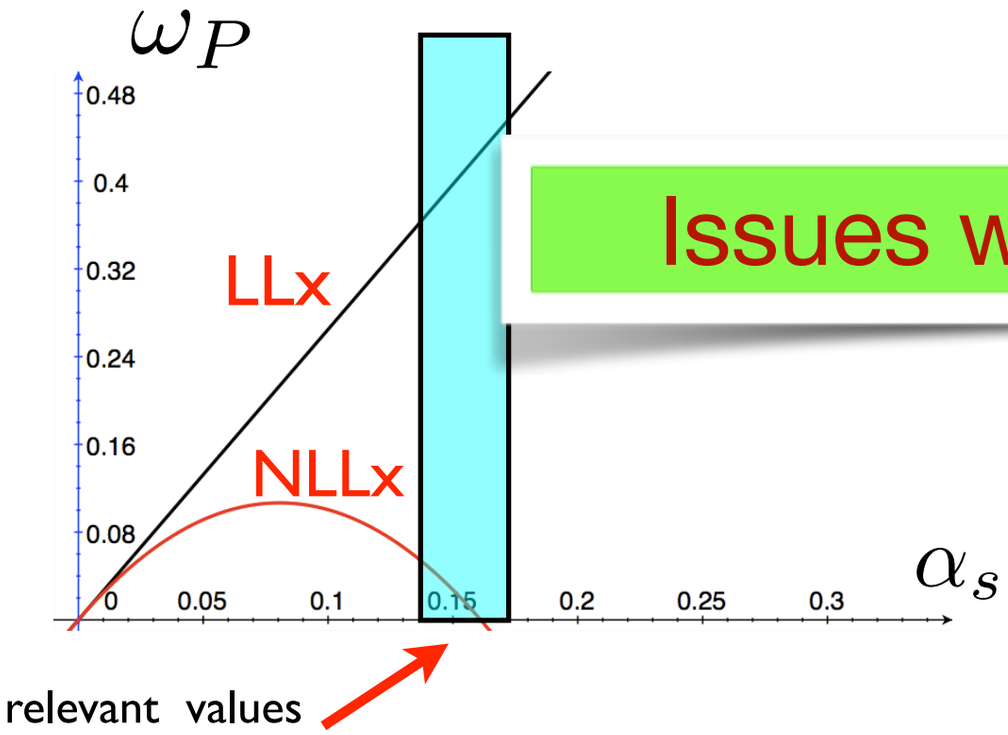

Issues with convergence…

LLx vs NLLx BFKL solution for the gluon Green's function

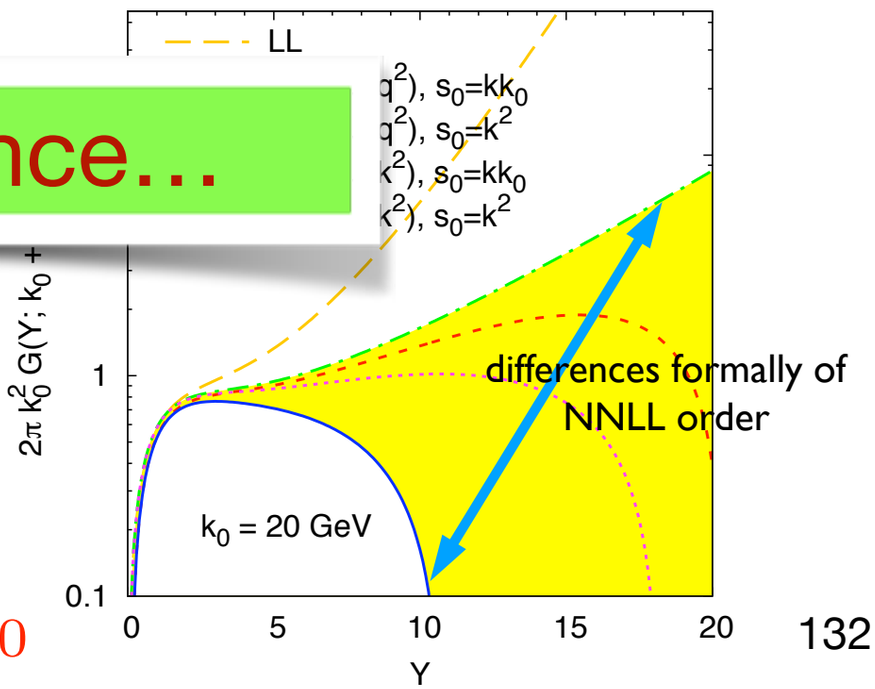

$Y = \ln s/s_0$

Why NLLx is so large in BFKL?

- Strong coupling constant is **not** a naturally small parameter in the Regge limit: $s \gg |t|, \Lambda^2_{QCD}$ but $\alpha_s(\mu^2),\ \mu^2 \neq s$

- Regge limit is inherently nonperturbative.

- Compare DGLAP (collinear approach): $Q^2 \gg \Lambda^2$ and $\alpha_s(Q^2) \ll 1$

- No momentum sum rule, since the evolution is local in x. In DGLAP: momentum sum rule satisfied at each order due to the initial assumption of the collinearity of the partons and the non-locality of the evolution in x.

- Approximations in the phase space (multi-Regge kinematics, quasi multi-Regge kinematics, etc..) cannot be recovered by the (fixed number of) the higher orders of expansion in the coupling constant.

Low x resummation

Ciafaloni, Colferai, Salam, AS
Altarelli, Ball, Forte; Thorne; Thorne, White

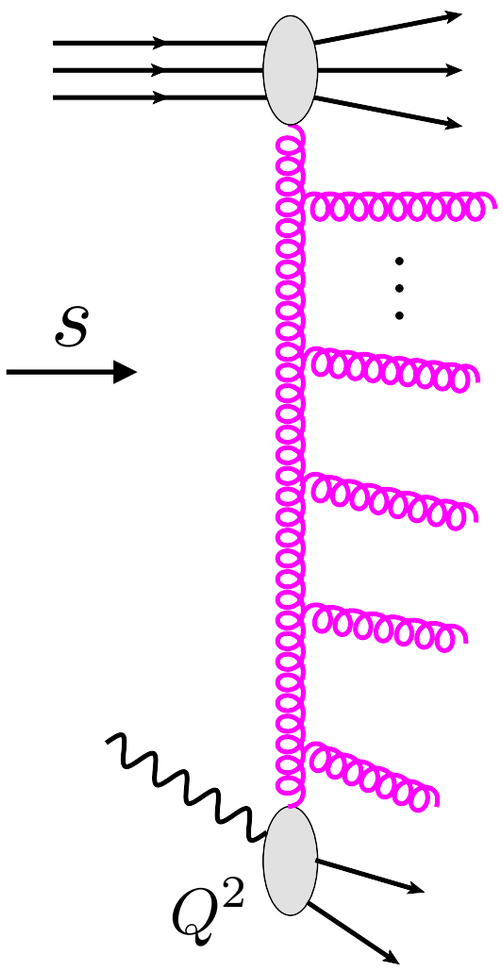

Combine the information from both expansions

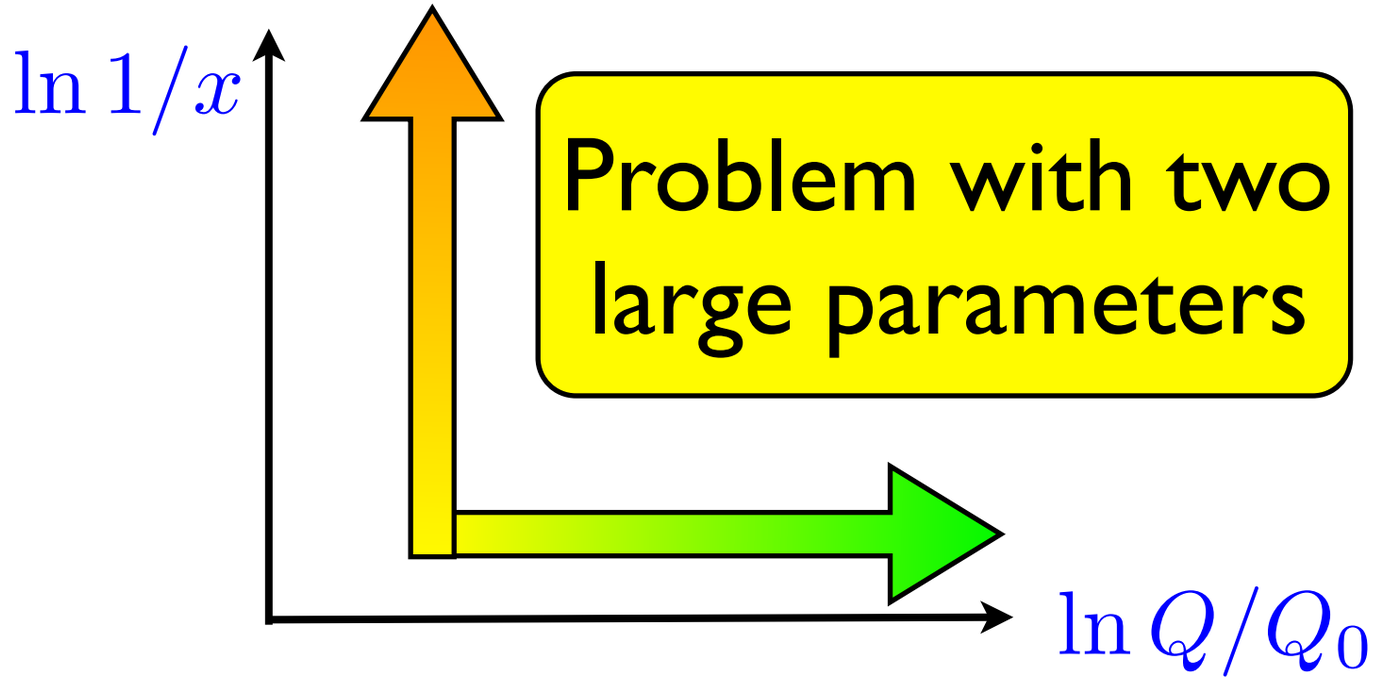

$\left(\frac{\alpha_s N_c}{\pi} \ln \frac{1}{x}\right)^n$ logarithms of energy

$\left(\frac{\alpha_s N_c}{\pi} \ln \frac{Q}{Q_0}\right)^n$ logarithms of scale (related to transverse momentum)

Resummation

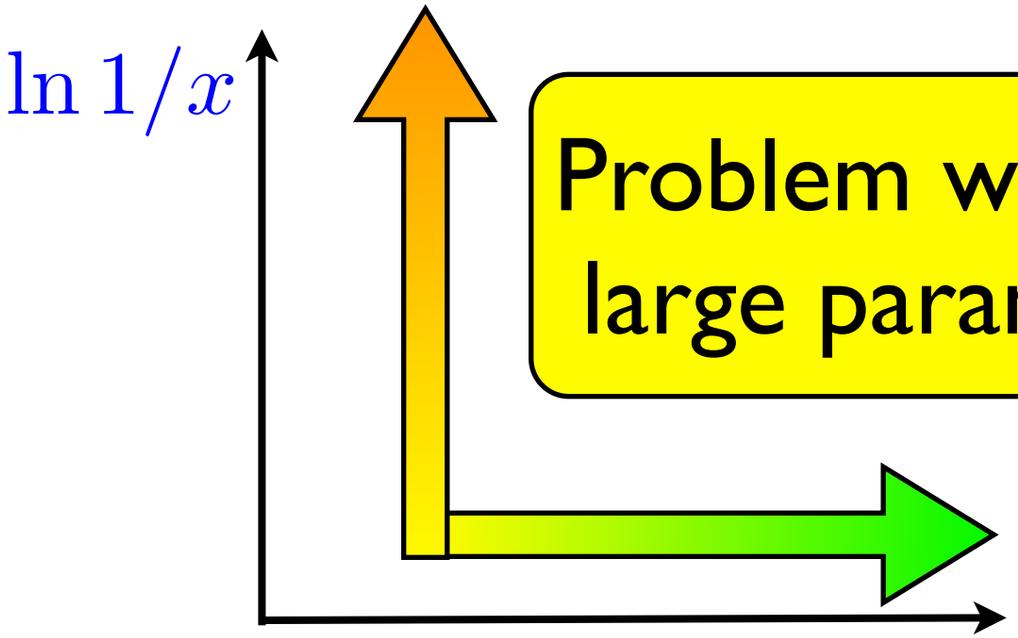

Problem with two large parameters

$$\left(\frac{\alpha_s N_c}{\pi}\ln\frac{1}{x}\right)^n$$

$$\left(\frac{\alpha_s N_c}{\pi}\ln\frac{Q}{Q_0}\right)^n$$

Mellin variables: $\gamma \leftrightarrow \ln k_T^2$ $\omega \leftrightarrow \ln 1/x$

Kernel in Mellin space $\chi(\gamma) = \int dk'^2 K(k^2, k'^2)\left(\frac{k'^2}{k^2}\right)^\gamma$

Anomalous dimension $\gamma(\omega) = \int_0^1 dz z^\omega P(z)$

Resummation

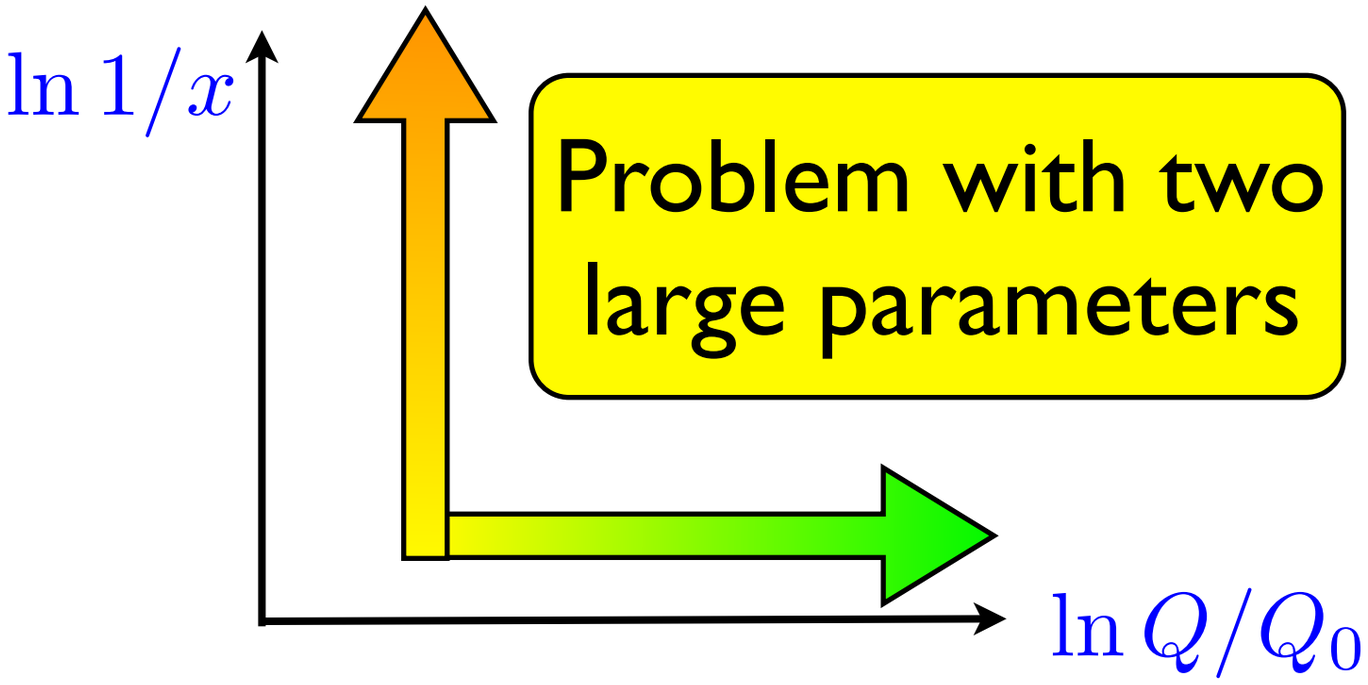

$$\left(\frac{\alpha_s N_c}{\pi}\ln\frac{1}{x}\right)^n$$ energy

$$\left(\frac{\alpha_s N_c}{\pi}\ln\frac{Q}{Q_0}\right)^n$$ scale (related to transverse momentum)

Mellin variables: $\gamma \leftrightarrow \ln k_T^2$ $\omega \leftrightarrow \ln 1/x$

Kernel in Mellin space $$\chi(\gamma) = \int dk'^2 K(k^2, k'^2)\left(\frac{k'^2}{k^2}\right)^\gamma$$

Anomalous dimension $$\gamma(\omega) = \int_0^1 dz z^\omega P(z)$$

Resummation

linear case

Anderson,Gustafson,Kharraziha,Samuelson Z.Phys. C71(1996) 613

Kwiecinski, Martin, Sutton Z.Phys. C71(1996) 585; Kwiecinski,Martin,AS Phys.Rev. D56 (1997) 3991

Salam JHEP 9807 (1998) 19;

Ciafaloni,Colferai,Salam,AS Phys.Rev. D68(2003) 114003

Altarelli,Ball,Forte Nucl.Phys. B575(2000) 313; Bonvini,Marzani,Perano Eur. Phys. J C76(2016) 597.

Thorne Phys. Rev. D64 (2001) 074005

Sabio-Vera Nucl. Phys. B722 (2005) 65.

Brodsky,Fadin,Kim,Lipatov,Pivovarov JETP Lett. 70 (1999) 155.

nonlinear case

Motyka,AS Phys. Rev.D79(2009) 085016; Beuf Phys.Rev.D89(2014) 074039

Iancu,Madrigal,Mueller,Soyez; Phys.Lett. B744 (2015) 293;Lappi,Mantysaari Phys.Rev.D93(2016) 094004

General setup for resummation

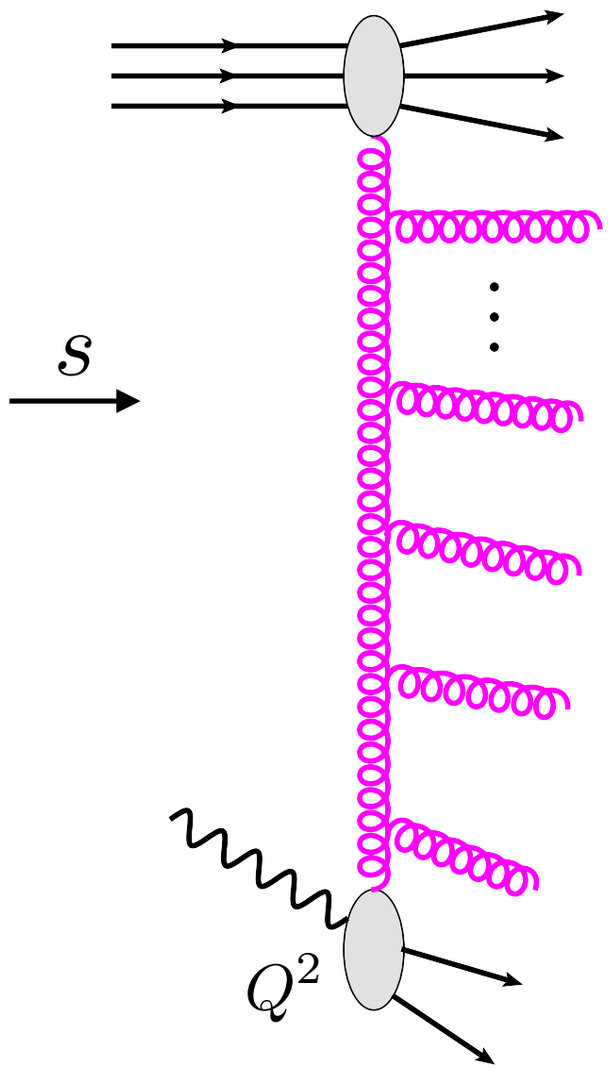

- Kinematical constraints: impose constraints coming from the kinematics by the analysis of individual diagrams.
- DGLAP splitting function recovered at fixed order of large logarithms of scale.
- LLx and NLLx BFKL terms are included.
- Subtraction procedure in order to avoid the double counting.
- Momentum sum rule for the resummed splitting function must be satisfied.
- Running coupling in the BFKL evolution.

LLx BFKL

Representation of the kernel $\mathcal{K} = \sum_{n=0}^{\infty} \bar{\alpha}_s^{n+1} \mathcal{K}_n \qquad \bar{\alpha}_s \equiv \frac{N_c \alpha_s}{\pi}$

Mellin variables: $\gamma \leftrightarrow \ln k_T^2 \qquad \omega \leftrightarrow \ln 1/x$

BFKL eq: $$\mathcal{F}(x,k_T) = \mathcal{F}^{(0)}(x,k_T) + \int_x^1 \frac{dz}{z} \int d^2k'_T \, \mathcal{K}(k_T,k'_T) \, \mathcal{F}(\frac{x}{z},k'_T)$$

LLx BFKL

Representation of the kernel $\mathcal{K} = \sum_{n=0}^{\infty} \bar{\alpha}_s^{n+1} \mathcal{K}_n \qquad \bar{\alpha}_s \equiv \frac{N_c \alpha_s}{\pi}$

Mellin variables: $\gamma \leftrightarrow \ln k_T^2 \qquad \omega \leftrightarrow \ln 1/x$

BFKL eq: $$\mathcal{F}(x,k_T) = \mathcal{F}^{(0)}(x,k_T) + \int_x^1 \frac{dz}{z} \int d^2k'_T \, \mathcal{K}(k_T,k'_T)\, \mathcal{F}(\frac{x}{z},k'_T)$$

LLx kernel in Mellin space

$$\chi_0(\gamma) = 2\psi(1) - \psi(\gamma) - \psi(1-\gamma)$$

Polygamma function

$$\psi(\gamma) = \frac{\Gamma'(\gamma)}{\Gamma(\gamma)}$$

LLx BFKL

Representation of the kernel $\mathcal{K} = \sum_{n=0}^{\infty} \bar{\alpha}_s^{n+1} \mathcal{K}_n$ $\bar{\alpha}_s \equiv \frac{N_c \alpha_s}{\pi}$

Mellin variables: $\gamma \leftrightarrow \ln k_T^2$ $\omega \leftrightarrow \ln 1/x$

BFKL eq: $$\mathcal{F}(x,k_T) = \mathcal{F}^{(0)}(x,k_T) + \int_x^1 \frac{dz}{z} \int d^2k'_T \, \mathcal{K}(k_T,k'_T)\, \mathcal{F}(\frac{x}{z},k'_T)$$

LLx kernel in Mellin space

Polygamma function $\psi(\gamma) = \frac{\Gamma'(\gamma)}{\Gamma(\gamma)}$

$$\chi_0(\gamma) = 2\psi(1) - \psi(\gamma) - \psi(1-\gamma)$$

$$\overline{\mathcal{F}}(\omega,k_T) = \int_0^1 dx\, x^{\omega-1}\, \mathcal{F}(x,k_T) \qquad \tilde{\mathcal{F}}(\omega,\gamma) = \int_0^\infty dk_T^2 \left(k_T^2\right)^{-\gamma-1} \bar{\mathcal{F}}(\omega,k_T)$$

LLx BFKL

Representation of the kernel $\mathcal{K} = \sum_{n=0}^{\infty} \bar{\alpha}_s^{n+1} \mathcal{K}_n$ $\bar{\alpha}_s \equiv \frac{N_c \alpha_s}{\pi}$

Mellin variables: $\gamma \leftrightarrow \ln k_T^2$ $\omega \leftrightarrow \ln 1/x$

BFKL eq: $$\mathcal{F}(x,k_T) = \mathcal{F}^{(0)}(x,k_T) + \int_x^1 \frac{dz}{z} \int d^2k'_T \, \mathcal{K}(k_T,k'_T)\, \mathcal{F}(\frac{x}{z},k'_T)$$

LLx kernel in Mellin space

$$\chi_0(\gamma) = 2\psi(1) - \psi(\gamma) - \psi(1-\gamma)$$

Polygamma function $\psi(\gamma) = \frac{\Gamma'(\gamma)}{\Gamma(\gamma)}$

$$\overline{\mathcal{F}}(\omega,k_T) = \int_0^1 dx\, x^{\omega-1}\, \mathcal{F}(x,k_T) \qquad \tilde{\mathcal{F}}(\omega,\gamma) = \int_0^\infty dk_T^2 \left(k_T^2\right)^{-\gamma-1} \bar{\mathcal{F}}(\omega,k_T)$$

BFKL equation in Mellin space:

$$\tilde{\mathcal{F}}(\omega,\gamma) = \tilde{\mathcal{F}}^{(0)}(\omega,\gamma) + \frac{\overline{\alpha}_s}{\omega}\chi_0(\gamma)\tilde{\mathcal{F}}(\omega,\gamma)\,,$$

Solution to BFKL equation

Solution to the algebraic equation in Mellin space

$$\tilde{\mathcal{F}}(\omega,\gamma) = \frac{\tilde{\mathcal{F}}^{(0)}(\omega,\gamma)}{1-\frac{\bar{\alpha}_s}{\omega}\chi(\gamma)}$$

The asymptotic behavior in x space will be determined by the position of the singularity

$$\omega(\gamma) = \bar{\alpha}_s \chi(\gamma)$$

Solution to BFKL equation

Solution to the algebraic equation in Mellin space

$$\tilde{\mathcal{F}}(\omega,\gamma) = \frac{\tilde{\mathcal{F}}^{(0)}(\omega,\gamma)}{1-\frac{\bar{\alpha}_s}{\omega}\chi(\gamma)}$$

The asymptotic behavior in x space will be determined by the position of the singularity

$$\omega(\gamma) = \bar{\alpha}_s\chi(\gamma)$$

The solution

$$\mathcal{F}(x,k_T) = \frac{1}{2\pi i}\int_{c-i\infty}^{c+i\infty} d\gamma (k_T^2)^\gamma R(\gamma) x^{-\omega(\gamma)}$$

The residue $R(\gamma)$

Solution to BFKL equation

Solution to the algebraic equation in Mellin space

$$\tilde{\mathcal{F}}(\omega,\gamma)=\frac{\tilde{\mathcal{F}}^{(0)}(\omega,\gamma)}{1-\frac{\bar{\alpha}_s}{\omega}\chi(\gamma)}$$

The asymptotic behavior in x space will be determined by the position of the singularity

$$\omega(\gamma)=\bar{\alpha}_s\chi(\gamma)$$

The solution

$$\mathcal{F}(x,k_T)=\frac{1}{2\pi i}\int_{c-i\infty}^{c+i\infty}d\gamma(k_T^2)^\gamma R(\gamma)x^{-\omega(\gamma)}$$

The residue $R(\gamma)$

Plots of $\chi_0(\gamma)=2\psi(1)-\psi(\gamma)-\psi(1-\gamma)$

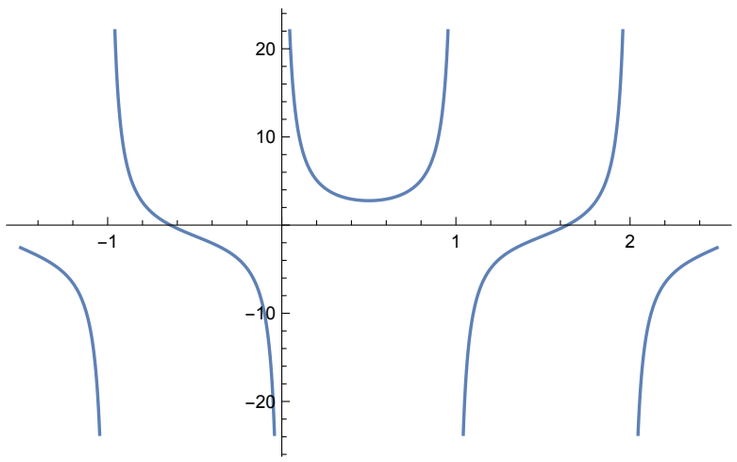

Real axis

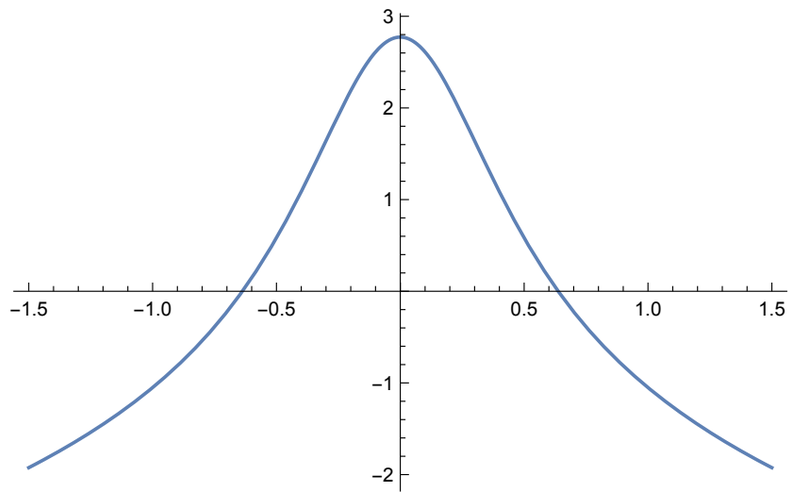

Imaginary axis at c=1/2

Solution to BFKL equation

Solution to the algebraic equation in Mellin space

$$\tilde{\mathcal{F}}(\omega,\gamma)=\frac{\tilde{\mathcal{F}}^{(0)}(\omega,\gamma)}{1-\frac{\bar{\alpha}_s}{\omega}\chi(\gamma)}$$

The asymptotic behavior in x space will be determined by the position of the singularity

$$\omega(\gamma)=\bar{\alpha}_s\chi(\gamma)$$

The solution

$$\mathcal{F}(x,k_T)=\frac{1}{2\pi i}\int_{c-i\infty}^{c+i\infty}d\gamma(k_T^2)^\gamma R(\gamma)x^{-\omega(\gamma)}$$

The residue $R(\gamma)$

Plots of $\chi_0(\gamma)=2\psi(1)-\psi(\gamma)-\psi(1-\gamma)$

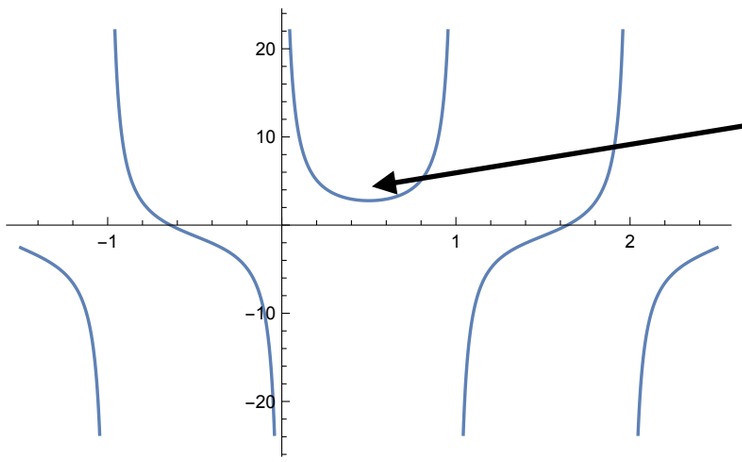

Saddle point

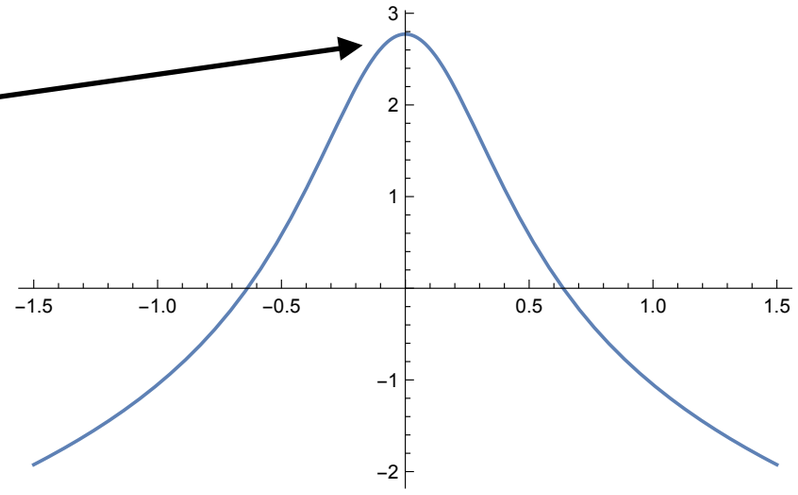

Real axis

Imaginary axis at c=1/2

Solution to BFKL equation

Solution to the algebraic equation in Mellin space

$$\tilde{\mathcal{F}}(\omega,\gamma)=\frac{\tilde{\mathcal{F}}^{(0)}(\omega,\gamma)}{1-\frac{\bar{\alpha}_s}{\omega}\chi(\gamma)}$$

The asymptotic behavior in x space will be determined by the position of the singularity

$$\omega(\gamma)=\bar{\alpha}_s\chi(\gamma)$$

The solution

$$\mathcal{F}(x,k_T)=\frac{1}{2\pi i}\int_{c-i\infty}^{c+i\infty}d\gamma(k_T^2)^\gamma R(\gamma)x^{-\omega(\gamma)}$$

The residue $R(\gamma)$

Plots of $\chi_0(\gamma)=2\psi(1)-\psi(\gamma)-\psi(1-\gamma)$

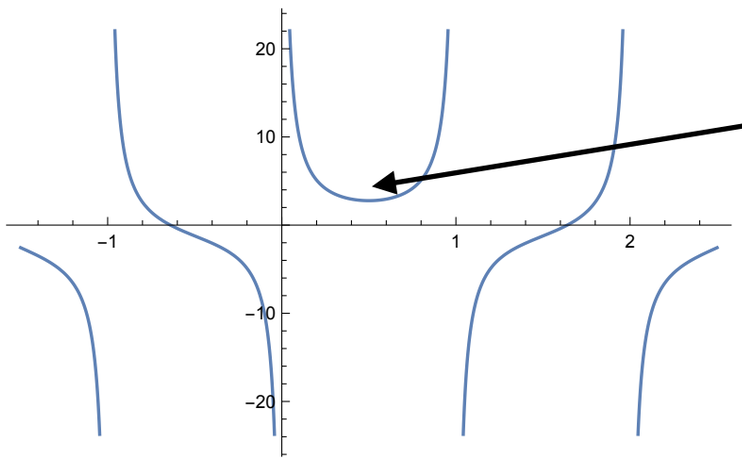

Saddle point

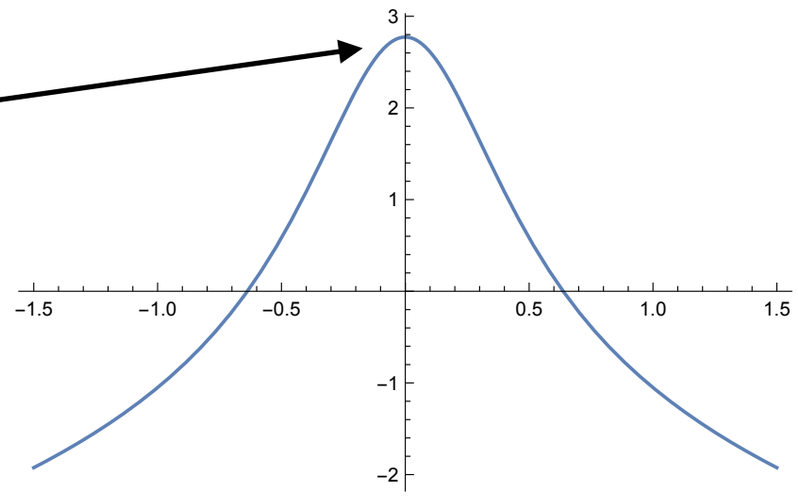

Real axis

Imaginary axis at c=1/2

The saddle point at γ=1/2

Small x behavior given by $\omega_{IP}=\bar{\alpha}_s\chi_0(1/2)=\bar{\alpha}_s 4\ln 2$

Collinear poles

LLx kernel in Mellin space

$$\chi_0(\gamma) = 2\psi(1) - \psi(\gamma) - \psi(1-\gamma)$$

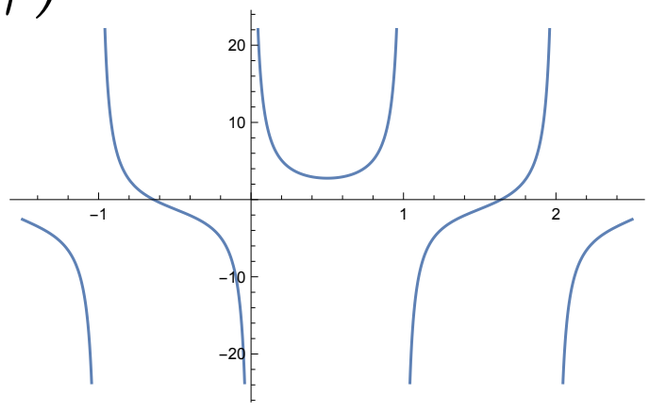

Collinear poles

LLx kernel in Mellin space

$$\chi_0(\gamma) = 2\psi(1) - \psi(\gamma) - \psi(1-\gamma)$$

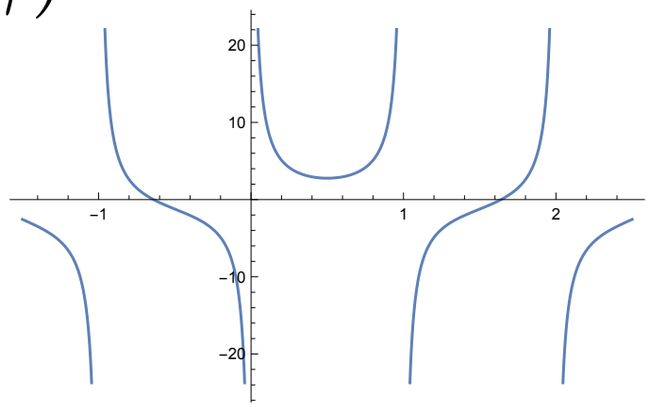

Collinear approximation:

$$\chi_0(\gamma) \sim \frac{1}{\gamma} + \frac{1}{1-\gamma}$$

Single poles only at LIx level.

Collinear poles

LLx kernel in Mellin space

$$\chi_0(\gamma) = 2\psi(1) - \psi(\gamma) - \psi(1-\gamma)$$

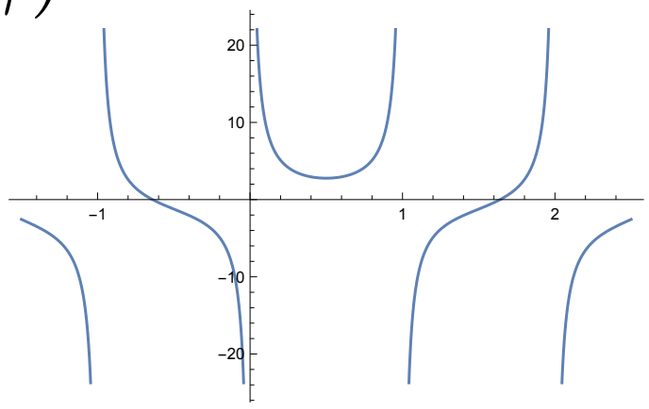

Collinear approximation:

$$\chi_0(\gamma) \sim \frac{1}{\gamma} + \frac{1}{1-\gamma}$$

Single poles only at LIx level.

Physical interpretation: BFKL does not have ordering in transverse momenta. Contains thus (among) others two extreme cases

Collinear poles

LLx kernel in Mellin space

$$\chi_0(\gamma) = 2\psi(1) - \psi(\gamma) - \psi(1-\gamma)$$

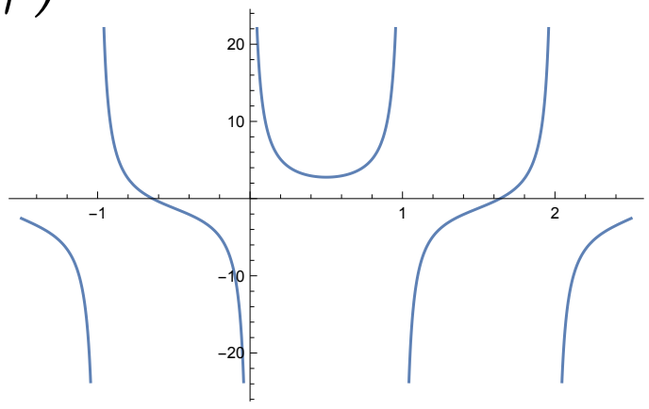

Collinear approximation:

$$\chi_0(\gamma) \sim \frac{1}{\gamma} + \frac{1}{1-\gamma}$$

Single poles only at LIx level.

Physical interpretation: BFKL does not have ordering in transverse momenta. Contains thus (among) others two extreme cases

Consider scattering of two virtual photons (could be realized in electron-positron collider)

Collinear poles

LLx kernel in Mellin space

$$\chi_0(\gamma) = 2\psi(1) - \psi(\gamma) - \psi(1-\gamma)$$

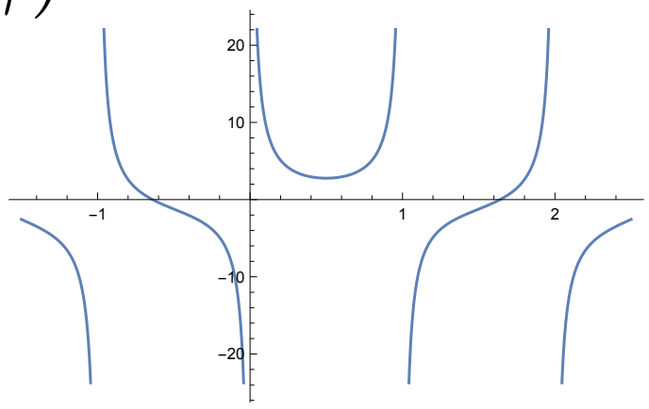

Collinear approximation:

$$\chi_0(\gamma) \sim \frac{1}{\gamma} + \frac{1}{1-\gamma}$$

Single poles only at LIx level.

Physical interpretation: BFKL does not have ordering in transverse momenta. Contains thus (among) others two extreme cases

Consider scattering of two virtual photons (could be realized in electron-positron collider)

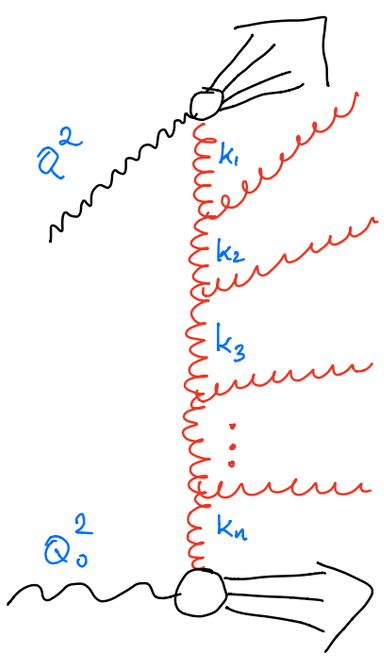

Collinear limit

$$Q^2 \gg k_1^2 \gg k_2^2 \gg \cdots \gg k_n^2 \gg Q_0^2$$

Collinear poles

LLx kernel in Mellin space

$$\chi_0(\gamma) = 2\psi(1) - \psi(\gamma) - \psi(1-\gamma)$$

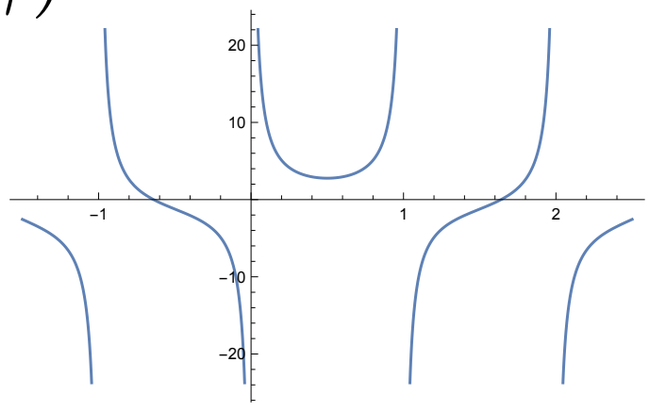

Collinear approximation:

$$\chi_0(\gamma) \sim \frac{1}{\gamma} + \frac{1}{1-\gamma}$$

Single poles only at LIx level.

Physical interpretation: BFKL does not have ordering in transverse momenta. Contains thus (among) others two extreme cases

Consider scattering of two virtual photons (could be realized in electron-positron collider)

Collinear limit

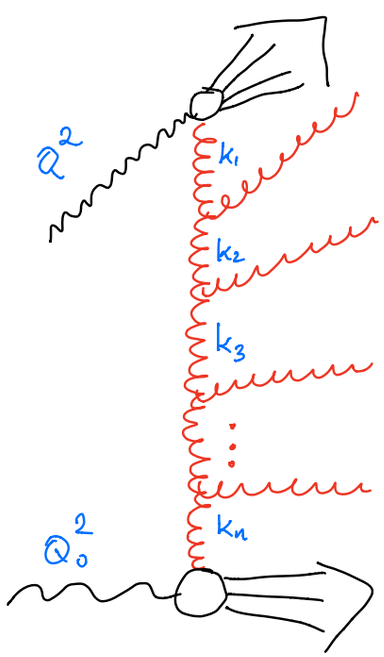

$$Q^2 \gg k_1^2 \gg k_2^2 \gg \cdots \gg k_n^2 \gg Q_0^2$$

Anti-collinear limit

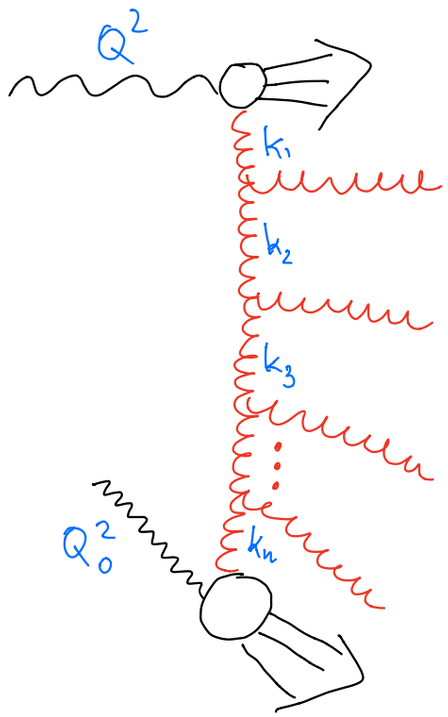

$$Q^2 \ll k_1^2 \ll k_2^2 \ll \cdots \ll k_n^2 \ll Q_0^2$$

LLx + NLLx

Representation of the kernel $\mathcal{K} = \sum_{n=0}^{\infty} \bar{\alpha}_s^{n+1} \mathcal{K}_n$ $\bar{\alpha}_s \equiv \frac{N_c \alpha_s}{\pi}$

Mellin variables: $\gamma \leftrightarrow \ln k_T^2$ $\omega \leftrightarrow \ln 1/x$

LLx kernel in Mellin space

$$\chi_0(\gamma) = 2\psi(1) - \psi(\gamma) - \psi(1-\gamma)$$

LLx + NLLx

Representation of the kernel $\mathcal{K} = \sum_{n=0}^{\infty} \bar{\alpha}_s^{n+1} \mathcal{K}_n$ $\bar{\alpha}_s \equiv \frac{N_c \alpha_s}{\pi}$

Mellin variables: $\gamma \leftrightarrow \ln k_T^2$ $\omega \leftrightarrow \ln 1/x$

LLx kernel in Mellin space

$$\chi_0(\gamma) = 2\psi(1) - \psi(\gamma) - \psi(1-\gamma)$$

running coupling

triple poles

double poles

NLLx kernel in Mellin space

$$\chi_1(\gamma) = -\frac{b}{2}[\chi_0^2(\gamma) + \chi_0'(\gamma)] - \frac{1}{4}\chi_0''(\gamma) - \frac{1}{4}\left(\frac{\pi}{\sin\pi\gamma}\right)^2 \frac{\cos\pi\gamma}{3(1-2\gamma)}\left(11 + \frac{\gamma(1-\gamma)}{(1+2\gamma)(3-2\gamma)}\right)$$
$$+ \left(\frac{67}{36} - \frac{\pi^2}{12}\right)\chi_0(\gamma) + \frac{3}{2}\zeta(3) + \frac{\pi^3}{4\sin\pi\gamma}$$
$$- \sum_{n=0}^{\infty}(-1)^n\left[\frac{\psi(n+1+\gamma) - \psi(1)}{(n+\gamma)^2} + \frac{\psi(n+2-\gamma) - \psi(1)}{(n+1-\gamma)^2}\right]$$

Strictly speaking at NLLx this is not an eigenvalue. Still, one can consider Mellin transform of the kernel.

Collinear poles at NLL

$$\chi_1^{\rm coll}(\gamma) = -\frac{1}{2\gamma^3} - \frac{1}{2(1-\gamma)^3} + \frac{A_1(0)}{\gamma^2} + \frac{A_1(0)-b}{(1-\gamma)^2}$$

double and triple poles of the NLL part

LO DGLAP anomalous dimension $\gamma_{gg}^{(0)}(\omega) = \frac{\bar\alpha_s}{\omega} + \bar\alpha_s A_1(\omega)$ $\qquad A_1(\omega) = -\frac{11}{12} + \mathcal{O}(\omega)$

Difference of about 7% at most between collinear approximation and full NLL kernel

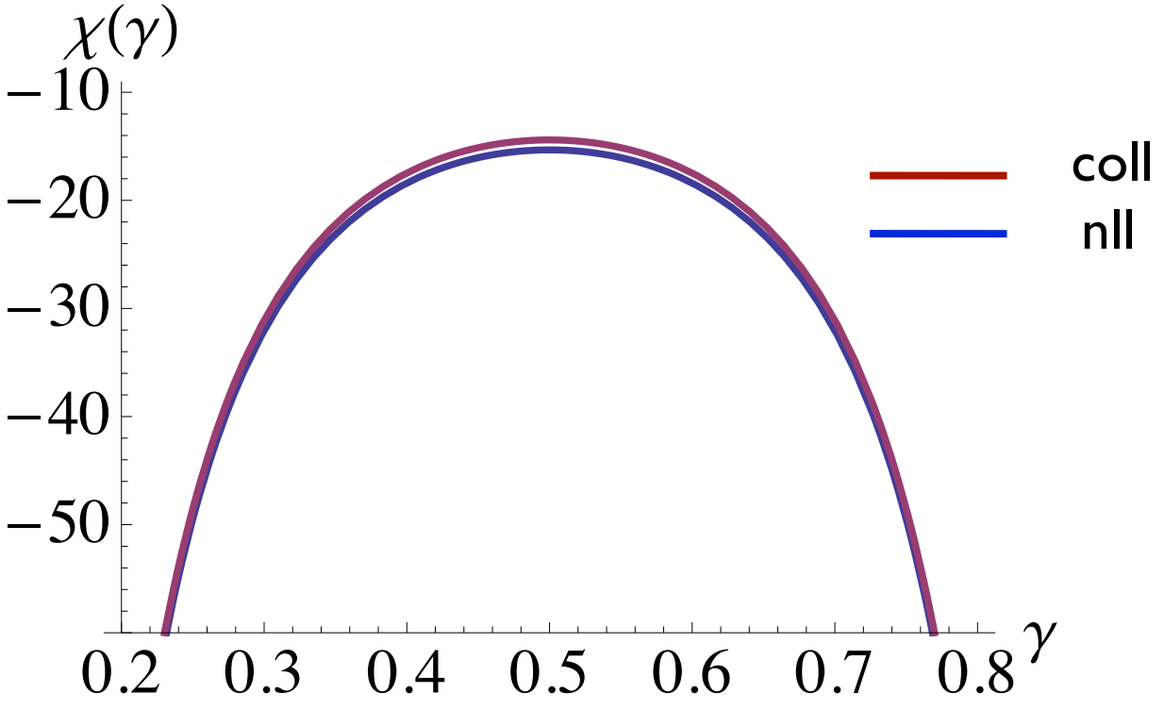

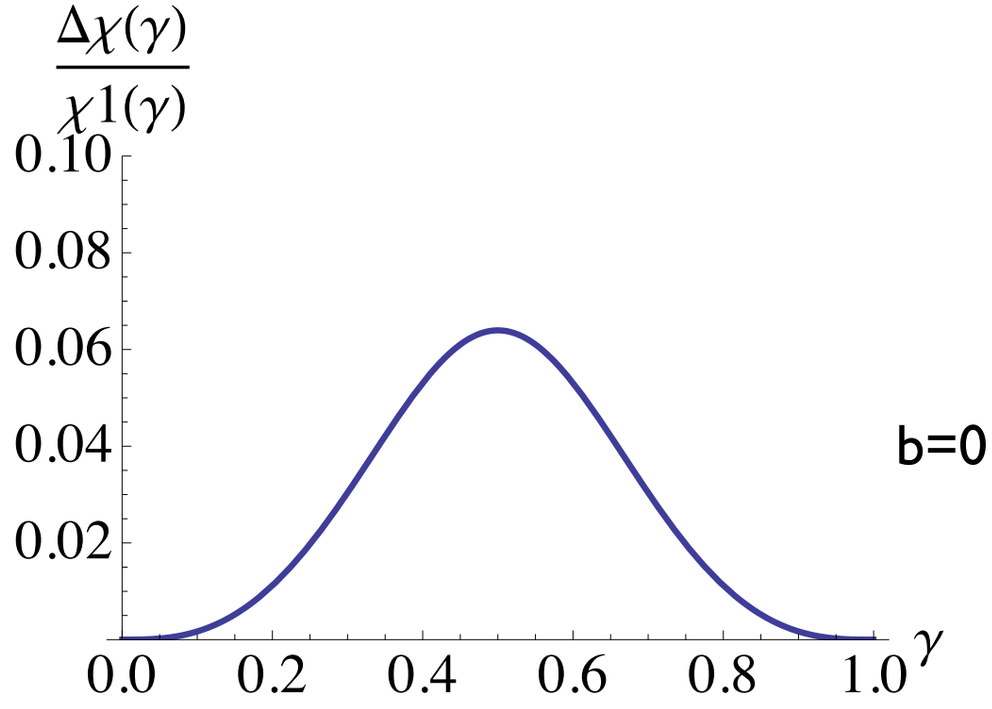

Note that NLL kernel is large and negative, this is the origin of the instability

Collinear poles at NLL

$$\chi_1^{\rm coll}(\gamma) = -\frac{1}{2\gamma^3} - \frac{1}{2(1-\gamma)^3} + \frac{A_1(0)}{\gamma^2} + \frac{A_1(0)-b}{(1-\gamma)^2}$$

double and triple poles of the NLL part

LO DGLAP anomalous dimension $\gamma_{gg}^{(0)}(\omega) = \frac{\bar{\alpha}_s}{\omega} + \bar{\alpha}_s A_1(\omega)$ $\qquad A_1(\omega) = -\frac{11}{12} + \mathcal{O}(\omega)$

Difference of about 7% at most between collinear approximation and full NLL kernel

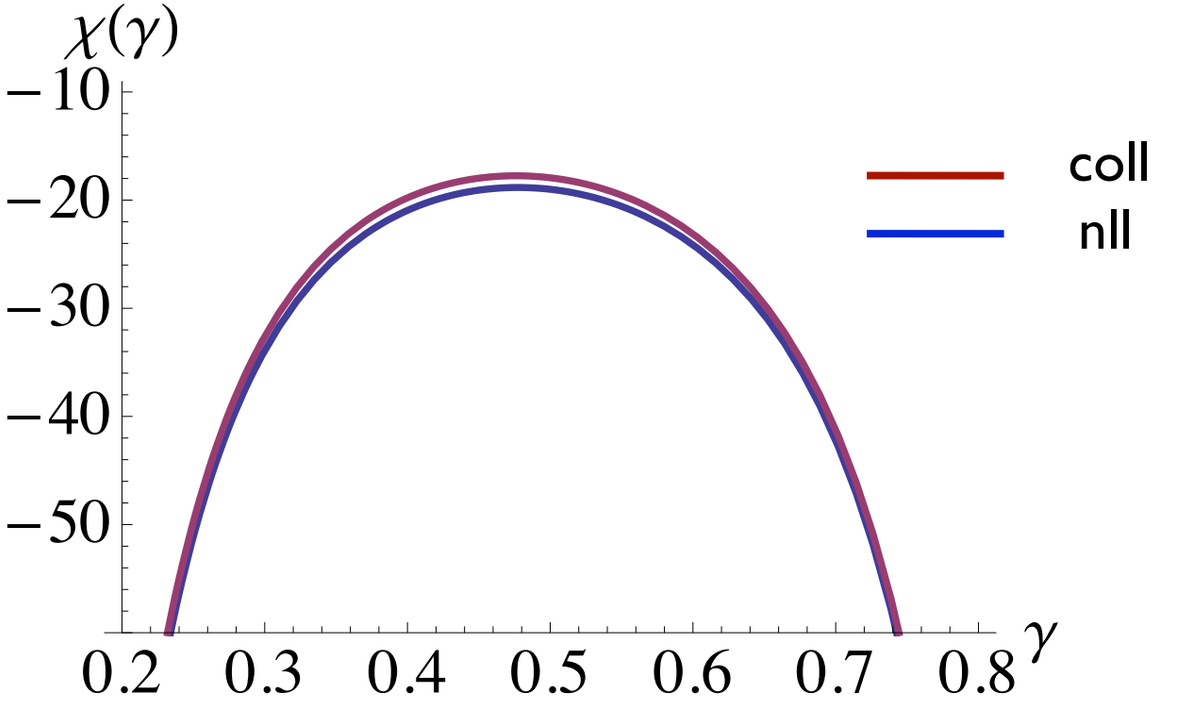

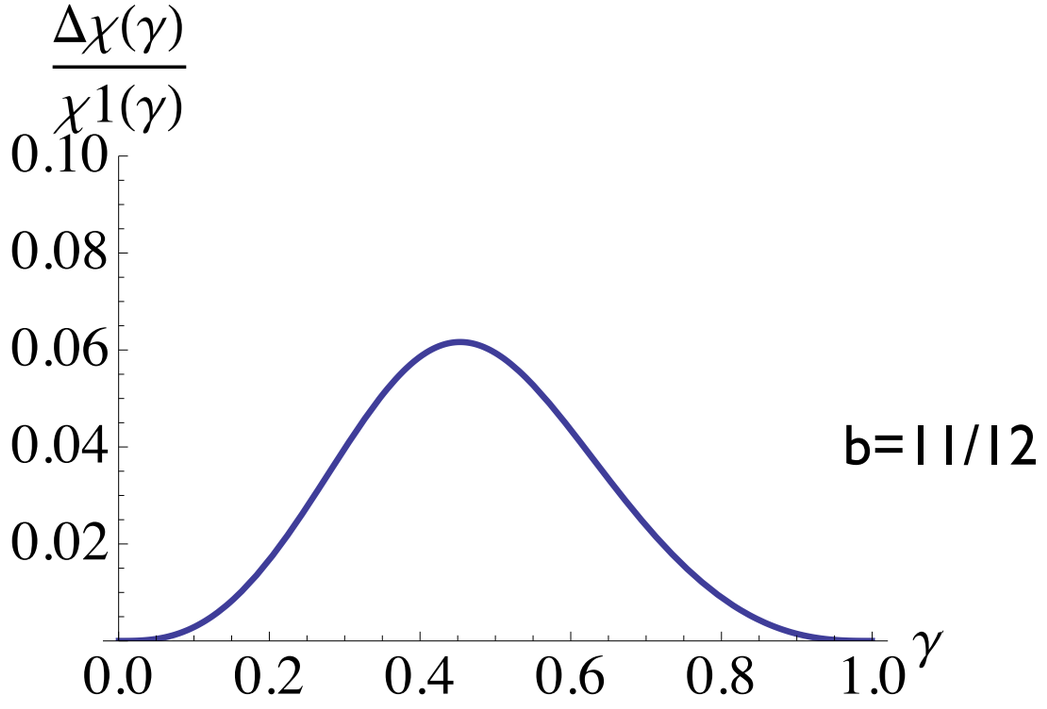

Note that NLL kernel is large and negative, this is the origin of the instability

Collinear poles at NLL

$$\chi_1^{\rm coll}(\gamma) = -\frac{1}{2\gamma^3} - \frac{1}{2(1-\gamma)^3} + \frac{A_1(0)}{\gamma^2} + \frac{A_1(0)-b}{(1-\gamma)^2}$$

double and triple poles of the NLL part

LO DGLAP anomalous dimens

Difference of abo

ω_P

$\mathcal{O}(\omega)$

NLL kernel

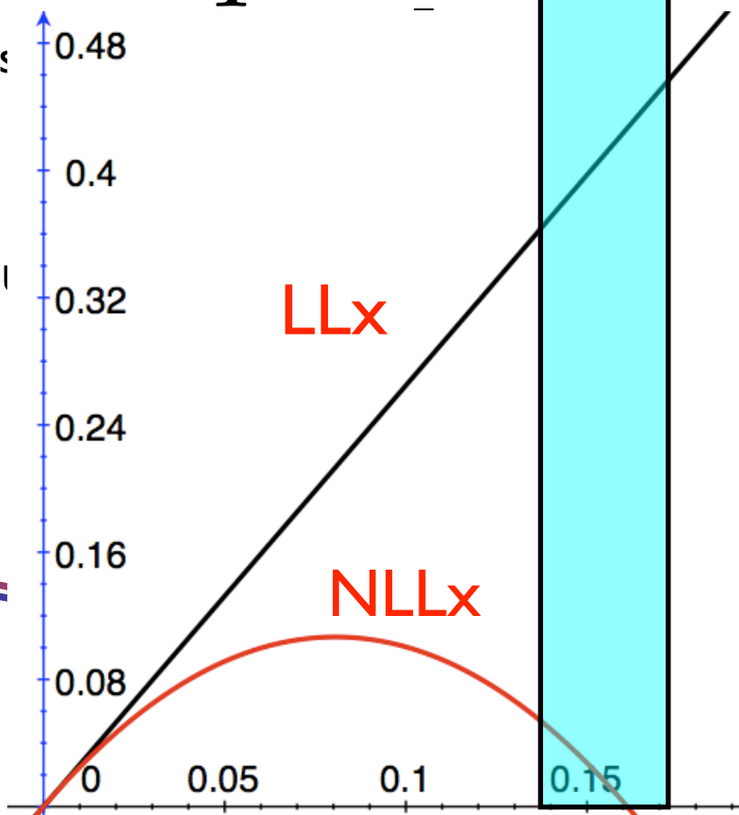

$$\omega_{IP}^{NLLx} \simeq \bar{\alpha}_s 4\ln 2(1-6.5\bar{\alpha}_s)$$

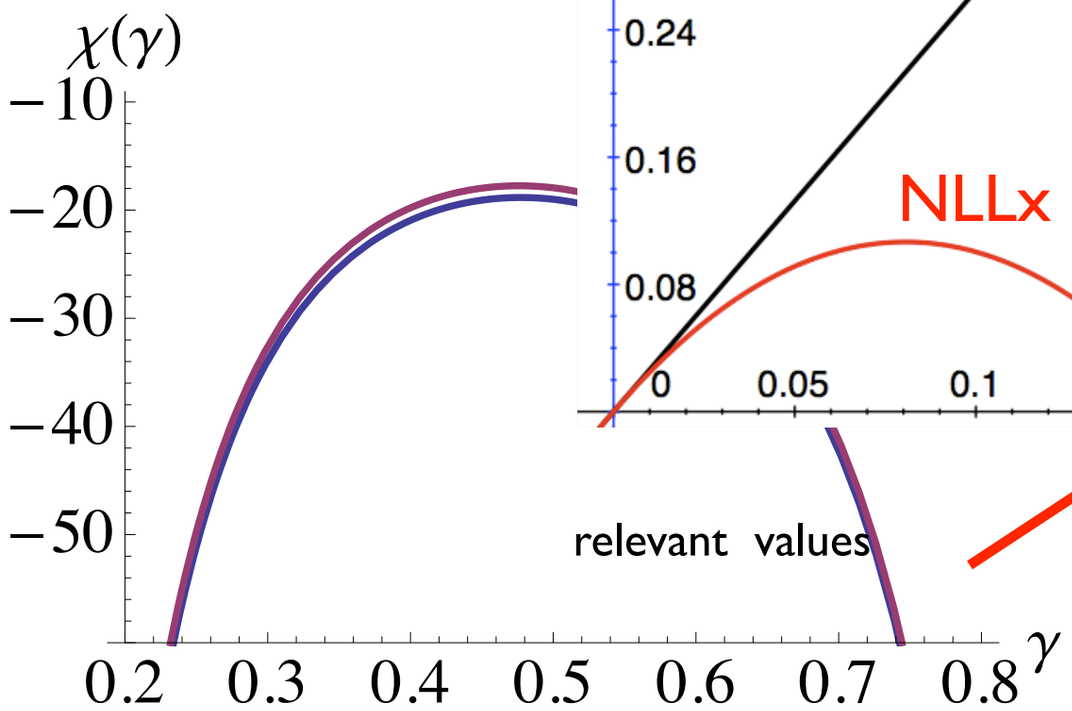

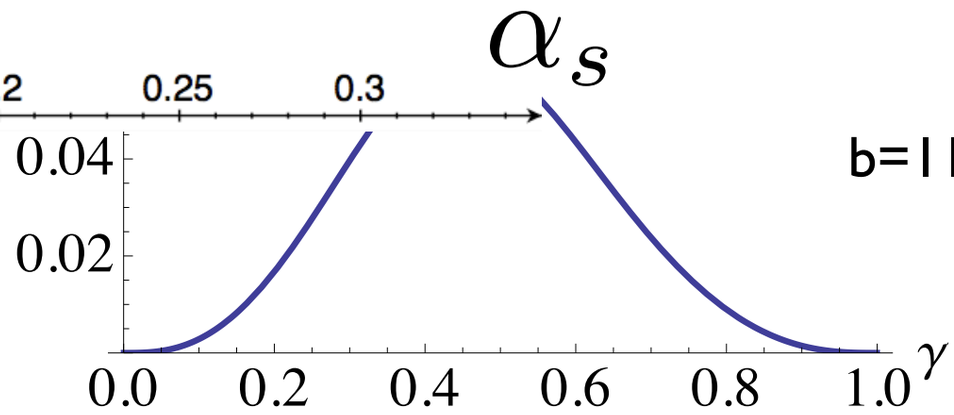

b=11/12

Note that NLL kernel is large and negative, this is the origin of the instability

Origin of poles at NLL

What is the origin of the double and triple collinear poles at NLL?

- ✦ Triple collinear poles: kinematical constraint which limits the transverse momenta of the exchanged gluons.

- ✦ Triple collinear poles: related to the scale choice in the BFKL equation.

- ✦ Double collinear poles: terms which originate from the non-singular in z parts of the DGLAP splitting function which appear at this order.

- ✦ Double collinear poles with coefficient equal to beta function: terms from the running coupling (recall that LIx BFKL has fixed coupling)

Kinematical constraint

Consider BFKL equation

Unlimited integral over transverse momentum

$$\mathcal{F}(x,k_T) = \mathcal{F}^{(0)}(x,k_T) + \int_x^1 \frac{dz}{z} \int d^2k'_T \mathcal{K}(k_T,k'_T)\,\mathcal{F}(\frac{x}{z},k'_T)$$

Explicit form:

$$\mathcal{F}(x,k) = \mathcal{F}^{(0)}(x,k) + \bar{\alpha}_s k^2 \int_x^1 \frac{dz}{z} \int \frac{dk'^2}{k'^2} \left[\frac{\mathcal{F}(x/z,k')}{|k'^2 - k^2|} - \frac{\mathcal{F}(x/z,k)}{} + \frac{F(x/z,k)}{\sqrt{4k'^4+k^4}} \right]$$

Real

Virtual

Kinematical constraint

Consider BFKL equation

Unlimited integral over transverse momentum

$$\mathcal{F}(x,k_T) = \mathcal{F}^{(0)}(x,k_T) + \int_x^1 \frac{dz}{z} \int d^2k'_T \, \mathcal{K}(k_T,k'_T)\, \mathcal{F}(\frac{x}{z},k'_T)$$

Explicit form:

$$\mathcal{F}(x,k) = \mathcal{F}^{(0)}(x,k) + \bar{\alpha}_s k^2 \int_x^1 \frac{dz}{z} \int \frac{dk'^2}{k'^2} \left[\frac{\mathcal{F}(x/z,k')}{|k'^2 - k^2|} - \frac{\mathcal{F}(x/z,k)}{} + \frac{F(x/z,k)}{\sqrt{4k'^4 + k^4}} \right]$$

Real **Virtual**

Rung in the BFKL cascade:

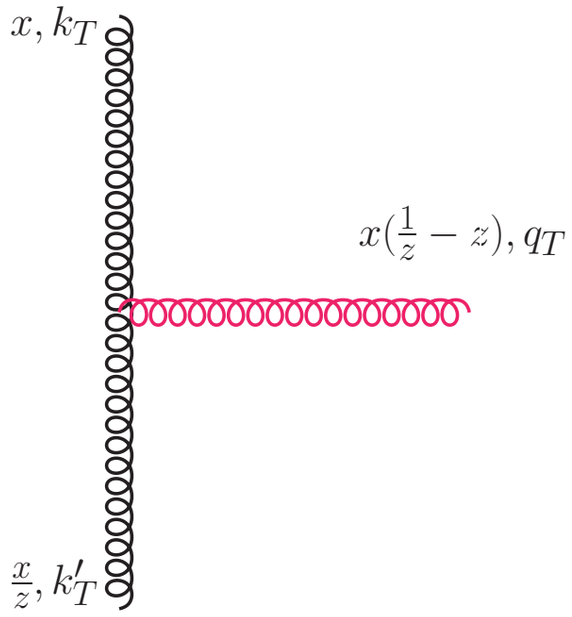

High energy approximation:
Virtualities of the exchanged gluons are dominated by their transverse momenta

$$|k^2| \simeq k_T^2$$

This leads to the **kinematical constraint**:

$$k_T'^2 < \frac{k_T^2}{z}$$

Transverse momentum is limited!

BFKL with kinematical constraint

$$\mathcal{F}(x,k) = \mathcal{F}^{(0)}(x,k) + \bar{\alpha}_s k^2 \int_x^1 \frac{dz}{z} \int \frac{dk'^2}{k'^2} \left[\frac{\mathcal{F}(x/z,k')\,\theta(k^2/z - k'^2) - \mathcal{F}(x/z,k)}{|k'^2 - k^2|} + \frac{F(x/z,k)}{\sqrt{4k'^4 + k^4}} \right]$$

Kinematical constraint
In real part

$$\chi(\gamma,\omega) = \int_0^\infty \frac{d\rho}{\rho} \left[\frac{\rho^\gamma \theta(1-\rho) + \rho^{\gamma-\omega}\theta(\rho-1) - 1}{|\rho - 1|} + \frac{1}{\sqrt{4\rho^2+1}} \right]$$

Kernel in Mellin space

$$\chi(\gamma,\omega) = 2\psi(1) - \psi(\gamma) - \psi(1-\gamma+\omega)$$

Contains shift of the pole by other Mellin variable: all order correction

Scale choices

HE factorization for the cross section

$$\sigma_{AB}(s;Q,Q_0) = \int \frac{d\omega}{2\pi i} \frac{d^2\boldsymbol{k}}{\boldsymbol{k}^2} \frac{d^2\boldsymbol{k}_0}{\boldsymbol{k}_0^2} \left(\frac{s}{QQ_0}\right)^{\omega} h_\omega^A(Q,\boldsymbol{k})\, \mathcal{G}_\omega(\boldsymbol{k},\boldsymbol{k}_0)\, h_\omega^B(Q_0,\boldsymbol{k}_0)$$

BFKL equation for the gluon Green's function

$$\omega \mathcal{G}_\omega(\boldsymbol{k},\boldsymbol{k}_0) = \delta^2(\boldsymbol{k}-\boldsymbol{k}_0) + \int \frac{d^2\boldsymbol{k}'}{\pi}\, \mathcal{K}_\omega(\boldsymbol{k},\boldsymbol{k}')\, \mathcal{G}_\omega(\boldsymbol{k}',\boldsymbol{k}_0)$$

$$G(x;\mathbf{k}_T,\mathbf{k}_{T0}) = \int \frac{d\omega}{2\pi i} \left(\frac{\nu}{k_T k_{T0}}\right)^{\omega} G_\omega(\mathbf{k}_T,\mathbf{k}_{T0}) = \int \frac{d\omega}{2\pi i} \left(\frac{\nu}{k_T^2}\right)^{\omega} \left(\frac{k_T}{k_{T0}}\right)^{\omega} G_\omega(\mathbf{k}_T,\mathbf{k}_{T0})$$

Different possible scale choices:

symmetric (ex. two jets) $\quad \nu_0 = k k_0 \qquad k \sim k_0$

DIS type configuration $\quad \nu_0 = k^2 \qquad k \gg k_0$

$\nu_0 = k_0^2 \qquad k \ll k_0$

Shift of poles

Similarity transformation

$$\mathcal{G}_\omega \to \left(\frac{k_>}{k_<}\right)^\omega \mathcal{G}_\omega$$

$$\mathcal{K}_\omega(k,k') \to \mathcal{K}^u_\omega(k,k') = \mathcal{K}_\omega(k,k')\left(\frac{k}{k'}\right)^\omega , \qquad \nu_0 = k^2 ,$$

$$\mathcal{K}_\omega(k,k') \to \mathcal{K}^l_\omega(k,k') = \mathcal{K}_\omega(k,k')\left(\frac{k'}{k}\right)^\omega , \qquad \nu_0 = k'^2 ,$$

Shift of poles (asymmetric case): suitable for DIS case

$$\chi(\gamma,\omega) = 2\psi(1) - \psi(\gamma) - \psi(1-\gamma+\omega)$$

↓ Change of scales

Shift of poles (symmetric case): suitable for the two scale process

$$\chi(\gamma,\omega) = 2\psi(1) - \psi(\gamma+\frac{\omega}{2}) - \psi(1-\gamma+\frac{\omega}{2})$$

Shifts are equivalent to the kinematical constraints imposed on the transverse momenta in the ladder

Triple poles from shifts

$\gamma \leftrightarrow \ln k_T^2$ $\omega \leftrightarrow \ln 1/x$

LL case with shifts

$$\chi(\gamma,\omega) = 2\psi(1) - \psi(\gamma + \frac{\omega}{2}) - \psi(1-\gamma+\frac{\omega}{2})$$

Triple poles from shifts

$\gamma \leftrightarrow \ln k_T^2$ $\omega \leftrightarrow \ln 1/x$

LL case with shifts

$$\chi(\gamma,\omega) = 2\psi(1) - \psi(\gamma + \frac{\omega}{2}) - \psi(1-\gamma+\frac{\omega}{2})$$

Expand :

$$\chi(\gamma,\omega) = 2\psi(1) - \psi(\gamma + \frac{\omega}{2}) - \psi(1-\gamma+\frac{\omega}{2}) = \chi_0 + \chi^{(1)}\frac{\omega}{2} + \frac{1}{2!}\chi^{(2)}\left(\frac{\omega}{2}\right)^2 + \dots$$

Triple poles from shifts

$\gamma \leftrightarrow \ln k_T^2$ $\omega \leftrightarrow \ln 1/x$

LL case with shifts

$$\chi(\gamma,\omega) = 2\psi(1) - \psi(\gamma + \frac{\omega}{2}) - \psi(1-\gamma+\frac{\omega}{2})$$

Expand :

$$\chi(\gamma,\omega) = 2\psi(1) - \psi(\gamma + \frac{\omega}{2}) - \psi(1-\gamma+\frac{\omega}{2}) = \chi_0 + \chi^{(1)}\frac{\omega}{2} + \frac{1}{2!}\chi^{(2)}\left(\frac{\omega}{2}\right)^2 + \dots$$

Use the solution: $\omega(\gamma) = \bar{\alpha}_s \chi(\gamma)$

Triple poles from shifts

$\gamma \leftrightarrow \ln k_T^2$ $\omega \leftrightarrow \ln 1/x$

LL case with shifts

$$\chi(\gamma,\omega) = 2\psi(1) - \psi(\gamma + \frac{\omega}{2}) - \psi(1-\gamma+\frac{\omega}{2})$$

Expand :

$$\chi(\gamma,\omega) = 2\psi(1) - \psi(\gamma + \frac{\omega}{2}) - \psi(1-\gamma+\frac{\omega}{2}) = \chi_0 + \chi^{(1)}\frac{\omega}{2} + \frac{1}{2!}\chi^{(2)}\left(\frac{\omega}{2}\right)^2 + \dots$$

Use the solution: $\omega(\gamma) = \bar{\alpha}_s \chi(\gamma)$

Need to take it at LL order to get NLL terms:

$$\omega_0 = \bar{\alpha}_s \chi_0$$

Triple poles from shifts

$\gamma \leftrightarrow \ln k_T^2$ $\omega \leftrightarrow \ln 1/x$

LL case with shifts

$$\chi(\gamma,\omega) = 2\psi(1) - \psi(\gamma + \frac{\omega}{2}) - \psi(1-\gamma+\frac{\omega}{2})$$

Expand :

$$\chi(\gamma,\omega) = 2\psi(1) - \psi(\gamma + \frac{\omega}{2}) - \psi(1-\gamma+\frac{\omega}{2}) = \chi_0 + \chi^{(1)}\frac{\omega}{2} + \frac{1}{2!}\chi^{(2)}\left(\frac{\omega}{2}\right)^2 + \dots$$

Use the solution: $\omega(\gamma) = \bar{\alpha}_s \chi(\gamma)$

Need to take it at LL order to get NLL terms:

$$\omega_0 \;=\; \bar{\alpha}_s \chi_0$$

Contribution at NLL is:

$$\chi_1(\gamma) = \frac{1}{2}\chi^{(1)}\chi_0 = \frac{1}{2}\left[\psi^{(1)}(\gamma) + \psi^{(1)}(1-\gamma)\right]\left[2\psi(1) - \psi(\gamma) - \psi(1-\gamma)\right]$$

Triple poles from shifts

$\gamma \leftrightarrow \ln k_T^2$ $\omega \leftrightarrow \ln 1/x$

LL case with shifts

$$\chi(\gamma,\omega) = 2\psi(1) - \psi(\gamma + \frac{\omega}{2}) - \psi(1-\gamma+\frac{\omega}{2})$$

Expand :

$$\chi(\gamma,\omega) = 2\psi(1) - \psi(\gamma + \frac{\omega}{2}) - \psi(1-\gamma+\frac{\omega}{2}) = \chi_0 + \chi^{(1)}\frac{\omega}{2} + \frac{1}{2!}\chi^{(2)}\left(\frac{\omega}{2}\right)^2 + \dots$$

Use the solution: $\omega(\gamma) = \bar{\alpha}_s \chi(\gamma)$

Need to take it at LL order to get NLL terms:

$$\omega_0 \;=\; \bar{\alpha}_s \chi_0$$

Contribution at NLL is:

$$\chi_1(\gamma) = \frac{1}{2}\chi^{(1)}\chi_0 = \frac{1}{2}\left[\psi^{(1)}(\gamma) + \psi^{(1)}(1-\gamma)\right]\left[2\psi(1) - \psi(\gamma) - \psi(1-\gamma)\right]$$

Most leading poles are cubic poles:

$$\chi_1(\gamma) \simeq -\frac{1}{2\gamma^3} - \frac{1}{2(1-\gamma)^3}$$

Double poles from DGLAP

DGLAP splitting function at LO (collinear)

$$N_f = 0$$

$$P(z) = \bar{\alpha}_s \left(\frac{1-z}{z} + \frac{z}{(1-z)_+} + z(1-z) + \frac{11}{12}\delta(1-z) \right)$$

Double poles from DGLAP

DGLAP splitting function at LO (collinear)

$$N_f = 0$$

$$P(z) = \bar{\alpha}_s \left(\frac{1-z}{z} + \frac{z}{(1-z)_+} + z(1-z) + \frac{11}{12}\delta(1-z) \right)$$

DGLAP splitting function in Mellin space - anomalous dimension:

$$P(\omega) = \bar{\alpha}_s \left(\frac{1}{\omega} - \frac{1}{\omega+1} + \frac{1}{\omega+2} - \frac{1}{\omega+3} - \Psi(\omega+2) - \gamma_E + \frac{11}{12} \right)$$

Double poles from DGLAP

DGLAP splitting function at LO (collinear)

$$N_f = 0$$

$$P(z) = \bar{\alpha}_s \left(\frac{1-z}{z} + \frac{z}{(1-z)_+} + z(1-z) + \frac{11}{12}\delta(1-z) \right)$$

DGLAP splitting function in Mellin space - anomalous dimension:

$$P(\omega) = \bar{\alpha}_s \left(\frac{1}{\omega} - \frac{1}{\omega+1} + \frac{1}{\omega+2} - \frac{1}{\omega+3} - \Psi(\omega+2) - \gamma_E + \frac{11}{12} \right)$$

Most singular part is also present in LL BFKL:

$$P(z) = \bar{\alpha}_s \frac{1}{z} \qquad\qquad P(\omega) = \bar{\alpha}_s \frac{1}{\omega}$$

Double poles from DGLAP

DGLAP splitting function at LO (collinear)

$$N_f = 0$$

$$P(z) = \bar{\alpha}_s \left(\frac{1-z}{z} + \frac{z}{(1-z)_+} + z(1-z) + \frac{11}{12}\delta(1-z) \right)$$

DGLAP splitting function in Mellin space - anomalous dimension:

$$P(\omega) = \bar{\alpha}_s \left(\frac{1}{\omega} - \frac{1}{\omega+1} + \frac{1}{\omega+2} - \frac{1}{\omega+3} - \Psi(\omega+2) - \gamma_E + \frac{11}{12} \right)$$

Most singular part is also present in LL BFKL:

$$P(z) = \bar{\alpha}_s \frac{1}{z} \qquad\qquad P(\omega) = \bar{\alpha}_s \frac{1}{\omega}$$

The first term in expansion in ω appears at NLL BFKL

$$P(\omega) = \bar{\alpha}_s \left(\frac{1}{\omega} + A(\omega) \right) \qquad\qquad P(\omega) \simeq \bar{\alpha}_s \left(\frac{1}{\omega} - \frac{11}{12} \right) + \mathcal{O}(\omega^2)$$

Double poles from DGLAP

NLLx kernel in Mellin space

$$\chi_1(\gamma) = -\frac{b}{2}[\chi_0^2(\gamma) + \chi_0'(\gamma)] - \frac{1}{4}\chi_0''(\gamma) - \frac{1}{4}\left(\frac{\pi}{\sin\pi\gamma}\right)^2 \frac{\cos\pi\gamma}{3(1-2\gamma)}\left(11 + \frac{\gamma(1-\gamma)}{(1+2\gamma)(3-2\gamma)}\right)$$
$$+ \left(\frac{67}{36} - \frac{\pi^2}{12}\right)\chi_0(\gamma) + \frac{3}{2}\zeta(3) + \frac{\pi^3}{4\sin\pi\gamma}$$
$$- \sum_{n=0}^{\infty}(-1)^n\left[\frac{\psi(n+1+\gamma)-\psi(1)}{(n+\gamma)^2} + \frac{\psi(n+2-\gamma)-\psi(1)}{(n+1-\gamma)^2}\right]$$

Double poles from DGLAP splitting function

$$\frac{A(0)}{\gamma^2} + \frac{A(0)}{(1-\gamma)^2}$$

$$A(0) = -\frac{11}{12}$$

Large negative contribution

Resumming DGLAP in BFKL

How to resum these poles?

Recall BFKL equation

$$\tilde{\mathcal{F}}(\omega,\gamma) = \tilde{\mathcal{F}}^{(0)}(\omega,\gamma) + \frac{\overline{\alpha}_s}{\omega}(\chi_0(\gamma) + \bar{\alpha}_s\chi_1(\gamma))\tilde{\mathcal{F}}(\omega,\gamma)\,,$$

The kernel

$$\frac{\overline{\alpha}_s}{\omega}(\chi_0(\gamma) + \bar{\alpha}_s\chi_1(\gamma))$$

Resumming DGLAP in BFKL

How to resum these poles?

Recall BFKL equation

$$\tilde{\mathcal{F}}(\omega,\gamma) = \tilde{\mathcal{F}}^{(0)}(\omega,\gamma) + \frac{\overline{\alpha}_s}{\omega}(\chi_0(\gamma) + \bar{\alpha}_s\chi_1(\gamma))\tilde{\mathcal{F}}(\omega,\gamma)\,,$$

The kernel

$$\frac{\overline{\alpha}_s}{\omega}(\chi_0(\gamma) + \bar{\alpha}_s\chi_1(\gamma))$$

Consider the DGLAP kernel (collinear + anti-collinear)

$$\frac{\overline{\alpha}_s}{\omega}\frac{1}{\gamma} + \bar{\alpha}_s A(\omega)\frac{1}{\gamma} + \frac{\overline{\alpha}_s}{\omega}\frac{1}{1-\gamma} + \bar{\alpha}_s A(\omega)\frac{1}{1-\gamma}$$

Resumming DGLAP in BFKL

How to resum these poles?

Recall BFKL equation

$$\tilde{\mathcal{F}}(\omega,\gamma) = \tilde{\mathcal{F}}^{(0)}(\omega,\gamma) + \frac{\overline{\alpha}_s}{\omega}(\chi_0(\gamma) + \bar{\alpha}_s\chi_1(\gamma))\tilde{\mathcal{F}}(\omega,\gamma)\,,$$

The kernel

$$\frac{\overline{\alpha}_s}{\omega}(\chi_0(\gamma) + \bar{\alpha}_s\chi_1(\gamma))$$

Consider the DGLAP kernel (collinear + anti-collinear)

$$\frac{\overline{\alpha}_s}{\omega}\frac{1}{\gamma} + \bar{\alpha}_s A(\omega)\frac{1}{\gamma} + \frac{\overline{\alpha}_s}{\omega}\frac{1}{1-\gamma} + \bar{\alpha}_s A(\omega)\frac{1}{1-\gamma}$$

Consider the following modified kernel:

$$\frac{\overline{\alpha}_s}{\omega}\chi_0(\gamma) + \bar{\alpha}_s A(\omega)\frac{1}{\gamma} + \bar{\alpha}_s A(\omega)\frac{1}{1-\gamma}$$

Resumming DGLAP in BFKL

How to resum these poles?

Recall BFKL equation

$$\tilde{\mathcal{F}}(\omega,\gamma) = \tilde{\mathcal{F}}^{(0)}(\omega,\gamma) + \frac{\overline{\alpha}_s}{\omega}(\chi_0(\gamma) + \bar{\alpha}_s\chi_1(\gamma))\tilde{\mathcal{F}}(\omega,\gamma)\,,$$

The kernel

$$\frac{\overline{\alpha}_s}{\omega}(\chi_0(\gamma) + \bar{\alpha}_s\chi_1(\gamma))$$

Consider the DGLAP kernel (collinear + anti-collinear)

$$\frac{\overline{\alpha}_s}{\omega}\frac{1}{\gamma} + \bar{\alpha}_s A(\omega)\frac{1}{\gamma} + \frac{\overline{\alpha}_s}{\omega}\frac{1}{1-\gamma} + \bar{\alpha}_s A(\omega)\frac{1}{1-\gamma}$$

Consider the following modified kernel:

$$\frac{\overline{\alpha}_s}{\omega}\chi_0(\gamma) + \bar{\alpha}_s A(\omega)\frac{1}{\gamma} + \bar{\alpha}_s A(\omega)\frac{1}{1-\gamma}$$

LL BFKL

Resumming DGLAP in BFKL

How to resum these poles?

Recall BFKL equation

$$\tilde{\mathcal{F}}(\omega,\gamma) = \tilde{\mathcal{F}}^{(0)}(\omega,\gamma) + \frac{\overline{\alpha}_s}{\omega}(\chi_0(\gamma) + \bar{\alpha}_s\chi_1(\gamma))\tilde{\mathcal{F}}(\omega,\gamma)\,,$$

The kernel

$$\frac{\overline{\alpha}_s}{\omega}(\chi_0(\gamma) + \bar{\alpha}_s\chi_1(\gamma))$$

Consider the DGLAP kernel (collinear + anti-collinear)

$$\frac{\overline{\alpha}_s}{\omega}\frac{1}{\gamma} + \bar{\alpha}_s A(\omega)\frac{1}{\gamma} + \frac{\overline{\alpha}_s}{\omega}\frac{1}{1-\gamma} + \bar{\alpha}_s A(\omega)\frac{1}{1-\gamma}$$

Consider the following modified kernel:

$$\frac{\overline{\alpha}_s}{\omega}\chi_0(\gamma) + \bar{\alpha}_s A(\omega)\frac{1}{\gamma} + \bar{\alpha}_s A(\omega)\frac{1}{1-\gamma}$$

LL BFKL

LO non-singular DGLAP (collinear+anti-collinear)

Resumming DGLAP in BFKL

$$\frac{\overline{\alpha}_s}{\omega}\chi_0(\gamma)+\bar{\alpha}_s A(\omega)\frac{1}{\gamma}+\bar{\alpha}_s A(\omega)\frac{1}{1-\gamma}\simeq\frac{\overline{\alpha}_s}{\omega}\left(\chi_0(\gamma)+\omega A(0)\frac{1}{\gamma}+\omega A(0)\frac{1}{1-\gamma}\right)$$

$$\simeq\frac{\overline{\alpha}_s}{\omega}\left(\chi_0(\gamma)+\bar{\alpha}_s\chi_0(\gamma)A(0)\frac{1}{\gamma}+\bar{\alpha}_s\chi_0(\gamma)A(0)\frac{1}{1-\gamma}\right)\simeq\frac{\overline{\alpha}_s}{\omega}\left(\chi_0(\gamma)+\bar{\alpha}_s A(0)\frac{1}{\gamma^2}+\bar{\alpha}_s A(0)\frac{1}{(1-\gamma)^2}\right)$$

Double poles!

Resumming DGLAP in BFKL

$$\frac{\overline{\alpha}_s}{\omega}\chi_0(\gamma)+\bar{\alpha}_s A(\omega)\frac{1}{\gamma}+\bar{\alpha}_s A(\omega)\frac{1}{1-\gamma}\simeq\frac{\overline{\alpha}_s}{\omega}\left(\chi_0(\gamma)+\omega A(0)\frac{1}{\gamma}+\omega A(0)\frac{1}{1-\gamma}\right)$$

$$\simeq\frac{\overline{\alpha}_s}{\omega}\left(\chi_0(\gamma)+\bar{\alpha}_s\chi_0(\gamma)A(0)\frac{1}{\gamma}+\bar{\alpha}_s\chi_0(\gamma)A(0)\frac{1}{1-\gamma}\right)\simeq\frac{\overline{\alpha}_s}{\omega}\left(\chi_0(\gamma)+\bar{\alpha}_s A(0)\frac{1}{\gamma^2}+\bar{\alpha}_s A(0)\frac{1}{(1-\gamma)^2}\right)$$

Double poles!

By combining the BFKL LL and LO non-singular splitting function from DGLAP one can resum the large contributions from NLL BFKL.

Need DGLAP collinear + anti-collinear terms

Resumming DGLAP in BFKL

$$\frac{\overline{\alpha}_s}{\omega}\chi_0(\gamma)+\bar{\alpha}_s A(\omega)\frac{1}{\gamma}+\bar{\alpha}_s A(\omega)\frac{1}{1-\gamma}\simeq\frac{\overline{\alpha}_s}{\omega}\left(\chi_0(\gamma)+\omega A(0)\frac{1}{\gamma}+\omega A(0)\frac{1}{1-\gamma}\right)$$

$$\simeq\frac{\overline{\alpha}_s}{\omega}\left(\chi_0(\gamma)+\bar{\alpha}_s\chi_0(\gamma)A(0)\frac{1}{\gamma}+\bar{\alpha}_s\chi_0(\gamma)A(0)\frac{1}{1-\gamma}\right)\simeq\frac{\overline{\alpha}_s}{\omega}\left(\chi_0(\gamma)+\bar{\alpha}_s A(0)\frac{1}{\gamma^2}+\bar{\alpha}_s A(0)\frac{1}{(1-\gamma)^2}\right)$$

Double poles!

By combining the BFKL LL and LO non-singular splitting function from DGLAP one can resum the large contributions from NLL BFKL.

Need DGLAP collinear + anti-collinear terms

The remaining double poles stem from running of the coupling:

$$\chi_1(\gamma)=-\frac{b}{2}[\chi_0^2(\gamma)+\chi_0'(\gamma)]-\frac{1}{4}\chi_0''(\gamma)-\frac{1}{4}\left(\frac{\pi}{\sin\pi\gamma}\right)^2\frac{\cos\pi\gamma}{3(1-2\gamma)}\left(11+\frac{\gamma(1-\gamma)}{(1+2\gamma)(3-2\gamma)}\right)$$
$$+\left(\frac{67}{36}-\frac{\pi^2}{12}\right)\chi_0(\gamma)+\frac{3}{2}\zeta(3)+\frac{\pi^3}{4\sin\pi\gamma}$$
$$-\sum_{n=0}^{\infty}(-1)^n\left[\frac{\psi(n+1+\gamma)-\psi(1)}{(n+\gamma)^2}+\frac{\psi(n+2-\gamma)-\psi(1)}{(n+1-\gamma)^2}\right]\ .$$

Resummed kernel

$$\tilde{\mathcal{K}}_\omega = \bar{\alpha}_s(\boldsymbol{q}^2) K_0^\omega + \omega \bar{\alpha}_s(k_>^2) K_{\rm c}^\omega + \bar{\alpha}_s^2(k_>^2) \tilde{K}_1^\omega$$

Running coupling

LL with shifts

non-singular DGLAP

NLL with subtractions

$$\chi_0^\omega = 2\psi(1) - \psi(\gamma + \tfrac{\omega}{2}) - \psi(1 - \gamma + \tfrac{\omega}{2})$$

$$\chi_{\rm c}^\omega(\gamma) = \frac{A_1(\omega)}{\gamma + \frac{\omega}{2}} + \frac{A_1(\omega)}{1 - \gamma + \frac{\omega}{2}} \,,$$

$$\begin{aligned}
\tilde{\chi}_1(\gamma) &= \chi_1(\gamma) - \chi_0^0(\gamma)[\chi_0^1(\gamma) + \chi_{\rm c}^0(\gamma)] - \chi_0^{\rm run}(\gamma) \\
&= \chi_1(\gamma) + \frac{1}{2}\chi_0(\gamma)\frac{\pi^2}{\sin^2(\pi\gamma)} - \chi_0(\gamma)\frac{A_1(0)}{\gamma(1-\gamma)} + \frac{b}{2}(\chi_0' + \chi_0^2)
\end{aligned}$$

NLL

Subtraction of cubic poles

Subtraction of double poles from DGLAP

Subtraction of double poles from r.c.

Additional subtraction needed to satisfy the momentum sum rule.

All the calculations are actually done in momentum space

Resummed kernel in x,k_T

$$\int_x^1 \frac{dz}{z} \int dk'^2\ \tilde{\mathcal{K}}(z;k,k') f(\frac{x}{z},k')$$
$$= \int_x^1 \frac{dz}{z} \int dk'^2 \left[\bar{\alpha}_s(\boldsymbol{q}^2) K_0^{\rm kc}(z;\boldsymbol{k},\boldsymbol{k}') + \bar{\alpha}_s(k_>^2) K_{\rm c}^{\rm kc}(z;k,k') + \bar{\alpha}_s^2(k_>^2)\tilde{K}_1(k,k')\right] f(\frac{x}{z},k')$$

LL BFKL with consistency constraint

$$\int_x^1 \frac{dz}{z} \int dk'^2\ \left[\bar{\alpha}_s(\boldsymbol{q}^2) K_0^{\rm kc}(z;\boldsymbol{k},\boldsymbol{k}')\right] f(\frac{x}{z},k')$$
$$= \int_x^1 \frac{dz}{z} \int \frac{d^2\boldsymbol{q}}{\pi \boldsymbol{q}^2}\ \bar{\alpha}_s(\boldsymbol{q}^2) \left[f(\frac{x}{z},|\boldsymbol{k}+\boldsymbol{q}|)\Theta(\frac{k}{z}-k')\Theta(k'-kz) - \Theta(k-q) f(\frac{x}{z},k)\right]$$

non-singular DGLAP with consistency constraint

$$\int_x^1 \frac{dz}{z} \int dk'^2\ \bar{\alpha}_s(k_>^2) K_{\rm c}^{\rm kc}(z;k,k') f(\frac{x}{z},k')$$
$$= \int_x^1 \frac{dz}{z} \int_{(kz)^2}^{k^2} \frac{dk'^2}{k^2}\ \bar{\alpha}_s(k^2) z\frac{k}{k'} \tilde{P}_{gg}(z\frac{k}{k'}) f(\frac{x}{z},k')$$
$$+ \int_x^1 \frac{dz}{z} \int_{k^2}^{(k/z)^2} \frac{dk'^2}{k'^2}\ \bar{\alpha}_s(k'^2) z\frac{k'}{k} \tilde{P}_{gg}(z\frac{k'}{k}) f(\frac{x}{z},k')\ ,$$

Resummed kernel in x,k_T

NLL BFKL with subtractions

$$\int_x^1 \frac{dz}{z} \int dk'^2\ \bar{\alpha}_s^2(k_>^2)\tilde{K}_1(k,k')f(\frac{x}{z},k')$$

$$= \frac{1}{4}\int_x^1 \frac{dz}{z} \int dk'^2\ \bar{\alpha}_s^2(k_>^2)\Bigg\{$$

$$\left(\frac{67}{9}-\frac{\pi^2}{3}\right)\frac{1}{|k'^2-k^2|}\left[f(\frac{x}{z},k'^2)-\frac{2k_<^2}{(k'^2+k^2)}f(\frac{x}{z},k^2)\right]+$$

$$\Bigg[-\frac{1}{32}\left(\frac{2}{k'^2}+\frac{2}{k^2}+\left(\frac{1}{k'^2}-\frac{1}{k^2}\right)\log\left(\frac{k^2}{k'^2}\right)\right)+\frac{4\mathrm{Li}_2(1-k_<^2/k_>^2)}{|k'^2-k^2|}$$

$$-4A_1(0)\mathrm{sgn}(k^2-k'^2)\left(\frac{1}{k^2}\log\frac{|k'^2-k^2|}{k'^2}-\frac{1}{k'^2}\log\frac{|k'^2-k^2|}{k^2}\right)$$

$$-\left(3+\left(\frac{3}{4}-\frac{(k'^2+k^2)^2}{32k'^2k^2}\right)\right)\int_0^\infty \frac{dy}{k^2+y^2k'^2}\log|\frac{1+y}{1-y}|$$

$$+\frac{1}{k'^2+k^2}\left(\frac{\pi^2}{3}+4\mathrm{Li}_2(\frac{k_<^2}{k_>^2})\right)\Bigg]f(\frac{x}{z},k')\Bigg\}$$

$$+\frac{1}{4}6\zeta(3)\int_x^1\frac{dz}{z}\ \bar{\alpha}_s^2(k^2)f(\frac{x}{z},k)\ .$$

+additional subtractions to satisfy momentum sum rule

Resummation: results

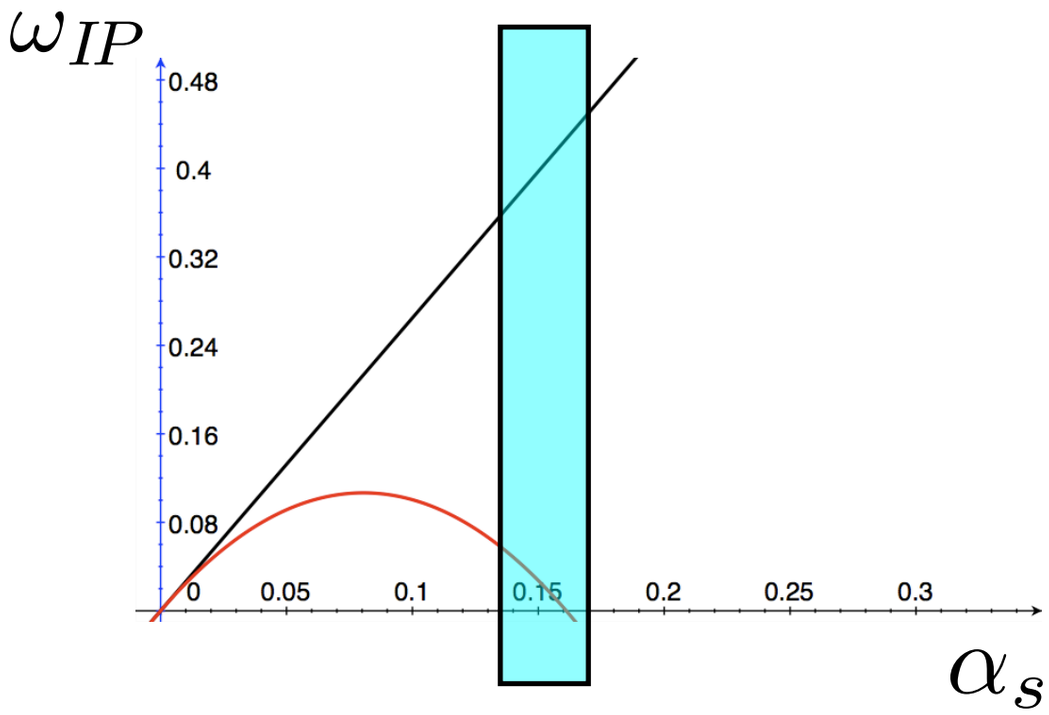

$$\mathcal{F}_g(x, k_T) \sim x^{-\omega_{IP}}$$

$$\sigma^{\gamma^* p} \sim s^{\omega_{IP}}$$

Stable result

$$\omega_{IP} \sim 0.2 - 0.3$$

Significant reduction with respect to LLx

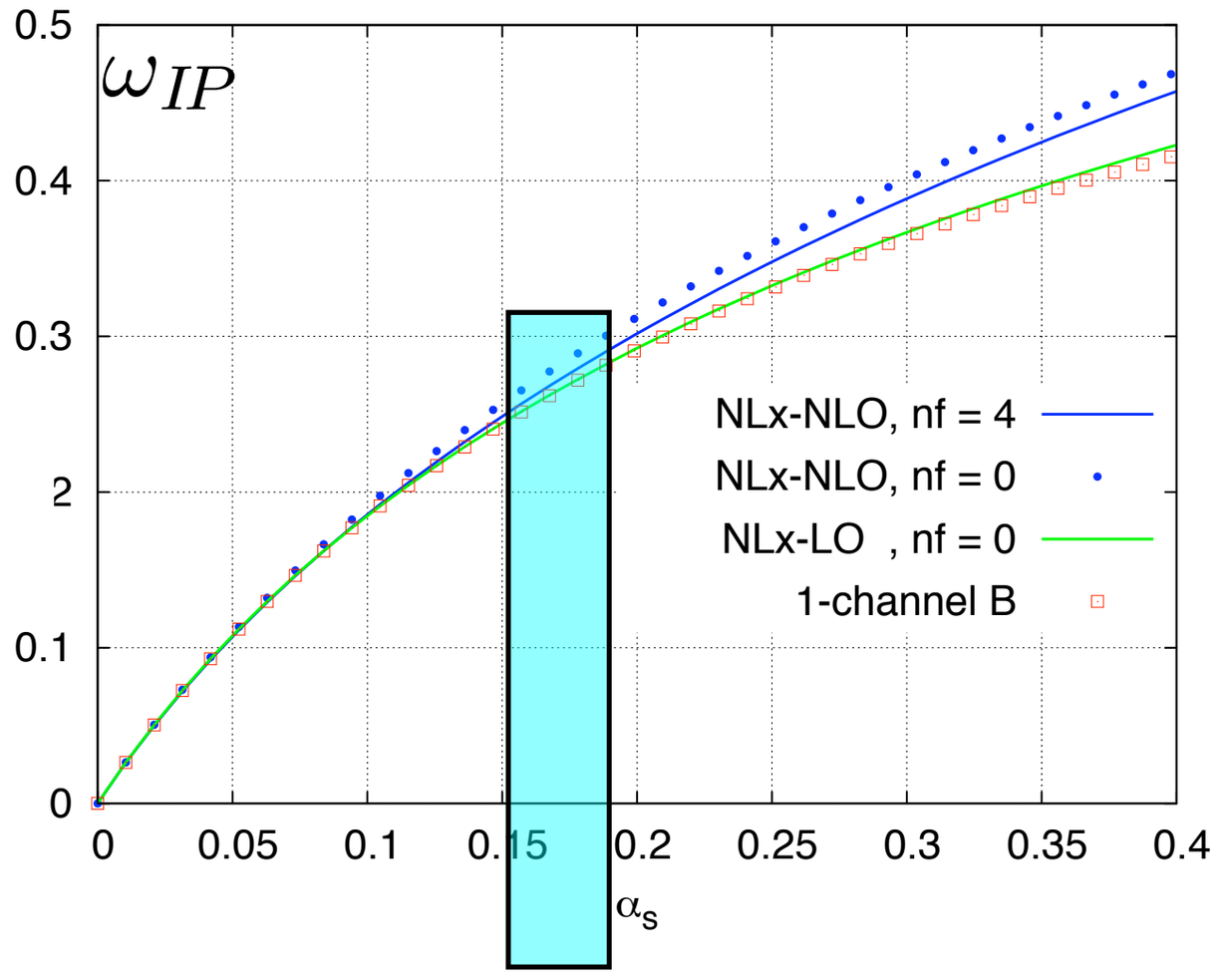

Ciafaloni, Colferai, Salam, AS

Frozen coupling features

$$\bar{\alpha}_s \chi_\omega(\gamma, \bar{\alpha}_s) = \bar{\alpha}_s(\chi_0^\omega + \omega \chi_{\rm c}^\omega) + \bar{\alpha}_s^2 \tilde{\chi}_1^\omega$$

Effective characteristic function: $\omega = \bar{\alpha}_s \chi_{\rm eff}^{(0)}(\gamma, \bar{\alpha}_s)$

Fixed point (independent of the coupling). Energy momentum conservation

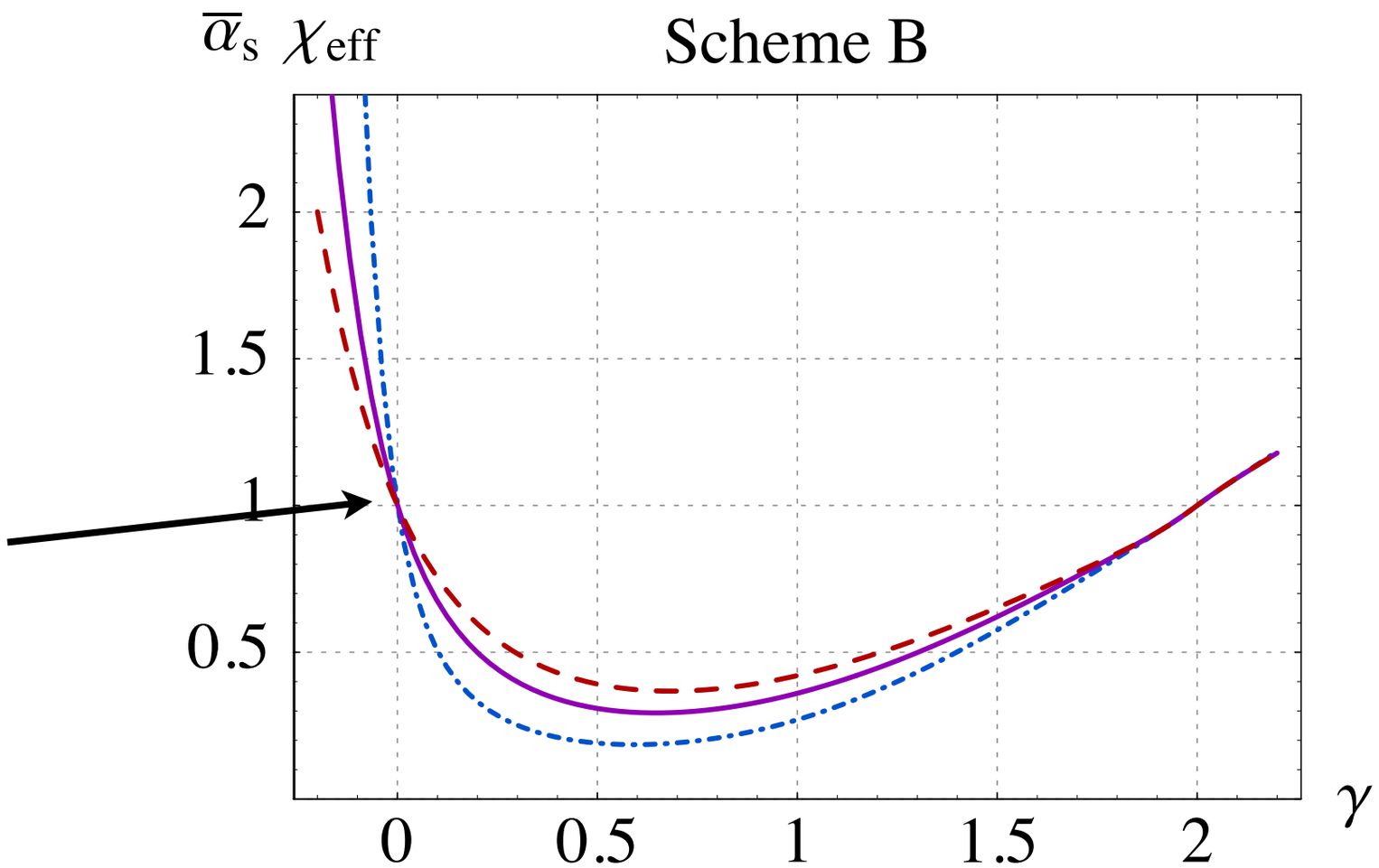

Gluon Green's function

Solution to the BFKL equation (gluon Green's function). Single channel: gluons only.

$$G(Y;k_{1\perp},k_{2\perp}) = \delta^{(2)}(k_{1\perp}-k_{2\perp}) + \int_0^Y dy \int d^2k'_\perp \, \mathcal{K}(k_{1\perp},k'_\perp)\, G(Y;k'_\perp,k_{2\perp})$$

Suitable for the two scale process : Mueller - Navelet jets, $\gamma^*\gamma^*$ scattering

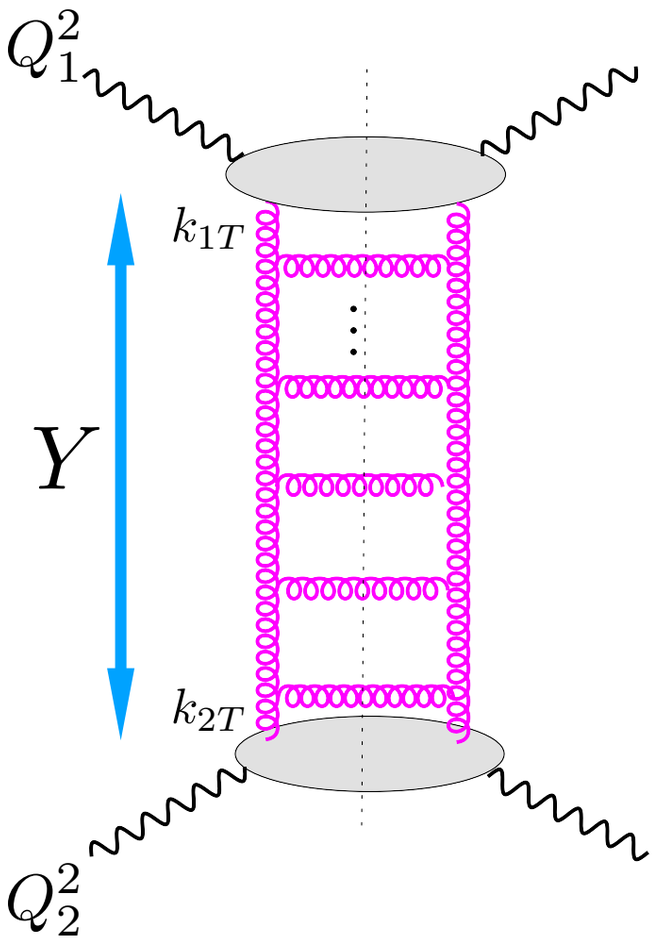

Gluon Green's function

Solution to the BFKL equation (gluon Green's function). Single channel: gluons only.

$$G(Y;k_{1\perp},k_{2\perp}) = \delta^{(2)}(k_{1\perp}-k_{2\perp}) + \int_0^Y dy \int d^2k'_\perp \, \mathcal{K}(k_{1\perp},k'_\perp)\, G(Y;k'_\perp,k_{2\perp})$$

Suitable for the two scale process : Mueller - Navelet jets, γ*γ* scattering

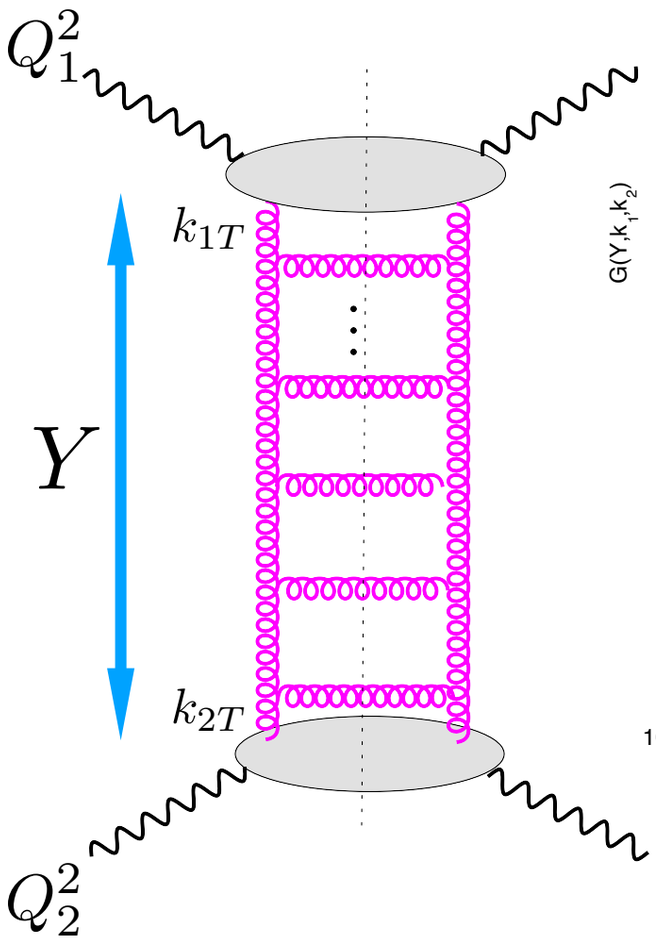

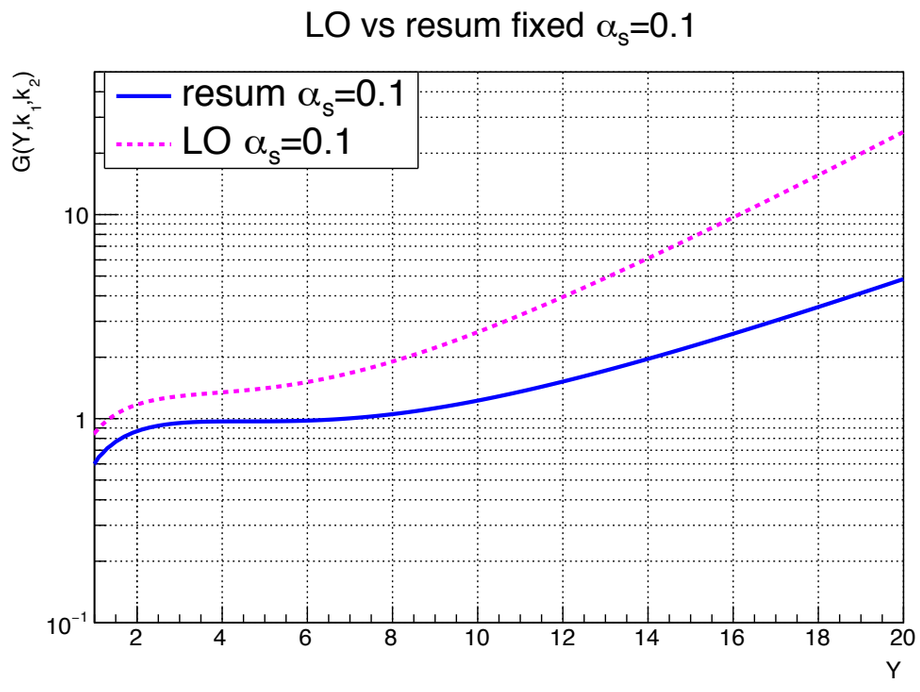

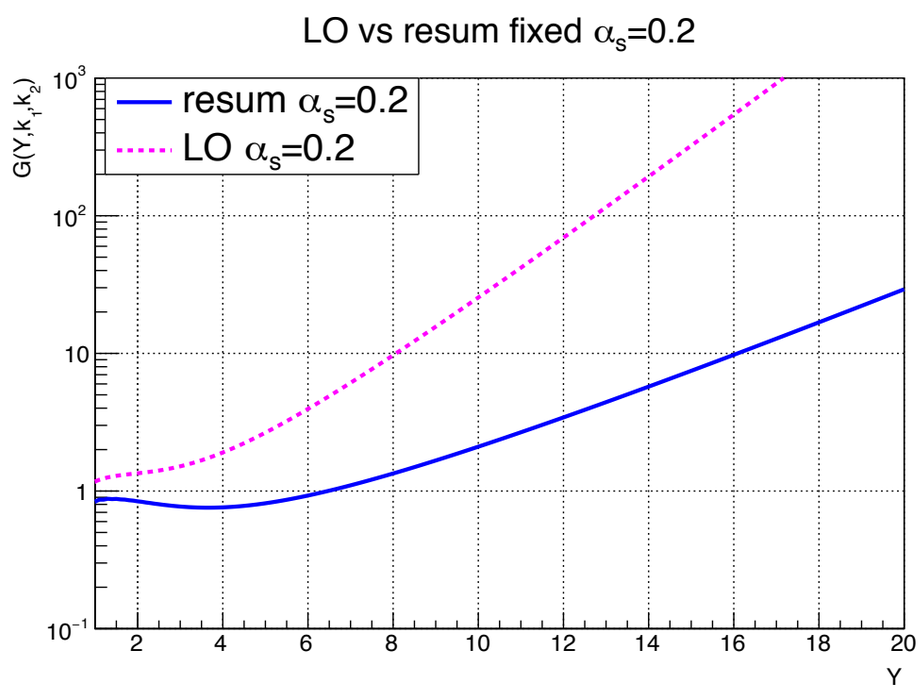

Large suppression of the solution in the resummed case as compared to LLx

Gluon Green's function

$$G(Y;k_{1\perp},k_{2\perp}) = \delta^{(2)}(k_{1\perp}-k_{2\perp}) + \int_0^Y dy \int d^2k'_\perp \, \mathcal{K}(k_{1\perp},k'_\perp)\, G(Y;k'_\perp,k_{2\perp})$$

Different scale choices

$(k_{1T} = k_{2T} \equiv k_{T0})$

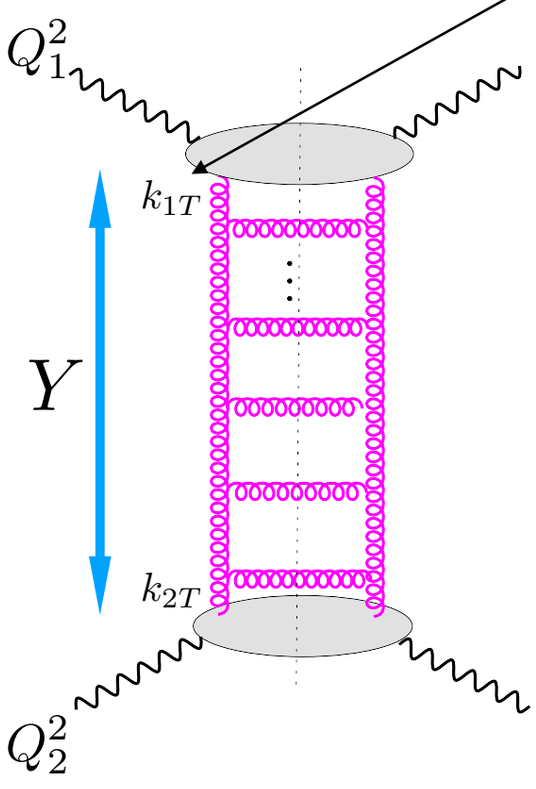

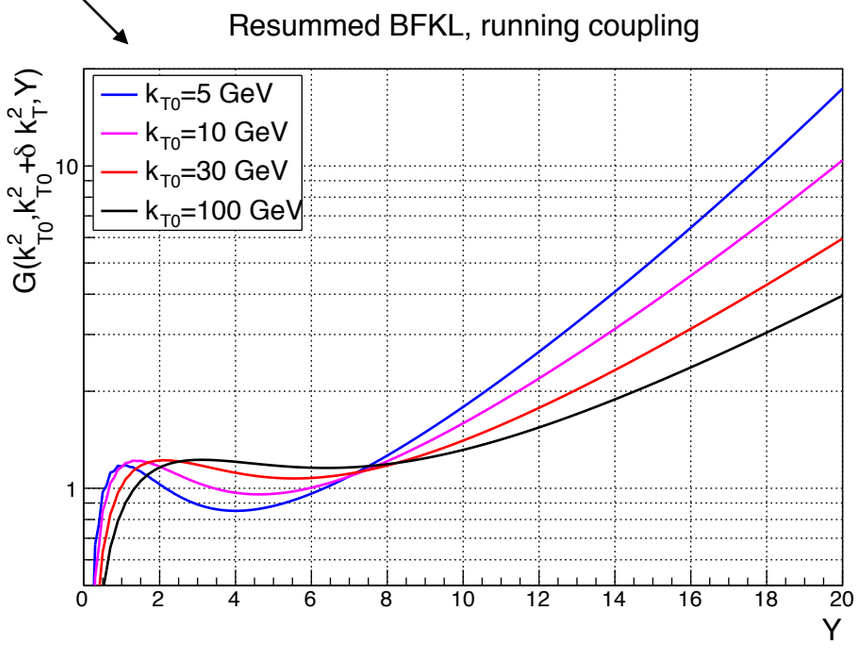

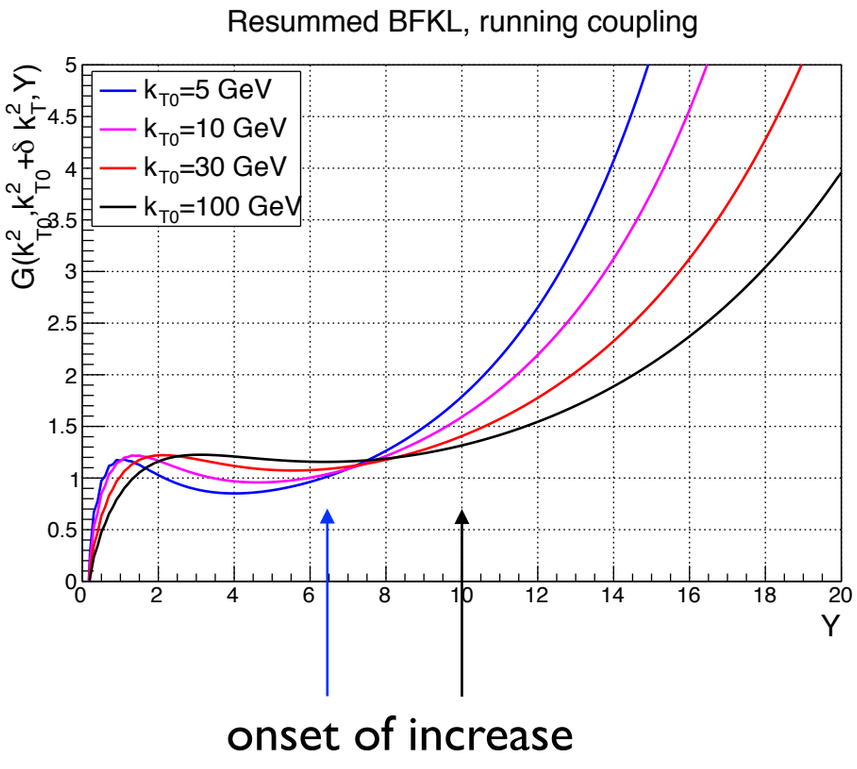

Resummation not only causes the decrease of the intercept, how fast the cross section grows, but also delays the onset of the rise.
Large preasymptotic effects

Ciafaloni, Colferai, Salam, AS
Frankfurt, Strikman, AS

Resummed splitting function

- Deconvolution of the integral equation.
- Calculate the integrated density: $xg(x,Q^2) = \int^{Q^2} dk_T^2\, G^{(s_0=k_T^2)}(x;k_T,k_{0T})$
- Solve numerically for the splitting function:

$$\frac{dg(x,Q^2)}{d\log Q^2} = \int \frac{dz}{z} P_{\rm eff}(z,Q^2)\, g(\frac{x}{z},Q^2)$$

At large values of Q^2 the results should be independent of the regularization of the coupling and the choice of k_0 .

Factorization in Q^2 of the non-perturbative and perturbative contributions.

Resummed splitting function

Gluon-gluon splitting function has logarithmic enhancements at small x

$$xP_{gg}(x) = \sum_{n=1} a_n \alpha_s^n \ln^{n-1} \frac{1}{x} + \sum_{n=2} b_n \alpha_s^n \ln^{n-2} \frac{1}{x} + \dots$$

LLx NLLx

First small x logarithmic term which belongs to NLLx hierarchy recovered at NNLO

$$-1.54 \bar{\alpha}_s^3 \ln 1/x$$

Resummation at small x is inevitable.

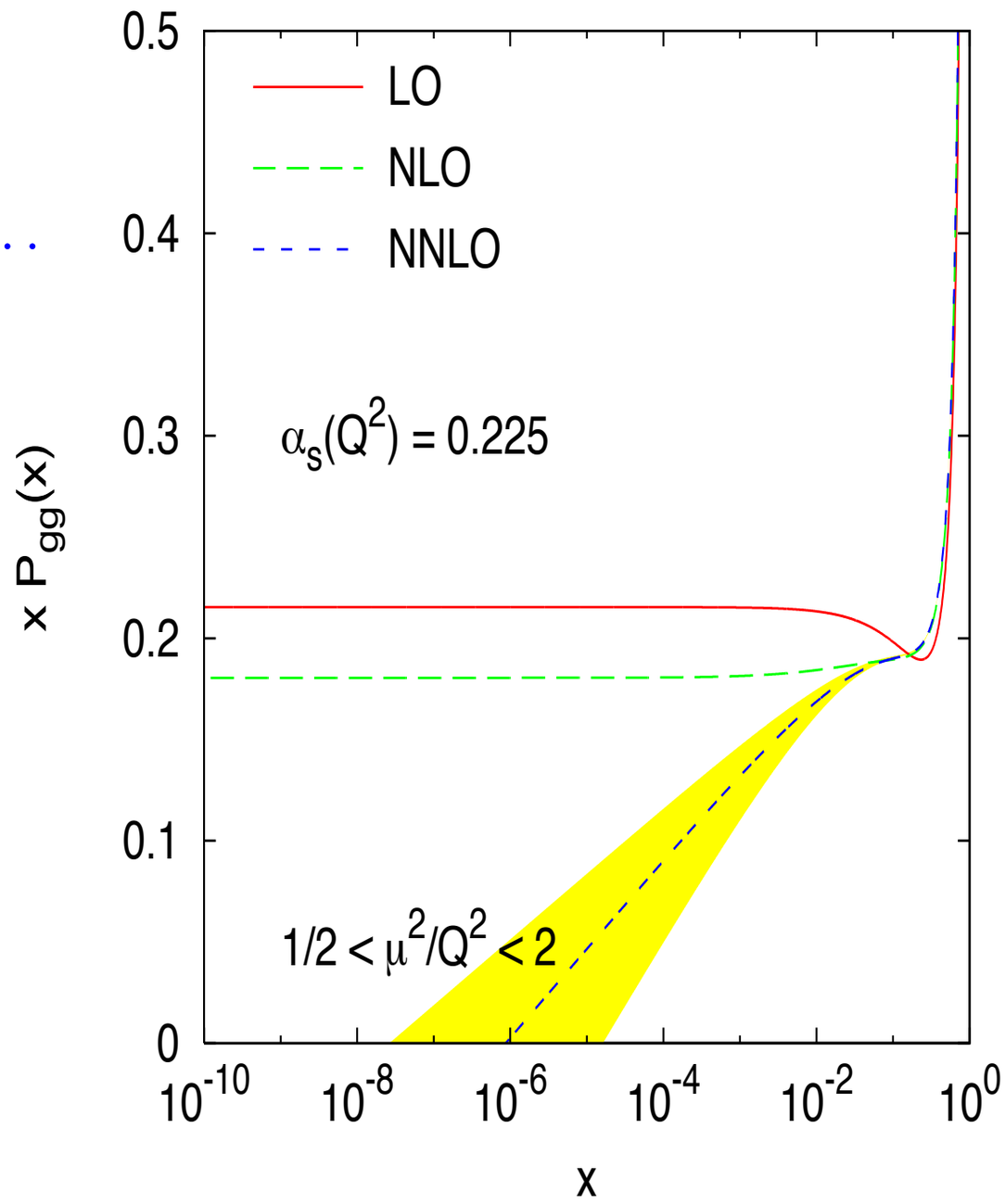

Resummed splitting function

Gluon-gluon splitting function has logarithmic enhancements at small x

$$xP_{gg}(x) = \sum_{n=1} a_n \alpha_s^n \ln^{n-1} \frac{1}{x} + \sum_{n=2} b_n \alpha_s^n \ln^{n-2} \frac{1}{x} + \dots$$

LLx NLLx

First small x logarithmic term which belongs to NLLx hierarchy recovered at NNLO

$$-1.54 \bar{\alpha}_s^3 \ln 1/x$$

Resummation at small x is inevitable.

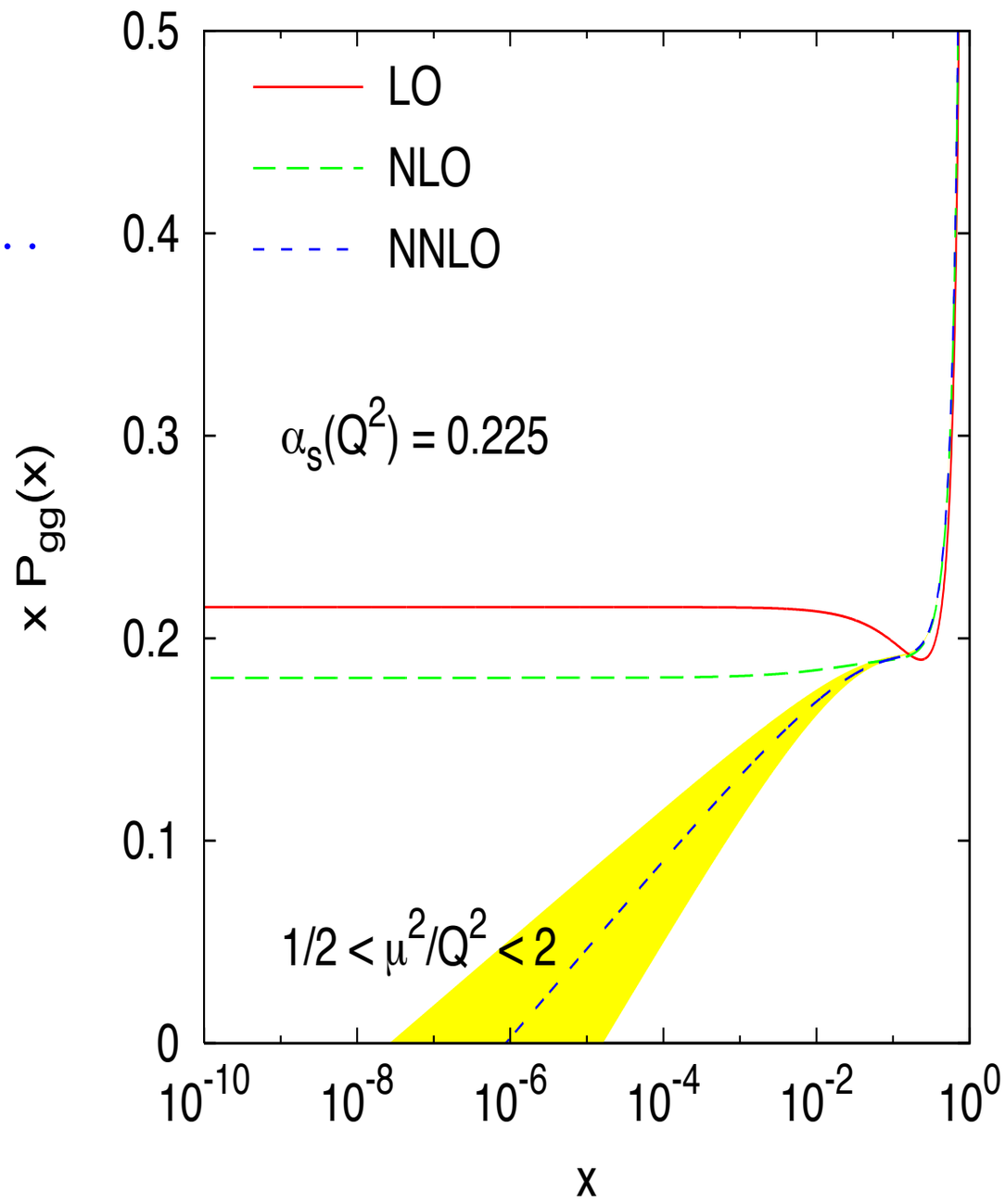

Moch, Vermaseren, Vogt

Resummed splitting function

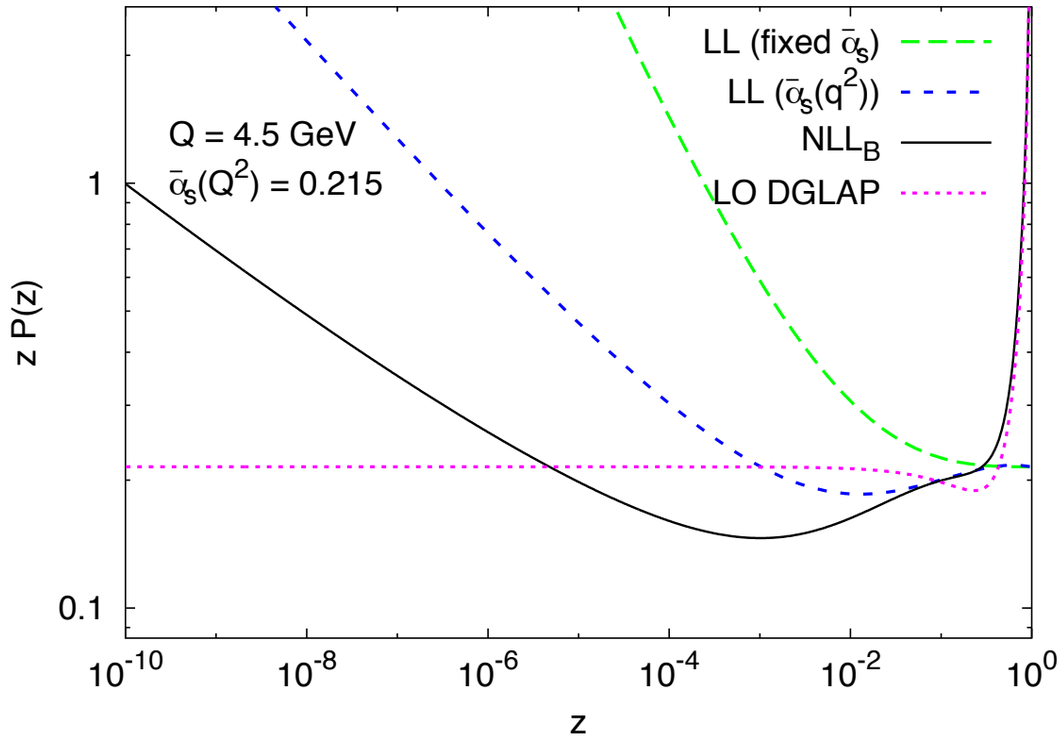

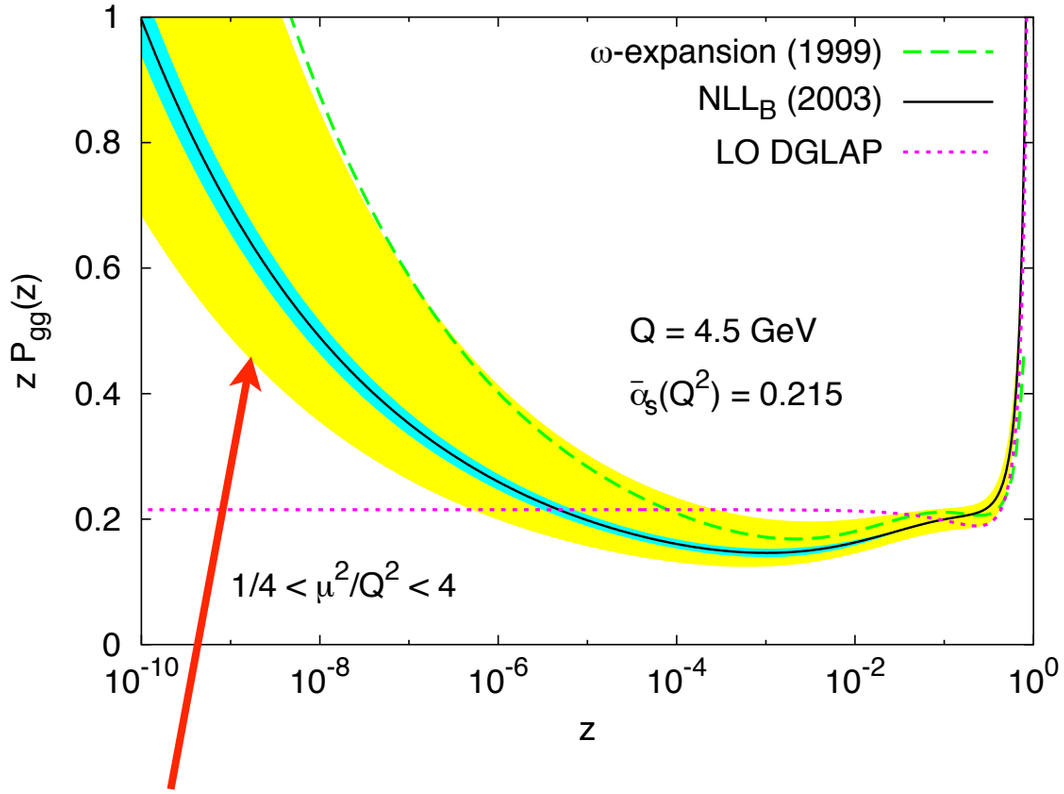

Dependence on the renormalization scale

- Small x growth delayed to much smaller values of x (beyond HERA)
- Interesting feature: a dip seen at around $x \simeq 10^{-3}$
- Is this universal feature ?
- The same feature seen in other schemes of resummation (Altarelli,Ball,Forte; Thorne).
- Need to understand the origin of the dip.

Where the dip comes from?

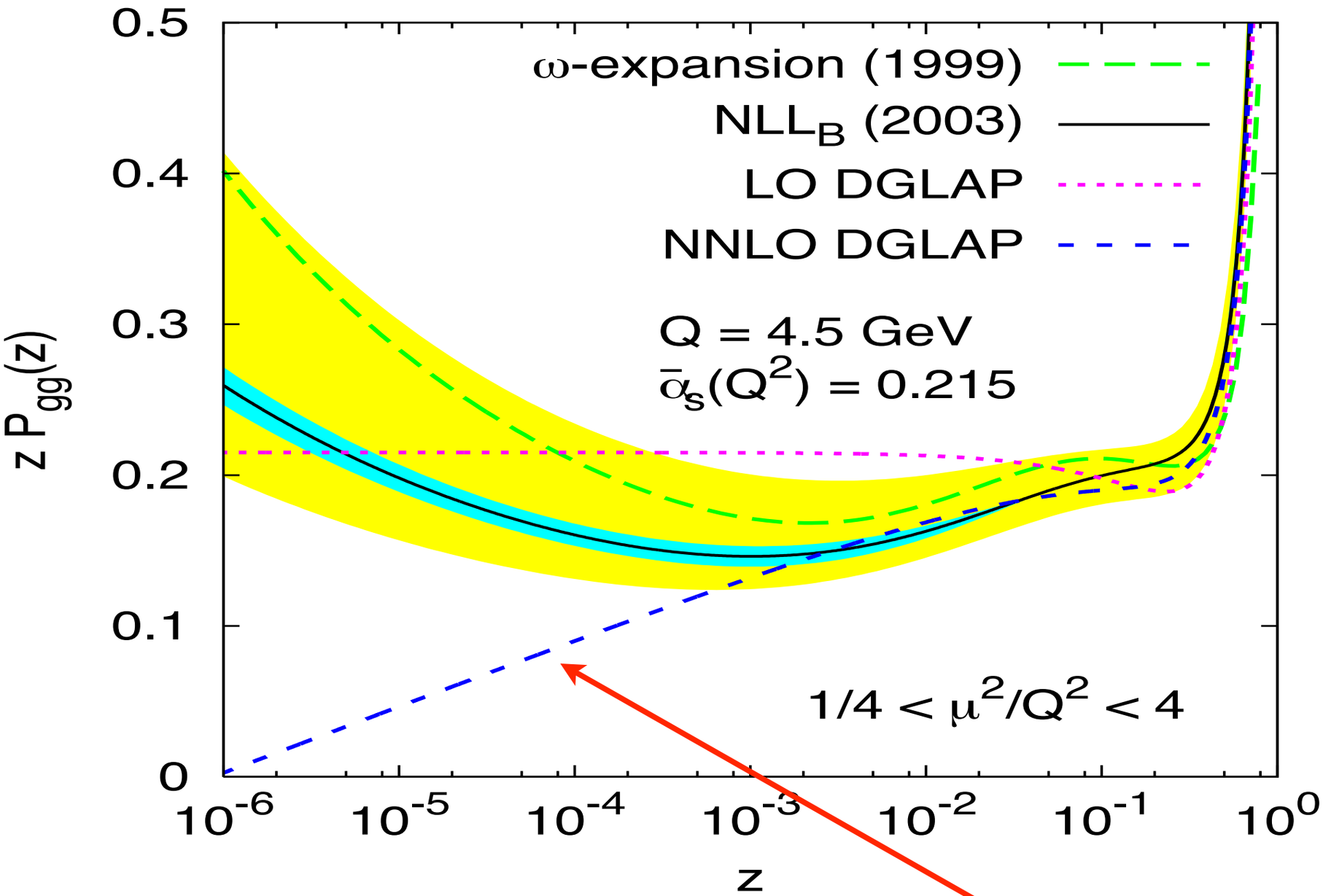

$$-1.54\bar{\alpha}_s^3 \ln 1/x$$

Initial decrease seems to be consistent with the small x NNLO term.

Resummed splitting function

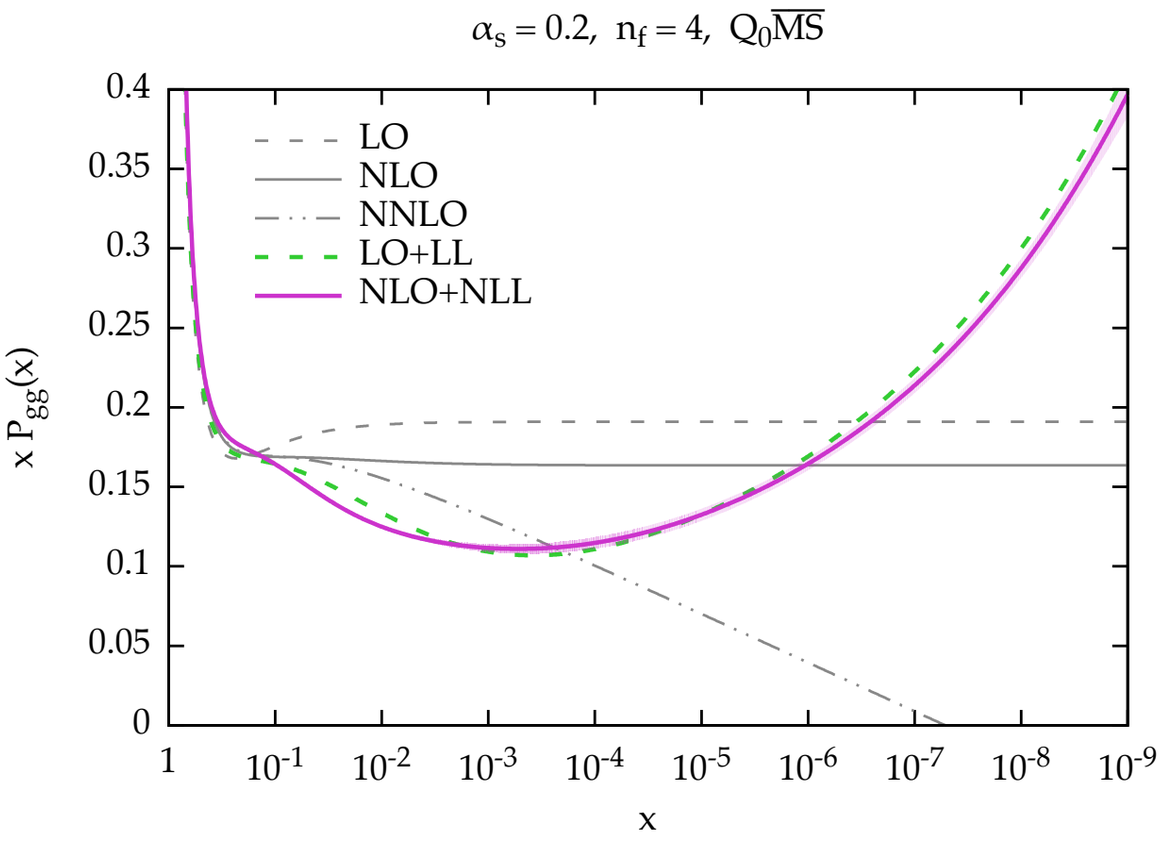

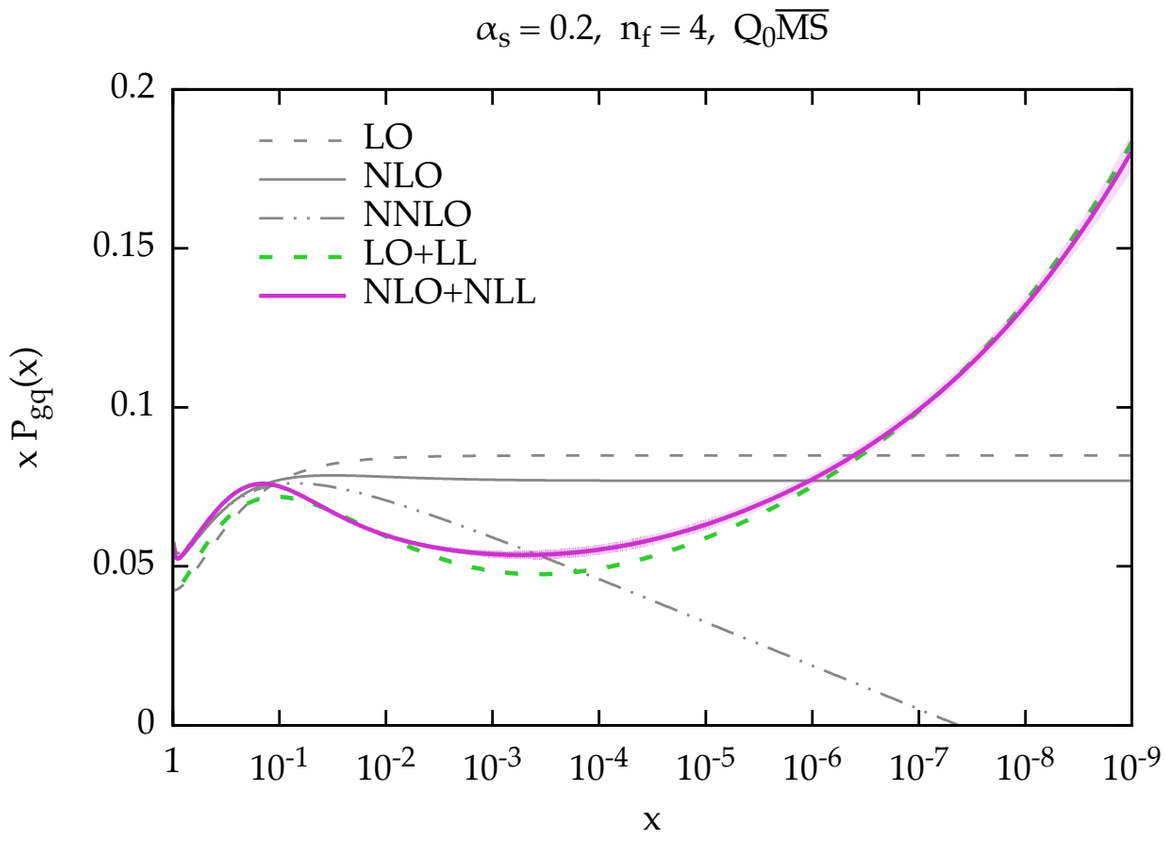

The same feature visible in other schemes of resummation

Understanding the structure of the splitting function

Perturbative terms in the splitting function

	LLx	NLLx	NNLLx	…	
α_s	x	–	–		
α_s^2	0	n_f	–		
α_s^3	0	x	x		const.
α_s^4	x	x	x		$\ln 1/x$
α_s^5	0	x	x		$\ln^2 1/x$
⋮					$\ln^3 1/x$

Understanding the structure of the splitting function

Perturbative terms in the splitting function

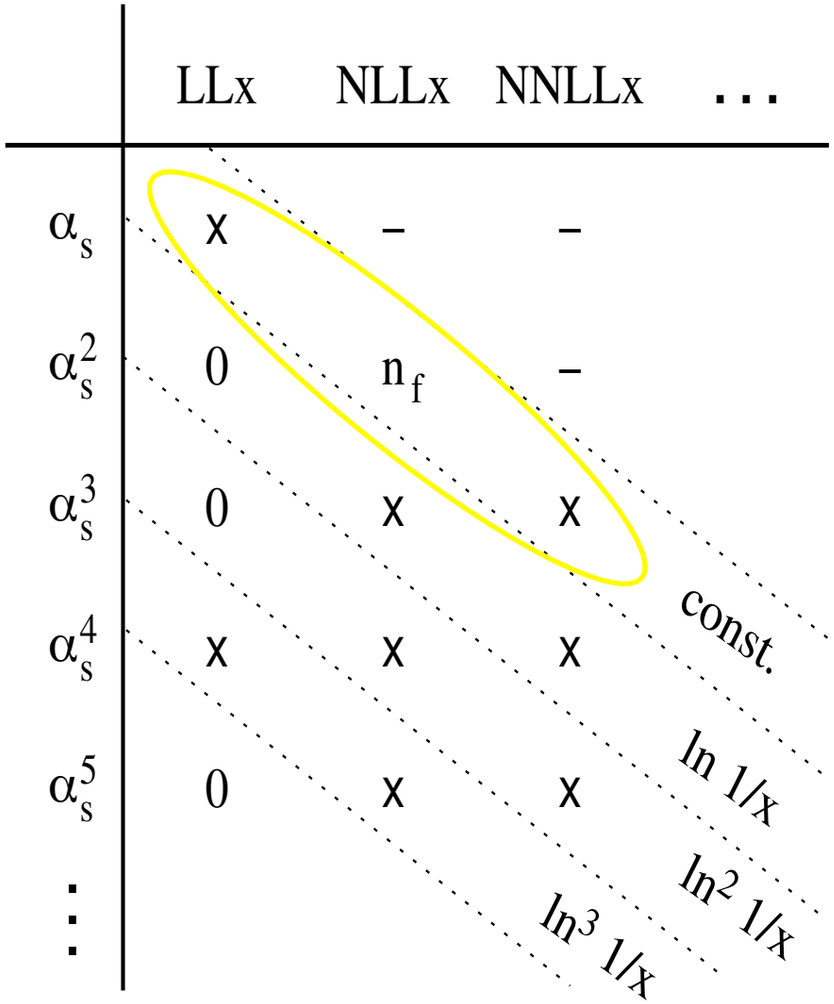

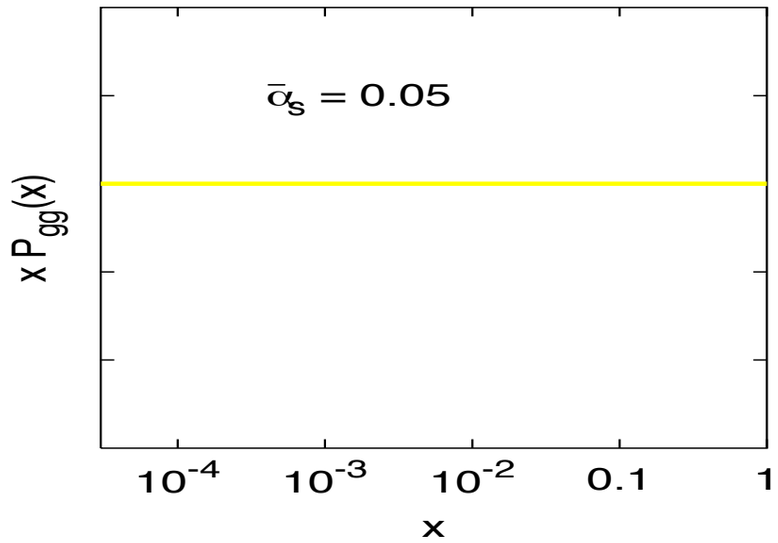

Understanding the structure of the splitting function

Perturbative terms in the splitting function

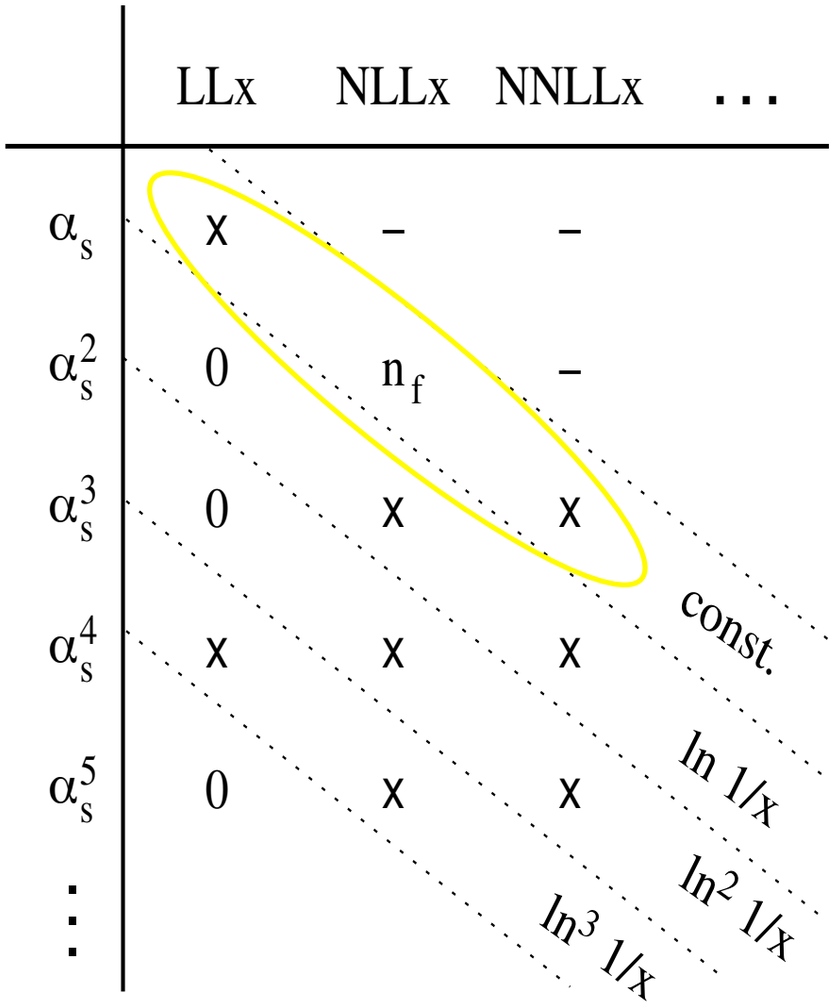

Understanding the structure of the splitting function

Perturbative terms in the splitting function

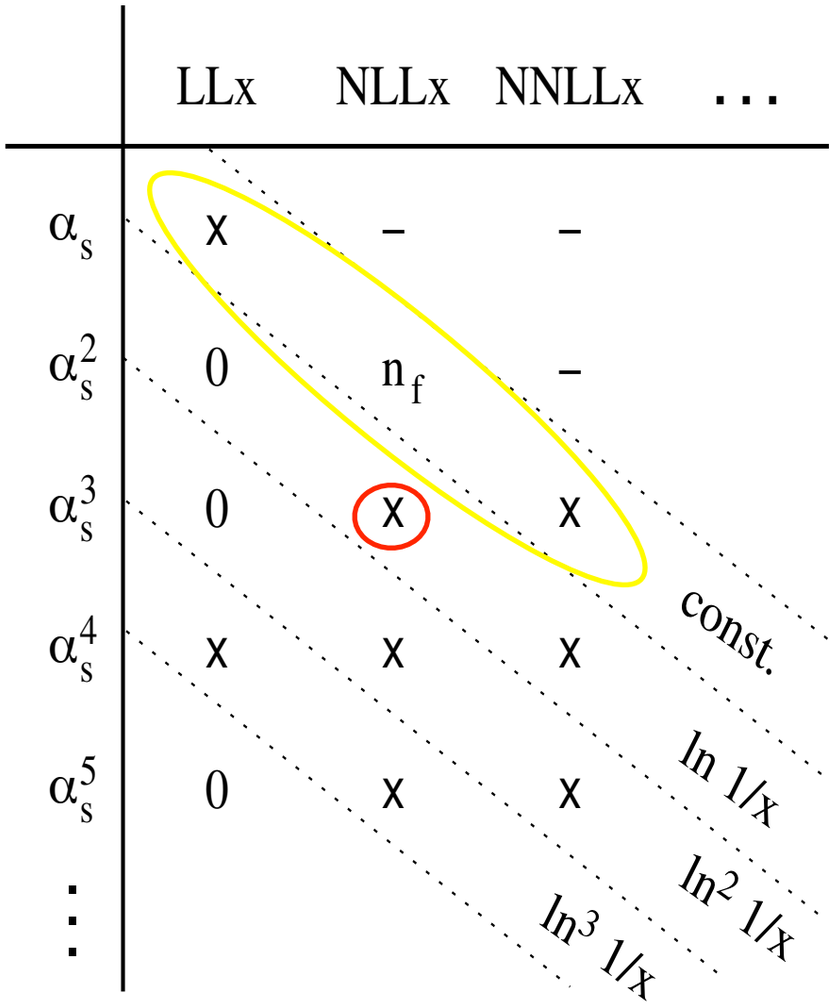

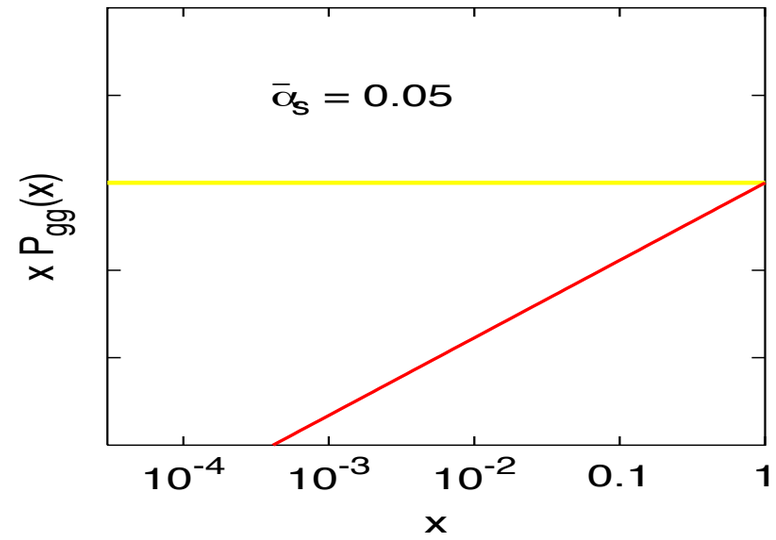

Understanding the structure of the splitting function

Perturbative terms in the splitting function

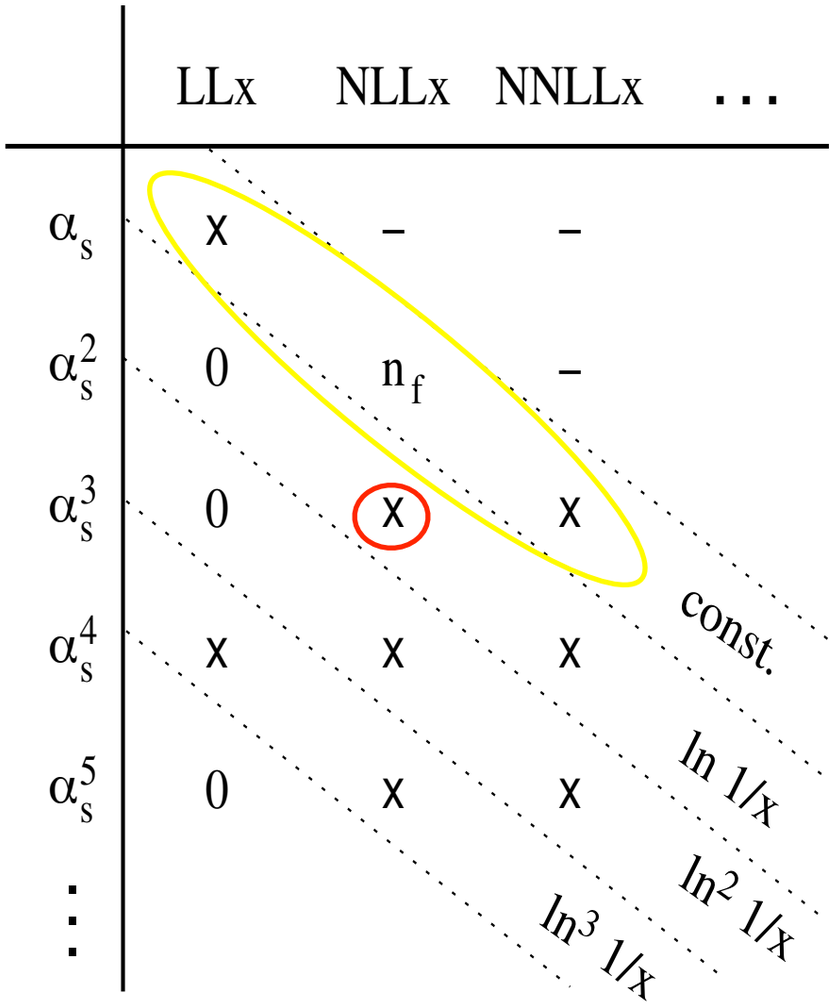

Understanding the structure of the splitting function

Perturbative terms in the splitting function

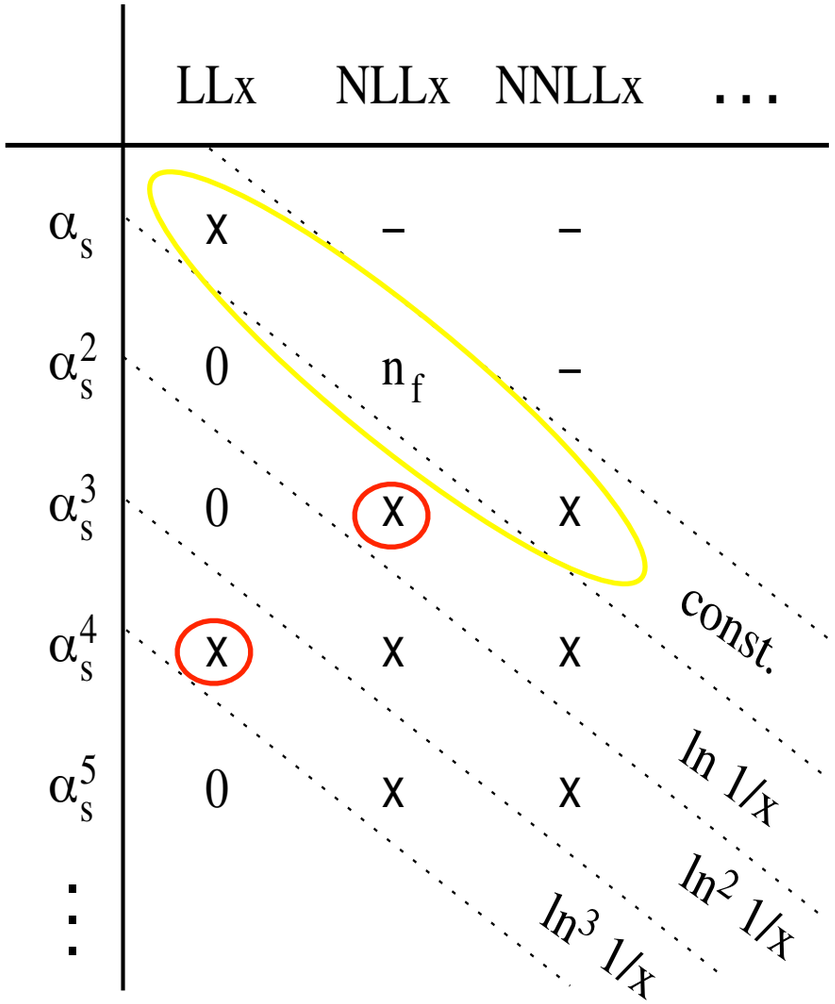

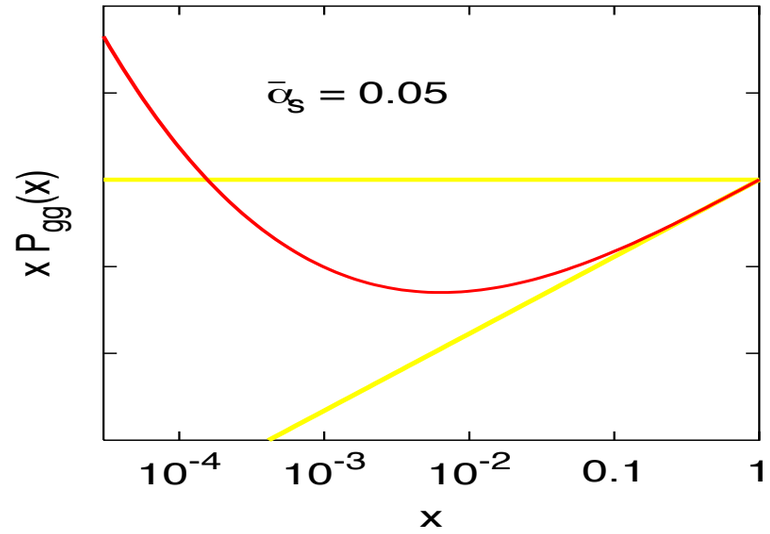

Understanding the structure of the splitting function

Perturbative terms in the splitting function

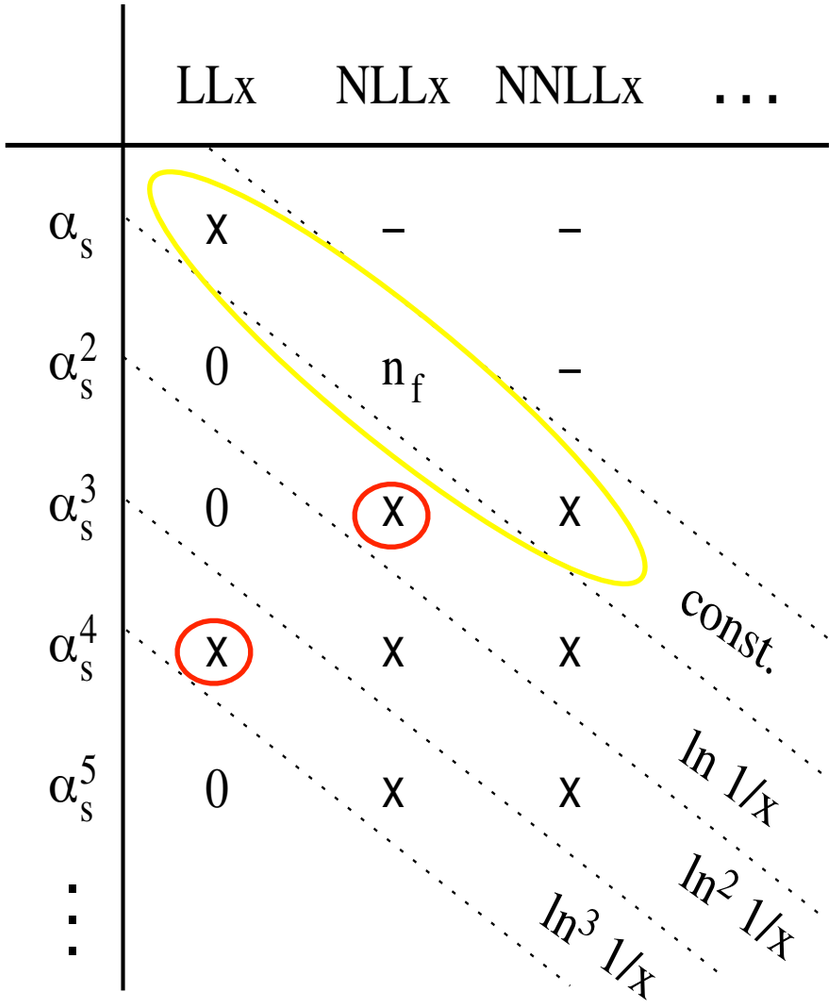

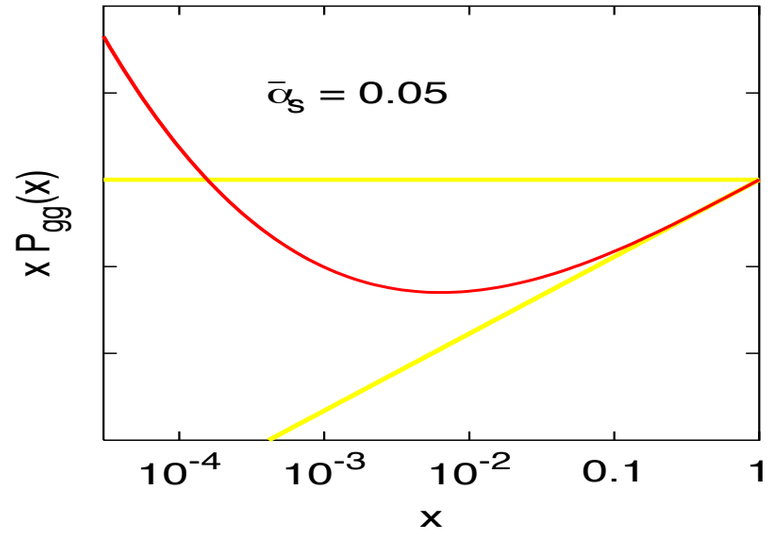

$$-1.54\bar{\alpha}_s^3 \ln 1/x \; + \; 0.401\bar{\alpha}_s^4 \ln^3 1/x$$

Understanding the structure of the splitting function

Perturbative terms in the splitting function

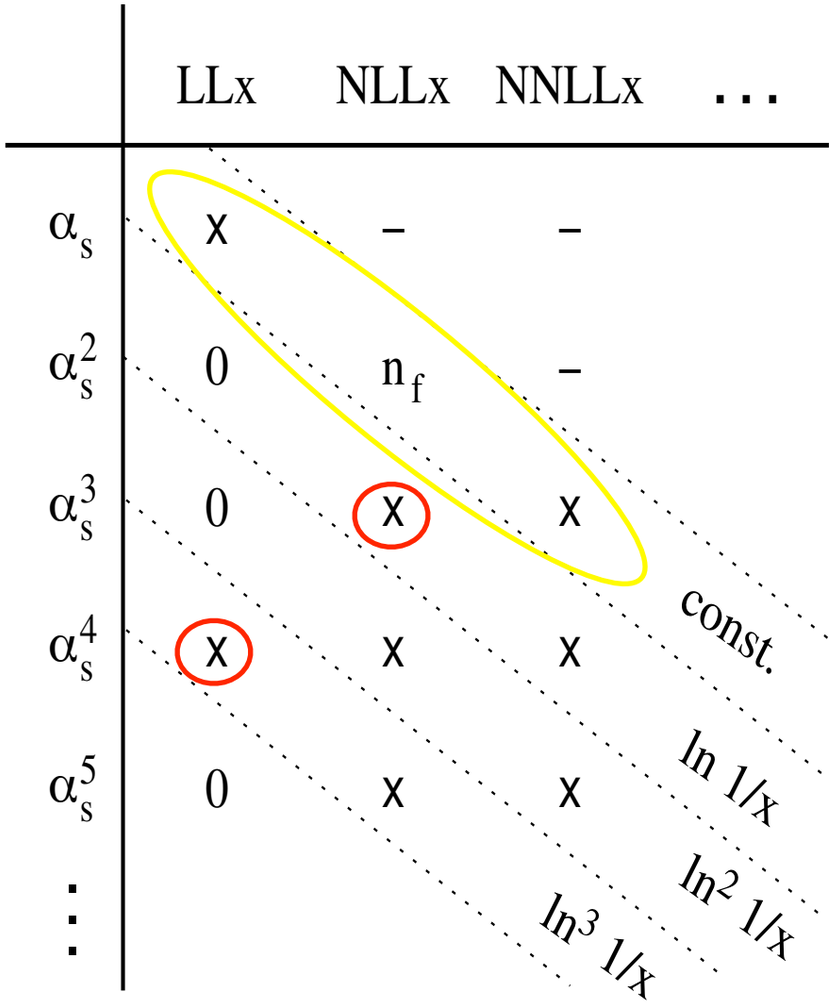

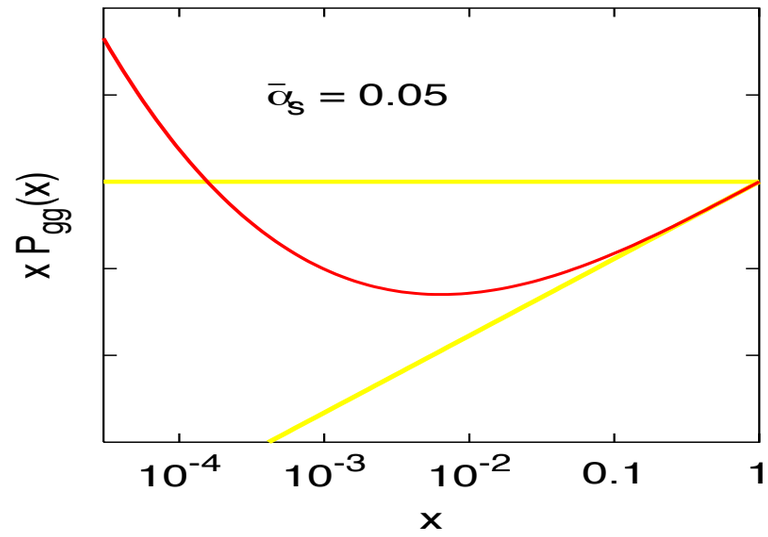

$$-1.54\bar{\alpha}_s^3 \ln 1/x \; + \; 0.401\bar{\alpha}_s^4 \ln^3 1/x$$

There is a minimum when

$$\alpha_s \ln^2 \frac{1}{x} \sim 1 \longrightarrow \ln \frac{1}{x} \sim \frac{1}{\sqrt{\alpha_s}}$$

Understanding the structure of the splitting function

Perturbative terms in the splitting function

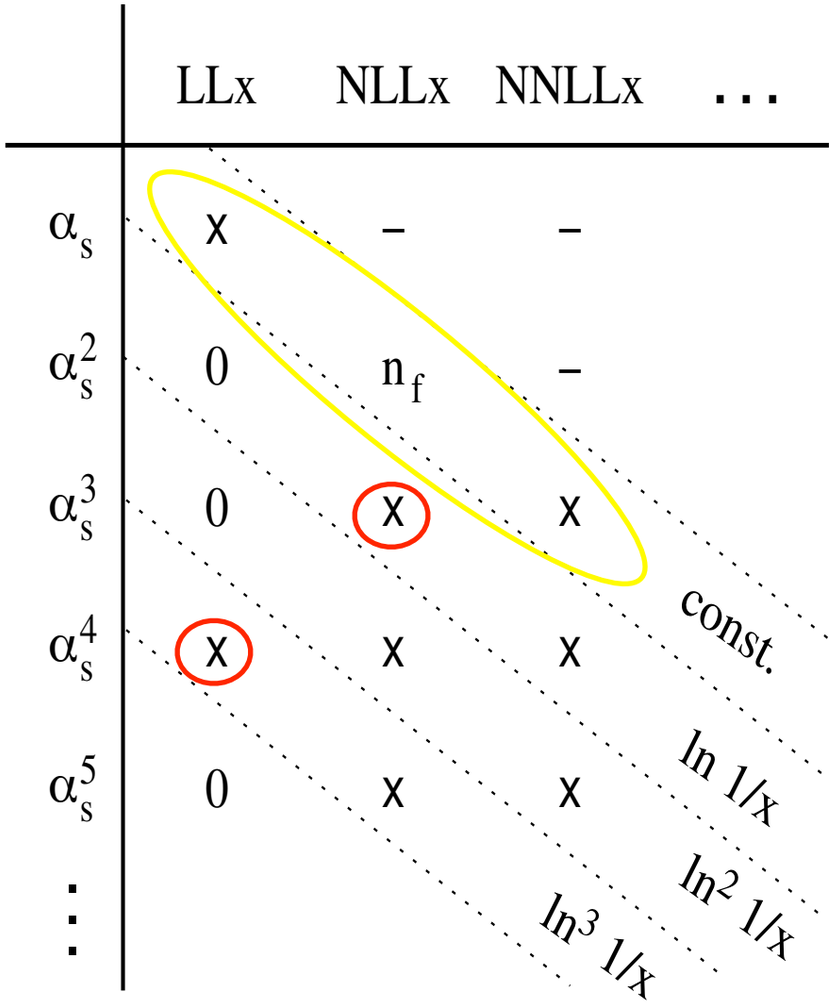

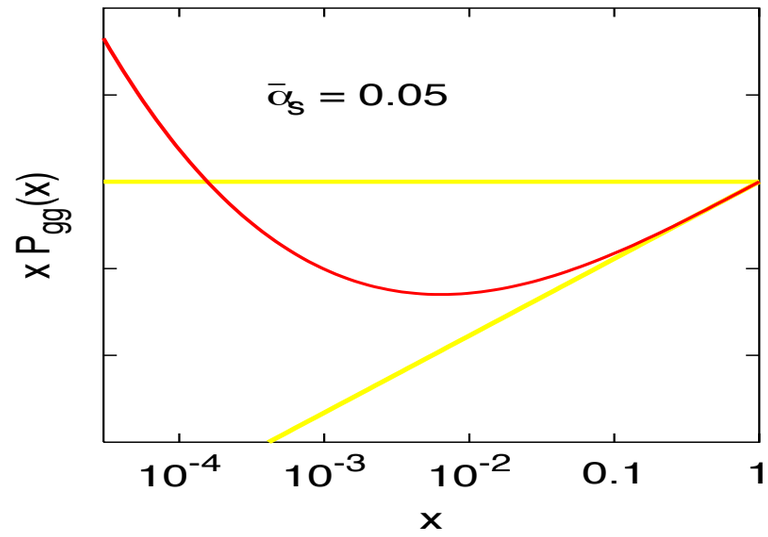

$$-1.54\bar{\alpha}_s^3 \ln 1/x \; + \; 0.401\bar{\alpha}_s^4 \ln^3 1/x$$

In general: dip comes from the interplay between NNLO and the resummation.

There is a minimum when

$$\alpha_s \ln^2 \frac{1}{x} \sim 1 \longrightarrow \ln \frac{1}{x} \sim \frac{1}{\sqrt{\alpha_s}}$$

Resummation impact on the DIS data

Ball,Bertoni,Bonvini,Marzani,Rojo,Rottoli

Resummation (implemented in ABF scheme) leads to the improvement the description of the structure function data F_2 for low x and Q.

Better than fixed order NLO, NNLO.

Better description of the longitudinal structure function F_L.

Resummation cures the problem of the negative gluon density at low x which occurred at fixed NNLO order

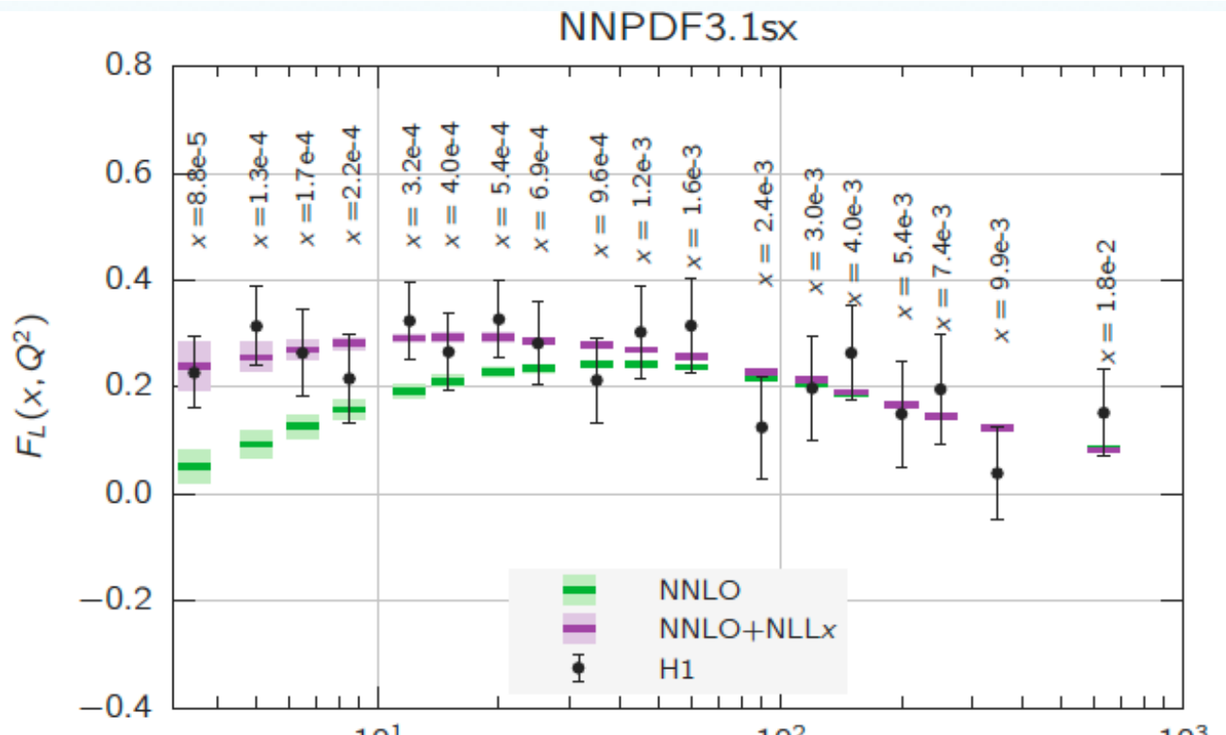

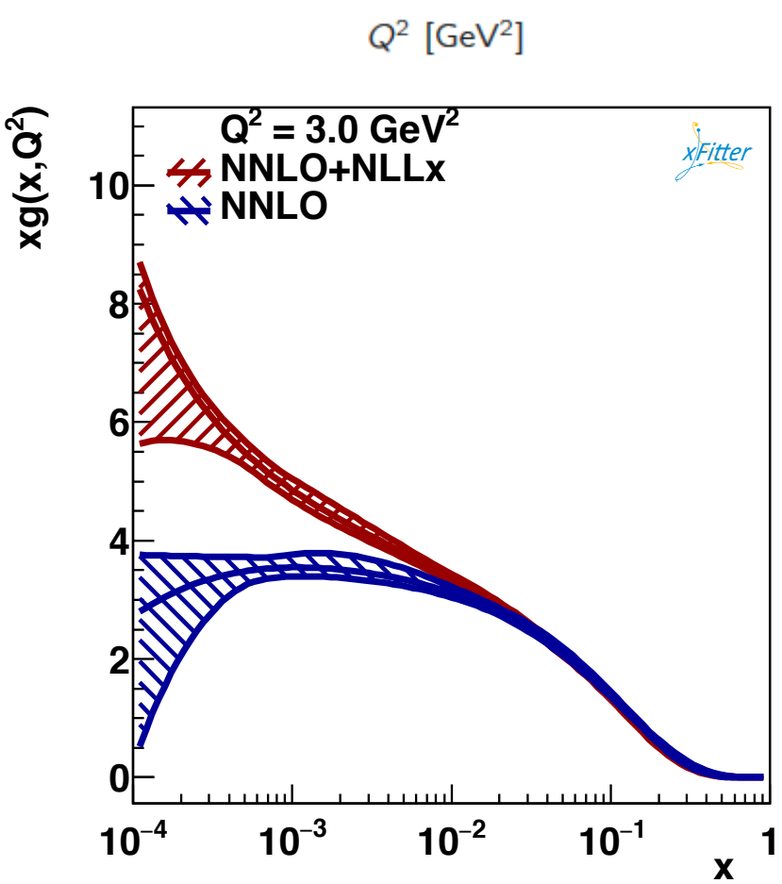

xFitter Developer's team

What happens at NNLL BFKL?

Currently the NNLL in BFKL is known in N=4 sYM but not in QCD

Gromov, Levkovich-Maslyuk, Sizov, Velizhanin,
Caron-Huot, Herranen

Structure of poles

$$\chi_2^{sYM} = \frac{1}{2\gamma^5} - \frac{\zeta(2)}{\gamma^3} - \frac{9\zeta(3)}{4\gamma^2} - \frac{29\zeta(4)}{8\gamma} + \mathcal{O}(1)$$

+ symmetric structure for poles at $\gamma = 1$

What happens at NNLL BFKL?

Currently the NNLL in BFKL is known in N=4 sYM but not in QCD

Gromov, Levkovich-Maslyuk, Sizov, Velizhanin, Caron-Huot, Herranen

Structure of poles

$$\chi_2^{sYM} = \frac{1}{2\gamma^5} - \frac{\zeta(2)}{\gamma^3} - \frac{9\zeta(3)}{4\gamma^2} - \frac{29\zeta(4)}{8\gamma} + \mathcal{O}(1)$$

+ symmetric structure for poles at $\gamma = 1$

Compare with NLL for N=4 sYM

$$\chi_1^{sYM} = -\frac{1}{2\gamma^3} - 1.79 + \mathcal{O}(\gamma)$$

The highest pole in NLL coincides at N=4 sYM and in QCD, other poles are different. Notably there are no double and single poles in N=4 sYM theory

What happens at NNLL BFKL?

Currently the NNLL in BFKL is known in N=4 sYM but not in QCD

Gromov, Levkovich-Maslyuk, Sizov, Velizhanin, Caron-Huot, Herranen

Structure of poles

$$\chi_2^{sYM} = \frac{1}{2\gamma^5} - \frac{\zeta(2)}{\gamma^3} - \frac{9\zeta(3)}{4\gamma^2} - \frac{29\zeta(4)}{8\gamma} + \mathcal{O}(1)$$

+ symmetric structure for poles at $\gamma = 1$

Compare with NLL for N=4 sYM

$$\chi_1^{sYM} = -\frac{1}{2\gamma^3} - 1.79 + \mathcal{O}(\gamma)$$

The highest pole in NLL coincides at N=4 sYM and in QCD, other poles are different. Notably there are no double and single poles in N=4 sYM theory

Since the cubic poles occur due to the shifts of the poles in the kernel, can one generate the highest poles at NNLL from the shifts as well?

Shifts at NNLL in N=4 sYM

$$\chi(\gamma,\omega) = 2\psi(1) - \psi(\gamma+\frac{\omega}{2}) - \psi(1-\gamma+\frac{\omega}{2}) = \chi_0 + \chi^{(1)}\frac{\omega}{2} + \frac{1}{2!}\chi^{(2)}\left(\frac{\omega}{2}\right)^2 + \dots\,,$$

Need to take terms up to NLL in ω

$$\omega_1 = \bar{\alpha}_s\chi_0 + \bar{\alpha}_s^2\chi_1$$

Which gives the following contribution to NNLL kernel

$$\chi_2 = \frac{1}{4}\left(\chi^{(1)}\right)^2\chi_0 + \frac{1}{8}\chi^{(2)}\left(\chi_0\right)^2$$

Shifts at NNLL in N=4 sYM

$$\chi(\gamma,\omega) = 2\psi(1) - \psi(\gamma + \frac{\omega}{2}) - \psi(1-\gamma+\frac{\omega}{2}) = \chi_0 + \chi^{(1)}\frac{\omega}{2} + \frac{1}{2!}\chi^{(2)}\left(\frac{\omega}{2}\right)^2 + \dots ,$$

Need to take terms up to NLL in ω

$$\omega_1 = \bar{\alpha}_s\chi_0 + \bar{\alpha}_s^2\chi_1$$

Which gives the following contribution to NNLL kernel

$$\chi_2 = \frac{1}{4}\left(\chi^{(1)}\right)^2\chi_0 + \frac{1}{8}\chi^{(2)}\left(\chi_0\right)^2$$

Expanding around the poles leads to the result

$$\chi_2 = \frac{1}{2\gamma^5} + \frac{\zeta(2)}{\gamma^3} + \frac{2\zeta(3)}{\gamma^2} + O\left(\frac{1}{\gamma}\right)$$

Shifts at NNLL in N=4 sYM

$$\chi(\gamma,\omega) = 2\psi(1) - \psi(\gamma + \frac{\omega}{2}) - \psi(1-\gamma+\frac{\omega}{2}) = \chi_0 + \chi^{(1)}\frac{\omega}{2} + \frac{1}{2!}\chi^{(2)}\left(\frac{\omega}{2}\right)^2 + \dots ,$$

Need to take terms up to NLL in ω

$$\omega_1 = \bar{\alpha}_s\chi_0 + \bar{\alpha}_s^2\chi_1$$

Which gives the following contribution to NNLL kernel

$$\chi_2 = \frac{1}{4}\left(\chi^{(1)}\right)^2\chi_0 + \frac{1}{8}\chi^{(2)}\left(\chi_0\right)^2$$

Expanding around the poles leads to the result

$$\chi_2 = \frac{1}{2\gamma^5} + \frac{\zeta(2)}{\gamma^3} + \frac{2\zeta(3)}{\gamma^2} + O\left(\frac{1}{\gamma}\right)$$

Compare with exact result:

$$\chi_2^{sYM} = \frac{1}{2\gamma^5} - \frac{\zeta(2)}{\gamma^3} - \frac{9\zeta(3)}{4\gamma^2} - \frac{29\zeta(4)}{8\gamma} + \mathcal{O}(1)$$

Shifts at NNLL in N=4 sYM

$$\chi(\gamma,\omega)=2\psi(1)-\psi(\gamma+\frac{\omega}{2})-\psi(1-\gamma+\frac{\omega}{2})=\chi_0+\chi^{(1)}\frac{\omega}{2}+\frac{1}{2!}\chi^{(2)}\left(\frac{\omega}{2}\right)^2+\dots\,,$$

Need to take terms up to NLL in ω

$$\omega_1=\bar{\alpha}_s\chi_0+\bar{\alpha}_s^2\chi_1$$

Which gives the following contribution to NNLL kernel

$$\chi_2=\frac{1}{4}\left(\chi^{(1)}\right)^2\chi_0+\frac{1}{8}\chi^{(2)}\left(\chi_0\right)^2$$

Expanding around the poles leads to the result

$$\chi_2=\frac{1}{2\gamma^5}+\frac{\zeta(2)}{\gamma^3}+\frac{2\zeta(3)}{\gamma^2}+O\left(\frac{1}{\gamma}\right)$$

Compare with exact result:

$$\chi_2^{sYM}=\frac{1}{2\gamma^5}-\frac{\zeta(2)}{\gamma^3}-\frac{9\zeta(3)}{4\gamma^2}-\frac{29\zeta(4)}{8\gamma}+\mathcal{O}(1)$$

Most singular terms coincide, also absence of quartic poles. The cubic poles are not reproduced.

Summary

Summary

- ✦ Higher orders in the high energy expansion - BFKL physics - are very large and lead to unstable results

Summary

- ✦ Higher orders in the high energy expansion - BFKL physics - are very large and lead to unstable results

- ✦ Resummation is needed, dominant contributions come from the DGLAP anomalous dimension, improved kinematics and running coupling

Summary

- ✦ Higher orders in the high energy expansion - BFKL physics - are very large and lead to unstable results
- ✦ Resummation is needed, dominant contributions come from the DGLAP anomalous dimension, improved kinematics and running coupling
- ✦ Resummation leads to stable results, slows down the evolution significantly

Summary

- ✦ Higher orders in the high energy expansion - BFKL physics - are very large and lead to unstable results
- ✦ Resummation is needed, dominant contributions come from the DGLAP anomalous dimension, improved kinematics and running coupling
- ✦ Resummation leads to stable results, slows down the evolution significantly
- ✦ This will slow down the approach to dense regime, delay the onset of saturation

Summary

- ✦ Higher orders in the high energy expansion - BFKL physics - are very large and lead to unstable results

- ✦ Resummation is needed, dominant contributions come from the DGLAP anomalous dimension, improved kinematics and running coupling

- ✦ Resummation leads to stable results, slows down the evolution significantly

- ✦ This will slow down the approach to dense regime, delay the onset of saturation

- ✦ Structure function data seem to indicate the need for resummation; can have much bigger effects at higher energies. Cures the problem of the negative gluon

Summary

- ✦ Higher orders in the high energy expansion - BFKL physics - are very large and lead to unstable results
- ✦ Resummation is needed, dominant contributions come from the DGLAP anomalous dimension, improved kinematics and running coupling
- ✦ Resummation leads to stable results, slows down the evolution significantly
- ✦ This will slow down the approach to dense regime, delay the onset of saturation
- ✦ Structure function data seem to indicate the need for resummation; can have much bigger effects at higher energies. Cures the problem of the negative gluon
- ✦ N=4 sYM results suggest that the ansatz for resummation is correct, at least in this case as it reproduces the leading terms.